

Biological and Medical Physics, Biomedical Engineering

Soroush Nazarpour *Editor*

Thin Films and Coatings in Biology

 Springer

Biological and Medical Physics, Biomedical Engineering

Editor-in-Chief

Elias Greenbaum, Oak Ridge National Laboratory, Oak Ridge, TN, USA

Editorial Board

M. Aizawa, Department of Bioengineering, Tokyo Institute of Technology, Yokohama, Japan
Olaf Sparre Andersen, Department of Physiology Biophysics & Molecular Medicine, Cornell University, New York, USA
Robert H. Austin, Department of Physics, Princeton University, Princeton, NJ, USA
James Barber, Department of Biochemistry, Imperial College of Science, Technology and Medicine, London, England
Howard C. Berg, Department of Molecular and Cellular Biology, Harvard University, Cambridge, MA, USA
Victor Bloomfield, Department of Biochemistry, University of Minnesota, St. Paul, MN, USA
Robert Callender, Department of Biochemistry, Albert Einstein College of Medicine, Bronx, NY, USA
Britton Chance, Department of Biochemistry/Biophysics, University of Pennsylvania, Philadelphia, PA, USA
Steven Chu, Berkeley National Laboratory, Berkeley, CA, USA
Louis J. DeFelice, Department of Pharmacology, Vanderbilt University, Nashville, TN, USA
Johann Deisenhofer, Howard Hughes Medical Institute, The University of Texas, Dallas, TX, USA
George Feher, Department of Physics, University of California, San Diego, La Jolla, CA, USA
Hans Frauenfelder, Los Alamos National Laboratory, Los Alamos, NM, USA
Ivar Giaever, Rensselaer Polytechnic Institute, Troy, NY, USA
Sol M. Gruner, Cornell University, Ithaca, NY, USA
Judith Herzfeld, Department of Chemistry, Brandeis University, Waltham, MA, USA
Mark S. Humayun, Doheny Eye Institute, Los Angeles, CA, USA
Pierre Joliot, Institute de Biologie Physico-Chimique, Fondation Edmond de Rothschild, Paris, France
Lajos Keszthelyi, Institute of Biophysics, Hungarian Academy of Sciences, Szeged, Hungary
Robert S. Knox, Department of Physics and Astronomy, University of Rochester, Rochester, NY, USA
Aaron Lewis, Department of Applied Physics, Hebrew University, Jerusalem, Israel
Stuart M. Lindsay, Department of Physics and Astronomy, Arizona State University, Tempe, AZ, USA
David Mauzerall, Rockefeller University, New York, NY, USA
Eugenie V. Mielczarek, Department of Physics and Astronomy, George Mason University, Fairfax, VA, USA
Markolf Niemz, Medical Faculty Mannheim, University of Heidelberg, Mannheim, Germany
V. Adrian Parsegian, Physical Science Laboratory, National Institutes of Health, Bethesda, MD, USA
Linda S. Powers, University of Arizona, Tucson, AZ, USA
Earl W. Prohofsky, Department of Physics, Purdue University, West Lafayette, IN, USA
Andrew Rubin, Department of Biophysics, Moscow State University, Moscow, Russia
Michael Seibert, National Renewable Energy Laboratory, Golden, CO, USA
David Thomas, Department of Biochemistry, University of Minnesota Medical School, Minneapolis, MN, USA

For further volumes:

<http://www.springer.com/series/3740>

The fields of biological and medical physics and biomedical engineering are broad, multidisciplinary and dynamic. They lie at the crossroads of frontier research in physics, biology, chemistry, and medicine. The Biological and Medical Physics, Biomedical Engineering Series is intended to be comprehensive, covering a broad range of topics important to the study of the physical, chemical and biological sciences. Its goal is to provide scientists and engineers with textbooks, monographs, and reference works to address the growing need for information.

Books in the series emphasize established and emergent areas of science including molecular, membrane, and mathematical biophysics; photosynthetic energy harvesting and conversion; information processing; physical principles of genetics; sensory communications; automata networks, neural networks, and cellular automata. Equally important will be coverage of applied aspects of biological and medical physics and biomedical engineering such as molecular electronic components and devices, biosensors, medicine, imaging, physical principles of renewable energy production, advanced prostheses, and environmental control and engineering.

Soroush Nazarpour
Editor

Thin Films and Coatings in Biology

 Springer

Editor
Soroush Nazarpour
Group NanoXplore Inc.
Montreal, QC
Canada

ISSN 1618-7210
ISBN 978-94-007-2591-1 ISBN 978-94-007-2592-8 (eBook)
DOI 10.1007/978-94-007-2592-8
Springer Dordrecht Heidelberg New York London

Library of Congress Control Number: 2013943464

© Springer Science+Business Media Dordrecht 2013

This work is subject to copyright. All rights are reserved by the Publisher, whether the whole or part of the material is concerned, specifically the rights of translation, reprinting, reuse of illustrations, recitation, broadcasting, reproduction on microfilms or in any other physical way, and transmission or information storage and retrieval, electronic adaptation, computer software, or by similar or dissimilar methodology now known or hereafter developed. Exempted from this legal reservation are brief excerpts in connection with reviews or scholarly analysis or material supplied specifically for the purpose of being entered and executed on a computer system, for exclusive use by the purchaser of the work. Duplication of this publication or parts thereof is permitted only under the provisions of the Copyright Law of the Publisher's location, in its current version, and permission for use must always be obtained from Springer. Permissions for use may be obtained through RightsLink at the Copyright Clearance Center. Violations are liable to prosecution under the respective Copyright Law. The use of general descriptive names, registered names, trademarks, service marks, etc. in this publication does not imply, even in the absence of a specific statement, that such names are exempt from the relevant protective laws and regulations and therefore free for general use.

While the advice and information in this book are believed to be true and accurate at the date of publication, neither the authors nor the editors nor the publisher can accept any legal responsibility for any errors or omissions that may be made. The publisher makes no warranty, express or implied, with respect to the material contained herein.

Printed on acid-free paper

Springer is part of Springer Science+Business Media (www.springer.com)

Contents

1	Introduction: What are Coatings?	1
	Soroush Nazarpour	
2	Biocompatibility of Thin Films	11
	Mareike Zink	
3	Modern Porous Coatings in Orthopaedic Applications	69
	Rachel M. Frank, David Fabi and Brett R. Levine	
4	Biofunctional Coatings for Dental Implants	105
	Xi Chen, Yuping Li and Conrado Aparicio	
5	Nano-Bio Structures Developed via Electrophoresis	145
	Cyrus Zamani	
6	Diamond-Like Carbon Coated on Polymers for Biomedical Applications	171
	Atsushi Hotta and Terumitsu Hasebe	
7	Surface Modification of Biodegradable Polyesters for Soft and Hard Tissue Regeneration	229
	Hesameddin Mahjoubi, Sara Abdollahi and Marta Cerruti	
8	Thin Film Biosensors	265
	Hatice Ceylan Koydemir, Haluk Külah and Canan Özgen	

9 Thin Film Coatings as Electrodes in Neuroscience	301
Saida Khan, Ahsan Mian and Golam Newaz	
10 Scanning Electrochemical Microscopy Applied to Cancer Related Studies	331
Isabelle Beaulieu and Janine Mauzeroll	
Index	363

Chapter 1

Introduction: What are Coatings?

Soroush Nazarpour

Thin film and coating science and technology is by far one of the oldest arts dating back to metal ages of ancient history. Consider the Egyptian Gold plating or Mali Empire Blood coating, which has been practiced continuously for several millennia. Egyptian covers their sculptures to preserve them from chemical degradation and Sculptors from the extraordinarily wealthy ancient Mali Empire, once the source of nearly half the world's gold, at times coated their works of art with blood of animals shed during ancient ceremonies. Throughout the history, our ancestors applied coatings of different materials and liquids to generate desirable properties such as durability, mechanical strength, and optical appearance. During the years, coating industry becomes more and more advanced as such, turned to a crucial segment of today's technology. Outnumbered applications in the area of protection, decoration, optics, electronics, energy, and biomedicine have been developed and coating market grows with a rapid pace. Thousands of articles are being published every year justifying novel applications of advanced coatings and thin films. Of those, bio-coating requires a special attention due to the fact that it deals with human life. Interest of funding agencies and governors to dedicate large financial budget in order to develop nanobiotechnology during the last 20 years in US and Canada, and last 10 years in UK and Europe reveals this importance. This book is a snapshot of recent improvements in this area and collects the fresh ideas of experts, those that push forward the boundary of bio-coating science and technology.

In general, the surface of materials is routinely exposed to various environmental influences. These surfaces are subjected to Humidity, wear, corrosion, and interact with light and electromagnetic fields. Therefore, the choice of appropriate material that withstands these severe working conditions becomes too limited. Changing the properties of the surface enables us to continue the usage of conventional metals. For instance, beauty, outstanding electrical conductivity, and

S. Nazarpour (✉)
President and CEO of Group Nano Xplore Inc, 2050 Rue Dandurand,
Suite 004, Montreal, QC H2G1Y9, Canada
e-mail: nazarpour@nanoxplore.ca

Fig. 1.1 This ankh amulet is plated with gold. The Ankh is a symbol of eternal life and power bestowing boons of health, protection and authority to the bearer



chemical stability of Gold introduce it as a potential candidate for several applications, however, its high cost does not justify its usage as the base material. Hence, coatings of Gold on the rather cheaper metal such as steel generates an opportunity for a surface with tailored properties (Fig. 1.1).

In general terms, substrate is the base material that is being coated and coating is the solid or liquid body which exhibits a significantly lower geometrical extension in one dimension than in the remaining two spatial dimensions. The properties of the film or coating have to differ significantly from the bulk. Generally coatings are assumed to be thick films with thickness of at least $1\ \mu\text{m}$, whereas films with thickness lower than $1\ \mu\text{m}$ are “thin films”. Therefore, by reducing the thickness from several hundreds micrometer to a few nanometers, bulk turns into coating and after that, thin films. From the technological point of view the miniaturization of mechanic, electronic, optic and optoelectronic components permanently increases the surface to volume ratio of the involved materials. This results into severe changes in the properties of coatings and thin films in comparison with their bulk counterparts. This reduction changes the material’s properties such as increase of electrical resistivity and decrease of melting point. A recent tutorial review by Emil Roduner [1], reveals the importance of the size of nanomaterials and the reasoning behind the abnormal change of their properties due to the reduction of the surface to volume ratio (surface effect) and quantum size effect that results into changes of the electrical properties and density of states of nanomaterials.

Coating posses a massive market with several large segments. The global market for coatings is forecast to reach \$107 billion in value by the year 2017 with UV-cure coating and coating for medical devices and health industry as one of the most rapid growing segments. Recent market reports estimate that medical device coating and surface modification treatment industry will reach nearly \$8 billion by 2017. Indeed, The biomaterials sector is rapidly expanding and significant advances have been made in the technology of biomedical coatings and materials, which provide a means to improve the wear of joints, change the biological interaction between implant and host and combine the properties of various

materials to improve device performance. Rapid growth of this market proved that it was only a matter of time before some marketing Wall Street companies jumped onto the nanotechnology bandwagon and created a fund to capture the field's expected growth. A clue to visualize the progress of fast growing bio-coating field is the arrangements in NSF, NIH, and NCI/NASA to support nanobotechnology research proposals. Many of the government agencies granting funds for nanobiotechnology are well aware of the potential commercial applications of the supported projects. In fact, a common theme among the program solicitations issued by these agencies is the application and commercialization of the fruits of nanobio research. Both the NIH and NSF have announced Small Business Innovation Research (SBIR) programs to help support work being done in small business settings. And NIH and NSF encourage businesses applying for these awards to collaborate with nonprofit research organizations. If the recent past is any indication of things to come, the funding future for nanobiotechnology looks extremely bright as well as its potential for commercialization.

Having said all, interesting properties of coatings and thin films in biology as well as lack of a strong and complete book inspired authors to draft this book. This book intends to fulfill the recent gap in the literature where final applicable ideas are missing and to categorize the recent progresses and spectacular findings from the scientific point of view. Having said that the purpose of this book is to orientate the future scientific efforts on thin films and coatings toward industrial application in biology, some examples such as application of Diamond like carbon in biology and coating for dental implants will be deeply studied. Essentially, tailoring the structural properties and fabrication process of coatings and layers can pave the way for healing and organ replacement. For instance, great effort is already being done to generate artificial skins fully integrated with multifunctional nanosensors. These skins have the ability to sense even small change in surrounding climate and can foster the reliability of the underneath electronic parts when a robot is replaced with a human in hazardous situation such as fire fighting and radioactive polluted regions. Potential application of thermoelectric layers in future nanorobots which may flow between blood cells to detect the enzymes and cancerous cells could be one of the several future break through on this field that are still far from commercialization and need further studies.

1.1 Thin Films and Coating Deposition Techniques

Basically all sorts of coatings and thin film deposition process and characterization techniques require a special environment such as vacuum, a reduced environment, or a chemical solution. This environment assists ad-atoms to reach into the substrate and impinge onto that. Ad-atoms diffuse on the surface and coalesce to form a semi-continuous and continuous film. Growth depends on energetically favorable sites at the surface. At a surface an ad-atom may find kink sites, steps, clusters, vacancies, impurities to impinge. These sites are energetically favorable for

ad-atoms to diffuse into. Since diffusion is a thermally activated process, substrate temperature is an important factor defining the growth mode. Depending upon substrate temperature, three mechanisms have been postulated for thin film growth. At high substrate temperature, ad-atoms diffuse rapidly into kinks and steps resulting into step growth (Fig. 1.2a). This type of growth is called layer by layer leading to a highly textured film and even an epitaxial layer when lattice dimensions of film and substrate are comparable. At low substrate temperatures, ad-atoms have a limited surface mobility and form 2D islands (b). Third scenario represents a layer-by-layer growth (Frank–van der Merwe growth) that follows with a island growth (Volmer–Weber growth). This growth mode is so called Stranski–Krastanov, which is an intermediary process characterized by both 2D layer and 3D island growth (c). Transition from the layer-by-layer to island-based growth occurs at a critical layer thickness, which is highly dependent on the chemical and physical properties, such as surface energies and lattice parameters, of the substrate and film [2, 3]. In this growth mode, mobility of ad-atoms is limited by reaching an ad-atom to an atomic step (Effect of the Ehrlich–Schwoebel barrier, [4]).

1.1.1 Chemical and Electrochemical Techniques

These are those types of deposition in which ions in a solution are moved by an electric field (sometimes electroless) to coat an electrode. The process uses electrical current to reduce cations of a desired material from a solution and coat a conductive object with a thin layer of the material, such as a metal.

- Anodizing

Anodizing is a process that a natural oxide grows over the surface of a metal in order to improve its surface properties such as corrosive. Anodizing normally

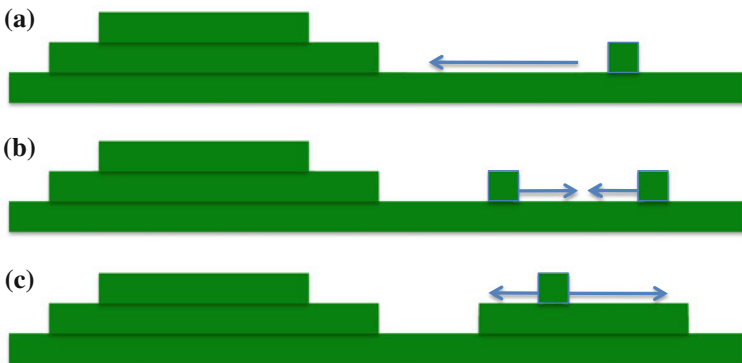


Fig. 1.2 **a** Frank–van der Merwe growth, **b** Volmer–Weber growth, and **c** Stranski–Krastanov growth

applies onto metallic implants such as Aluminum and Titanium to improve their biocompatibility.

- Conversion coating

Conversion coating is a passivation process that generates metallic oxides on a surface by rinsing the surface into acids such as chromic acid. This technique has outnumbered application as corrosion inhibitor, primer, decorative finish, or to retain electrical conductivity. Main techniques of conversion coatings are:

- Chromate conversion coating
- Plasma electrolytic oxidation (Plasma is the source to general electrochemical reaction on the surface. This is a similar process to Anodizing)
- Phosphate conversion coating (In phosphating process, Phosphoric acid is the source to generate oxides over steel)
- Ion beam mixing

In order to adhere a deposited film onto a substrate, ion beam could be used to irradiate onto the film. Irradiation generates the required energy to strengthen the bonds in the interface of single- or multi-layered films.

- Plating

Plating is one the most known and old deposition techniques in which a metal is deposited onto a conductive surface. A known application of plating is finishing gold and silver. Recent efforts to deposit few atoms using plating pushed this technique into nanoscale [5].

- Sol-gel

This process involves the transition of a solution system from a liquid “sol” (mostly colloidal) into a solid “gel” phase. “sol” acts as the precursor for an integrated network of either discrete particles or network of polymers in order to fabricate materials such as metal oxides.

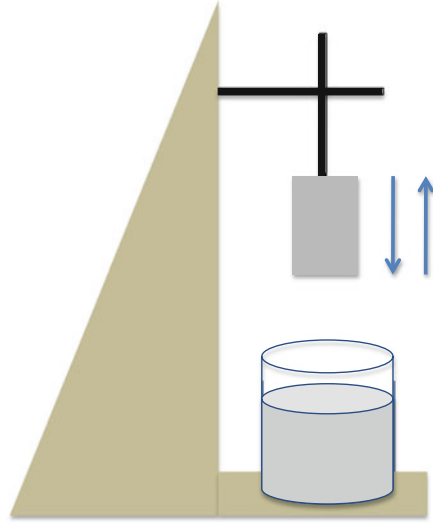
- Dip-coating

This is the process that substrate enters into the bath of liquid and exits, as a result, a uniform layer of the solvent stick onto the substrate. This is a common process for measuring cell adhesion (Fig. 1.3).

1.1.2 Chemical Vapor Deposition

Chemical Vapor Deposition (CVD) is a technique to deposit films and coatings using chemical reactions of gaseous reactants on or near the vicinity of a heated substrate surface. This deposition techniques can provide highly pure materials

Fig. 1.3 Schematic of dip coating



with structural control at atomic or nanometer scale level. CVD covers processes such as:

- Plasma enhanced chemical vapor deposition (PECVD)

PECVD, as one of the fastest deposition techniques, is widely used for fabrication of nitride and carbides of metals for several applications such as anti-corrosive and wear resistant coatings.

- Atomic layer deposition (ALD)

ALD is winning process when thickness control in the range of Angstrom is important. This technique is extendible to large substrates since precursors are gas phase molecules, and they fill all space independent of substrate geometry and do not require line- of-sight to the substrate. Complete information regarding ALD could be found at the work of George [6].

- Atmospheric pressure CVD (APCVD) and Low-pressure CVD (LPCVD)

Depending upon the operating pressure of CVD, film uniformity could be controlled. Reducing the operating pressure from atmospheric pressure to ultra high vacuum reduces unnecessary gas reactions in the chamber, and enhances the film uniformity across the wafer.

- Metalorganic chemical vapor deposition (MOCVD)

MOCVD is a complex deposition process in which a metal organic precursor such as Dimethyles of metals is used to generate a chemical reaction rather than physical adsorption. It is been widely used in semiconductor and manufacturing.

1.1.3 Physical Vapor Deposition

PVD is a process based on condensation of the film's vapor onto the substrate at normally high vacuum. Depending upon the source of energy for evaporation of the material, different categories could be schemed.

- Electron beam physical vapor deposition (EBPVD)

In this process, tungsten filament generates electron beams that bombard the deposition material (anode), under high vacuum. As a result, deposition material turns into gas and impinges onto the substrate (cathode), and generates a layer. Deposition rate could vary from a few nanometers to micrometers per minute.

- Sputtering

In sputtering, high energy particles (normally Ar⁺) bombard the target resulting into some sputtered particles with wide range of energy. These particles move within the chamber ballistically and absorb on the substrate. With this technique, several types of materials could be deposited. This is a rapid and scalable process with several applications in health and biology such as Au or carbon deposition for making the biological samples conductive for electron imaging or calcium deposition for osteoblast cells.

- Pulsed laser deposition (PLD)

PLD is a process that a high power pulsed laser hits the target and evaporates it at ultra high vacuum. In fact, laser ablates the target and generates a plasma plume of high-energy particles on the substrate. As a result, ablated materials impinge on the substrate, nucleate, coalesce, and grow (Fig. 1.4).

1.1.4 Spray Deposition

Spraying is a process in which powders of materials such as ceramics or molten metals spray onto a substrate to generate a thick layer of the sprayed material. Spray deposition is categorized depending upon the type of energy source. Coatings prepared by spray deposition have extensive applications as biocompatible coatings.

- Flame spraying—Combustion powder coating

Flame spray is basically the first spraying technique. In the flame-spraying torch, fuel gas reacts with oxygen and the chemical energy of combustion generate a hot flame. Powders, rods, and wires could be injected into hot flame and be deposited over the substrate. Flame temperatures are in the range from 3000 to 3400 K with velocity equal to 8–10 m/s. This process has outnumbered

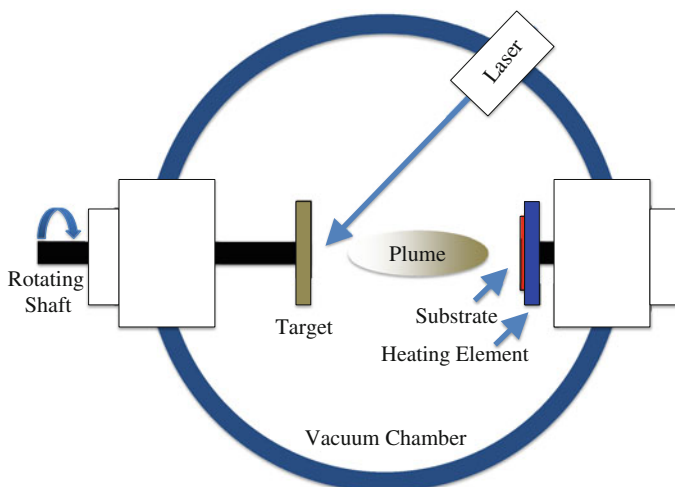


Fig. 1.4 Schematic of a PLD system

applications in the health and biological applications such as fabrication of bio-compatible coatings (e.g. TiO_2).

- Plasma spraying

In this process, rather than a hot flame, plasma is the source of energy for deposition. The temperature of the plasma torch normally reaches to 14,000 K generating a velocity of 800 m/s. High temperatures of the plasma provide the possibility for deposition of high melting point materials. This process received a great attention in biology and health due to enabling the deposition of bioceramics and surface modification of metallic implants.

- High velocity oxygen fuel (HVOF)

In HVOF, fuel gas or liquid and oxygen are injected into the combustion chamber. An ignition initiates the combustion. The powder is introduced into the jet chamber to be sprayed over the substrate. Depending upon the choice of fuel, flame temperature would vary. Normally it reaches around 3,000 K and a velocity of 2,000 m/s. Higher velocity of incidence increases the adhesive properties of the deposited coating. Many kinds of polymer and nanocomposites could be deposited with HVOF.

1.2 Thin Films and Coatings in Biology

In this book, well-known researchers and experts in bio-coating include their recent achievements and break-through in the field. First chapter dedicates to the very important subject of biocompatibility of thin films. In this chapter,

biocompatibility of different types of materials has been studied with a special attention into the characteristics of advanced materials such as shape memory alloys and carbon nanotube. Second chapter reveals the application of modern coatings in orthopedic applications. This chapter has been written by R. M. Frank, D. Fabi, and B. R. Levine who all are medical doctors and add insights into the book from a medical point of view. [Chapter 3](#) deals with the recent development in the field of dental implant using biofunctional coatings. [Chapter 4](#) introduce a novel technique for preparation of nano-bio- structures such as thin films using electrophoresis. [Chapter 5](#) targets Diamond-Like Carbon and their capabilities for biomedical applications. [Chapter 6](#) deals with biodegradable coatings and layers for tissue regeneration and precisely explains the importance of surface modification and its methods. [Chapter 7](#) greatly discuss about the outstanding application of thin films in biosensing and sensing strategies for biomolecular detection, as well as an interesting insight into *lab-on-a-chip* and *human-on-a-chip* systems. [Chapter 8](#) explains how arrays of electrodes can make a big difference in neuroscience by detecting brain signals. Metallic, polymeric, and carbon nanotube-based electrodes were well explained. Last but not least, [Chapter 9](#) pushes the boundaries of cancer detection using scanning electrochemical microscopy. Method, apparatus, and challenges on the way were all been explained.

References

1. Roduner, E.: Size matters: why nanomaterials are different. *Chem. Soc. Rev.* **35**, 583–592 (2006)
2. Venables, J.: *Introduction to Surface and Thin Film Processes*. Cambridge University Press, Cambridge (2000). ISBN 0-521-62460-6
3. Pimpinelli, A., Jacques, V.: *Physics of Crystal Growth*. Cambridge University Press, Cambridge (1998). ISBN 0-521-55198-6
4. Schwoebel, R.L.: Step motion on crystal surfaces. *J. Appl. Phys.* **37**(10), 3682–3686 (1966)
5. Kuo, H.S., Hwang, I.S., Fu, T.Y., Wu, J.Y., Chang, C.C., Tsong, T.T.: Preparation and characterization of single-atom tips. *Nano Lett.* **4**(12), 2379–2382 (2004)
6. George, S.M.: Atomic layer deposition: an overview. *Chem. Rev.* **110**, 111–131 (2010)

Chapter 2

Biocompatibility of Thin Films

Mareike Zink

Abstract The interaction of soft living matter with different substrate materials such as thin films made of metals, ceramics and carbon-based materials have attracted more and more interest over the last decades. Thin films yield the potential to build miniaturized devices for tissue regeneration, implants, stents, as well as drug delivery systems. However, the interaction of materials with cells and tissue must first be investigated in detail to ensure safe and long-time handling when implanted within the human body. This chapter describes the basics of biocompatibility and bioactivity of thin films and gives a short introduction how behavior and viability of cells and tissue in contact with different materials are assessed. In fact, biocompatibility properties in terms of corrosion resistance and the in vitro and in vivo performance of thin films made of metals, alloys, ceramics, carbon-based materials and nanostructured films will be discussed, as well as their application. This chapter ends with an outlook on future applications and requirements to supply new thin film based materials for medical applications in a fast growing market of miniaturized devices for diagnosis and therapy.

2.1 Introduction: Biocompatibility and its Assessments

Thin films and coatings of many different materials offer a wide range of applications in biology and medicine. Prerequisite is the integrity of the soft living matter in contact with the material, which is the scope of this chapter. Because of the variety of biological systems, the term *biocompatibility* has many different definitions. Generally, biocompatibility is meant to describe an “appropriate” interaction of living matter such as single cells and tissue with other non-living

M. Zink (✉)

Faculty of Physics and Earth Sciences, Institute of Experimental Physics 1,
University of Leipzig, Linnéstr. 5, 04103 Leipzig, Germany
e-mail: zink@physik.uni-leipzig.de

materials. It can consider the performance of a material *in vitro*, i.e. cell/tissue-material interaction in a Petri dish, or *in vivo*, i.e. within the living body of an animal or human.

Initially, biocompatibility was referred to the effect a material has on a biological system, while nowadays the term is employed to describe (1) an appropriate response of the host tissue and living system to the material, and (2) the response of the material due to contact with living matter [1]. Additionally, the term *bioactivity* is introduced to describe biocompatible materials onto which cells and tissue can adhere. A material is named *hemocompatible* or *haemocompatible* if it possesses adequate response in contact with blood.

There are several possibilities why materials feature good or bad biocompatibility. Surface structure and roughness determine cell adhesion properties and can enhance or suppress corrosion and degradation. *Biodegradation* describes the chemical dissolution of material by biological means, e.g. under physiological conditions *in vitro* and *in vivo*. Cell cultures and the human body are corrosive environments. They contain large quantities of chloride ions, which can promote ion release from the substrate or implanted material. Biocompatibility depends on how many ions dissolve, if these ions are toxic at the released concentration, and how quickly corrosion proceeds. Many metal ions can cause the formation of blood platelets increasing the risk of thrombosis or bind to proteins disabling their function.

Generally, three different assessments to study corrosion properties are employed. The easiest experiment *in vitro* is soaking the material in simulated body fluid (SBF). Here the material is exposed to a saline fluid with similar salt concentrations as present in the body for a certain period under physiological conditions at 37 °C and pH 7.4. Subsequently, the concentration of ions released from the material into the fluid is measured, and possible changes of the material surface can be examined with microscopy techniques and energy dispersive X-ray spectroscopy (EDX). In order to investigate corrosion rates in more detail, potential differences between the anodic and cathodic site of two electrodes—the test material and a reference—can be determined by potentiodynamic and potentiostatic measurements. In the potentiodynamic test, the sample material is placed in a test solution, which can be pure water or strong acids, and the potential difference between the sample and reference electrode is increased while monitoring the current. When pitting corrosion and damage of the sample electrode occur, the potential scan direction is reversed. This breakdown potential denotes the voltage at which the surface layer of the sample is corrupted and destruction of the materials starts. Furthermore, the voltage at which the current density decreases to an extremely low value gives the repassivation potential when a protective surface layer is formed.

In contrast to the pitting corrosion assessment, potentiostatic tests assess only the repassivation behavior of a material. A sample with an initially damaged surface is placed in a solution together with a reference electrode, and the potential difference between them is lowered while monitoring the current density. At very low densities, a new protective layer has formed and no corrosion occurs anymore.

Passivation by oxidization plays an important role in the biocompatibility of metal surfaces because metal oxides often feature much better corrosion resistances compared to their un-oxidized counterparts.

Determining only the corrosion behavior of a material does not give adequate information about possible responses with living matter. Nevertheless, if a material with high contents of nickel and other toxic ingredients is highly corrosive under physiological conditions, it is for sure that it cannot be used for biomedical purposes. First biocompatibility tests with living material are usually carried out with single cells in vitro. Here one has to distinguish between cell lines and primary cells. Cell lines are immortalized cells which are often standardized with specific cellular features. They exhibit a very good test system and are usually recommended by national guidelines, such as the American Food and Drug Administration and the ISO guidelines for assessing biocompatibility. In contrast, primary cells extracted from humans display specific features of cells much better than cell lines. However, they are difficult to handle, expensive and quickly change their characteristics in cell culture. Furthermore, handling must be approved by an ethics committee.

Fibroblasts are the most common type of cells in connective tissue. The fibroblast cell line NIH 3T3 is a well-known test system and often employed for first-step biocompatibility assessments. HUVEC (Human Vascular Endothelial Cell) is a cell line of endothelial cells that play an important role in the formation of blood vessels. To this end, these cells in contact with a sample material display a test system for hemocompatibility assessment. Neuronal cells from the brain can be used to determine the interaction of materials employed for neuro-stimulating electrodes. Very important is the interaction of osteoblast cells with implant materials. Osteoblasts are bone-forming cells, while osteoclast cells are responsible for bone resorption.

In in vitro tests cells are usually seeded onto the test material and their proliferation behavior, morphological changes, adhesion, as well as cytotoxic effects are monitored. In a first step cell adhesion to the material is eye-catching under the microscope. Surfaces which are non-toxic but do not allow cells to adhere however, lead to the induction of apoptosis because all cells—beside blood cells—need substrate materials to attach. Cells that do adhere display different morphological features on different materials and surface structures which give rise to adhesion strength. Large and well-spread cells are usually stronger attached to the substrate than small and rounded cells. However, for non-transparent substrate materials, cells appear to be invisible under the microscope, phase contrast imaging techniques cannot be used and fluorescent dyes must be employed to visualize the cells.

A simple viability assay is the application of calcein acetoxymethyl ester (AM) and propidium iodide (PI). Calcein AM is a live staining dye for viable cells. It permeates the membrane of a cell and is converted to strongly green fluorescent calcein when hydrolyzed by intracellular esterases in live cells. Cells are then imaged by fluorescence or confocal laser scanning microscopy. In contrast, PI can

only enter apoptotic cells and can be used to detect these cells by imaging their red fluorescent nuclei.

A well-established method to label cells and count them to investigate proliferation and cell division rates is the MTT test. During the test, adherent cells are exposed to the agent MTT (3-(4,5-dimethylthiazol-2-yl)-2,5-diphenyltetrazolium bromide) which is converted to insoluble purple formazan that can be imaged by fluorescence techniques. The stronger the signal, the more viable cells are present in the culture dish. In contrast, the Trypan Blue assay, which is applied similarly, only stains dead cells, and is thus a dye exclusion method.

Cytotoxic effects that result in necrosis and apoptosis can be determined *in vitro* by measuring the mRNA profiles of tumor necrosis factor (TNF)- α and interleukin, e.g. (IL)-1 β and IL-6 with polymerase chain reaction (PCR). TNF- α , IL-1 β and IL-6 are cytokines and important signaling molecules when inflammation responses and cell death occur due to foreign materials and ions in the cellular surrounding.

However, even if cytotoxic effects are absent, good performance of an implant material is not ensured. Bioactivity and strong bonding of bone to prosthesis is a prerequisite for a long-time stability and durability of an artificial joint. In order to investigate possible reactions of bone cells with substrate materials *in vitro*, measuring alkaline phosphatase activity is a good marker for biocompatibility. Alkaline phosphatase activity of cells results in the deposition of extra-cellular calcium of osteoblast cells. Calcium is then transformed to bone-forming material on the substrate surface.

In vivo the performance of implant materials to replace joints or fixate bone is enhanced if osteoblast activity is stimulated by simultaneous reduction of osteoclast function. An *osseconducting* surface promotes bone growth in terms of osteoblast proliferation, which is important to suppress bone shrinkage due to osteoclast activity and failure of prostheses. If hard bone tissue can directly attach to a substrate material without the formation of a soft tissue layer, (e.g. fibrous tissue) it allows *osseointegration*, which is the most natural contact with best life-time perspective between implant and bone. *Osteoconduction*, as well as *osseointegration* can be promoted by changing the surface structure of an implant or by coating it with *osseointegration* supporting materials.

The strength of the bonding between bone and the implant *in vivo* can be addressed with pushout and pullout test. Here a force is applied to the implant to push or pull the material out of the bone. The higher the force needed to remove the implant, the better the bonding. However, over time the interface between the implant and the tissue can change. Inflammation, the formation of fibrous tissues that encapsulate the material can occur even years after initial implantation, as well as the occurrence of tumors, immune cell responses and allergies. Thus, the biocompatibility of all materials—bulk or thin films—must be carefully addressed and monitored on long and short time scales *in vitro* and *in vivo*.

2.2 Biocompatible Thin Films

The biocompatibility of many different thin films and coatings has attracted medical research for decades. Good biocompatible coating can improve the lifetime of implant materials, while free-standing thin films offer the possibility to build miniaturized devices. To this end, corrosion resistance and the interaction of single cells and tissue with various materials made of metals, metal alloys, ceramics and carbon-based materials have been studied and are addressed in the following sections.

2.2.1 *Metal and Metal-Alloys Thin Films*

Metals are employed to stabilize bone fracture, replace joints or stenting coronary arteries due to diseases. Biocompatibility of the materials is mainly determined by the corrosion resistance since the release of metal ions can cause severe inflammations and even shock syndromes in low amounts. Ion release is often hampered by the formation of oxide surface layers that passivate the material. Nowadays many different metals and alloys ranging from titanium, silver, gold, platinum and magnesium, as well as rare earth elements are employed as bulk in medicine, while thin films for miniaturized devices such as drug delivery systems are more and more applied.

2.2.1.1 Titanium and Titanium Alloys

Titanium is the most important and mostly employed material for biomedical devices. It is corrosion resistant under usual physiological conditions, has a relatively low modulus, good fracture toughness and is easy to machine. Bulk titanium is mainly used for hard tissue replacement such as prostheses, dental implants, bone screws and plates, pacemakers and artificial hearts. Although in vitro tests with many different cell types exhibit good biocompatibility, cells adhere, grow and proliferate well on titanium surfaces, the in vivo performance is often facing problems especially for long-time perspectives [2]. After implantation of titanium within the human body, neutrophils and macrophages are generally detected around the implant, followed by the presence of foreign body giant cells—a first step in foreign body reaction and encapsulation. In contrast, titanium allergies and hyperreactivity rarely occur after implantation.

Smooth titanium surfaces are hardly bioactive and do not promote osseointegration and bone integration in vivo, which can result in prosthesis fall out after some years. Thus, titanium thin films and coatings on bone replacement and fixation devices are not suitable to improve the lifetime of the device. Several surface treatments such as plasma straying, sputtering, etching and anodical oxidization (Fig. 2.1) increase the surface roughness up to the micrometer level,

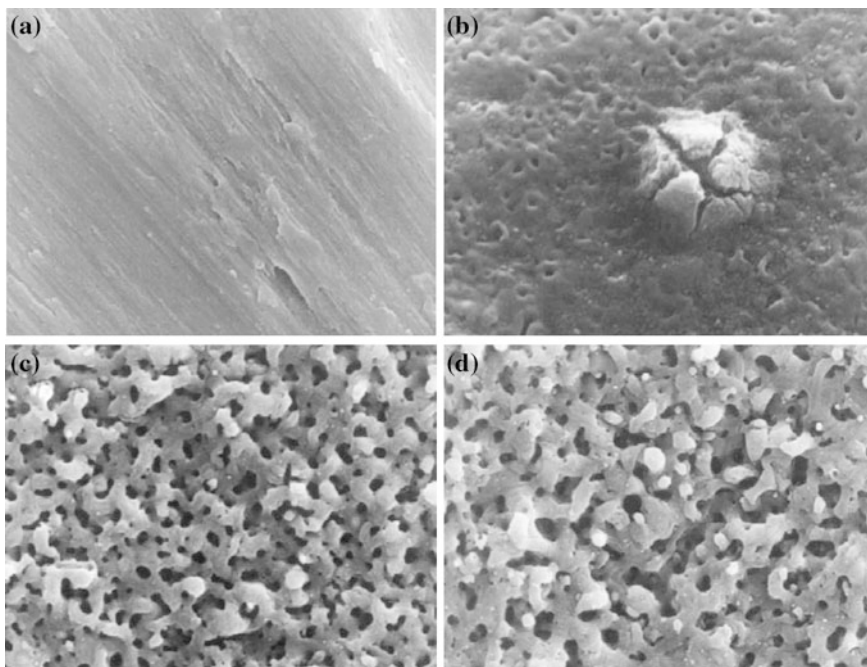


Fig. 2.1 SEM photographs of (a) titanium surfaces without treatment and anodically oxidized at (b) 90 V, (c) 155 V, (d) 180 V in 1 M H_2SO_4 for 1 min. Reprinted from [4], Copyright (2004), with permission from Elsevier

which then promotes bone healing, cell attachment and prevents quick prosthesis failure. In vitro studies with MG63 osteoblast-like cells exhibit an average roughness of 4 μm ideal for cell behavior [3]. Moreover, surface roughness on the nanometer scale promotes bacteria adhesion and influences bacterial retention. Thus, if very smooth titanium thin films are employed, the ability of human pathogenic bacteria to adhere to the surface should be taken into account to suppress possible inflammatory response due to contamination.

Improving the surface properties of titanium to ensure osseointegration is mainly employed for younger patients who require replacement surgery, while for older patients bone cement at the interface of titanium and bone tissue is inserted. Enhanced corrosion resistance is gained by the formation of oxide layers on the surface. Titanium oxide (titania) is a native oxide layer, which is bioinert and exhibits excellent biocompatibility. Nanophase titania ceramics are corrosion resistant, can enhance osteoblast proliferation and promote apatite formation. However, thick titania layers achieve weak chemical bonding to the underlying bulk titanium and also have a weak bone-bonding ability.

Corrosion resistance of titanium is further improved by ion implantation with several metals. Nickel and molybdenum implantation promote the passivation of

titanium surfaces in acidic environments, while tantalum implantation suppresses dissolution of pure titanium in boiling sulfuric acid solution [5]. Ti-Ta alloys exhibit even better corrosion properties the higher the tantalum content. Formation of a passive Ta_2O_5 on the film surface obtains high stability even in HCl solution without drawbacks in the biocompatibility and cell behavior with respect to pure titanium and Ti-6Al-4V surfaces [6].

Thin foil of pure titanium was one of the first materials employed for cardiovascular stents. Since it is not sufficiently radiopaque (visible in X-ray images) in finer structures and shows other disadvantages, nowadays TiNi is the material of choice for stents as discussed later in this chapter. Another important alloy is Ti-6Al-4V, which shows similar biocompatibility features as pure titanium.

Ti-6Al-4V is the most common titanium alloy in medical applications, such as prostheses, because it possesses high corrosion resistance and higher fracture toughness but similar stiffness and thermal properties than titanium. MC3T3-E1 mouse osteoblasts proliferate and grow well on Ti-6Al-4V surfaces, while these properties strongly depend on surface roughness: On very smooth surfaces, cells grow better but show a decrease in cell adhesion in terms of smaller projected cell areas [7]. Thermal surface treatment to increase the oxide layer thickness even reduces possible inflammatory processes and enhances in vitro cell response. However, human umbilical vein endothelial cells (HUVEC) seeded onto untreated and heat-subjected Ti-6Al-4V surfaces not only express intercellular adhesion molecule-1 (ICAM-1) and vascular cell adhesion molecule-1 (VCAM-1) important for good attachment and spreading, but also TNF- α release is detectable. Tumor necrosis factor (TNF)- α is a marker for inflammatory responses of the cells, which is less expressed on heat treated Ti-6Al-4V surfaces with thick oxide layers. However, signs of apoptosis are present a few days after plating the cells [8]. In vivo tissue response is mainly characterized by the formation of a fibrous capsule around the implant as similarly found for pure titanium devices.

Although the surface of Ti-6Al-4V can be easily modified by UV radiation to suppress the adhesion of bacteria on the surface without impairing cell performance, this alloy is hardly used as thin film in medicine. Thin films and coatings usually aim to improve the foreign body response and to reduce inflammatory and allergic reactions. Ti-6Al-4V is not suitable to fulfill these requirements with respect to bioceramics and carbon-based materials. To this end, titanium and titanium alloys are usually employed as bulk material due to their high strength and additionally coated with ceramics and polymers to improve osseointegration or hemocompatibility.

In contrast, titanium nitride is an important coating material for stainless steel to improve corrosion and wear resistance. However, TiN coatings hardly change corrosion behavior of titanium and Ti-6Al-4V [9]. Furthermore, freestanding TiN thin films bare the potential for microelectrode materials and are investigated in contact with primary neuronal cells. Primary neurons from hippocampus attach and proliferate well on thin TiN films. Neuronal network formation appears preferentially on nitrogen rich substrates, while smooth surfaces additionally promote neuronal interconnections [10]. Moreover, TiN shows good

hemocompatibility and also promotes adhesion and proliferation of human pluripotent mesenchymal stem cells (hMSCs). Since these cells contribute to the regeneration of the bone, TiN coatings and thin films might offer new possibilities for bone healing from a materials science perspective.

2.2.1.2 Stainless Steel

Nowadays, various compositions of stainless steel are employed for medical devices due to favorable mechanical properties, corrosion resistance, biocompatibility and low costs. However, high concentrations of chloride ions at physiological conditions can result in ion release and corrosion of stainless steel, causing tissue inflammation and failure of the device.

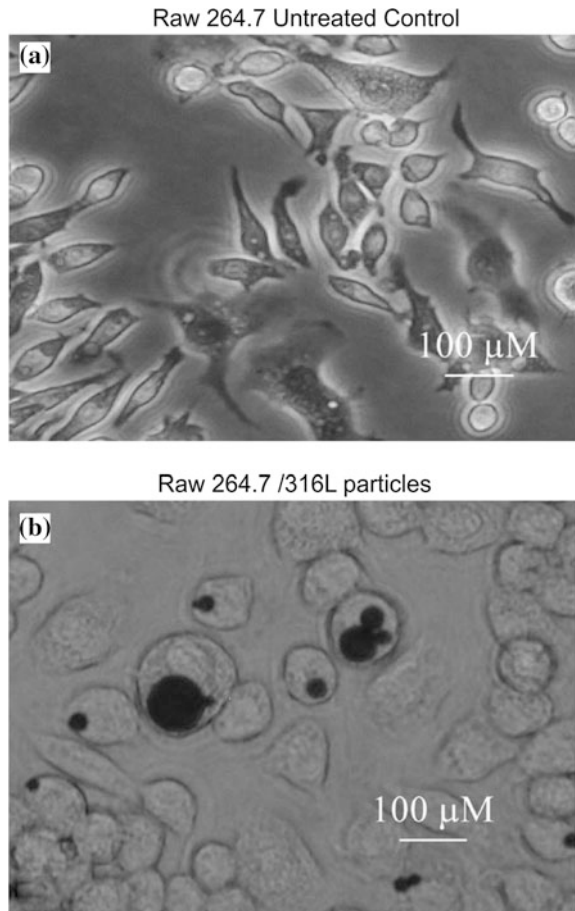
316L stainless steel with a composition of 0.025 C, 17.5 Cr, 13.0 Ni, 1.06 Mn, 2.66 Mo, 0.60 Si, 0.008 S, 0.023 P and 65.124 wt % Fe is mostly used for medical purposes, such as hip prostheses, orthopedic screws and wires, while thin foils are employed for stents and vascular devices. However, great effort is still under way to suppress metal ion release of iron, chromium and especially nickel to reduce cytotoxic effects and platelet formation of the blood. Although the nickel content of 316L stainless steel is much lower compared to NiTi, which is an important material for stents, the corrosion potential and Ni release is much higher for stainless steel, regardless of the pH value and loading range employed to stress the material [11].

Surface passivation of 316L stainless steel with oxides before in vitro and in vivo use is a promising technique to improve corrosion resistance. Several techniques, such as thermal and electrochemical treatment to reform oxide layers, show only limiting improvements. Nitrogenation and amorphous oxidation are good alternatives, which exhibit successful passivation. Here a more uniform and compact oxide layer is formed on the surface, which reduces ion release and pitting corrosion [12].

Another way for enhanced biocompatibility is the reduction of the nickel content. Ni-free austenitic stainless steel shows better corrosion resistance in minimum essential medium (MEM) compared to phosphate buffered saline (PBS). However, corrosion resistance is still lower compared to titanium [13]. Alternatively, small amounts of the rare earth element lanthanum (0.01–0.08 %) improve pitting corrosion resistance in tests with simulated blood plasma and Hank's saline solution, which might be attributed to enhanced passivation of the surface [14].

Smooth muscle cells exposed to corrosion products of 316L stainless steel exhibit morphological changes and induce apoptosis for nickel concentrations above 11.7 ppm [15]. The mRNA profiles of (tumor necrosis factor) TNF- α and (interleukin) IL-1 β —two of the most important signaling molecules for inflammatory response, necrosis and apoptosis—are employed to investigate murine macrophages RAW 264.7 reaction in contact with 316L stainless steel and the nitrogenated alloy. Cells exposed to 316L particles on micrometer size display a rounded, unphysiological morphology, which is not observed for nitrogenated

Fig. 2.2 Phase contrast microscopy of RAW 264.7 cells. **a** Untreated control cells. **b** Cells that have phagocytosed 316L particles after 24 h. Cells exposed to 316L particles display rounded morphology regardless of whether they have consumed a particle. Reprinted from [16], Copyright (2005), with permission from Elsevier



particles (Fig. 2.2) [16]. The investigation of particles in contact with cells is especially important to study the effect of wear debris on cell viability. However, also bulk 316L stainless steel affects cells by possible induction of apoptosis, while cell viability and growth is improved after nitrogenation. However, nitriding stainless steel with different processing techniques influence cellular response to a great extent and studies with human osteoblast and fibroblast cells on low temperature plasma nitrided 316L stainless steel show a dramatic decrease in proliferation compared to untreated and carbon-doped stainless steel [17].

In order to further validate the *in vitro* performance of stainless steel, vascular endothelial cells represent a good model system to study the response at the interface of the blood stream and tissue. Human umbilical vein endothelial cells (HUVEC) and human peripheral blood mononuclear cells (PBMC) exposed to AISI 316 stainless steel, glow-discharged nitriding surfaces and nitriding + post-oxidizing samples possess differences in proliferation and apoptosis. All samples

exhibit higher surface hardness and better corrosion resistance in phosphate buffered saline. In contact with HUVEC, especially the nitrided + post-oxidized samples promote higher proliferation rates, while PMBC seeded onto untreated and nitrided + post-oxidized surfaces show increased apoptosis, characterized by a marked rise in TNF- α and IL-6 release [18]. Here it must be taken into account that the sterilization method of AISI 316L stainless steel prior to cell culture influences cell proliferation. Sterilization by autoclaving causes the formation of surface oxide films in contrast to UV radiation, which passivates the surface and results in better biocompatibility and cell growth.

The interaction of vascular tissue and cells with 316L stainless steel is of major importance for the application as coronary stent material. Thrombogenicity under physiological conditions is studied *ex vivo* in a porcine model by investigating fibrin(ogen) adsorption and platelet adhesion. Comparison with NiTi stents shows that 316L stainless steel stents possess a much higher risk of acute and subacute stents thrombosis [19]. Additionally, stainless steel stents are usually conventional balloon expandable devices, which require high pressure to adapt the shape for the required function and obtain a certain risk for vessel injury.

New stainless steel compositions with negligible nickel content in contact with osteoblast cells decrease TNF- α , as well as IL-6, an inducer of osteoclast activity and bone resorption. While adhesion of cells and osseointegration of bone tissue to stainless steel is much worse compared to bioactive glasses, many ceramics and titanium, P558 austenitic nickel reduced stainless steel reveal much better osseointegration properties *in vivo* than Ti-6Al-4V [20]. P558 does not affect microhardness of pre-existing bone and offers great potential for future application.

Although 316L stainless steel is approved for *in vivo* application and together with titanium the most employed medical material, it often causes inflammation and the formation of fibrous capsules. Thus, stainless steel is usually not used as coating or thin film material to improve biocompatibility. Thin foils of stainless steel are still the gold standard for stents, while NiTi stents are more and more applied. However, as bulk material stainless steel screws have the advantage that the surgeon can feel the onset of plastic deformation important to avoid overtightening, which is not noticeable with titanium screws. Due to the low costs of stainless steel and good fracture toughness, its application as bulk and thin film material for medical purposes is still of major importance. More devices might even be developed in combination with bioactive coatings and new passivation techniques to reduce corrosion and improve cell adhesion *in vivo*.

2.2.1.3 Silver

The application of silver-based materials within the human body, e.g. for surgical instruments and implants, already started in the 19th century. However, until now possible cell damaging effects are still under debate. On the other hand,

antimicrobial activity of silver is well known and the antibacterial effect offers a wide range of applications to reduce the risk of infections and inflammations after implantation. One prominent example is an orthopedic external fixation pin which is often confronted with bacterial colonization.

In vitro cell tests in contact with silver show contradicting results. NIH 3T3 fibroblasts and osteoblast-like cells plated on silver coated stainless steel show good spreading. A larger number of cells is found on the silver film compared to control experiments on stainless steel pins after 4 days [21]. Genotoxic and cytotoxic effects are not present on silver, nor proliferation rate changes or protein activities. In contrast, studies with the same fibroblast cell line on silver coated glass coverslips obtained no cell attachment, which cannot be attributed to cytotoxic effects since cells in the same culture dish on glass substrates in contact with the silver sample still proliferated [22]. Furthermore, incubation of THP-1 human monocytes exposed to silver for 4 weeks clearly reveal alterations in growth and division with a significant slow-down in proliferation due to silver ions release [23]. Macromolecular concentrations are also capable of causing severe distortion of bone marrow cells.

Similar contradicting results occur in in vivo assessments. Silver-impregnated catheters placed subcutaneously or percutaneously in the neck of rats showed good responses in terms of low bacterial infections, foreign body reactions without occurrence of abscesses [24]. The results are corroborated for silver coated dialysis catheters implanted in rats and pigs. However, clinical trials of these devices do not show any statistically improved outcome and less infections compared to uncoated catheters [25].

Silver-coated megaendoprostheses in a rabbit model proved reduced infection rates without toxicological side effect [26]. In contrast, studies on muscle microvascular response with silver implanted in hamsters show severe disruption of endothelial integrity. Massive leukocyte extravasation, inflammation and edema occur [27]. Negative side-effects are mainly attributed to silver ion release and the dose of ions must be reduced as much as possible. To this end, bulk silver devices, such as prostheses, are incapable to replace titanium-based implants although antibacterial effects are a valuable property to reduce the risk of inflammation.

On the other hand, silver-coated polyester grafts employed in clinical trials with patients suffering from aortic infections demonstrate favorable outcome, while here the antimicrobial efficiency of the graft is in the focus of the study and determines the success of the implant. However, long-term studies on possible toxic effects from silver ion release are important for safe use.

To take advantage of the antimicrobial activity of silver without cell damaging effects from large quantities of silver ions, coatings with small amounts of silver can be employed. Titanium/silver thin films of 2 μm thickness with 0.7–9 % silver content coated via physical vapor deposition on pure titanium show no cytotoxic effects on osteoblast and epithelial cells in vitro. In contrast, *Staphylococcus epidermis* and *Klebsiella pneumoniae* weakly adhere and the formation of microorganisms on the surface is clearly hampered [28]. Thus, doping surfaces of load bearing implants and other medical devices with small amounts of silver instead of

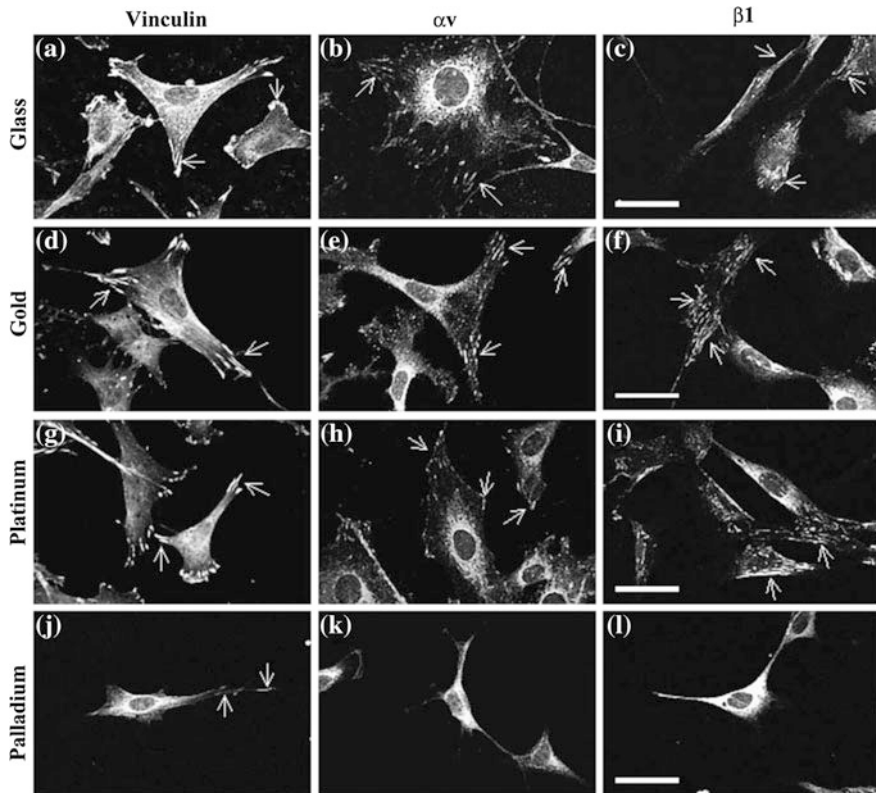


Fig. 2.3 Immunolocalisation of vinculin and integrins αv and $\beta 1$ in Swiss mouse 3T3 fibroblast cells grown on glass, gold, platinum and palladium substrata for 24 h. Antibody staining is visualized using confocal microscopy. Focal contacts (*arrows*) are clearly seen in all combinations except in cells grown on palladium and stained with antibodies to the integrins. Scale bar = 20 μm . Reproduced with permission, from [22]. Copyright international federation for cell biology

using large quantities of silver and bulk materials offers the possibility to benefit from the antibacterial properties without risking inflammatory and cytotoxic effects.

2.2.1.4 Gold

Gold shows extreme corrosion resistance under many different environmental conditions, such as in saline solution and body environment. Fibroblasts spread and proliferate very well on glass-coated substrates and express αv and $\beta 1$ integrin for strong adhesion to the substrate (Fig. 2.3) [22]. Bulk gold devices are expensive and usually too soft for many orthopedic and dental applications. To this end, gold containing alloys and thin films are employed to increase in vivo

performance. For example, Au-Pd is an important dental alloy, which shows better corrosion resistance the higher the Au content.

Gold thin film microelectrode arrays employed *in vitro* offers the possibility to monitor signals of electrogenic neuronal cells and investigate electrophysical activity of the neuronal network. The *in vivo* performance of thin film gold electrodes depends on surface roughness and shape of the device, which also influence alternating current impedance—an important characteristics of the electrode.

Gold is radiopaque, and thus a gold layer on conventional stents could improve precise positioning into the coronary lesion. *In vitro* tests with gold coated stents show reduced platelet activity important to reduce thrombotic risks. However, clinical trials with gold coated stents employed for coronary replacement compared to stainless steel stents obtain an increased risk of thrombosis and restenosis, in particular [29]. *In vivo* assessments of gold coated NIR stents in porcine coronary arteries result in hyperplastic and inflammatory reactions four weeks after implantation [30]. Performance is improved by postplating thermal processing to smooth the surface. However, until now gold coated stents are hardly used for the treatment of coronary diseases because stainless steel and especially NiTi stents are generally cheaper and show very good hemocompatibility.

2.2.1.5 Platinum

Platinum and its alloys offer a wide range of application due to inertness and high tensile strength. Thin films of platinum with good mechanical resistance coated on titanium surfaces can be employed for spinal fixation, hip and knee implants. Platinum exhibits the best corrosion resistance together with gold. However, early *in vitro* studies with MC3T3-E1 osteogenic cells show that platinum-coated titanium inhibits calcification and the formation of mineral deposition of the implant surface, important for many orthopedic applications [31]. Thus, platinum coated implants do not improve *in vivo* performance and osseointegration compared to conventional titanium prostheses.

In contrast, fibroblast cells spread and proliferate well on platinum substrates and express many focal contacts. An important factor of fibroblast morphology and division rate is the surface roughness, which influences cell behavior for all kinds of substrate materials. Cells grown on smooth platinum surfaces with a root-mean-square roughness below 1 nm are more elongated in shape and proliferate faster than cells on surfaces with 23 nm roughness [32]. Interestingly, proliferation of glial cells is not affected by surface roughness within this range, while only the cell morphology varies.

The study of glial and neuronal cells on platinum films is especially interesting because platinum is conductive and radiopaque, which makes it a potential material for the application as electrodes. Neuronal cell lines cultured on flat and nanostructured platinum thin films with laser ablated holes of 100 nm spacing exhibit cellular attachment and the formation of neuronal networks [33].

In contrast, investigations with primary neurons show that these platinum surfaces do not support cell attachment.

In vivo studies of implanted platinum-coated electrodes within the brain of small mammalian animals exhibit good acceptance of the body without inflammatory response. These electrodes enable faradic currents to flow through the tissue-implant-interface. To avoid faradic reactions, which might cause tissue trauma, electrodes made of layers comprising different materials, such as platinum coated on chromium/gold sputtered films on polyimide are possible [34]. Floating electrode arrays composed of platinum thin films, which are not anchored to the skull, are capable to record low field potentials. New neuronal devices combine the good electronic properties of platinum with those of iridium. Furthermore, iridium oxide has a higher charge capacity than pure platinum and allows smaller electrodes. Especially regenerative multi-electrode arrays composed of Pt-Ir can be fabricated with many different designs. Besides conventional platinum neuro-electrodes, they promote early and stable interfacing of neural activity by simultaneously less inflammatory responses and reactive gliosis after implantation within the brain. Thus, these materials offer new perspectives for direct interfacing of transected peripheral nerves with advanced robotic prosthetic.

Nowadays, easy manufacturing of platinum-based thin films and coatings allows their applications as electro-medical material not only for neuronal devices, but also for pacemakers, implanted defibrillators, hearing assist devices, catheter ablation and stents [35], which are already commercially available.

2.2.1.6 Magnesium

Magnesium is a lightweight metal with similar mechanical properties to bone. It has a higher fracture toughness than bioceramics, is not inert and corrosion resistant and degrades in salty environment. Magnesium is found in bone and stored in other tissues such as muscles, which makes it a good candidate for in vivo use.

First attempts with magnesium-coated implants were performed in vivo in 1907. Over the following decades it turned out that magnesium does not cause toxic effects and inflammations. It can stimulate bone formation, while corrosion of the material within the body is so fast that the implants resolve within days. In vitro tests with bone marrow cells also obtained cell stimulating effects on proliferation and viability on magnesium substrates. Soaking of magnesium in saline solution promotes precipitation of calcium phosphates and enhances osteoconductivity. Formation of calcium phosphate layers might also slow down the corrosion process in vivo. However, further in vitro assessments concluded that magnesium causes more cytotoxic effects in cell culture compared to in vivo experiments. Degradation of magnesium results in strong pH changes and hydrogen production, which are regulated by the local environment within the body but not during cell culture experiments. Here cells are killed by osmotic

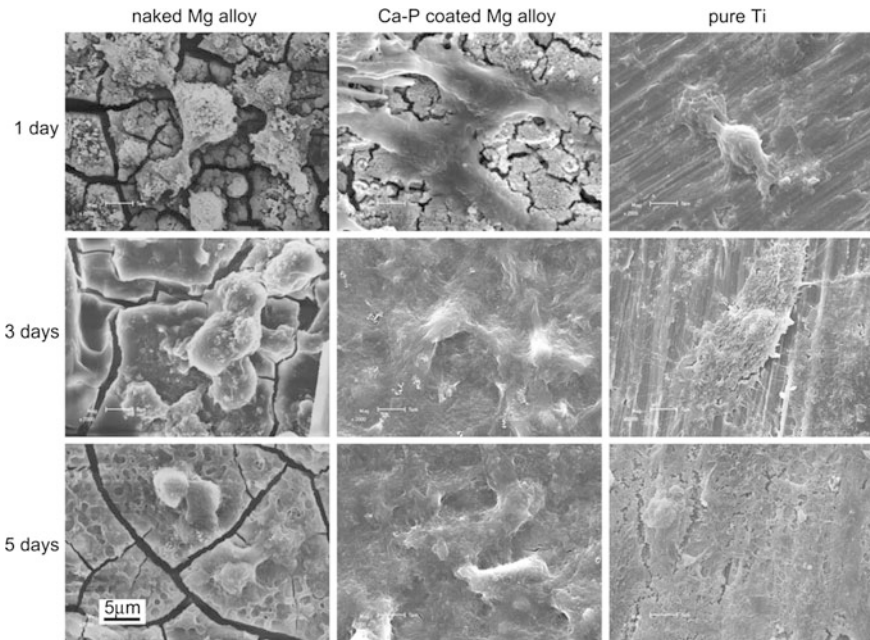


Fig. 2.4 Morphology of L929 cells after 1, 3, and 5 days incubation on different substrate materials. Reprinted from [37], Copyright (2009), with permission from Elsevier

shock [36]. Corrosion and dissolution of the magnesium sample can be slowed down by the addition of serum to the culture medium.

Further in vitro studies exhibit better biocompatibility of calcium supplemented magnesium, which increases viability of primary osteoblast cells. Another possibility for decreased degradation and improved cell response is the addition of small quantities of other elements up to 4 wt %. Here especially rare earth elements have a drastic effect. Magnesium with 2 wt % of cerium, lanthanum, neodymium and praseodymium (LAE442) exhibits a significant decrease in resolution rate, and entire degradation of the implant was observed after 18 weeks. Additionally, osteoconductive properties are still maintained, and LAE442 could already prove successful application in orthopedics. Alternatively, Mg alloys are coated with bioceramics such as Ca-P which are well tolerated by the body (Fig. 2.4).

2.2.1.7 Hafnium, Niobium, Tantalum and Rhenium

Although currently used titanium implants together with many different coatings, such as ceramics and carbon-based materials, show good in vivo performance, other metals are tested for their application as prostheses material. New load-bearing orthopedic devices require bioactive materials with high mechanical strength and corrosion resistance onto which bone tissue can adhere and which

promotes osseointegration. Metallic biomaterials employed as coating or bulk material for prostheses might offer new perspectives for long-time survival of the device, which have not been reached with titanium so far.

Wires of 97 % hafnium, 99.9 % niobium, 99.95 % tantalum and 99.97 % rhenium implanted in the subcutaneous connective tissue in the abdominal region of Wistar rats show promising tissue response (Fig. 2.5). Only few signs of inflammatory processes are present, while the implants are encapsulated with fibrous tissue [38]. Implantation within the bone marrow of the femur exhibits excellent corrosion resistance and no dissolution of Hf, Nb, Ta and Re occurs. Around the implants calcification is observed together with the formation of new bone within 4 weeks. The overall soft and hard tissue response is similar to the reaction on titanium. Good biocompatibility in terms of osseointegration-properties of hafnium on time-scales of 24 weeks is already corroborated for abdominal wall implants in rabbits. Wear resistance and debris formation is an important issue when applying Hf, Nb, Ta and Re for prostheses, which must be addressed *in vivo* in the future.

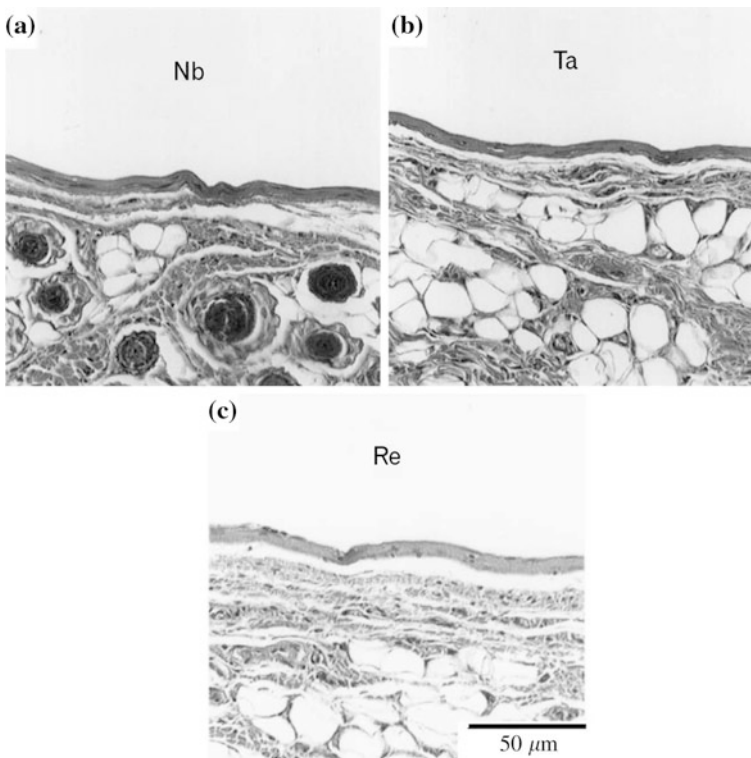


Fig. 2.5 Tissue response to Nb, Ta and Re implants in subcutaneous tissue after 4 weeks: (a) Nb; (b) Ta; (c) Re. Reprinted from, Copyright (2009), with permission from Elsevier. Reprinted from [38], Copyright (2001), with permission from Elsevier

Tantalum and niobium coatings of 316L stainless steel improve corrosion resistance under physiological environment. Possible applications of tantalum and tantalum oxide thin films as stents and other blood-contacting devices are addressed in vitro by culturing human umbilical vein endothelial cells (HUVEC) on their surfaces. Cells adhere very well, spread and proliferate much better compared to cell on 316L stainless steel [39]. Studies with human alveolar bone derived cells corroborated biocompatibility of niobium coatings on stainless steel. Nowadays tantalum metal stents are already available for endovascular surgery.

2.2.2 Shape Memory Alloys Thin Films

Smart materials that deform under temperature change or external magnetic fields offer a broad range of applications. Shape memory alloys can be employed for new miniaturized devices for stents and tissue actuation, surgery and diagnostics. Nitinol—NiTi shape memory material—deforms by small variation of temperature, while Fe-Pd ferromagnetic shape memory alloys strain in external magnetic fields. However, especially Ni is cytotoxic, and corrosion and Ni release together with inflammatory processes and cell responses in vitro and in vivo must be carefully addressed.

2.2.2.1 Thermal Shape Memory Alloys: Nitinol

NiTi, widely known as nitinol, is a smart functional material, which exhibits the thermal shape memory effect—thus, it recovers its shape after heating above a certain temperature. Furthermore, it is superelastic and can fully return to its original shape after deformation to tensile strains of 8 % due to transformation between the martensitic (low temperature) and austenitic (high temperature) crystal structure.

Mostly employed nitinol consists of Ni and Ti concentrations near equiatomic composition. Manufacturing of large bulk components made of pure NiTi is complicated and expensive. Thus, the application as coating materials and thin films is a suitable alternative. Very thin coating are often processed by magnetron sputtering, while larger thickness is usually achieved by different vacuum plasma spraying techniques. The production procedure is important for the subsequent application because it influences surface roughness, as well as the formation of oxide layers on the film surface. Oxidization is mainly determined by temperature exposure during spraying, which then influences corrosion behavior of the sample.

Although nitinol comprises a large Ni compound, the probability for ion release is low. Ni and Ti atoms are arranged in a regular crystal lattice with high atomic forces. Large energies are needed to release single ions from the bulk material. Furthermore, Ti is more readily oxidized than Ni, and generally TiO₂ layers on the surface of nitinol are present. These thin films further protect the environment

from Ni release [40]. For good biocompatibility the stability of the oxide layer and wear resistance are crucial. To this end, corrosion investigations of NiTi have been performed with many different fluids ranging from organic and body fluids to chloride acids. However, contradictory results are reported from very high corrosion resistance better than stainless steel to poor corrosive properties [41]. Differences in experimental outcome are mainly attributable to variations in sample production and not experimental differences such as temperature and pH variations.

In fact, exposure to H_2O_2 for 22 h results in a high Ni content up to 27 % in the oxide surface layer. These layers can obtain thickness up to 70 nm, while samples immersed in Hank's and physiological solutions contain only minimal Ni concentrations within the titanium oxide layer. These oxide coatings grow during immersion, which also promotes the formation of calcium phosphate layers. Surface passivation and quick TiO_2 formation is enhanced by heat treatment and aging [10], while homogeneous smooth thin oxide surfaces show better corrosion resistance compared to those with large roughness, scratches and grooves. A simple way of surface passivation by TiO_2 formation is autoclaving the nitinol sample at temperatures above 100 °C before in vitro or in vivo application.

Comparison of NiTi coatings produced with three different spray techniques (high velocity oxy-fuel—HVOF –, vacuum plasma spraying—VPS –, and atmospheric plasma spray quenching—APS+Q) show strong dependence of corrosion on surface conditions: VPS and HVOP surfaces obtain roughness of 4.8 ± 0.6 and 8.2 ± 0.9 nm, respectively, while APS+Q coatings are even rougher with 13.1 ± 1.7 nm and are characterized by coating cracks (Fig. 2.6) [42]. Electrolyte penetration through these cracks results in homogeneous wettability of the sample and enhances corrosion behavior. VPS processed samples with smoothest surfaces present best corrosion resistance. Repassivation after removal of the oxide layer undergoing wear, e.g. in orthopedic and orthodontic applications, is essential for in vivo performance. Potentiodynamic corrosion tests indicate that NiTi undergoes slower repassivation kinetics than Co-based and Ti-alloys.

Under physiological conditions smooth NiTi alloys without surface cracks show a very high corrosion resistance, which explains the success in vitro and in vivo cell and tissue experiments. In this context, surface roughness correlates with platelet adhesion in blood and thrombogenicity. Superhydrophilicity of thin film nitinol with film thickness below 10 microns minimizes risk of thrombus [43]. Compared to commercially employed bulk nitinol with thickness larger than 30 microns for endovascular devices, especially stents, nitinol thin films offer great potential for improved hemocompatibility due to various possibilities in surface treatments such as polishing. Here surface roughness below 5 nm can be reached to reduce platelet formation, in contrast to 500 nm roughness after electropolishing. Good hemocompatibility and biocompatibility of austenitic and martensitic NiTi thin films in contact with human vascular endothelial cells also supports safe application of nitinol for miniaturized vascular devices [40].

Many tests in which cells are seeded onto NiTi substrate to investigate viability, proliferation and morphology showed good biocompatibility of the material.

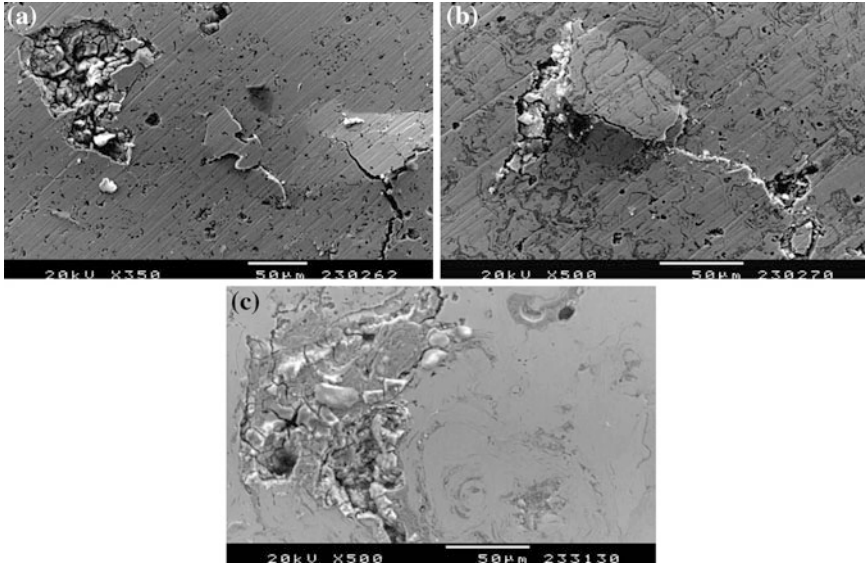


Fig. 2.6 Pitting phenomena on the as-polished (a) VPS, (b) HVOF, and (c) APS+Q coatings. Reprinted from [42], Copyright (2009), with permission from Elsevier

Different cells types such as primary fibroblast cells and cell lines, primare human epithelial cells and osteoblast-like cells in direct contact with nitinol grow well and proliferate. As mentioned before, surface treatments of the samples before cell tests influence corrosion and, in line, cell viability. Surfaces with only very small amounts of Ni therefore show very good performance in contact with cells, while untreated samples that corrode during testing induce moderate cytotoxicity. Surface passivation by calcium-phosphate coating is a possibility to enhance cell growth and proliferation. However, adhesion between the coating and the nitinol is generally weak and must be improved for application in vivo.

Genotoxicity assessment further proved save application of the material in vitro. No sign of DNA damage of primary blood lymphocytes is observed. Orthodontic application of nitinol implanted within the human oral mucosa leads to moderate genotoxic effects and an increase in blood Ni content. Other in vivo tests with NiTi implanted in the skin, bone and muscle in Guinea pigs, rats, mice and rabbits, as well as humans show no signs of cytotoxicity, no sensitizing and negligible irritations [40]. Negative side-effects for orthodontic patients with NiTi implants can mainly be attributed to Ni allergy. Osseointegration and bone ingrowth into NiTi surfaces is promoted for nanoporous nitinol implants [44]. Employing the shape memory effect and straining of the device in vivo further stimulates bone growth.

However, detecting the amount of Ni release in vivo is a challenging task and the individual environmental exposures must be taken into account. Measurements of Ni release in vitro determined contradicting values ranging from 490 to

14 mm²/ml and even one order of magnitude smaller [41]. The highest concentration is mostly found after 48 h, in line with a decrease in cell proliferation on this time scale. When transferring this result to cytotoxic reactions in vivo, exchange with body fluids would lead to a significantly lower local Ni concentration. Thus, a good biocompatibility of NiTi—bulk and thin films—because of only small amounts of Ni release is suggested.

To adapt corrosion properties to different environmental and experimental conditions, variations in ion release is obtained by doping nitinol thin films with small quantities of oxygen, carbon, zinc, zirconium and molybdenum. The implantation depth influences the Ni content on the surface and corrosion of the material. Implantation of Zr, for instance, improves corrosion, while recovery of the martensitic phase and the superelasticity is affected. Depending on the implanted ions and the concentration, the shape memory effect and recovery of the shape after deformation can be inhibited.

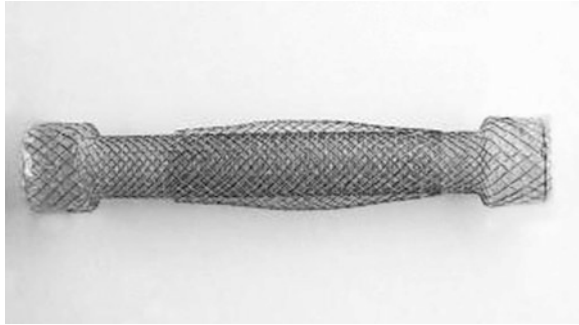
Ternary elements, especially Cu influence not only the mechanical properties of the material and can result in a narrower hysteresis and superior elasticity, but also changes corrosion behavior. Ternary nitinol, such as NiTiTa and NiTiCu, both show adequate biocompatibility, while copper release and cytotoxic effects of NiTi₄₂Cu₇ are observed [45]. Tantalum addition improves corrosion resistance of nitinol and promotes endothelial proliferation [46]. Since the superelastic hysteresis stress is lower for ternary NiTiCu than binary NiTi, biocompatible coatings or surface passivation that do not influence the thermal shape memory transformation might offer a wide range of applications as miniaturized medical devices with long-term life time.

Long-term host body responses on binary NiTi devices, especially stents (Fig. 2.7), give no signs of cytotoxicity or worse performance than stainless steel or titanium alloys. The ability to adapt the materials shape to the environment together with possible shape changes due to temperature changes are unique properties essential for vascular applications. Stents are usually made of pure NiTi or coated with e.g. ceramics to improve cell attachment. Here the interaction of the thin film with the underlying material determines the in vivo performance, because the coating must still allow shape changes of the device without rupture. In contrast to coatings, surface structuring can influence substrate-tissue interaction. In vivo tests with micropatterned NiTi stents show good endothelial tissue generation through the patterns of the thin film device without any abnormalities or thrombosis [48].

The first NiTi actuated micropump for drug delivery was reported in 1997. Here two nitinol thin films were separated by a silicon spacer. Heating and opening of the pump released liquid agents with flow rates of 49 µl/min at operating voltage and currents of 6 V and 0.9 A, respectively [49]. Nowadays, nitinol drug delivery systems of MEMS (microelectromechanical systems) sizes are possible, e.g. made of free-standing NiTi thin films or nitinol wires that allow flow rates of several hundred microliters.

Recently the application of nitinol thin films as intraocular clips for ophthalmic microsurgery is investigated. Animal models with Yucatan mini-pigs show that 70 days after surgery these clips are well tolerated by the iris and show as good

Fig. 2.7 Niti-S stent with a double-layer configuration, consisting of an inner polyurethane layer and an outer uncovered nitinol wire. Reprinted from [47], Copyright (2006), with permission from Elsevier



responses without any sign of cytotoxicity as conventionally used polypropylene suture [50]. Further studies are under way for future application of nitinol in ophthalmic surgery in humans.

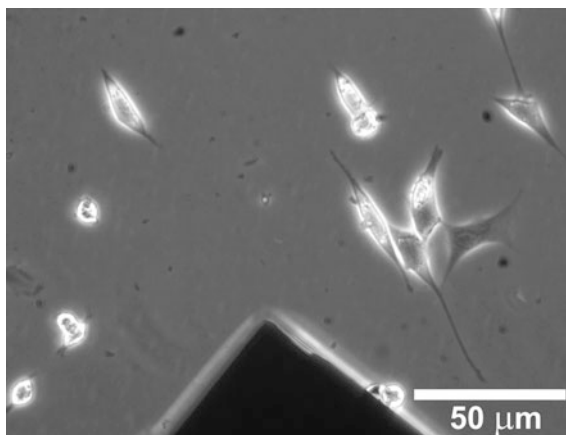
2.2.2.2 Ferromagnetic Shape Memory Alloys

Ferromagnetic magnetic shape memory (FMSM) alloys are an exciting new class of smart materials that can yield magnetically switchable strains up to ten percent at constant temperatures and frequencies from quasi-static up to some kilohertz. Macroscopic, viz. bulk FMSM and their actuation in external magnetic fields are well established, while miniaturization of the FMSM effect within thin films are still almost unresolved. Free-standing FMSM alloys, which constitute not only the “superelastic” thermal shape memory effect, but also magnetically switchable shape changes, could pave the way for magnetically controlled stents, vena cava filters, abdominal aortic aneurysm devices, and atrial septal defect occlusion devices without possible temperature damaging effects. However, the biocompatibility of the material must first be proved well to avoid inflammatory processes and cell death when incorporated in the human body.

Two classes of FMSM materials exist: Ni-Mn-Ga and Fe-Pd alloys. Corrosion behavior of FMSM alloys was first investigated for the initially discovered Ni-Mg-Ga. Bulk samples were soaked in saline solutions at pH 7.4 and 37 °C to mimic conditions present in the human body. After 12 h pitting is visible—a clear sign of corrosion and destruction of the initially smooth surface [51]. Furthermore, thin films of Ni-Mn-Ga deposited on SiO₂ wafer in contact with NIH 3T3 fibroblasts showed cytotoxic effect, viz. cells in a Petri dish together with the thin films died or pathologically transformed due to corrosion of the Ni-Mn-Ga film, dissolution of Ni and Mg ions and uptake of the cells (Fig. 2.8). Thus, Ni-Mn-Ga alloys are not biocompatible and their application for medical devices requires appropriate coatings to suppress ion release, but still promotes shape changes when external magnetic fields are applied.

Besides Ni-Mn-Ga, Fe-Pd based FMSM thin films are a highly promising class of material due to their chemical composition of less toxic Fe and Pd particles.

Fig. 2.8 NIH 3T3 fibroblast cells cultured in a plastic Petri dish into which a single crystalline Ni–Mn–Ga thin film (*black triangle*) is placed. Some dead cells are seen (*small light spherical objects*), whereas the viable cells attached to the culture dish are smaller compared to control cells and obtain a spindle-like shape due to cytotoxic effects after ion release from the Ni–Mn–Ga film



Recently, the in vitro biocompatibility of single crystalline $\text{Fe}_{70}\text{Pd}_{30}$ FSMA films grown on MgO single crystal substrates were conducted by simulated body fluid (SBF) and cell viability tests. The FSMA films were immersed in SBF for 65 h at 37 °C. Less than 0.001 mg/L Pd ions are detected throughout, whereas the Fe concentration clearly increases an order of magnitude, thus reflecting a higher reactivity of Fe in the Fe–Pd alloy, as expected. Additionally, apatite-like materials aggregation on the surface becomes present, which is very important for tissue-bonding and the adhesion of cells on the substrate (Fig. 2.9) [52].

The interaction of NIH 3T3 fibroblasts with $\text{Fe}_{70}\text{Pd}_{30}$ was employed by seeding the cells onto the films and investigate cell morphology and viability employing fluorescent dyes to visualize cells on the films. After 65 h cells were stained with calcein AM (stains live cells in green) and with propidium iodide (PI, for apoptotic cells with nuclei fluorescing in red). During culture cells adhere and proliferate on the surface of the films, and only very few apoptotic cells can be found. Immunohistochemical staining of the actin cytoskeleton and the focal contacts provided

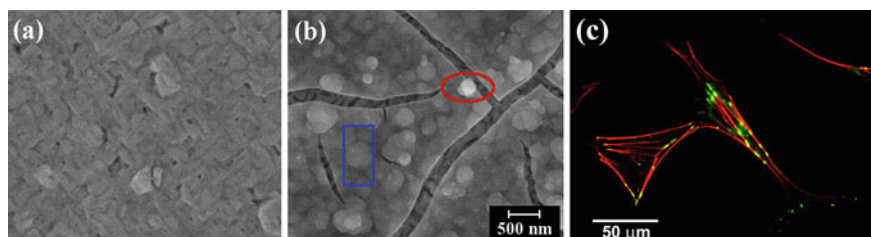


Fig. 2.9 $\text{Fe}_{70}\text{Pd}_{30}$ thin film before (a) and after soaking in SBF for 65 h (b). The *circle* and *rectangle* mark precipitation of apatite-like material deposition. (c) NIH 3T3 cells attached to the $\text{Fe}_{70}\text{Pd}_{30}$ surface. The stress fibers of the actin cytoskeleton (*red*) are well pronounced—an indicator for good adhesion. The focal contacts, the sites of adhesions, are shown in *green*

evidence that the cells are well spread on the substrate, exhibit well-defined stress fibers and obtain a normal morphology (Fig. 2.9c).

Additionally, after cell detachment from the films, no morphological, structural, and chemical changes of the films, which could interfere with their functionality, are detected. The results suggest that Fe-Pd membranes are biocompatible and even bioactive [52], whereas bioactive coatings might even improve cell-substrate interaction for in vivo applications in the future.

2.2.3 Carbon-Based Thin Films

Carbon-based materials, such as diamond-like carbon, carbon nitride and nanocrystalline diamond, are excellent candidates for coatings of biomedical devices, e.g. in joint replacement, stents and dental roots. Carbon-based coatings are usually composed only of the biocompatible elements C, N and H, which do not cause cytotoxic effect by dissolution of corrosion products as often found for metal implants. However, skin irritation or hypersensitivity reactions might occur, which can result in inflammations and failure of the device. To this end, biocompatibility in vitro and in vivo must be carefully addressed for the different types of tissue in contact with.

2.2.3.1 Diamond-Like Carbon

Diamond-like carbon (DLC) is an amorphous carbon material, which is chemically inert with high corrosion resistance, hardness, low frictional coefficient and high wear resistance. It displays some characteristics of diamond, while DLC is not as hard and comprises a different microstructure. Carbon-carbon interaction bonds can be of sp^2 form (graphene) or tetragonal sp^3 (diamond). The structure allows incorporation of different materials, such as hydrogen, copper, silver and vanadium [53].

Many different fabrication techniques are employed to produce DLC coatings: Ion beam deposition, chemical vapor deposition, magnetron and ion beam sputtering, and pulsed laser deposition [54]. The biocompatibility of DLC was first addressed in the early 90 s. Fibroblasts seeded on DLC and hydrogenated amorphous carbon films attach and spread well, while no indications of cytotoxicity and inflammations are present. Interactions of human macrophages and monocytes show identical results. Among these cells, human ML-1 hematopoietic myoblasts and human embryo kidney (HEK) 293 cells spread well on DLC coatings with identical morphologies as control cells under usual culture conditions. Although no signs of toxicity and inflammations are obtained, one day after seeding 60 % of all ML-1 and HEK 293 cells are viable compared to 90 % of the control cells [55].

Good biocompatibility in terms of unchanged morphology, cell spreading and proliferation is also corroborated for fibroblast and osteoblast cells exposed to

DLC coatings with silicon intermediate layers. Incorporation of titanium within hydrogenated films enhances osteoblast proliferation and reduces osteoclast activity. In contrast, doping of toxic elements such as copper or vanadium inhibits cell attachment and proliferation [56].

Investigations of DLC films in contact with blood are important to study protein absorption, blood coagulation and the risk of thrombosis. Inhibition of platelet and fibrinogen adhesion is a prerequisite for safe application of carbon-based cardiovascular devices *in vivo*, while enhanced albumin adhesion reduces the number of adhering platelets. DLC coatings show lower platelet adhesion compared to carbon nitride films and control experiments with polymethyl methacrylate (PMMA) films. Additionally, rapid binding of albumin and passivation of DLC films for fibrinogen adsorption are promoted by high chemical heterogeneity of the surface. This good hemocompatibility is promising for future applications as coating material for artificial hearts [57].

In contrast to diamond, DLC coatings exhibit an intrinsic smooth surface due to the amorphous structure, and thus display less debris formation during excessive wear important for orthopedic application such as artificial joints. *In vivo* assessments in rats and other small mammals show good acceptance of DLC coated implants made of stainless steel, titanium and polymers in contact with bone, muscular and cardiovascular tissue. DLC coated steel rods for bone fixation in humans do not show any signs of corrosion and inflammation of the surrounding tissue. In fact, non-hydrogenated DLC coated metal implants exhibit a decreased corrosion rate up to 100,000 times lower than for uncoated devices, while the wear rate is also reduced up to 1,000,000 times [58]. However, contradictory results on wear resistance ranging from weak to strong wear resistance are still under debate. Different experimental outcomes are attributed to variations in test conditions, e.g. under which liquid lubricant wear is employed. Furthermore, some studies show no improvement in the *in vivo* performance of DLC coated stainless steel, used e.g. for shoulder joint balls or coated femoral heads. One of the major problems with DLC coating results from bad adhesion of the film to the implant in aqueous solution.

DLC coating adhesion to a substrate material like stainless steel is an important issue for the application as stent materials (Fig. 2.10). Stents are placed in an artery to open the blood tube by inflating the stent after implantation. *In vivo* tests showed very good performance of DLC-coated stents with no signs of thrombosis and inflammation even after one year. However, recent investigations observed no advantage of DLC coated stents compared to conventional stainless steel-based materials. As well as for orthopedic applications, adhesion of the coating is weak and deformation of the stent during opening of the artery can cause detachment of the DLC film and failure of the device.

Besides an improved DLC bonding to the underlying material, future applications focus on doping DLC films with toxic components such as copper for antibacterial purposes. They can be employed for contact lenses to avoid biofilm formation and contamination. Other applications are coating devices with DLC for microsurgery and neuronal implants to reduce scar formation within the brain.

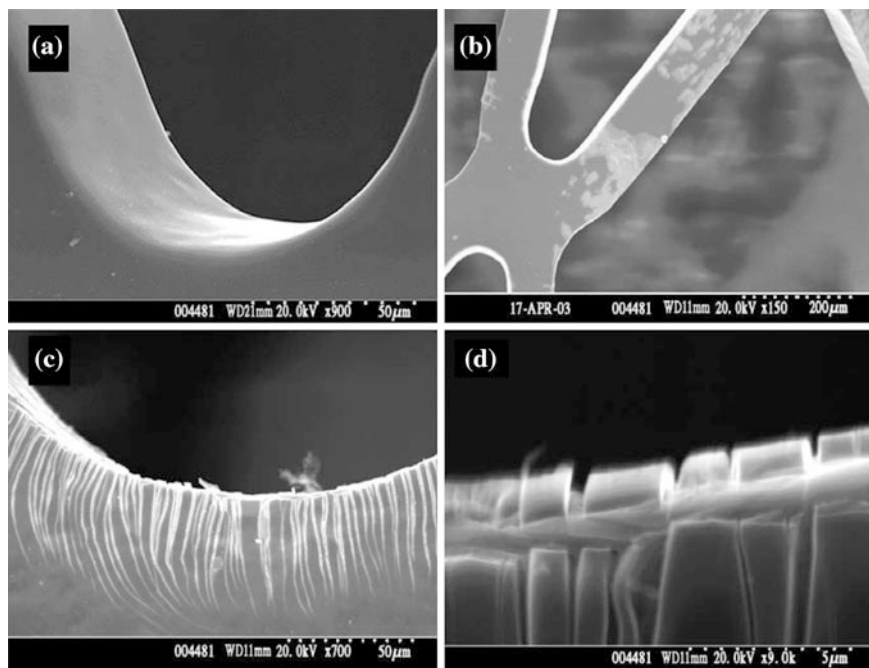


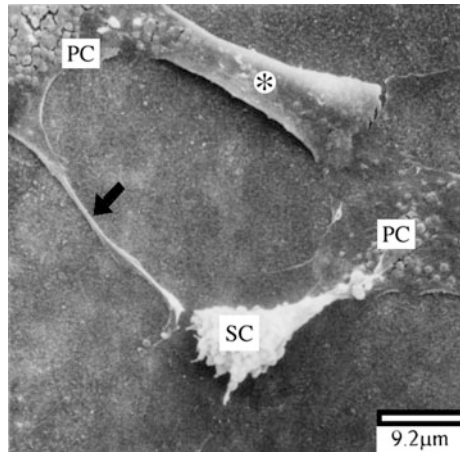
Fig. 2.10 a DLC coating deposited onto an unexpanded stent, b after expansion, c, d showing crack initiation. Reprinted from [59], Copyright (2005), with permission from Elsevier

2.2.3.2 Carbon Nitride Thin Films

Similar to DLC, amorphous carbon nitride (CN) obtains a sp^3 and sp^2 bonded structure, while a C/N ration of 0.2–2.0 can be produced experimentally. Only few studies have addressed its biocompatibility in contact with cells and tissue so far, although CN comprises similar mechanical and corrosion resistance features than DLC—thus perfectly matching the requirements for medical applications. Usually, CN films are prepared by reactive magnetron sputtering from a graphite target yielding an extreme hardness of 40–60 GPa.

Osteoblast cells seeded onto CN films spread and proliferate well as shown in Fig. 2.11. The morphology of fibroblasts attached onto CN is unchanged compared to cells on DLC and control experiments, while for all substrate materials no signs of cytotoxicity are observed. Contradictory studies determine a strong decrease in cell number for osteoblast cells on CN films coated to stainless steel. However, these observations might result from weak adhesion of the CN coating, which failed during cell culture and detached from the steel [60]. During exposure to blood, CN promotes higher coagulation of fibrinogen but less adhesion than control experiments with PMMA. However, systematic *in vitro* and *in vivo* assessments are still lacking for future applications of CN coated devices.

Fig. 2.11 SEM morphology of osteoblast cells on amorphous CN film deposited on silicon in 1 week of culture. Spindle-shaped cell *SC* and well-spread polygonal cells *PC* maintained physical contact with each other through filopodia (*arrow*) or lamellopodia (*asterisk*). Reprinted from [55], Copyright (2000), with permission from Elsevier



2.2.3.3 Nanocrystalline Diamond Thin Films

Crystalline diamond offers a wide range of applications because its structure can be tuned from micrometer grain sizes up to nano- and ultra-nanocrystalline with 2–5 nm grains and root-mean-square surface roughness of 10–20 nm. Nanocrystalline diamond (NCD) and ultra-nanocrystalline diamond (UNCD) thin films mimic the surface roughness of bone, together with a high chemical and corrosion resistance, fracture toughness and hardness. Although it is composed of the same element as diamond-like carbon, its biocompatibility must be clearly evaluated because variations in surface structure, as well as electronic properties and surface energies can lead to unexpected interactions with cells and tissue.

In vitro studies with MG63 osteoblast-like cells and bone marrow cells on NCD films demonstrate improved cell spreading behavior and proliferation compared to cells cultured on polystyrene tissue culture dishes. Additionally, the expression of extracellular matrix proteins important for bone formation is stimulated. In fact, proliferation and alkaline phosphatase activity of human osteoblasts is enhanced on nanometer grain size films in contrast to submicron crystalline diamond [61].

Further evaluations with L929 mouse and human gingival fibroblasts reveal no cytotoxic effects on NCD, while the two cell types exhibit different morphological features on the films (Fig. 2.12): human gingival cells are well spread with an elongated morphology, while L929 cells exhibit lower cytoplasmic extensions and a higher proliferation rate [62]. However, proliferation of both fibroblast cell lines is accelerated compared to control cells on conventional plastic culture plates.

Neural stem cells seeded on hydrogen-terminated UNCD spontaneously undergo neuronal differentiation and proliferate [63]. In contrast, these cells differentiate into oligodendrocytes on oxygen-terminated UNCD. Tuning stem cell differentiation by doping ultra-nanocrystalline diamond films with different elements raises the potential for future application as neuronal microelectronic devices. One possibility is the coating with UNCD of retinal microchips to restore

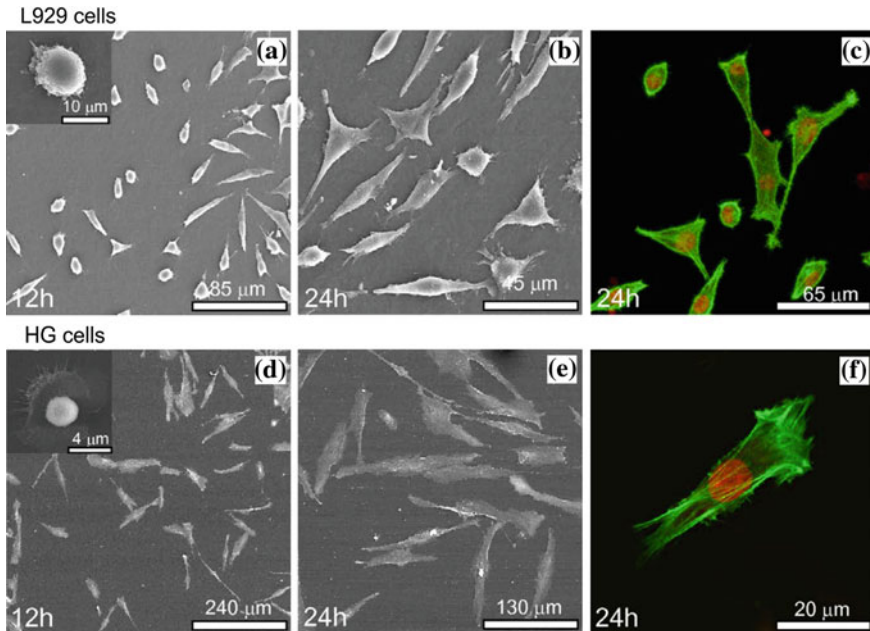


Fig. 2.12 Morphological appearance of L929 mouse and human gingival fibroblast cells cultured on the NCD coating, at 12 and 24 h of culture. **a, b, d** and **e**: SEM (inset in **a** and **d**: 1 h); **c** and **f**: Confocal laser scanning microscopy images, actin filaments (*green*) and nucleus (*red*) staining. Reprinted from [62], Copyright (2009), with permission from Elsevier

vision. Silicon retinal chips with UNCD thin films including 1 % hydrogen have already been tested in rabbit eyes for 4–6 months and showed good biocompatibility [64]. To combine the advantages of NCD and amorphous carbon thin films, such as very smooth surfaces together with high yield strengths, hybrid materials offer new perspectives for medical devices.

2.2.4 Bioceramic Thin Films

Bioceramics are usually porous and fragile materials, which cannot be exposed to high mechanical loads. However, they can exhibit good corrosion resistance and improve bioactivity of surfaces when used as thin films and coated onto implants and prostheses. Due to lack of bioactivity and osteoconductive properties, the lifetime of metal-, especially titanium-based orthopedic and dental implants, is often limited to 10–15 years. Bioceramic thin films coated on the titanium surface can improve these bone-integration properties and promote bone growth.

The surface structure of ceramics can be tuned from smooth layers to porous networks to support tissue ingrowth and improved bonding. However, ceramics such as alumina and zirconia can promote osteolysis, viz. increased osteoclast activity and resorption of bone materials *in vivo*. Their application must be carefully examined. Ceramics employed within the human body are divided into three groups: (1) Bioinert ceramics, e.g. oxides and silica ceramics; (2) resorbable ceramics, e.g. calcium phosphates, and (3) bioactive ceramics, e.g. hydroxyapatite and bioglasses.

Hydroxyapatite (HA), the most common bioceramic, is a bone-like material, which can be coated by sputter deposition, plasma spraying, hydrothermal techniques, hydrolysis of other calcium phosphates and sol–gel synthesis. In general, sol–gel-derived bioceramic coatings offer several advantages with respect to other techniques such as easy fabrication of an uniform layer with complex geometric shape. These coatings comprise adequate mechanical properties important for medical devices due to their nanocrystalline structure. Nevertheless, different fabrication processes result in variations of surface morphology and film thickness, which must be adapted to the requirements of the implant. The most common bioceramic thin films and coatings, their corrosion resistance, and biocompatibility features are discussed in the following sections.

2.2.4.1 Calcium Phosphate

Degradable bioceramics implanted within the human body change their structure and eventually fully dissolve by allowing bone in-growth and replacement of the artificial material with natural tissue. Prominent examples are calcium phosphate based materials which have caught the most attention because of their excellent biocompatibility and compositional similarities to natural bone [65]. Thin Ca-P films attached to implants made of titanium, its alloys, and other metals promote osteogenic cell attachment and proliferation. Additionally the expression of extracellular matrix proteins by the cells is stimulated to produce an apatite layer for further bone-healing after implantation. Thus, calcium phosphates are often employed for stimulation of bone regeneration, e.g. after joint replacement. However, these ceramics cannot bear high loads and are therefore unsuitable for the application as bulk materials for prostheses, but are widely used as coating materials on titanium and its alloys to improve *in vivo* performance.

Several calcium phosphate ceramics show different solubility under physiological conditions: Tetracalcium Phosphate ($\text{Ca}_4\text{P}_2\text{O}_9$) > Amorphous Calcium Phosphate > α -Tricalcium Phosphate- $(\text{Ca}_3(\text{PO}_4)_2)$ > β -Tricalcium Phosphate- $(\text{Ca}_3(\text{PO}_4)_2)$ > Hydroxyapatite (no degradation under physiological conditions). The different calcium phosphate compositions vary in their mechanical strength, physiochemical properties, and thus *in vivo* performance and their behavior in bone integration.

Manufacturing of these ceramic coatings on titanium implants usually starts with grid-blasting the implant to increase surface roughness. High roughness

promotes the interaction and bonding strength of the Ca-P coating. Additionally, dental implants are generally etched to further produce cavities. Afterwards, the material is soaked in a simulated body fluid containing a supersaturated calcium and phosphate solution, which leads to precipitation and the formation of a Ca-P layer on the titanium surface. However, many other methods are employed for fast and cost-effective production of Ca-P coated implants.

Atmospheric plasma spraying of Ca-P coatings of titanium surfaces at temperature greater than 10,000 °C is a widely used method to produce layer thickness of 30–200 µm within minutes [66, 67]. However, the fast cooling after production can result in heterogeneities of Ca-P-phases, and thus differences in dissolution rates in vivo. Additionally, this manufacturing is not very effective for small devices such as dental implants. The high temperature during production also lacks the possibility to incorporate biological agents within the coating material.

Dense and uniform coating thickness of 0.5–3.0 µm can be obtained with sputter coating of a multi-component Ca-P ceramic target [68]. The surface Ca/P ratio can vary from 1.6 to 2.6, and the surface morphology is adaptable to different requirements by annealing at several hundred degrees Celsius. However, this technique is expensive and time consuming that other methods are mostly applied.

An alternative is electrochemical deposition which allows the deposition of dense, porous or nanostructured Ca-P coatings (Fig. 2.13) [69, 70]. Here the implant material is placed in supersaturated Ca-P solutions. Near the electrode, a local pH increase is induced, which leads to precipitation and the formation of a Ca-P layer on the implant surface. A platinum electrode acts as the anode and the titanium implant as the cathode, which can be employed to coat complex surface structures at rapid deposition rates. The incorporation of bioactive molecules, such as proteins, is possible but limited, if further postheating is employed to improve the coating structure and bonding to the implant material.

Most of the described drawbacks can be avoided with sol-gel techniques that require low processing temperatures and result in stoichiometric, homogeneous and pure coatings [72]. Uniform fine-grained structures with coating thickness up to 1 µm can be obtained. Thicker coatings are possible with the biomimetic process of Ca-P coating, which uses natural biomineralization and the precipitation of Ca-P onto the implant surface. Similar to the formation of ceramic coating in simulated body fluids, the implant is placed in saturated calcium and phosphate solutions with the addition of a weak acid gas. Bubbling of the solution increases the pH value and the nucleation of Ca-P crystals is larger compared to simple SBF soaking. The layers of up to 30 µm thickness are similar to bone-like apatite: well-bonded to the implant and can include bone growth stimulating factors. Furthermore, the composition is more soluble in physiological fluids.

Although the formation of bone-like apatite is promoted on Ca-P coated titanium, proliferation rates of osteoblast-like cells in vitro are higher on pure titanium surfaces [73, 74]. However, a significantly larger mineralized extracellular matrix on the Ca-P coated surface with embedded collagen fibers forms, which is important for good in vivo performance. Furthermore, Ca-P coatings

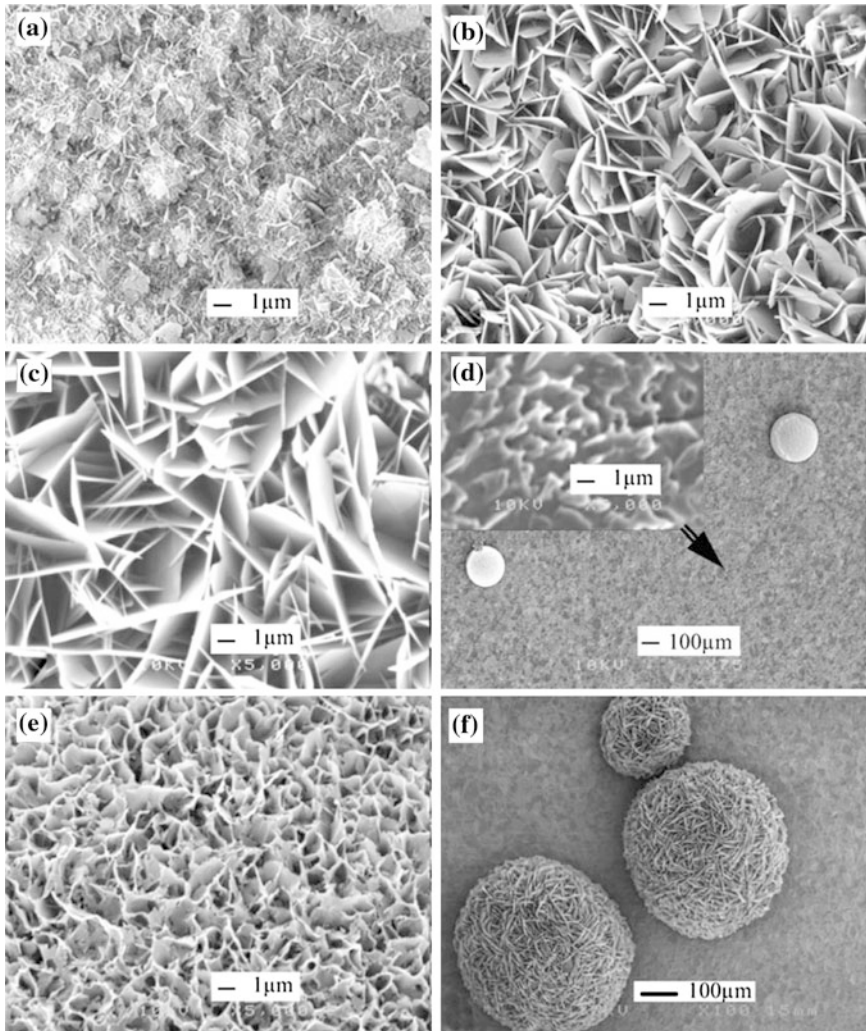


Fig. 2.13 Morphology of the biomimetic Ca-P deposition: (a) Ca-P layer on electrochemically-treated surface after 2 h immersion; (b) Ca-P layer on electrochemically-treated surface after 6 h immersion; (c) Ca-P layer on electrochemically-treated surface after 24 h immersion; (d) non-treated titanium surface after 24 h immersion with a few isolated Ca-P particles; (e) high magnification of Ca-P particles in d; and (f) non-treated titanium surface after 72 h immersion. Reprinted from [71], Copyright (2005), with permission from Elsevier

promote differentiation of osteogenic cells, while cell response depends on the crystallinity and surface morphology of the coating.

In contrast to osteoblast adhesion on Ca-P coated and pure Ti surfaces *in vitro*, animal tests and clinical studies with patients demonstrate that biomimetic Ca-P coatings obtain a stronger bonding to the implant compared to uncoated titanium

implants. Already 1–2 months after implantation, the ceramic is surrounded by mature bone and no resorption is usually observed. Currently it is still under debate whether the overall dissolution behavior important for bone formation is a solution-mediated process or driven by cell-mediated processes [75].

The limiting factors for the application of Ca-P *in vivo* are mainly the brittleness, low mechanical resistance and tensile strength. Ceramics with porosity up to 90 % stimulate bone ingrowth, while leading to mechanical instabilities. In fact, minimum pore sizes of 100 μm are required due to cell sizes, but diameters $>300 \mu\text{m}$ are recommended to promote formation of capillaries and vascularization [76]. Different filler materials are employed to improve mechanical stability, stop crack formation, and still support resorption and bone growth. New Ca-P-based composites made of biphasic calcium phosphate with up to 30 wt % mullite ($3\text{Al}_2\text{O}_3 \cdot 2\text{SiO}_2$) addition are a candidate with improved mechanical strength [77]. The biocompatibility of such material has already been demonstrated *in vitro*, while clinical trials are still outstanding. Future Ca-P based ceramics aim to enhance bioactivity by activating genes, delivering biological agents, and improving mechanical performance and bioactivity.

2.2.4.2 Hydroxyapatite

Hydroxyapatite (HA) is the most often used calcium phosphate coating for biomedical implant materials. Its chemical structure $\text{Ca}_{10}(\text{PO}_4)_6(\text{OH})_2$ and a Ca/P wt. ratio of 2.151 make it an excellent bioactive ceramic with a similar composition to bone mineral. At physiological pH of 7.4 HA is the most thermodynamically stable Ca-P which is not resorbable. It is therefore often used as coating material to stimulate cell attachment *in vitro* and bone formation and growth *in vivo*. HA promotes efficient implant fixation and implant-to-bone bonding shortly after implantation because of excellent osteoconductivity, as well as fast bone remodeling.

Compared to natural apatite, HA lacks several ions such as Na^+ , K^+ , Mg^{2+} , Fe^{2+} , F^- and Cl^- which results in different crystallinity and mechanical strength. HA films show the best resistance for lower (1N) and higher (3N) load with respect to SiO_2 and TiO_2 [78, 79]. However, HA thin films have a low tensile strength and fracture toughness compared to bone, which can be improved by sintering HA coatings on metallic substrates such as titanium (Fig. 2.14) or Ti-6Al-4V alloys, bioactive glass ceramics, as well as titanium nanotubes. Plasma-assisted fabrication allows large variations in grain size and crystallinity [80]. However, these films are highly porous, brittle and often detach from the underlying material. Further difficulties in film attachment can occur when oxide layers are formed on the implant surface prior to coating, which often occurs during deposition of growing pure crystalline HA films at several hundred degrees Celsius [81]. Adhesion and density can be improved by ion-implantation techniques at low temperatures, as well as radio frequency magnetron sputtering.

Fig. 2.14 Hydroxyapatite ceramic-coated furlong total hip arthroplasty stem. Reprinted from [82], Copyright (2010), with permission from Elsevier



Soaking of sintered HA in SBF at 37 °C reveals formation of bone-like apatite on the surface, while the deposition kinetics depend on the surface charges of the initial HA material. Different sintering temperatures influence the surface potential, and thus trigger nucleation of HA precipitates. The HA surface has a negative surface charge which interacts with the positive calcium ions in the fluid to form the Ca-rich nanocrystalline calcium phosphate with positive surface charge. This calcium phosphate on the HA surface interacts with the negative phosphate ions in the SBF to form the Ca-poor nanocrystalline calcium phosphate, which crystallizes into bone-like apatite [83] important for osseointegration.

Good bioactivity is corroborated by *in vitro* cell tests. Mesenchymal stem cells and mouse osteoblast cells seeded onto HA coated substrates show good adhesion and proliferation behavior [80, 84]. After 8 days the interaction of osteoblasts with the HA surface results in the formation of a thick layer of extracellular matrix and bone nodules. *In vivo* cell attachment can be improved even further when immobilized cell adhesion proteins, such as laminin, are incorporated into the HA layer [85].

Small amounts of elements such as silicon and magnesium, which are found in natural bone, can be doped to HA coatings to influence dissolution rates and improve bone formation processes. *In vivo* and *in vitro* testing of silicon-substituted hydroxyapatite (Si-HA) with approximately 1 wt % Si obtain that Si-HA improves early bonding of the bone to the implant surface with respect to pure HA coatings [86]. Amorphous or nanocrystalline Si-HA coatings up to 700 nm thick on titanium substrates can be fabricated by magnetron co-sputtering [87], while subsequent heat treatment results in improved crystallinity. Such films employed as substrate materials *in vitro* promote proliferation and attachment of osteoblast

cells compared to as-deposited samples. Metabolic activity and mineralization of the cell layer demonstrate bioactive properties *in vitro* which could already be verified *in vivo* (Fig. 2.15): Silicon doped HA shows excellent performance in animal testing in terms of bone bonding and remodeling, as well as mechanical stability [88], which offers further application for bioactive coatings of load-bearing devices such as hip prostheses in the future.

A new approach for further improvement of tissue-implant-bonding with HA coatings uses electric changes to stimulate bone ingrowth. Piezoelectricity in bone was first proposed and measured by Fukada and Yasuda in 1957 [89]. They suggested that shear forces within the bone lead to slipping of collagen fibers that result in generation of electric dipoles and thus electric fields. Since surface changes of cell substrates influence protein absorption, and in line cell adhesion and migration, osteoblast proliferation and bone formation can be stimulated by employing charged HA coatings *in vitro* and *in vivo* [90]. Negatively charged HA surfaces especially enhance osteoblast proliferation, whereas positively charged surfaces reduce cell division rates. Besides, an increase in cell migration can be stimulated on both positive and negative surfaces, which is attributable to charge induced variation of actin filaments within the cellular cytoskeleton.

In vivo studies on charged HA coatings of bone implants confirm positive effects on increased bone ingrowth. Compared to non-charged HA surfaces, positively as well as negatively charged HA films promote the formation of fibrin layers for osteoconduction. This promising cell response on piezoelectric materials

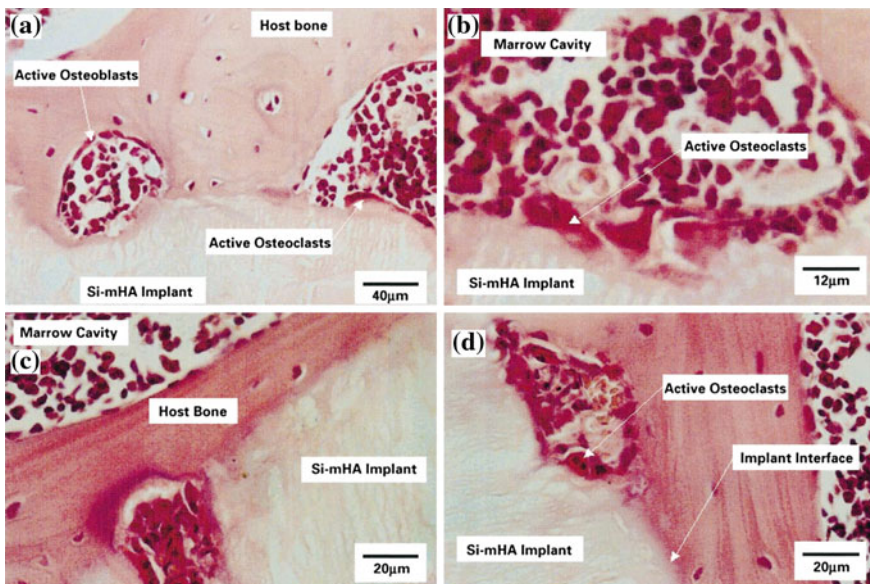


Fig. 2.15 Histological sections illustrating the Si-microporous HA marrow cavity interface after six weeks implantation into the femur of adult Wistar rats. Reprinted from [88], Copyright (2001), with permission from Elsevier

can also be found for other charged bioceramics such as BaTiO_3 surfaces. The integration of electrically charged surfaces into biomedical devices offers great potential not only for promotion of tissue attachment and bone formation, but also for drug delivery systems and leaves room for future work.

2.2.4.3 Silicon-Based Ceramics and Bioglass[®]

Bioglasses composed of various quantities of SiO_2 , Na_2O , CaO and P_2O_5 were first investigated in the late 1950s by L. L. Hench who is still working on bioceramics as Emeritus Professor at Imperial College London. Initially, bioglasses were developed to replace diseased or damaged tissues. The first bioactive glass, 45S5 Bioglass[®], is composed of 45 wt % SiO_2 , 24.5 wt % Na_2O , 24.5 wt % CaO and 6 wt % P_2O_5 . Nowadays, bioglasses with many different quantities of these and other oxides are available. Although bioactive glass scaffolds obtain a low resistance to fracture, they are employed as bulk materials as well as thin film coatings for implant materials with great success. Their applications range from coating to bulk material prostheses, as well as tissue engineering for articular cartilage and skin repair.

Bioglasses can be bioinert and get encapsulated within fibrous tissue for >65 mol % SiO_2 , resolve within 30 days or binds to bone, while all these properties depend on composition. 45S5 Bioglass[®] promotes the formation of hydroxyapatite layers on its surface in contact with body fluids and osteoblast cells. Although ion release of Si, Ca, Na and P takes place, it turns out that 45S5 Bioglass[®] enhances ATP generation, up-regulation of genes, promotes alkaline phosphatase activity and osteocalcin, as well as collagen I synthesis. Proliferation of osteoblast cells is promoted due to Si-induced osteoblast cell cycle shortening [91]. The good biocompatibility of 45S5 Bioglass[®] is attributed to the relatively small amount of silica and in turn larger quantities of Na_2O and CaO with a high $\text{CaO}/\text{P}_2\text{O}_5$ ratio. In contrast, larger amounts of silicon in MBG 85 glasses ($85\text{SiO}_2\text{-}10\text{CaO-}5\text{P}_2\text{O}_5$) reduce osteoblast cell division. Different cells types such as osteoblasts, fibroblasts and endothelial cells adhere well to the surface of various bioactive glass compositions, thus excellent bioactivity in contact with a wide range of tissues is the reason for applying bioglasses as coating materials in implantology.

Bioactive glasses employed as coatings on prostheses made of titanium and other materials often suffer the formation of cracks in the surface layer, which may result in severe injury of the patient. These cracks often appear due to corrosion of the material and can be avoided when a thin layer of HA forms up till the point when osteoblasts adhere to the surface. Since SiO_2 controls the bioactivity of the bioglass, variations of the composition promote success of the coating and foreign body response. Drawbacks of 45S5 Bioglass obtained in vitro are slow degradation rates and conversion to an apatite material. Thus, conversion is often incomplete; SiO_2 can remain within the scaffold causing long-term side effects [92].

New bioglass coatings use various quantities of SiO_2 , CaCO_3 , MgCO_3 , Na_2CO_3 , K_2CO_3 and NaH_2PO_4 for bioactive coatings on titanium devices, which are realized, e.g. by pulsed laser deposition [93]. When soaking these coated materials in simulated body fluid, a loss of Ca, Mg, P and Si ions occurs within the first 2–3 days, accompanied with a relative increase of Si in the surface layer. Subsequently, increase in PO_4^{3-} results in bone-like HA formation within 14 days.

Implanted 45S5 bioactive glasses in vivo release Na^+ and Ca^+ ions, which promote apatite formation and stimulate angiogenesis [94]. Silicon release cannot be avoided, and even months after implantation, silicon is still present in several organs and bones. However, the very small quantities are supposed to be harmless. Higher SiO_2 contents, as used for the designated 13–93 bioglass, lead to better processing properties and support osteoblast proliferation to the same extent as found for 45S5 Bioglass. However, 13–93 bioglass possesses even slower degradation rates.

In line with in vitro assessments, 45S5 Bioglass and glasses with MgO and K_2O content such as 13–93 bioglass promote cell adhesion (Fig. 2.16), rapid bone formation and even faster osteoblast proliferation than synthetic HA. Implanted bioactive glasses placed within the femur of mammalian animals exhibited very good osteoconductive and osteoinductive properties, namely new bone growth promotion along the implant surface. In fact, conversion into HA-like material is accelerated with increasing B_2O_3 content. For example, borosilicate 13–93B1 fully converts to HA. However, some in vitro studies find that borite glasses show worse biocompatibility in terms of a lower ability to promote cell growth and function due to the release of boron ions. Nevertheless, the microstructure of the bioglass surface such as roughness, porosity and pore size plays a vital role in tissue infiltration. New approaches use mesenchymal stem cells seeded onto the bioglass. These cells adhere well to the substrate material and support bone infiltration in vivo.

Besides new bone growth, bioglasses can promote the formation of new blood vessels (angiogenesis) because they stimulate vascular endothelial growth factor (VEGF) and basic fibroblast growth factor (bFGF). Surfaces such as polystyrene coated with low concentrations of 45S5 Bioglass exhibit enhanced proliferation of fibroblasts in vitro compared to uncoated surfaces. In vivo experiments in rat with implanted poly(glycolic acid) meshes in rat obtained improved neovascularization within 28 and 42 days [92]. Additionally, the borosilicate bioglass 13–93B3 also promotes angiogenesis. It appears to be non-toxic according to experiments in small mammalian animals.

These results show that the addition of ions to clinically applied silicon-based bioglasses might enhance specific biological function and responses of the surrounding tissue in vivo. Many different ions are doped to the bioglasses, such as zinc, strontium, copper, cobalt and gold. Ion addition changes dissolution rates of the material, in line with cell adhesion properties and certain gene expressions of the cells. Current investigations aim to combine the promotion of cell function together with adequate mechanical properties of the bulk glass or coating of the implant for clinical applications by varying the bioglass composition.

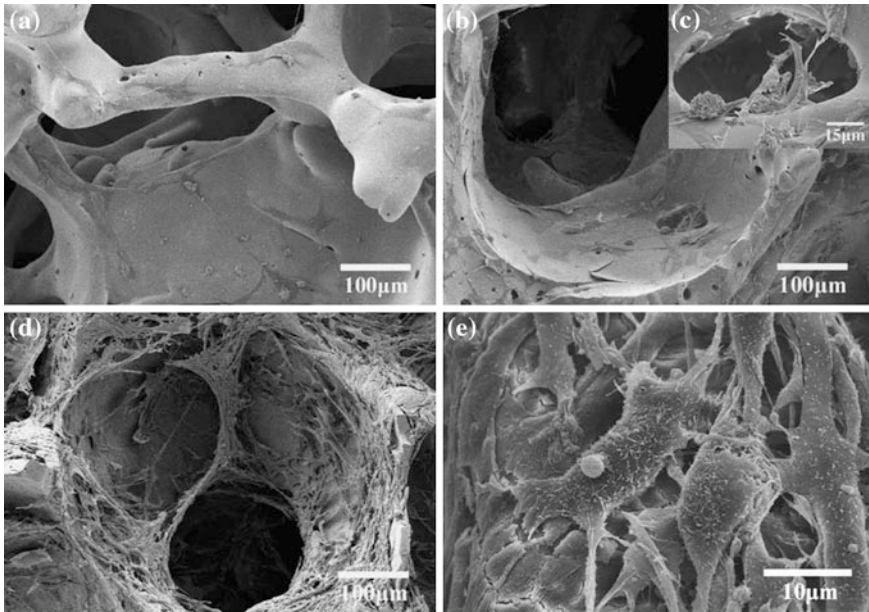


Fig. 2.16 SEM images of silicate-based bioactive glasses, designated 13-93, with a modified 45S5 bioglass composition, seeded with MC3T3-E1 cells and cultured for: (a) 2 days; (b, c) 4 days; and (d, e) 6 days. Reprinted from [95], Copyright (2008), with permission from Elsevier

2.2.4.4 Alumina

Although titanium/titania-based materials are commonly used as implant materials together with calcium-phosphate-based coatings, other ceramics are under investigation that exhibit excellent biocompatibility together with different mechanical properties, wear resistance and weight. Alumina ceramics (Al_2O_3) are bioinert and exhibit low surface roughness, high hardness for scratch resistance and fracture toughness, as well as high wettability, which can be achieved by a high material density, high purity and small grains. In contrast to titania implants, alumina-on-alumina bearings show improved sliding characteristics and a low wear debris generation. Thus, they are among the most resistant to wear in total hip replacement [96]. Nevertheless, coating of medical devices with alumina-based ceramics is hardly investigated until now, and little is known on the interaction of single cells with smooth alumina surfaces.

Since the first alumina-based hip arthroplasty in 1970, most studies have focused on the biocompatibility in vivo. New fabrication methods such as the Morse taper technology together with technological progress in prosthesis design lead to very promising alumina-on-alumina bearings showing very good performance as hip arthroplasties with about 85 % survival after 20 years [97]. The previously observed increase in osteolysis and aseptic loosening after surgery

could be limited by reducing the amount of wear particles around the bearing. Replacement of such alumina implants is easy and usually no foreign body reaction occurs. However, these medical devices are expensive and efficient surgical training is necessary.

In vitro studies with osteoblast and human coronary artery smooth muscle cells corroborate good cellular attachment and proliferation on alumina films [98, 99]. Extracellular matrix proteins, such as osteocalcin, as well as type I and V collagen are expressed by bone cells attached to alumina substrates, which maintain normal cellular morphology. Although a dense cell layer with well-spread cells can be obtained after some days of cell culture, the proliferation rate is slightly reduced compared to cells cultured on glass substrates. Similar cell division behavior can be seen on zirconia substrates, while on both bioceramics more than 90 % of the cells are viable. Thus, the observed bone resorption in vivo is mainly attributable to prosthetic debris, which can stimulate biological reactions leading to osteolysis. Cytotoxic effects can be neglected as alumina is a well-established biocompatible and bioactive material.

2.2.4.5 Zirconia

Zirconia (ZrO_2) is a bioinert ceramic with a high strength, wear and corrosion resistance. Small amounts of yttria (2–3 %) stabilize the tetragonal zirconia phase, which is characterized by low porosity, high bending and compression strength and mechanical stability. Further aging of the material to the monoclinic phase structurally stabilizes the material with a compression resistance of about 2 GPa, similar to stainless steel. This makes it an ideal candidate for dental implants. In fact, the brittleness of alumina and failure of alumina-based hip prosthesis can be avoided when zirconia is used with the appropriate microstructure [100]. To this end, for more than 30 years the biocompatibility of zirconia has been addressed in vitro and in vivo.

SBF tests show excellent corrosion resistance of tetragonal ZrO_2 thin films deposited on silicon wafers. Immersion within the SBF leads to the nucleation of bone-like apatite onto the films, while the nanostructured surface is believed to be the key factor that apatite is induced to precipitate on the surface [101]. SBF investigation zirconia deposited on hydrogels show that apatite formation is supposed to be induced by Zr–OH groups in a zirconia hydrogel layer that forms on the metal upon exposure to NaOH in the body fluid.

In vitro biocompatibility of different structural forms of zirconia has been addressed with different fibroblast cell lines, lymphocytes, monocytes, macrophages and osteoblasts. Fibroblasts adhere well to zirconia substrates and proliferate (Fig. 2.17), whereas wear debris leads to dose-dependent cytotoxic effects. Mutagenicity evaluations prove that zirconia does not generate genetic mutations of fibroblast cells [102]. In fact, for human monocytes differentiated into macrophages, zirconia powders are less cytotoxic compared to alumina powders [100]. Moreover, macrophage mortality is dependent on particle size, increasing with size

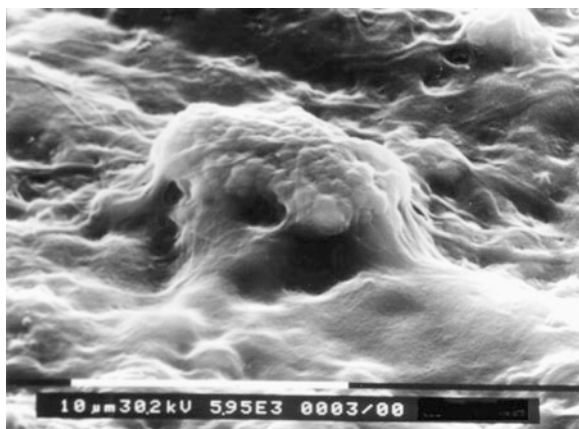
(>2 μm) and concentration. Small zirconia particles do not cause severe cytotoxicity or inflammation processes on lymphocytes, monocytes and macrophages. Furthermore, bone marrow mesenchymal stem cells are observed to grow and proliferate on the surface of zirconia thin films, in line with the good cell growth and gene expression of MG-63 osteoblast-like cells.

Biocompatibility assays with different osteoblast cells such as rat osteoblasts, MG-63 and CAL-72 osteoblast-like cells provide good adhesion properties of cells on zirconia surfaces and high viability in contact with zirconia powders. Osteoblast division and growth is thereby dependent on surface roughness and wettability. Compared to osteoblast behavior on pure alumina surfaces or in contact with powder, zirconia provides better biocompatibility features as cells proliferate faster and show less cytotoxic effects.

The interaction of soft and hard tissue with zirconia pins, bars and coated implant materials has been studied in various animals such as mice, rats, dogs and monkeys. In contact with soft tissue, e.g. muscles, fibrous tissue encapsulates the zirconia polycrystalline samples [100]. No signs of pathologic tissue reaction are evident, which is also observed for other physical structures of zirconia. Yttria stabilized zirconia implanted into hard tissue, e.g. the femur of monkeys, also proves the good biocompatibility of the material since no inflammatory processes and toxic effects occur. Moreover, the bone tissue strongly attaches to zirconia coated surfaces.

Clinical trials mainly employed the performance of zirconia—bulk and coatings—as materials for dental abutments. The good bioactivity leads to a reduced marginal bone loss around the peri-implant compared to titanium devices. Bonding of the dental implant with the bone is investigated by measuring the rotational freedom. A small rotation below 3° , as found for zirconia and titanium, is a good indicator for strong tissue bonding. In comparison, osseointegration of alumina implants is worse and larger rotation angles are evident [102]. However, treatments to increase surface roughness before implantation are essential to promote bone attachment and long-term stability. Nowadays, zirconia is especially used for

Fig. 2.17 Scanning electron microscopy observation of fibroblasts cultured on zirconia: cells grow on the whole zirconia surface, covering it with a cellular layer. A cellular body covered by cytoplasm is discernible (magnification 7,400 \times). Reprinted from [102], Copyright (2007), with permission from Elsevier



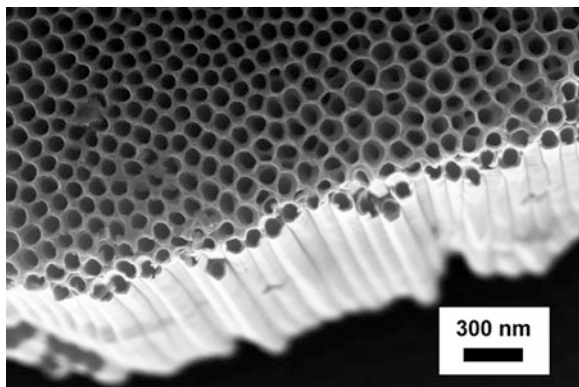
dental implantology as bulk material or thin film coated to e.g. titanium to improve cell adhesion and osseointegration. Zirconia surfaces also accumulate fewer bacteria than titanium. Odontology also uses zirconia-based materials because of aesthetical issues [103].

2.2.5 Nanotube-Structured Arrays

Nanotubes are nano-sized structures which assemble by self-organization of atoms during processing. The tubes can vary in length and diameter from a few nanometers up to several hundred and even microns. The most common nanotubes are carbon nanotubes and titan dioxid nanotubes. While carbon nanotubes (CNT) are usually produced as single fibers or bundles forming a random network, TiO_2 nanotubes are films of well-organized and aligned nanotubes that build up an array (Fig. 2.18).

Although carbon as well as titania materials are well established as biocompatible materials, there are several aspects which can influence biocompatibility and cause harm: Considering single nanotubes as a type of nanoparticles, (1) the ratio surface area/mass ratio of the nanoparticle is large, which increases the possibility of absorption and transport of cytotoxic substances. (2) The particle retention time can be large, i.e. the particle stays in long contact with the tissue which can result is increased uptake of toxic substances. (3) Nanoparticles can show an improved reactivity [104], which is already proved for titania nanotubes. However, nanotubes can be used to assemble various surface structures, which can stimulate cell proliferation and adhesion. These nanotube structures are easily tunable in terms of length and diameter and are thus adaptable to various in vitro and in vivo applications.

Fig. 2.18 Scanning electron micrograph of TiO_2 nanotube array composed of parallel aligned nanotubes



2.2.5.1 Carbon Nanotubes

Carbon nanotubes (CNT) are molecular scale wires exhibiting useful physical properties for numerous potential applications including electronics as well as miniaturized biotechnological devices. CNT can be processed by various techniques including arc-discharge sublimation, laser ablation, catalytic decomposition, and high-pressure carbon monoxide and chemical vapor deposition, which yield large quantities of nanotubes. The electrical properties are sensitive to surface charge transfer and changes in the electrostatic surroundings, important for the application as electronic biosensors and electrostimulation devices during tissue formation and cell culture. CNT can exist as single-walled (SWNT) and multi-walled (MWNT) nanotubes (Fig. 2.19). Both types are characterized by high tensile strength, ultra-light weight and excellent thermal and chemical stability, making them perfect candidates for medical devices. Although carbon is already used for biomedical applications such as bone fixation materials and coating of metal implants for improved corrosion resistance, the performance of cells and tissue in contact with CNT cannot directly be derived from biocompatibility assessments of other carbon materials. Nanostructured surfaces can often lead to cytotoxic effect due to increased surface areas, which are exposed to tissue and cells, and thus must be tested *in vitro* and *in vivo*.

In vitro biocompatibility tests examine the interaction of living cells with CNT by employing (1) aqueous solution of CNT with various concentrations in contact with cells or (2) by attaching CNT to a substrate material which is then used for cell culture. The influence of CNT on cell viability and adhesion depends to a great extent on the concentration of the CNT in the cell culture medium and the incubation time because cells tend to take up nano-sized particles. However, for CNTs in cell culture medium also the structure and the diameter of the nanotubes are a major determinant of cell viability. Neuronal and lung cells treated with concentrations ranging from 25 to 100 $\mu\text{g/ml}$ for 24 h show a decrease in proliferation, while MWNT with diameters from 9 to 30 nm and length up to tens of micrometers are more biocompatible compared to SWNT in bundles with

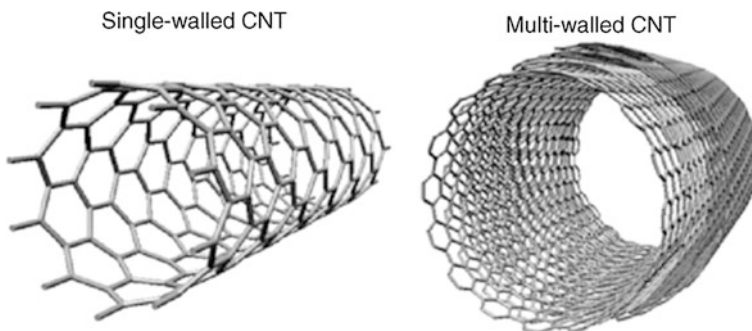


Fig. 2.19 Sketch of single-walled and multi-walled carbon nanotubes. Reprinted from [105], Copyright (2012), with permission from Elsevier

diameters up to 25 nm and length over 3 μm . Even if these cells proliferate in the presence of CNT, studies on the uptake of SWCN and MWNT with human epidermal keratinocyte (HaCaT and HEK) cells (Fig. 2.20) clearly show an increased production of pro-inflammatory cytokine IL-8 release [106] and accelerated oxidative stress [107] pointing towards a reduction of cell viability. Together with the obtained changes in cell morphology, cellular uptake of CNT by epidermal keratinocytes is correlated to dermal toxicity, which is also obtained for other cell types.

CNT uptake during biocompatibility assessments can be suppressed by attaching the nanotubes to a substrate material onto which the cells are seeded. These studies are especially important for the understanding of CNT employed as coating materials for implants. Due to the unique electronic properties of CNT, the interaction of neuronal cell with nanotube decorated substrates is of high interest. Here not only the viability of the cells is examined, but also the formation of neuronal networks by the growth of neurites and axons. Astrocytes which are mainly responsible for scar tissue formation around implanted neuronal devices show an increased adhesion and proliferation on carbon-nanofiber (CNF) substrates with fiber diameters >100 nm [108]. Thus, smaller CNFs bear the potential as coatings for devices implanted within the brain to suppress adhesion and thus scar tissue formation. Further chemical functionalization of nanostructured CNF substrates is possible to increase and stimulate cell proliferation and neuronal network formation.

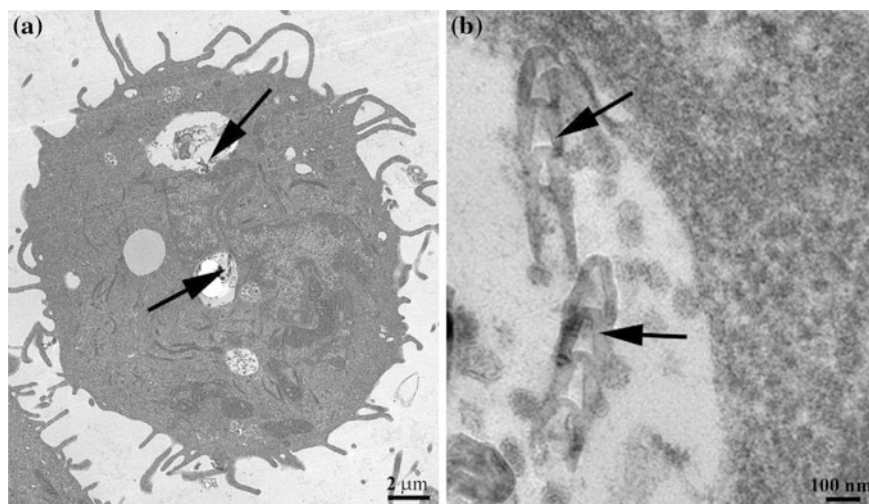


Fig. 2.20 Transmission electron micrograph of human epidermal keratinocytes. **a** Low magnification of a keratinocyte for precise location of the vacuoles containing MWCNT (arrows). **b** High magnification of vacuole to demonstrate that MWCNT retain their structure. Reprinted with from [106], Copyright (2005), with permission from Elsevier

Similar biocompatibility features can be found for osteoblast cells, whereas these cells show increased proliferation on CNF-based substrates with fiber diameters below 100 nm. Good biocompatibility is also confirmed for fibroblast cells on MWCN decorated substrates [109]. Additionally, these substrates stimulate alkaline phosphatase activity and the deposition of extra-cellular calcium deposition of osteoblast cells. Thus, they bear the potential as thin film attached to orthopedic devices to promote tissue bonding. However, the interaction of the bulk material with the nanofiber decoration must be investigated in detail to ensure strong attachment and suppress possible rupture.

Since in-growth of osteoblasts into implant materials such as hip prostheses improves the long-term performance of the tissue-implant interaction, three-dimensional surface structures can account for better cell adhesion in vitro and in vivo. Three-dimensionally structured MWNT substrates as shown in Fig. 2.21 [110] are examples of surface morphologies composed of MWNT which are proved to be biocompatible and allow cell adhesion and proliferation in vitro.

Even after the promising in vitro biocompatibility tests of CNT, workers involved in manufacturing and handling CNT-based materials often show severe side effects such as skin irritations and lung inflammations. Although patch tests on volunteers in which filter papers saturated with water suspension of unrefined CNT were exposed to the skin for 96 h showed no skin irritations [111], nanotube uptake by human epidermal keratinocytes can induce cytotoxic effects. In vivo assessments on the effect of SWNT and MWNT by intratracheal instillation on mouse, rat and guinea pig lungs exhibit severe health risks due to lung inflammation with indices of apoptosis, lung lesions characterized by interstitial granulomas and significant evidence of pulmonary toxicity [112–114]. CNT inhalation is more inflammatory than carbon black but causes less harm than asbestos fibers [115]. Even though the uptake of single carbon nanotube fibers by single cells can lead to apoptosis and inflammatory processes, the response of cells to CNF including substrates, which bind the fibers to suppress migration of the material out of the substrate into the cells and tissue, is promising and bears the potential for the application of CNF as biomedical sensors.

2.2.5.2 Titanium Dioxide Nanotubes

Nanotubes made of TiO_2 are self-assembled nanostructures which can be achieved by various techniques such as sol–gel methods, template-assigned methods, metal–organic physical vapor deposition and seeded growth. The most common and easiest production technique is anodization of titanium in adequate electrolytes. Here an electrochemical oxidation reaction of a titanium foil is employed, which leads to a self-organized alignment of TiO_2 nanotubes attached to the substrate foil. Ultrasonic treatments, heating and drying procedures can be used afterwards to detach the nanotubes, as well as remove debris from the surface, changing the nanotube structure and the array morphology from e.g. *nanoporous* nanotubes into *free-standing* nanotube thin films (Fig. 2.22). Environmental conditions during

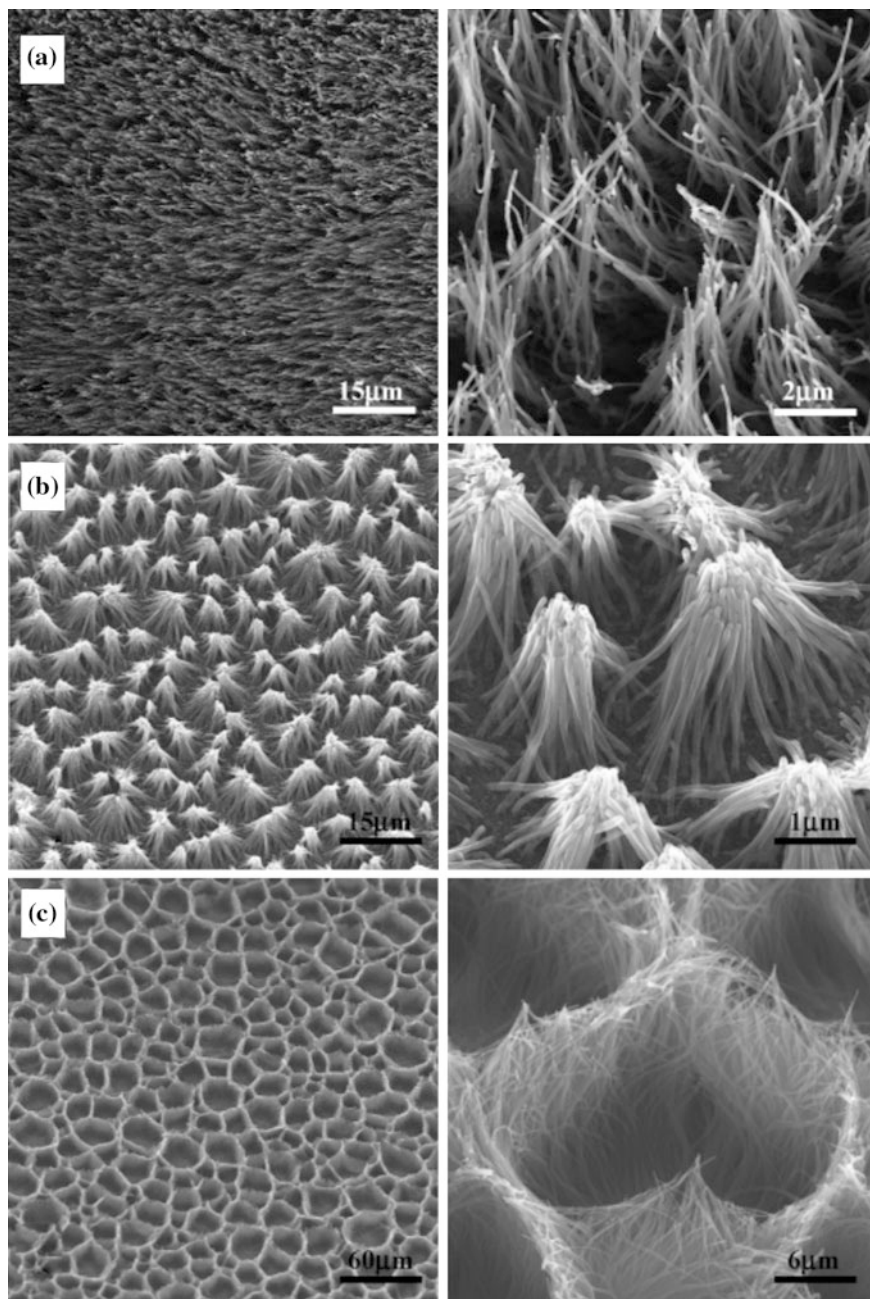


Fig. 2.21 Examination by SEM of the different MWCNT-based structures. **a** Perpendicular aligned carbon nanotubes. **b** The latter after a physicochemical treatment forming pyramid-like structure with basal planes of ca. 3 μm. **c** Network of crosslinked carbon nanotube walls forming cavities. Reprinted with permission from [110], Copyright (2004) American chemical society

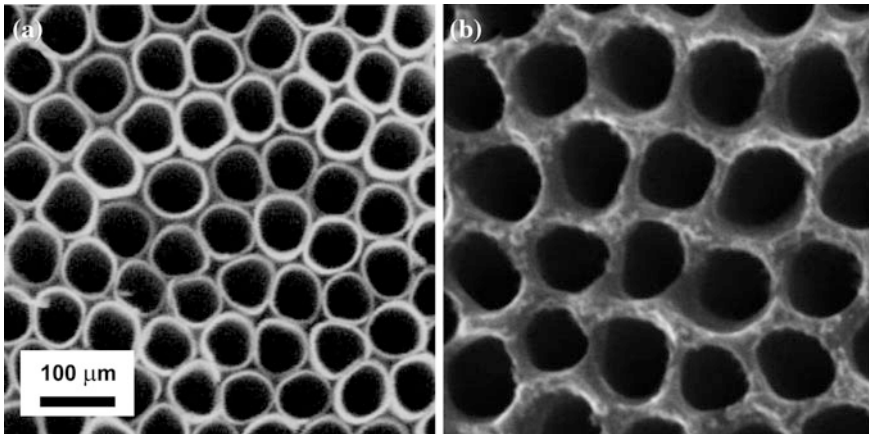


Fig. 2.22 TiO₂ nanotube arrays. **a** Free-standing nanotubes, **b** nanoporous nanotubes

anodization like the composition of the electrolyte, as well as oxidation times determine the nanotube diameter, wall thickness and surface roughness. Currently, nanotube diameters ranging from a few nanometers up to ~ 500 nm and nanometer length of 1 mm are possible.

Since titanium and titania are biocompatible and commonly used for biomedical devices and implants, testing the interaction of TiO₂ nanotube thin films with living matter can offer new perspectives for biomedical applications and miniaturized devices because surface parameters are easily tunable and adaptable to various conditions. After the discovery of TiO₂ nanotubes in 1999 by Zwillig et al., *in vitro* biocompatibility assessments were already performed by the beginning of the 20th century. These tests focused on the one hand on the interaction of single cells with nanotube arrays of different tube diameters, as well as materials aggregation on the nanotube surface during simulated body fluid tests. Although the length of the applied nanotube substrates does not influence the outcome of the tests because the cells are in contact with the open tube ends, thin film arrays with tube length of a few hundred nanometers are usually used because they are easily and quickly produced.

In vitro cell tests have been performed with many different cell types and nanotube morphologies. In comparison to flat titania substrates, cells can adhere to the nanotube surfaces much better, proliferate and migrate if the right nanotube diameters are employed. Otherwise these arrays act as passive surfaces that suppress cell attachment because nanotube arrays provide nanoscale cues that facilitate cellular probing, cell sensing and migration. However, the nanostructure does not only influence the attachment of cell adhesion molecules to the nanotube surface, but also physical properties such as surface energy and wetting behavior. Since hydrophilic surfaces promote cell adhesion, the super-hydrophilicity of TiO₂ nanotube arrays [116] improves cell survival and proliferation.

In vitro studies proved 15 nm nanotubes in diameter ideal for cell stimulating effects of mesenchymal and hematopoietic stem cells, as well as osteoblast and

osteoclast cells [117]. In fact, integrin clustering and thus, the formation of focal adhesion complexes is of the size of 10 nm, which leads to optimal fitting of the cell to the substrate geometry, whereas larger diameters up to 100 nm can cause cell fate. However, these nanotube diameters can be used for biomedical devices with passivated surfaces for which cell adhesion is not desired.

Besides, other studies on the interaction of osteoblast cells with nanotube thin films proved diameters in the range of 30–100 nm favorable for cellular adhesion. This contradiction is still a matter of debate and might be attributed to different production procedures of the substrates, which result in variations of chemical depositions remaining within the pores after anodization, as well as changes in surface roughness and surface pretreatments.

Directly correlated with cellular adhesion is the regulation of cell morphology. The regular nanotube structure leads to a well-organized actin cytoskeleton and the formation of filopodia that probe the surface and can protrude into the nanopores [118, 119], which furthermore increases the cell-substrate interaction. In comparison to flat titania film, endothelial cells on TiO₂ nanotube arrays with diameters from 30 to 100 nm are smaller and more elongated. This polarized shape promotes migration via the ability to exert larger traction forces to the substrate. Thus, cells on nanotubes migrate faster compared to cells on flat surfaces, an important feature e.g. to improve wound healing. Similar observations are made for osteoblast cells which exhibit weaker adhesion on 100 nm tubes and an elongated shape in comparison to 30 nm tubes. This cell polarization results in up-regulation of alkaline phosphatase activity important for bone formation [120]. Besides, vascular smooth muscle cells show a slowed proliferation on nanotube films compared to endothelial cells. Both cell types exhibit a decreased expression of molecules involved in inflammation and coagulation with respect to cells grown on flat TiO₂ surfaces [121, 122]. The up- and down-regulation of certain genes is dependent on surface properties and influenced by nanotube diameters, which can be used to improve in vivo performance by varying surface morphologies of prostheses and stents.

Furthermore, improved response of osteoblast cells with TiO₂ nanotubes can be achieved by coating the surface with bone-like apatite. Alternatively, osteoblast function and stimulation can result in the formation of an apatite layer by protein expression of the cells themselves. Simulated body fluid tests also corroborate the ability to build up apatite layers of several microns thickness onto the nanotubes, while compact TiO₂ films do not support apatite formation.

Nevertheless, although the good bioactivity of TiO₂ nanotube arrays has already be proven, in vivo tests are necessary to address possible inflammatory response and foreign body reaction. First investigations were performed with nanotubes with diameters of 30 nm, which were implanted into the front skull of domestic pigs [123]. In comparison to pure untreated titanium surfaces, TiO₂ nanotubes enhance osteoblast function and bone formation. However, the bonding of the nanotube array to the underlying titanium is weak. Future studies must address this issue to avoid detachment and, thus failure of the material in vivo.

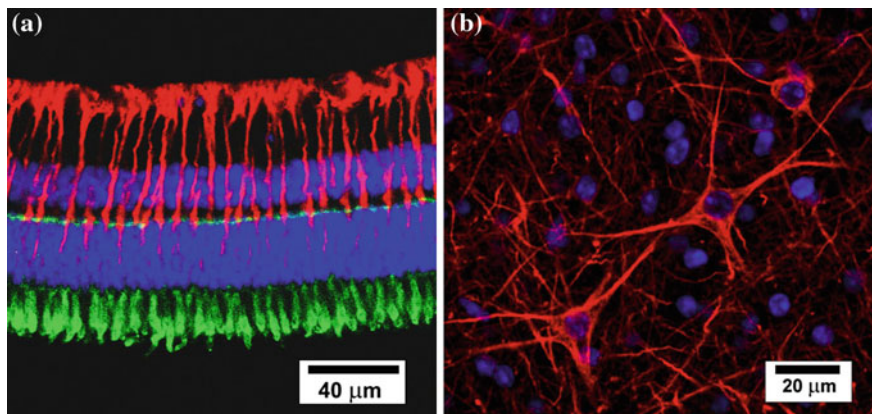


Fig. 2.23 Confocal laser scanning microscopy image of adult guinea pig retina (a) and adult murine brain slice (b) after 14 days culture on TiO₂ nanotube arrays. The structure of the retina with the glial Müller cells (red), cell nuclei (blue) and photoreceptors (green) is fully maintained after culture, as well as the neuronal network of the brain slice from neocortex with neurofilaments (red) and neuronal cell nuclei (blue)

Interestingly, recent experiments show that TiO₂ nanotube arrays feature perfect characteristics for long-term organotypic culture of adult neuronal tissue [116]. Organotypic tissue culture is a perfect alternative to in vivo animal tests; however, long-term culture of adult tissue is an unsolved problem for many decades. Superhydrophilic nanostructured TiO₂ substrates with tunable surface morphologies offer ideal conditions for culturing adult retinal explants (Fig. 2.23a) and adult brain slices (Fig. 2.23b) as recently shown. Even after two weeks, the neuronal tissue structures are maintained without any signs of degeneration, which paves the way for in vitro retina and brain tissue regeneration.

2.2.6 Nanoporous Thin Films

Besides nanotube structured materials made of TiO₂, other nanostructured thin films made of metal oxides such as silicon and aluminum oxides bare the potential for drug delivery systems and microelectronic devices, including filtration and microdialysis systems and immunoisolation devices. Although these materials are biocompatible as discussed above, the surface structure in terms of roughness, pore size and wall thickness play a crucial role in cell adhesion and viability of the surrounding tissue.

Similar to TiO₂ nanotube arrays, nanoporous Al₂O₃ and SiO₂ membranes can be produced with parallel aligned tubes of nanometer diameter, while porous thin films with even larger pores up to millimeters are possible. Nanotube arrays of

these oxides are produced by anodization, and large pores with tortuous morphology by e.g. powder sintering or microfabrication.

Several studies clearly show that many different cell types such as neuronal and ovary cell lines, as well as primary rat hepatocyte cells adhere and proliferate better on nanoporous silicon compared to unstructured glass substrates. Good cell attachment is also reported for pheochromocytoma PC12 and human lens epithelial cells [124]. Surface modification with collagen coating even enhances adhesion of these cells.

Ultrathin nanoporous silica membranes with 15 nm thickness show very good biocompatibility as cell culture substrate materials for fibroblasts and primary vascular endothelial cells. Nevertheless, it must be taken into account that the membrane degrades under cell culture conditions within one to four days depending on the thickness of oxide layer on the surface [125]. Further passivation to slow down dissolution rates offers a wide range of application especially for drug delivery systems. Compared to polymeric membranes these nanoporous thin films are 1,000 fold thinner, and thus allow a much better permeability to small solutes.

The possibility to link nanoporous ultrathin silica membranes to microfluidic devices has already attracted the application to study neuronal behavior and networking. Hybrid systems composed of ultrathin nanoporous silica with alternating laminin and poly-D-lysine or fibronectin layers show good biocompatibility. Neurons adhere, proliferate and connect via the formation of dendrites [126]. Since the mammalian eye is a complex structure composed of many different cell types such as neurons, glial and epithelial cells, the interaction of the membranes with eye tissue is an interesting issue. Nanoporous silica thin films implanted under the rat conjunctiva become embedded by a thin fibrous layer, while hardly any signs of inflammation or vascularization occur 8 weeks after implantation. Although degradation of the material occurs, the nanoporous silica membranes are still detectable under the microscope at that time. Primary corneal epithelial cell grow and adhere very well on these substrates *in vitro* as seen in Fig. 2.24. Culturing primary corneal epithelial cells on nanoporous silica thin films, and subsequently implanting this hybrid material under the rat conjunctiva was shown as a method to successfully transport cells into ocular tissue spaces. Since nanoporous silica films fully dissolve after some time, they can act as carriers to improve therapeutic treatments [127].

Nanoporous alumina thin films have also already shown to support cell attachment and proliferation of many different cell types. However, neurotoxicity of aluminum is still a matter of debate and the application of aluminum films within the brain must be carefully addressed. *In vivo* tests with nanoporous alumina thin films implanted in the peritoneal cavity of rats result in inflammatory response, while this reaction can be minimized by coating the film with polyethylene glycol (PEG) [128]. New approaches employ layer-by-layer nanoporous thin films of metals or metal oxides in combination with organic materials to adapt the required features, such as degradation rates, adhesion to the tissue, and of course biocompatibility. Since investigations and research on these thin films are

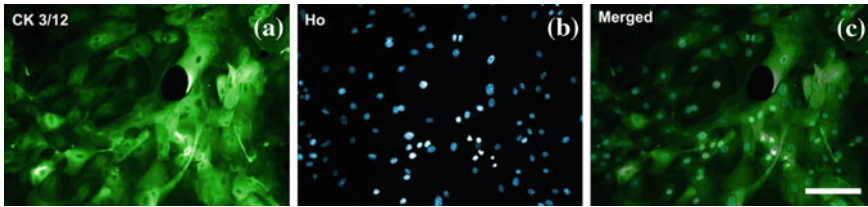


Fig. 2.24 Immunocytochemistry on human ocular cells grown out from human corneal rim explants at 2 weeks cultured on nanoporous silicon membranes. Fluorescence micrograph of cells stained for cytokeratins 3/12 (a) and the nuclei with Hoechst 33342 (b). (c) Shows the merged image. Scale bar 100 μm . Reprinted from [127], Copyright (2009), with permission from Elsevier

new and have just started the last couple of years, many new miniaturized medical devices are possible and will be tested in the future.

2.3 Conclusion and Future Perspective

For more than a century bulk metals have been employed for biomedical purposes, while bioglasses and bioceramics were first introduced in the 50th. Nevertheless, the application of thin films in medicine, such as orthopedics, dentistry and surgery, was established only a few decades ago because of improved production and characterization techniques, as well as further need due to scientific progress. Thin films and coatings offer the possibility to combine favorable mechanical properties of a bulk material with improved biocompatibility and bioactivity of the coating material to enhance tissue response and cell adhesion together with suppressed inflammatory processes and allergies. However, even nowadays it is still impossible to implant materials with bioactive coatings, especially joint replacement materials that last a life time, thus longer than the current time spans of about 15 years due to bone shrinkage and loosening of the prosthesis or even implant destruction from corrosion.

In 2009 327,000 total hip and 676,000 total knee replacements were performed only in the USA, and it is assumed that the number of total joint replacements will double within the next few years. Thus, new products which are well tolerated by the human body together with osseointegrative properties offer a great market potential to satisfy the demand of medical devices. Besides corrosion resistance and bioactivity, thin films and coatings on hip and knee prostheses must fulfill the following prerequisites: (1) They must be attached very well to the underlying bulk materials, and (2) they must be wear resistant that debris does not occur during walking. Especially thin film attachment is often still difficult to obtain, and is e.g. one reason why TiO_2 nanotubes have not been used as thin films atop titanium implants to promote cell adhesion and osseointegration.

An alternative is the application of currently employed materials in combination with new functionalization, e.g. mechanical deformation of the device to

stimulate cell growth and adhesion. Ferritic stainless steel fibers sintered together to a fibrous network attached to an underlying metal prosthesis is currently under investigation for its biocompatibility [129]. The orientation of the fibers changes under an external magnetic field, which causes mechanical stress acting onto the bone tissue at the interface. This stress promotes bone cell proliferation and bone ingrowth into the fiber network for improved and strong bonding to the implant.

Mechanical stimulation of new bone formation by thermal and ferromagnetic shape memory thin films attached to the surface of joint prostheses are future applications with great potential because the thermal shape memory alloy Ni-Ti and the magnetic shape memory alloy Fe-Pd show good biocompatibility features together with cell actuation effects. However, especially coating of thin film shape memory alloys are challenging to realize when the shape-changing properties should be maintained. The shape memory effect must not be hindered by the substrate material, while detachment during shape changes must not occur.

Free-standing shape memory thin films employed for cardiac catheterizations offer a potential of several million US-\$ sales volume with more than 1.1 million applications per year in the USA. New approaches for good attachment to the blood vessel together with reduced platelet formation come from the investigation of soft materials coated onto the stent material. For example, polymers and proteins, such as fibronectin-containing polymers that include the RGD binding motif from the extracellular matrix, might offer new perspectives to promote cellular attachment to the blood vessel, while polymers with surface passivation properties suppress adsorption of particles within the blood and reduce the risk of thrombosis.

Great potential of miniaturized medical devices lies in the development of brain electrodes for neuronal stimulation. The number of patients with Parkinson disease in the USA is estimated between 500,000 and one million and at least 50,000 new diagnoses each year. While many new drugs to reduce symptoms are under investigation, the application of microelectronic devices implanted into the brain already show the future potential of electro-stimulation treatment. Difficulties lie in the biocompatibility and the interaction of the neuronal tissue with the electrode material. On the one hand good adhesion of the device is important for current transfer; on the other hand mainly glial cells surround the electrode and adhere to it, which often results in glial scars of the damaged tissue after implantation. Fibrous scaffold substrates are shown to enhance neurite formation and axon regrowth, which might be a good alternative to conventional electrodes. Nevertheless, the electronic properties of the fibrous electrodes must be well addressed, as well as the electronic coupling to the neuronal tissue. Additionally, recent studies obtained that neuronal cells perform invers durotaxis, thus they prefer soft substrate materials to migrate and adhere to. New hybrid electrodes with soft, but conductible coatings that promote neuronal cell adhesion instead of glial cell attachment might improve the performance and the life time of the device in the brain.

Hybrid materials made of many different materials with a biocompatible coating also offer new perspectives for regenerative medicine. Pure fixation of bone after fracture is not the overall goal anymore. New approaches use resorbable materials to promote new tissue formation, while the inert part of the device

enhances mechanical stability. Further possibility is the combination of stem cells attached to a bioactive coating of a medical device. Stem cells can enhance the regenerative mechanisms of the body and improve the long-term prognosis of the medical device. Stem cell differentiation can be promoted by variations of substrate surface structures: Culturing these cells on nanostructured substrates such as TiO₂ nanotubes guides differentiation towards certain cell properties, which are triggered by the substrate itself.

Surface structured resorbable thin films offer the possibility for the application as drug carriers together with the advantage of tuning stem cell differentiation by the underlying surface topography. The films dissolve after implantation and the stem cells support the regenerative mechanisms of the human body. Moreover, combinations of mechanically and chemically modified substrates that promote single cell motility and adhesion, durotaxis (cell guidance by substrate stiffness) and chemotaxis (cell guidance by chemical gradients), offer future perspectives in nerve regeneration and the stimulation of anti-inflammatory responses.

At the end of this chapter it should be mentioned that biocompatibility of thin films is not only essential for application of medical devices implanted within the human body, but also offers great potential for reduction of animal experiments and tests. Tissue engineering has developed approaches on the basis of thin films and hybrid materials to mimic physiological conditions close to the in vivo environment. Bioreactors for example, which represent physiologic flow features are employed to study the cardiac cycle and heart valve function. Recently, nanostructured TiO₂ thin films have been shown to represent perfect surface characteristics to culture adult neuronal tissue for at least two weeks—much longer than previously attained times before tissue distortion occurred [116]. Organotypic cultures of adult tissue display a good test system to study the effect of drugs in vitro, as well as tissue regeneration properties, while here tests with living animals can be reduced in the preclinical phase. Thus, varying and tuning the surface structures of already employed thin films made of metals, alloys and ceramics offer a wider range of future applications with the advantage that the biocompatibility of these materials are already known and new, time and cost expensive tests can be cut down.

References

1. J. Black, *Biological performance of materials: Fundamentals of biocompatibility* (CRC Press, Taylor & Francis Group, Boca Raton, 2006)
2. X. Liu, P.K. Chu, C. Ding, Surface modification of titanium, titanium alloys, and related materials for biomedical applications. *Mat. Sci. Eng. R.* **47**, 49–121 (2004)
3. M. Bächle, R.J. Kohal, A systematic review of the influence of different titanium surfaces on proliferation, differentiation and protein synthesis of osteoblast-like MG63 cells. *Clin. Oral Implan. Res.* **15**, 683–692 (2004)
4. B. Yang, M. Uchida, H.-M. Kim, X. Zhang, T. Kokubo, Preparation of bioactive titanium metal via anodic oxidation treatment. *Biomaterials* **25**, 1003–1010 (2004)

5. Y. Sugizaki, T. Yasunaga, H. Tomari, Improvement of corrosion resistance of titanium by co-implantation. *Surf. Coat. Tech.* **83**, 167–174 (1996)
6. Y.L. Zhou, M. Niinomi, T. Akahori, H. Fukui, H. Toda, Corrosion resistance and biocompatibility of Ti-Ta alloys for biomedical applications. *Mater. Sci. Eng., A* **398**, 28–36 (2005)
7. P. Linez-Bataillon, F. Monchau, M. Bigerelle, H.F. Hildebrand, In vitro MC3T3 osteoblast adhesion with respect to surface roughness of Ti6Al4V substrates. *Biomol. Eng.* **19**, 133–141 (2002)
8. S. Bruni, M. Martinesi, M. Stio, C. Treves, T. Bacci, F. Borgioli, Effects of surface treatment of Ti-6Al-4V titanium alloy on biocompatibility in cultured human umbilical vein endothelial cells. *Acta Biomater.* **1**, 223–234 (2005)
9. A.L. Paschoal, E.C. Vanâncio, L.C.F. de Canale, O. Lopes da Silva, D. Huerta-Vilca, A. de Jesus Motheo, Metallic biomaterials TiN-coated: Corrosion analysis and biocompatibility. *Artif. Organs.* **27**, 461–464 (2003)
10. L.A. Cyster, K.G. Parker, T.L. Parker, D.M. Grant, The effect of surface chemistry and nanotopography of titanium nitride (TiN) films on primary hippocampal neurones. *Biomaterials* **25**, 97–107 (2004)
11. H. Huang, Corrosion resistance of stressed NiTi and stainless steel orthodontic wires in acid artificial saliva. *J. Biomed. Mater. Res. A.* **66A**, 829–839 (2003)
12. C.-C. Shih, C.-M. Shih, Y.-Y. Su, L.H.J. Su, M.-S. Chang, S.-J. Lin, Effect of surface oxide properties on corrosion resistance of 316L stainless steel for biomedical applications. *Corros. Sci.* **46**, 427–441 (2004)
13. G. Rondelli, P. Torricelli, M. Fini, R. Giardino, In vitro corrosion study by EIS of a nickel-free stainless steel for orthopaedic applications. *Biomaterials* **26**, 739–744 (2005)
14. H. Yang, K. Yang, B. Zhang, Pitting corrosion resistance of La added 316L stainless steel in simulated body fluids. *Mater. Lett.* **61**, 1154–1157 (2007)
15. C. Shih, C. Shih, Y. Chen, Y. Su, J. Shih, C. Kwok, S. Lin, Growth inhibition of cultured smooth muscle cells by corrosion products of 316L stainless steel wire. *J. Biomed. Mater. Res.* **57**, 200–207 (2001)
16. L.O. Bailey, S. Lippiatt, F.S. Biancanello, S.D. Ridder, N.R. Washburn, The quantification of cellular viability and inflammatory response to stainless steel alloys. *Biomaterials* **26**, 5296–5302 (2005)
17. K. Bordjijh, J.-Y. Jouzeau, D. Mainard, E. Payan, J.-P. Delagoutte, P. Netter, Evaluation of the effect of three surface treatments on the biocompatibility of 316L stainless steel using human differentiated cells. *Biomaterials* **17**, 491–500 (1996)
18. M. Martinesi, S. Bruni, M. Stio, C. Treves, T. Bacci, F. Borgioli, Biocompatibility evaluation of surface-treated AISI 316L austenitic stainless steel in human cell cultures. *J. Biomed. Mater. Res. A.* **80A**, 131–145 (2007)
19. B. Thierry, Y. Merhi, L. Bilodeau, C. Trépanier, M. Tabrizian, Nitinol versus stainless steel stents: acute thrombogenicity study in an ex vivo porcine model. *Biomaterials* **23**, 2997–3005 (2002)
20. M. Fini, N. Nicoli Aldini, P. Torricelli, G. Giavaresi, V. Borsari, H. Lenger, J. Bernauer, R. Giardino, R. Chiesa, A. Cigada, A new austenitic stainless steel with negligible nickel content: An in vitro and in vivo comparative investigation. *Biomaterials* **24**, 4929–4939 (2003)
21. M. Bosetti, A. Massè, E. Tobin, M. Cannas, Silver coated materials for external fixation devices: in vitro biocompatibility and genotoxicity. *Biomaterials* **23**, 887–892 (2002)
22. N. Turner, M. Armitage, R. Butler, G. Ireland, An in vitro model to evaluate cell adhesion to metals used in implantation shows significant differences between palladium and gold or platinum. *Cell Biol. Int.* **28**, 541–547 (2004)
23. J.C. Wataha, P.E. Lockwood, A. Schedle, Effect of silver, copper, mercury, and nickel ions on cellular proliferation during extended, low-dose exposures. *J. Biomed. Mater. Res.* **52**, 360–364 (2000)

24. M. Böswald, K. Mende, W. Bernschneider, S. Bonakdar, H. Ruder, H. Kissler, E. Sieber, J.-P. Guggenbichler, Biocompatibility testing of a new silver-impregnated catheter in vivo. *Infection* **27**, S38–S42 (1999)
25. E.J. Tobin, R. Bambaauer, Silver coating of dialysis catheters to reduce bacterial colonization and infection. *Ther. Apher. Dial.* **7**, 504–509 (2003)
26. G. Gosheger, J. Harges, H. Ahrens, A. Streitburger, H. Buerger, M. Erren, A. Gonsel, F.H. Kemper, W. Winkelmann, C. von Eiff, Silver-coated megaendoprostheses in a rabbit model—an analysis of the infection rate and toxicological side effects. *Biomaterials* **25**, 5547–5556 (2004)
27. C.N. Kraft, M. Hansis, S. Arens, M.D. Menger, B. Vollmar, Striated muscle microvascular response to silver implants: A comparative in vivo study with titanium and stainless steel. *J. Biomed. Mater. Res.* **49**, 192–199 (2000)
28. A. Ewald, S.K. Glückermann, R. Thull, U. Gbureck, Antimicrobial titanium/silver PVD coatings on titanium. *BioMed. Eng. Online* **5**, 22 (2006)
29. A. Kastrati, A. Schömg, J. Dirschinger, J. Mehilli, N. von Welser, J. Pache, H. Schühlen, T. Schilling, C. Schmitt, F.J. Neumann, Increased risk of restenosis after placement of gold-coated stents: Results of a randomized trial comparing gold-coated with uncoated steel stents in patients with coronary artery disease. *Circulation* **101**, 2478–2483 (2000)
30. E.R. Edelman, P. Seifert, A. Groothuis, A. Morss, D. Bornstein, C. Rogers, Gold-coated NIR stents in porcine coronary arteries. *Circulation* **103**, 429–434 (2001)
31. Y. Itakura, T. Tajima, S. Ohoke, J. Matsuzawa, H. Sudo, S. Yamamoto, Osteocompatibility of platinum-plated titanium assessed in vitro. *Biomaterials* **10**, 489–493 (1989)
32. C.P. Pennisi, C. Sevcencu, A. Dolatshahi-Pirouz, M. Foss, J.L. Hansen, A.N. Larsen, V. Zachar, F. Besenbacher, K. Yoshida, Responses of fibroblasts and glial cells to nanostructured platinum surfaces. *Nanotechnology* **20**, 385103 (2009)
33. S. Thanawala, O. Palyvoda, D. Georgiev, S.P. Khan, I.A. Al-Homoudi, G. Newaz, G. Auner, A neural cell culture study on thin film electrode materials. *J. Mater. Sci. Mater. Med.* **18**, 1745–1752 (2007)
34. S. Mailley, M. Hyland, P. Mailley, J.A. McLaughlin, E.T. McAdams, Thin film platinum coated electrodes for neurostimulation: In vitro approach of safe neurostimulation parameters. *Bioelectrochemistry* **63**, 359–364 (2004)
35. A. Cowley, B. Woodward, A healthy future: Platinum in medical applications. *Platinum Met. Rev.* **55**, 98–107 (2011)
36. J. Fischer, D. Pröfrock, N. Hort, R. Willumeit, F. Feyerabend, Improved cytotoxicity testing of magnesium materials. *Mater. Sci. Eng., B* **176**, 830–834 (2011)
37. L. Xu, F. Pan, G. Yu, L. Yang, E. Zhang, K. Yang, In vitro and in vivo evaluation of the surface bioactivity of a calcium phosphate coated magnesium alloy. *Biomaterials* **30**, 1512–1523 (2009)
38. H. Matsuno, A. Yokoyama, F. Watari, M. Uo, T. Kawasaki, Biocompatibility and osteogenesis of refractory metal implants, titanium, hafnium, niobium, tantalum and rhenium. *Biomaterials* **22**, 1253–1262 (2001)
39. Y.X. Leng, J.Y. Chen, P. Yang, H. Sun, J. Wang, N. Huang, The biocompatibility of the tantalum and tantalum oxide films synthesized by pulse metal vacuum arc source deposition. *Nucl. Instrum. Meth. B.* **242**, 30–32 (2006)
40. S. Shabalovskaya, J. Anderegg, J. Van Humbeeck, Critical overview of nitinol surfaces and their modifications for medical applications. *Acta Biomater.* **4**, 447–467 (2008)
41. M. Es-Souni, M. Es-Souni, H. Fischer-Brandies, Assessing the biocompatibility of NiTi shape memory alloys used for medical applications. *Anal. Bioanal. Chem.* **381**, 557–567 (2005)
42. J.M. Guilemany, N. Cinca, S. Dosta, A.V. Benedetti, Corrosion behaviour of thermal sprayed nitinol coatings. *Corros. Sci.* **51**, 171–180 (2009)
43. C.P. Kealey, S.A. Whelan, Y.J. Chun, C.H. Soojung, A.W. Tulloch, K.P. Mohanchandra, D. Di Carlo, D.S. Levi, G.P. Carman, D.A. Rigberg, In vitro hemocompatibility of thin film nitinol in stenotic flow conditions. *Biomaterials* **31**, 8864–8871 (2010)

44. A. Bansiddhi, T.D. Sargeant, S.I. Stupp, D.C. Dunand, Porous NiTi for bone implants: A review. *Acta Biomater.* **4**, 773–782 (2008)
45. M. Es-Souni, M. Es-Souni, H.F. Brandies, On the transformation behaviour, mechanical properties and biocompatibility of two NiTi-based shape memory alloys: NiTi42 and NiTi42Cu7. *Biomaterials* **22**, 2153–2161 (2001)
46. W. Haider, N. Munroe, C. Pulletikurthi, P.K. Singh Gill, S. Amruthaluri, A comparative biocompatibility analysis of ternary nitinol alloys. *J. Mater. Eng. Perform.* **18**, 760–764 (2009)
47. E.M.L. Verschuur, M.Y.V. Homs, E.W. Steyerberg, J. Haringsma, P.J. Wahab, E.J. Kuipers, P.D. Siersema, A new esophageal stent design (Niti-S stent) for the prevention of migration: A prospective study in 42 patients. *Gastrointest. Endosc.* **63**, 134–140 (2006)
48. Y.J. Chun, D.S. Levi, K.P. Mohanchandra, M.C. Fishbein, G.P. Carman, Novel micro-patterning processes for thin film NiTi vascular devices. *Smart Mater. Struct.* **19**, 105021 (2010)
49. D. Reynaerts, J. Peirs, H. van Brussel, An implantable drug-delivery system based on shape memory alloy micro-actuation. *Sensor. Actuat. A: Phys.* **61**, 455–462 (1997)
50. J.L. Olson, R. Velez-Montoya, M. Erlanger, Ocular biocompatibility of nitinol intraocular clips. *IOVS* **53**, 354–360 (2012)
51. L.L. Stepan, D.S. Levi, E. Gans, K.P. Mohanchandra, M. Ujihara, G.P. Carman, Biocorrosion investigation of two shape memory nickel based alloys: Ni-Mn-Ga and thin film NiTi. *J. Biomed. Mater. Res. A.* **82A**, 768–776 (2007)
52. Y. Ma, M. Zink, S.G. Mayr, Biocompatibility of single crystalline Fe₇₀Pd₃₀ ferromagnetic shape memory films. *Appl. Phys. Lett.* **96**(3), 213703 (2010)
53. R. Hauert, A review of modified DLC coatings for biological applications. *Diam. Relat. Mater.* **12**, 583–589 (2003)
54. G. Dearnaley, J.H. Arps, Biomedical applications of diamond-like carbon (DLC) coatings: A review. *Surf. Coat. Tech.* **200**, 2518–2524 (2005)
55. F.Z. Cui, D.J. Li, A review of investigations on biocompatibility of diamond-like carbon and carbon nitride films. *Surf. Coat. Tech.* **131**, 481–487 (2000)
56. R.K. Roy, K. Lee, Biomedical applications of diamond-like carbon coatings: A review. *J. Biomed. Mater. Res. B: Appl. Biomat.* **83B**, 72–84 (2007)
57. A. Grill, Diamond-like carbon coatings as biocompatible materials—an overview. *Diam. Relat. Mater.* **12**, 166–170 (2003)
58. T. Veli-Matti, Amorphous carbon as a bio-mechanical coating—mechanical properties and biological applications. *Diam. Relat. Mater.* **10**, 153–160 (2001)
59. P.D. Maguire, J.A. McLaughlin, T.I.T. Okpalugo, P. Lemoine, P. Papakonstantinou, E.T. McAdams, M. Needham, A.A. Ogwu, M. Ball, G.A. Abbas, Mechanical stability, corrosion performance and bioresponse of amorphous diamond-like carbon for medical stents and guidewires. *Diam. Relat. Mater.* **14**, 1277–1288 (2005)
60. R. Olivares, S.E. Rodil, H. Arzate, In vitro studies of the biomineralization in amorphous carbon films. *Surf. Coat. Tech.* **177–178**, 758–764 (2004)
61. L. Yang, B.W. Sheldon, T.J. Webster, The impact of diamond nanocrystallinity on osteoblast functions. *Biomaterials* **30**, 3458–3465 (2009)
62. M. Amaral, P.S. Gomes, M.A. Lopes, J.D. Santos, R.F. Silva, M.H. Fernandes, Cytotoxicity evaluation of nanocrystalline diamond coatings by fibroblast cell cultures. *Acta Biomater.* **5**, 755–763 (2009)
63. Y.-C. Chen, D.-C. Lee, C.-Y. Hsiao, Y.-F. Chung, H.-C. Chen, J.P. Thomas, W.-F. Pong, N.-H. Tai, I.-N. Lin, I.-M. Chiu, The effect of ultra-nanocrystalline diamond films on the proliferation and differentiation of neural stem cells. *Biomaterials* **30**, 3428–3435 (2009)
64. X. Xiao, J. Wang, C. Liu, J.A. Carlisle, B. Mech, R. Greenberg, D. Guven, R. Freda, M.S. Humayun, J. Weiland, O. Auciello, In vitro and in vivo evaluation of ultrananocrystalline diamond for coating of implantable retinal microchips. *J. Biomed. Mater. Res. B: Appl. Biomat.* **77B**, 273–281 (2006)

65. P. Layrolle, *Comprehensive biomaterials: Calcium phosphate coatings* (Elsevier, Amsterdam, 2011). Chap. 1.112
66. C.P.A.T. Klein, J.G.C. Wolke, J.M.A. de Blicck-Hogervorst, K. de Groot, Calcium phosphate plasma-sprayed coatings and their stability: An in vivo study. *J. Biomed. Mater. Res.* **28**, 909–917 (1994)
67. M. Shirkhazadeh, Bioactive calcium phosphate coatings prepared by electrodeposition. *J. Mater. Sci. Lett.* **10**, 1415–1417 (1991)
68. Y. Yang, K.-H. Kim, J.L. Ong, A review on calcium phosphate coatings produced using a sputtering process—an alternative to plasma spraying. *Biomaterials* **26**, 327–337 (2005)
69. S.M. Best, A.E. Porter, E.S. Thian, J. Huang, Bioceramics: Past, present and for the future. *J. Eur. Ceram. Soc.* **28**, 1319–1327 (2008)
70. X. Lu, Y. Leng, TEM study of calcium phosphate precipitation on bioactive titanium surfaces. *Biomaterials* **25**, 1779–1786 (2004)
71. Q. Zhang, Y. Leng, Electrochemical activation of titanium for biomimetic coating of calcium phosphate. *Biomaterials* **26**, 3853–3859 (2005)
72. G. Heness, B. Ben-Nissan, Innovative bioceramics. *Mater. Forum* **27**, 104–114 (2004)
73. Y.-J. Lee, J.S. Ko, H.-M. Kim, The role of cell signaling defects on the proliferation of osteoblasts on the calcium phosphate apatite thin film. *Biomaterials* **27**, 3738–3744 (2006)
74. D. Perizzolo, W.R. Lacefield, D.M. Brunette, Interaction between topography and coating in the formation of bone nodules in culture for hydroxyapatite- and titanium-coated micromachined surfaces. *J. Biomed. Mater. Res.* **56**, 494–503 (2001)
75. A.J. Ambard, L. Mueninghoff, Calcium phosphate cement: Review of mechanical and biological properties. *J. Prosthodont.* **15**, 321–328 (2006)
76. V. Karageorgiou, D. Kaplan, Porosity of 3D biomaterial scaffolds and osteogenesis. *Biomaterials* **26**, 5474–5491 (2005)
77. S. Nath, S. Kalmodia, B. Basu, In vitro biocompatibility of novel biphasic calcium phosphate-mullite composites. *J. Biomater. Appl.* (2011). doi:[10.1177/0885328211412206](https://doi.org/10.1177/0885328211412206)
78. W. Zhang, W. Liu, Y. Liu, C. Wang, Tribological behaviors of single and dual sol–gel ceramic films on Ti–6Al–4V. *Ceram. Int.* **35**, 1513–1520 (2009)
79. W. Zhang, C. Wang, W. Liu, Characterization and tribological investigation of sol–gel ceramic films on Ti–6Al–4V. *Wear* **260**, 379–386 (2006)
80. S. Xu, J. Long, L. Sim, C.H. Diong, K. Ostrikov, RF plasma sputtering deposition of hydroxyapatite bioceramics: Synthesis, performance, and biocompatibility. *Plasma Process. Polym.* **2**, 373–390 (2005)
81. V. Nelea, H. Pelletier, D. Müller, N. Broll, P. Mille, C. Ristoscu, I. Mihailescu, Mechanical properties improvement of pulsed laser-deposited hydroxyapatite thin films by high energy ion-beam implantation. *Appl. Surf. Sci.* **186**, 483–489 (2002)
82. P. Chandran, M. Azzabi, J. Miles, M. Andrews, J. Bradley, Furlong hydroxyapatite-coated hip prosthesis vs the Charnley cemented hip prosthesis. *J. Arthroplasty* **25**, 52–57 (2010)
83. H.-M. Kim, T. Himeno, T. Kokubo, T. Nakamura, Process and kinetics of bonelike apatite formation on sintered hydroxyapatite in a simulated body fluid. *Biomaterials* **26**, 4366–4373 (2005)
84. F. Sima, C. Ristoscu, D. Caiteanu, C.N. Mihailescu, N. Stefan, I.N. Mihailescu, G. Prodan, V. Ciupina, E. Palcevskis, J. Krastins, L.E. Sima, S.M. Petrescu, Biocompatibility and bioactivity enhancement of Ce stabilized ZrO₂ doped HA coatings by controlled porosity change of Al₂O₃ substrates. *J. Biomed. Mater. Res. Part B Appl. Biomater.* **96**, 218–224 (2011)
85. A. Oyane, K. Hyodo, M. Uchida, Y. Sogo, A. Ito, Preliminary in vivo study of apatite and laminin-apatite composite layers on polymeric percutaneous implants. *J. Biomed. Mater. Res. B: Appl. Biomater.* **97B**, 96–104 (2011)
86. E.S. Thian, J. Huang, S.M. Best, Z.H. Barber, W. Bonfield, Silicon-substituted hydroxyapatite: The next generation of bioactive coatings. *Mater. Sci. Eng., C* **27**, 251–256 (2007)

87. E.S. Thian, J. Huang, S.M. Best, Z.H. Barber, W. Bonfield, Magnetron co-sputtered silicon-containing hydroxyapatite thin films—an *in vitro* study. *Biomaterials* **26**, 2947–2956 (2005)
88. S. Langstaff, M. Sayer, T.J. Smith, S.M. Pugh, Resorbable bioceramics based on stabilized calcium phosphates. Part II: Evaluation of biological response. *Biomaterials* **22**, 135–150 (2001)
89. E. Fukada, I. Yasuda, On the piezoelectric effect of bone. *J. Phys. Soc. Jpn.* **12**, 1158–1162 (1957)
90. F.R. Baxter, C.R. Bowen, I.G. Turner, A.C.E. Dent, Electrically active bioceramics: a review of interfacial responses. *Ann. Biomed. Eng.* **38**, 2079–2092 (2010)
91. A. Hoppe, N.S. Güldal, A.R. Boccaccini, A review of the biological response to ionic dissolution products from bioactive glasses and glass-ceramics. *Biomaterials* **32**, 2757–2774 (2011)
92. M.N. Rahaman, D.E. Day, B. Sonny Bal, Q. Fu, S.B. Jung, L.F. Bonewald, A.P. Tomsia, Bioactive glass in tissue engineering. *Acta Biomater.* **7**, 2355–2373 (2011)
93. C. Berbecaru, H.V. Alexandru, A. Ianculescu, A. Popescu, G. Socol, F. Sima, I. Mihailescu, Bioglass thin films for biomimetic implants. *Appl. Surf. Sci.* **255**, 5476–5479 (2009)
94. Q. Fu, E. Saiz, M.N. Rahaman, A.P. Tomsia, Bioactive glass scaffolds for bone tissue engineering: state of the art and future perspectives. *Mater. Sci. Eng. C: Mater. Biol. Appl.* **31**, 1245–1256 (2011)
95. Q. Fu, M.N. Rahaman, B.S. Bal, R.F. Brown, D.E. Day, Mechanical and *in vitro* performance of 13–93 bioactive glass scaffolds prepared by a polymer foam replication technique. *Acta Biomater.* **4**, 1854–1864 (2008)
96. A. Hamadouche Meunier, R. Nizard, D. Hannouche, P. Bizot, L. Sedel, Alumina-on-alumina articulation in total hip arthroplasty: From bench-side to bedside. *Semin. Arthroplasty.* **17**, 125–133 (2006)
97. D. Hannouche, A. Zaoui, F. Zadegan, L. Sedel, R. Nizard, Thirty years of experience with alumina-on-alumina bearings in total hip arthroplasty. *Int. Orthop.* **35**, 207–213 (2010)
98. Y. Josset, Z. Oum’Hamed, A. Zarrinpour, M. Lorenzato, J.J. Adnet, D. Laurent–Maquin, *In vitro* reactions of human osteoblasts in culture with zirconia and alumina ceramics. *J. Biomed. Mater. Res.* **47**, 481–493 (1999)
99. D.S. Finch, T. Oreskovic, K. Ramadurai, C.F. Herrmann, S.M. George, R.L. Mahajan, Biocompatibility of atomic layer-deposited alumina thin films. *J. Biomed. Mater. Res. A.* **87**, 100–106 (2008)
100. M. Hisbergues, S. Vendeville, P. Vendeville, Zirconia: Established facts and perspectives for a biomaterial in dental implantology. *J. Biomed. Mater. Res. B: Appl. Biomater.* **88B**, 519–529 (2009)
101. X. Liu, A. Huang, C. Ding, P.K. Chu, Bioactivity and cytocompatibility of zirconia (ZrO₂) films fabricated by cathodic arc deposition. *Biomaterials* **27**, 3904–3911 (2006)
102. P.F. Manicone, P. Rossi Iommetti, L. Raffaelli, An overview of zirconia ceramics: Basic properties and clinical applications. *J. Dent.* **35**, 819–826 (2007)
103. A.-L. Gomes, J. Montero, Zirconia implant abutments: A review. *Med. Oral Patol. Oral Cir. Bucal.* **16**, e50–e55 (2011)
104. S.K. Smart, A.I. Cassady, G.Q. Lu, D.J. Martin, The biocompatibility of carbon nanotubes. *Carbon* **44**, 1034–1047 (2006)
105. Y. Zhang, Y. Bai, B. Yan, Functionalized carbon nanotubes for potential medicinal applications. *Drug Discov. Today.* **15**, 428–435 (2010)
106. N.A. Monteiro-Riviere, R.J. Nemanich, A.O. Inman, Y.Y. Wang, J.E. Riviere, Multi-walled carbon nanotube interactions with human epidermal keratinocytes. *Toxicol. Lett.* **155**, 377–384 (2005)
107. A.A. Shvedova, V. Castranova, E.R. Kisin, D. Schwegler-Berry, A.R. Murray, V.Z. Gandelsman, A. Maynard, P. Baron, Exposure to carbon nanotube material: assessment of nanotube cytotoxicity using human keratinocyte cells. *J. Toxicol. Environ. Health A.* **66**, 1909–1926 (2003)

108. J.L. McKenzie, M.C. Waid, R. Shi, T.J. Webster, Decreased functions of astrocytes on carbon nanofiber materials. *Biomaterials* **25**, 1309–1317 (2004)
109. J. Chłopek, B. Czajkowska, B. Szaraniec, E. Frackowiak, K. Szostak, F. Béguin, In vitro studies of carbon nanotubes biocompatibility. *Carbon* **44**, 1106–1111 (2006)
110. M.A. Correa-Duarte, N. Wagner, J. Rojas-Chapana, C. Morszeck, M. Thie, M. Giersig, Fabrication and biocompatibility of carbon nanotube-based 3D networks as Scaffolds for cell seeding and growth. *Nano Lett.* **4**, 2233–2236 (2004)
111. A. Huczko, H. Lange, Carbon nanotubes: Experimental evidence for a null risk of skin irritation and allergy. *Fuller. Sci. Techn.* **9**, 247–250 (2001)
112. A. Huczko, H. Lange, M. Bystrzejewski, P. Baranowski, H. Grubek-Jaworska, P. Nejman, T. Przybyłowski, K. Czumińska, J. Glapiński, D.R.M. Walton, H.W. Kroto, Pulmonary toxicity of 1-D nanocarbon materials. *Fuller. Nanotub. Car. N.* **13**, 141–145 (2005)
113. C.-W. Lam, J.T. James, R. McCluskey, R.L. Hunter, Pulmonary toxicity of single-wall carbon nanotubes in mice 7 and 90 days after intratracheal instillation. *Toxicol. Sci.* **77**, 126–134 (2004)
114. D.B. Warheit, B.R. Laurence, K.L. Reed, D.H. Roach, G.A.M. Reynolds, T.R. Webb, Comparative pulmonary toxicity assessment of single-wall carbon nanotubes in rats. *Toxicol. Sci.* **77**, 117–125 (2004)
115. J. Muller, F. Huaux, N. Moreau, P. Misson, J.-F. Heilier, M. Delos, M. Arras, A. Fonseca, J.B. Nagy, D. Lison, Respiratory toxicity of multi-wall carbon nanotubes. *Toxicol. Appl. Pharm.* **207**, 221–231 (2005)
116. V. Dallacasagrande, M. Zink, S. Huth, A. Jakob, M. Müller, A. Reichenbach, J.A. Käs, S.G. Mayr, Tailoring substrates for long-term organotypic culture of adult neuronal tissue. *Adv. Mater.* **24**, 2399–2403 (2012)
117. P. Roy, S. Berger, P. Schmuki, TiO₂ nanotubes: Synthesis and applications. *Angew. Chem. Int. Ed. Engl.* **50**, 2904–2939 (2011)
118. M. Arnold, E.A. Cavalcanti-Adam, R. Glass, J. Blümmel, W. Eck, M. Kantlehner, H. Kessler, J.P. Spatz, Activation of integrin function by nanopatterned adhesive interfaces. *Chem. Phys. Chem.* **5**, 383–388 (2004)
119. K.S. Brammer, S. Oh, J.O. Gallagher, S. Jin, Enhanced cellular mobility guided by TiO₂ nanotube surfaces. *Nano Lett.* **8**, 786–793 (2008)
120. K.S. Brammer, S. Oh, C.J. Cobb, L.M. Bjursten, H. van der Heyde, S. Jin, Improved bone-forming functionality on diameter-controlled TiO₂ nanotube surface. *Acta Biomater.* **5**, 3215–3223 (2009)
121. L. Peng, A.J. Barczak, R.A. Barbeau, Y. Xiao, T.J. LaTempa, C.A. Grimes, T.A. Desai, Whole genome expression analysis reveals differential effects of TiO₂ nanotubes on vascular cells. *Nano Lett.* **10**, 143–148 (2010)
122. L. Peng, M.L. Eltgroth, T.J. LaTempa, C.A. Grimes, T.A. Desai, The effect of TiO₂ nanotubes on endothelial function and smooth muscle proliferation. *Biomaterials* **30**, 1268–1272 (2009)
123. C. von Wilmsowky, S. Bauer, R. Lutz, M. Meisel, F.W. Neukam, T. Toyoshima, P. Schmuki, E. Nkenke, K.A. Schlegel, In vivo evaluation of anodic TiO₂ nanotubes: An experimental study in the pig. *J. Biomed. Mater. Res. B: Appl. Biomater.* **89B**, 165–171 (2009)
124. S.P. Low, K.A. Williams, L.T. Canham, N.H. Voelcker, Evaluation of mammalian cell adhesion on surface-modified porous silicon. *Biomaterials* **27**, 4538–4546 (2006)
125. A.A. Agrawal, B.J. Nehilla, K.V. Reisig, T.R. Gaborski, D.Z. Fang, C.C. Striemer, P.M. Fauchet, J.L. McGrath, Porous nanocrystalline silicon membranes as highly permeable and molecularly thin substrates for cell culture. *Biomaterials* **31**, 5408–5417 (2010)
126. H. Ai, H. Meng, I. Ichinose, S.A. Jones, D.K. Mills, Y.M. Lvov, X. Qiao, Biocompatibility of layer-by-layer self-assembled nanofilm on silicone rubber for neurons. *J. Neurosci. Meth.* **128**, 1–8 (2003)
127. S.P. Low, N.H. Voelcker, L.T. Canham, K.A. Williams, The biocompatibility of porous silicon in tissues of the eye. *Biomaterials* **30**, 2873–2880 (2009)

128. K.E. la Flamme, K.C. Popat, L. Leoni, E. Markiewicz, T.J. la Tempa, B.B. Roman, C.A. Grimes, T.A. Desai, Biocompatibility of nanoporous alumina membranes for immunoisolation. *Biomaterials* **28**, 2638–2645 (2007)
129. V.N. Malheiro, R.L. Spear, R.A. Brooks, A.E. Markaki, Osteoblast and monocyte responses to 444 ferritic stainless steel intended for a magneto-mechanically actuated fibrous scaffold. *Biomaterials* **32**, 6883–6892 (2011)

Chapter 3

Modern Porous Coatings in Orthopaedic Applications

Rachel M. Frank, David Fabi and Brett R. Levine

Abstract The development of porous metals and coatings for orthopaedic applications has revolutionized the medical field. The ability to bond metallic implants to bone has spawned the advancements in total joint arthroplasty we have experienced over the last 4 decades. Early success was obtained as factors (pore size, coefficient of friction, modulus of elasticity) necessary for osseointegration were just being discovered. Despite good results, initial implant designs were fabricated utilizing traditional coatings (i.e. sintered beads, fiber metal, plasma spray), which have several inherent limitations, including relatively high moduli of elasticity, low coefficient of frictions and intermediate porosity. In order to improve upon these limitations and capitalize on modern techniques for implant fabrication several new porous metals have been recently introduced in orthopaedics. Tritanium (Stryker, Mahwah, NJ), Regenerex (Biomet, Warsaw, IN), StikTite (Smith and Nephew, Memphis, TN), Gription (Depuy, Warsaw, IN), Biofoam (Wright Medical, Arlington, TX), and Trabecular Metal (Zimmer, Warsaw, IN) are currently available for orthopaedic surgery applications. These materials have moved us into the era metallic foams that possess a characteristic appearance similar to cancellous bone. The open-cell internal structure of these metals afford several interesting biomaterial properties, including; high volumetric porosity (60–80 %), low modulus of elasticity and high surface frictional characteristics. The following chapter reviews the mode of fabrication, properties and applications in orthopaedic surgery for this new class of highly porous metals.

R. M. Frank · D. Fabi · B. R. Levine (✉)

Adult Reconstruction Specialist and General Orthopaedic Surgeon San Diego
Orthopaedic Associates Medical Group San Diego, Rush University Medical Center,
Chicago, CA 92103, US
e-mail: brettlevinemd@gmail.com

3.1 Introduction

The development of porous metals and coatings for orthopaedic applications has revolutionized the medical field. The ability to bond metallic implants to bone has spawned the advancements in total joint arthroplasty we have experienced over the last several decades. Early success was obtained as factors necessary for adequate osseointegration, such as pore size, coefficient of friction, and modulus of elasticity, were discovered. Despite initial encouraging results, early implant designs were fabricated utilizing traditional coatings such as sintered beads, fiber metal mesh, and titanium plasma spray, all of which have several inherent limitations including relatively high moduli of elasticity, low coefficient of friction, and intermediate porosity. In order to improve upon these limitations and capitalize on contemporary implant fabrication techniques, several new porous metals available for use as orthopaedic implants have been recently introduced. Such products, including Tritanium (Stryker, Mahwah, NJ), Regenerex (Biomet, Warsaw, IN), StikTite (Smith and Nephew, Memphis, TN), Gription (Depuy, Warsaw, IN), Biofoam (Wright Medical, Arlington, TX), and Trabecular Metal (Zimmer, Warsaw, IN) are currently available for orthopaedic surgery applications, including implants in the hip [1–29], knee [30–47], spine [48–66], and shoulder [67].

The advent of these coatings emanated from the concerns regarding late loosening of cemented implants, particularly total hip replacement components. These coatings paved the way for orthopaedic implants to enter the era of metallic foams that possess a characteristic appearance similar to cancellous bone, allowing for rapid and enhanced biologic fixation as opposed to cemented implants and traditional coatings. Unlike cemented implants, biologic fixation is achieved with these coatings as bone grows into the porous structure, which in turn, may increase the long-term survival. Specifically, the open-cell internal structure and nano-texture of these metals affords several favorable biomaterial properties, including high volumetric porosity (60–80 %), low modulus of elasticity, high surface frictional characteristics and possibly greater resistance to bacterial adhesion. The following chapter reviews the mode of fabrication, properties, and applications in orthopaedic surgery for this new class of highly porous metals.

3.2 Brief History of Porous Orthopaedic Implants

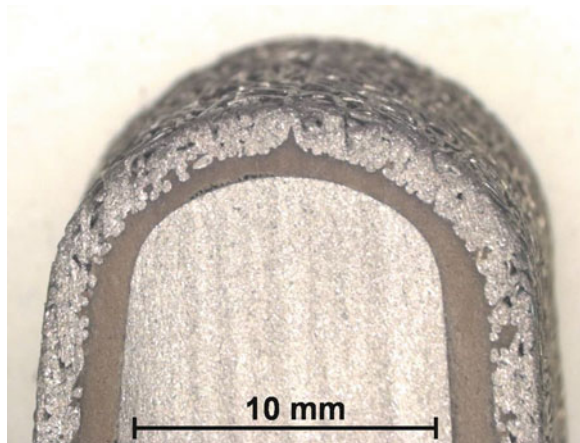
The concept of bone ingrowth fixation has been around since the early 1900s. Application of porous-coated implants as a vehicle for bone ingrowth was introduced in the 1940s, with applications in total hip arthroplasty described in the 1980s. The move toward the creation and advancement of porous-coated implants stemmed from the clinical desire to address the limitations associated with cemented implants, with a goal of improving implant survivorship and improved fixation.

In the 1960s, Cerosium, a porous calcium aluminate ceramic impregnated with an epoxy resin, was introduced and was considered to be the first porous material mechanically strong enough to be considered in orthopaedic load-bearing applications [68]. While Cerosium carried a stiffness closer to that of bone, its sub-optimal pore size did not promote bone ingrowth, and ultimately this material was not utilized clinically. Nevertheless, its discovery did lead to further advancements in the field throughout the early 1960s and 1970s. At that time, it became clear to researchers that both pore size as well as material strength were key in promoting bone ingrowth. In 1969, Lueck et al. [69] reported the development and insertion of a porous, commercially pure titanium fiber-metal mesh composite material (Fig. 3.1), the basis for several implants still in clinical use today [70–72]. This titanium fiber-metal composite material demonstrated improved biomaterial properties, including sufficient strength, a relatively high level of porosity (in the range of 40–50 %), and a large range of elastic strain [69]. During this same time period, other researchers developed and advanced the technology of porous cobalt-chromium (CoCr) surfaces for use as coatings in orthopaedic implants, many of which form the basis for use in today’s orthopaedic industry [68, 73–86].

Other materials, including porous stainless steel as an implant in bone [18] as well as porous polymers as prosthetic coatings [87–89] were investigated as potential materials for improved bone ingrowth, however certain shortcomings prohibited their widespread clinical applications. While stainless steel porous coatings provided rigid fixation and pore sizes adequate for osseous integration, the material was found to undergo excessive *in vivo* corrosion. Similarly, several porous polymers, including porous polysulfone, porous polyethylene and Proplast (a Teflon/graphite fiber material composite) were found to have inadequate strength, unacceptable wear, and high failure rates [87–89].

Overall, porous coatings have found widespread success and utilization in the field of joint replacement, particularly in cementless total hip arthroplasty (THA) and total knee arthroplasty (TKA). Long-term biologic fixation has consistently

Fig. 3.1 Cross-section of a composite stem with fiber metal mesh pads coating the outer surface. (Courtesy of Zimmer, Warsaw, IN)



been achieved via porous coated implants, and thus has been thought to address the concerns regarding the longevity of cemented orthopaedic implants. Moreover, these technologies have been expanded for use in revision THA/TKA components, total shoulder replacement components, and spine implants. Despite good clinical results, traditional porous coatings possess a number of shortcomings. This has spurred the development of a new generation of porous materials to address these limitations while expanding clinical applications and indications.

3.3 The Ideal Porous Metal

The ideal porous metal/coating would have an open-cell structure, high porosity, and microstructure resembling that of cancellous bone (spongy bone). Additionally, an ideal porous coating would possess a low modulus of elasticity and high frictional characteristics (surface coefficient of friction close to 1). By resembling the native material characteristics of bone, the ideal implant would be more biologically compatible and result in earlier and increased volumes of bone ingrowth. Further, the ideal porous metal would be able to stand alone as an independent structure, rather than solely as a porous coating. Finally, manufacturing costs of such a material would need to be reasonable and implantation relatively simple, precise and reproducible. Currently, no perfect coating/material exists that satisfies all these criteria, and further long-term studies analyzing the safety and efficacy of existing implants are needed.

3.4 Traditional Porous Metals

First generation (conventional) porous metals consist of *cobalt-chrome (CoCr) alloy sintered beads, diffusion-bonded fiber-metal mesh, cancellous structured titanium, and titanium plasma spray*. These traditional materials generally have a relatively low porosity in the range of 30–50 %, a high modulus of elasticity (all assume the modulus of their bonded substrate metal), and low surface-friction characteristics (Table 3.1) [90]. A wide variety of implantable devices have been made with these conventional metals, each with successful long-term results as described below. However, despite a proven history for porous coating applications, these traditional porous metals are not suitable to be used as bulk structural materials for implants, bone augmentation, or as a bone graft substitute [90].

3.4.1 Cobalt-Chrome (CoCr) Alloy Sintered Beads

Porous coating with Cobalt-Chrome (CoCr) alloy sintered beads was an attractive early first generation porous metal due to its biomaterial properties of inertness,

Table 3.1 Material properties for traditional and new generation of porous metals available for clinical use in orthopaedic surgery

Material property	CoCr beads	Fiber metal mesh	Cancellous structured titanium	Porous tantalum	Regenerex	Tritanium	StikTite	Gription	Biofoam
Modulus of elasticity (GPa)	210	106-115	106-115	2.5-3.9*	1.6*	106-115	106-115	3.5*	2.9*
Average pore size	100-400	100-400	520	550	300	546	200	300	530
Porosity (%)	30-50	40-50	50-60	75-85	67	72	60	63	60-70
Coefficient of friction	0.53	0.63	N/A	0.88	N/A	1.01	~0.89	1.2	0.58

*These values are for the stand-alone material without a substrate/non-modular implants

biocompatibility, and mechanical durability [86]. Currently, the fabrication process of CoCr beads begins with the production of spherical CoCr metal powders via gas atomization. These beads are then sintered to the implant substrate or surface. This part of the process is somewhat imprecise, and can produce coatings of variable thickness, even within the same production. Thus, fully coated CoCr beaded femoral stems produced with this technology, when measured with a hole gauge, have been found to be 1/3 smaller than, 1/3 equal to, and 1/3 larger than the desired size. This porous surface's mechanical properties include an average pore size of 100–400 microns, a modulus of elasticity of 210 GPa, a 30–50 % porosity, and a coefficient of friction of 0.53.

Applications for CoCr beaded porous coatings primarily include THA components (acetabular and femoral implants), TKA components, and total disc replacement prostheses in spine surgery. Results reported in the literature regarding clinical use of CoCr beaded acetabular components have been variable, with revision rates ranging from 4 % [91] (average follow-up 8.5 years) to 11 % (average follow-up 2–10 years), with variable rates of aseptic loosening. Nevertheless, these rates improve upon the 42 % incidence of aseptic loosening seen in cemented acetabular components at similar follow-up interval of 12 years [92]. Despite good clinical results the transfer of forces to the acetabulum often leads to stress shielding that is apparent at the time of revision surgery.

CoCr beaded femoral stem components have garnered superior clinical success with regard to survival and fixation when compared with the acetabular implants. In a report of 100 consecutive CoCr beaded porous stems (Prodigy stem, Depuy, Warsaw, IN), 82 hips were available for follow-up at an average 11.4 years post implantation, and at this time all stems demonstrated bone ingrowth without a single stem requiring revision surgery [93]. Other reports have described survival rates of up to 95 % following implantation of CoCr beaded stems at 11.4 years [94] and up to 17 years post-operatively [95]. Despite concerns for proximal stress shielding and thigh pain around stiff femoral stems (modulus mismatch), this design has been quite successful at long-term follow-up. Further long-term study is needed to assess the degree of bony ingrowth following implantation of CoCr beaded implants, as the reported low rates of ingrowth (or fibrous ingrowth) may prove detrimental to long-term clinical results [96–98].

3.4.2 Fiber Metal Mesh

As previously mentioned, Lueck et al. originally described the manufacturing and implantation of a porous commercially pure titanium fiber-metal mesh composite material that is still being used in contemporary TKA and THA procedures [69–71, 99–101]. This porous aggregate is fabricated by molding and sintering short titanium metal fibers; porosity is controlled by either the initial molding pressure or by successive repressing after the sintering treatment [71]. The pressed products are then heat-treated in a vacuum annealing furnace and finally molded

Fig. 3.2 Fully coated femoral stem with titanium fiber metal mesh coating



over a solid core structure [71]. Fiber-metal mesh possesses an average pore size of 100–400 microns, a modulus of elasticity in the range of 106–115 GPa (based upon bound substrate), a porosity on the level of 40–50 %, and a coefficient of friction of 0.63.

Fiber metal coatings (Fig. 3.2) are available for THA components (femoral stem and acetabular cup implants) and TKA components with encouraging clinical outcomes. Recently, Klein et al. [102] reported a 100 % bone osseous integration rate following THA with a collarless, tapered, fiber metal proximally coated femoral stem (Fiber metal taperTM, Zimmer, Warsaw, IN) at an average 6.7 years post-operatively. Similarly, Lachiewicz et al. [103] reported an implant survival rate of 100 % at an average 10.5 years following THA with a second-generation fiber-metal proximally coated femoral stem. In long-term follow-up studies of the Harris-Galante femoral stem, Anseth et al. [104] reported an overall 87.7 % survival rate at 17 years post-operatively, which also included the revision of failed acetabular components as well. Finally, Hamilton et al. [105] revealed an 89.3 % survivorship at an average 15 years post-implantation in a study of 83 first-generation Harris-Galante acetabular cups.

In addition to primary total joint replacement surgery, fiber metal coatings have been used reliably in revision THA procedures. Della Valle et al. [106] reported on 138 acetabular revisions with a fiber metal mesh acetabular component at a mean follow-up of 15 years and found an overall survivorship of 81 % at 15 years with

revision for *any* reason as an endpoint. Of note, this survivorship rate increased to 96 % when loosening or radiographic evidence of loosening was considered as an endpoint. Similarly, other authors have reported 84–95 % survival rates at an average 12 years post-operatively following acetabular revisions utilizing a fiber metal acetabular component [107, 108]. Similar to CoCr implants, the degree of bony ingrowth in fiber metal mesh composite materials requires further study, though some retrieval study data has demonstrated average ingrowth of rates of 12 % [109].

Disadvantages of fiber metal mesh composite materials include its reported fragmentation at up to 11–15 years post operatively [110], possibly leading to long-term cup failure via gross loosening and its inability to be employed as an independent structure. Increased porosity and decreased modulus of elasticity may prove to be potential areas for improvement in the amount of biologic bony fixation provided by newer designs of fiber metal mesh composite materials.

3.4.3 Cancellous Structured Titanium

Another well-studied traditional porous metal is cancellous structured titanium (CSTi). The production of this metal coating involves the sintering of commercially pure titanium powder onto a titanium or CoCr alloy substrate at a high temperature and pressure. Overall, CSTi contains biomaterial properties similar to human cancellous bone with interconnecting pores that allow for bone ingrowth, thereby providing excellent strength and fatigue characteristics. CSTi possesses an average pore size of 520 microns, a modulus of elasticity of 106–115 GPa (also assumes that of its titanium-bound substrate), and a porosity of 50–60 %.

CSTi has been used extensively as a coating in orthopaedic implants, primarily in the field of THA and TKA with demonstrated success in long-term clinical outcomes studies. For example, Udomkiat et al. [111] reported the outcomes of 110 primary THA cases utilizing CSTi porous-coated acetabular cups at an average follow-up of 10.2 years. The authors found the 12 year survival rate of the acetabular shell was 99.1 % and 98 % in patients rated their outcomes as good to excellent, respectively. Similarly, Hoffman et al. [112] reported on the outcomes of 100 primary THA cases utilizing Natural-hip stems (Zimmer, Warsaw, IN) with proximal CSTi porous coatings. The authors in this series found no femoral component subsidence, loosening, or revision procedures. Despite these encouraging outcomes, other authors have reported early implant subsidence (i.e., within the first two months post-operatively) [113].

With regard to TKA implants, CSTi porous coated implants have been shown to have encouraging long-term clinical outcomes. Recently, Hoffman et al. [114] reported on 176 knees following TKA with the Natural-Knee CSTi porous-coated total knee implant (Zimmer, Warsaw, IN) at an average follow-up of 12 years. With bony attachment as the outcome, survivorship of these implants was found to be 95.1 %. Of note, in these components, the substrate consisted of a cobalt-

chrome alloy, as opposed to the traditional substrate of titanium for which CSTi was originally developed.

Similar to the other first generation porous metal coatings, further retrieval and/or postmortem analyses are necessary to determine the extent of bony ingrowth within CSTi coated implants [115, 116]. Overall, the literature seems to demonstrate promising clinical outcomes following THA/TKA with CTSi porous coated implants. While the biomaterial properties of CTSi are similar to cancellous bone and are thus favorable with regard to biologic fixation, concerns regarding component migration remain, as well as this material's inability to be used as a stand-alone structure.

3.4.4 Porous Plasma Spray

Plasma spray is another type of porous coating originally fabricated in the 1960s and 1970s, and currently in clinical use today [117]. Currently, this type of porous coating is manufactured by plasma-flame spraying of commercially pure titanium constructs. Plasma-flame spray coating is produced via subjecting particles of commercially pure titanium to high temperature plasma and casting them in a molten state onto their respective surface. This results in a roughened, irregular surface of interconnecting particles and porosities, which are then bonded to the underlying metal substrate via a vacuum sintering process [118]. This manufacturing process permits the titanium alloy to maintain 90 % of its fatigue strength, compared to less than 50 % for sintered or diffusion-bonded materials [119]. Such strength becomes clinically relevant out of trepidation for delamination and debonding of other traditional porous materials.

Porous plasma spray titanium coatings for THA (Fig. 3.3) have proven to be a safe and predictable material as demonstrated in long-term follow-up studies. For example, Lombardi et al. [120] retrospectively reported on the outcomes of 1,866 patients (out of a total cohort of 2,000 patients) who underwent THA with titanium plasma spray femoral components. The authors noted survival of the implant, with

Fig. 3.3 Porous titanium plasma spray coating on an explanted acetabular component. Notice areas of bone ongrowth at the periphery of the cup



any stem revision as the endpoint, to be 98.6 % at 5 years, 98.4 % at 10 years, 97.1 % at 15 years, and 95.5 % at 20 years utilizing the Kaplan–Meier method. Further, some authors have shown that porous plasma spray coated THA implants (Mallory-Head) perform better than sintered bead cementless THA implants (PCA) as well as cemented THA components [119]. The latest generation of flat-taper wedge (so-called “broach only”) femoral components are typically coated with a porous plasma spray for most if not all implant companies.

3.4.5 Summary of Traditional Porous Metals

Several rigorous investigations have been conducted in an attempt to determine the best porous coating amongst all the traditional coating options. Overall, the data has shown that bone ingrowth behavior is similar for all conventional porous materials and that intimate bony contact is required to achieve long-term biologic fixation. Despite the early clinical success of conventional porous metal coatings, there remain multiple areas for improvement, including increasing porosity, which would ultimately increase the maximum interfacial strength that can form via bone ingrowth [90]. Further, these types of traditional materials do not possess the material characteristics that would allow their use as bulk structural material for bone implantation or as a bone graft substitute [90]. Historically these materials have required close and complete contact with the host bone to assure osseointegration; however, in the revision setting this is not always possible. This has spawned the advent of a new generation of porous materials with goal of optimizing success in the face of limited host bone implant contact. Additionally, due to limited bone bank supplies and cost there remains a demand for various forms of bone graft substitutes.

3.5 New Porous Metals

Due to the inherent limitations of traditional porous metals as described above, numerous open-cell structured metals have been developed in an attempt to improve bone ingrowth while maintaining mechanical strength. The creation of an open-cell structured metal involves the manufacturing of a reticulated skeleton composed of vitreous carbon, polyurethane foam, or other organic substrates with subsequent deposition of titanium or tantalum (highly biocompatible, self-passivating and inert transition metals) onto the surface. A key advantage is that the skeleton scaffolds can be fashioned into nearly limitless sizes and shapes for utilization in a vast assortment of orthopaedic applications. Overall, these types of porous coatings possess characteristics resembling that of cancellous bone with

high surface coefficients of friction, improved porosity levels, and relatively low moduli of elasticity. The precise generation of such coatings also affords a complex nanostructure that contributes to the material properties and possible resistance to bacterial adhesion. Given these properties, metallic foams would ideally serve as a porous surface coating and possible bone graft substitute with the potential to create a long-lasting metallic-osseous bond with substantial levels of bone ingrowth.

3.6 Titanium-Based Metallic Foams

3.6.1 *Regenerex (Biomet, Warsaw, IN)*

Biomet (Warsaw, IN) has developed a highly porous, low modulus titanium metal construct referred to as Regenerex. Their coating and stand alone metallic foam was first applied clinically in early 2007. This highly porous metal is manufactured via coating of an organic binding agent scaffold with a titanium alloy. Of note, this is the same titanium alloy as used in Biomet's porous plasma spray technology, which has maintained a long successful history in joint replacement surgery. A unique feature of Regenerex when compared to traditional porous metals is that not only can this titanium metal construct be utilized as a coating, but it can also be utilized as an independent implant [44, 121]. Regenerex possesses favorable characteristics that demonstrate a high compressive strength coupled with flexibility, allowing for improved biologic fixation. The metallic foam has an overall porosity of 67 % with pore sizes ranging from 100 to 600 microns (average of 300 microns) and a modulus of elasticity of 1.6 GPa [44]. The surface roughness is on average 2485.6 Ra, which is much coarser than that of conventional porous materials. When utilized as a coating, Regenerex maintains a 3496.32 psi adhesion strength (well above the ASTM standard guidelines) to the underlying titanium skeleton (company website unpublished data).

Currently, Regenerex implants are available in THA, TKA, and total shoulder arthroplasty (TSA) surgery (Fig. 3.4). Further, Regenerex acetabular augments can serve as structural, stand-alone bone graft substitutes in revision THA due to the material's highly porous open-cell makeup, mechanical strength, and low modulus of elasticity. Similar options are available for revision knee surgery, with porous tibial and femoral cones that are utilized to fill cavitory and segmental bony defects. While exciting in theory, the main clinical limitation of Regenerex based implants is the paucity of peer-reviewed clinical data available regarding short, medium, and long-term clinical outcomes following implantation. The majority of data comes from internal files at Biomet, and thus it is difficult to determine the implant's success given inherent biases in data reporting.



Fig. 3.4 *Top Row* Close-up picture of Regenerex and high-power photomicrograph of the titanium metallic foam. *Bottom Row* Revision cones (serve as bone graft substitute) for total knee arthroplasty surgery and primary cementless tibial and femoral components. (Courtesy of Biomet, Warsaw, IN)

3.6.2 Biofoam (Wright Medical, Arlington, TN)

Biofoam is another metallic foam that was introduced clinically in 2007 by Wright Medical (Arlington, TN). This metal is a titanium-based, metallic foam with an open-cell structure, available in both bulk form as well as a bonded surface coating. The average pore cell size of Biofoam is $530\ \mu\text{m}$ and its porosity in the range of 60–70 %. Per the manufacturer's description, this level of porosity creates an osteoconductive matrix ideal for rapid bony ingrowth. The compressive

strength lies between that of cortical and cancellous bone (86 MPa), allowing for flexibility and strength with dynamic loading. It possesses a high coefficient of friction allowing for stabilization and decreased micromotion at the bone-implant interface, as well as a low modulus of elasticity of 2.7 GPa, close to that of cancellous bone.

In vivo animal studies have been performed using this titanium foam to determine shear strength and time to bone ingrowth. In one study, cylindrical implants were inserted into canine femoral diaphyses and were compared to implants fabricated from sintered titanium beads. At 12 weeks, the mean shear strength was higher for Biofoam compared to beaded implants (not statistically significant), as was the average percentage of bone ingrowth (statistically significant). In another similar study, Biofoam was compared to conventional metal beaded surfaces with regard to shear strength, bone ingrowth, bone apposition, and bone attachment mode of failure in metaphyseal bone were evaluated. Failure was seen in the surrounding bone with Biofoam implants as opposed to failure at the bone implant interface in sintered beaded controls, implying that the bone-implant interface strength of Biofoam implants was greater than the strength of the surrounding bone. It should be noted that all of this data has been collected and presented from within Wright Medical, and is not currently available as part of the peer reviewed literature.

Biofoam is primarily available as a wedge system used for correcting bony deformities and re-aligning osteotomy procedures, and was previously available as part of a fixation surface for tibial baseplates in TKA and acetabular cups in THA (Fig. 3.5). Similar to many of the newer open-cell porous materials, there is no current peer-reviewed literature available on the clinical outcomes of Biofoam, and as such, caution must be used in interpreting its success.



Fig. 3.5 Titanium foam coated tibial baseplate and acetabular components currently available for clinical use

3.6.3 Tritanium (*Stryker, Mahwah, NJ*)

Tritanium is an open-cell, highly porous, three-dimensional coating/material manufactured by Stryker (Mahwah, NJ) and is currently used in clinical orthopaedic practice. This metallic foam is a biologically-inspired reticulated porous titanium coating, manufactured from a commercially pure titanium matrix. Processing of this material begins with a machined polyurethane foam shell, which is then coated with commercially pure titanium using a Low Temperature Arc Vapor Deposition (LTAVD). Of note, the coating thickness is variable, which can alter stiffness and pore size, both of which can ultimately alter clinical performance. The LTAVD coated foam shell undergoes a forging process to a Ti-6Al-4 V alloy shell, after which a final sintering is performed with the addition of anatomically positioned screw holes.

With regard to its biomaterial properties, Tritanium maintains porosity of 72 %, an average pore size of 546 microns, and a high coefficient of friction of 1.01. In a canine model comparing Tritanium to conventional CoCr beaded surfaces, Tritanium had higher bone penetration and greater tensile strength than the beaded surfaces. Further, nearly all titanium foam channels were inhabited with new bone permeating throughout the porous surface's interstices as demonstrated via microscopic evaluation [24]. Other similar animal studies (both rabbit and canine models) have further demonstrated the bone ingrowth potential of Tritanium acetabular cups [24].

Currently, Tritanium is available in the form of coating for THA acetabular components (Fig. 3.6). In addition, Tritanium was recently introduced as available as stand-alone augments for revision THA. Unlike the previously mentioned open-cell porous materials, limited peer-reviewed literature describing clinical outcomes following Tritanium coated implants is available. In a recent prospective study, Ramappa et al. [9] analyzed 43 acetabular revisions using Tritanium coated acetabular components and revealed 96 % osseointegration at 6 weeks post-



Fig. 3.6 High-power photomicrograph of Tritanium metallic coating and its application to a primary total hip acetabular component. (Courtesy of Stryker, Mahwah, NJ)

operatively. In this cohort, one acetabular cup failed via aseptic loosening and protrusion medially in a patient with a pelvic discontinuity (extensive bone loss). While promising with regard to its biomaterial properties, Tritanium is currently limited by its lack of peer-reviewed outcomes data. Further research and development is clearly warranted to determine possible future applications of this promising material.

3.6.4 Gription (Depuy, Warsaw, IN)

Gription is a recently released, ultra-porous, super-textured, commercially pure titanium coating material currently used in multiple areas of orthopaedic surgery including THA and TKA. Released by Depuy (Warsaw, IN) as an improvement on the already successful Porocoat™ porous coating, Gription fabrication is thought to involve attaching titanium shards to the underlying Porocoat surface in an attempt to roughen the surface, increase the coefficient of friction, and ultimately increase bone-implant stability under high loads. The coating itself is composed of super-textured asperity topography (STAT), which combines macro and micro-texture topographies in an effort to create an environment prime for bone ingrowth and

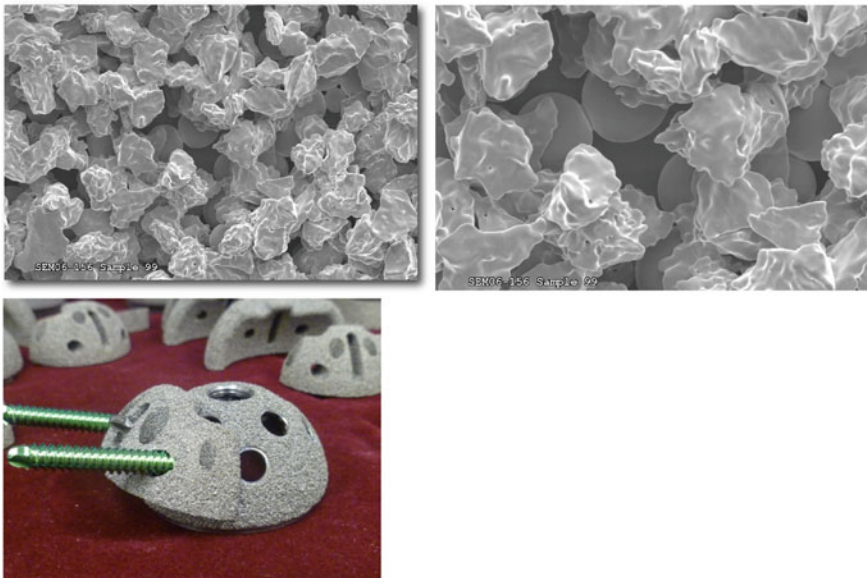


Fig. 3.7 High power photographs of Gription coating—note the intricate nanotexture of the metallic struts. Current applications include acetabular components and augments, pictured here. (Courtesy of Depuy, Warsaw, IN)

proliferation. The biomaterial properties of Gription improve upon conventional coatings with a 63 % porosity, average pore size of 300 microns, and coefficient of friction of 1.2, which is currently the highest of all contemporary open-cell structured metallic coatings. These properties have the potential to improve initial fixation (improves stability), long-term fixation (improves bone ingrowth), and mechanical integrity (improves biomechanical strength).

Currently, Gription is used as the surface coating material in the Pinnacle acetabular cup system, in the Trilock femoral stem implant, as well as in revision TKA metaphyseal sleeves. Further, Gription titanium foam augments, buttresses, and shims are now available for revision THA (Fig. 3.7) in patients with severe acetabular bone loss as part of the Pinnacle revision system for THA (Depuy, Warsaw, IN). Similarly, Gription titanium foam cones are available as both femoral and tibial augments in patients with severe bone loss in the setting of revision TKA. Due to its relatively recent launch, there is no peer-reviewed literature available regarding the clinical outcomes associated with implants coated with Gription. Nevertheless, early success with acetabular components for primary and revision THA led to the expansion of this coating to femoral stems and primary and revision TKA as well as the creation of stand-alone Gription titanium foam implants.

3.6.5 StikTite (Smith and Nephew, Memphis, TN)

StikTite (Smith and Nephew, Memphis, TN) is an open-cell, highly porous metallic coating used in orthopaedic implants. StikTite is comprised of a sintered asymmetrical three-dimensional titanium powder coating, designed to improve the scratch-fit feel encountered during insertion of the implant. The biomaterial properties of StikTite include a porosity of 60 % with an average pore size of 200 microns and a coefficient of friction between approximately 0.9 (cortical bone) and 1.4 (cancellous bone). Unpublished data reports excellent biomaterial properties with StikTite as compared to trabecular metal, in regards to coefficient of friction and initial fixation strength.

Clinically, StikTite is only available as an acetabular coating on the relatively new R3 shell, with new applications currently under development. While there is relatively little clinical data available on the clinical performance of StikTite, a recent study by Bourne et al. [122] analyzed the R3 acetabular cup in a prospective study using radiostereometric analysis (RSA). The authors found less micromotion in the R3 cup coated with StikTite compared to a sintered bead porous coating (Roughcoat); further, the authors reported a higher coefficient of friction in the StikTite coated R3 cup than in the specimens coated with trabecular metal.

3.7 Tantalum-Based

3.7.1 Trabecular Metal (Zimmer, Warsaw, IN)

Trabecular metal is an open-cell, highly-porous construct manufactured by Zimmer (Warsaw, IN). It is made from tantalum, a transition metal, which is relatively inert in vivo, as evidenced by its long-term use in various medical devices including pacemaker electrodes, foil and mesh for nerve repair, and cranioplasty plates [21, 45, 57]. Porous tantalum is created via the pyrolysis of a thermosetting polymer foam precursor that creates a low-density, reticulated, vitreous carbon skeleton [90]. The reticulated polymer foam precursor naturally forms a repeating dodecahedron structural array of regular pores. Commercially pure tantalum is then deposited on this interconnected carbon scaffold using a complex process of chemical vapor deposition and infiltration. This process involves heating the tantalum to a gaseous state and then depositing it evenly on the struts as a solid material. Together, this process creates a highly-porous coating with a configuration similar to cancellous bone (Fig. 3.8).

Typically, strut coating ranges from 40 to 60 microns, however the thickness can be changed to alter pore size and mechanical properties of the metallic foam. Trabecular metal possesses mechanical properties of low stiffness, increased porosity, and a high coefficient of friction. The coefficient of friction has been found to be 0.88 and modulus of elasticity has been found to be 3 GPa for the bulk porous foam. Trabecular metal orthopaedic implants possess an average pore size of 400–600 microns and a volume porosity of 75–85 % (99 % tantalum, 1 % vitreous carbon by weight) [21, 45, 57]. Despite a low modulus of elasticity and highly porous structure, trabecular metal is able to withstand physiologic loads and support bone ingrowth under such stresses (Table 3.2) [123]. Further, tantalum has been shown to be corrosion resistant, with a theoretical benefit of decreased stress shielding, the potential for immediate postoperative weight bearing, and a more normal pattern of bone remodeling adjacent to the component.

Fig. 3.8 High power photomicrograph of the dodecahedron array of porous tantalum. Notice the roughened nanotexturing that lends a high coefficient of friction to this metallic foam. (Courtesy of Zimmer, Warsaw, IN)

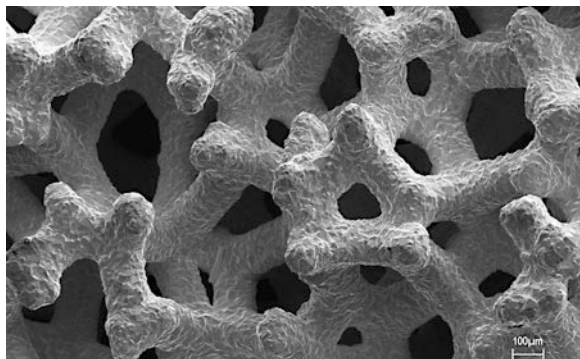


Table 3.2 Material properties of porous tantalum compared to other metals commonly used in orthopaedics

	Modulus of elasticity (Gpa)	Ultimate strength (MPa)	Yield strength (MPa)	Compressive strength (MPa)	Tensile strength (MPa)	Bending strength (MPa)	Elongation (%)	Reduction of Area (%)
Porous tantalum	2.5-3.9	50-110	35-51	50-70	63	110	n/a	n/a
Unalloyed tantalum (F560)	186	207-517	138-345	n/a	n/a	n/a	2-30	n/a
Ti-6Al-4 V (F1472)	106-115	860	758	n/a	n/a	n/a	8	14
Co-28Cr-6Mo (F75)	210	655-889	445-517	n/a	n/a	n/a	8	8
UHMWPE (F648)	12.6	35	21	n/a	n/a	n/a	300	n/a



Fig. 3.9 Wide array of orthopaedic applications exist for porous tantalum including primary and revision THA, primary and revision TKA and total and reverse shoulder arthroplasty. (Courtesy of Zimmer, Warsaw, IN)

A major advantage of trabecular metal is its wider availability in various orthopaedic applications as compared to the other open-celled structured porous materials (Fig. 3.9). This is because the carbon scaffold can be manufactured in a variety of shapes and sizes, after which the tantalum metal can be deposited on its surface, via a deposition process described above. Current orthopaedic applications [57] include use in acetabular components, femoral stems, tibia components, patellar components, spine implants, and humeral stems in TSA. Further, trabecular metal can be used as a stand-alone material in a variety of ways, including acetabular augments, patellar augments, and osteonecrosis implants.

The biologic properties of trabecular metal have been thoroughly evaluated in the basic science literature. With regard to bone ingrowth, Bobyn et al. reported a bone ingrowth rate of 80 % in a canine model at retrieval one year following implantation of acetabular components. Furthermore, the authors demonstrated, on histological analysis, haversian remodeling within the pores at the time of retrieval. Finally, the authors biomechanically demonstrated superior shear fixation strength in samples with trabecular metal as compared to samples with sintered CoCr beads [90, 124]. Similarly, trabecular metal has shown favorable results with fibrous tissue ingrowth within the pores of the metal coating. Fibrous tissue ingrowth is of growing importance to the development of megaprotheses [124], in which ligamentous, tendinous, and even vascularized soft tissue may incorporate into the trabecular metal pores, increasing implant stability and strength. This may lead to better outcomes in revision/oncology hip surgery with successful abductor reattachment as well as the possibility of extensor mechanism reconstruction via patella tendon fixation to a proximal tibial replacement in revision/oncology knee surgery. Previous studies have again demonstrated superior fibrous tissue ingrowth in trabecular metal coated implants as compared to sintered beaded porous coated implants (canine model).

Porous tantalum has also been labeled as chondroconductive [57, 125] in several in vitro based studies. As originally defined by Gordon et al. [126], chondroconductivity is essentially providing a scaffolding for growth of cartilage

and supporting structures. In their animal model, canine and emu chondrocytes were placed on porous tantalum segments from a commercially available acetabular component. Quantitative histomorphometry techniques were applied to the culture samples and the authors found evidence of tissue growth into and onto the porous tantalum after 4 weeks. Of note, only samples from dynamic cultures showed evidence of hyaline cartilage and matrix formation; cultures taken from static samples did not show detectable matrix formation or collagen. In another animal model study performed by Mardones et al. [127], periosteum from rabbits was placed on porous tantalum cylinders. Following 6 weeks of culture under chondrogenic conditions, the authors found hyaline-like cartilage outgrowth on the surface of the cylinders with associated fibrous growth within the tantalum scaffold pores. Biomechanical testing of these chondral-porous composites compared to native rabbit femoral condyle osteochondral plugs showed similar performance with regard to stress and strain. While the results from these *in vitro* studies clearly cannot be directly translated into a true *in vivo* outcome, the results are certainly encouraging with regard to the creation of a cartilaginous-tantalum composite for future resurfacing and arthroplasty-based procedures.

Both acetabular components (modular, monoblock and all-porous tantalum; \pm screw fixation) and femoral stem implants utilizing trabecular metal coatings are available for use in both primary and revision THA. Additionally, a wide variety of trabecular metal augmentation implants are available that can be used as structural bone graft substitutes [128–130]. Porous tantalum implants of all applications have been reported on to a greater extent than any of the other metallic foams in the latest generation of orthopaedic implants [21, 45, 57]. In a recent series of 43 revision THA procedures, Weeden et al. [131] investigated the use of porous tantalum acetabular components. Of note, in 26 of the 43 revisions, acetabular augments were used. At an average of 2.8 years follow-up, 42 of the 43 components were stable (98 %) and 1 failed due to septic loosening. Longer-term outcomes following THA with porous tantalum monoblock acetabular components have been encouraging, with no radiographic evidence of failure or loosening at 8–10 years following implantation [10].

Other authors have reported similar encouraging outcomes following the use of porous tantalum acetabular components in both primary and revision THA procedures. In 2002, Christie [26] described the outcomes of 54 THA operations using a porous tantalum monoblock acetabular component; amongst these cases they reported an only 1 % dislocation rate at latest follow-up [26]. Similarly in 2003, Lewis et al. [132] reported on 259 monoblock THA procedures with porous tantalum acetabular components with a follow-up period of 24–60 months. In this time frame, the authors reported a 9 % dislocation rate, with 245 THAs being stable without screws at the most recent follow-up. Gruen et al. [133] reported on a total of 414 THA procedures utilizing monoblock porous tantalum acetabular component at an average 33 months (minimum 24 months) following surgery. Initial postoperative radiographs in this cohort revealed 19 % of hips with acetabular gaps in 100 zones, while at final follow-up, 84 % of the zones with gaps were completely filled in with host bone. There was no radiographic evidence of

gap progression, periacetabular radiolucencies, or lysis, and no revision procedures had been performed. In 2005, Bargiotas et al. [134] reported on 102 monoblock THA procedures (90 primary, 12 revision) utilizing porous acetabular components with peripheral screw augmentation. At average follow-up of 50 months, the authors reported no dislocations and a 1 % revision rate. Also in 2005, Unger et al. [22] described the outcomes following 50 THA procedures with porous tantalum monoblock acetabular components. At an average 42 months post-operatively, the authors reported a 7 % dislocation rate and 7 % reoperation rate. While osseointegration has not been a concern with this monoblock component several limitations can be noted from these studies including; inability to use highly-cross linked polyethylene, increased dislocation rates due to prominent liner edge and inability to perform and isolated liner exchange in the future.

More recently, Macharas et al. [20] reported on 86 monoblock THA procedures with porous tantalum coated acetabular components at an average 7.3 years following implantation. The authors found no cases of osteolysis nor did they find any evidence of radiolucent lines on radiographic follow-up. Perhaps most encouraging is a recent long-term computed tomography (CT) based study examining specifically for the presence of osteolysis following THA. In 2011, Moen et al. [135] retrospectively reported on 51 patients who had a THA using a monoblock porous tantalum acetabular cup. At an average 10.3 years following surgery, 0/51 patients had CT evidence of osteolysis. In 2012, Nakashima et al. [136] reported on 82 hips (79 patients) at an average 61.2 months following primary THA with a porous tantalum modular acetabular component. At final follow-up, no periacetabular osteolysis was noted, and the survival rate of the implant was 100 %. The authors did describe 15 hips (18.3 %) with filling gaps on initial postoperative radiographs, however all gaps showed adequate bone filling within 12 months.

When compared with primary THA operations, revision procedures utilizing porous tantalum coated acetabular components have produced similar encouraging outcomes. In 2005, Sporer and Paprosky [137] reported on 28 revision THA procedures with a porous coated acetabular component at approximately 36 months follow-up. In this cohort, the authors reported a 1 % dislocation rate as well as 1 % reoperation rate. All revisions in this cohort were for Paprosky type IIIA defects. The same group reported on the use of the porous tantalum revision shell as an “internal plate” to treat pelvic discontinuity and acetabular fractures in cases of revision THA [138]. Out of a cohort of 13 hips, 12 hips demonstrated radiographic stability without the need for repeat surgery at an average follow-up of 2.6 years post-operatively. Mardones et al. [139] described 114 revision THA procedures using porous coated acetabular components at an average 2 years following surgery and noted 97.3 % with complete incorporation of host bone. The authors did report a 4 % dislocation rate and a 6 % reoperation rate in this series (note, this data represents individually published subsets of the published results by Bobyn et al. [140] as described below). In the original study by Bobyn et al. [140], 261 revision THAs with porous coated acetabular components were followed for an average 24–48 months. Remarkably, the authors reported an absence of radiolucent lines as well as stable reconstruction in 260/261 hips with one patient experiencing

Table 3.3 Outcomes of primary and revision total hip arthroplasty procedures using porous tantalum acetabular components

Author	Years	Component	N	Follow-up	Dislocation (%)	Reoperation (%)	Notes
Lewis	2003	Monoblock	250	24–60 m	9	n/a	245 THAs stable without screw fixation
Gruen	2005	Monoblock	574	33 m	6	10	Initial postop XR with 19 % of hips with acetabular gaps in 100 zones; final XR showed 84 % of these gaps completely filled. No RLL or osteolysis
Bargiotas	2005	Monoblock	102	50 m	0	1	Includes 90 primary, 12 secondary procedures
Macheras	2005	Monoblock	86	7.3 y	0	0	No RLL or osteolysis
Sporer	2006	Revision	28	36 m	1	1	Paprosky Tpe IIIA defects
Sporer	2005	Revision	13	31 m	0	0	Proposky Type IIIB defects
Unger	2005	Monoblock	60	42 m	7	7	5 revision monoblock cups used with screw augmentation
Mardones	2005	Revision	114	24 m	4	6	97.3 % complete incorporation
Bobynd	2004	Revision	261	24–48 m	n/a	1	1 failure (pelvic discontinuity)
Malkani	2005	Revision	18	24 m	1	2	94.4 % with evidence of bone ingrowth
Moen	2011	Monoblock	51	10.3 y	0	0	None with CT evidence of osteolysis
Nakashima	2012	Modular acetabular component	82	61.2 m	0	0	No periacetabular osteolysis

migration with pelvic discontinuity. Finally, in 2005, Malkani et al. [141] described 18 revision THA procedures utilizing porous coated acetabular components at an average 2 years following surgery. At final follow-up, the authors reported 17/18 hips (94.4 %) with evidence of bone ingrowth and a reoperation rate of 2 %. A summary of these outcomes for both primary and revision THA procedures using porous coated acetabular components is provided in Table 3.3.

With regard to TKA surgery, both tibial (modular mono block) and patella components (monoblock) utilizing trabecular metal coatings are available for clinical use. A variety of tibial cones, femoral cones, and standard augments can be used in the revision TKA setting to provide structural support and to manage complex bony deficiencies [42, 142].

A variety of clinical and radiographic studies have evaluated the utilization of porous tantalum coated TKA components with promising results. Bobyn et al. [140] described 101 monoblock tibia porous tantalum components at 6–24 month follow-up after primary TKA (72 cemented, 29 uncemented). Upon the final report there were no described complications or revisions. Siffri et al. also described their use of monoblock porous tantalum tibia components in 53 primary TKAs (all cemented). The authors found that at a minimum of 2 years postoperatively, 0/53 patients had evidence of radiolucent lines or osteolysis on radiographs, while 1/53 patients required revision surgery. In 2004, Stulberg et al. [143] reported on 43 knee augments utilizing porous tantalum augments and found that at 1–5 years postoperatively, four revision procedures were required (2 cases of aseptic loosening and 2 cases of infection). Two studies describing the use of porous tantalum salvage patella components have also been described. In 2003, Nelson et al. [144] described 20 cases at an average 23 months following surgery and found that the average arc of motion increased from 102.8° to 108.4° following surgery. Of note, 11 of the 20 patients did have reported complications, including 3 patella fractures and 8 cases of post-operative knee pain. In 2004, Nasser et al. [47] also described 11 cases of revision knee arthroplasty with porous tantalum salvage patella components. At an average 32 months following surgery, the authors described an improvement in the average range of motion from 62° to 103°. In this series, 1/11 patients experienced a traumatic patella fracture postoperatively and no revision procedures were described. These authors were able to conclude that the salvage patella performed better when there was a remaining bed of cancellous bone to fix the component to and not just fibrous tissue.

Recently, Meneghini et al. [42] reported on the utilization of porous tantalum cones for structural support in 15 revision TKA procedures. At an average 34 months post-operatively, the authors found no evidence of loosening; and, all cases demonstrated osseointegration. Similarly, in 2009, Long et al. [41] described 16 cases of revision TKA utilizing porous tantalum tibial cones at an average 31 months (minimum 24 months) following implantation. These revision procedures were performed for either aseptic loosening (13) or staged reimplantation for infection (3). At final follow-up, 14 knees were noted to be functioning well with signs of stable osteointegration into the cones. Of note, 2 knees experienced recurrent sepsis and required removal of the cone. Recently in 2011, Howard et al. [33] reported on their early results following the use of porous tantalum femoral cones in 24 revision TKAs at an average 33 months (minimum 24 months) following implantation. These revision procedures were performed for a variety of reasons, including aseptic loosening (11), staged reimplantation for infection (7), severe osteolysis (3), periprosthetic fracture (2), and severe instability (1). The authors reported improvements in the Knee Society score from 55 to 81 at final

follow-up as well as good radiographic fixation of the cone at an average 35 months in 20/20 patients (not all patients had adequate radiographs). A summary of these outcomes for both primary and revision TKA procedures using porous coated acetabular components is provided in Table 3.4.

Another important clinical application of trabecular metal is the porous tantalum rod, available for the treatment of early stages of femoral head osteonecrosis. During the pre-collapse stages of the disease process, a porous tantalum coated rod can support the overlying cartilage as the areas of osteonecrosis regenerates with promising clinical outcomes [145, 146]. The overall goal is to provide the overlying cartilage with some amount of subchondral support while the avascular lesion attempts to reconstitute itself within the femoral head. Of note, subtrochanteric fracture after implantation of a porous tantalum rod in this patient population has been reported [147], and thus caution must be exercised when using this prosthesis in this patient population. Overall, further long-term outcomes studies are warranted to determine the medium and long-term outcomes and potential complications associated with the use of porous tantalum coated rods in patients with femoral head osteonecrosis.

Encouraging results have been demonstrated in both animal model [59, 60, 65] and clinical [64] studies examining spinal fusion with porous tantalum cages. In a goat model, Sidhu et al. studied the effects of porous tantalum blocks with and without recombinant bone morphogenic protein-2 (rhBMP-2) in anterior cervical interbody fusion, and noted a positive trend with improved bone ingrowth in the rhBMP-2 group. In a pig model, Zou et al. described bone ingrowth and successful lumbar spinal fusion utilizing porous tantalum rings and cages. When compared to carbon-fiber cages, the authors found pedicle screw fixation of the fusion level in specimens with porous tantalum cages afforded improved fusion rates and bone ingrowth rates. Further, the authors reported less bone graft requirements and enhanced remodeling effects in the porous tantalum group.

In a prospective, randomized clinical trial conducted by Wigfield et al. [64] the use of porous tantalum implants in patients undergoing cervical interbody fusion was studied. While the study's enrollment was initially halted out of concern for possible delayed or non-fusion outcomes in the porous tantalum groups, ultimately all patients achieved successful fusion at 12 months. In another recent prospective, randomized clinical trial, Lofgren et al. [51] compared the results of anterior cervical decompression and fusion (ACDF) with trabecular metal implantation to ACDF with the Smith-Robinson (SR) autograft technique. The authors reported shorter operative times with TM implantation ($P = 0.001$), however the fusion rates were lower in the trabecular metal group ($P < 0.05$). Perhaps most important to note, however, is that the authors demonstrated no statistically significant differences in clinical outcomes between the two groups. Similar findings were reported in a recent study by Kasliwal et al. [50] in their multicenter investigation analyzing the outcomes following porous tantalum cervical interbody fusion. At 2-year follow-up, the authors found decreased fusion rates and increased risk of device fragmentation in patients in the tantalum group as compared with the

Table 3.4 Outcomes of primary and revision total knee arthroplasty procedures using porous tantalum tibia, patella, or argument components

Author	Years	Component	N	Follow-up	Complications	Reoperations	Notes
Boby Sifri	2004	Monoblock tibia	101	6–24 m	n/a	None	No RLL or osteolysis on Xrays
	2006	Monoblock tibia	53	Min 24 m	1 MUA, 1 intraop fracture	One	
Boby Stulberg	2004	Monoblock patella	69	12–24 m	n/a	None	
	2004	Knee augments	43	1–5 y	2 aseptic loosening, 2 infections	4	
Nasser	2004	Salvage patella	11	32 m	1 traumatic patella fracture	None	ROM improved 62 to 103
Nelson	2003	Salvage patella	20	23 m	3 patella postop	3 revisions (2 extensor mechanism repairs, 1 patella clunk debridement)	102.8 to 108.4
					3 patella fractures, 8 postop anterior knee pain		
Meneghini	2009	Porous tantalum cones revision TKA	15	34 m	None	None	No loosening, no osteolysis, all with osteo integration
Long	2009	Porous tantalum tibial cones revision TKA	16	31 m	2 recurrent sepsis and removal of cones	2 removal of cones	Other 14 with good functioning and osteointegration
Howard	2011	Porous tantalum femoral cones revision TKA	24	33 m	None	None	Improvements in Knee Society scores 55 to 81, 20/20 with xrays available with good integration

control group of iliac autograft fusion. Thus, further long-term study is needed to determine the efficacy and safety of porous tantalum applications in the spine.

While certainly advantageous with regard to its similar biomaterial properties, nearly unlimited potential for fabricating shapes, and encouraging long-term clinical and radiographic outcomes (>10 years) [10], the manufacturing cost for tantalum is relatively high, and as such, the material is not as readily available as titanium. The manufacturing process itself, however, is relatively “green” in that the tantalum that is left over from the process is recycled to the semiconductor industry as an oxide powder and the water is pure and passed down the drain.

3.8 Safety of Metal in Orthopaedic Surgery

A discussion on the application of porous metals in orthopaedic surgery would not be complete without mention of the possible pitfalls associated in general with the use of metallic implants. In particular, the potential development of adverse local tissue reaction (ALTR) and metallosis due to the release of metallic debris locally and systemically has received substantial attention in both the academic and public arenas. While not associated specifically with porous metals, such as those described in this chapter, it is crucial to understand the potential unwanted local [148] and/or systemic effects [149–154] of metal debris release. Additionally, while porous tantalum as a bulk form is inert, there are always concerns regarding tantalum and titanium debris and its local reactivity. Therefore when using augments, cones and sleeves it is best to currently use a small coating of cement between the rough edges of these adjacent porous surfaces. With regard to metal-on-metal total hip arthroplasty applications, some more recent, longer-term outcomes studies in the literature have suggested that elevated serum ion levels have no lasting clinical effects, and that the level of ions actually decreases over time, however this warrants further study with randomized, level I studies [155–157]. Interestingly, recent work by Berntein et al. [158] has shown that increases in serum metal ions do not alter the levels of oxidative stress markers found in the serum. Certainly, further basic science and clinical research is warranted to evaluate possible associations between porous coated implants and release of metallic debris both locally and systemically as well as to evaluate if release of debris causes any significant lasting clinical effects.

3.9 Future Developments

The recent advancements in the research and development of porous coatings for use in bone and soft tissue implant procedures have initiated a new and exciting era of porous materials in orthopaedic surgery. As newer porous coated implants (open-

cell) are adapted into everyday clinical practice, it will become easier to analyze a given component's potential for success at long-term follow-up. Furthermore, new applications for porous coated implants remain under investigation and include bone graft substitutes, tendon reconstruction, cartilage restoration and as drug delivery agents. While current reports are encouraging, improved long-term clinical outcomes studies are needed to better understand the role of newer porous coated implants in the field of orthopaedic surgery.

References

1. Fernandez-Fairen M, Murcia A, Iglesias R, Sevilla P, Manero JM, Gil FJ. Analysis of tantalum implants used for avascular necrosis of the femoral head: a review of five retrieved specimens. *J Appl Biomater Biomech*. Mar 15 2012:0
2. Baad-Hansen, T., Kold, S., Olsen, N., Christensen, F., Soballe, K.: Excessive distal migration of fiber-mesh coated femoral stems. *Acta Orthop* **82**(3), 308–314 (2011)
3. Oh, K.J., Pandher, D.S.: A new mode of clinical failure of porous tantalum rod. *Indian J Orthop*. **44**(4), 464–467 (2010)
4. Meneghini, R.M., Meyer, C., Buckley, C.A., Hanssen, A.D., Lewallen, D.G.: Mechanical stability of novel highly porous metal acetabular components in revision total hip arthroplasty. *J. Arthroplasty* **25**(3), 337–341 (2010)
5. Meneghini, R.M., Ford, K.S., McCollough, C.H., Hanssen, A.D., Lewallen, D.G.: Bone remodeling around porous metal cementless acetabular components. *J. Arthroplasty* **25**(5), 741–747 (2010)
6. Macheras, G.A., Kateros, K., Koutsostathis, S.D., Tsakotos, G., Galanakis, S., Papadakis, S.A.: The trabecular metal monoblock acetabular component in patients with high congenital hip dislocation: A prospective study. *J. Bone Joint Surg. Br.* **92**(5), 624–628 (2010)
7. Liu, G., Wang, J., Yang, S., Xu, W., Ye, S., Xia, T.: Effect of a porous tantalum rod on early and intermediate stages of necrosis of the femoral head. *Biomed. Mater.* **5**(6), 065003 (2010)
8. Fernandez-Fairen, M., Murcia, A., Blanco, A., Merono, A., Murcia Jr, A., Ballester, J.: Revision of failed total hip arthroplasty acetabular cups to porous tantalum components: a 5-year follow-up study. *J. Arthroplasty* **25**(6), 865–872 (2010)
9. Ramappa, M., Bajwa, A., Kulkarni, A., McMurtry, I., Port, A.: Early results of a new highly porous modular acetabular cup in revision arthroplasty. *Hip Int.* Jul-Sep **19**(3), 239–244 (2009)
10. Macheras, G., Kateros, K., Kostakos, A., Koutsostathis, S., Danomaras, D., Papagelopoulos, P.J.: Eight- to ten-year clinical and radiographic outcome of a porous tantalum monoblock acetabular component. *J. Arthroplasty* **24**(5), 705–709 (2009)
11. Tanzer, M., Bobyn, J.D., Krygier, J.J., Karabasz, D.: Histopathologic retrieval analysis of clinically failed porous tantalum osteonecrosis implants. *J. Bone Joint Surg. Am.* **90**(6), 1282–1289 (2008)
12. Malizos, K.N., Bargiotas, K., Papatheodorou, L., Hantes, M., Karachalios, T.: Survivorship of monoblock trabecular metal cups in primary THA : Midterm results. *Clin. Orthop. Relat. Res.* **466**(1), 159–166 (2008)
13. Kim, W.Y., Greidanus, N.V., Duncan, C.P., Masri, B.A., Garbuz, D.S.: Porous tantalum uncemented acetabular shells in revision total hip replacement: two to four year clinical and radiographic results. *Hip Int.* **18**(1), 17–22 (2008)

14. Nadeau, M., Seguin, C., Theodoropoulos, J.S., Harvey, E.J.: Short term clinical outcome of a porous tantalum implant for the treatment of advanced osteonecrosis of the femoral head. *Mcgill J Med.* **10**(1), 4–10 (2007)
15. Klika, A.K., Murray, T.G., Darwiche, H., Barsoum, W.K.: Options for acetabular fixation surfaces. *J. Long Term Eff. Med. Implants* **17**(3), 187–192 (2007)
16. Grelsamer RP.: Applications of porous tantalum in total hip arthroplasty. *J Am Acad Orthop Surg.* **15**(3):137; author reply 137–138
17. Veillette, C.J., Mehdian, H., Schemitsch, E.H., McKee, M.D.: Survivorship analysis and radiographic outcome following tantalum rod insertion for osteonecrosis of the femoral head. *J. Bone Joint Surg. Am.* **88**(Suppl 3), 48–55 (2006)
18. Sporer, S.M., Paprosky, W.G.: The use of a trabecular metal acetabular component and trabecular metal augment for severe acetabular defects. *J. Arthroplasty* **21**(6), 83–86 (2006). Suppl 2
19. Rose, P.S., Halasy, M., Trousdale, R.T., et al.: Preliminary results of tantalum acetabular components for THA after pelvic radiation. *Clin. Orthop. Relat. Res.* **453**, 195–198 (2006)
20. Macheras, G.A., Papagelopoulos, P.J., Kateros, K., Kostakos, A.T., Baltas, D., Karachalios, T.S.: Radiological evaluation of the metal-bone interface of a porous tantalum monoblock acetabular component. *J. Bone Joint Surg. Br.* **88**(3), 304–309 (2006)
21. Levine, B., Della Valle, C.J., Jacobs, J.J.: Applications of porous tantalum in total hip arthroplasty. *J. Am. Acad. Orthop. Surg.* **14**(12), 646–655 (2006)
22. Unger, A.S., Lewis, R.J., Gruen, T.: Evaluation of a porous tantalum uncemented acetabular cup in revision total hip arthroplasty: clinical and radiological results of 60 hips. *J. Arthroplasty* **20**(8), 1002–1009 (2005)
23. Chalkin, B., Minter, J.: Limb salvage and abductor reattachment using a custom prosthesis with porous tantalum components. *J. Arthroplasty* **20**(1), 127–130 (2005)
24. Frenkel, S.R., Jaffe, W.L., Dimaano, F., Iesaka, K., Hua, T.: Bone response to a novel highly porous surface in a canine implantable chamber. *J. Biomed. Mater. Res. B Appl. Biomater.* **71**(2), 387–391 (2004)
25. Karrholm J, Anderberg C, Snorrason F, et al. Evaluation of a femoral stem with reduced stiffness. A randomized study with use of radiostereometry and bone densitometry. *J Bone Joint Surg Am.*; **84**-A(9), 1651–1658 (2002)
26. Christie, M.J.: Clinical applications of Trabecular Metal. *Am J Orthop (Belle Mead NJ).* **31**(4), 219–220 (2002)
27. Bobyn, J.D., Toh, K.K., Hacking, S.A., Tanzer, M., Krygier, J.J.: Tissue response to porous tantalum acetabular cups: A canine model. *J. Arthroplasty* **14**(3), 347–354 (1999)
28. Karrholm, J., Herberts, P., Hultmark, P., Malchau, H., Nivbrant, B., Thanner, J.: Radiostereometry of hip prostheses. Review of methodology and clinical results. *Clin. Orthop. Relat. Res.* **344**, 94–110 (1997)
29. Ciccotti, M.G., Rothman, R.H., Hozack, W.J., Moriarty, L.: Clinical and roentgenographic evaluation of hydroxyapatite-augmented and nonaugmented porous total hip arthroplasty. *J. Arthroplasty* **9**(6), 631–639 (1994)
30. Kamath, A.F., Gee, A.O., Nelson, C.L., Garino, J.P., Lotke, P.A., Lee, G.C.: Porous tantalum patellar components in revision total knee arthroplasty minimum 5-year follow-up. *J. Arthroplasty* **27**(1), 82–87 (2012)
31. Sambaziotis C, Lovy AJ, Koller KE, Bloebaum RD, Hirsh DM, Kim SJ. Histologic Retrieval Analysis of a Porous Tantalum Metal Implant in an Infected Primary Total Knee Arthroplasty. *J Arthroplasty* (2011)
32. Kamath, A.F., Lee, G.C., Sheth, N.P., Nelson, C.L., Garino, J.P., Israelite, C.L.: Prospective results of uncemented tantalum monoblock tibia in total knee arthroplasty: minimum 5-year follow-up in patients younger than 55 years. *J. Arthroplasty* **26**(8), 1390–1395 (2011)
33. Howard, J.L., Kuder, J., Lewallen, D.G., Hanssen, A.D.: Early results of the use of tantalum femoral cones for revision total knee arthroplasty. *J. Bone Joint Surg. Am.* **93**(5), 478–484 (2011)

34. Haidukewych, G.J., Hanssen, A., Jones, R.D.: Metaphyseal fixation in revision total knee arthroplasty: Indications and techniques. *J. Am. Acad. Orthop. Surg.* **19**(6), 311–318 (2011)
35. O'Keefe, T.J., Winter, S., Lewallen, D.G., Robertson, D.D., Poggie, R.A.: Clinical and radiographic evaluation of a monoblock tibial component. *J. Arthroplasty* **25**(5), 785–792 (2010)
36. Minoda, Y., Kobayashi, A., Iwaki, H., Ikebuchi, M., Inori, F., Takaoka, K.: Comparison of bone mineral density between porous tantalum and cemented tibial total knee arthroplasty components. *J. Bone Joint Surg. Am.* **92**(3), 700–706 (2010)
37. Troyer, J., Levine, B.R.: Proximal tibia reconstruction with a porous tantalum cone in a patient with charcot arthropathy. *Orthopedics.* **32**(5), 358 (2009)
38. Tigani, D., Sabbioni, G., Raimondi, A.: Early aseptic loosening of a porous tantalum knee prosthesis. *Chir. Organi Mov.* **93**(3), 187–191 (2009)
39. Sheth, N.P., Lonner, J.H.: Clinical use of porous tantalum in complex primary total knee arthroplasty. *Am J Orthop (Belle Mead NJ)* **38**(10), 526–530 (2009)
40. Meneghini RM, Lewallen DG, Hanssen AD. Use of porous tantalum metaphyseal cones for severe tibial bone loss during revision total knee replacement. Surgical technique. *J Bone Joint Surg Am*, **91**(Pt 1), 131–138 (2009), Suppl 2
41. Long, W.J., Scuderi, G.R.: Porous tantalum cones for large metaphyseal tibial defects in revision total knee arthroplasty: A minimum 2-year follow-up. *J. Arthroplasty* **24**(7), 1086–1092 (2009)
42. Meneghini, R.M., Lewallen, D.G., Hanssen, A.D.: Use of porous tantalum metaphyseal cones for severe tibial bone loss during revision total knee replacement. *J. Bone Joint Surg. Am.* **90**(1), 78–84 (2008)
43. Klein, G.R., Levine, H.B., Hartzband, M.A.: Removal of a well-fixed trabecular metal monoblock tibial component. *J. Arthroplasty* **23**(4), 619–622 (2008)
44. Lombardi Jr, A.V., Berasi, C.C., Berend, K.R.: Evolution of tibial fixation in total knee arthroplasty. *J. Arthroplasty* **22**(4 Suppl 1), 25–29 (2007)
45. Levine, B., Sporer, S., Della Valle, C.J., Jacobs, J.J., Paprosky, W.: Porous tantalum in reconstructive surgery of the knee: A review. *J Knee Surg.* **20**(3), 185–194 (2007)
46. Ries, M.D., Cabalo, A., Bozic, K.J., Anderson, M.: Porous tantalum patellar augmentation: The importance of residual bone stock. *Clin. Orthop. Relat. Res.* **452**, 166–170 (2006)
47. Nasser, S., Poggie, R.A.: Revision and salvage patellar arthroplasty using a porous tantalum implant. *J. Arthroplasty* **19**(5), 562–572 (2004)
48. Sinclair SK, Konz GJ, Dawson JM, Epperson RT, Bloebaum RD. Host bone response to polyetheretherketone versus porous tantalum implants for cervical spinal fusion in a goat model. *Spine (Phila Pa)*. May 1 2012, **37**(10):E571–580 (1976)
49. Fernandez-Fairen M, Murcia A, Torres A, Hernandez-Vaquero D, Menzie AM. Is anterior cervical fusion with a porous tantalum implant a cost-effective method to treat cervical disc disease with radiculopathy? *Spine (Phila Pa 1976)*. Mar 29 2012
50. Kasliwal MK, Baskin DS, Traynelis VC. Failure of porous tantalum cervical interbody fusion devices: Two-year results from a prospective, randomized, multicenter clinical study. *J Spinal Disord Tech*. Dec 21 (2011)
51. Lofgren, H., Engquist, M., Hoffmann, P., Sigstedt, B., Vavruch, L.: Clinical and radiological evaluation of Trabecular Metal and the Smith-Robinson technique in anterior cervical fusion for degenerative disease: a prospective, randomized, controlled study with 2-year follow-up. *Eur. Spine J.* **19**(3), 464–473 (2010)
52. Frigg, A., Dougall, H., Boyd, S., Nigg, B.: Can porous tantalum be used to achieve ankle and subtalar arthrodesis?: a pilot study. *Clin. Orthop. Relat. Res.* **468**(1), 209–216 (2010)
53. Maccauro, G., Iommetti, P.R., Muratori, F., Raffaelli, L., Manicone, P.F., Fabbriani, C.: An overview about biomedical applications of micron and nano size tantalum. *Recent Pat. Biotechnol.* **3**(3), 157–165 (2009)
54. Guan, Y., Yoganandan, N., Maiman, D.J., Pintar, F.A.: Internal and external responses of anterior lumbar/lumbosacral fusion: Nonlinear finite element analysis. *J Spinal Disord Tech.* **21**(4), 299–304 (2008)

55. Lin, C.Y., Wirtz, T., LaMarca, F., Hollister, S.J.: Structural and mechanical evaluations of a topology optimized titanium interbody fusion cage fabricated by selective laser melting process. *J Biomed Mater Res A*. **83**(2), 272–279 (2007)
56. Zou, X., Li, H., Zou, L., Mygind, T., Lind, M., Bunger, C.: Porous tantalum trabecular metal scaffolds in combination with a novel marrow processing technique to replace autograft. *Adv. Exp. Med. Biol.* **585**, 197–208 (2006)
57. Levine, B.R., Sporer, S., Poggie, R.A., Della Valle, C.J., Jacobs, J.J.: Experimental and clinical performance of porous tantalum in orthopedic surgery. *Biomaterials* **27**(27), 4671–4681 (2006)
58. Bunger, M.H., Foss, M., Erlacher, K., et al.: Bone nanostructure near titanium and porous tantalum implants studied by scanning small angle X-ray scattering. *Eur Cell Mater.* **12**, 81–91 (2006)
59. Zou X, Li H, Teng X, et al. Pedicle screw fixation enhances anterior lumbar interbody fusion with porous tantalum cages: an experimental study in pigs. *Spine (Phila Pa 1976)*. Jul 15, **30**(14):E392–399 (2005)
60. Zou, X., Li, H., Bunger, M., Egund, N., Lind, M., Bunger, C.: Bone ingrowth characteristics of porous tantalum and carbon fiber interbody devices: An experimental study in pigs. *Spine J.* **4**(1), 99–105 (2004)
61. Kokubo T. Metallic materials stimulating bone formation. *Med J Malaysia*. May 2004, **59** Suppl B:91–92 (2004)
62. Zou, X., Xue, Q., Li, H., Bunger, M., Lind, M., Bunge, C.: Effect of alendronate on bone ingrowth into porous tantalum and carbon fiber interbody devices: An experimental study on spinal fusion in pigs. *Acta Orthop. Scand.* **74**(5), 596–603 (2003)
63. Zou, X., Li, H., Baatrup, A., Lind, M., Bunger, C.: Engineering of bone tissue with porcine bone marrow stem cells in three-dimensional trabecular metal: in vitro and in vivo studies. *APMIS Suppl.* **109**, 127–132 (2003)
64. Wigfield, C., Robertson, J., Gill, S., Nelson, R.: Clinical experience with porous tantalum cervical interbody implants in a prospective randomized controlled trial. *Br. J. Neurosurg.* **17**(5), 418–425 (2003)
65. Sidhu, K.S., Prochnow, T.D., Schmitt, P., Fischgrund, J., Weisbrode, S., Herkowitz, H.N.: Anterior cervical interbody fusion with rhBMP-2 and tantalum in a goat model. *Spine J.* **1**(5), 331–340 (2001)
66. Levi AD, Choi WG, Keller PJ, Heiserman JE, Sonntag VK, Dickman CA. The radiographic and imaging characteristics of porous tantalum implants within the human cervical spine. *Spine (Phila Pa 1976)*. Jun 1, **23**(11):1245–1250; discussion 1251 (1998)
67. Higuera, C.A., Inoue, N., Lim, J.S., et al.: Tendon reattachment to a metallic implant using an allogenic bone plate augmented with rhOP-1 vs. autogenous cancellous bone and marrow in a canine model. *J. Orthop. Res.* **23**(5), 1091–1099 (2005)
68. Smith, L.: Ceramic-plastic material as a bone substitute. *Arch. Surg.* **87**, 653–661 (1963)
69. Lueck, R.A., Galante, J., Rostoker, W., Ray, R.D.: Development of an open pore metallic implant to permit attachment to bone. *Surg Forum.* **20**, 456–457 (1969)
70. Galante, J., Rostoker, W., Lueck, R., Ray, R.D.: Sintered fiber metal composites as a basis for attachment of implants to bone. *J. Bone Joint Surg. Am.* **53**(1), 101–114 (1971)
71. Lambert, E., Galante, J., Rostoker, W.: Fixation of skeletal replacement by fiber metal composites. *Clin. Orthop. Relat. Res.* **87**, 303–310 (1972)
72. Sumner, D.R., Kienapfel, H., Jacobs, J.J., Urban, R.M., Turner, T.M., Galante, J.O.: Bone ingrowth and wear debris in well-fixed cementless porous-coated tibial components removed from patients. *J. Arthroplasty* **10**(2), 157–167 (1995)
73. Boby, J.D., Cameron, H.U., Abdulla, D., Pilliar, R.M., Weatherly, G.C.: Biologic fixation and bone modeling with an unconstrained canine total knee prosthesis. *Clin. Orthop. Relat. Res.* **166**, 301–312 (1982)
74. Boby, J.D., Pilliar, R.M., Cameron, H.U., Weatherly, G.C.: The optimum pore size for the fixation of porous-surfaced metal implants by the ingrowth of bone. *Clin Orthop Relat Res.* Jul-Aug **150**, 263–270 (1980)

75. Bobynd, J.D., Pilliar, R.M., Cameron, H.U., Weatherly, G.C.: Osteogenic phenomena across endosteal bone-implant spaces with porous surfaced intramedullary implants. *Acta Orthop. Scand.* **52**(2), 145–153 (1981)
76. Bobynd, J.D., Pilliar, R.M., Cameron, H.U., Weatherly, G.C., Kent, G.M.: The effect of porous surface configuration on the tensile strength of fixation of implants by bone ingrowth. *Clin. Orthop. Relat. Res.* **149**, 291–298 (1980)
77. Cameron, H., Macnab, I., Pilliar, R.: Porous surfaced vitallium staples. *S. Afr. J. Surg.* **10**(2), 63–70 (1972)
78. Cameron, H.U., Macnab, I., Pilliar, R.M.: A porous metal system for joint replacement surgery. *Int. J. Artif. Organs* **1**(2), 104–109 (1978)
79. Cameron, H.U., Pilliar, R.M., MacNab, I.: The effect of movement on the bonding of porous metal to bone. *J. Biomed. Mater. Res.* **7**(4), 301–311 (1973)
80. Cameron, H.U., Pilliar, R.M., Macnab, I.: The rate of bone ingrowth into porous metal. *J. Biomed. Mater. Res.* **10**(2), 295–302 (1976)
81. Cameron, H.U., Yoneda, B.T., Pilliar, R.M., Macnab, I.: The effect of early infection on bone ingrowth into porous metal implants. *Acta Orthop Belg.* **43**(1), 71–74 (1977)
82. Hungerford, D.S., Kenna, R.V., Krackow, K.A.: The porous-coated anatomic total knee. *Orthop. Clin. North Am.* **13**(1), 103–122 (1982)
83. Kienapfel, H., Martell, J., Rosenberg, A., Galante, J.: Cementless Gustilo-Kyle and BIAS total hip arthroplasty: 2- to 5-year results. *Arch. Orthop. Trauma Surg.* **110**(4), 179–186 (1991)
84. Pilliar, R.M., Cameron, H.U., Binnington, A.G., Szivek, J., Macnab, I.: Bone ingrowth and stress shielding with a porous surface coated fracture fixation plate. *J. Biomed. Mater. Res.* **13**(5), 799–810 (1979)
85. Pilliar, R.M., Cameron, H.U., Macnab, I.: Porous surface layered prosthetic devices. *Biomed. Eng.* **10**(4), 126–131 (1975)
86. Welsh, R.P., Pilliar, R.M., Macnab, I.: Surgical implants. The role of surface porosity in fixation to bone and acrylic. *J. Bone Joint Surg. Am.* **53**(5), 963–977 (1971)
87. Spector, M., Flemming, W.R., Kreutner, A.: Bone growth into porous high-density polyethylene. *J. Biomed. Mater. Res.* **10**(4), 595–603 (1976)
88. Spector, M., Michno, M.J., Smarook, W.H., Kwiatkowski, G.T.: A high-modulus polymer for porous orthopedic implants: Biomechanical compatibility of porous implants. *J. Biomed. Mater. Res.* **12**(5), 665–677 (1978)
89. Tullos, H.S., McCaskill, B.L., Dickey, R., Davidson, J.: Total hip arthroplasty with a low-modulus porous-coated femoral component. *J. Bone Joint Surg. Am.* **66**(6), 888–898 (1984)
90. Bobynd, J.D., Stackpool, G.J., Hacking, S.A., Tanzer, M., Krygier, J.J.: Characteristics of bone ingrowth and interface mechanics of a new porous tantalum biomaterial. *J. Bone Joint Surg. Br.* **81**(5), 907–914 (1999)
91. Smith, S.E., Estok 2nd, D.M., Harris, W.H.: Average 12-year outcome of a chrome-cobalt, beaded, bony ingrowth acetabular component. *J. Arthroplasty* **13**(1), 50–60 (1998)
92. Mulroy Jr, R.D., Harris, W.H.: The effect of improved cementing techniques on component loosening in total hip replacement. An 11-year radiographic review. *J. Bone Joint Surg. Br.* **72**(5), 757–760 (1990)
93. Hennessy, D.W., Callaghan, J.J., Liu, S.S.: Second-generation extensively porous-coated THA stems at minimum 10-year followup. *Clin. Orthop. Relat. Res.* **467**(9), 2290–2296 (2009)
94. Sakalkale, D.P., Eng, K., Hozack, W.J., Rothman, R.H.: Minimum 10-year results of a tapered cementless hip replacement. *Clin. Orthop. Relat. Res.* **362**, 138–144 (1999)
95. Yoon, T.R., Rowe, S.M., Kim, M.S., Cho, S.G., Seon, J.K.: Fifteen- to 20-year results of uncemented tapered fully porous-coated cobalt-chrome stems. *Int. Orthop.* **32**(3), 317–323 (2008)
96. Cook, S.D., Barrack, R.L., Thomas, K.A., Haddad Jr, R.J.: Quantitative analysis of tissue growth into human porous total hip components. *J. Arthroplasty* **3**(3), 249–262 (1988)

97. Engh, G.A., Bobyn, J.D., Petersen, T.L.: Radiographic and histologic study of porous coated tibial component fixation in cementless total knee arthroplasty. *Orthopedics* **11**(5), 725–731 (1988)
98. Vigorita, V.J., Minkowitz, B., Dichiaro, J.F., Higham, P.A.: A histomorphometric and histologic analysis of the implant interface in five successful, autopsy-retrieved, noncemented porous-coated knee arthroplasties. *Clin. Orthop. Relat. Res.* **293**, 211–218 (1993)
99. Spector, M.: Historical review of porous-coated implants. *J. Arthroplasty* **2**(2), 163–177 (1987)
100. Gustilo RB, Kyle RF. Revision of femoral component loosening with titanium ingrowth prosthesis and bone grafting. *Hip*, 342–346 (1984)
101. Landon, G.C., Galante, J.O., Maley, M.M.: Noncemented total knee arthroplasty. *Clin. Orthop. Relat. Res.* **205**, 49–57 (1986)
102. Klein, G.R., Levine, H.B., Nafash, S.C., Lamothe, H.C., Hartzband, M.A.: Total hip arthroplasty with a collarless, tapered, fiber metal proximally coated femoral stem: minimum 5-year follow-up. *J. Arthroplasty* **24**(4), 579–585 (2009)
103. Lachiewicz, P.F., Soileau, E.S., Bryant, P.: Second-generation proximally coated titanium femoral component: minimum 7-year results. *Clin. Orthop. Relat. Res.* **465**, 117–121 (2007)
104. Anseth, S.D., Pulido, P.A., Adelson, W.S., Patil, S., Sandwell, J.C., Colwell Jr, C.W.: Fifteen-year to twenty-year results of cementless Harris-Galante porous femoral and Harris-Galante porous I and II acetabular components. *J. Arthroplasty* **25**(5), 687–691 (2010)
105. Hamilton, W.G., Calendine, C.L., Beykirch, S.E., Hopper Jr, R.H., Engh, C.A.: Acetabular fixation options: first-generation modular cup curtain calls and caveats. *J. Arthroplasty* **22**(4 Suppl 1), 75–81 (2007)
106. Della Valle CJ, Berger RA, Rosenberg AG, Galante JO. Cementless acetabular reconstruction in revision total hip arthroplasty. *Clin Orthop Relat Res*, (420), 96–100 (2004)
107. Jones CP, Lachiewicz PF. Factors influencing the longer-term survival of uncemented acetabular components used in total hip revisions. *J Bone Joint Surg Am*, **86**-A(2), 342–347 (2004)
108. Leopold, S.S., Rosenberg, A.G., Bhatt, R.D., Sheinkop, M.B., Quigley, L.R., Galante, J.O.: Cementless acetabular revision. Evaluation at an average of 10.5 years. *Clin. Orthop. Relat. Res.* **369**, 179–186 (1999)
109. Pidhorz, L.E., Urban, R.M., Jacobs, J.J., Sumner, D.R., Galante, J.O.: A quantitative study of bone and soft tissues in cementless porous-coated acetabular components retrieved at autopsy. *J. Arthroplasty* **8**(2), 213–225 (1993)
110. Mayman, D.J., Gonzalez Della Valle, A., Lambert, E., et al.: Late fiber metal shedding of the first and second-generation Harris Galante acetabular component. A report of 5 cases. *J. Arthroplasty* **22**(4), 624–629 (2007)
111. Udomkiat P, Dorr LD, Wan Z. Cementless hemispheric porous-coated sockets implanted with press-fit technique without screws: average ten-year follow-up. *J Bone Joint Surg Am*, **84**-A(7), 1195–1200 (2002)
112. Hofmann, A.A., Feign, M.E., Klauser, W., VanGorp, C.C., Camargo, M.P.: Cementless primary total hip arthroplasty with a tapered, proximally porous-coated titanium prosthesis: A 4- to 8-year retrospective review. *J. Arthroplasty* **15**(7), 833–839 (2000)
113. Luites, J.W., Spruit, M., Hellemond, G.G., Horstmann, W.G., Valstar, E.R.: Failure of the uncoated titanium ProxiLock femoral hip prosthesis. *Clin. Orthop. Relat. Res.* **448**, 79–86 (2006)
114. Hofmann, A.A., Evanich, J.D., Ferguson, R.P., Camargo, M.P.: Ten- to 14-year clinical followup of the cementless Natural Knee system. *Clin. Orthop. Relat. Res.* **388**, 85–94 (2001)
115. Bloebaum, R.D., Bachus, K.N., Jensen, J.W., Hofmann, A.A.: Postmortem analysis of consecutively retrieved asymmetric porous-coated tibial components. *J. Arthroplasty* **12**(8), 920–929 (1997)

116. Bloebaum, R.D., Rhodes, D.M., Rubman, M.H., Hofmann, A.A.: Bilateral tibial components of different cementless designs and materials. Microradiographic, backscattered imaging, and histologic analysis. *Clin. Orthop. Relat. Res.* **268**, 179–187 (1991)
117. Hahn, H., Palich, W.: Preliminary evaluation of porous metal surfaced titanium for orthopedic implants. *J. Biomed. Mater. Res.* **4**(4), 571–577 (1970)
118. Turner, T.M., Sumner, D.R., Urban, R.M., Rivero, D.P., Galante, J.O.: A comparative study of porous coatings in a weight-bearing total hip-arthroplasty model. *J. Bone Joint Surg. Am.* **68**(9), 1396–1409 (1986)
119. Bourne, R.B., Rorabeck, C.H., Burkart, B.C., Kirk, P.G.: Ingrowth surfaces. Plasma spray coating to titanium alloy hip replacements. *Clin. Orthop. Relat. Res.* **298**, 37–46 (1994)
120. Lombardi Jr, A. V., Berend, K.R., Mallory, T.H., Skeels, M.D., Adams, J.B.: Survivorship of 2000 tapered titanium porous plasma-sprayed femoral components. *Clin. Orthop. Relat. Res.* **467**(1), 146–154 (2009)
121. Karageorgiou, V., Kaplan, D.: Porosity of 3D biomaterial scaffolds and osteogenesis. *Biomaterials* **26**(27), 5474–5491 (2005)
122. Bourne RB, McCalden RW, Naudie D, Charron KD, Yuan X, Holdsworth DW. The next generation of acetabular shell design and bearing surfaces. *Orthopedics*, ,31 (12 Suppl 2) (2008)
123. Zardiackas, L.D., Parsell, D.E., Dillon, L.D., Mitchell, D.W., Nunnery, L.A., Poggie, R.: Structure, metallurgy, and mechanical properties of a porous tantalum foam. *J. Biomed. Mater. Res.* **58**(2), 180–187 (2001)
124. Hacking, S.A., Bobyn, J.D., Toh, K., Tanzer, M., Krygier, J.J.: Fibrous tissue ingrowth and attachment to porous tantalum. *J. Biomed. Mater. Res.* **52**(4), 631–638 (2000)
125. Levine, B.: A new era in porous metals: Applications in orthopaedics. *Adv. Eng. Mater.* **10**(9), 788–792 (2008)
126. Gordon, W.J., Conzemius, M.G., Birdsall, E., et al.: Chondroconductive potential of tantalum trabecular metal. *J. Biomed. Mater. Res. B Appl. Biomater.* **75**(2), 229–233 (2005)
127. Mardones, R.M., Reinholz, G.G., Fitzsimmons, J.S., et al.: Development of a biologic prosthetic composite for cartilage repair. *Tissue Eng.* **11**(9–10), 1368–1378 (2005)
128. Paprosky, W.G., O'Rourke, M., Sporer, S.M.: The treatment of acetabular bone defects with an associated pelvic discontinuity. *Clin. Orthop. Relat. Res.* **441**, 216–220 (2005)
129. Paprosky, W.G., Sporer, S.S., Murphy, B.P.: Addressing severe bone deficiency: What a cage will not do. *J. Arthroplasty* **22**(4 Suppl 1), 111–115 (2007)
130. Sporer, S.M., O'Rourke, M., Paprosky, W.G.: The treatment of pelvic discontinuity during acetabular revision. *J. Arthroplasty* **20**(4), 79–84 (2005). Suppl 2
131. Weeden, S.H., Schmidt, R.H.: The use of tantalum porous metal implants for Paprosky 3A and 3B defects. *J. Arthroplasty* **22**(6 Suppl 2), 151–155 (2007)
132. Lewis RJ, O'Keefe TJ, Unger AS. A monoblock trabecular metal acetabulum; two to five year results. 70th AAOS Annual Meeting. Dallas, TX (2005)
133. Gruen, T.A., Poggie, R.A., Lewallen, D.G., et al.: Radiographic evaluation of a monoblock acetabular component: A multicenter study with 2- to 5-year results. *J. Arthroplasty* **20**(3), 369–378 (2005)
134. Bargiotas K, Konstantinos M, Karachalios T, Hantes M, Varitimidis SE. Total Hip Arthroplasty using trabecular metal acetabular component: middle term results. 72nd Annual AAOS Meeting. Washington, DC (2005)
135. Moen, T.C., Ghate, R., Salaz, N., Ghodasra, J., Stulberg, S.D.: A monoblock porous tantalum acetabular cup has no osteolysis on CT at 10 years. *Clin. Orthop. Relat. Res.* **469**(2), 382–386 (2011)
136. Nakashima Y, Mashima N, Imai H, et al. Clinical and radiographic evaluation of total hip arthroplasties using porous tantalum modular acetabular components: 5-year follow-up of clinical trial. *Modern rheumatology/the Japan Rheumatism Association.* Mar 7 (2012)

137. Sporer S, Paprosky W. Acetabular revision using a trabecular metal acetabular component for severe acetabular bone loss associated with a pelvic discontinuity. 15th Annual AAHKS Meeting. Dallas, TX (2005)
138. Sporer, S.M., Paprosky, W.G.: Acetabular revision using a trabecular metal acetabular component for severe acetabular bone loss associated with a pelvic discontinuity. *J. Arthroplasty* **21**(6 Suppl 2), 87–90 (2006)
139. Mardones R, Talac R, Hanssen A, Lewallen DG. Use of a porous tantalum revision shell in revision total hip arthroplasty. 72nd Annual AAOS Meeting. Dallas, TX (2005)
140. Bobyn JD, Poggie RA, Krygier JJ, et al. Clinical validation of a structural porous tantalum biomaterial for adult reconstruction. *J Bone Joint Surg Am*, **86-A** Suppl 2, 123–129 (2004)
141. Malkani AL, Crawford C, Baker D. Acetabular component revision using a trabecular metal implant. 72nd Annual AAOS Meeting. Washington, DC (2005)
142. Radnay, C.S., Scuderi, G.R.: Management of bone loss: Augments, cones, offset stems. *Clin. Orthop. Relat. Res.* **446**, 83–92 (2006)
143. Stulberg SD. The use of porous tantalum components in revision tka—A five year follow-up study. 71st AAOS Annual Meeting. San Francisco, CA (2004)
144. Nelson, C.L., Lonner, J.H., Lahiji, A., Kim, J., Lotke, P.A.: Use of a trabecular metal patella for marked patella bone loss during revision total knee arthroplasty. *J. Arthroplasty* **18**(7 Suppl 1), 37–41 (2003)
145. Shuler, M.S., Rooks, M.D., Roberson, J.R.: Porous tantalum implant in early osteonecrosis of the hip: preliminary report on operative, survival, and outcomes results. *J. Arthroplasty* **22**(1), 26–31 (2007)
146. Tsao, A.K., Roberson, J.R., Christie, M.J., et al.: Biomechanical and clinical evaluations of a porous tantalum implant for the treatment of early-stage osteonecrosis. *J. Bone Joint Surg. Am.* **87**(Suppl 2), 22–27 (2005)
147. Fung, D.A., Frey, S., Menkowitz, M., Mark, A.: Subtrochanteric fracture in a patient with trabecular metal osteonecrosis intervention implant. *Orthopedics* **31**(6), 614 (2008)
148. Pandit H, Glyn-Jones S, McLardy-Smith P, et al. Pseudotumours associated with metal-on-metal hip resurfacings. *The Journal of bone and joint surgery. British volume*, **90**(7), 847–851, (2008)
149. Hallab N, Merritt K, Jacobs JJ. Metal sensitivity in patients with orthopaedic implants. *The Journal of bone and joint surgery. American volume*, 001, **83-A**(3), 428–436 (2001)
150. Hallab, N.J., Mikecz, K., Vermes, C., Skipor, A., Jacobs, J.J.: Orthopaedic implant related metal toxicity in terms of human lymphocyte reactivity to metal-protein complexes produced from cobalt-base and titanium-base implant alloy degradation. *Mol. Cell. Biochem.* **222**(1–2), 127–136 (2001)
151. Jacobs, J.J., Skipor, A.K., Campbell, P.A., Hallab, N.J., Urban, R.M., Amstutz, H.C.: Can metal levels be used to monitor metal-on-metal hip arthroplasties? *The Journal of arthroplasty* **19**(8), 59–65 (2004). Suppl 3
152. Savarino, L., Granchi, D., Ciapetti, G., et al.: Effects of metal ions on white blood cells of patients with failed total joint arthroplasties. *J. Biomed. Mater. Res.* **47**(4), 543–550 (1999)
153. Jacobs JJ, Skipor AK, Doorn PF, et al. Cobalt and chromium concentrations in patients with metal on metal total hip replacements. *Clinical orthopaedics and related research* (329 Suppl), S256–263 (1996)
154. Antoniou J, Zukor DJ, Mwale F, Minarik W, Petit A, Huk OL. Metal ion levels in the blood of patients after hip resurfacing: a comparison between twenty-eight and thirty-six-millimeter-head metal-on-metal prostheses. *The Journal of bone and joint surgery. American volume*, **90**, 142–148 (2008), Suppl 3
155. Bernstein M, Desy NM, Petit A, Zukor DJ, Huk OL, Antoniou J. Long-term follow-up and metal ion trend of patients with metal-on-metal total hip arthroplasty. *International orthopaedics*. Jun 9 (2012)
156. Nikolaou, V.S., Petit, A., Debiparshad, K., Huk, O.L., Zukor, D.J., Antoniou, J.: Metal-on-metal total hip arthroplasty—five- to 11-year follow-up. *Bulletin of the NYU hospital for joint diseases* **69**(Suppl 1), S77–S83 (2011)

157. Tkaczyk, C., Petit, A., Antoniou, J., Zukor, D.J., Tabrizian, M., Huk, O.L.: Significance of elevated blood metal ion levels in patients with metal-on-metal prostheses: An evaluation of oxidative stress markers. *The Open Orthopaedics Journal* **4**, 221–227 (2010)
158. Bernstein, M., Walsh, A., Petit, A., Zukor, D.J., Huk, O.L., Antoniou, J.: Femoral head size does not affect ion values in metal-on-metal total hips. *Clin. Orthop. Relat. Res.* **469**(6), 1642–1650 (2011)

Chapter 4

Biofunctional Coatings for Dental Implants

Xi Chen, Yuping Li and Conrado Aparicio

Abstract Success of dental implant materials depends on their integration into the adjacent soft and hard tissues where critical interactions take place at the interface between the surface of the metal and the biological components. The properties of the dental implant surface, such as surface morphology, surface energy, and chemistry affect cell responses and tissue regeneration. Therefore, modifications of the surfaces of the implant to minimize the nonspecific adsorption of proteins and to mediate bone osseointegration and tissue healing are research subjects of major interest. One promising approach consists of functionalizing dental implant materials by incorporating biological molecules with known bioactivities. Bioactive components such as extracellular matrix proteins, growth factors, and peptides have been covalently immobilized on surfaces to investigate their potential benefit in the clinical success of dental implants. The immobilization by means of primary bonds between the surface and the biomolecules can enhance stability and retention of the biomolecules on the implant and preserve biological activity compared to physically adsorbed molecules. We introduce here methodologies to covalently anchor biomolecules on the surface of dental implants. We thoroughly review the chemical strategies and biomolecules used as well as their effects on different biological responses of interest, such as osteoblasts response to improve osseointegration, antimicrobial properties, and in vivo integration. The stable immobilization of biomolecules on implants to form a bioactive surface can be an effective and novel approach to achieve implantation success in all clinical scenarios.

X. Chen · Y. Li · C. Aparicio (✉)

MDRCBB—Minnesota Dental Research Center for Biomaterials and Biomechanics,
Department of Restorative Sciences, School of Dentistry, 16-250a Moos Health Science
Tower, 515 Delaware St. S.E, Minneapolis 55455, USA
e-mail: apari003@umn.edu

4.1 Introduction

4.1.1 *Need for Improving Surface Properties of Dental Implants*

Commercially pure titanium (c.p. Ti) is the dominant material for making dental implants because it is biocompatible by combining very high corrosion resistance in contact with biological fluids and appropriate mechanical properties, namely high strength, high fracture toughness, and relatively low modulus of elasticity [1, 2]. In the last three decades, titanium dental implants have become successful for the replacement of teeth lost due to decay, trauma or disease. Generally, more than 90 % of implant success rates are achieved after 10–15 years of implantation [3, 4]. The most important factor for dental implant success is the osseointegration of the metallic device; i.e., the formation of a strong and long-lasting connection between the implant surface and the peri-implant bone that results in a stable mechanical fixation of the implant in the bone bed [5].

In spite of the high rate of dental implant success, surface modification of implants remains a very active area of research [6–8] as titanium is a bioinert material with passive interactions with the biological environment. Titanium does not trigger any specific positive reactions in the surrounding biological environment to improve the process of bone healing [9]. As a result, implants get osseointegrated following an osseoconductive process that ends up with a successful performance that entirely relies in mechanical considerations. However, the process of osseointegration is also fully dependent on the biological interactions at the metal surface. The process starts with wetting of the surface and rapid adsorption of biologically active molecules, and follows with recruitment of osseoprogenitor cells that finally orchestrate the regeneration of the tissue [10] and facilitates the reduction of the foreign body reaction [11, 12].

All of those biological interactions can hence be conditioned by the properties of the implant surface and thus, implants have room for improvement as:

- Under healthy conditions the process of bone regeneration is very slow and is far from allowing early or immediate loading of implants [13]. That has significant implications in terms of reduced patient morbidity and health care costs [14].
- It is counter indicated to place these implants in patients that present compromised clinical scenarios (in elderly, smokers, traumatic damage, systemic diseases) [15] and
- Infection of the surface of implants may result in short or long-term failure of the implants in place [6].

Surface modification of titanium dental implants in order to enhance its osseointegration, peri-implant bone regeneration, and/or antimicrobial properties includes several approaches and techniques (Fig. 4.1). Among them, the most traditional surface treatments to modify topography at the micro and nanoscale, to

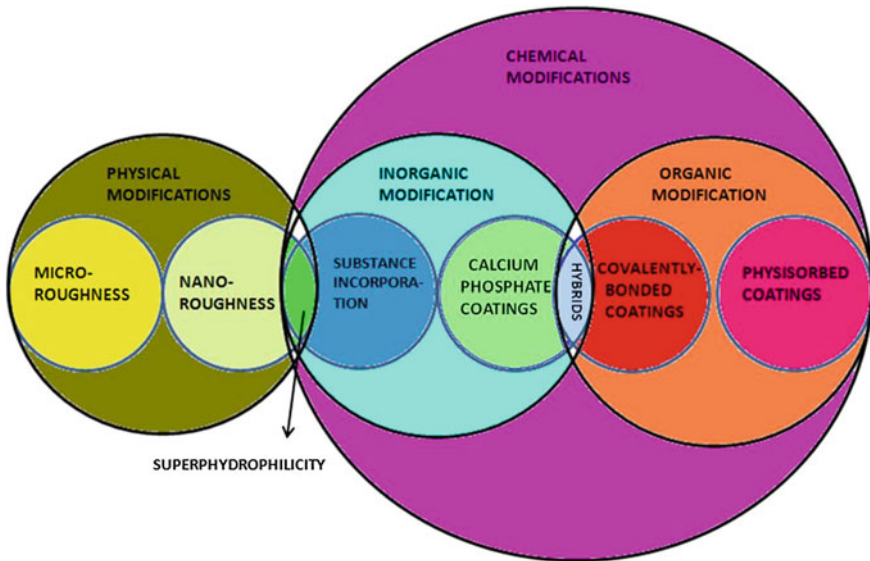


Fig. 4.1 Classification of strategies to modify or coat titanium surfaces to improve clinical performance of dental implants

increase hydrophilicity, or to obtain inorganic coatings made of calcium phosphates not only are still actively investigated but have found already room in the market. Those are briefly presented in the next section of this introduction.

4.1.2 Traditional Approaches to Modify Dental Implant Surfaces

The increase of surface micro-roughness was the first attempt to improve osseointegration with the rationale that direct contact of rough implants with newly-formed bone would result in higher micromechanical retention than a smooth or as-machined implant. As a matter of fact, this has been proved to be a successful approach, and implant surface topography is nowadays modified in commercially available products [7, 8] by chemical etching [16], by grit-blasting [17], by plasma-spraying titanium coatings [18], by electrochemical processes with different solutions [19], or by a combination of some of them [20]. Later, intensive and prolific research assessed other beneficial effects in the biological response to rough metallic surfaces, such as improved cellular attachment and osteoblast-like cell activity [21–23], selective protein adsorption, and collagen synthesis [24] as well as more intensive bone implant contact and higher mechanical retention than as-machined implants when implanted *in vivo* [12, 23, 25]. We concluded that $R_a = 4.5 \mu\text{m}$ was optimal for cell response and protein adsorption [26, 27], but

this is still a controversial subject [8] and nowadays most of dental implant systems have a microrough surface with values of $R_a = 1\text{--}5\ \mu\text{m}$.

More recently the exploration of the benefits of modifying the topography of metallic implants with nanofeatures with different size, distribution, and shape has become a hot topic of research [28, 29]. The simplest process to incorporate nanotopographical details to an implant surface is by etching titanium with a mixture of acids. Recent studies showed that surfaces with nanoscale features stimulate additional biological effects *in vitro* and *in vivo*, e.g., by producing an accelerating integration [30]. In fact, micro and nanorough surfaces have been recently used in some commercial products with good clinical results that, however, have not yet reached the clinical evidence stage [30, 31].

Increasing surface roughness influences other important physicochemical properties. For instance, it increases surface energy, which has a strong impact on the interactions of the metal with the surrounding biological system [32]. Of current clinical interest is the development of metallic surfaces that have high surface energy with superhydrophilic properties. Those surfaces are obtained by a process that delivers a metallic surface permanently free of hydrocarbons, which are hydrophobic in nature and that otherwise can be readily adsorbed on the titanium surface. The resulting superhydrophilic surfaces have been claimed to accelerate early processes of bone healing [33] as fibronectin, osteocalcin, and growth factors are preferentially adsorbed on them, thereby favoring bone growth right at the surface of the implant [34]. Other approaches to increase surface energy and hydrophilicity of titanium that produced promising *in vitro* and *in vivo* outcomes have been recently developed, such as the use of ultraviolet irradiation [35].

Another group of traditional surface treatments for dental implants has focused on coating the surface of titanium with a layer of calcium-phosphates [7, 36] as none of the previously introduced surface treatments change the intrinsic bioinert chemical characteristics of the titanium surfaces and are limited in their ability to accelerate and improve osseointegration. The deposition of bioactive calcium-phosphate minerals, such as apatite, can enhance implant performance at an early stage after implantation by an osseoinductive process of regeneration around the implant. This is because the biological nature of apatites, which represent the mineral phase in bone, have the potential to actively signal the cells that interrogate the surface after implantation.

A first generation of thick coatings applied on titanium dental implants by a plasma-sprayed or electrodeposition processes showed that response [37]. But later, it was also demonstrated that the chemical and structural heterogeneity of the layers obtained resulted in heterogeneous degradation of the layer and eventually mechanical failure and delamination [38]. As a result of the process of degradation, *in vivo* reactivity of delaminated fragments from the calcium-phosphate layer resulted in adverse tissue reactions and failure of the implants at mid- and long-term after implantation [39].

To avoid the problems of the thick calcium-phosphate layers deposited by plasma-spray at high temperatures, a series of new treatments to obtain thin layers at room temperature using biomimetically-inspired processes was published

during the 1990s [40–44]. The traditional biomimetic treatments for obtaining a bioactive layer of calcium-phosphates are widely based on etching the surface of titanium to obtain a nanoporous, highly reactive, and strongly negatively charged surface. In some cases the etched surface is thermally treated to mechanically stabilize the oxides formed [45]. Then, the treated surface is immersed at 37 °C in a solution with controlled supersaturation levels of calcium and phosphate, such as Kokubo’s Simulated Body Fluid (SBF) [46]. As a result of a cascade of ionic and electrostatic interactions between SBF and the surface, the local pH at the surface increases and thus, the relative supersaturation of the solution with respect to apatite increases. That triggers a sequential electrostatic attraction of calcium and phosphate ions to the metallic surface and precipitation of a continuous coating of carbonated apatite that is strongly bonded to the metal [47]. One important consideration is that, as described, the surfaces can be coated with apatite by immersion in SBF before implantation, but the etched surface implanted *in vivo* is also able to induce the formation of the apatite layer and thus, it is potentially bioactive [48].

As a further step, we developed a new surface treatment, *2Step*, for titanium dental implants that combines microroughness and potential bioactivity by first, grit blasting, and second, alkaline etching and thermally treating the implant surface. We demonstrated the potential bioactivity of the *2Step* surfaces [49] by growing *in vitro* HA layers in SBF and assessing that the preferential nucleation of apatite crystals took place on the bottom of the microrough features. This phenomenon accelerated the *in vitro* formation of the apatite layer in comparison to smooth surfaces with the same chemical treatment. Those implant surfaces were also tested to prove that they induce preferential differentiation of MG63 cells into the osteoblastic lineage [50]. We recently concluded that the *2Step* implants accelerated bone tissue regeneration and increased mechanical retention in mandible and maxilla of minipigs at short periods of implantation in comparison with microrough, HF-etched, and as-machined titanium implants [48]. This was mostly attributed to the ability of *2Step* implants to form *in vivo* a layer of apatitic mineral that coated the implant and could rapidly stimulate (1) bone nucleation directly on the implant surface; and (2) bone growth from the implant surface (Fig. 4.2).

4.2 Functionalization of Dental Implants with Biochemical Coatings

Currently, surface modification of dental implants using biochemical methods bring an attractive new approach to promote implant success as it aims inducing specific cell and tissue responses using critical biological components (Fig. 4.3). The regeneration of bone highly depends on the communication between cells and extracellular matrix components. Thus, the extracellular matrix proteins and its components, growth factors and bone morphogenetic proteins govern various key

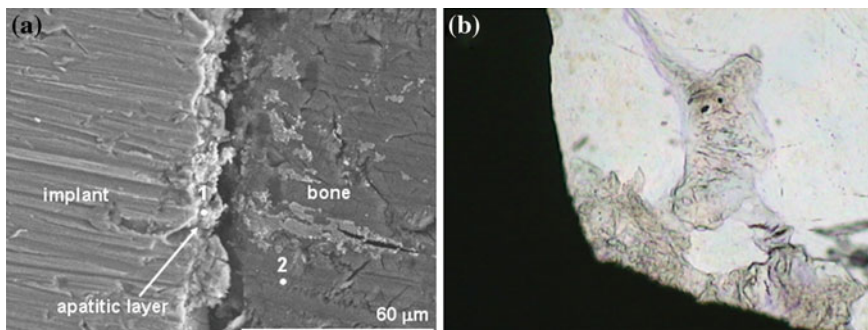


Fig. 4.2 **a** SEM picture of the interface between a 2Step implant and bone after 10 weeks of implantation. The image shows the presence of an apatitic layer on top of the 2Step cpTi implant. Locations used for microprobe chemical analysis on the apatitic layer (point 1) and bone (point 2) had Ca/P molar ratio of 1.70 and 1.66, respectively; **b** Representative histology ($\times 80$) of a 2Step dental implant after 2 weeks of implantation showing the growth of immature bone from the surface of the implant and that nucleated on top of the surface. Reproduced with permission from [48]

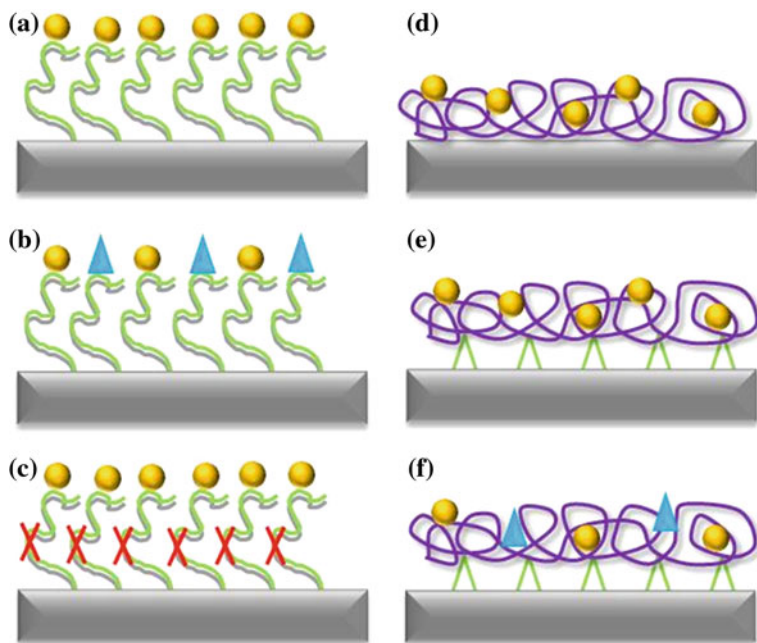


Fig. 4.3 Different approaches to coat titanium dental implants with bioactive peptides and proteins. **a** Covalently-bonded peptides with one bioactive signal (o); **b** Co-immobilization of peptides with multiple bioactivities (o, Δ); **c** Immobilization of peptides incorporating an enzyme-cleavable motif (X); **d** Physical adsorption of proteins; **e** Covalently-bonded proteins with one bioactive signal (o); **f** Covalently-bonded proteins with multiple bioactivities (o, Δ)

biological events, including cell adhesion, proliferation and differentiation. Immobilization of bioactive molecules on the surface of the implant potentially provides control over the tissue implant interface with further improvement of cell communication; tissue and bone repair.

These approaches depend on key factors for being effective on displaying biomolecules on the surface of a dental implant and retaining the molecular bioactivity. The specific chemistry used to retain the molecule on the surface and the selection and further modification of the biomolecule to also favor chemical and mechanical stability of the coating are among the most important ones. The rest of this chapter thoroughly reviews the newest strategies based on stable functional coatings made of different biomolecules of interest.

4.2.1 Methods for Immobilizing Biomolecules on Implant Surfaces

The methods for surface modification of biomaterials with biomolecules are not only an alternative to physicochemical and morphological modification, but also a supplement to improve dental implant performance. Those methods are based on current understanding of the biology and biochemistry of cellular function and differentiation, especially on lessons learned from the mechanisms of cells adherent to substrates [51] and the role of biomolecules in regulating cell differentiation and remodeling of tissues. The goal of biological surface modification is to immobilize proteins, peptides and polysaccharides on biomaterials to induce specific cell and tissue response [14] as well as minimize the unspecific adsorption of tissue fluid proteins [52]. The display of those molecules on the surface of dental implants should enhance peri-implant bone healing and/or prevent bacteria colonization of the surface [6].

To design a methodology to decorate the surface of a dental implant with biomolecules there are two main factors to be considered to improve their clinical performance: (1) the temporal stability of the bioactive molecules presented at the implant-tissue interface; and (2) the density and accessibility of the bioactive sites. Cells need to interact with the implant for a certain period of time to initiate cellular events, implying the biomolecules must be stable at the interface during that period. The concentration of the bioactive molecules must be above threshold levels to successfully induce the targeted cellular activity [53].

There are three main methods for surface immobilization of biomolecules [54] that have been extensively studied for coating surfaces for dental implant applications. The simplest one is by physical absorption of the organic molecules onto the surface, which can be achieved by immersing the substrate into a solution of the bioactive molecule. Another method consists of embedding the biomolecules into a bioresorbable material that is used for coating the implant surface. The third

method, which is the focus of this chapter relies on directly conjugate the biomolecules to the surface by covalent bonding or molecular self-assembly.

The simplicity of physical adsorption of biomolecules on the implant surface is the most attractive characteristic of this strategy. However, the physical adsorption method provides little control over both the density and the retention with time of the biomolecules on the surface. As the microenvironment around the implant changes during its time of application and the attachment of the molecules depends on secondary weak bonds—hydrogen bonds, electrostatic attraction, etc., the adsorbed molecules on the implant surface can be easily detached from the surface by desorption or displacement by other molecules. Thus, the surface can rapidly lose their bioactive properties. That makes this method far from ideal to fabricate a stable and long lasting coating. Others have proved that titanium surfaces coated with physically-adsorbed bone morphogenic protein lost 96 % of their bioactivity after the first hours in contact with biological fluids [55]. Moreover, this method can not precisely control the surface density and/or orientation of the molecules, which are vital for regulating the interactions of the implant with the biological agents—proteins, cells, tissues. The conformation of the biomolecules can also change during time and thus, lose their bioactivity [56].

Alternatively, covalently bonding biomolecules to implant surfaces provides coatings that are more stable and more resistant to disruption not only under harsh physiological conditions but also during fabrication of the coating and implantation at the time of the surgery. Overall, this can help for preserving the biological activity of the bound biomolecules [57].

The covalent bonding of the biomolecules also provides the potential to control their density and orientation, e.g., aligning and/or exposing the appropriate active sites at the interface, and thus provoking a more specific and rapid host reaction [58, 59]. The way the orientation and density of the immobilized molecules can be controlled depends on:

- the characteristics of the metallic substrate, in this case the nature of the passivating titanium oxide that naturally covers the surface and that provides plenty of hydroxyl groups under adequate fabrication conditions. Functional groups such as amino, carboxyl, and thiol can also be deposited on metallic surfaces by plasma treatment [60], by photo-initiated polymerization, by chemical etching [59], or by ion beam etching [61], which could be further used to attach biomolecules.
- the chemistry/molecule used as a linker between the surface and the biomolecule, which in some cases incorporates additional properties—hydrophobicity, electrostatic charges, etc.
- the design/modification of the biomolecule to be anchored, which in many cases includes additional chemical groups to physically separate the biomolecule from the coated surface and thus, facilitating the access of the cells to the bioactive cues.

The rest of this section presents the chemical strategies—functional groups and molecular linkers—that have been mostly used to functionalize titanium with active molecules for dental applications. The next section thoroughly reviews the biomolecules that have been investigated with strategies for designing more specific and effective bioactive coatings and, hence, the main applications of those coatings are also introduced.

4.2.2 Coupling of Biomolecules with Silane Agents

Silane coupling agents have been used to anchor peptides, enzymes and adhesive proteins on different biomaterials, such as Ti, NiTi, Ti-6Al-4V and Co-Cr-Mo [59, 62–65]. Covalent anchoring of biomolecules by silane chemistry is a simple and versatile method to modify surface properties. Silane coupling agents with different end functional groups are attached via reaction with the oxidized metal surface, which is activated to display reactive groups. The functional groups of the silane molecule at the opposite end are used to couple the bioactive molecules, either directly or via a cross-linker molecule. Generally, the process of silanization with biomolecules can be grouped into four types of directed reactions, namely thiol-, amino-, carboxyl-, and chloro- (Fig. 4.4) according to the functional end group in the silane molecule. The selection of the chemical group is based on the active residues of the biomolecules that are aimed to be used in the immobilization process. The ductile alkyl spacers on silane agents; i.e., the central part of the molecule can partially absorb the biomaterial-tissue interfacial stresses and may be also used to appropriately orientate and expose the bioactive molecules at the biomaterial interface in an arrangement to induce the desired tissue responses. Additionally, the alkyl spacer can also be used to adjust the hydrophobic properties of the final coating [66].

Silanes with different terminal functionalities deposited on model substrates such as gold can form stable self-assembled monolayers (SAMs), but the

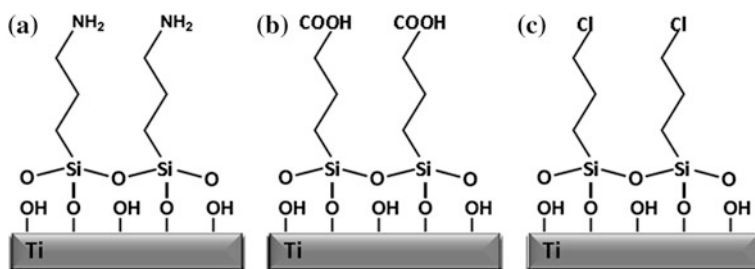


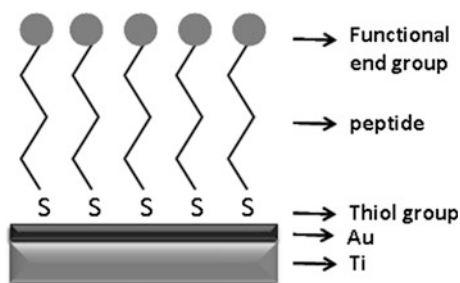
Fig. 4.4 Silane coupling agents with different functional end groups: **a** amine-, **b** carboxyl-, **c** chloro- that have been used to covalently-anchor biological molecules on Ti surfaces using appropriate chemistry and, in some cases, specific design of the biofunctional molecules

formation of SAMs on imperfect surfaces of polycrystalline metals such as dental implants, has proved to be a more difficult task. To graft silane agents to polycrystalline metal oxides the surface of the metal is first activated to form hydroxyl groups. Etching or plasma treatment of the titanium surface are often used to that purpose. Then hydrolysis of the alkoxy groups of the silane followed by condensation of the surface hydroxyls with the formed silanols at the silane molecules occur. On the one hand, in hydrous conditions, hydrolysis of the alkoxy groups occur immediately in solution, provoking condensation between silanols before contacting with the metal surface and thus, resulting in an uncontrollable and inhomogeneous polymerized silane multilayer. On the other hand, in anhydrous conditions, hydrolysis and condensation only occur when the silane molecules directly contact with the H₂O layer adsorbed on the metal oxide surface. Consequently, the silane monomers polymerize before reaching the metal oxide surface, preventing the formation of a uniform silane layer on polycrystalline metal surfaces. Nevertheless, anhydrous silanization has been found to yield better coverage and higher stability of coupled silanes compared to hydrous silanization [67].

Conventional, well established, and commercially-exploited techniques for immobilization of biomolecules on synthetic substrates use carbodiimides and glutaraldehydes as linkers to anchor terminal amino groups of biomolecules to silane agents [59, 68], or maleimides to biomolecules with cysteinethiol groups [61, 69].

The titanium surface can be also modified by surface-initiated atom-transfer radical polymerization (ATRP) of vinyl monomers [70]. Atom transfer radical polymerization (ATRP) is a recently-developed conveniently-controlled radical polymerization method [71–73]. ATRP fabricates polymers with narrowly-dispersed molecular weights because the method allows for the polymerization and block copolymerization of a wide range of functional monomers in a controlled manner. In addition, the tolerance of ATRP to polar functionality allows the direct polymerization of functional monomers without protection and deprotection procedures. Functional monomers such as poly(ethylene glycol)methacrylate, (2-dimethylamino)-ethyl methacrylate, and 2-hydroxyethyl methacrylate as well as their block copolymers can be tethered on the titanium surface to form polymer brushes by first silane coupling the surface with an agent that contains the ATRP initiator. Through the transferring of the ATRP initiator, such as chloride, functional monomers can be anchored to the surface in desired amount and orientation. The surface initiated ATRP produce a polymer-coated titanium surface with well-controlled hydrophilicity/hydrophobicity [70] that can be converted into carboxyl or amine groups. Those groups can then be further used to immobilize the target biomolecules, such as antibacterial agents or proteins of interest [74].

Fig. 4.5 Peptides with biofunctional end groups can be self-assembled on Au-coated titanium surfaces by incorporating thiol groups to covalently interact with the gold coating



4.2.3 Coupling of Biomolecules with Thiols Forming Self-Assembled Monolayers

Titanium can be coated with a thin layer of gold to further introduce alkanethiols coupling agents to the metal surface. Gold surfaces are not toxic to living cells and biocompatible with conditions used for cell culture. Covalent binding of thiols on gold surfaces is a simple and cost efficient method for surface modification [75]. Peptides with terminal cysteine groups can be covalently bonded to gold through the thiol groups of cysteine to form monolayers (Fig. 4.5).

Recently, self-assembled monolayers of alkane phosphates or phosphonates have been used on titanium or titanium alloy surfaces via reaction of phosphonic acids with their native oxides [76]. However, the harsh conditions needed, such as the use of anhydrous organic solvents and high temperatures might not be compatible with the stability of the biomolecules. The use of bisphosphonic acids with greater affinity to titanium surface to form monolayers on titanium has been also reported [77], as it requires less harsh conditions to be incorporated on the metallic surface.

4.2.4 Coupling of Biomolecules Using Tresyl Chloride Activation

Immobilizing biomolecules to various hydroxyl groups by using highly reactive sulfonyl chlorides, such as 2,2,2-trifluoroethanesulfonyl chloride (tresyl chloride) has been reported [78]. This process involves casting the tresyl chloride solution on the titanium substrate for two days followed by protein immobilization through the interaction between the amino groups of the protein and the tresyl chloride activated hydroxyl groups on the titanium surface.

4.2.5 Use of Spacer Assistant for Coupling Biomolecules

The non-treated titanium surfaces and most of the ones coated with biomolecules following the aforementioned methods lack the property of resisting unspecific protein adsorption from the biological medium. The massive uncontrolled adsorption of proteins from the medium can form an effective barrier on the metal surface that may hinder the desired interactions between the bioactive molecules and cells during the process of healing and tissue regeneration. One effective way to minimize unspecific protein adsorption onto titanium surfaces that has been now vastly investigated is the use of a poly (L-lysine)-graft-poly (ethylene glycol) (PLL-g-PEG) molecules in an assembly on the surface of the biomaterial mediated by electrostatic attractions [79–81]. Once the titanium surface is coated with PLL-g-PEG, the biomolecules can be covalently attached via vinyl sulfone-cysteine coupling reaction to the PEG side chains [82]. The result is a coating that blocks non-specific protein adsorption while promoting appropriate cell interactions.

4.2.6 Oligonucleotide Mediated Immobilization of Biomolecules

A novel and recently developed method for surface modification of titanium and titanium alloys is based on the immobilization of bioactive molecules using electrochemically fixed nucleic acids [83, 84]. In this method, the first step is the regioselectively adsorption of nucleic acid single strands on the air-formed passive layer of titanium alloys via 5'-terminally phosphorylated sites. Adsorption is followed by anodic polarization during which the single stranded nucleic acids; i.e., the anchor strands are entrapped and fixed on the titanium oxide layer by partial incorporation. The next step is the hybridization of the anchor strands with complementary strands that will be further conjugated with bioactive molecules.

This method, as a difference to all previously introduced, does not use an additional chemical agent for surface modification and thus, it is free from potential hazards that those synthetic linkers pose when applied in vivo. In addition, the release behavior of the bioactive molecules can be controlled by adjusting the hybrid stability. The successful use of this method for anchoring osteogenic growth factors on titanium and their slow release from the surfaces has been reported and positively compared to physically adsorbed biomolecules [85].

4.3 Biomolecules to Coat Titanium for Improving the Clinical Performance of Dental Implants

There is a debate on whether using short synthetic peptides or long chain extracellular matrix (ECM) proteins is the best approach for designing biomaterials that guide cell response for tissue engineering and regenerative medicine (Fig. 4.3). The ECM of bone, which is synthesized, deposited and mineralized by osteoblasts, consists of 90 % collagenous proteins (type I collagen 97 % and type V collagen 3 %) and 10 % non-collagenous proteins (osteocalcin, osteonectin, bone sialoproteins, proteoglycans, osteopontin, fibronectin, growth factors, etc.) [86]. ECM proteins mediate cell response—adhesion, proliferation and differentiation. Peptides are the functional motifs in ECM proteins which have specific bioactive functions, such as recognizing corresponding integrins on the cell membrane and thus, attach to them. Both ECM proteins [87–89] and short peptides [90–92] were proved to be effective in enhancing cell performance after being used to coat the surface of biomaterials. Both have advantages and disadvantages from both, the biological and chemical point of view.

The most advantageous property of peptides is that they are small and chemically defined [93], which implies that they can be easily synthesized, modified or reconstructed. By using techniques such as solid phase peptide synthesis (SPPS), peptides of up to 30–50 aminoacids can be routinely prepared with good yields [94]. Peptides with diverse functions, such as cell adhesion induction, enzyme-controlled, or antimicrobial properties can be precisely conjugated to biomaterial surfaces comparing with large molecules, such as proteins. Also, non-native chemistries and functional groups can also be conveniently incorporated in the peptide sequence with no much difficulty [93]. However, the short length of peptides limits their ability to selectively acquire the most desired conformation to achieve their bio-function. Also, although they might be retained in higher amounts than proteins and other larger biomolecules, the achievement of full coverage of the surface is challenging. Thus, they can be readily cleaved from the surface by proteases unless specific strategies, such as some of the ones introduced below, that aim to overcome this drawback are used to immobilize them.

Proteins have the main advantage that they carry the whole biochemical information needed for retaining the desired conformation and multiple biofunctions and not just part of it, as it is the case for short peptides. For instance, SPARC contains both hydroxyapatite bonding sequence (glutamic acid-rich sequence) and plasmin cleavable sequences; and bone sialoprotein possesses both hydroxyapatite bonding domain and cell recruitment domain. Therefore, ECM proteins have the intrinsic potential of contributing to multi-functionalization of titanium surfaces. However, most of the aforementioned advantages for the use of peptides are significant hurdles for the ease of use and appropriate performance of macromolecules attached to titanium surfaces as ECM proteins are difficult to be reconstructed, synthesized, and modified. Additionally, proteins from animal origin raise concerns about infection and immunological undesired reactions, which

requires significant attention and expenses to be highly purified [93]. The alternative recombinant synthesis is a high-investment and expensive methodology for producing these same molecules.

4.3.1 Peptides

4.3.1.1 Peptides to Enhance Cell Recruitment

RGD-Containing Peptides

Extracellular matrix governs various cellular events of cells, including cell adhesion, proliferation and differentiation [95]. A heterodimeric cell membrane receptor family known as integrins is involved in cell adhesion to extracellular matrix proteins [96] by interacting with short amino acid sequences present in molecules of the ECM. Especially, the RGD (Arginine-Glycine-Aspartate) amino acid sequence is identified as a key mediator of cell adhesion through interaction with integrins at the cell membrane [97]. RGD peptide is found in most ECM molecules including fibronectin, vitronectin, type I collagen, osteopontin and bone sialoprotein [98]. Thus, synthetic peptides that contain the RGD amino acid sequence can induce and thus, enhance cell attachment [91]. Covalently immobilized peptides with RGD sequences to implant surfaces has been recognized as a strategy for enhancing cell interaction with implants [69] and is the most used one in the category of coatings with biological molecules.

The RGD cell-adhesive sequences derived from fibronectin have been widely investigated. It has reported that the binding ability of fibronectin to cells can be due to the tetrapeptide L-arginyl-glycyl-L-aspartyl-L-serine (RGDS), a sequence which is a part of the cell adhesion domain of fibronectin [91]. Synthetic peptides containing GRGDSP (glycine-arginine-glycine-aspartate-serine-proline) can regulate cell attachment activity of the parent molecule [99] and have been used to modify the surface of titanium with enhanced cell attachment. However, these biomimetic strategies yielded only marginal enhancement in tissue healing in vivo.

Peptides with RGD motifs and sequences containing GRGDSP derived from human vitronectin are known to affect osteoblast adhesion by activating $\alpha 2\beta 1$, $\alpha 1\beta 1$, $\alpha v\beta 3$ and other integrins expressed on osteoblasts and osteoclasts [92]. Titanium alloy surfaces with immobilized RGD sequences displayed significantly increased levels of osteocalcin and pro-collagen I α 1 mRNAs, compared with the untreated Ti6Al4 V.

RGD-containing peptides derived from bone sialoprotein induced high cell adhesion strength [100]. A peptide with 15 amino acids having an RGD sequence which is unique to bone sialoprotein was linked to amino functionalized surfaces. The effects of the RGD-peptide on cell adhesion were compared with those induced by the arginine-glycine-glutamate (RGE) peptide. The cell detachment study using a radial flow apparatus showed that the RGD-grafted surface induced

significantly higher cell adhesion strength than the RGE-grafted surface. The cell contact area and focal contact patches on the periphery of the bone cells were considerably enhanced by the RGD-containing peptide surface as well.

Fibronectin type III 7th to 10th domain (FNIII7-10) attached to titanium surfaces using silanization and poly(oligo(ethylene glycol) methacrylate) polymerization was recently evaluated for in vitro osteoblastic cell differentiation and in vivo osseointegration [101]. Results demonstrated that $\alpha 5\beta 1$ -integrin-specific fibronectin fragment FNIII7-10-functionalized titanium improved implant osseointegration compared to RGD-functionalized and unmodified titanium. Moreover, bioactive peptides promoting integrin binding specificity regulated marrow-derived progenitor osteoblastic differentiation and enhanced healing response and integration.

Synergistic RGD and PHSRN Peptides

More recently, a Proline-Histidine-Serine-Arginine-Asparagine (PHSRN) sequence in the 9th type III repeating unit of fibronectin was found to have synergistic effect with RGD in improving cell adhesion. Many authors have demonstrated that multi-component peptide systems containing both RGD (the primary recognition site for $\alpha 5\beta 1$ integrin) and PHSRN (the synergistic site for $\alpha 5\beta 1$ integrins, in fibronectin 9th type III repeating unit) were more efficient in increasing cell adhesion, spreading, proliferation, and differentiation than the RGD peptide alone [102–107]. In the native conformation of fibronectin, RGD and PHSRN are spaced by approximately 40 aminoacids [103]. Therefore, the distance between PHSRN and RGD and the conformation of that part of the protein are important for the synergistic interaction of the two peptides. Ochsenhirt et al. [108] reported that the alternation of the concentration of RGD and PHSRN on the functionalized surface led to changes in the RGD-PHSRN distance and thus, influenced cell performance. They assessed that the distance which most closely mimicked the natural RGD-PHSRN distance significantly enhanced cell spreading. Vogel showed that small mechanical forces, in the range of tens of pN, can partially unfold fibronectin and change the RGD-PHSRN distance [109, 110]. A switch in integrin specificity from $\alpha 5\beta 1$ in non stretched status to $\alpha v\beta 3$ in stretched status was followed by this conformational change [109, 110]. In addition, structure, conformation, orientation and spatial distribution of RGD and PHSRN peptides are all important parameters in affecting the bioactivity of the modified surface.

Non RGD-Peptides

The triple-helical type I collagen-mimicking peptide with glycine-phenylalanine-hydroxyproline-glycine-glutamate-glycine-arginine (GFOGER) has been investigated by Reyes et al. [111]. Integrin $\alpha 2\beta 1$ can recognize the GFOGER motif in residues 502–508 of the $\alpha 1(I)$ chain of type I collagen. The adhesion of cells is

entirely dependent on the triple-helical conformation of the ligand in a similar way to what happens to native collagen. Results showed that immobilized peptides exhibited higher cell adhesion activity than physically adsorbed peptides. The GFOGER peptide promoted cell adhesion, mimicked the post-adhesion signaling characteristics of collagen surfaces that involves interaction with $\alpha_2\beta_1$ the integrins and further enhances cell differentiation.

The heparin-binding motif of human vitronectin precursor, phenylalanine-arginine-histidine-arginine-asparagine-arginine-lysine-tyrosine (FRHRNRKGY) was also investigated by being covalently immobilized on titanium surfaces [112]. Results demonstrated that FRHRNRKGY peptide preferentially promoted human osteoblast cell adhesion on the functionalized metal surfaces.

4.3.1.2 Peptides to Enhance Biomineralization

Osteoinductive surfaces that will produce osteogenesis around dental implants have been pursued to significantly improve their clinical performance. This is because it accelerates the process of osseointegration and can induce direct bonds between the surface of the implant and the newly-formed bone. The aforementioned inorganic coatings made of calcium-phosphates aim to do so by mimicking the extracellular matrix of bone in one of its components; i.e., its mineral phase. One further step to obtain biomimetic coatings incorporating calcium phosphates is the use of organic components known to have a role in ECM mineralization [113] to coat titanium surfaces and regulate nucleation and growth of the calcium-phosphates that form on the functionalized surface of the implant [65].

Benesch et al. reviewed proteins and corresponding peptides that have relevant roles in controlling biomineralization at different stages of tissue regeneration for different hard tissues in our body. Those are non-collagenous proteins that associate to collagen, which in its fibrillar assembly serves as a template for bone mineral nucleation and growth [114].

Osteopontin [115–117] and statherin [118–120] can inhibit mineral nucleation and growth by recognition of the mineral surface and adsorption on it. We have immobilized on titanium a recombinant molecule that contains the 15-aminoacid N-terminus peptide of the salivary protein statherin to take advantage of its affinity to calcium-phosphates [65]. We demonstrated that surfaces with the conjugated statherin-derived peptide were able to nucleate and control growth of calcium phosphate nanominerals and induced preferential differentiation of osteoblasts-like cells compared to non-coated surfaces and surfaces with physical adsorbed molecules.

Osteocalcin also inhibits nucleation and growth of apatite crystals in vitro, but considering its late appearance during bone formation, it might be important in bone remodeling [121, 122].

Glutamic acid rich sequences of osteonectin and, most significantly bone sialoprotein are responsible for improvement of mineralization [123, 124]. Sialoprotein is an effective apatite nucleator in vitro. The functional motifs in bone

sialoprotein are long sequences of glutamic acids –E4, E6 and E8–. Therefore, a highly negatively charged multi-Glutamic acid peptide sequence is supposed to be able to enhance surface mineralization and hence improve osteoblast differentiation.

4.3.1.3 Antibiotics and Antimicrobial Peptides

Infections are the most prevalent cause of failure for dental implants and orthopedic prosthesis. The inflammatory response to bacteria on the implant surface is called peri-implantitis, which may finally result in bone loss and implant failure. Peri-implantitis can happen immediately after oral surgery or months or years later. The literature has shown that peri-implantitis can affect up to 14 % of implants after 5 years; however, the relevant incidence may be higher due to poor clinical diagnosis and the short duration of reporting clinical studies [125]. The implant surface has a higher risk of infection comparing with natural tooth surface because it accumulates serum proteins which promote bacterial adherence and colonization faster. This is even more prone to happen on the current devices as they all incorporate microroughness surfaces that further facilitate bacteria attachment.

Existing approaches for surface modification of implants to reduce bacterial formation include the immobilization of antibiotics [126, 127]. Gentamicin have been loaded into nanotubes [128], poly (D,L-lactide) coating [129] or porous hydroxyapatite coatings [130] on titanium implants. The antibiotic-hydroxyapatite-coatings exhibited significant improvement in infection prevention [131]. Antibiotics have been normally physically adsorbed on titanium surfaces for ease of processing and prevention of degradation of the molecules that some fabrication methods would provoke; e.g., high temperatures when incorporated on plasma-sprayed hydroxyapatite coatings. The physical absorption process; however, limits the loaded amount and release characteristics of the drugs. Loading antibiotics in HA coatings, for example, led to 80–90 % of the total loaded drug being released during the first 60 min in contact with fluids [132, 133] and drugs loaded into nanotubes were fully released in 50–150 min [128]. Surfaces incorporating chlorhexidine [134], silver [135], poly lysine [136] and chitosan [137] have all been developed. Recently, Vancomycin has been successfully covalently-bonded to titanium and its antibacterial activity is retained even after incubation in PBS for at least 11 months [138–141]. Comparing with the non covalent coatings that quickly release antibiotics, covalently-bonded antibiotics remained active for notably longer periods.

Although antibiotics coated on titanium proved to be effective, their use is controversial because of their potential host cytotoxicity and bacterial resistance. For instance, Weber and Lautenbach [142] noted that 41 % of bacteria isolated postoperatively were resistant to gentamicin following the application of gentamicin-impregnated bone cement. Other investigations also showed drug resistance of bacteria isolated from orthopedic implants [143]. In addition, although

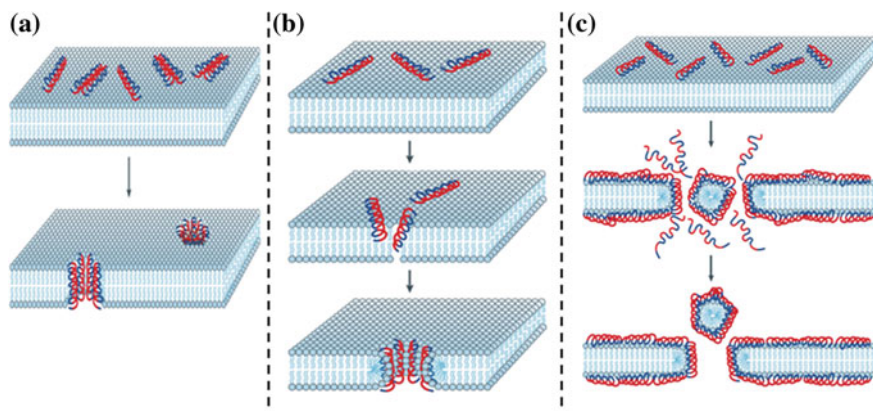


Fig. 4.6 Current models of the mechanism of antimicrobial induced-killing peptides; **a** Barrel-stave model; **b** Toroidal pore model; **c** Carpet model. Adapted with permission from [237]

antibiotics are normally thought to be biocompatible, their potential in inducing host cytotoxicity have been also widely reported [144–148].

The use of antimicrobial peptides (AMPs) have recently raised as an alternative antimicrobial approach with strong potential to improve dental implants performance when immobilized on titanium. Naturally, the bacterial flora in the oral cavity is mediated by the human innate immune system, which is rich in antimicrobial proteins and peptides [149, 150]. These AMPs can kill bacteria directly through membrane disruption, or act as immune modulators by enhancing bacteria clearance using our innate defense system [151] (Fig. 4.6). The advantages of using AMPs over antibiotics are 1) they are of human origin; hence, with potential low host cytotoxicity. This is still disputable because some reports showed that certain AMPs, such as LL-37, can freely translocate into cells and carry passenger molecules into their nuclei [152, 153]. More studies are needed to evaluate subtle toxicities of AMPs. 2) The co-evolution of AMPs with bacteria suggested low bacterial resistance. In addition, the immunomodulatory properties of AMPs would not be affected by antimicrobial resistance because of the irrelevance of direct bacteria killing. 3) The exceptionally broad activity of AMPs indicates that a single peptide can have activity against gram-negative and gram positive bacteria, fungi, and even viruses and parasites [151]. However, the disadvantage of AMPs involves the potential liability to proteases, which indicates the possibility of being proteolytically degraded by enzymes secreted by the microbial flora.

Over 45 AMPs with different antimicrobial mechanisms have already been identified from the human immune system, ranging from small cationic peptides to enzymes and large agglutinating proteins [149]. They may act as metal ion chelators, protease inhibitors, or promoters of enhanced bacterial agglutination [149].

A few AMPs are in current clinical use, such as polymyxin B, which is in clinical use for ophthalmic infections. But there are few reports regarding the application of AMPs on titanium surfaces to prevent peri-implant infection.

Kazemzadeh-Narbat et al. [154] used physically-adsorbed AMPs on micro-porous calcium-phosphate coated titanium surfaces and proved that had efficient antimicrobial activity and acceptable biocompatibility. However, again, physical adsorption of AMPs resulted in a rapid burst out of the agent from the surface, which quickly lost its antimicrobial ability. In addition, non-covalent coatings may develop a concentration gradient from the surface that would lead to the development of drug resistance as bacteria get the possibility of gradually respond to the antimicrobial challenge [155, 156]. Recently, the same research group built up a covalently anchored antimicrobial coating on titanium surfaces based on hydrophilic polymer brushes conjugated with the AMPs [157]. The hydrophilic polymer brushes were tethered on titanium using ATRP. The surfaces were maleimide functionalized, and cysteine modified AMPs were finally conjugated to the coatings. These tethered AMPs demonstrated excellent in vitro and in vivo antimicrobial activity with no toxicity to osteoblasts. We have also immobilized AMPs derived from the parotid secretory protein using silane chemistry. Our results proved the sustained antimicrobial activity of the AMPs, resistance to form bacteria biofilm, and appropriate cytocompatibility [158].

It is worth noting that AMPs may suffer conformational changes after being tethered on the surface. It has been previously suggested that soluble AMPs change their conformation when interacted with bacterial membrane and their subsequent incorporation is one mechanism for their antimicrobial activities [159, 160]. Gao et al. [157] confirmed this hypothesis by demonstrating the alteration of CD spectra of soluble AMPs after interacting with a modal bacterial lipid membrane. Most interestingly the unlikely soluble AMPs, such as polymer brush conjugated AMPs changed conformation to a substantially less degree. The spatial confinements of AMPs after being tethered could hinder their complete penetration into the bacterial membrane. Therefore, the induced disturbance to the bacteria membrane may trigger other cell death mechanisms that finally confer their antimicrobial effect.

4.3.1.4 Enzyme-Cleavable Peptides

The importance of proteolytic susceptibility of peptides relies on their ability of building up a degradable system conducted by enzyme secreted by cells. The degradation of coatings can trigger controlled release of important motifs that would add another level of sophistication to the coatings on dental implants. For example, many implant related infections occur not only as a consequence of the initial exposure during the surgery but also after a long time of implantation, from months to years, as bacteria enter into the body through the lungs or wounds and find the surface of the implant an ideal location to be colonized. A coating with controlled and sustained release of antimicrobial agents is an obvious improved system to work towards the long-term success of dental implants.

Biodegradable polymers, such as poly(lactic-*co*-glycolic acid) (PLGA), have been widely utilized as degradable carriers in drug delivery and the application of

antibiotics loaded on PLGA for periodontitis treatment have been also investigated [161–163]. PLGA degradation is mediated by hydrolysis and thus, with no specific control. On the contrary, given that most of enzymes are cell secreted, the release of antimicrobials mediated by enzyme-cleavable peptides is therefore “cell mediated”, in a process that simulates the natural degradation of the ECM.

Two main categories of proteolyzable peptides are matrix metalloproteases (MMP)-cleavable and plasmin-cleavable peptides [93]. MMP family are produced by plenty of cells such as activated inflammatory cells (neutrophils and macrophages), epithelial cells and fibroblasts. Besides, osteoclasts can secrete MMPs to degrade collagen and other components of the ECM of soft tissues, which is the main problem related to periodontitis. Therefore, with the continuous secretion of MMPs in the peri-implant environment by inflammatory cells in early implantation stages and osteoclasts in late bone formation stages, MMP-cleavable peptides are suitable candidates for antimicrobial agent controlled-release systems. Plasmin acts during wound healing to degrade provisional fibrin matrix generated during clot formation. It is secreted by blood endothelial cells and platelets. The wound healing process following implantation may activate plasmin in the peri-implant environment and thus, cleave suitable plasmin-cleavable peptides.

The most widely used MMP-cleavable peptides are GPQG↓IAGQ and GPQG↓IWGQ. GPQG↓IAGQ is the MMP substrate site found within the alpha chain of type I collagen, and GPQG↓IWGQ incorporates an amino acid substitution (A/W) to enhance enzymatic activity [164]. Other important peptides include VPMS↓MR and its modified VPMS↓MRG and VPMS↓MRGG sequences [93]. Patterson and Hubbell [165] used a combinatorial method of oriented peptide libraries to test degradation rate of 17 MMP sensitive amino acid sequences. They used GPQG↓IAGQ (GPQG↓IWGQ) as reference peptides, and they assessed different degradation times for all tested MMP sensitive sequences ranging from less than 2 days to more than 10 days when incubated with MMPs. When incubated with cells, EGTKKGHK was degraded after 26 days, which constituted the fastest time for degradation, whereas GPQG↓IAGQ took the longest time to be fully degraded. Therefore, proper selection of the MMP-cleavable peptide can be done according to the degradation time needed to optimize the antimicrobial delivery process. It is worth noting that 3D hydrogels incorporating the MMP-cleavable peptides with the fastest degradation times increased cell spreading and proliferation.

The most widely used plasmin-cleavable peptide is HPVE↓LLAR. This peptide is also sensitive to a number of MMPs (MMP-2, MMP-7, MMP-9 and MMP-13) [93]. Many of the plasmin-cleavable peptides are derived from secreted protein acidic rich in cysteine (SPARC). SPARC, also referred to as BM-40 or osteonectin, is a ECM protein that has been discovered to bind hydroxyapatite to type I collagen in bone. As a large protein with 4 domains, SPARC contains both hydroxyapatite bonding sequence (glutamic acid-rich sequence) and plasmin-cleavable sequences which makes this protein a target for further research. Patterson [166] also tested the degradation time of a total of 12 peptides derived from SPARC and demonstrated their different degradation rates when submitted to

plasmin-rich media. Again, this shows the potential for time control of antimicrobial agent release. However, peptide sensitivity to proteases is not the only factor that may determine release rates of the molecules of interest. For instance, the concentration of protease on the surface and the number of cleavable sites tethered on the implant surface should also be considered [167].

MMP- and plasmin-cleavable systems have been already tested in several hydrogel models. Aulisa et al. [168] developed a self-assembly method for peptides that were organized with triblock ABA structure in which the central B domain contained alternating hydrophilic and hydrophobic amino acids. On the one hand, the hydrophobic amino acids can drive peptides to be packed together to form “hydrophobic sandwich” structures. On the other hand, the hydrophilic amino acids are the functional motifs, such as MMP-cleavable sites. Proteolytic degradation was confirmed by mass spectrometry and transmission electron microscopy [169]. Galler et al. [170] tested self-assembled peptide-amphiphile nanofibers as scaffolds for pulpal stem cells. These peptide amphiphiles were designed with 4 functional groups: an alkyl tail, an enzyme-cleavable site, a glutamic acid for calcium binding, and a RGD group for cell recruitment. Other researches used polyethylene glycol diacrylate (PEGDA) monomer with MMP sensitive crosslinkers to form a degradable PEGDA hydrogel network [167]. Those experiments, either through self assembly [171] or UV crosslinking, were aimed to be applied as scaffolds for tissue engineering and regenerative medicine. The covalent bonding of MMP-cleavable peptides on solid substrates has been just rarely investigated. Tokatlian et al. reported on the immobilization of GPQG|IAGQ coated nanoparticles on tissue culture plastic surfaces using biotin and streptavidin as cross-linking system [172].

4.3.1.5 Multifunctional Coatings with a Combination of Peptides

As previously discussed, surface modification of titanium surface to improve osseointegration of dental implants by improving cell recruitment and differentiation, biomineral formation, or antimicrobial activity has been widely investigated. However, the fabrication of advanced multifunctional coatings that bear both bone regenerative and antimicrobial signals is an ambitious and desired goal that has been seldom pursued. It is a challenging task, though, as it requires original designs for the bioactive molecules as well as the methodological steps to obtain a robust and active coating.

The competition between bacterial adhesion and tissue integration was described by Gristina [173] as the “race for the surface”. The general concept is that if the bacteria first colonize the surface of the implant to form a biofilm they win the race as bacteria in biofilms are difficult to eradicate and become resistant to antimicrobial agents. Thus, cells from the tissue in regeneration can not displace bacteria from the surface, which leads to decreased tissue integration, occurrence of infection, and failed osseointegration. Therefore, the simultaneous prevention of bacteria adhesion and promotion of cell recruitment and differentiation on the

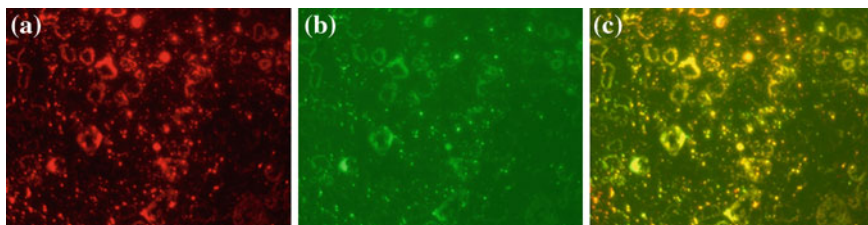


Fig. 4.7 Dual-functional coatings on Ti by co-immobilization of PHSRN- (*red/dark* tag-labeled in **a**) and RGD-containing (*green/light* tag-labeled in **b**) oligopeptides. The overlapping of the two fluorescent signals at the surface of the dual-functional coating gave a *yellow/brighter* figure shown in **(c)**

implant surface can be regarded as crucial in facilitating cells to win the race and improve clinical performance of dental implants [174].

A post-implantation period of 6 h has been identified as the “decisive period” when an implant is particularly susceptible to bacteria colonization [175]. To properly balance osseointegration and antimicrobial activity on the surface of the implant, prevention of bacterial adhesion and stimulation of cellular response should be accomplished in early stages after implantation. A barrier of hydrophilic polymers, either anionic (dextran [176] or hyaluronic acid [137, 177]) or highly flexible (polyethylene glycol (PEG) [178, 179]) have been used on Ti surfaces to control bacterial adhesion. They notably hinder protein adsorption as well as bacterial and cell adhesion due to their non-fouling properties that are acquired by either electrostatic repulsion or formation of a hydration shell. Those polymers are susceptible to further functionalization with bioactive molecules to stimulate osseointegration. By further incorporating cell integrin specific receptors, such as RGD or bone morphogenetic proteins, which are not recognizable by main bacteria in implant infection [180], simultaneous increased of osteoblastic functions and decreased bacteria adhesion were observed [181, 182].

Multifunctional coatings with a mixture of peptides with other combinations of bioactivities have been also recently studied. For instance, we fabricated silanized titanium surfaces with combination in parallel of RGD and PHSRN peptides that demonstrated the targeted synergistic effect of the two peptides on osteoblast adhesion [183] (Fig. 4.7).

4.3.2 ECM Proteins

4.3.2.1 Collagen

Collagen is the major component of connective tissues and accounts for approximately 30 % of all proteins in the human body. Collagen is often found in every major tissue that requires strength and flexibility, such as tendons, skin, bones, and

fascia. Collagen plays a critical role in the evolution of large complex organisms where it provides an insoluble scaffold for shape and form, for the attachment of macromolecules, glycoproteins, hydrated polymers and inorganic ions, as well as cell attachment. Collagen type I and its active peptides play an important role in osteoblast response [96]. Collagen can accelerate cell adhesion [184] and promote osteoblast proliferation and differentiation [185].

Collagen and collagen fibrils have been covalently bonded to the surface of titanium implants by silane chemistry. Collagen type I immobilized to titanium surfaces using acrylic acid grafting enhanced early osseointegration in *in vivo* studies [186]. A significant increase rate of bone growth and bone-to-implant contact in rabbit femur on collagen modified titanium implants was assessed in comparison to non-coated surfaces. That was even though a lower proliferation rate of SaOS-2 and a non-significant difference in alkaline phosphatase production was previously detected for the collagen-coated titanium surfaces.

The effect of collagen-modified surfaces on osseointegration of trabecular bone has also been studied [187]. Results indicated that a significant increase in bone-to-implant contact and enhanced bone in-growth can be achieved with collagen-coated implants when compared to control titanium surfaces. Since bone formation around implants is highly dependent on the recruitment of undifferentiated mesenchymal cells with osteogenic differentiation capability, it was suggested that the collagen layer on implants provided biological advantages over the non-coated surfaces to adhere and proliferate mesenchymal cells.

The covalent immobilization of type I collagen on implant surfaces can increase their enzymatic and mechanical stability [188]. It has been recently reported that the stability of the collagen on the substrate plays an important role on cellular response [189]. Fibrillar type I collagen was covalently attached via activated metal surfaces and aspartic and glutamic acid residues in type I collagen that were activated using an EDC/NHS cross-linking system. An increase in cell adhesion was found on collagen modified surfaces in comparison to non-coated oxidized surfaces. Osteoblast-like cells proliferation was also significantly enhanced on collagen modified titanium and cobalt alloys. However, a significantly increased cell proliferation on collagen-coated commercially pure titanium was not found compared with non-coated surfaces of the same metal. In this case, it was suggested that type I collagen is an attractive material for orthopedic and dental implant coatings due to its osteoconductivity and its potential to serve as a bio-compatible carrier for bioactive molecules.

4.3.2.2 Non-Collagenous ECM Proteins

Fibronectin and Laminin

Fibronectin is a high molecular weight (400 kDa) glycoprotein having two homologous subunits which are held by two disulfide bonds near the carboxyl termini. Fibronectin is expressed during early stages of bone development to

promote bone mineralization [190, 191]. Endo et al. [62] reported on covalent-immobilization of human plasma fibronectin on NiTi substrates using silane chemistry and its effect on cell response. The results showed a significant increase on fibroblast spreading on the coated surfaces. We recently also assessed that fibronectin-coated titanium surfaces significantly influenced adhesion and differentiation of SaOS-2 cells both at the gene expression and protein production levels [44, 192].

Laminin-5, a component of basement membranes, plays a crucial role in the assembly and maintenance of hemidesmosomes which connect the gingival epithelium to dental implants [193]. Laminin has been used to promote the formation of a biological seal around the transmucosal portion of dental implants. The laminin-5-derived peptide coating strongly favored the formation of hemidesmosomes [194, 195]. Lange et al. [196] immobilized laminin and human epidermal growth factor (EGF) to promote adhesion of epithelial cells. Laminin and EGF showed inhibition on adsorption of salivary proteins and bacteria while enhanced epithelial adhesion.

Growth Factors

While RGD-peptides have been the molecules most largely investigated to mediate adhesion of cells to substrates, immobilized growth factors have been the selected ones to study modulation of subsequent cell functions, such as proliferation, differentiation, and activity on biomaterial surfaces [197]. However, compared to investigations with peptides, only a few reports have focused on chemical immobilization of growth factors on implant surfaces. Most of the published work is on physical adsorption and/or local administration of these proteins both in *in vitro* and *in vivo* experiments.

Platelet-derived growth factor and insulin-like growth factor have been applied to the insertion site of titanium dental implants and implanted in dogs with a notable increase in bone regeneration [198]. EGF was immobilized on polystyrene plates and induced phosphorylation of the RGF receptor [199]. Immobilized EGF was as effective as a soluble growth factor in stimulating DNA synthesis in hepatocytes, too [200].

Bone morphogenetic proteins (BMP) belong to the TGF- β superfamily. They were originally identified as active components in bone extracts capable of inducing bone formation at ectopic sites. Three members of the family, namely BMP-2, BMP-4 and BMP-7 are expressed in bone. BMPs are able to regulate Runx2 activity through several ways, for example, through Protein Kinase D [201] or SMAD pathway [202], to regulate osteoblast differentiation.

BMP-2 has been known to play an important role in bone-healing processes and to enhance therapeutic efficacy. BMP-2 is one of the most effective osseoinductive factors as demonstrated in many works in the literature [203]. It has been successfully applied in repairing segmental defects and alveolar bone defects in conjunction with implants [204, 205] and Seol et al. [206] used a synthetic binding

motif to BMP-2 and showed that surfaces modified with BMP-2 enhanced cell attachment and significantly increased bone growth when implanted in canine mandibles in vivo compared to untreated titanium surfaces.

BMP-4 can induce osteoblastic responses in non-osteoblastic cells [207]. BMP-4 was immobilized on NH₂-rich metal surfaces. Significant amounts of BMP-4 were retained on the functionalized surfaces, which resulted in higher osteoblastic activity when compared with surfaces with no biomolecules or with lower density of initial NH₂ groups [60]. Some researchers have suggested that BMPs are better to regulate bone growth around dental implants than the widely used RGD peptide because RGDs are cell unspecific [14, 208] whereas BMPs are not. However, as a locally distributed growth factor, the long term effects of BMPs to systemic organs need to be further investigated [209].

ECM Glycosaminoglycans

Proteoglycans and their glycosaminoglycans interact with ECM molecules like collagen and bone cells like osteoblasts and osteoclasts. These molecules further mediate the attachment of cytokines and growth factors to the ECM or the cell surface [210]. However, the interactions of proteoglycans and glycosaminoglycans with cytokines and growth factors are complex in nature. A glycosaminoglycan and chondroitin sulphate enhanced bone remodeling at peri-implant interfaces when co-adsorbed with collagen [211].

Hyaluronan, also called hyaluronic acid, is a linear polysaccharide with bio-activity during cell proliferation, repair and regeneration [212]. Even though hyaluronan-functionalized titanium surfaces inhibited osteoblast adhesion, the interaction of hyaluronan with its receptors on cell surface is modulated by interactions with cytokines transiently expressed on wound healing [213]. Hyaluronan covalently coupled to titanium surfaces induced a significant improvement in bone-to-implant contact and bone ingrowth after 4 weeks of implantation in vivo studies [214]. Those improvements were more notable on trabecular bone than on cortical bone.

Biom mineralization-Related Proteins with Potential Application as Coatings for Dental Implants

Glycosylated proteins with RGD motifs. Investigations on ECM proteins with bone/teeth specific functions led to the discovery of the SIBLINGS family (Small Integrin-Binding LIgand N-linked Glycoprotein), which included Bone sialoprotein (BSP), dentin matrix protein 1 (DMP1), dentin sialophosphoprotein (DSPP), enamel (ENAM), matrix extracellular phosphoglycoprotein (MEPE), and osteopontin (OPN) [215]. All proteins of the SIBLINGS family contain an RGD sequence which is able to bind to integrin receptors on the cell membrane, as described in a previous section of this chapter. The family is also characterized by

extensive post translational modifications including N- and O-linked oligosaccharides, many of them rich in sialic acid [216]. Two members of the SIBLINGS family that have specific roles in bone regeneration are OPN and BSP.

OPN is expressed in osteoblasts just prior to mineralization. It has high affinity for calcium and it can mediate cell matrix interactions as it contains the RGD motif. OPN plays a notable role on binding osteoclasts to hydroxyapatite, thus causing bone resorption. An osteopontin knock-out mouse model showed significance resistance to bone resorption [217]. Other reports indicated that OPN is required for bone resorption as it increases angiogenesis, vascularization, and accumulation of osteoclasts [218].

BSP is a highly phosphorylated protein which is rich in polyglutamic regions. Thus, BSP is an effective apatite nucleator in vitro [219, 220]. BSP has been shown to be linear with minimal secondary structure [221, 222], but it contains several spatially segmented motifs that can bind collagen [223, 224], matrix metalloproteinases [225], hydroxyapatite [226] and cell membrane integrins [227, 228]. The spatiotemporal expression of BSP at sites of de novo bone indicates its effect in the onset of mineralization [229]. Studies showed that interference of BSP and osteoblast binding by addition of anti-BSP antibody led to compromised osteoblast differentiation and reduced mineralization [230]. In contrast, increased BSP expression improved osteoblast differentiation as well as mineralized nodule formation [231].

gamma-carboxylated (GLA) proteins. Vitamin K dependent γ -carboxylase can add carboxyl groups to glutamic acids and thus form GLA proteins. Two acidic carboxyl groups in GLA contribute to calcium binding activity. Two major members in this family are Matrix Gla protein (MGP) and osteocalcin (OCN). OCN is specifically secreted by osteoblasts and osteoclasts in bone while MGP is also highly expressed in cartilage and arteries. MGP is a powerful mineralization inhibitor. MGP deficient mice showed severe calcification of arteries and cartilage [232]. Osteocalcin also inhibits nucleation and growth of apatite crystals in vitro, but considering its late appearance during bone formation, it might be important in bone remodeling [121].

Alkaline phosphatase (ALP) has a prominent role in bone formation with multiple functions, including local regulation of phosphate supersaturation [233, 234]. ALP has been already covalently-anchored to an oxide layer of titanium using silane chemistry without losing its enzymatic activity [59].

Osteonectin was one of the first ECM proteins postulated to have bone specific functions [235]. The name “osteonectin” means bone connector because this protein has a strong affinity for both collagen and inorganic calcium-phosphate minerals. It is theorized to be a positive regulator of bone formation by improving mineral nucleation. Experiments in mice showed that mutation of the osteonectin gene caused osteopenia—resulting from low bone turnover—with defects in both osteoblast and osteoclast activity [236]. A glutamate-rich region in osteonectin has been suggested to be the site for hydroxyapatite bonding [123].

Elastin-like recombinamers with bone-mineralizing peptide sequences. Recombinant polymers with bio-mimetic activities can be covalently coated on Ti

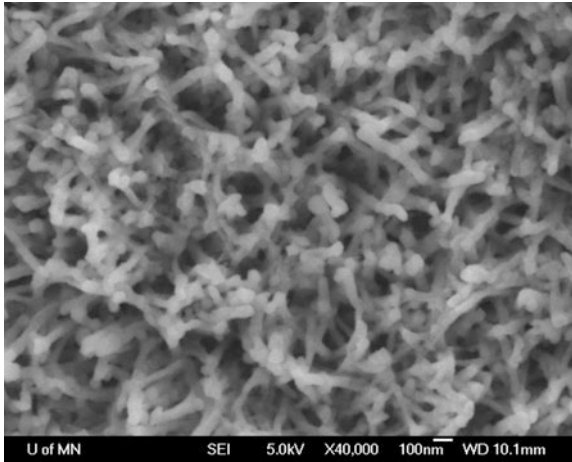


Fig. 4.8 SEM image of a Ti surface etched, coated with a recombinant carrying a peptide sequence derived from statherin, and mineralization during 7 days through an enzymatically-controlled biomimetic process. The image shows a coarse mineralized nanorod-like texture that suggested that calcium phosphate minerals formed specifically around the surface of functionalized Ti preserving the original nanorough texture

surfaces. In our lab, we have covalently-functionalized nano-rough Ti surface with a genetically synthesized elastin-like recombinamers carrying a peptide sequence derived from statherin (HSS), a multifunctional salivary protein. We further mineralized the HSS coatings using a enzymatically-controlled biomimetic mineralization process, in which the obtained homogeneous layer of mineral preserved the nano-rough topography of the metallic substrate (Fig. 4.8) [65]. This mineral layer was composed of amorphous calcium phosphate nanoparticles of 10–40 nm in diameter. Cell culture studies demonstrated that the cellular adhesion was improved on the HSS-coated Ti after 7 days of biomineralization. Furthermore, cell differentiation to osteoblasts (expression of ALP and OCN) was stimulated during 21 days of culture. The biomimetic mineralized Ti surfaces that were covalently-functionalized with statherin derived recombinant biopolymers possessed compositional and topographical features mimicking the natural bone, and are of potential interest for implant applications.

4.4 Outlook

Even though titanium has been now used for several decades to produce dental implants there is still significant research dedicated to improve its interactions with cells and tissues. Among the different strategies reviewed here, we believe that those focusing on obtaining multifunctional coatings are the ones with the highest

potential to significantly impact clinical performance of dental implants in the near future. In that respect, the use of biomolecules to be covalently anchored to the metal surface is a very attractive strategy as it provides with the desired versatility and extraordinary specificity. However, notable achievements are still to be accomplished before these coatings will be available in the dental office. For instance, the most effective chemical strategies for the immobilization of the molecules to increase implant shelf life and avoid rapid degradation of the coating after implantation as well as the methods of sterilization to be applied need to be further studied. In years to come it is expected that researchers of different disciplines—engineering, chemistry, biology, dentistry—will continue developing together new dental implants to expand their application and to improve their clinical outcome both at short and long term after implantation.

References

1. Brunski, J.B.: Classes of materials used in medicine. Metals. In: Rutner, B., Hoffman, A., Schoen, F., Lemons, J. (eds.) *Biomaterials Science, an Introduction to Materials in Medicine*. Academic Press, San Diego (1996)
2. Ratner, B.D.: A perspective on titanium biocompatibility. In: Brunette, D.M., Tengvall, P., Textor, M., Thomsen, P. (eds.) *Titanium in medicine: Material science, surface science, engineering, biological responses and medical applications*, pp. 1–12. Springer-Verlag, Berlin Heidelberg (2001)
3. Lindquist, L.W., Carlsson, G.E., Jemt, T.: A prospective 15-year follow-up study of mandibular fixed prostheses supported by osseointegrated implants—clinical results and marginal bone loss. *Clin. Oral Implan. Res.* **7**, 329–336 (1996)
4. Schwartz-Arad, D., Kidron, N., Dolev, E.: A long-term study of implants supporting overdentures as a model for implant success. *J. Periodontol.* **76**, 1431–1435 (2005)
5. Branemark, P.I., Hansson, B.O., Adell, R., et al.: Osseointegrated implants in the treatment of the edentulous jaw. Experience from a 10-year period. *Scandinavian journal of plastic and reconstructive surgery. Supplementum* **16**, 1–132 (1977)
6. Bumgardner, J.D., Adatrow, P., Haggard, W.O., et al.: Emerging antibacterial biomaterial strategies for the prevention of peri-implant inflammatory diseases. *Int. J. Oral. Max. Impl.* **26**, 553–560 (2011)
7. Le Guehennec, L., Soueidan, A., Layrolle, P., et al.: Surface treatments of titanium dental implants for rapid osseointegration. *Dent. Mater.* **23**, 844–854 (2007)
8. Schliephake, H., Scharnweber, D.: Chemical and biological functionalization of titanium for dental implants. *J. Mater. Chem.* **18**, 2404–2414 (2008)
9. Williams, D.F.: Titanium for medical applications. In: Brunette, D.M., Tengvall, P., Textor, M., Thomsen, P. (eds.) *Titanium in Medicine: Material Science, Surface Science, Engineering, Biological Responses and Medical Applications*, pp. 13–24. Springer-Verlag, Berlin Heidelberg
10. Kasemo, B.: Biological surface science. *Surf. Sci.* **500**, 656–677 (2002)
11. Castner, D.G., Ratner, B.D.: Biomedical surface science: Foundations to frontiers. *Surf. Sci.* **500**, 28–60 (2002)
12. Elmengaard, B., Bechtold, J.E., Soballe, K.: In vivo study of the effect of RGD treatment on bone ongrowth on press-fit titanium alloy implants. *Biomaterials* **26**, 3521–3526 (2005)
13. Wang, H.L., Ormianer, Z., Palti, A., et al.: Consensus conference on immediate loading: The single tooth and partial edentulous areas. *Implant Dent.* **15**, 324–333 (2006)

14. Puleo, D.A., Nanci, A.: Understanding and controlling the bone-implant interface. *Biomaterials* **20**, 2311–2321 (1999)
15. Buser, D.: Titanium for dental applications (II): Implants with roughened surfaces. In: Brunette, D.M., Tengvall, P., Textor, M., Thomsen, P. (eds.) *Titanium in Medicine: Material Science, Surface Science, Engineering, Biological Responses and Medical Applications*, pp. 875–887. Springer-Verlag, Berlin Heidelberg (2001)
16. Klokkevold, P.R., Johnson, P., Dadgostari, S., et al.: Early endosseous integration enhanced by dual acid etching of titanium: a torque removal study in the rabbit. *Clin. Oral Implan. Res.* **12**, 350–357 (2001)
17. Ivanoff, C.J., Hallgren, C., Widmark, G., et al.: Histologic evaluation of the bone integration of TiO₂ blasted and turned titanium microimplants in humans. *Clin. Oral. Implan. Res.* **12**, 128–134 (2001)
18. Sutter, F., Schroeder, A., Buser, D.A.: The new concept of ITI hollowcylinder and hollowscrew implants. Part 1. Engineering and design. *Int. J. Oral Maxillofac. Implants.* **3**, 161–172 (1988)
19. Sul, Y.T., Johansson, C.B., Petronis, S., et al.: Characteristics of the surface oxides on turned and electrochemically oxidized pure titanium implants up to dielectric breakdown: the oxide thickness, micropore configurations, surface roughness, crystal structure and chemical composition. *Biomaterials* **23**, 491–501 (2002)
20. Buser, D., Nydegger, T., Hirt, H.P., et al.: Removal torque values of titanium implants in the maxilla of miniature pigs. *Int. J. Oral Maxillofac. Implants* **13**, 611–619 (1998)
21. Boyan, B.D., Hummert, T.W., Dean, D.D., et al.: Role of material surfaces in regulating bone and cartilage cell response. *Biomaterials* **17**, 137–146 (1996)
22. Han, C.-H., Johansson, C.B., Wennerberg, A., et al.: Quantitative and qualitative investigations of surface enlarged titanium and titanium alloys implants. *Clin. Oral Implan. Res.* **9**, 1–10 (1998)
23. Martin, J.Y., Schwartz, Z., Hummert, T.W., et al.: Effect of titanium surface-roughness on proliferation, differentiation, and protein-synthesis of human osteoblast-like cells (Mg63). *J. Biomed. Mater. Res.* **29**, 389–401 (1995)
24. Pegueroles, M., Aparicio, C., Bosio, M., et al.: Spatial organization of osteoblasts fibronectin-matrix on titanium surface-effects of roughness, chemical heterogeneity, and surface free energy. *Acta. Biomater.* **6**, 291–301 (2010)
25. Cochran, D.L., Schenk, R.K., Lussi, A., et al.: Bone response to unloaded and loaded titanium implants with a sandblasted and acid-etched surface: A histometric study in the canine mandible. *J. Biomed. Mater. Res.* **40**, 1–11 (1998)
26. Aparicio, C., Gil, F.J., Fonseca, C., et al.: Corrosion behaviour of commercially pure titanium shot blasted with different materials and sizes of shot particles for dental implant applications. *Biomaterials* **24**, 263–273 (2003)
27. Pegueroles, M., Gil, F.J., Planell, J.A., et al.: The influence of blasting and sterilization on static and time-related wettability and surface-energy properties of titanium surfaces. *Surf. Coat. Tech.* **202**, 3470–3479 (2008)
28. Mendonca, G., Mendonca, D.B.S., Aragao, F.J.L., et al.: Advancing dental implant surface technology—from micron- to nanotopography. *Biomaterials* **29**, 3822–3835 (2008)
29. Variola, F., Brunski, J.B., Orsini, G., et al.: Nanoscale surface modifications of medically relevant metals: State-of-the art and perspectives. *Nanoscale* **3**, 335–353 (2011)
30. Palmquist, A., Omar, O.M., Esposito, M., et al.: Titanium oral implants: surface characteristics, interface biology and clinical outcome. *J. R. Soc. Interface* **7**, S515–S527 (2010)
31. Junker, R., Dimakis, A., Thoneick, M., et al.: Effects of implant surface coatings and composition on bone integration: a systematic review. *Clin. Oral Implan. Res.* **20**, 185–206 (2009)
32. Rupp, F., Scheideler, L., Olshanska, N., et al.: Enhancing surface free energy and hydrophilicity through chemical modification of microstructured titanium implant surfaces. *J. Biomed. Mater. Res. A* **76A**, 323–334 (2006)

33. Schwarz, F., Herten, M., Sager, M., et al.: Bone regeneration in dehiscence-type defects at chemically modified (SLActive[®]) and conventional SLA titanium implants: A pilot study in dogs. *J. Clin. Periodontol.* **34**, 78–86 (2007)
34. Zhao, G., Schwartz, Z., Wieland, M., et al.: High surface energy enhances cell response to titanium substrate microstructure. *J. Biomed. Mater. Res. A* **74A**, 49–58 (2005)
35. Ueno, T., Yamada, M., Suzuki, T., et al.: Enhancement of bone-titanium integration profile with UV-photofunctionalized titanium in a gap healing model. *Biomaterials* **31**, 1546–1557 (2010)
36. Borsari, V., Fini, M., Giavaresi, G., et al.: Osteointegration of titanium and hydroxyapatite rough surfaces in healthy and compromised cortical and trabecular bone: In vivo comparative study on young, aged, and estrogen-deficient sheep. *J. Orthop. Res.* **25**, 1250–1260 (2007)
37. Geesink, R.G.T., Degroot, K., Klein, C.P.A.T.: Chemical implant fixation using hydroxyl-apatite coatings—the development of a human total hip-prosthesis for chemical fixation to bone using hydroxyl-apatite coatings on titanium substrates. *Clin. Orthop. Relat. Res.* 147–170 (1987)
38. Hulshoff, J.E., Hayakawa, T., Van Dijk, K., et al.: Mechanical and histologic evaluation of Ca-P plasma-spray and magnetron sputter-coated implants in trabecular bone of the goat. *J. Biomed. Mater. Res.* **36**, 75–83 (1997)
39. Lee JR, L., Beirne, O.: Survival of hydroxyapatite-coated implants: A meta-analytic review. *J. Oral Maxillofac. Surg.* **58**, 1372–1379 (2000)
40. Kim, H.M., Miyaji, F., Kokubo, T., et al.: Preparation of bioactive Ti and its alloys via simple chemical surface treatment. *J. Biomed. Mater. Res.* **32**, 409–417 (1996)
41. Li, P.J., Degroot, K.: Calcium-phosphate formation within sol-gel prepared Titania in-vitro and in-vivo. *J. Biomed. Mater. Res.* **27**, 1495–1500 (1993)
42. Li, P.J., Ducheyne, P.: Quasi-biological apatite film induced by titanium in a simulated body fluid. *J. Biomed. Mater. Res.* **41**, 341–348 (1998)
43. Ohtsuki, C., Iida, H., Hayakawa, S., et al.: Bioactivity of titanium treated with hydrogen peroxide solutions containing metal chlorides. *J. Biomed. Mater. Res.* **35**, 39–47 (1997)
44. Wen, H.B., Dewijn, J.R., Liu, Q., et al.: A simple method to prepare calcium phosphate coatings on Ti6Al4 V. *J. Mater. Sci. Mater. M* **8**, 765–770 (1997)
45. Kim, H.M., Miyaji, F., Kokubo, T., et al.: Preparation of bioactive Ti and its alloys via simple chemical surface treatment. *J. Biomed. Mater. Res.* **32**, 409–417 (1996)
46. Kokubo, T., Takadama, H.: How useful is SBF in predicting in vivo bone bioactivity? *Biomaterials* **27**, 2907–2915 (2006)
47. Nishiguchi, S., Kato, H., Fujita, H., et al.: Titanium metals form direct bonding to bone after alkali and heat treatments. *Biomaterials* **22**, 2525–2533 (2001)
48. Aparicio, C., Padros, A., Gil, F.J.: In vivo evaluation of micro-rough and bioactive titanium dental implants using histometry and pull-out tests. *J. Mech. Behav. Biomed. Mater.* **4**, 1672–1682 (2011)
49. Aparicio, C., Manero, J.M., Conde, F., et al.: Acceleration of apatite nucleation on microrough bioactive titanium for bone-replacing implants. *J. Biomed. Mater. Res. A* **82A**, 521–529 (2007)
50. Aparicio, C., Gil, F.J., Planell, J.A., et al.: Human-osteoblast proliferation and differentiation on grit-blasted and bioactive titanium for dental applications. *J. Mater. Sci. Mater. M* **13**, 1105–1111 (2002)
51. Albelda, S.M., Buck, C.A.: Integrins and other cell-adhesion molecules. *Faseb J.* **4**, 2868–2880 (1990)
52. Ratner, B.D.: New ideas in biomaterials science—a path to engineered biomaterials. *J. Biomed. Mater. Res.* **27**, 837–850 (1993)
53. Massia, S.P., Hubbell, J.A.: An rgd spacing of 440 nm is sufficient for integrin alpha-V-beta-3-mediated fibroblast spreading and 140 nm for focal contact and stress fiber formation. *J. Cell Biol.* **114**, 1089–1100 (1991)

54. García, A.J.: Surface modification of biomaterials. In: Atala, A., Lanza, R., Thomson, J.A., Nerem, R. (eds.) *Principles of Regenerative Medicine* (2nd edn), pp. 663–673. Elsevier/Academic Press, San Diego (2011)
55. Hall, J., Sorensen, R.G., Wozney, J.M., et al.: Bone formation at rhBMP-2-coated titanium implants in the rat ectopic model. *J. Clin. Periodontol.* **34**, 444–451 (2007)
56. Bekos, E.J., Ranieri, J.P., Aebischer, P., et al.: Structural-changes of bovine serum-albumin upon adsorption to modified fluoropolymer substrates used for neural cell attachment studies. *Langmuir* **11**, 984–989 (1995)
57. Tebbe, D., Thull, R., Gbureck, U.: Influence of spacer length on heparin coupling efficiency and fibrinogen adsorption of modified titanium surfaces. *Biomed. Eng. Online.* **6**(1), 31 (2007)
58. Nadkarni, V.D., Pervin, A., Linhardt, R.J.: Directional immobilization of heparin onto beaded supports. *Anal. Biochem.* **222**, 59–67 (1994)
59. Nanci, A., Wuest, J.D., Peru, L., et al.: Chemical modification of titanium surfaces for covalent attachment of biological molecules. *J. Biomed. Mater. Res.* **40**, 324–335 (1998)
60. Puleo, D.A., Kissling, R.A., Sheu, M.S.: A technique to immobilize bioactive proteins, including bone morphogenetic protein-4 (BMP-4), on titanium alloy. *Biomaterials* **23**, 2079–2087 (2002)
61. Rezanian, A., Johnson, R., Lefkow, A.R., et al.: Bioactivation of metal oxide surfaces. 1. Surface characterization and cell response. *Langmuir* **15**, 6931–6939 (1999)
62. Endo, M., Takagaki, K., Nakamura, T.: A new avenue of proteoglycan studies—of glycosaminoglycan chains using endo-type glycosidases. *Seikagaku* **67**, 1269–1282 (1995)
63. Puleo, D.A.: Activity of enzyme immobilized on silanized Co-Cr-Mo. *J. Biomed. Mater. Res.* **29**, 951–957 (1995)
64. Puleo, D.A.: Retention of enzymatic activity immobilized on silanized Co-Cr-Mo and Ti-6Al-4 V. *J. Biomed. Mater. Res.* **37**, 222–228 (1997)
65. Li, Y., Aparicio, C., Rodriguez-Cabello, C., et al.: Bio-mineralization of nanorough titanium covalently-coated with statherin-derived recombinant biopolymers. *J. Dent. Res. (Spec. Iss. B)*, **89**, 3574 (2010)
66. Schuler, M., Trentin, D., Textor, M., et al.: Biomedical interfaces: Titanium surface technology for implants and cell carriers. *Nanomedicine (Lond)* **1**, 449–463 (2006)
67. Porte-Durrieu, M.C., Guillemot, F., Pallu, S., et al.: Cyclo-(DfKRG) peptide grafting onto Ti-6Al-4 V: Physical characterization and interest towards human osteoprogenitor cells adhesion. *Biomaterials* **25**, 4837–4846 (2004)
68. Puleo, D.A.: Biochemical surface modification of Co-Cr-Mo. *Biomaterials* **17**, 217–222 (1996)
69. Xiao, S.J., Textor, M., Spencer, N.D., et al.: Immobilization of the cell-adhesive peptide Arg-Gly-Asp-Cys (RGDC) on titanium surfaces by covalent chemical attachment. *J. Mater. Sci. Mater. Med.* **8**, 867–872 (1997)
70. Zhang, F., Xu, F.J., Kang, E.T., et al.: Modification of titanium via surface-initiated atom transfer radical polymerization (ATRP). *Ind. Eng. Chem. Res.* **45**, 3067–3073 (2006)
71. Kamigaito, M., Ando, T., Sawamoto, M.: Metal-catalyzed living radical polymerization. *Chem. Rev.* **101**, 3689–3745 (2001)
72. Matyjaszewski, K., Miller, P.J., Shukla, N., et al.: Polymers at interfaces: Using atom transfer radical polymerization in the controlled growth of homopolymers and block copolymers from silicon surfaces in the absence of untethered sacrificial initiator. *Macromolecules* **32**, 8716–8724 (1999)
73. Matyjaszewski, K., Xia, J.H.: Atom transfer radical polymerization. *Chem. Rev.* **101**, 2921–2990 (2001)
74. Zhang, F., Shi, Z.L., Chua, P.H., et al.: Functionalization of titanium surfaces via controlled living radical polymerization: From antibacterial surface to surface for osteoblast adhesion. *Ind. Eng. Chem. Res.* **46**, 9077–9086 (2007)

75. Mrksich, M., Chen, C.S., Xia, Y.N., et al.: Controlling cell attachment on contoured surfaces with self-assembled monolayers of alkanethiolates on gold. *Proc. Natl. Acad. Sci. USA* **93**, 10775–10778 (1996)
76. Gawalt, E.S., Avaltroni, M.J., Koch, N., et al.: Self-assembly and bonding of alkanephosphonic acids on the native oxide surface of titanium. *Langmuir* **17**, 5736–5738 (2001)
77. Danahy, M.P., Avaltroni, M.J., Midwood, K.S., et al.: Self-assembled monolayers of alpha, omega-diphosphonic acids on Ti enable complete or spatially controlled surface derivatization. *Langmuir* **20**, 5333–5337 (2004)
78. Hayakawa, T., Yoshinari, M., Nagai, M., et al.: X-ray photoelectron spectroscopic studies of the reactivity of basic terminal OH of titanium towards tresyl chloride and fibronectin. *Biomed. Res. Tokyo* **24**, 223–230 (2003)
79. Huang, N.P., Michel, R., Voros, J., et al.: Poly (L-lysine)-g-poly(ethylene glycol) layers on metal oxide surfaces: Surface-analytical characterization and resistance to serum and fibrinogen adsorption. *Langmuir* **17**, 489–498 (2001)
80. Kenausis, G.L., Voros, J., Elbert, D.L., et al.: Poly (L-lysine)-g-poly (ethylene glycol) layers on metal oxide surfaces: Attachment mechanism and effects of polymer architecture on resistance to protein adsorption. *J. Phys. Chem. B* **104**, 3298–3309 (2000)
81. Tosatti, S., De Paul, S.M., Askendal, A., et al.: Peptide functionalized poly (L-lysine)-g-poly (ethylene glycol) on titanium: resistance to protein adsorption in full heparinized human blood plasma. *Biomaterials* **24**, 4949–4958 (2003)
82. Vandevonede, S., Voros, J., Hubbell, J.A.: RGD-Grafted poly-L-lysine-graft-(polyethylene glycol) copolymers block non-specific protein adsorption while promoting cell adhesion. *Biotechnol. Bioeng.* **82**, 784–790 (2003)
83. Beutner, R., Michael, J., Forster, A., et al.: Immobilization of oligonucleotides on titanium based materials by partial incorporation in anodic oxide layers. *Biomaterials* **30**, 2774–2781 (2009)
84. Michael, J., Beutner, R., Hempel, U., et al.: Surface modification of titanium-based alloys with bioactive molecules using electrochemically fixed nucleic acids. *J. Biomed. Mater. Res. B* **80B**, 146–155 (2007)
85. Schliephake, H., Botel, C., Forster, A., et al.: Effect of oligonucleotide mediated immobilization of bone morphogenic proteins on titanium surfaces. *Biomaterials* **33**, 1315–1322 (2012)
86. De Jonge, L.T., Leeuwenburgh, S.C.G., Wolke, J.G.C., et al.: Organic-inorganic surface modifications for titanium implant surfaces. *Pharm. Res. Dordr* **25**, 2357–2369 (2008)
87. Bierbaum, S., Hempel, U., Geissler, U., et al.: Modification of Ti6Al4 V surfaces using collagen I, III, and fibronectin. II. Influence on osteoblast responses. *J Biomed Mater Res A* **67A**, 431–438 (2003)
88. Ku, Y., Chung, C.P., Jang, J.H.: The effect of the surface modification of titanium using a recombinant fragment of fibronectin and vitronectin on cell behavior. *Biomaterials* **26**, 5153–5157 (2005)
89. Steele, J.G., Johnson, G., Mcfarland, C., et al.: Roles of serum vitronectin and fibronectin in initial attachment of human vein endothelial-cells and dermal fibroblasts on oxygen-containing and nitrogen-containing surfaces made by radiofrequency plasmas. *J. Biomat. Sci. Polym. E* **6**, 511–532 (1994)
90. Carson, A.E., Barker, T.H.: Emerging concepts in engineering extracellular matrix variants for directing cell phenotype. *Regen. Med.* **4**, 593–600 (2009)
91. Pierschbacher, M.D., Ruoslahti, E.: Cell attachment activity of fibronectin can be duplicated by small synthetic fragments of the molecule. *Nature* **309**, 30–33 (1984)
92. Ruoslahti, E.: RGD and other recognition sequences for integrins. *Annu. Rev. Cell Dev. Biol.* **12**, 697–715 (1996)
93. Collier, J.H., Segura, T.: Evolving the use of peptides as components of biomaterials. *Biomaterials* **32**, 4198–4204 (2011)

94. Coin, I., Beyermann, M., Bienert, M.: Solid-phase peptide synthesis: From standard procedures to the synthesis of difficult sequences. *Nat. Protoc.* **2**, 3247–3256 (2007)
95. Cooper, L.F., Deporter, D., Wennerberg, A., et al.: What physical and/or biochemical characteristics of roughened endosseous implant surfaces particularly enhance their bone-implant contact capability? *Int. J. Oral Max. Impl.* **20**, 307–312 (2005)
96. Lebaron, R.G., Athanasiou, K.A.: Extracellular matrix cell adhesion peptides: Functional applications in orthopedic materials. *Tissue Eng.* **6**, 85–103 (2000)
97. Itoh, D., Yoneda, S., Kuroda, S., et al.: Enhancement of osteogenesis on hydroxyapatite surface coated with synthetic peptide (EEEEEEPRGDT) in vitro. *J. Biomed. Mater. Res.* **62**, 292–298 (2002)
98. Grzesik, W.J., Robey, P.G.: Bone-matrix rgd glycoproteins—immunolocalization and interaction with human primary osteoblastic bone-cells in-vitro. *J. Bone Miner. Res.* **9**, 487–496 (1994)
99. Pierschbacher, M.D., Hayman, E.G., Ruoslahti, E.: Cell attachment to fibronectin and the extracellular-matrix. *In Vitro Cell Dev. B* **20**, 255–265 (1984)
100. Rezanian, A., Thomas, C.H., Branger, A.B., et al.: The detachment strength and morphology of bone cells contacting materials modified with a peptide sequence found within bone sialoprotein. *J. Biomed. Mater. Res.* **37**, 9–19 (1997)
101. Petrie, T.A., Raynor, J.E., Reyes, C.D., et al.: The effect of integrin-specific bioactive coatings on tissue healing and implant osseointegration. *Biomaterials* **29**, 2849–2857 (2008)
102. Aucoin, L., Griffith, C.M., Pleizier, G., et al.: Interactions of corneal epithelial cells and surfaces modified with cell adhesion peptide combinations. *J. Biomat. Sci. Polym. E* **13**, 447–462 (2002)
103. Benoit, D.S.W., Anseth, K.S.: The effect on osteoblast function of colocalized RGD and PHSRN epitopes on PEG surfaces. *Biomaterials* **26**, 5209–5220 (2005)
104. Feng, Y.Z., Mrksich, M.: The synergy peptide PHSRN and the adhesion peptide RGD mediate cell adhesion through a common mechanism. *Biochemistry-US* **43**, 15811–15821 (2004)
105. Kao, W.J., Lee, D., Schense, J.C., et al.: Fibronectin modulates macrophage adhesion and FBGC formation: The pole of RGD, PHSRN, and PRRARV domains. *J. Biomed. Mater. Res.* **55**, 79–88 (2001)
106. Kokkoli, E., Ochsenhirt, S.E., Tirrell, M.: Collective and single-molecule interactions of alpha (5) beta (1) integrins. *Langmuir* **20**, 2397–2404 (2004)
107. Mardilovich, A., Kokkoli, E.: Biomimetic peptide-amphiphiles for functional biomaterials: The role of GRGDSP and PHSRN. *Biomacromolecules* **5**, 950–957 (2004)
108. Ochsenhirt, S.E., Kokkoli, E., McCarthy, J.B., et al.: Effect of RGD secondary structure and the synergy site PHSRN on cell adhesion, spreading and specific integrin engagement. *Biomaterials* **27**, 3863–3874 (2006)
109. Collier, J.H., Rudra, J.S., Gasiorowski, J.Z., et al.: Multi-component extracellular matrices based on peptide self-assembly. *Chem. Soc. Rev.* **39**, 3413–3424 (2010)
110. Vogel, V.: Mechanotransduction involving multimodular proteins: Converting force into biochemical signals. *Annu. Rev. Bioph. Biom.* **35**, 459–488 (2006)
111. Reyes, C.D., Garcia, A.J.: Engineering integrin-specific surfaces with a triple-helical collagen-mimetic peptide. *J. Biomed. Mater. Res. A* **65A**, 511–523 (2003)
112. Bagnò, A., Piovano, A., Dettin, M., et al.: Human osteoblast-like cell adhesion on titanium substrates covalently functionalized with synthetic peptides. *Bone* **40**, 693–699 (2007)
113. Benesch, J., Mano, J.F., Reis, R.L.: Proteins and their peptide motifs in acellular apatite mineralization of scaffolds for tissue engineering. *Tissue Eng. Part B-Rev.* **14**, 433–445 (2008)
114. Weiner, S., Traub, W.: Organization of hydroxyapatite crystals within collagen fibrils. *FEBS Lett.* **206**, 262–266 (1986)
115. He, G., Ramachandran, A., Dahl, T., et al.: Phosphorylation of phosphophoryn is crucial for its function as a mediator of biomineralization. *J. Biol. Chem.* **280**, 33109–33114 (2005)

116. Steitz, S.A., Speer, M.Y., Mckee, M.D., et al.: Osteopontin inhibits mineral deposition and promotes regression of ectopic calcification. *Am. J. Pathol.* **161**, 2035–2046 (2002)
117. Wada, T., Mckee, M.D., Steitz, S., et al.: Calcification of vascular smooth muscle cell cultures inhibition by osteopontin. *Circ. Res.* **84**, 166–178 (1999)
118. Ohta, K., Monma, H., Tanaka, J., et al.: Interaction between hydroxyapatite and proteins by liquid chromatography using simulated body fluids as eluents. *J. Mater. Sci. Mater. Med.* **13**, 633–637 (2002)
119. Raj, P.A., Johnsson, M., Levine, M.J., et al.: Salivary statherin—dependence on sequence, charge, hydrogen-bonding potency, and helical conformation for adsorption to hydroxyapatite and inhibition of mineralization. *J. Biol. Chem.* **267**, 5968–5976 (1992)
120. Wikel, K., Burke, E.M., Perich, J.W., et al.: Hydroxyapatite mineralization and demineralization in the presence of synthetic phosphorylated pentapeptides. *Arch. Oral Biol.* **39**, 715–721 (1994)
121. Hunter, G.K., Hauschka, P.V., Poole, A.R., et al.: Nucleation and inhibition of hydroxyapatite formation by mineralized tissue proteins. *Biochem. J.* **317**, 59–64 (1996)
122. Yao, K.L., Todescan, R., Sodek, J.: Temporal changes in matrix protein-synthesis and messenger-rna expression during mineralized tissue formation by adult-rat bone-marrow cells in culture. *J. Bone Miner. Res.* **9**, 231–240 (1994)
123. Fujisawa, R., Wada, Y., Nodasaka, Y., et al.: Acidic amino acid-rich sequences as binding sites of osteonectin to hydroxyapatite crystals. *Bba. Protein Struct. Mol.* **1292**, 53–60 (1996)
124. Stubbs, J.T., Mintz, K.P., Eanes, E.D., et al.: Characterization of native and recombinant bone sialoprotein: Delineation of the mineral-binding and cell adhesion domains and structural analysis of the RGD domain. *J. Bone Miner. Res.* **12**, 1210–1222 (1997)
125. Norowski, P.A., Bumgardner, J.D.: Biomaterial and antibiotic strategies for peri-implantitis. *J. Biomed. Mater. Res. B* **88B**, 530–543 (2009)
126. Huang, H.L., Chang, Y.Y., Lai, M.C., et al.: Antibacterial TaN-Ag coatings on titanium dental implants. *Surf. Coat. Tech.* **205**, 1636–1641 (2010)
127. Zhao, L.Z., Chu, P.K., Zhang, Y.M., et al.: Antibacterial coatings on titanium implants. *J. Biomed. Mater. Res. B* **91B**, 470–480 (2009)
128. Papat, K.C., Eltgroth, M., Latempa, T.J., et al.: Decreased staphylococcus epidermidis adhesion and increased osteoblast functionality on antibiotic-loaded Titania nanotubes. *Biomaterials* **28**, 4880–4888 (2007)
129. Lucke, M., Schmidmaier, G., Sadoni, S., et al.: Gentamicin coating of metallic implants reduces implant-related osteomyelitis in rats. *Bone* **32**, 521–531 (2003)
130. Jahoda, D., Nyc, O., Pokorny, D., et al.: Antibiotic treatment for prevention of infectious complications in joint replacement. *Acta Chir. Orthopaedicae Et Traumatologiae Cechoslovaca* **73**, 108–114 (2006)
131. Alt, V., Bitschnau, A., Osterling, J., et al.: The effects of combined gentamicin-hydroxyapatite coating for cementless joint prostheses on the reduction of infection rates in a rabbit infection prophylaxis model. *Biomaterials* **27**, 4627–4634 (2006)
132. Radin, S., Campbell, J.T., Ducheyne, P., et al.: Calcium phosphate ceramic coatings as carriers of vancomycin. *Biomaterials* **18**, 777–782 (1997)
133. Yamamura, K., Iwata, H., Yotsuyanagi, T.: Synthesis of antibiotic-loaded hydroxyapatite beads and invitro drug release testing. *J. Biomed. Mater. Res.* **26**, 1053–1064 (1992)
134. Kim, W.H., Lee, S.B., Oh, K.T., et al.: The release behavior of CHX from polymer-coated titanium surfaces. *Surf. Interface Anal.* **40**, 202–204 (2008)
135. Chen, W., Liu, Y., Courtney, H.S., et al.: In vitro anti-bacterial and biological properties of magnetron co-sputtered silver-containing hydroxyapatite coating. *Biomaterials* **27**, 5512–5517 (2006)
136. Harris, L.G., Tosatti, S., Wieland, M., et al.: Staphylococcus aureus adhesion to titanium oxide surfaces coated with non-functionalized and peptide-functionalized poly (L-lysine)-grafted-poly(ethylene glycol) copolymers. *Biomaterials* **25**, 4135–4148 (2004)

137. Chua, P.H., Neoh, K.G., Kang, E.T., et al.: Surface functionalization of titanium with hyaluronic acid/chitosan polyelectrolyte multilayers and RGD for promoting osteoblast functions and inhibiting bacterial adhesion. *Biomaterials* **29**, 1412–1421 (2008)
138. Antoci, V., Adams, C.S., Hickok, N.J., et al.: Vancomycin bound to Ti rods reduces periprosthetic infection—preliminary study. *Clin. Orthop. Relat. Res.* **461**, 88–95 (2007)
139. Antoci, V., Adams, C.S., Parvizi, J., et al.: Covalently attached vancomycin provides a nanoscale antibacterial surface. *Clin. Orthop. Relat. Res.* **461**, 81–87 (2007)
140. Antoci Jr, V., Adams, C.S., Parvizi, J., et al.: The inhibition of staphylococcus epidermidis biofilm formation by vancomycin-modified titanium alloy and implications for the treatment of periprosthetic infection. *Biomaterials* **29**, 4684–4690 (2008)
141. Antoci, V., King, S.B., Jose, B., et al.: Vancomycin covalently bonded to titanium alloy prevents bacterial colonization. *J. Orthop. Res.* **25**, 858–866 (2007)
142. Weber, F.A., Lautenbach, E.E.G.: Revision of infected total hip-arthroplasty. *Clin. Orthop. Relat. R.* **211**, 108–115
143. Tunney, M.M., Ramage, G., Patrick, S., et al.: Antimicrobial susceptibility of bacteria isolated from orthopedic implants following revision hip surgery. *Antimicrob. Agents Ch.* **42**, 3002–3005 (1998)
144. Antoci, V., Adams, C.S., Hickok, N.J., et al.: Antibiotics for local delivery systems cause skeletal cell toxicity in vitro. *Clin. Orthop. Relat. Res.* **462**, 200–206 (2007)
145. Ince, A., Schutze, N., Hendrich, C., et al.: Effect of polyhexanide and gentamycin on human osteoblasts and endothelial cells. *Swiss Med.Wkly.* **137**, 139–145 (2007)
146. Ince, A., Schutze, N., Hendrich, C., et al.: In vitro investigation of orthopedic titanium-coated and brushite-coated surfaces using human osteoblasts in the presence of gentamycin. *J. Arthroplasty* **23**, 762–771 (2008)
147. Naal, F.D., Salzmann, G.M., Von Knoch, F., et al.: The effects of clindamycin on human osteoblasts in vitro. *Arch. Orthop. Trauma Surg.* **128**, 317–323 (2008)
148. Salzmann, G.M., Naal, F.D., Von Knoch, F., et al.: Effects of cefuroxime on human osteoblasts in vitro. *J. Biomed. Mater. Res. A* **82**, 462–468 (2007)
149. Gorr, S.U., Abdolhosseini, M.: Antimicrobial peptides and periodontal disease. *J. Clin. Periodontol.* **38**, 126–141 (2011)
150. Krisanaprakornkit, S., Khongkhunthian, S.: The role of antimicrobial peptides in periodontal disease. *Public Health 21st C.* 73–103 (2010)
151. Hancock, R.E.W., Sahl, H.G.: Antimicrobial and host-defense peptides as new anti-infective therapeutic strategies. *Nat. Biotechnol.* **24**, 1551–1557 (2006)
152. Lau, Y.E., Rozek, A., Scott, M.G., et al.: Interaction and cellular localization of the human host defense peptide LL-37 with lung epithelial cells. *Infect. Immun.* **73**, 583–591 (2005)
153. Sandgren, S., Wittrup, A., Cheng, F., et al.: The human antimicrobial peptide LL-37 transfers extracellular DNA plasmid to the nuclear compartment of mammalian cells via lipid rafts and proteoglycan-dependent endocytosis. *J. Biol. Chem.* **279**, 17951–17956 (2004)
154. Kazemzadeh-Narbat, M., Kindrachuk, J., Duan, K., et al.: Antimicrobial peptides on calcium phosphate-coated titanium for the prevention of implant-associated infections. *Biomaterials* **31**, 9519–9526 (2010)
155. Campoccia, D., Montanaro, L., Speziale, P., et al.: Antibiotic-loaded biomaterials and the risks for the spread of antibiotic resistance following their prophylactic and therapeutic clinical use. *Biomaterials* **31**, 6363–6377 (2010)
156. Walsh, C.: Molecular mechanisms that confer antibacterial drug resistance. *Nature* **406**, 775–781 (2000)
157. Gao, G.Z., Lange, D., Hilpert, K., et al.: The biocompatibility and biofilm resistance of implant coatings based on hydrophilic polymer brushes conjugated with antimicrobial peptides. *Biomaterials* **32**, 3899–3909 (2011)
158. Holmberg, K.V., Hegde, R., Abdolhosseini, M., et al.: Antimicrobial-peptide biofunctionalized titanium for dental implants. *J. Dent. Res.* **90**, 1722 (2011)

159. Jelokhani-Niaraki, M., Prenner, E.J., Kay, C.M., et al.: Conformation and interaction of the cyclic cationic antimicrobial peptides in lipid bilayers. *J. Pept. Res.* **60**, 23–36 (2002)
160. Wieczorek, M., Jenssen, H., Kindrachuk, J., et al.: Structural studies of a peptide with immune modulating and direct antimicrobial activity. *Chem. Biol.* **17**, 970–980 (2010)
161. Bromberg, L.E., Buxton, D.K., Friden, P.M.: Novel periodontal drug delivery system for treatment of periodontitis. *J. Controlled Release* **71**, 251–259 (2001)
162. Owen, G.R., Jackson, J.K., Chehroudi, B., et al.: An in vitro study of plasticized poly (lactic-co-glycolic acid) films as possible guided tissue regeneration membranes: Material properties and drug release kinetics. *J. Biomed. Mater. Res A* **95A**, 857–869 (2010)
163. Srirangarajan, S., Mundargi, R.C., Ravindra, S., et al.: Randomized, controlled, single-masked, clinical study to compare and evaluate the efficacy of microspheres and gel in periodontal pocket therapy. *J. Periodontol.* **82**, 114–121 (2011)
164. Nagase, H., Fields, G.B.: Human matrix metalloproteinase specificity studies using collagen sequence-based synthetic peptides. *Biopolymers* **40**, 399–416 (1996)
165. Patterson, J., Hubbell, J.A.: Enhanced proteolytic degradation of molecularly engineered PEG hydrogels in response to MMP-1 and MMP-2. *Biomaterials* **31**, 7836–7845 (2010)
166. Patterson, J., Hubbell, J.A.: SPARC-derived protease substrates to enhance the plasmin sensitivity of molecularly engineered PEG hydrogels. *Biomaterials* **32**, 1301–1310 (2011)
167. Tokatlian, T., Shrum, C.T., Kadoya, W.M., et al.: Protease degradable tethers for controlled and cell-mediated release of nanoparticles in 2- and 3-dimensions. *Biomaterials* **31**, 8072–8080 (2010)
168. Aulisa, L., Dong, H., Hartgerink, J.D.: Self-assembly of multidomain peptides: Sequence variation allows control over cross-linking and viscoelasticity. *Biomacromolecules* **10**, 2694–2698 (2009)
169. Tauro Jr, L.B., Ss, Lateef, Ra, Gemeinhart: Matrix metalloprotease selective peptide substrates cleavage within hydrogel matrices for cancer chemotherapy activation. *Peptides* **29**, 1965–1973 (2008)
170. Galler, K.M., Aulisa, L., Regan, K.R., D'souza, R.N., Hartgerink, J.D.: Self-assembling multidomain peptide hydrogels: designed susceptibility to enzymatic cleavage allows enhanced cell migration and spreading. *J. Am. Chem. Soc.* **132**, 1965–1973 (1973)
171. Chau, Y., Luo, Y., Cheung, A.C.Y., et al.: Incorporation of a matrix metalloproteinase-sensitive substrate into self-assembling peptides—a model for biofunctional scaffolds. *Biomaterials* **29**, 1713–1719 (2008)
172. Lai, Y.X., Xie, C., Zhang, Z., et al.: Design and synthesis of a potent peptide containing both specific and non-specific cell-adhesion motifs. *Biomaterials* **31**, 4809–4817 (2010)
173. Gristina, A.G.: Biomaterial-centered infection—microbial adhesion versus tissue integration. *Science* **237**, 1588–1595 (1987)
174. Neoh, K.G., Hu, X., Zheng, D., et al.: Balancing osteoblast functions and bacterial adhesion on functionalized titanium surfaces. *Biomaterials* **33**, 2813–2822 (2012)
175. Hetrick, E.M., Schoenfish, M.H.: Reducing implant-related infections: active release strategies. *Chem. Soc. Rev.* **35**, 780–789 (2006)
176. Shi, Z., Neoh, K.G., Kang, E.T., et al.: Titanium with surface-grafted dextran and immobilized bone morphogenetic protein-2 for inhibition of bacterial adhesion and enhancement of osteoblast functions. *Tissue Eng. Part A* **15**, 417–426 (2009)
177. Kim, J., Kim, I.S., Cho, T.H., et al.: Bone regeneration using hyaluronic acid-based hydrogel with bone morphogenetic protein-2 and human mesenchymal stem cells. *Biomaterials* **28**, 1830–1837 (2007)
178. Holland, N.B., Qiu, Y.X., Ruegsegger, M., et al.: Biomimetic engineering of non-adhesive glycocalyx-like surfaces using oligosaccharide surfactant polymers. *Nature* **392**, 799–801 (1998)
179. Vacheethasane, K., Marchant, R.E.: Surfactant polymers designed to suppress bacterial (*Staphylococcus epidermidis*) adhesion on biomaterials. *J. Biomed. Mater. Res.* **50**, 302–312 (2000)

180. Maddikeri, R.R., Tosatti, S., Schuler, M., et al.: Reduced medical infection related bacterial strains adhesion on bioactive RGD modified titanium surfaces: A first step toward cell selective surfaces. *J. Biomed. Mater. Res. A* **84A**, 425–435 (2008)
181. Garcia, A.J., Reyes, C.D.: Bio-adhesive surfaces to promote osteoblast differentiation and bone formation. *J. Dent. Res.* **84**, 407–413 (2005)
182. Groll, J., Fiedler, J., Engelhard, E., et al.: A novel star PEG-derived surface coating for specific cell adhesion. *J. Biomed. Mater. Res. Part A* **74A**, 607–617 (2005)
183. Chen, X., Sevilla, P., Aparicio, C.: Surface biofunctionalization by covalent co-immobilization of oligopeptides. *Colloids Surf. B.* **107**, 189–197 (2013)
184. Geissler, U., Hempel, U., Wolf, C., et al.: Collagen type I-coating of Ti6Al4 V promotes adhesion of osteoblasts. *J. Biomed. Mater. Res.* **51**, 752–760 (2000)
185. Roehlecke, C., Witt, M., Kasper, M., et al.: Synergistic effect of titanium alloy and collagen type I on cell adhesion, proliferation and differentiation of osteoblast-like cells. *Cells Tissues Organs* **168**, 178–187 (2001)
186. Morra, M., Cassinelli, C., Cascardo, G., et al.: Surface engineering of titanium by collagen immobilization. Surface characterization and in vitro and in vivo studies. *Biomaterials* **24**, 4639–4654 (2003)
187. Morra, M., Cassinelli, C., Cascardo, G., et al.: Collagen I-coated titanium surfaces: Mesenchymal cell adhesion and in vivo evaluation in trabecular bone implants. *J. Biomed. Mater. Res. A* **78A**, 449–458 (2006)
188. Muller, R., Abke, J., Schnell, E., et al.: Surface engineering of stainless steel materials by covalent collagen immobilization to improve implant biocompatibility. *Biomaterials* **26**, 6962–6972 (2005)
189. Muller, R., Abke, J., Schnell, E., et al.: Influence of surface pretreatment of titanium- and cobalt-based biomaterials on covalent immobilization of fibrillar collagen. *Biomaterials* **27**, 4059–4068 (2006)
190. Couchourel, D., Escoffier, C., Rohanizadeh, R., et al.: Effects of fibronectin on hydroxyapatite formation. *J. Inorg. Biochem.* **73**, 129–136 (1999)
191. Garcia, A.J., Ducheyne, P., Boettiger, D.: Effect of surface reaction stage on fibronectin-mediated adhesion of osteoblast-like cells to bioactive glass. *J. Biomed. Mater. Res.* **40**, 48–56 (1998)
192. Pegueroles, M., Aguirre, A., Engel, E., et al.: Effect of blasting treatment and Fn coating on MG63 adhesion and differentiation on titanium: a gene expression study using real-time RT-PCR. *J. Mater. Sci. Mater. Med.* **22**, 617–627 (2011)
193. El-Ghannam, A., Starr, L., Jones, J.: Laminin-5 coating enhances epithelial cell attachment, spreading, and hemidesmosome assembly on Ti-6Al-4 V implant material in vitro. *J. Biomed. Mater. Res.* **41**, 30–40 (1998)
194. Werner, S., Huck, O., Frisch, B., et al.: The effect of microstructured surfaces and laminin-derived peptide coatings on soft tissue interactions with titanium dental implants. *Biomaterials* **30**, 2291–2301 (2009)
195. Werner, S., Kocgozlu, L., Huck, O., et al.: Epithelial cell adhesion on a new laminin-5 functionalized porous titanium material. *Int. J. Artif. Organs* **31**, 639–649 (2008)
196. Lange, K., Herold, M., Scheideler, L., et al.: Investigation of initial pellicle formation on modified titanium dioxide (TiO₂) surfaces by reflectometric interference spectroscopy (RIfS) in a model system. *Dent. Mater.* **20**, 814–822 (2004)
197. Rezanian, A., Healy, K.E.: Biomimetic peptide surfaces that regulate adhesion, spreading, cytoskeletal organization, and mineralization of the matrix deposited by osteoblast-like cells. *Biotechnol. Prog.* **15**, 19–32 (1999)
198. Lynch, S.E., Buser, D., Hernandez, R.A., et al.: Effects of the platelet-derived growth-factor insulin-like growth factor-i combination on bone regeneration around titanium dental implants—results of a pilot-study in beagle dogs. *J. Periodontol.* **62**, 710–716 (1991)
199. Ito, Y., Chen, G.P., Imanishi, Y.: Micropatterned immobilization of epidermal growth factor to regulate cell function. *Bioconjug. Chem.* **9**, 277–282 (1998)

200. Kuhl, P.R., Griffiths, L.G.: Tethered epidermal growth factor as a paradigm for growth factor-induced stimulation from the solid phase. *Nat. Med.* **2**, 1022–1027 (1996)
201. Jensen, E.D., Gopalakrishnan, R., Westendorf, J.J.: Bone morphogenetic protein 2 activates protein kinase d to regulate histone deacetylase 7 localization and repression of runx2. *J. Biol. Chem.* **284**, 2225–2234 (2009)
202. Yamaguchi, A., Komori, T., Suda, T.: Regulation of osteoblast differentiation mediated by bone morphogenetic proteins, hedgehogs, and Cbfa1. *Endocr. Rev.* **21**, 393–411 (2000)
203. Suzawa, M., Takeuchi, Y., Fukumoto, S., et al.: Extracellular matrix-associated bone morphogenetic proteins are essential for differentiation of murine osteoblastic cells in vitro. *Endocrinology* **140**, 2125–2133 (1999)
204. Fiorellini, J.P., Buser, D., Riley, E., et al.: Effect on bone healing of bone morphogenetic protein placed in combination with endosseous implants: A pilot study in beagle dogs. *Int. J. Periodont. Rest.* **21**, 41–47 (2001)
205. Marukawa, E., Asahina, I., Oda, M., et al.: Functional reconstruction of the non-human primate mandible using recombinant human bone morphogenetic protein-2. *Int. J. Oral Max. Surg.* **31**, 287–295 (2002)
206. Seol, Y.J., Park, Y.J., Lee, S.C., et al.: Enhanced osteogenic promotion around dental implants with synthetic binding motif mimicking bone morphogenetic protein (BMP)-2. *J. Biomed. Mater. Res. A* **77A**, 599–607 (2006)
207. Leong, L.M., Brickell, P.M.: Bone morphogenetic protein-4. *Int. J. Biochem. Cell B* **28**, 1293–1296 (1996)
208. Morra, M.: Biochemical modification of titanium surfaces: Peptides and ECM proteins. *Eur. Cells Mater.* **12**, 1–15 (2006)
209. Schmidmaier, G., Wildemann, B., Ostapowicz, D., et al.: Long-term effects of local growth factor (IGF-I and TGF-beta 1) treatment on fracture healing—a safety study for using growth factors. *J. Orthop. Res.* **22**, 514–519 (2004)
210. Ruoslahti, E.: Proteoglycans in cell regulation. *J. Biol. Chem.* **264**, 13369–13372 (1989)
211. Rammelt, S., Illert, T., Bierbaum, S., et al.: Coating of titanium implants with collagen, RGD peptide and chondroitin sulfate. *Biomaterials* **27**, 5561–5571 (2006)
212. Zou, X.N., Li, H.S., Chen, L., et al.: Stimulation of porcine bone marrow stromal cells by hyaluronan, dexamethasone and rhBMP-2. *Biomaterials* **25**, 5375–5385 (2004)
213. Chen, W.Y.J., Abatangelo, G.: Functions of hyaluronan in wound repair. *Wound Repair Regen* **7**, 79–89 (1999)
214. Morra, M., Cassinelli, C., Cascardo, G., et al.: Covalently-linked hyaluronan promotes bone formation around Ti implants in a rabbit model. *J. Orthop. Res.* **27**, 657–663 (2009)
215. Fisher, L.W., Fedarko, N.S.: Six genes expressed in bones and teeth encode the current members of the SIBLING family of proteins. *Connect. Tissue Res.* **44**, 33–40 (2003)
216. Young, M.F.: Bone matrix proteins: Their function, regulation, and relationship to osteoporosis. *Osteoporos. Int.* **14**, S35–S42 (2003)
217. Yoshitake, H., Rittling, S.R., Denhardt, D.T., et al.: Osteopontin-deficient mice are resistant to ovariectomy-induced bone resorption. *P. Natl. Acad. Sci. USA* **96**, 8156–8160 (1999)
218. Asou, Y., Rittling, S.R., Yoshitake, H., et al.: Osteopontin facilitates angiogenesis, accumulation of osteoclasts, and resorption in ectopic bone. *Endocrinology* **142**, 1325–1332 (2001)
219. Boskey, A., Spevak, L., Tan, M., et al.: Dentin sialoprotein (DSP) has limited effects on in vitro apatite formation and growth. *Calcif. Tissue Int.* **67**, 472–478 (2000)
220. Hunter, G.K., Goldberg, H.A.: Nucleation of hydroxyapatite by bone sialoprotein. *Proc. Natl. Acad. Sci. USA* **90**, 8562–8565 (1993)
221. Fisher, L.W., Torchia, D.A., Fohr, B., et al.: Flexible structures of SIBLING proteins, bone sialoprotein, and osteopontin. *Biochem. Biophys. Res. Commun.* **280**, 460–465 (2001)
222. Tye, C.E., Rattray, K.R., Warner, K.J., et al.: Delineation of the hydroxyapatite-nucleating domains of bone sialoprotein. *J. Biol. Chem.* **278**, 7949–7955 (2003)
223. Fujisawa, R., Kuboki, Y.: Affinity of bone sialoprotein and several other bone and dentin acidic proteins to collagen fibrils. *Calcif. Tissue Int.* **51**, 438–442 (1992)

224. Tye, C.E., Hunter, G.K., Goldberg, H.A.: Identification of the type I collagen-binding domain of bone sialoprotein and characterization of the mechanism of interaction. *J. Biol. Chem.* **280**, 13487–13492 (2005)
225. Karadag, A., Ogbureke, K.U.E., Fedarko, N.S., et al.: Bone sialoprotein, matrix metalloproteinase 2, and alpha (v) beta (3) integrin in osteotropic cancer cell invasion. *J. Natl. Cancer Inst.* **96**, 956–965 (2004)
226. Goldberg, H.A., Warner, K.J., Li, M.C., et al.: Binding of bone sialoprotein, osteopontin and synthetic polypeptides to hydroxyapatite. *Connect. Tissue Res.* **42**, 25–37 (2001)
227. Byzova, T.V., Kim, W., Midura, R.J., et al.: Activation of integrin alpha (V) beta (3) regulates cell adhesion and migration to bone sialoprotein. *Exp. Cell Res.* **254**, 299–308 (2000)
228. Grzesik, W.J., Robey, P.G.: Bone matrix RGD glycoproteins: immunolocalization and interaction with human primary osteoblastic bone cells in vitro. *J. Bone Miner. Res.* **9**, 487–496 (1994)
229. Chen, J., Shapiro, H.S., Sodek, J.: Development expression of bone sialoprotein mRNA in rat mineralized connective tissues. *J. Bone Miner. Res.* **7**, 987–997 (1992)
230. Cooper, L.F., Yliheikkilä, P.K., Felton, D.A., et al.: Spatiotemporal assessment of fetal bovine osteoblast culture differentiation indicates a role for BSP in promoting differentiation. *J. Bone Miner. Res.* **13**, 620–632 (1998)
231. Gordon, J.A., Tye, C.E., Sampaio, A.V., et al.: Bone sialoprotein expression enhances osteoblast differentiation and matrix mineralization in vitro. *Bone* **41**, 462–473 (2007)
232. Luo, G., Ducy, P., McKee, M.D., et al.: Spontaneous calcification of arteries and cartilage in mice lacking matrix GLA protein. *Nature* **386**, 78–81 (1997)
233. Beertsen, W., Vandenbos, T., Niehof, J.: Mineralization of dentinal collagen sheets complexed with alkaline-phosphatase and integration with newly formed bone following subperiosteal implantation over osseous defects in rat calvaria. *Bone Miner.* **20**, 41–55 (1993)
234. Bellows, C.G., Aubin, J.E., Heersche, J.N.M.: Initiation and progression of mineralization of bone nodules formed invitro—the role of alkaline-phosphatase and organic phosphate. *Bone Miner.* **14**, 27–40 (1991)
235. Termine, J.D., Kleinman, H.K., Whitson, S.W., et al.: Osteonectin, a bone-specific protein linking mineral to collagen. *Cell* **26**, 99–105 (1981)
236. Delany, A.M., Amling, M., Priemel, M., et al.: Osteopenia and decreased bone formation in osteonectin-deficient mice. *J. Clin. Invest.* **105**, 1325–1325, 915 (2000)
237. Brogden, K.A.: Antimicrobial peptides: Pore formers or metabolic inhibitors in bacteria? *Nat. Rev. Microbiol.* **3**, 238–250 (2005)

Chapter 5

Nano-Bio Structures Developed via Electrophoresis

Cyrus Zamani

Abstract In recent decades, application of electric fields for manipulation of biological particles has been witnessing a rapid growth. Electrophoresis, in particular, now is a phenomenon with widespread use in biological applications and processes for manipulation of biological species such as cells, enzymes and proteins. Electrophoretic deposition (EPD) is a cheap and versatile technique based on electrophoresis in which charged particles suspended in a liquid medium move toward a substrate and deposit there following the electric field lines. Historically, only DC fields have been tried for material deposition since it was theoretically accepted that AC electric fields cause particles oscillate at their position due to field reversal in each half cycle. Recently, however, researchers showed that alternating fields can also be employed for material deposition, a fact which attracted the attention of scientists to its potentiality in separation, trapping, assembling, transportation and characterization of nano/bio particles. Works on bio-particles are performed in a wide range of frequencies. However, low frequencies (below 10 kHz) are not preferred for manipulation of bio-species. Thus, experimental and theoretical studies have been focused on application of high frequency AC electric fields so far. Ceramic particles, in contrast, are not sensitive to non-aqueous medium without the risk of electrolysis and working at low frequencies becomes possible. Therefore, low frequency AC electrophoretic deposition (LFACEPD) is considered as a promising process for manipulation and controlled deposition of bioactive ceramic oxide thin films. This chapter deals with electrophoretic manipulation of oxide nanoparticles—through experiments as well as theoretical computations—for being deposited as bioactive thin films on substrates of various conductivities introducing some phenomena arising in such systems.

C. Zamani (✉)

Department of Electrònica, Universitat de Barcelona, 08028 Barcelona, Spain
e-mail: czamani@el.ub.es

5.1 Introduction

The need for small-size products forced researchers in academia and industry to dedicate their time to the effective methods for downsizing components during the last decade. This, of course, requires processes which can be adapted to the miniaturization trends. Compared to conventional devices, advanced miniaturized instruments are expected to operate in a faster and more efficient manner. Started with electronic parts, downsizing is now extended to all product categories and scientific fields including chemical and biological systems. Thus, thanks to nanotechnology, large size and expensive equipment are now being substituted with portable products which in many cases are even offered for personal use. The miniaturization strategies are mainly based on substitution of bulk materials with thick or thin films (of the same material or modified compositions). Biomedical and biological thin and thick films are produced through various methods such as spin coating [1], electrospray deposition [2] pulsed laser deposition [3, 4], Langmuir–blodgett [5–7], sputtering [8], layer by layer assembly [9–13], and sol-gel [14] successfully which give coatings in the range of a few nanometers to several millimeters depending on the technique and adjusted parameters (see Table 5.1). Each method comes with its advantages and drawbacks. But all these methods require expensive specialty equipment. Electrophoretic deposition (EPD), on the other hand, is considered as one of those enabling technologies which does not require sophisticated systems, a fact which has attracted the attention of scientists to extend its field of applications from ceramic particles to biological species. Usually, EPD is used for coating purposes although it has been also introduced as a near-net-shape manufacturing process [15–17]. In addition to its traditional use in separation of bioparticles such as proteins and DNA [18], successful deposition of thick and thin films of bioactive materials and biological species is already reported [19–22]. Electrophoretic deposition is now used as an industrial process. However, the process is not fully understood and many aspects

Table 5.1 Typical thickness ranges obtained by using various coating processes

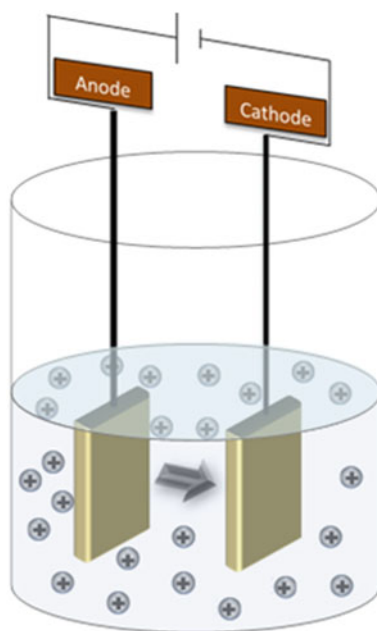
Process	Typical thickness range
Powder metallurgy	>50 microns
Screen printing	>10 microns
Dip coating	50–1,000 microns
Thermal spraying	>10 microns
CVD and PVD	0.5–50 microns
Sol-gel	5 nm–10 microns
Sputtering and ion implantation	10 nm–1 micron
Pulsed laser deposition (PLD)	1–200 nm
Electrophoresis	100 nm–100 microns

remain challenging [23]. This chapter tries to review the applications of electrophoretic set-ups in deposition of thick and thin nanobiomaterials. The main focus will be on the non-uniform AC electric fields which appear to be the most promising area in particle manipulation and deposition.

5.2 Electrophoresis: Principles

Migration of charged species under the influence of an electric field is called electrophoresis. The phenomenon occurs in a liquid medium in which, particles are suspended. It is generally said that positively charged particles move towards negative electrode (cathode) while negatively charged particles are attracted by positive electrode (anode), Fig. 5.1; thus resulting into deposition of the materials in the form of thick or thin films. Electrophoretic deposition (EPD) is, therefore, considered as a two-step (i.e. particle movement and subsequent deposition on electrode) material-processing technique with several parameters which should be optimized to obtain the desired product. Deposited material is, usually, a powder compact which needs further densification process. The phenomenon has been the topic of many publications and is already reviewed in many aspects [24–31]. In this section, therefore, the process is briefly described in order to provide the basic knowledge needed for manipulation of nano/bio particles for their deposition and in vivo applications.

Fig. 5.1 Schematic illustration of a simple electrophoretic setup. Charged particles move towards oppositely-charged electrode



5.3 Governing Equations

In electrophoresis, only charged particles can move in response to the applied field. Particle velocity is dictated by the net charge surrounding the particle which is different from the surface charge. In fact, formation of a double layer in the vicinity of the particle surface with oppositely-charged ions and the corresponding zeta potential determine its speed inside the liquid medium.

A charged particle (q) exposed to uniform electric field (E) will experience the force (F) defined as follows (known as electrophoretic force):

$$\vec{F}_e = q\vec{E} \quad (5.1)$$

The electrophoretic force is opposed by a friction force, a retardation force due to the effect of applied field on counter ions, and a relaxation force originated from displacement between the centers of positive and negative charges (asymmetric double layer), Fig. 5.2. The classical approach to solve the electrophoretic system ignores all decelerating forces except friction force so that:

$$F_{tot} = \vec{F}_e + \vec{F}_f \quad (5.2)$$

\vec{F}_f is the friction force exerted by the suspending medium and can be calculated from:

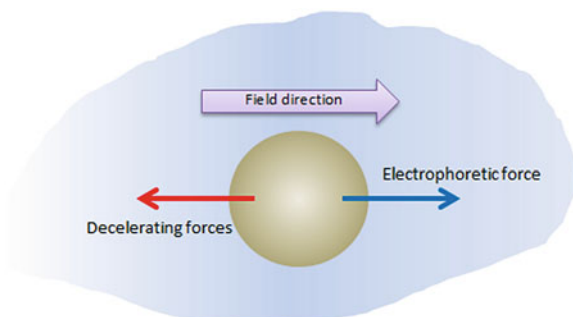
$$\vec{F}_f = -f\vec{v} \quad (5.3)$$

where f and \vec{v} are friction coefficient and particle velocity vector. The friction coefficient, itself, is a function of particle's shape and size and can cause particle to reach a terminal velocity (\vec{v}):

$$\vec{v} = \frac{q\vec{E}}{f} \quad (5.4)$$

The ability of particles to move through the suspending medium is determined with its mobility defined as:

Fig. 5.2 Forces exerted on a particle in an electrophoretic assembly



$$\mu = \frac{\bar{v}}{\bar{E}} \quad (5.5)$$

In electrophoresis, it is assumed that with addition of particles, the solution is polarized. To have the system completely known, electrical potential, fluid flow, and conservation of mass (represented by Poisson, Navier-Stokes, and Nernst-Planck equations respectively) should be solved simultaneously. This is a difficult task as no analytical solution exists. Therefore the following equation (proposed by Henry) gives an estimate of the mobility for low surface charge density particles:

$$\mu = \left[\frac{2\varepsilon\xi}{3\eta} \right] f(\kappa a) \quad (5.6)$$

where ε , ξ , η , a , and κ are dielectric constant of the solution, zeta-potential, solution's viscosity, Particle radius, and the inverse of Debye-length respectively [32]. Debye-length (κ^{-1}) is a deterministic feature of the aqueous systems containing charged particles [33]. Poisson-Boltzmann equation (PB) is used to predict the Debye-length:

$$\kappa^{-1} = \left(\frac{2e^2 z^2 n_\infty}{\varepsilon k_B T} \right)^{-1/2} \quad (5.7)$$

where e , z , n_∞ , k_B , and T are the charge of electron, valence of the ionic species, ionic concentration, Boltzmann constant, and temperature respectively.

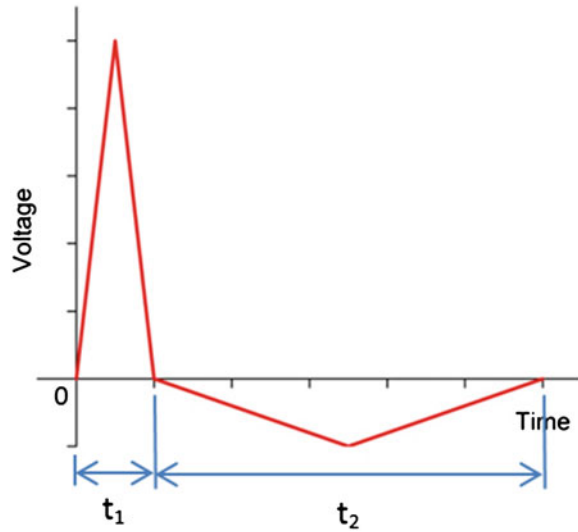
For extremely small particles, κ is small (κ^{-1} becomes too large) that κa approaches zero and $f(\kappa a)$ reaches its limit ($f(\kappa a) = 1$). For large particles, on the other hand, $f(\kappa a) = 1.5$ [34].

5.4 DC and AC Electrophoresis

When working with linear fields, DC currents can drive particles toward the oppositely signed electrode. Symmetric AC fields, however, make particles oscillate around a fixed point. Until recently, it was believed that employing AC fields does not result in electrophoresis and this, forced scientists stay away of AC fields for electrophoretic deposition.

Recently, the possibility of electrophoretic in AC fields was reported where researchers make use of modified alternating current in such a way that a net electrophoresis occurs [35–37]. Here, the signals are different in positive and negative part though the net integral is zero in a full cycle (Fig. 5.3). Therefore the relationship between electrophoretic mobility and the electric field is no longer linear, a fact which produces net particle movement in the medium. If the system parameters are adjusted properly (so that a sufficiently asymmetric field is

Fig. 5.3 A typical non-symmetric AC cycle. In a full cycle, the net integral is zero (equal area for positive and negative signals)



produced), this behavior can be used in creating deposited layers through directing suspended particles towards substrates.

5.5 Dielectrophoresis

In electrophoresis, charged particles move following the field lines. In other words, electric charges are needed for the particle to be affected by the field. Dielectrophoresis (the term first used by Pohl [38]), however, occurs when neutral dielectric particles (suspended in a liquid medium) are subjected to a non-uniform electric field resulting to its polarization [39, 40]. This surface charge redistribution gives particle the chance to move in the applied field (Fig. 5.4).

Dielectrophoresis (DEP) has the potentiality to manipulate all kinds of particles whether charged or neutral [41]. The disadvantage is that, in DEP, polarization forces are weak. Thus, large field gradients are needed in order to have the particles moving inside the system. Manipulation of particles will require a force balance in which DEP force is balanced with the drag force (originated from hydrodynamic interaction between particles in the medium), the Brownian motion (random motion of particles in response to temperature), and the buoyancy force (the force exerted by the fluid which opposes the particle weight). In other words, the total force experienced by particle can be written as:

$$F_{Total} = F_{DEP} + F_{Drag} + F_{Brownian} + F_{Bouyancy} \quad (5.8)$$

The drag force is a linear function of particle velocity and depends on the particle shape and fluid's viscosity. For a spherical particle of radius "a":

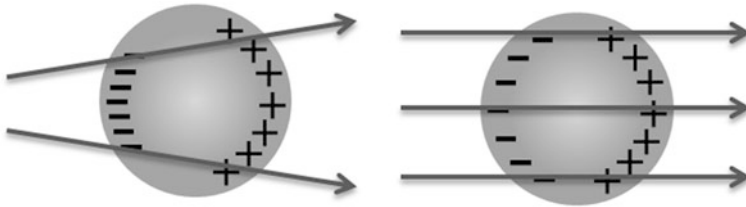


Fig. 5.4 Polarization and movement of dielectric particles by dielectrophoresis. Non-uniform fields polarize neutral particles and help them move. The field gradient plays a key role in particle trajectory

$$F_{Drag} = -6\pi\eta aU \tag{5.9}$$

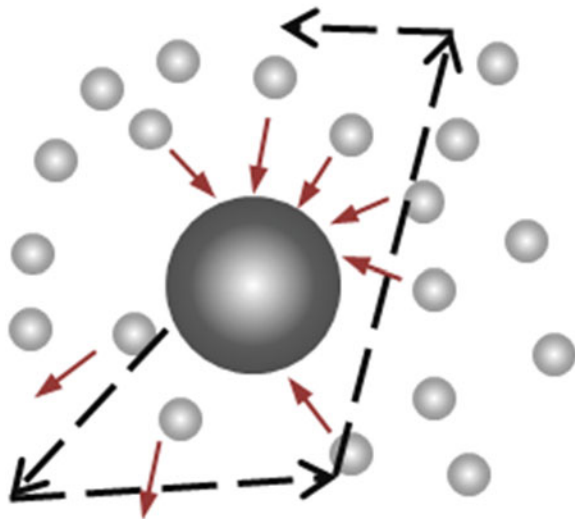
where η is the viscosity and U is the particle velocity. The shape dependence is already discussed by several researchers [42–45]. The equation, moreover, does not consider the fluid heating.

Particles suspended in a fluid are continuously hit by the fluid’s molecules. These impingements gain importance especially when particles are extremely small in size. Random impingements result in particle movement in random paths, a phenomenon called Brownian motion, Fig. 5.5.

Based on the Einstein’s theory of Brownian motion, the main parameter in the random displacement of small particles is the diffusion coefficient (D) and particles follow a Gaussian profile:

$$|\Delta x|^2 = 2Dt \tag{5.10}$$

Fig. 5.5 Random movement of the particle suspended in a solution. Impingement of the fluid’s molecules with particles make them move randomly



$$D = \frac{kT}{f} \quad (5.11)$$

Δx is the displacement, k is the Boltzmann constant (1.38×10^{-16} erg/K), T is temperature, and f is the friction factor. Then, the force is determined to be:

$$F_{Brownian} = \zeta \sqrt{\frac{2kTf}{\Delta t}} \quad (5.12)$$

where ζ possesses a random value between 0 and 1, and Δt is the time interval.

The friction factor is different for particles of different geometries. Values are compared in Table 5.2 [46–49].

Finally, the buoyancy force is calculated based on the following equation:

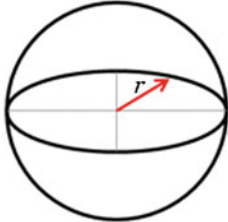

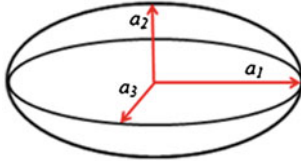
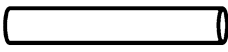
$$F_{Buoyancy} = g(\rho_{particle} - \rho_{medium})V_{particle} \quad (5.13)$$

For spherical particle of radius “ a ”:

$$F_{Buoyancy} = \frac{4}{3}\pi a^3 \Delta \rho g \quad (5.14)$$

where g is the gravitational acceleration and $\Delta \rho$ is the density difference between the particle and the suspending medium. For sub-micron particles, the buoyancy

Table 5.2 Friction factors for different geometries

Particle geometry	Friction factor (f)	Illustration
Spherical ($a_1 = a_2 = a_3 = r$)	$f = 6\pi\eta r$	
Disk ($a_1 = a_2 = r \gg a_3$) moving face parallel to a_3	$f = 16\eta r$	
Disk ($a_1 = a_2 = r \gg a_3$) moving edge perpendicular to a_3	$f = \frac{32}{3}\eta r$	
Disk ($a_1 = a_2 = r \gg a_3$) random movement	$average\langle f \rangle = 12\eta r$	
Ellipsoid ($a_1 \gg a_2 = a_3$) moving parallel to a_1	$f = \frac{8\pi\eta a_1}{2 \ln(2a_1/a_2) - 1}$	
Ellipsoid ($a_1 \gg a_2 = a_3$) moving perpendicular to a_1	$f = \frac{16\pi\eta a_1}{2 \ln(2a_1/a_2) - 1}$	
Ellipsoid ($a_1 \gg a_2 = a_3$) random movement	$average\langle f \rangle = \frac{6\pi\eta a_1}{2 \ln(2a_1/a_2)}$	
Cylinder (nanotube) ($a_1 = a_2 = d/2, a_3 = l$)	$f = \frac{3\pi\eta l}{\ln(2l/d)}$	

force is neglected since it is overcome by other forces. The force, however, finds a great importance when particles increase in mass which may result into their sedimentation.

The force exerted on a particle in an AC field can be expressed as [50]:

$$F_{DEP} = \Gamma \cdot \epsilon_m \text{Re}\{K_f\} \nabla |E|^2 \quad (5.15)$$

In this equation, Γ is a factor which shows the dependency on particle geometry, ϵ_m is the real part of the permittivity of the liquid medium, K_f is a parameter which depends on the complex permittivities of the medium and the suspended particle, and E is the electric field. When dealing with spherical particles, K_f is called Clausius-Mossotti factor defined as:

$$K_f = \frac{\epsilon_p^* - \epsilon_m^*}{\epsilon_p^* + 2\epsilon_m^*} \quad (5.16)$$

where ϵ_p^* and ϵ_m^* are complex permittivity of the particle and medium respectively. K_f is a unique property of the particle in the medium which is used for particle manipulation [39].

In the case of isotropic spherical homogeneous particles, Eq. 5.15 can be rewritten as [51]:

$$F_{DEP} = 2\pi\epsilon_m a^3 \text{Re}[K(\omega)] \nabla |E|^2 \quad (5.17)$$

Equation 5.17 holds true only for DC or stationary AC fields. To calculate the time-averaged force, both magnitude and phase of the field components should be taken into account. Thus, the generalized form of the equation will be [39, 51]:

$$F_{DEP} = 2\pi\epsilon_m a^3 \{ \text{Re}[K(\omega)] \nabla |E|^2 + \text{Im}[K(\omega)] \sum E^2 \nabla \varphi \} \quad (5.18)$$

In the case of bacteria and cells, mobile ions in their structure determine their conductivity so that:

$$\epsilon_p^* = \epsilon_0 \epsilon_p - \frac{j\sigma_p}{\omega} \quad (5.19)$$

In reality, few species come in a spherical homogeneous form and the majority of particles especially biological materials are inhomogeneous. Therefore, above models need some modifications for being applicable to biological species. The most-widely used model for these materials is a multishell structure which can be adapted to several categories of biological materials. Cells and bacteria are modeled this way. Depending on the structure, different number of shells is defined. In the case of viable cells with nucleus, the same model can be used assuming a shell for the membrane around the nucleus which is then simplified to a simple spherical model, Fig. 5.6. Detailed analysis of such structures is presented in [40, 51] and is not discussed here.

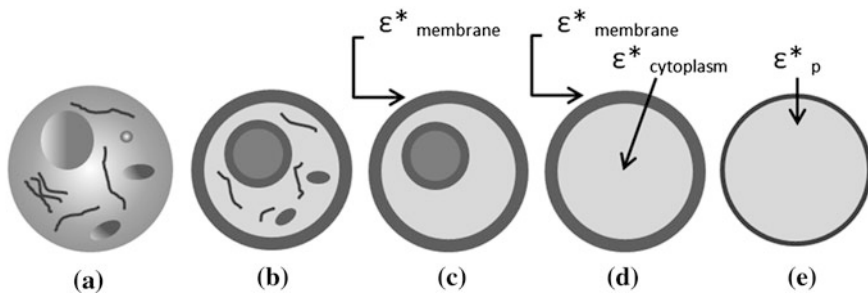


Fig. 5.6 A cell can be simplified for modeling. **a, b** The schematic illustration of the cell and its cross section. **c, d** The whole cell internal sub-structure with cytoplasm is approximated with an effective permittivity ($\epsilon^*_{\text{cytoplasm}}$) and the membrane possesses its own complex permittivity ($\epsilon^*_{\text{membrane}}$). **e** Finally, the entire structure is calculated using an equivalent complex permittivity (ϵ^*_p) assuming a simple sphere (reproduced from [51] with permission)

Elongated particles are immediately aligned with the electric field lines as it is schematically illustrated in Fig. 5.7. For elongated cylindrical particles the Claussius-Mossotti factor and the geometry dependent parameter (Γ) are determined using following equations [52]:

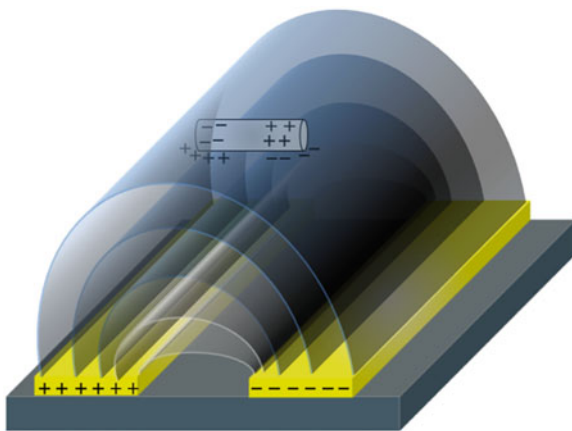
$$K_f = \frac{\epsilon_p - \epsilon_m}{\epsilon_m} \quad (5.20)$$

And

$$\Gamma = \frac{\pi}{6} r^2 l \quad (5.21)$$

In which, r is radius and l is the length of the cylinder. This is the case for many biological and biomimetic materials. For an ellipsoid aligned with the field, DEP force (Eq. 5.15) is determined from:

Fig. 5.7 A nanotube under dielectrophoresis aligned following the field lines. The net force exerted on the nanotube can result in particle movement towards high field or low field regions (i.e. downward or upward respectively)



$$F_{DEP} = \frac{2\pi abc}{3} \varepsilon_m \text{Re}[K(\omega)] \nabla E^2 \quad (5.22)$$

where

$$K(\omega) = \frac{\varepsilon_p^* - \varepsilon_m^*}{\left(\varepsilon_p^* - \varepsilon_m^*\right) A_\alpha + \varepsilon_m^*} \quad (5.23)$$

a , b , and c are ellipsoid's semi-axes. α represents either the x , y , or z axis and A is the depolarization factor [26]. Needle-shape viruses (like tobacco mosaic virus) and many other biological species can be approximated using prolate ellipsoids ($a > b = c$).

Thus, deposition of thick or thin films of bioparticles in the form of cylinders (e.g. carbon nanotubes [52, 53]), ellipsoids [54, 55], and filaments (e.g. actin [50], some bacterial cells [56]) may be formulated using above equations. All these equations assume a uniform and stable particle distribution in the suspension which, in turn, is a challenging work especially for carbon nanotubes [57].

5.6 EPD of Thin Bioactive Films

Almost all classes of materials—whether organic or inorganic—are successfully deposited via electrophoresis. Examples are metals, oxides, nitrides, borides, and different families of polymeric materials such as resins, polyamides, polyurethanes, and various categories of copolymers [58].

Among numerous applications of EPD process, traditionally, the most evident works are done in coating of surfaces. Biomedical applications started with deposition of coatings on metallic substrates (stainless steels, titanium and titanium alloys) for implants. In such applications, the coating is expected to offer a bioactive surface (to support the ingrowth and osseointegration) with a high degree of compatibility to the touching issue. Also, it acts as a barrier preventing direct contact of the metallic implant with live tissues thus blocking the release of dangerous metal ions. In this scenario, hydroxyapatite (HA) has a long history and a great number of works have been concentrated on this material with the formula $\text{Ca}_{10}(\text{PO}_4)_6(\text{OH})_2$. The reason is its similarity to the main mineral component of the bones and its ability to integrate in bone structure without the risk of dissolution.

HA coatings are deposited in the form of porous thick films. The porous structure is a must for osseointegration (direct connection between bone and the implant). EPD is widely employed in preparation of such structures where fine particles of PTFE or polystyrene (PS) are used as templates [59, 60]. The advantage of utilizing polymers is that they facilitate low temperature processing of materials. These templates are then burned out leaving pores inside the coating. Also, patterned HA coatings can be prepared for biosensing or other applications [61].

Apart from the classical case of HA, there exist several other categories of biomedical materials deposited in the form of thick or thin films via EPD. Other bioactive materials such as silicate glass, and bioceramics (e.g. zirconia, alumina, nacre), Biocomposites (e.g. composites of HA with Fe_3O_4 , CaO, CaCO_3 , or polymer bioceramic composites), and functionally graded coatings are also reported [62–67].

Electrochemical processes can accomplish several desirable effects for bio-applications. In fact, using such methods it is possible to engineer the surface morphology in order to enhance its bioactivity, and in vivo corrosion resistance. Moreover, EPD processes are able to create coatings with controlled porous structure for a programmable drug release inside the body [68]. Among different classes of materials, those with mesoporous structure can offer a combination of properties such as porous structure, mechanical strength and biocompatibility. Mesoporous bioactive glass (MBG) is the most important material studied for in vitro applications. The tunable pore size and controllable structure of the pores, introduce this category of materials as a new generation of biomaterials for bone reconstruction and regeneration, drug delivery, tissue engineering and even tumor treatment [69–72]. The reason for this selection is that with implanting MBGs inside the human body, a layer of hydroxycarbonate apatite (HCA, which makes the inorganic part of the bone) is formed on the surface (i.e. a good bioactivity). A TEM image of a thin film of MBG presented in Fig. 5.8 shows the ordered mesostructure of the material with nanometric pore size. In Fig. 5.9, a mesoporous silica layer is depicted which is covered by protein through EPD. Adsorption of protein on the host surface is the first stage of integration between the host and biomaterial and is of great importance since a good bonding is needed to guarantee the growth of the tissue.

Fig. 5.8 TEM image of MBG revealing ordered mesostructure suitable for in vitro applications

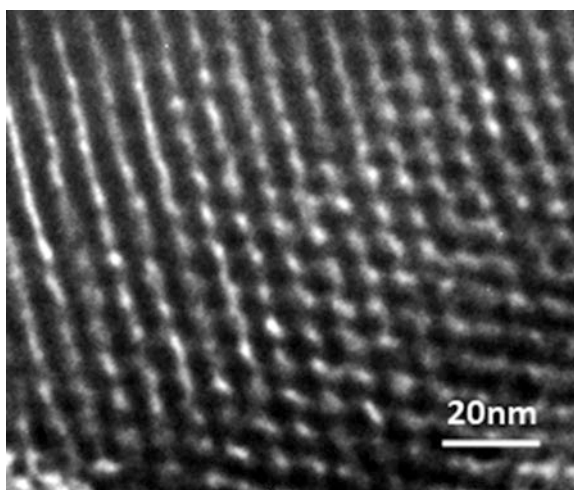
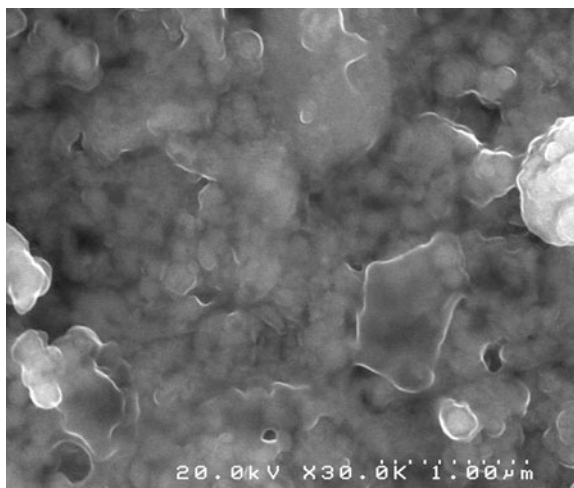


Fig. 5.9 SEM image of mesoporous silica with enhanced bioactivity. The protein layer covers the surface



5.7 EPD of Biological Entities

Technologies based on Electrophoresis are unique since they enable us to work in a wide range of size from a few nanometers to several microns covering all biological species from DNA to bacteria. Almost all biological species can be manipulated by using electrophoresis. This is due to the fact that biological materials are either charged or they can be polarized easily. From size characteristics point of view, fortunately, a great number of members of the biomaterials' family lie in the acceptable range (nm-microns) for EPD since they can be prepared in the form of colloidal suspensions. Red blood cells, viruses, bacteria, DNA, all and all are examples of such bioparticles. Usually, single molecules are a few nanometers in size. Therefore, thin molecular layers can be deposited if a proper technique is employed.

In addition to biological species, synthetic materials such as zirconia [73] and carbon nano-tubes [74] have also gained a big attention due to their excellent mechanical properties and compatibility to human-body. The extraordinary combination of high strength and flexibility and their resistance to corrosion introduces carbon nano-tubes as distinguished candidates for biological applications. Thus, a great effort is ongoing for deposition of thick and thin films of such materials as well as other bioactive ceramics on different substrates both for in vitro as well as in vivo applications. The majority of these works are based on DEP technique.

5.8 Film Deposition: Simulation and Practice

Prediction of nano/bio particle trajectory is a must for processes such as sorting bio species and bio-sensing. Manipulation and deposition of nanosized bioparticles through electrophoretic processes require a deep knowledge on the behavior of the system under study. In the case of biological systems, water is the preferred medium. Water, however, is hydrolyzed when DC field are applied (this, in practice, occurs at voltages about 3–4 V or above), a problem which may result in high current densities and ruins the integrity of coating due to the formation of hydrogen and oxygen bubbles on the electrode surface. To solve this problem, several tricks are tried by researchers such as addition of chemical materials to the system [75], application of membranes [76], absorbing hydrogen using palladium electrode [77], or working at low voltages [78]. To these, the utilization of non-aqueous solutions as the solvent should be added [79]. Nevertheless, none of the proposed methods can prevent water decomposition and other strategies are needed to overcome this. Hirata suggested that AC electric fields at frequencies of about 10 kHz can be used to deposit thick alumina layers from aqueous systems [80] although his results confirm deposition through a diffusional mechanism instead of an electrophoretic process. Neirinck et al. employed high frequency AC fields for deposition of α -Al₂O₃ films [37]. They stated that although in AC field particles are exerted to the field reversal in each half-cycle, the field for re-suspending deposited particles is smaller than the deposition counterpart, thus only particles weakly connected to the deposited layer are re-suspended. This gives dense layers. The first report on deposition of Si thick films using non-uniform low frequency AC field was published by Gardeshzadeh et al. [81]. Aimed at understanding the deposition mechanism for extending results to nanobiotechnology, Riahifar et al. preformed a detailed study on electrophoretic deposition of nano-bioparticles in non-uniform AC electric fields [82]. They analyzed the system carefully taking all forces and possible phenomena into account and reached to this conclusion that in a system comprised of parallel planar electrodes, there exists a region above the electrode surface where particles can reach electrode surface following the field lines while particles outside this volume keep in their position oscillating around a fixed point. Inside this region—called electric field affected zone (EFAZ)—the field is strong enough to overcome other forces pushing them towards the substrate where they can deposit, Fig. 5.10. Therefore, different trajectories are seen for particles located at different distances from electrode edge so that some particles have no chance to reach to the substrate, Fig. 5.11. The Brownian motion takes the role only if the particle size is below 50 nm which is much smaller than the size of many biological species. Therefore, it is expected that following the same trend, thin films of biological materials can also be deposited.

Based on their findings, increasing frequency leaves no time for the particles to move towards the substrate, so the chance of deposition is decreased. The process starts from the electrode edge where the field is intense and as the time passes by,

Fig. 5.10 Particles located at various distances from the electrode surface experience different electrophoretic forces. Nano/bio particles close to the surface have a great chance to deposit on the substrate since they are subjected to substantially intense field. Values in micrometers show the distances from electrode surface (reproduced from [83])

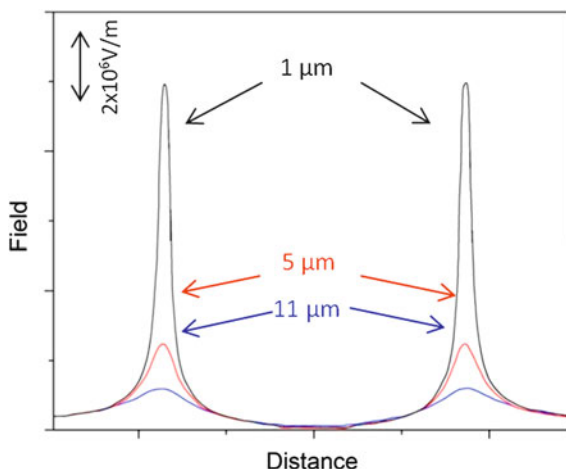
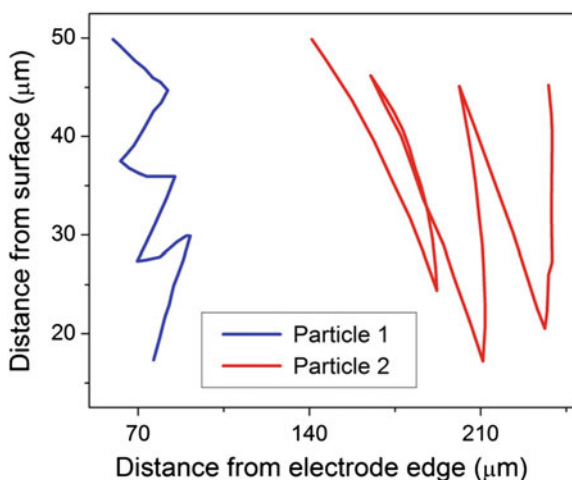


Fig. 5.11 Trajectory of two particles located at different positions with respect to the electrode edge. Both particles start at the same elevation. Particle 1 moves towards electrode which may result into deposition. In contrast, particle 2 does not have any chance to reach to the surface (reproduced from [83])



the deposited area is extended inside the gap, Fig. 5.12. It should be noted that particles may also be pushed by the tangential force exerted by electroosmosis so that a deposition band (parallel to the electrode edge) can be formed away from the gap space [84]. For frequencies above 10 kHz, particles can aggregate forming pearl chains. In this case, the field-induced force between particles is proportional to $r^3 \epsilon_m |u^*|^2 E^2$ where u^* is the Clausius–Mossotti factor [85]. For non-spherical particles, the stability conditions are satisfied only when the elongated particle is aligned with the longest axis along the field lines (the phenomenon is also called electro-rotation and originates from the torque produced in the dipole as a result of the separation of charge centers). An example of such chains are shown in Fig. 5.13 where the chains of CdO are clearly seen in the SEM images.

Fig. 5.12 Film formation process in a dielectrophoresis assembly with in-plane electrodes. Deposition starts from electrode edges where the field is intense. After reaching to the gap, the film starts to form and grow until the gap is filled (reproduced with permission from [83])

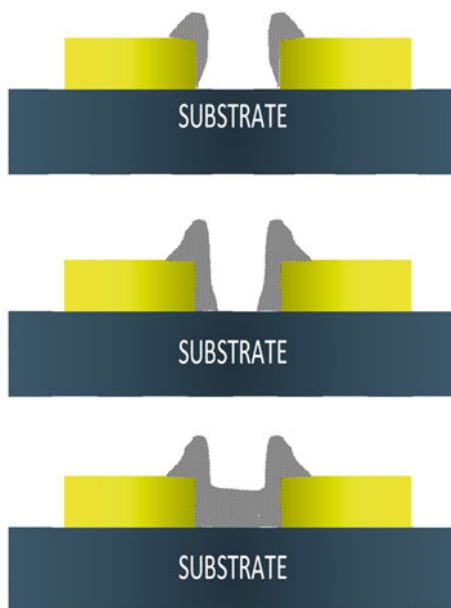


Fig. 5.13 A thin film of CdO nanoparticles bridging the gap. Pearl chain is a well-suited structure for nano/bio sensing

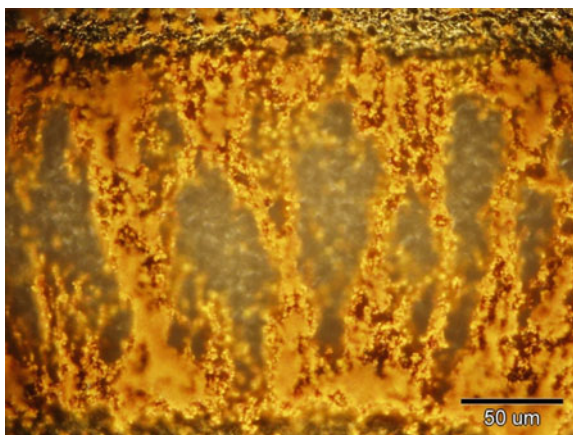


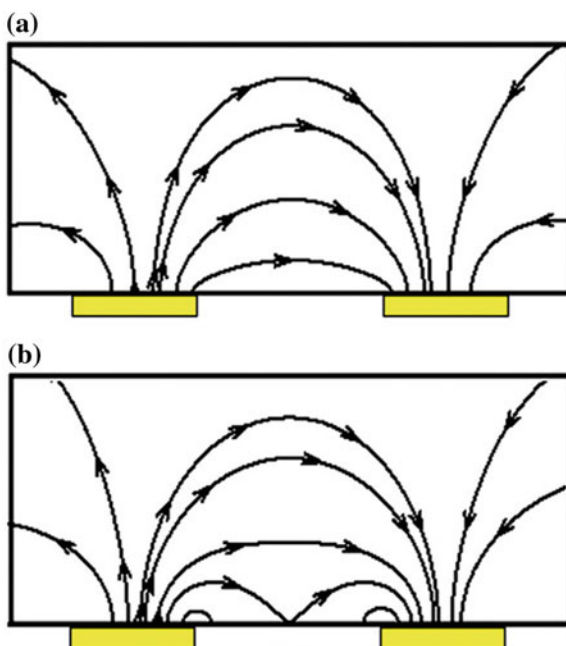
Table 5.3 summarizes the observed mechanisms in different frequency intervals.

5.9 EPD-Deposited Films: Emerging Applications

One of the interesting findings of Riahifar et al. is the possibility of deposition on non-conducting substrates. Figure 5.14 depicts the field lines for 2 types of substrates, i.e. an insulator (non-conductive) and an insulator with surface charges

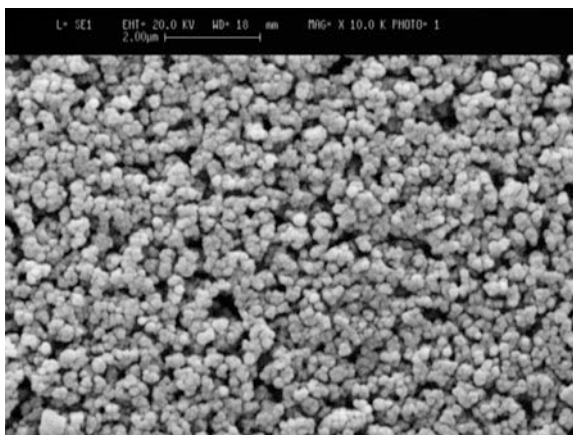
Table 5.3 Deposition mechanisms and possible applications of electrophoretically deposited layers

Frequency range	Proposed mechanism	Application
<1 Hz	Oscillatory EP force (only electrodes are covered)	Coating implants (equivalent to DC)
1 to 10 Hz	Unsteady-state liquid flow (gap filling)	Micro-patterning
10 Hz to 10 kHz	AC-electroosmosis	Bioparticle separation, screening nanomaterials
>10 kHz	Pearl chain formation	Thin and thick films for nano-bio sensing

Fig. 5.14 Effect of substrate conductivity on field lines for an electrophoretic assembly with in-plane electrodes [86]

(conductive) [86, 87]. Both simulations and experiments suggest deposition on insulator surfaces with some charges on the surface (which is the case for many ceramic materials). This feature may be used in deposition of thin or thick biological films on ceramic implants. An image of TiO_2 nanoparticles deposited on alumina substrate is presented in Fig. 5.15 where a rather homogeneous film is obtained. Titania is a photoactive anti-pathogenic material presenting itself as a disinfectant for viruses and bacteria. Usually, such biocide films are deposited via sophisticated techniques such as CVD or sputtering [88, 89]. Now, these processes may be substituted with EPD as a cheap, simple, and reliable method.

Fig. 5.15 Mesostructured TiO_2 film deposited via electrophoresis for in vitro applications



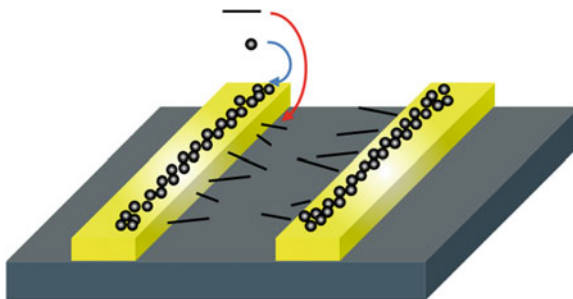
5.10 Particle Separation and Sorting

As an important task in biology, bio species are sorted before being deposited on the substrate. Separation of biospecies using DEP has almost a half century of history [90].

The field of bioseparation is now of great importance not only in biology, but also in engineering, protection of global environment, recycling and other discipline. This, however, falls beyond the topic of this chapter and is not discussed here. Instead, the focus will be on particle sorting for film deposition.

In an electrophoretic setup, sorting and separation of bioparticles and their immobilization or deposition on the surface is done through adjusting process parameters in a way that a combination of dielectrophoresis and AC-electroosmosis forces provides different paths for particles of different size, geometry or chemical properties. This results to formation of organized films of sorted species in various locations of the system as it is indicated schematically in Fig. 5.16. In this figure (valid for low frequencies) DEP forces are in competition with the fluid flow induced by electroosmosis. High degree of polarization occurred in rod-like particles leads to strong interactions between particle and electrode edge following

Fig. 5.16 Sorting nanobioparticles according to their geometries. Non-spherical particles move towards the electrode edge where the field is more intense. On the other hand, spherical objects tend to cover the surface



the field line intensities. So the DEP force can overcome other present forces and rods move towards the edge and deposit there inside the gap. In the case of spherical particles, however, swim away from the electrode edge, following the fluid flow [91, 92].

5.11 Biosensing

Invented in 1916, biosensors—employed for bioanalysis—are considered as valuable tools of biotechnology and medical sciences, agriculture and military (for homeland security). Biosensors are known with several names like biochips, immunosensors, glucometers etc. and are defined as (IUPAC definition): “An electrochemical biosensor is a self-contained integrated device, which is capable of providing specific quantitative or semi-quantitative analytical information using a biological recognition element (biochemical receptor) which is retained in direct spatial contact with an electrochemical transduction element” [93]. Therefore, biosensors are members of chemical sensor family comprised of a biologically driven entity coupled to a transducer analyzing biochemical species.

There exist numerous types of biosensors. Usually, a bioelement is coupled to a sensor element in order to perform the sensing task. The bioelement (also called bioreceptor) which receives the analyte (virus, microorganism, etc.) can be a film made of molecules (e.g. an enzyme, DNA, protein, antibody) or a living biological system (e.g. tissues or cells). The effect generated by bioreceptor—as a result of its interaction with analyte—is converted to a measurable signal (electrochemical, optical, or mass detection) which is then used as the sensor response to the biological species touching its surface.

Today, the emphasis is on downsizing biosensors in order to receive a high signal-to-noise ratio. The strategy is based on application of methods which give small sensors with high selectivity, specificity and sensitivity. Thus, advanced

Fig. 5.17 Optical image of a thin film of TiO_2 deposited on alumina substrate with interdigitated electrodes. The device serves as an electrochemical (bio) sensor



miniaturized biosensors are armed with a single layer or composite thin films as bioelement [94–101]. Currently, EPD is the most widely accepted method for deposition of such layers [102–111]. The optical image of a TiO_2 thin film deposited on microelectrodes for biosensing is presented in Fig. 5.17. The electrode spacing is completely filled.

5.12 Energy

Environmental issues and the need to renewable and clean energy resources on one side, and problems such as the increasing demand, growing consumption and unstable conditions of many countries with the major reserves of fossil fuels, on the other side, are the main concern of energy sector and make the situation very challenging. Nowadays, therefore, there is a great tendency to work on energy-related issues, its production, storage, and transport. Biological thin films are now extensively studied for applications in green energy systems. Application of composite bio-films in advanced photovoltaic cells is converted to an emerging field of research and innovation introducing the next generation of photovoltaic systems called bio-photovoltaics (BPV). In bio-photovoltaic devices, a photosynthetic organism (made from a biological material such as algae and cyanobacteria) is used to convert the solar energy into electrical energy. This energy is then used to provoke a chemical reaction or simply, it runs a current or voltage across the system. In other words, the power is generated by harvesting electrons from photochemical and respiratory activities of photosynthetic microbes [112, 113]. The process is shown in Fig. 5.18 schematically. The advantage of such devices over

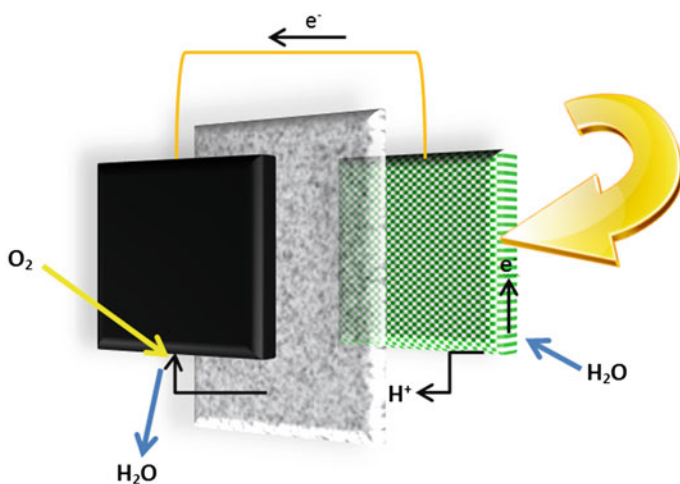


Fig. 5.18 Working principle of a bio-photovoltaic (BPV) device (schematic illustration)

existing PV cells is their low cost and more importantly, the ability to work continuously (i.e. day and night) and the drawback is their low efficiency.

BPVs, however, are still in laboratories needing intense research in order to have it commercialized. Recently, scientists in Cambridge University reported a prototype comprised of several small disk shape parts compacted in one sole assembly. In their design, both electrodes are constructed from films of carbon (cathode) and Algae (anode) separated by a proton exchange membrane [114]. Anode coating can be effectively performed by electrophoresis providing a thin film of biological material of adequate homogeneity.

5.13 Conclusions

Electrophoresis is introduced as a reliable method for deposition of thin and thick films of biomaterials for in vivo and in vitro conditions. Governing equations are briefly reviewed based on which, particle trajectory in AC-electric fields are modeled. Merits of the process for preparation of implants and bio-devices such as biosensors are mentioned.

References

1. Mitchell, J.S.: Spin-coated methacrylic acid copolymer thin films for covalent immobilization of small molecules on surface plasmon resonance substrates. *Eur. Polymer J.* **47**, 16–23 (2011)
2. Uematsu, I., Matsumoto, H., Morota, K., Minagawa, M., Tanioka, A., Yamagata, Y., Inoue, K.: Surface morphology and biological activity of protein thin films produced by electropray deposition. *J. Colloid Interface Sci.* **269**, 336–340 (2004)
3. Kecskeméti, G., Kresz, N., Smausz, T., Hopp, B., Nógrádi, A.: Pulsed laser deposition of pepsin thin films. *Appl. Surf. Sci.* **247**, 83–88 (2005)
4. Hopp, B., Smausz, T., Kecskeméti, G., Klini, A., Bor, Zs: Femtosecond pulsed laser deposition of biological and biocompatible thin layers. *Appl. Surf. Sci.* **253**, 7806–7809 (2007)
5. Sun, S., Ho-Si, P.-H., Jed Harrison, D.: Preparation of active Langmuir-Blodgett films of glucose oxidase. *Langmuir* **7**, 727–737 (1991)
6. Girard-Egrot, A.P., Godoy, S., Blum, L.J.: Enzyme association with lipidic Langmuir-Blodgett films: interests and applications in nanobioscience. *Adv. Colloid Interface Sci.* **116**, 205–225 (2005)
7. Kurella, A., Dahotre, N.B.: Review paper: Surface modification for bioimplants: the role of laser surface engineering. *J. Biomater. Appl.* **20**, 5–50 (2005)
8. Stan, G.E., Popescu, A.C., Mihailescu, I.N., Marcov, D.A., Mustata, R.C., Sima, L.E., Petrescu, S.M., Ianculescu, A., Trusca, R., Morosanu, C.O.: On the bioactivity of adherent bioglass thin films synthesized by magnetron sputtering techniques. *Thin Solid Films* **518**, 5955–5964 (2010)
9. Tomita, S., Sato, K., Anzai, J.: Layer-by-layer assembled thin films composed of carboxyl-terminated poly(amidoamine) dendrimer as a pH-sensitive nano-device. *J. Colloid Interface Sci.* **326**, 35–40 (2008)

10. Chu, J., Li, X., Zhang, J., Tang, J.: Fabrication and photoelectric response of poly(allylamine hydrochloride)/PM thin films by layer-by-layer deposition technique. *Biochem. Biophys. Res. Commun.* **305**, 116–121 (2003)
11. Ma, H., Peng, J., Han, Z., Yu, X., Dong, B.: A novel biological active multilayer film based on polyoxometalate with pendant support-ligand. *J. Solid State Chem.* **178**, 3735–3739 (2005)
12. Ding, B., Du, J., Hsieh, Y.-L.: Tubular multi-bilayer polysaccharide biofilms on ultra-thin cellulose fibers. *J. Appl. Polym. Sci.* **121**, 2526–2534 (2011)
13. Channasanon, S., Graisuwan, W., Kiatkamjornwong, S., Hoven, V.P.: Alternating bioactivity of multilayer thin films assembled from charged derivatives of chitosan. *J. Colloid Interface Sci.* **316**, 331–343 (2007)
14. Piveteau, L.-D., Girona, M.I., Schlapbach, L., Barbour, P., Boilot, J.-P., Gasser, B.: Thin films of calcium phosphate and titanium dioxide by a sol-gel route: a new method for coating medical implants. *J. Mater. Sci. Mater. Med.* **10**, 161–167 (1999)
15. Anné, G., Vanmeensel, K., Vleugels, J., Van der Biest, O.: Electrophoretic deposition as a novel near net shaping technique for functionally graded biomaterials. *Mater. Sci. Forum* **492–493**, 213–218 (2005)
16. Anné, G., Vanmeensel, K., Vleugels, J., Van der Biest, O.: Electrophoretic deposition as a novel near net shaping technique for functionally graded biomaterials. *Key Eng. Mater.* **314**, 213–218 (2006)
17. Van der Biest, O., Vandeperre, L., Put, S., Anné, G., Vleugels, J.: Laminated and functionally graded ceramics by electrophoretic deposition. *Key Eng. Mater.* **333**, 49–58 (2007)
18. Bousse, L., Cohen, C., Nikiforov, T., Chow, A., Kopf-Sill, A.R., Dubrow, R., Parce, J.W.: Electrokinetically controlled microfluidic analysis systems. *Annu. Rev. Biophys. Biomol. Struct.* **29**, 155–181 (2000)
19. Wei, M., Ruys, A.J., Milthorpe, B.K., Correll, C.C., Evans, J.H.: Electrophoretic deposition of hydroxyapatite coatings on metal substrate: a nano-particulate dual coating approach. *J. Sol-gel Sci. Technol.* **21**, 39–48 (2001)
20. Hasegawa, K., Kunugi, S., Tatsumisago, M., Minami, T.: Preparation of thick films by electrophoretic deposition using modified silica particles derived by sol-gel method. *J. Sol-gel Sci. Technol.* **15**, 243–249 (1999)
21. Shan, W., Zhang, Y., Yang, W., Ke, C., Gao, Z., Ye, Y., Tang, Y.: Electrophoretic deposition of nanosized zeolites in non-aqueous medium and its application in fabricating thin zeolite membranes. *Micropor. Mesopor. Mater.* **69**, 35–42 (2004)
22. Pallandre, A., de Lambert, B., Attia, R., Jonas, A.M., Viovy, J.-L.: Surface treatment and characterization: perspectives to electrophoresis and lab-on-chips. *Electrophoresis* **27**, 584–610 (2006)
23. Stappers, L., Zhang, L., Van der Biest, O., Franssaer, J.: The effect of electrolyte conductivity on electrophoretic deposition. *J. Colloid Interface Sci.* **328**, 436–446 (2008)
24. Fukada, Y., Nagarajan, N., Mekky, W., Bao, Y., Kim, H.-S., Nicholson, P.S.: Electrophoretic deposition—mechanisms, myths and materials. *J. Mater. Sci.* **39**, 787–801 (2004)
25. Sarkar, P., Nicholson, P.S.: Electrophoretic deposition (EPD): mechanisms, kinetics, and applications to ceramics. *J. Am. Ceram. Soc.* **79**(8), 1987–2002 (1996)
26. Hughes, M.P.: *Nanoelectromechanics in Engineering and Biology*. CRC Press, Boca Raton (2003)
27. Van Tassel, J.J., Randall, C.A.: Mechanisms of electrophoretic deposition. *Key Eng. Mater.* **314**, 167–174 (2006)
28. Ferrari, B., Moreno, R.: EPD kinetics: a review. *J. Eur. Ceram. Soc.* **30**, 1069–1078 (2010)
29. Besra, L., Liu, M.: A review on fundamentals and applications of electrophoretic deposition (EPD). *Prog. Mater. Sci.* **52**, 1–61 (2007)
30. Wang, X.-B., Huang, Y., Becker, F.F., Gascoyne, P.R.C.: A unified theory of dielectrophoresis and travelling wave dielectrophoresis. *J. Phys. D Appl. Phys.* **27**, 1571–1574 (1994)

31. Paunovic, M., Schlesinger, M.: *Fundamentals of Electrochemical Deposition*. Wiley-Interscience, New York (2006)
32. Masliyah, J.H., Bhattacharjee, S.: *Electrokinetic and Colloid Transport Phenomena*. Wiley (2006)
33. Tadmor, R., Hernández-Zapata, E., Chen, N., Pincus, P., Israelachvili, J.N.: Debye length and double-layer forces in polyelectrolyte solutions. *Macromolecules* **35**, 2380–2388 (2002)
34. Hamley, I.W.: *Introduction to Soft Matter—Revised Edition Synthetic and Biological Self-Assembling Materials*. Wiley (2007)
35. Neirincck, B., Fransaer, J., Vleugels, J., Van der Biest, O.: Aqueous electrophoretic deposition at high electric fields. *Key Eng. Mater.* **412**, 33–38 (2009)
36. Dukhin, A.S., Dukhin, S.S.: A periodic capillary electrophoresis method using an alternating current electric field for separation of macromolecules. *Electrophoresis* **26**, 2149–2153 (2005)
37. Neirincck, B., Fransaer, J., Van der Biest, O., Vleugels, J.: Aqueous electrophoretic deposition in asymmetric AC electric fields (AC-EPD). *Electrochem. Commun.* **11**, 57–60 (2009)
38. Pohl, H.A.: The motion and precipitation of suspensoids in divergent electric fields. *J. Appl. Phys.* **22**, 869–871 (1915)
39. Kua, C.H., Lam, Y.C., Yang, C., Youcef-Toumi, K.: *Review of Bio-Particle Manipulation Using Dielectrophoresis*. DSpace, MIT, Cambridge, Innovation in Manufacturing Systems and Technology collection, Singapore-MIT Alliance community (2005)
40. Jones, T.B.: *Basic Theory of Dielectrophoresis and Electrorotation*, IEEE Engineering in Medicine and Biology Magazine, Nov/Dec, 33–42 (2003)
41. Srivastava, S.K., Gencoglu, A., Minerick, A.R.: DC insulator dielectrophoretic applications in microdevice technology: a review. *Anal. Bioanal. Chem.* **399**, 301–321 (2011)
42. Douglas, J.F., Zhou, H.-X., Hubbard, J.B.: Hydrodynamic friction and the capacitance of arbitrarily shaped objects. *Phys. Rev. E* **49**(6), 5319–5331 (1994)
43. Swanson, E., Teller, D.C., de Haën, C.: Creeping flow translational resistance of rigid assemblies of spheres. *J. Chem. Phys.* **72**, 1623–1628 (1980)
44. Swanson, E., Teller, D.C.: The low Reynolds number translational friction of ellipsoids, cylinders, dumbbells, and hollow spherical caps. Numerical testing of the validity of the modified Oseen tensor in computing the friction of objects modeled as beads on a shell. *J. Chem. Phys.* **68**, 5097–5102 (1978)
45. Hubbard, J.B., Douglas, J.F.: Hydrodynamic friction of arbitrarily shaped Brownian particles. *Phys. Rev. E* **47**(5), R2983–R2986 (1993)
46. Wei, H., Craig, A., Huey, B.D., Papadimitrakopoulos, F., Marcus, H.L.: Electric field and tip geometry effects on dielectrophoretic growth of carbon nanotube nanofibrils on scanning probes. *Nanotechnology* **19**, 455303 (2008)
47. Morgan, H., Green, N.G.: *AC Electrokinetics: Colloids and Nanoparticles*. Research Studies Press, Philadelphia (2003)
48. Hulman, M., Tajmar, M.: The dielectrophoretic attachment of nanotube fibres on tungsten needles. *Nanotechnology* **18**, 145504 (2007)
49. Kim, J.-E., Han, C.-S.: Use of dielectrophoresis in the fabrication of an atomic force microscope tip with a carbon nanotube: a numerical analysis. *Nanotechnology* **16**, 2245–2250 (2005)
50. Asokan, S.B., Jawerth, L., Lloyd Carroll, R., Cheney, R.E., Washburn, S., Superfine, R.: Two-dimensional manipulation and orientation of actin-myosin systems with dielectrophoresis. *Nano Lett.* **3**(4), 431–437 (2003)
51. Pethig, R.: Review article—Dielectrophoresis: status of the theory, technology, and application. *Biomicrofluidics* **4**, 022811 (2010)
52. Dimaki, M., Bøggild, P.: Dielectrophoresis of carbon nanotubes using microelectrodes: a numerical study. *Nanotechnology* **15**, 1095–1102 (2004)

53. Lima, M.D., de Andrade, M.J., Bergmann, C.P., Roth, S.: Thin, conductive, carbon nanotube networks over transparent substrates by electrophoretic deposition. *J. Mater. Chem.* **18**, 776–779 (2008)
54. Gimsa, J.: A comprehensive approach to electro-orientation, electrodeformation, dielectrophoresis, and electrorotation of ellipsoidal particles and biological cells. *Bioelectrochemistry* **54**, 23–31 (2001)
55. Green, N.G., Jones, T.B.: Numerical determination of the effective moments of non-spherical particles. *J. Phys. D: Appl. Phys.* **40**, 78–85 (2007)
56. Neirinck, B., Van Mellaert, L., Fransaer, J., Van der Biest, O., Anné, J., Vleugels, J.: Electrophoretic deposition of bacterial cells. *Electrochem. Commun.* **11**, 1842–1845 (2009)
57. Hilding, J., Grulke, E.A., George Zhang, Z., Lockwood, F.: Dispersion of carbon nanotubes in liquids. *J. Dispersion Sci. Technol.* **24**(1), 1–47 (2003)
58. Van der Biest, O.O., Vandeperre, L.J.: Electrophoretic deposition of materials. *Annu. Rev. Mater. Sci.* **29**, 327–352 (1999)
59. Hamagami, J., Ato, Y., Kanamura, K.: Fabrication of highly ordered macroporous apatite coating onto titanium by electrophoretic deposition method. *Solid State Ionics* **172**, 331–334 (2004)
60. Yousefpour, M., Afshar, A., Chen, J., Zhang, X.: Electrophoretic deposition of porous hydroxyapatite coatings using polytetrafluoroethylene particles as templates. *Mater. Sci. Eng., C* **27**, 1482–1486 (2007)
61. Wang, R., Hu, Y.X.: Patterning hydroxyapatite biocoating by electrophoretic deposition. *J. Biomed. Mater. Res.* **67A**(1), 270–275 (2003)
62. Wang, R.: Pearl powder bio-coating and patterning by electrophoretic deposition. *J. Mater. Sci.* **39**, 4961–4964 (2004)
63. Boccaccini, A.R., Keim, S., Ma, R., Li, Y., Zhitomirsky, I.: Electrophoretic deposition of biomaterials. *J. R. Soc. Interface* **7**, S581–S613 (2010)
64. Rezwani, K., Chen, Q.Z., Blaker, J.J., Boccaccini, A.R.: Biodegradable and bioactive porous polymer/inorganic composite scaffolds for bone tissue engineering. *Biomaterials* **27**, 3413–3431 (2006)
65. Shirliff, V.J., Hench, L.L.: Bioactive materials for tissue engineering, regeneration and repair. *J. Mater. Sci.* **38**, 4697–4707 (2003)
66. Grandfield, K., Zhitomirsky, I.: Electrophoretic deposition of composite hydroxyapatite–silica–chitosan coatings. *Mater. Charact.* **59**, 61–67 (2008)
67. Das, T., Ghosh, D., Bhattacharyya, T.K., Maiti, T.K.: Biocompatibility of diamond-like nanocomposite thin films. *J. Mater. Sci. Mater. Med.* **18**, 493–500 (2007)
68. Cho, Y., Shi, R., Borgens, R.B., Ivanisevic, A.: Functionalized mesoporous silica nanoparticles-based drug delivery system to rescue acrolein-mediated cell death. *Nanomedicine* **3**(4), 507–519 (2008)
69. Vallet-Regí, M., Ruiz-González, L., Izquierdo-Barba, I., González-Calbet, J.M.: Revisiting silica based ordered mesoporous materials: medical applications. *J. Mater. Chem.* **16**, 26–31 (2006)
70. Melde, B.J., Johnson, B.J., Charles, P.T.: Mesoporous silicate materials in sensing. *Sensors* **8**, 5202–5228 (2008)
71. Arcos, D., Izquierdo-Barba, I., Vallet-Regí, M.: Promising trends of bioceramics in the biomaterials field. *J. Mater. Sci. Mater. Med.* **20**, 447–455 (2009)
72. Huang, W.-C., Hu, S.-H., Liu, K.-H., Chen, S.-Y., Liu, D.-M.: A flexible drug delivery chip for the magnetically-controlled release of anti-epileptic drugs. *J. Controlled Release* **139**, 221–228 (2009)
73. Oetzel, C., Clasen, R.: Preparation of zirconia dental crowns via electrophoretic deposition. *J. Mater. Sci.* **41**, 8130–8137 (2006)
74. Singh, I., Kaya, C., Shaffer, M.S.P., Thomas, B.C., Boccaccini, A.R.: Bioactive ceramic coatings containing carbon nanotubes on metallic substrates by electrophoretic deposition. *J. Mater. Sci.* **41**, 8144–8151 (2006)

75. Sakurada, O.: Electrophoretic bubble-free deposition on anodes from aqueous alumina and zirconia suspensions with hydroquinone: fabrication of alumina/zirconia graded composites. *J. Ceram. Soc. Jpn.* **112**(PacRim5 Special Issue), S153–S155 (2004)
76. Tabellion, J., Clasen, R.: Electrophoretic deposition from aqueous suspensions for near-shape manufacturing of advanced ceramics and glasses—applications. *J. Mat. Sci.* **39**, 803–811 (2004)
77. Uchikoshi, T., Ozawa, K., Hatton, B.D., Sakka, Y.: Dense, bubble-free ceramic deposits from aqueous suspensions by electrophoretic deposition. *J. Mater. Res.* **16**(2), 321–324 (2001)
78. Hayward, R.C., Saville, D.A., Aksay, I.A.: Electrophoretic assembly of colloidal crystals with optically tunable micropatterns. *Nature* **404**, 56–59 (2000)
79. Besra, L., Samantaray, P., Bhattacharjee, S., Singh, B.P.: Electrophoretic deposition of alumina on stainless steel from non-aqueous suspension. *J. Mater. Sci.* **42**, 5714–5721 (2007)
80. Hirata, Y., Nishimoto, A., Ishihara, Y.: Forming of alumina powder by electrophoretic deposition. *J. Ceram. Soc. Jpn.* **99**, 108–113 (1991)
81. Gardeshzadeh, A.R., Raissi, B., Marzbanrad, E.: Preparation of Si powder thick films by low frequency alternating electrophoretic deposition. *J. Mater. Sci.* **43**, 2507–2508 (2008)
82. Riahifar, R., Raissi, B., Marzbanrad, E., Zamani, C.: Effect of parameters on deposition pattern of ceramic nanoparticles in non-uniform AC electric field. *J. Mater. Sci.: Mater. Electron.* **22**, 40–46 (2011)
83. Riahifar, R.: Ceramic oxide nanoparticle trajectory modeling in AC electric fields. Department of Ceramics, Materials and Energy Research Center (MERC) Iran. PhD Thesis (2010)
84. Green, N.G., Ramos, A., González, A., Morgan, H., Castellanos, A.: Fluid flow induced by nonuniform ac electric fields in electrolytes on microelectrodes. III. Observation of streamlines and numerical simulation. *Phys. Rev. E* **66**, 026305 (2002)
85. Foster, K.R., Sauer, F.A., Schwan, H.P.: Electrorotation and levitation of cells and colloidal particles. *Biophys. J.* **63**, 180–190 (1992)
86. Riahifar, R., Marzbanrad, E., Raissi Dehkordi, B., Zamani, C.: Role of substrate potential on filling the gap between two planar parallel electrodes in electrophoretic deposition. *Mater. Lett.* **64**, 559–561 (2010)
87. Riahifar, R., Marzbanrad, E., Raissi, B., Zamani, C.: A new technique for micro-patterning of nanoparticles on non-conductive substrate by low frequency AC electrophoresis. *J. Mater. Sci.: Mater. Electron.* (2011). doi: [10.1007/s10854-011-0288-y](https://doi.org/10.1007/s10854-011-0288-y)
88. Evans, P., Sheel, D.W.: Photoactive and antibacterial TiO₂ thin films on stainless steel. *Surf. Coat. Technol.* **201**, 9319–9324 (2007)
89. Ishizaki, K., Sugita, Y., Iwasa, F., Minamikawa, H., Ueno, T., Yamada, M., Suzuki, T., Ogawa, T.: Nanometer-thin TiO₂ enhances skeletal muscle cell phenotype and behavior. *Int. J. Nanomed.* **6**, 2191–2203 (2011)
90. Hawk, H.A., Ira, P.: Separation of living and dead cells by dielectrophoresis science. *Science* **152**, 647–649 (1966)
91. Ramos, A., Morgan, H., Green, N.G., Castellanos, A.: AC electric-field-induced fluid flow in microelectrodes. *J. Colloid Interface Sci.* **217**, 420–422 (1999)
92. Riahifar, R., Marzbanrad, E., Raissi, B., Zamani, C., Kazemzad, M., Aghaei, A.: Sorting ZnO particles of different shapes with low frequency AC electric fields. *Mater. Lett.* **65**, 632–635 (2011)
93. Thévenot, D.R., Toth, K., Durst, R.A., Wilson, G.S.: Electrochemical biosensors: recommended definitions and classification. *Pure Appl. Chem.* **71**(12), 2333–2348 (1999)
94. Vo-Dinh, T., Cullum, B.: Biosensors and biochips: advances in biological and medical diagnostics. *Fresenius J. Anal. Chem.* **366**, 540–551 (2000)
95. Pohanka, M., Skládal, P.: Electrochemical biosensors—principles and applications. *J. Appl. Biomed.* **6**, 57–64 (2008)

96. Yogeswaran, U., Chen, S.-M.: A review on the electrochemical sensors and biosensors composed of nanowires as sensing material. *Sensors* **8**, 290–313 (2008)
97. Hall, R.H.: Biosensor technologies for detecting microbiological foodborne hazards. *Microbes Infect.* **4**, 425–432 (2002)
98. Jenison, R., La, H., Haeberli, A., Ostroff, R., Polisky, B.: Silicon-based biosensors for rapid detection of protein or nucleic acid targets. *Clin. Chem.* **47**(10), 1894–1900 (2001)
99. Mohanty, S.P., Kougiyanos, E.: Biosensors: a tutorial review. *IEEE Potentials* (March/April), 35–40 (2006)
100. Grieshaber, D., MacKenzie, R., Vörös, J., Reimhult, E.: Electrochemical biosensors—sensor principles and architectures. *Sensors* **8**, 1400–1458 (2008)
101. Zribi, A., Fortin, J. (ed.): *Functional Thin Films and Nanostructures for Sensors Synthesis, Physics, and Applications*. Springer (2009)
102. Velev, O.D., Kaler, E.W.: In situ assembly of colloidal particles into miniaturized biosensors. *Langmuir* **15**(11), 3693–3698 (1999)
103. Luo, X.-L., Xu, J.-J., Du, Y., Chen, H.-Y.: A glucose biosensor based on chitosan–glucose oxidase–gold nanoparticles biocomposite formed by one-step electrodeposition. *Anal. Biochem.* **334**, 284–289 (2004)
104. Fiorito, P.A., Córdoba de Torresi, S.I.: Optimized multilayer oxalate biosensor. *Talanta* **62**, 649–654 (2004)
105. Xu, Q., Zhu, J.-J., Hu, X.-Y.: Ordered mesoporous polyaniline film as a new matrix for enzyme immobilization and biosensor construction. *Anal. Chim. Acta* **597**, 151–156 (2007)
106. Li, F., Wang, Z., Chen, W., Zhang, S.: A simple strategy for one-step construction of bienzyme biosensor by in situ formation of biocomposite film through electrodeposition. *Biosens. Bioelectron.* **24**, 3030–3035 (2009)
107. Ammam, M., Fransaeer, J.: AC-electrophoretic deposition of glucose oxidase. *Biosens. Bioelectron.* **25**, 191–197 (2009)
108. Meng, D., Francis, L., Roy, I., Boccaccini, A.R.: Using electrophoretic deposition to identify protein charge in biological medium. *J. Appl. Electrochem.* **41**, 919–923 (2011)
109. Dhand, C., Sumana, G., Datta, M., Malhotra, B.D.: Electrophoretically deposited nano-structured polyaniline film for glucose sensing. *Thin Solid Films* **519**, 1145–1150 (2010)
110. Dhand, C., Singh, S.P., Arya, S.K., Datta, M., Malhotra, B.D.: Cholesterol biosensor based on electrophoretically deposited conducting polymer film derived from nano-structured polyaniline colloidal suspension. *Anal. Chim. Acta* **602**, 244–251 (2007)
111. Suehiro, J.: Fabrication and characterization of nanomaterial-based sensors using dielectrophoresis. *Biomicrofluidics* **4**, 022804 (2010)
112. McCormick, A.J., Bombelli, P., Scott, A.M., Philips, A.J., Smith, A.G., Fisher, A.C., Howe, C.J.: Photosynthetic biofilms in pure culture harness solar energy in a mediatorless biophotovoltaic cell (BPV) system. *Energy Environ. Sci.* **4**, 4699–4709 (2011)
113. Rosenbaum, M., Schröder, U.: Photomicrobial solar and fuel cells. *Electroanalysis* **22**(7–8), 844–855 (2010)
114. Driver, A., Bombelli, P.: Biophotovoltaics energy from algae. *Catalyst*, pp. 13–15, April (2011)

Chapter 6

Diamond-Like Carbon Coated on Polymers for Biomedical Applications

Atsushi Hotta and Terumitsu Hasebe

Abstract Diamond-like carbon (DLC) has been widely used for many industrial applications characterized by their outstanding physical properties such as high hardness, wear resistance, chemical inertness, and biological compatibility. As DLC consists only of carbon and hydrogen, DLC could be one of the strongest possible candidates for use as biomedical implants. DLC can also be effectively coated on materials, including polymeric surfaces in order to modify the polymers for highly-functionalized and highly-biocompatible materials. Considering biomedical applications, the base materials suitable for the deposition of DLC would be polymers which can create soft, flexible, highly absorbent, cost-effective, and hence human-friendly materials by carefully selecting and controlling the molecular structures of the polymers. In this chapter, the development process of DLC for biomedical applications was reviewed. The amorphous nature of DLC from the viewpoint of the chemical structures was introduced and the possibility of doping/alloying atomic elements such as fluorine (F) and silicon (Si) into DLC was discussed. The biocompatibility of the DLC and the alloyed DLC was then outlined. The interface characteristics between DLC and the base materials for the practical use of DLC were investigated, including the adhesion property and the surface fracture analysis of DLC. The adhesion property of DLC, when coated on polymers, was summarized, where the adhesion forces were found to be different from the types of the polymers. The fracture surfaces of DLC coated on polymers were also reviewed when the DLC-coated polymeric specimens were deformed, which would possibly damage the eventual permeation characteristics of the specimens. The gas and liquid permeation properties of DLC-coated polymers were also discussed. The permeation properties would be particularly significant when the DLC-coated

A. Hotta (✉)

Department of Mechanical Engineering, Keio University, Yokohama 223-8522, Japan
e-mail: hotta@mech.keio.ac.jp

T. Hasebe

Department of Radiology, Tokai University Hachioji Hospital/Tokai
University School of Medicine, Tokyo 190-0032, Japan

polymers were effectively used for e.g. drug-delivery systems and dermal (or transdermal) patches. All these experimental achievements should be highly important and widely applicable to the investigations of the next generation biomedical products using controlled microstructures of DLC/polymer composites.

6.1 Diamond-Like Carbon

6.1.1 DLC

Since the discovery of a diamond-like carbon film in 1971 by Aisenberg and Chabot [1], active research has been conducted on amorphous carbon films including diamond-like carbon (DLC). Amorphous carbon is a well-known material that possesses mixed molecular structures of sp^3 and sp^2 carbon bonds with hydrogen bonds. Over the last decade, especially DLC has been actively studied in the field of material science and engineering. DLC consists of dense amorphous carbon and/or hydrocarbon with high electrical resistivity, high refractive index, and high chemical inertness. The mechanical properties of this film lie between the properties of graphite and diamond; featuring a low-friction coefficient, low wear rate, high hardness, excellent tribological properties, and excellent corrosion resistance [2]. These distinguished mechanical, electrical, optical, and chemical properties have propelled the use of DLC coatings in the mechanical and electrical industries. Recently, DLC has been found useful in the food/beverage and biomedical fields due to its excellent properties such as high gas barrier property and high biocompatibility as well as many other useful mechanical properties. DLC coating is also considered advantageous for widespread use as e.g. a surface coating material for medical applications, such as coronary stents [3–5], heart valves [6] and orthopedic implants [7]. By varying the molecular compositions of amorphous carbon films, the physical properties of amorphous carbon films can be readily and uniquely controlled to achieve enhanced material qualities, where DLC presents high hardness, high electrical resistivity, high refractive index, low friction coefficients, low wear rates, and chemical inertness [8, 9]. Ferrari and Robertson carefully studied the compositions of DLC and successfully completed a ternary phase diagram of carbon films shown in Fig. 6.1 [10]. They also reported that when the carbon films contained few hydrogen bonds, the materials got harder and became well-suited for the hard-coating material applicable to cutting tools. Hydrogenated amorphous carbon (a-C:H) contains sp^3 , sp^2 as well as hydrogen bonds and the resulting materials or films become extremely smooth and flexible, hence a-C:H can be applied for lubricant components and flexible plastics. Owing to these attractive physical properties, amorphous carbon films including DLC and a-C:H in general are being widely used in the mechanical and electrical fields.

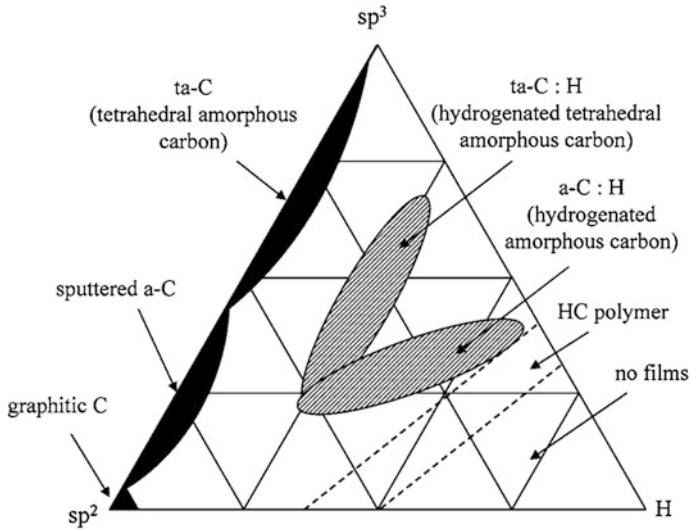


Fig. 6.1 The ternary phase diagram of amorphous carbons. The physical and the chemical properties of the amorphous carbons can be uniquely controlled by varying the compositions of sp^3 , sp^2 and, hydrogen bonds. [115]

DLC can be synthesized by various techniques such as radio frequency plasma enhanced chemical vapor deposition (RF-PECVD), plasma immersion ion implantation and deposition (PIIID) and filtered cathodic vacuum arc (FCVA) [11–13]. The properties of DLC are affected by the deposition techniques and the synthesis conditions employed. For example, PECVD is a commonly used laboratory technique with simple but proper control of the deposition parameters. The precise controls of the deposition parameters directly affect the chemical structures of the DLC films such as sp^3/sp^2 ratio and hydrogen content, changing the properties from polymer-like to diamond-like. The amorphous nature of DLC opens the possibility of incorporating elements such as Si, F, P, Ag and N [14–28], which imparts improved properties to DLC. Moreover, the properties can be controlled by the content of sp^3 , sp^2 and incorporated elements. For example, Kim et al. investigated the effect of Si incorporation on the wear-corrosion properties of DLC [19]. They reported that improved properties were obtained when the bonding ratio of sp^3/sp^2 was increased by increasing the Si content from 0 at. % to 2 at. %. Maguire et al. have demonstrated that Si incorporation enhanced the barrier properties of DLC, which was also beneficial to the bioresponse [23].

6.1.2 Polymers for DLC Coating

The demand for polymeric materials has also been increasing and highly functionalized polymers are much desired for wider applications to the production

materials ranging from biomaterials to eco-friendly materials. Thermoplastic polymers can be used as recyclable and biomedical materials due to the reprocessing nature of the thermoplasticity of the polymers. Polymers are also generally very flexible as compared with other non-polymeric materials such as metals and ceramics. Polymers are therefore regarded as base materials best suited for living organism. In fact, our living body can be considered as hydrogels where biogenic polymeric networks involve plenty of aqueous medium required for our complex life activity. An attempt of combining hard DLC with such soft polymers would expand the original capabilities of DLC and polymers. As was mentioned, DLC is one of many useful approaches that are industrially broadly used for the surface modification. The adhesion properties and the fracture mechanism are especially important for the polymers to be used with DLC. These are discussed later in [Sects. 6.2.1](#) and [6.2.2](#) in addition to the explanation as to the barrier properties of DLC-coated polymers for the application to gas barrier films and a new drug eluting system.

6.1.3 Biomedical Properties of DLC

6.1.3.1 General Consideration for the Biocompatibility of DLC

Biomedical devices have proven to be effective for the treatment of specific diseases and organ insufficiencies in the aging population. The healing response to implanted biomedical materials normally involves varying degrees and stages of inflammation and healing processes, which in some cases leads to serious device failure. Carbon can be generally well tolerated in the human body. It has been reported that DLC coatings did not induce any histological changes and that in fact they showed excellent biocompatibility in an *in vivo* implantation model [29]. Thrombogenic complications also remain as one of the major and unsolved problems for blood-contacting devices, such as cardiovascular and interventional devices (stents, guide wires, and catheters), and artificial organs. The initial local response to foreign materials and surfaces in the body is primarily catalyzed by surface-absorbed proteins that can trigger numerous processes, such as cellular activation, inflammatory and complement activation, and attraction of circulating platelets. To reduce the risk of platelet aggregation/thromboembolism and complications following the life-long course of anticoagulants, the improvement of the biocompatibility and hemocompatibility of the used biomaterials has been highly demanded. Surface coating is one highly efficient method of improving both the mechanical and the physical properties of the implants that are in direct contact with blood and tissue. Many groups have been consistently working on a variety of blood-compatible coatings, including a photoheparin formulation. Heparin is a potent anticoagulant purified for decades from ruminants or porcine tissues; however, with the emergence of bovine spongiform encephalopathy (BSE), or mad cow disease, only the porcine-derived heparin is allowed in the United States and

Europe. Regulators in Europe, the United States and Japan are also concerned about the possible side effects of the use of large amounts of heparin for patients, which makes it difficult or even discontinues to bring heparin-coated products to the market. Therefore, there has been an urgent need to develop non-biologic alternatives to heparin coating for medical devices. In fact, some companies made a decision to suspend the production of heparin-coated catheters and devices, which should be highly inconvenient and disadvantageous both for medical doctors and patients. Thus, there has been substantial interest in developing convenient and effective ways to modify the surfaces of metal and polymer implants that have been practically used, to increase the biocompatibility. A number of promising results for the surface modification by DLC coatings have been obtained by extensive *in vitro* and *in vivo* preclinical studies. For examples, less platelet adhesion and activation was found associated with a high albumin/fibrinogen adsorption ratio on the DLC surfaces. Such excellent biocompatibility of DLC films has also been confirmed in various types of cell culture [2, 5, 7, 30–34] and in animal models [7, 29]. DLC coating is therefore being considered for widespread use as a surface coating for coronary stents [3, 4], heart valves [6] and orthopedic implants [7] in clinical situations.

6.1.3.2 Biomedical Studies and Applications of DLC

The characteristics of DLC described above meet the criteria of biomaterials and thus provide an opportunity for DLC to be applied in the medical field [32, 35–39]. The potential for biomedical use can be determined by *in vitro* and *in vivo* studies which involve the interaction between the materials and biological cells or proteins. The first major event when a medical device comes into contact with blood is the adsorption of plasma proteins as well as tissue and complement factors. The presence of adsorbed proteins has a profound effect on the biocompatibility of materials and the interaction with blood components. The amount and the composition of the proteins adsorbed on the surface are also important for the evaluation of the hemocompatibility of the materials. As a rule, gamma globulin and fibrinogen promote platelet and leukocyte adhesion and possibly activation, whereas albumin tends to neutralize these effects. The ratio of adsorbed albumin to fibrinogen was reported to determine the hemocompatibility of biomaterials [32]. According to the report, platelet adhesion followed by aggregation and spreading is the process by which platelets form thrombus. Platelets respond to minimal stimulation and become activated when they come into contact with thrombogenic surface such as injured endothelium, subendothelium and artificial surfaces. Platelet activation is initiated by the interaction of an extracellular stimulus with platelet surface, which involves the coupling of the agonist to specific receptors on the platelet plasma membrane. During activation, platelets attach to the sample surface and they change shape by developing pseudopodia as their activation level increases. These activated platelets aggregate and lead to the thrombus formation on the material surface. The biocompatibility of DLC was investigated in the

1990s through cell culturing and observing biotolerance after implantation in animals [2, 38, 40]. Since then, a number of promising results have indicated good biocompatibility of DLC through in vitro and in vivo preclinical studies. For example, as mentioned above, less platelet adhesion and activation associated with a high albumin/fibrinogen adsorption ratio on DLC surfaces and the excellent biocompatibility of DLC were confirmed in various types of cell culture [7, 30, 31], while it has also been reported that DLC would not induce any histological changes, exhibiting excellent biocompatibility [29]. These studies have demonstrated that DLC presents no toxicity toward certain living cells without inflammatory response or loss of cell integrity. In fact, Saito et al. confirmed that DLC suppressed platelet adhesion and activation by in vitro experiments [41].

Owing to the detailed practical potential of DLC, manufacturers of various surgical implants have considered a number of biomedical applications of DLC as a surface coating material for coronary stents, heart valves and orthopedic implants in the clinical situations. Stents are expandable mesh tubes usually made of metals such as stainless steel, titanium alloy, cobalt chrome alloy, and nickel base alloy. The implantation of such stents is a widely accepted procedure for the treatments of artery diseases such as arteriosclerosis and cardiac infarction. Stents are carefully inserted into narrowed arteries before they are expanded to help the arteries open to restore the blood flow. Although the metals used for the stents are normally excellent in the mechanical properties while the implantation continues to be a growth area in the field of interventional procedures, the application of the stents is basically still limited. This is mainly because the stents suffer from the drawbacks such as occlusion, restenosis, and stent-related thrombosis. The major side-effects of the stents are thrombosis and allergic reactions due to the release of metal ions, which should be eventually prevented. Coating the stent surface with biocompatible and protective materials is thus an effective way and DLC has attracted much attention as such coating materials, having yielded a number of promising results. The thrombogenicity of stents is associated with platelets, predominantly with activated platelets. Patients undergoing coronary angioplasty and stenting procedures are known to be at higher risk for reocclusion and restenosis of the vessels when platelets express increased numbers of activation-dependent antigens. Shear forces and blood-biomaterial interaction induce the activation of platelets. Along with medical approaches and technical alterations to the interventional procedures such as intravascular ultrasound-guided stenting and high-pressure implantation techniques, a major focus of efforts to further reduce stent-associated thrombosis and in-stent restenosis has been given to the improvement of biocompatibility. One of the problems of vascular stenting is the thrombogenicity of stent metal itself. In situ thrombus formation sets the stage for the temporal cascade of molecular and cellular reactions that cause extracellular matrix deposition by modified smooth muscle cells and remodeling, which leads to restenosis due to intimal hyperplasia. All currently available stents are made of metal and the most recent available stents are manufactured using SUS316L stainless steel and nickel–titanium alloy (nitinol). Gutensohn et al. reported that a significant release of metal ions such as nickel and chromium was detected from

the surface of uncoated stent, which might enhance the platelet activation and leukocyte activation in the surrounding tissue [4]. Some *in vitro* and *in vivo* studies using DLC-coated stents have also been presented. Gutensohn et al. analyzed the intensity of platelet activation antigens CD62p and CD63 in *in vitro* experiment [4]. They showed that DLC coating onto SUS316L coronary stent resulted in a decrease in the concentrations of CD62p and CD63 antigens indicating low platelet activation on DLC and low tendency of thrombus formation. They also mentioned that the metal ion release from SUS316L stents may negatively affect the surface hemocompatibility, which could be suppressed by DLC coating. Schaefer et al. reported a successful implantation of DLC-coated nitinol stents [42]. There the DLC-coated stents were used for endovascular treatment of superficial femoral artery occlusive disease and their results showed a 100 % patency rate at 12 months after intervention. Because of the good hemocompatibility of DLC, some companies have already owned DLC-coated implants which are either commercially available or in the state of development. For example, Phytis, a medical device company, sells DLC-coated stents on which they report a reduced rate of restenosis due to DLC coating and necessary target revascularization in only 3.27 % of the lesions treated. Airolidi et al., on the other hand, reported that DLC-coated stents did not provide significant improvements over stainless steel stents [3]. They randomly compared DLC-coated stents with stainless steel stents during the treatment of coronary artery disease of 347 patients. The 6-month follow-up results showed no significant differences in rates of binary restenosis and cumulative major adverse cardiac events. Hence, to confirm the potential of DLC-coated stents, more systematic *in vitro* and *in vivo* analyses on the performance of DLC-coated stents should be required. In this article later, we will report that drug-eluting stent has a dramatic impact on endovascular therapy for coronary artery diseases. Avoiding systemic toxicity, stent-based local drug release at the site of vascular injury via a polymeric-coated stent is an attractive therapeutic method of achieving an effective local concentration of drug for a designed period. The safety and the efficacy of such an approach critically depend on the delicate combination of drugs, polymers, and the kinetics of release. Drug-eluting stent is a device releasing into the bloodstream with single or multiple bioactive agents that can deposit in the blood or affect tissues adjacent to the stent. Drugs can be simply linked to the stent surface, embedded and released from within the coated polymer materials or surrounded by and released through a carrier. The carrier can coat (strut-adherent) or span (strut-spanning) the stent struts. A recently published pooled analysis of 11 experimental trials suggested that drug-eluting stents showed benefits over bare metal stents by reducing the need for later revascularization and the risk of cardiac events [43]. Although the safety profiles of coronary drug-eluting stents did not seem to differ from those of bare metal stents in the short-to-medium term, concern has arisen about the potential for late stent thromboses related to a delayed endothelialization of the stent struts. McFadden et al. suggested that the potential risk of stent occlusions should be considered when the discontinuation of antiplatelet therapy was contemplated in patients with drug-eluting stents [44]. Their findings had potentially

serious clinical implications. Future stents should be made less thrombogenic and biocompatible by modifying the metallic surface or coating it with antithrombotic and/or antiproliferative agents or a membrane eluting antithrombotic and/or antiproliferative drugs. Therefore later in Sect. 6.4, a new coronary artery stent was proposed, consisting of DLC-coated polymer containing drug, which could overcome such current embarrassing biomedical situations.

6.1.4 Fluorine-Incorporated DLC and Other Doped DLC

Saito et al. synthesized fluorine-incorporated DLC (F-DLC) and verified that F-DLC significantly reduced platelet adhesion and activation when compared with DLC [41]. The scanning electron microscopic (SEM) images of adherent platelets of their experiment are shown in Fig. 6.2. As mentioned above, the ratio of adsorbed albumin to fibrinogen determines the hemocompatibility of biomaterials. Hasebe et al. investigated the ability of DLC and F-DLC to adsorb albumin and fibrinogen. As shown in Fig. 6.3, and found that a higher ratio of albumin to fibrinogen adsorption was observed on DLC when compared with polycarbonate (control) [17]. F-DLC presented an even higher ratio of albumin to fibrinogen adsorption, which could account for the excellent hemocompatibility of DLC as well as F-DLC. The detailed biocompatibility of F-DLC will be explained later in Sect. 6.1.6.

One of the major limitations of the hard coating technology is the emergence of micro-cracks on the coated surfaces [45]. After the hard coatings with possible high internal stress, interface cracks could lead to the complete delamination of the coating. The flaking of DLC coatings was occasionally observed not on the polymer substrates, but especially on the metal substrates due to the poor adhesion with metals and cracking. The crack spacing was observed to increase with thickness, being saturated beyond ~ 500 nm [23]. The DLC coatings must therefore be optimized in order to minimize the risk of film breakdown. Doping of some elements into DLC films or use of a-Si:H/a-Si:C:H interlayer possibly helps minimize the risk of an adhesion failure or film cracking. There have been several

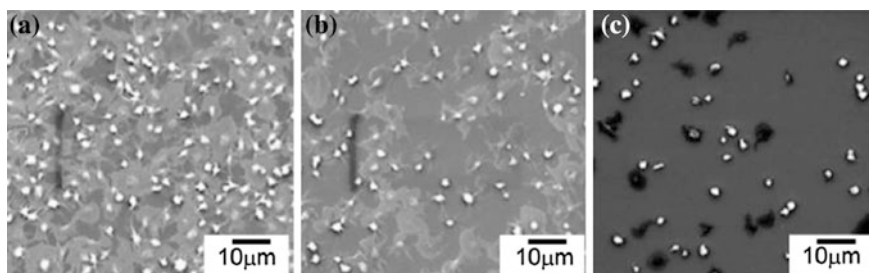


Fig. 6.2 SEM images of adherent platelets on **a** Si, **b** DLC, and **c** F-DLC surfaces [116]

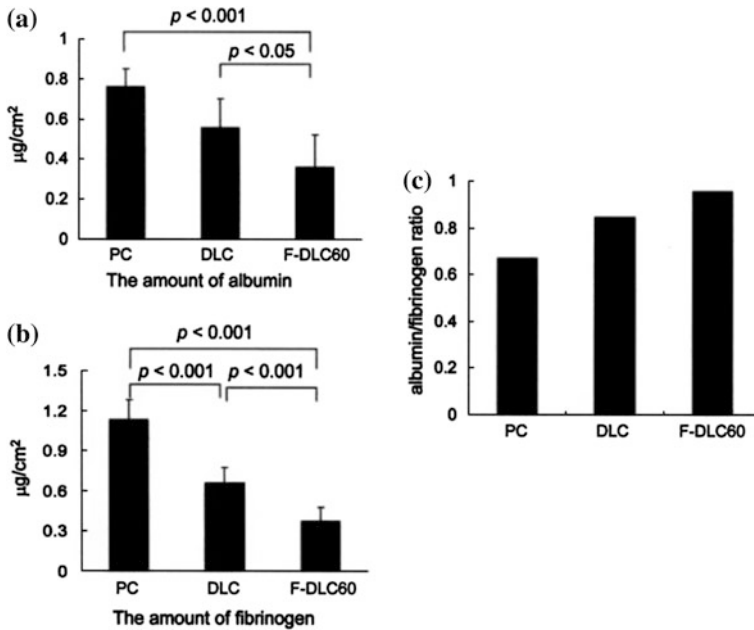


Fig. 6.3 Albumin (a) and fibrinogen (b) absorption on uncoated, DLC-coated and F-DLC coated PC substrates. Protein levels were assessed using the micro-BCA assay. The albumin/fibrinogen ratio is shown in (c) [116]

recent attempts to improve the tribological properties of DLC coatings by adding elements such as Si, F, N, O, W, V, Co, Mo, Ti, and B, or combinations of these elements into the film [32, 46]. Different film properties, such as tribological properties, electrical conductivity, surface energy, and biological reactions of cells, when in contact with surface, could therefore be continuously adapted to desired values. For example, surface fluorination of materials has generally been found to create surfaces with improved blood compatibility, hydrophobicity, and chemical stability [47]. It has been reported that the incorporation of fluorine into the DLC film greatly reduces the surface energy [48, 49] and the film hardness, largely preserving other DLC properties [50]. The elastic features of F-DLC would be advantageous for the coating of three-dimensional medical devices. Saito et al. have recently reported quantitative and morphological studies of platelet adhesion to DLC films or F-DLC-coated silicon (Si) and bare Si substrates incubated in platelet-rich plasma [41]. In the study, it was found that F-DLC showed the best antithrombogenicity among the tested samples. In addition, F-DLC coating reduced the number of platelets, which also inhibited platelet activation on the film surface with statistical significance. The same tendency of platelet attachment and activation has been confirmed on DLC or F-DLC films deposited on polymers as when using Si substrates. The data demonstrate that F-DLC is a promising

candidate for the coating material targeting blood contacting devices, such as cardiovascular interventional devices, artificial organs, and pacemakers.

6.1.5 Structural Analysis of F-DLC

As was mentioned above, F-DLC has recently drawn a great deal of attention as a more non-thrombogenic coating than conventional DLC for blood-contacting medical devices. The quantitative depth profiling of F-DLC film by X-ray photoelectron spectroscopy (XPS) was conducted in order to elucidate the effects of fluorine and fluorine distribution in F-DLC film in connection with the prevention of surface blood adhesion. F-DLC films were prepared on silicon substrates using the radio frequency plasma enhanced chemical vapor deposition method, and the thickness of films was detected as ~ 50 nm. 50-nm-thick F-DLC film samples were etched at 10-nm thickness intervals using argon plasma for each surface specimen to be examined by XPS. Each etched film layer was incubated thereafter with platelet-rich plasma isolated from human whole blood, and the platelet-covered area per unit area was evaluated for each surface. XPS spectra revealed the localization of doped fluorine in the topmost thin layer of the film. Platelet-covered areas represented progressively larger portions of the surfaces of deeper etched layers, corresponding to the decreasing fluorine content in such sample surfaces. These results indicated that the localized fluorine in the top-most thin layer was one of the key factors in the promotion of the non-thrombogenicity of F-DLC film.

A large number of medical devices such as hip joints, vascular grafts, artificial heart valves, interventional devices (stents, guidewires, and catheters), dental roots, and intraocular lenses have been gaining prominence with the development of medical engineering and are increasingly implanted into human bodies every year. However, almost all biomaterials are far from completely biostable or inert and thrombogenic complications remain among the main problems associated with blood-contacting devices. As was already mentioned, diamond-like carbon (DLC) has been actively studied, and a number of promising results have indicated the good biocompatibility, hemocompatibility, and non-thrombogenicity of DLC film [2, 5, 7, 30, 31, 33, 34]. In addition, we previously introduced the fluorine doping in DLC film (F-DLC) that markedly enhanced nonthrombogenicity in human blood [16, 41, 51]. The key factors for the nonthrombogenicity of F-DLC, such as those concerning mediated proteins, surface chemical properties, wettability, and surface structure will be summarized. The mechanisms of this non-thrombogenicity have not been fully elucidated. Here in this section, particularly the distribution of fluorine in F-DLC film was examined for the evaluation of the relationship between such distribution and the non-thrombogenic properties of F-DLC in human blood.

6.1.5.1 XPS Depth Profiles of F-DLC Film

Figure 6.4 shows the C1 s and F1 s XPS spectra for each F-DLC film surface. The horizontal axis corresponds to binding energy (eV) and the vertical axis to intensity (arb. unit). The spectrum of the top-most surface could be divided into four main peaks, which were centered at ~ 284.4 (C–C bond), ~ 287.0 (C–CF), ~ 289.0 (C–F) and ~ 292.0 eV (C–F₂), respectively. While the peak intensity figures for the C–C bond increased, those for bonds between carbon and fluorine such as C–CF, C–F, and C–F₂ decreased from the top-most surface through successively deeper etched layers. In addition, the peak intensity of the F1 s spectra dramatically decreased from the top-most surface to successively deeper etched layers. These results indicate that doped fluorine was localized in the top-most thin layer of the film. From the deconvolution of the C1 s spectrum, fluorine-to-carbon ratios (F/C) can easily be calculated based on the integrated intensity of the various components of the C1 s spectrum by the following equation:

$$\frac{F}{C} = \frac{3I_{CF_3} + 2I_{CF_2} + I_{CF}}{I_{C1s}} \quad (6.1)$$

where C1 s is the total area under the C1 s signal and C1x is the peak area of each fluorinated group [52]. The values of the XPS chemical composition (atomic percent) for F-DLC film samples were calculated based on the area of each peak of C bonds, which were expressed as the mean values of 3 replicates with its corresponding standard deviation. The values were compared using a t test, and the differences were considered statistically significant when p was less than 0.05. The fluorine contents in each F-DLC film layer were calculated, and the depth (nm) and the vertical axis to F/C (at. %) was analyzed. The values for F/C on the topmost surface, “–10”, “–20”, “–30” and “–40 nm,” were 23.2 ± 1.0 , 14.4 ± 1.3 ,

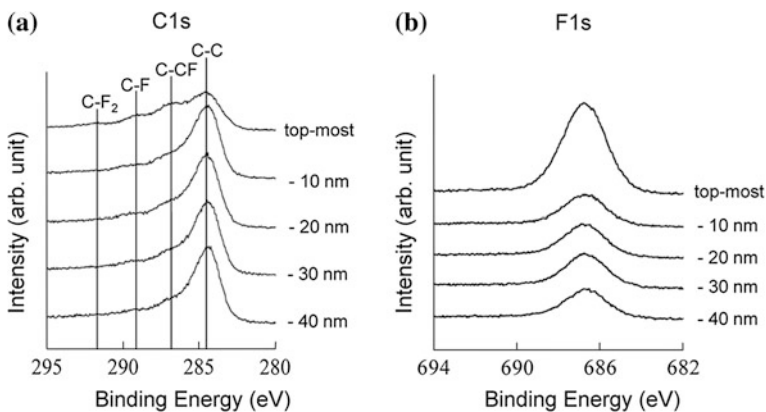


Fig. 6.4 C1 s and F1 s spectra from XPS for the top-most surface of F-DLC film and each exposed layer by argon etching process [117]

14.0 ± 1.3 , 14.4 ± 0.7 , and 14.7 ± 0.8 %, respectively. It was found that, among all surfaces, the F/C ratio for the top-most surface was the highest, and there were no significant differences in ratio among deeper layers. These results would be attributable to the competition between the attachment of CF_x species and the etching of fluorine atoms in the process of film growth [53–56]. It was reported that the higher electronegativity of fluorine with respect to hydrogen promoted the formation of C–F bonds (5.6 eV) that were stronger than C–H bonds (3.5 eV) [57]. These data indicate that the C–H bonds are broken more easily than the C–F bonds, which provides the opportunity for the substitution of fluorine for hydrogen, eventually leading to the stability of the film. In addition, increasing the fluorination of the film could contribute to the formation of C–F bonds rather than C–H bonds [58]. However, the formations of CF, CF_2 , and particularly CF_3 would lead to the termination of the carbon network, which could be an obstacle to the growth of the film. Therefore, fluorine atoms that were known to etch a fluorinated layer would definitely dominate the process of the ablation of the newly formed fluorinated layer during the deposition of the film, while both fluorine atoms and CF_x species could contribute to the formation of a fluorinated layer [53, 54, 56]. At the end of the deposition, such an ablation is less likely to occur, because the top-most surface is the terminal portion of the film and there will be no further need to help and induce the grow. As a result of higher bonding energy, the bonds saturated by fluorine atoms in the terminal positions do not allow for the substitution with hydrogen, particularly in the top-most surface reactions [59]. These phenomena can represent a possible reason why, among all surfaces, the top-most surface had the highest F/C ratio.

6.1.5.2 Contact Angle Measurement

From the results of the measurements of the contact angles of purified water droplets on the surfaces of F-DLC films, it was found that the contact angle was significantly higher for the top-most surface of F-DLC ($81 \pm 3^\circ$) than for the other etched surfaces of “–10”, “–20”, “–30”, and “–40 nm” surfaces, for which the values were $56 \pm 4^\circ$, $50 \pm 6^\circ$, $45 \pm 6^\circ$, and $50 \pm 4^\circ$, respectively (“the top-most surface” versus “each etched surface”; $p < 0.05$). The results indicate that the top-most surface was the most hydrophobic. This was highly due to the presence of polar bonds such as C–F and C–CF in the top-most surface, as was mentioned above.

6.1.5.3 Surface Roughness

R_a was observed via AFM for the top-most surface and each etched layer, and the resulting values for the top-most surface and the “–10”, “–20”, “–30” and “–40 nm” surfaces were 0.5 ± 0.1 , 1.1 ± 0.6 , 1.3 ± 0.5 , 1.3 ± 0.5 , and 0.7 ± 0.2 nm, respectively (“the top-most surface” versus “each etched surface”; $p < 0.05$). Although argon plasma etching increased surface roughness, all R_a values

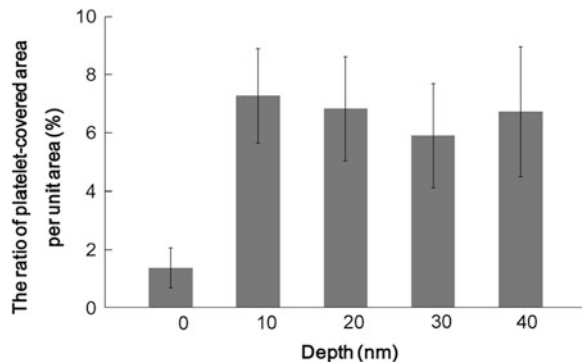
were less than 100 nm. According to the studies, which will also be introduced later [60], it was proven that this range of surface roughness (less than 100 nm) did not affect the degree of nonthrombogenicity of F-DLC film.

6.1.5.4 Platelet Adhesion and Activation

Using computer-aided image analysis, the number of adherent platelets and platelet-covered area were determined as markers of surface thrombogenicity. Both the number of platelets and changes in morphological shape in active platelets are factors relating to platelet-covered surface area of the substrate. Thus, calculating platelet-covered area/unit area provides an index that reflects platelet adhesion and activation. By investigating the representative optical microscopic images of adherent platelets on each surface, it was found that the number of adherent platelets was progressively higher for each deeper etched layer. Figure 6.5 indicates platelet-covered area per unit area ($67,500 \mu\text{m}^2$) for each surface of F-DLC film. Among all surfaces, the value for the top-most surface was the lowest, indicating that the platelet adhesion on the top-most surface was significantly inhibited as compared with that on other etched layers.

In summary, F-DLC films were deposited on Si substrates using the RFCVD method from a mixture of acetylene (C_2H_2) and hexafluoroethane (C_2F_6). Localized fluorine was observed in the several nanometers of the top-most thin layer via XPS measurements. This concentration of fluorine improved the water-shedding property of the film. This study was limited in that depth profiling focused particularly on fluorine distribution on an argon-etched surface measured via XPS. To obtain more precise information on the variation of composition with depth below the initial surface of F-DLC film, SIMS (secondary ion mass spectrometry) or Auger depth profiling would be more useful for the analysis of distribution of fluorine and other elements; however, in this case, with regard to practical applications relating to blood-contacting medical devices, the objective was to determine the exact effects of fluorine incorporated in DLC film by incubating each etched surface of F-DLC film with human blood. The results of the platelet

Fig. 6.5 Platelet-covered area per unit area at each layer with different depths of F-DLC film [117]



incubation study indicated that a fluorine-rich top-most surface dramatically inhibits platelet adhesion, and the number of adherent platelets increases with the decrease of the fluorine content. From this study, it can be concluded that the localization of fluorine in the top-most surface is a key factor in promoting the non-thrombogenicity of F-DLC film.

6.1.6 Biomedical Properties of F-DLC

The first major event when a medical device comes in contact with blood is the adsorption of plasma proteins. As was mentioned above, the protein adsorption on the material surface leads to the activation of the blood coagulation cascade and the inflammatory process, which could impair the lifetime of the material. Various efforts have been made to minimize protein adsorption and platelet adhesion. Diamond-like carbon (DLC) has indeed received much attention because of their antithrombogenicity. In addition, coating silicon substrates with fluorine-doped diamond-like carbon (F-DLC) was found to drastically suppress platelet adhesion and activation. In this section, the protein adsorption on the material surfaces was evaluated and the relationship between protein adsorption and platelet behaviors was clarified, using polycarbonate and DLC- or F-DLC-coated polycarbonate. The adsorption of albumin and fibrinogen were assessed using a colorimetric protein assay, and platelet adhesion and activation were examined using a differential interference contrast microscope. A higher ratio of albumin to fibrinogen adsorption was observed on F-DLC than on DLC and polycarbonate films, indicating that the F-DLC film should prevent thrombus formation more effectively. Platelet adhesion and activation on the F-DLC films were more strongly suppressed as the amount of fluorine doping was increased. These results show that the F-DLC coating may be highly useful for blood-contacting devices.

Blood-contacting medical devices are widely used to treat specific diseases; however, almost all biomaterials have been far from being completely biocompatible and inert. As was summarized above, the biocompatibility of blood-contacting devices is mainly related to the thrombotic response that they induce and the thrombogenic complications caused by the materials could eventually trigger life-threatening device failure. Platelet adhesion and activation following adsorption of proteins on foreign surfaces plays a central role in thrombosis. The first event when a medical device comes in contact with blood is the adsorption of plasma proteins [52]. This leads to the platelet adhesion and activation and subsequently to thrombus formation. Therefore, to determine the biocompatibility of a new material, blood protein adsorption on the material surfaces, and adhesion/activation of platelets must be assessed. To improve the blood compatibility of blood-contacting devices, surface modifications or surface coatings should be carefully considered. Heparin, as was mentioned above, is indeed a potent anti-coagulant purified for decades from ruminants or porcine tissues; however, with the emergence of bovine spongiform encephalopathy, or mad cow disease, only

porcine-derived heparin is allowed in the United States and Europe. Therefore, there is an urgent need to develop nonbiologic alternatives to heparin coating for medical devices. A fluorinated diamond-like carbon (F-DLC) coating on stainless steel (SUS316L) was found to present better biocompatibility than a DLC coating in an in vitro rotation model, using human whole blood [16]. Furthermore, doping fluorine into DLC films greatly reduced its Young's modulus and surface free energy [61, 62], while largely preserving its other properties [50]. The incorporation of fluorine also improved the flexibility of DLC [61, 62] which allowed its use in medical devices where the coating was subjected to substantial deformation and movement, such as in tubes, guidewires, and stents. In this section, we summarized the hemocompatibility of F-DLC films on a polycarbonate (PC) surface, which is commonly used in various blood-contacting medical devices. Several types of F-DLC films were synthesized on PC substrates by varying the ratio of hexafluoroethane (C_2F_6) and acetylene (C_2H_2). Accordingly, the abilities to adsorb albumin and fibrinogen were measured, and the adsorption and the morphology of platelets were investigated, which adhered to the surfaces, followed by the incubation with platelet-rich plasma (PRP).

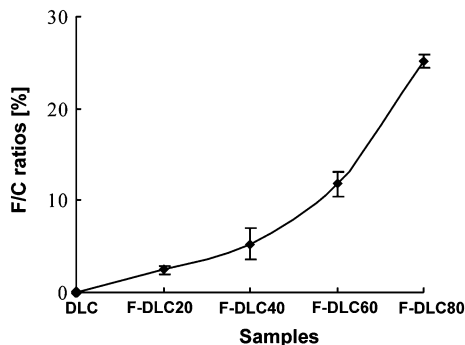
6.1.6.1 Characterization of Films

The chemical structure of the F-DLC films was examined by XPS. The C1 s spectrum of the F-DLC film could be deconvoluted into five Gaussian peaks corresponding to CF_3 (293.2 eV), CF_2 (290.95 eV), CF (288.8 eV), CCF_x (286.5 eV), and CC (284.9 eV). The absolute binding energies of CF_3 , CF_2 , CF, CCF_x , and CC are within previously reported ranges [57, 62–64] of 292.6–294, 290.3–292, 287.8–289.3, 285.5–287.3, and 283.4–285 eV, respectively. The ratio of fluorine to carbon atoms (F/C) can be calculated by Eq. (6.1) in Sect. 6.1.5.1 from the integrated intensity of the various components in the deconvoluted C1 s spectrum [52]. The results from the deconvolution of the C1 s spectrum are shown in Fig. 6.6. The values of XPS chemical composition (atomic percent) of F-DLC films were calculated by the area of each peak of C bonds and expressed as mean percent \pm standard deviation ($n = 3$). From the calculation, it was found that the main peaks of all F-DLC films were CC bond. As shown in Fig. 6.6, F-DLC20 and F-DLC40 films contained few fluorine bonds. The F-DLC60 film, however, had a much higher level of fluorine than the F-DLC20 and F-DLC40 films. Furthermore, the F-DLC80 film had a $\sim 25\%$ fluorine-to-carbon ratio.

6.1.6.2 Contact Angle Measurements

Contact angles of a drop of water (10 μ L) on F-DLC films were measured. The contact angle was significantly higher for PC (substrate) ($85.7^\circ \pm 1.3^\circ$) than for the substrates coated with DLC ($64.9^\circ \pm 1.6^\circ$), F-DLC20 ($65.1^\circ \pm 2.7^\circ$), F-DLC40 ($64.9^\circ \pm 1.6^\circ$), or F-DLC60 ($77.6^\circ \pm 2.9^\circ$) ($p < 0.05$). The contact

Fig. 6.6 F/C ratio in the F-DLC films determined by XPS [17]

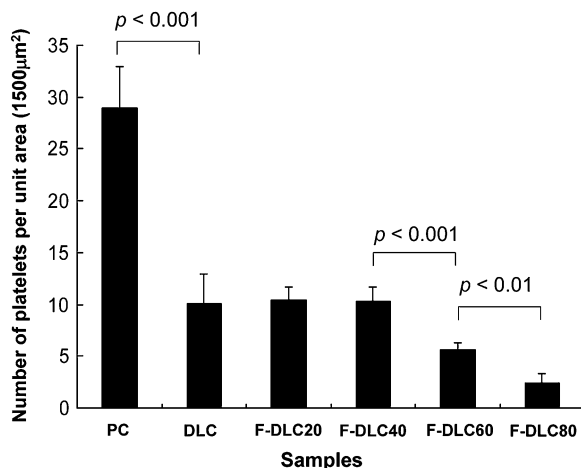


angle for F-DLC40 was the lowest, and it was nearly to the same as that for F-DLC20 (no statistical difference). The contact angle for the DLC-coated substrate was significantly lower than that for F-DLC20 or F-DLC40 ($p < 0.05$). The F-DLC60 group had a significantly higher contact angle ($77.6^\circ \pm 2.9^\circ$) than that of F-DLC20 or F-DLC40 ($p < 0.05$), and F-DLC80 had the highest contact angle ($90.9^\circ \pm 3.5^\circ$; $p < 0.05$ for F-DLC80 versus F-DLC60 and for F-DLC versus the PC substrate). The contact angles of F-DLC films increased as the ratio of C_2F_6 to C_2H_2 increased. According to Fig. 6.6 the fluorine-to-carbon (F/C) ratios in F-DLC20 and F-DLC40 films were much lower (nearly equal to 0) than those of F-DLC60 and F-DLC80. The F/C ratios were much higher in the F-DLC60 and F-DLC80 films, indicating that they were highly hydrophobic. The large ratios of fluorine-to-carbon could lead to a low surface energy on F-DLC films and increase the contact angles of water drops on them. The high hydrophobicity of F-DLC60 or F-DLC80 was consistent with their fluorine-to-carbon ratios (Fig. 6.6).

6.1.6.3 Platelet Adhesion

Figure 6.7 shows the number of platelets per unit area adhering to the surfaces of PC substrates and substrates coated with DLC, F-DLC20, F-DLC40, F-DLC60, and F-DLC80 films after 60-min incubation with PRP. The number of platelets adhering to DLC films was approximately one third of that on PC substrates; however, there were no significant differences in the number of adherent platelets between DLC, F-DLC20, and F-DLC40 films. The number of platelets adhering to F-DLC60 and F-DLC80 films was significantly lower than the number on DLC films. Thus, as the F/C ratios in the F-DLC films increased, the number of adherent platelets decreased.

Fig. 6.7 The number of platelets adhering per unit area ($1,500 \mu\text{m}^2$) after 60 min on PC substrates and substrates coated with DLC or F-DLC [17]



6.1.6.4 Platelet Activation

Representative DIC microscopic images of platelets on a PC substrate or substrates coated with DLC and F-DLC80 films are shown in Fig. 6.8a and Fig. 6.8b, respectively. The cellular morphology was divided into five grades according to Goodman et al. [65] and Allen et al. [66] as mentioned earlier. Many activated platelets in a spread state (grades 4 and 5) were adhered to the PC substrates (Fig. 6.8a). It was found that almost all platelets attached to DLC films were in grades 3 and 4. The morphologies of the platelets on F-DLC20, F-DLC40, and F-DLC60 films were analyzed. Inactivated platelets (grade 1) and slightly activated platelets (grade 2) were observed on F-DLC films, and a few of the platelets extended pseudopodia, indicating an early stage of activation (grade 3). Very few of the platelets adhering to F-DLC80 films were activated (Fig. 6.8b). Figure 6.9 shows the number of adherent platelets per unit area ($1,500 \mu\text{m}^2$) according to morphological grade. Platelets adhering to the PC surface were most frequently grade 5, whereas those on the DLC and F-DLC surfaces were mostly grade 2 and grades 1/2, respectively.

6.1.6.5 Protein Adsorption

The amount of albumin and fibrinogen adsorbed to the PC substrate and the substrates coated with DLC and F-DLC60 was measured using the micro-BCA assay (Fig. 6.3). As shown in Fig. 6.3a, the PC substrate adsorbed the highest level of albumin. The second highest adsorption was by the DLC-coated substrate, and the least was adsorbed by the F-DLC60-coated substrate. The same order of protein adsorption was observed using fibrinogen (Fig. 6.3b). A higher ratio of albumin to fibrinogen adsorption was observed on the substrate coated with F-DLC60 compared with the DLC-coated substrate or the PC substrate (Fig. 6.3c).

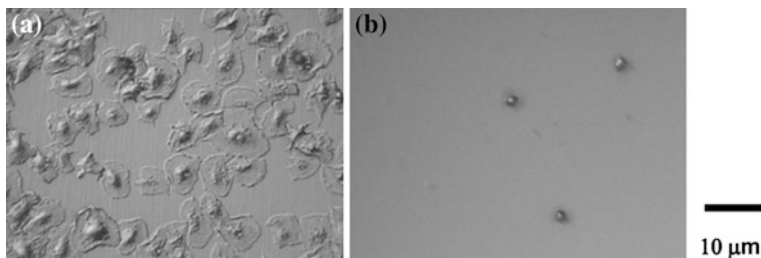
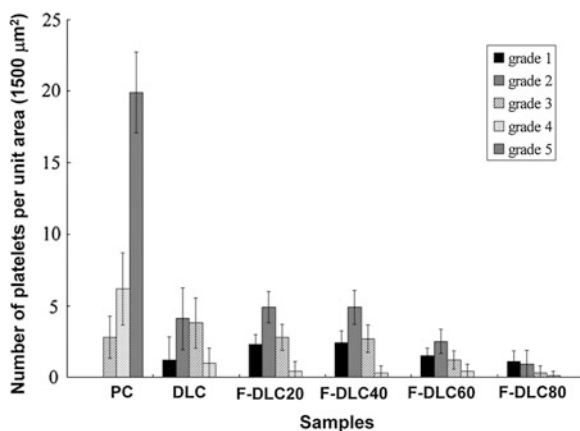


Fig. 6.8 Representative DIC microscopic images of platelets adhering to (a) PC substrates or substrates coated with (b) F-DLC80 after 60-min incubation [17]

Fig. 6.9 The number of platelets adhering per unit area ($1,500 \mu\text{m}^2$) after 60 min on PC substrates and substrates coated with DLC or F-DLC according to morphological grades [17]



These results indicate that the F-DLC60 coating should prevent the thrombus formation most effectively.

The adsorption of protein on uncoated PC and PC coated with DLC or F-DLC was investigated, and the relationship between protein adsorption and the adsorption and behavior of platelets was examined. When a foreign material is exposed to blood, it first adsorbs plasma proteins, leading to the activation of coagulation pathways or the adhesion and activation of platelets, and finally the formation of an insoluble fibrin network or thrombus. Because plasma proteins are rapidly adsorbed onto the surface of foreign biomaterials, they have profound effects on the biocompatibility of biomaterials and their interactions with blood components [67, 68]. It is generally recognized that platelet adhesion to surfaces is inhibited by the prior adsorption of albumin but enhanced by the adsorption of gamma globulin or fibrinogen [69]. Therefore, the amount and nature of the plasma proteins adsorbed on the surface are crucial determinants of the biocompatibility of biomaterials. Albumin and fibrinogen as plasma proteins were studied because the ratio of albumin to fibrinogen has been reported to be useful for assessing the biocompatibility of a biomaterial. Specifically, a higher ratio of albumin/fibrinogen corresponds to the lower number of adherent platelets on the

sample surfaces [35, 54]. Albumin is the major constituent of blood plasma and is one of the smallest plasma proteins. Many previous studies show that adsorption of albumin passivates biomaterial surfaces, reducing both proinflammatory and thrombogenic responses [70–72]. Fibrinogen is a key protein in the blood coagulation cascade, which enhances the adhesion and activation of platelets [58]. Fibrinogen supports platelet adhesion and aggregation through its binding to the platelet membrane glycoprotein GPIIb/IIIa [66], and its conformational changes at the cell surface are crucial for the interaction [53]. Moreover, fibrinogen has a critical role in attracting inflammatory cells to biomaterials [73]. The results introduced in this section showed that F-DLC60 films exhibited the highest albumin to fibrinogen ratio, which may be related to the low number of adhering platelets and, therefore, a low tendency to induce thrombus formation. From the experimental results, F-DLC films showed higher levels of CF bonds than CH bonds. The stable bonding of carbon and fluorine atoms in F-DLC films lowered the surface energy, which could result in the reduced adsorption of protein. The lower surface energy of the F-DLC films was also supported by the contact angle measurements. For example, F-DLC80 films were the most hydrophobic surfaces, indicating that they had the lowest surface energy. The plasma protein adsorption was significantly considered to be influenced by the interfacial energy between the implant surface and protein plasma. The reduction of the surface energy with varying F content was believed mainly due to the change of bonds in the film, that is, CC bond decreased and CF, CF₂ increased, which was also summarized in the previous section. Other studies have revealed that the roughness and the microstructure played negligible roles on affecting the film surface energy. DLC has been reported to have a higher albumin to fibrinogen adsorption ratio than Ti, TiN, and TiC surfaces, indicating that DLC may prevent thrombus formation [54]. Dion et al. also reported a higher albumin/fibrinogen adsorption ratio on DLC compared with silicone. Based on a review of the literature, Cui and Li stated that DLC and amorphous CN films showed good tissue and blood compatibility in vitro and that DLC had a high albumin/fibrinogen adsorption ratio [35]. Notably, the albumin to fibrinogen adsorption ratio for F-DLC was higher than that for DLC films, which were already known to suppress thrombus formation. A thrombus was formed by platelet adhesion followed by aggregation and spreading. As mentioned earlier, interaction of platelets with the foreign surfaces was determined by the nature of the proteins adsorbed on the biomaterial surfaces from the blood plasma. The numbers of platelets adhering to F-DLC60 and F-DLC80 films was drastically lower than with DLC, F-DLC20, and F-DLC40 films. In addition, the inclusion of fluorine in the DLC films inhibited platelet activation, with higher F/C ratios corresponding to greater inhibition of platelet activation. The tendency of platelets to adhere also corresponded with the albumin/fibrinogen adsorption ratio of the sample surface, and the higher albumin/fibrinogen ratio for the F-DLC corresponded to a suppression of platelet adhesion. Furthermore, the albumin/fibrinogen ratio also affected the behavior of the platelets: the higher the albumin/fibrinogen ratio, the lower the number of activated platelets. Upon platelet activation, a conformational change in GPIIb/IIIa led to the exposure of a high-affinity binding

site for soluble fibrinogen [74]. Binding of fibrinogen to GPIIb/IIIa led to platelet aggregation via fibrinogen-mediated crosslinking of GPIIb/IIIa on two different platelets. In this way, protein adsorption was closely connected to platelet activation and adhesion. We reported the adhesion and activation of platelets following incubation of silicon substrates and silicon coated with DLC or F-DLC with PRP [41]. In those experiments, the F-DLC coating dramatically reduced the number and the activation of adherent platelets. In contrast to silicon, which had a hydrophilic surface, PC had relatively a hydrophobic surface; however, despite the high hydrophobicity of PC, it bound and activated many more platelets than DLC-coated or F-DLC-coated PC. These results suggested that the wettability was not the only determinant of blood compatibility. Further investigation should be necessary to clarify which other factors were closely associated with biomaterial-induced thrombosis, including, for example, the specific chemical composition, the surface free energy, and the surface energy components (dispersive and polar components). In addition, further studies would also be to evaluate the availability of F-DLC coating for three-dimensional medical devices without the risk of film breakdown in various clinical settings.

In summary, PC substrates were coated with F-DLC films containing different amounts of fluorine by varying the ratio of C_2F_6 to C_2H_2 . The hemocompatibility of the F-DLC films was evaluated by analyzing the adhesion and the activation of adherent platelets. The correlation between the adsorption of blood protein and the behaviors of adherent platelets was clarified. F-DLC films presented lower numbers of adherent platelets and less platelet activation than PC and DLC-coated substrates. Increasing the doped amount of fluorine into the F-DLC films resulted in greater suppression of platelet adhesion and activation. Moreover, F-DLC had the highest ratio of albumin/fibrinogen adsorption. Therefore, the F-DLC coating may be useful for blood-contacting medical devices.

6.1.7 Effects of Surface Roughness on Anti-Thrombogenicity of DLC and F-DLC

It is widely believed that the surface roughness of biomaterials is a key factor that influences thrombogenicity. As was mentioned above, diamond-like carbon (DLC) is being considered for widespread clinical use as a surface coating for cardiovascular devices. We also already mentioned that fluorine doping in DLC films (F-DLC) markedly inhibits platelet adhesion and activation in human blood. To evaluate the effects of surface roughness of coatings on the thrombus formation, DLC and F-DLC films were deposited on the three different roughness-controlled polycarbonate (PC) substrates, and the platelet adhesion and the platelet activation were investigated on each substrate. The surface roughness of DLC-coated PC and F-DLC-coated PC ranged from 4.1 to 97 nm. In this range, there were no significant differences in the platelet-covered area among the three grades of differing

surface roughness for each coated surface. However, evaluation of the F-DLC films revealed significant reductions in platelet adhesion and activation when compared with DLC films for every grade of roughness, suggesting that the inherent chemical characteristics of the surface, such as wettability, interfacial free energy, and higher ratios of albumin/fibrinogen adsorption, might be more important in the mechanism of the non-thrombogenicity of F-DLC.

Biomedical devices, such as artificial hearts, and interventional tools (stents, guidewires, catheters, etc.) now play a major role in treating disease and organ insufficiency in the aging population. However, human immune reactions to biomaterials implanted in the body work against the intention to heal disease, and may even cause serious harm or death [16]. Thrombus generation on the surface of the blood-contacting medical devices is a particularly major problem. Thrombus formation not only hinders medical placement, but also acts as a trigger of cardiac infarction, brain infarction and loss of eyesight. Platelets play a central role in the hemostatic process, including recognizing the site of injury, recruiting additional platelets via intercellular signaling, adhering to one another, and interacting with the coagulation cascade to form a hemostatic plug [75]. Therefore, studying the interactions between platelets and the surface of biomaterials is necessary to overcome thrombogenic problems. For example, metallic stents are used as medical devices that can provide endovascular scaffolding to relieve vascular obstruction. They are commonly made of 316L stainless steel or nitinol (nickel–titanium alloy) and exert continuous radial pressure on diseased artery, resulting in a compression of atherosclerotic plaques, sealing of dissections, and vessel expansion. However, as was already mentioned, re-narrowing of the vessel remains a major problem after stent placement, and can trigger life-threatening device failure [41]. Interactions between metallic devices and living tissues (including blood and arteries) occurring at their interface and the surface properties of metallic devices play key roles in their safe, long-term implantation, while the material and surface patterns of intravascular stents play a pivotal role in activating platelets and triggering adherence of inflammatory cells that leads to the re-narrowing caused by neointimal hyperplasia [41]. Surface modification is one method of improving both the mechanical and physical properties of implants in direct contact with blood and tissue. Surface modification is a general concept that can be divided into surface treatments and surface coatings, or a combination of both. Surface treatments include mechanical and electrochemical polishing, ultrasonic cleaning, chemical etching and degreasing, as well as low pressure plasma etching, while surface coatings could be obtained by wet processes, such as dip coating, or dry processes, such as low pressure plasma deposition [76]. In such situation, diamond-like carbon (DLC) films have indeed attracted much attention as anti-thrombus coatings that reduce adhesion and activation of platelets [4, 16, 41, 77, 78]. Furthermore, as was mentioned, attempts to improve the anti-thrombus and physical properties have involved adding elements such as fluorine [16, 41, 79], silicon [25], phosphorus [20] and boron [80] to DLC. Also as was mentioned in the previous section, fluorinated DLC (F-DLC) films have performed particularly well in both blood adaptability and in vivo biocompatibility [79]. There should be

numerous mechanisms that prevent the adhesion and activation of platelets on DLC or doped-DLC, mediated proteins, chemical properties of the surfaces, wettability and surface structures. Surface roughness of biomaterials is also considered to be an important factor [81–84] in thrombosis. Hence polishing methods for material surfaces are an important subject of study in order to enhance the anti-thrombogenicity of biomaterials for medical applications [85], and many stent manufacturing companies believe that electrochemical polishing is vital for their products. However, there is little information on how roughness affects the thrombogenicity of DLC-coated substrates. Therefore the relationship between surface roughness of DLC and F-DLC, and hemocompatibility on incubation with platelet-rich plasma (PRP) isolated from human whole blood was investigated.

6.1.7.1 Polished SUS316L and Molded PC

SUS316L and molded PC with three different surface roughnesses were prepared. Ra was observed in a $50 \times 50 \mu\text{m}$ area, and the values are listed in Table 6.1. From the AFM images of SUS316L and PC, it was found that Ra was well controlled, ranging from 1 to 100 nm. The surface of SUS316L was well-followed by PC. Thus, the Ra of SUS316L closely corresponded to that of PC, indicating good transfer of the surface profile from SUS316L to PC. The Ra of DLC and F-DLC deposited on Ra-controlled PC substrates was measured by AFM and the values are also listed in Table 6.1.

6.1.7.2 Platelet Adhesion and Activation

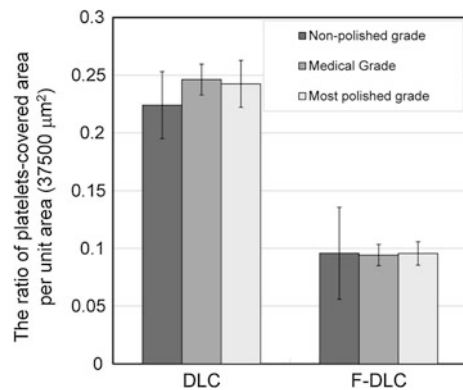
Platelets play a key role in biomaterial-associated thrombosis, and a reduction in platelet adhesion activation is vital for the eventual success of numerous blood-contacting medical applications. Hence the platelet adhesion was studied by Ra-controlled PC substrates (“Non-polished grade”, “Medical grade”, and “Most polished grade”) coated with DLC or F-DLC, and the relationship between surface roughness and behavior of human platelets was examined using the glutardialdehyde induced fluorescence technique (GIFT) [51]. GIFT uses the epifluorescence of glutardialdehyde-fixed platelets, as detected by fluorescence microscopy, and is suitable for opaque and transparent materials [51]. Early platelet activation produces cytoskeletal reorganization that results in characteristic cell shape

Table 6.1 Surface roughness (Ra) [nm] of each sample surface determined by AFM [60]

Roughness substrates	Non-polished grade	Medical grade	Most polished grade
SUS	100 ± 5	51 ± 16	2.2 ± 0.5
PC	83 ± 6	52 ± 13	3.7 ± 1.2
DLC	97 ± 4	27 ± 6	8.4 ± 0.3
F-DLC	81 ± 9	16 ± 4	4.1 ± 0.3

changes: platelets lose their discoid shape and begin to develop thin pseudopodia. At more advanced stages, they become large, spiny spheres completely covered by pseudopodia, and finally, become fully spread [65]. In the present study, using computer-aided image analysis, the number of adherent platelets and platelet-covered area was determined as markers of surface thrombogenicity. Both the number of platelets and the changes in morphological shape in active platelets contribute to the platelet-covered surface area of the substrate. Thus, calculating the platelet-covered area/unit area is an index that reflects platelet adhesion and activation. Representative fluorescence microscopic images of platelets on different grades of Ra-controlled PC substrates coated with DLC or F-DLC films were measured. The number of platelets adhering to F-DLC films was lower than the number on DLC films in every substrate with the same roughness. The ratio of platelets-covered area was measured by counting and analyzing the platelets per unit area ($37,500 \mu\text{m}^2$) adhering to the surfaces of substrates coated with DLC and F-DLC films after 60 min incubation with PRP, which was presented in Fig. 6.10. The proportion of platelet-covered area for F-DLC was significantly lower than that for DLC in each Ra-controlled substrate. Moreover, there were no significant differences in the proportion of platelet-covered area among the three Ra-controlled surfaces in either the DLC or F-DLC group. According to previous papers, there is a relationship between surface roughness and material thrombosis, as determined by qualitative SEM evaluation [81, 82, 84]; however, the effects of surface roughness at the nano-order scale on material thrombosis were not discussed. Tsunoda et al. [83] suggested that cellulose hollow-fiber dialysis membranes having rough surfaces had high platelet adhesion ratios and poor hemocompatibility, whereas those with smoother surfaces had lower platelet adhesion ratios and better hemocompatibility. They measured the surface roughness by AFM, and found a range of 10–100 nm. Therefore, in terms of the dialysis membrane surface, the difference in nano-order roughness had a clear effect on thrombogenicity. In the present study, the roughness of the tested surfaces of the samples ranged from 2 to 100 nm; however, there were no significant differences in thrombogenicity among the different grades of Ra-controlled PC substrates

Fig. 6.10 Ratio of platelet-covered area per unit area ($37,500 \mu\text{m}^2$) on the surfaces of substrates coated with DLC and F-DLC films after 60-min incubation with human platelet-rich plasma (PRP) [60]



coated with DLC or F-DLC film. In addition, platelet adhesion and activation on F-DLC was markedly suppressed when compared to those on DLC films in all roughness groups, which suggests that nano-order surface roughness (below 100 nm) of DLC and F-DLC had no obvious effects on non-thrombogenic properties when compared with the effect of fluorine doping. Coating with DLC or F-DLC appears to be a promising technique for blood-contacting devices [16, 41]. It is generally believed to be necessary for manufacturing companies to polish substrates using methods like electrochemical polishing or electrochemical buffing when producing biomaterials for blood-contacting medical devices. However, it is both expensive and time-consuming to polish the surface of three-dimensional substrates prior to deposition of DLC or F-DLC film. The results suggest that pursuing such high levels of smoothness should be unnecessary when DLC or F-DLC film is used as an antithrombogenic coating for blood-contacting medical devices. In this present study, the effects of surface roughness of DLC and F-DLC films under static conditions were evaluated using human PRP. This method is a simple screening technique for evaluating the thrombogenicity of newly developed biomaterials; however, thrombosis is fundamentally linked to thermodynamics, as blood transports cells and proteins to the thrombus and applies stresses that may disrupt the thrombus [84]. Thus, further studies are necessary to evaluate the relationship between the surface roughness of DLC and F-DLC and thrombogenicity under flow conditions.

In summary, the relationship between the surface roughness of DLC and F-DLC deposited on three types of Ra-controlled PC substrate and the degree of platelet adhesion and activation on the sample surfaces was investigated. AFM measurements revealed the surface roughness of DLC-coated PC and F-DLC-coated PC ranged from 4.1 to 97 nm (Ra). In this range, there were no significant differences in platelet-covered area among the three grades of surface roughness for each coated surface. However, evaluation of F-DLC films incubated with PRP showed significant reductions in platelet adhesion and activation when compared with DLC for every grade of roughness, thus suggesting that the inherent chemical characteristics of the surface, such as wettability, interfacial free energy and higher ratio of albumin/fibrinogen adsorption, might be more important in the mechanism of F-DLC non-thrombogenicity. However, further studies, including dynamic evaluation, are needed.

6.2 DLC on Polymers

6.2.1 Adhesion

In this section, the adhesion between DLC and polyethylene (PE), the most widely used plastic, was discussed. Polyethylene (PE) is a semi-crystalline polymer widely used in consumer products and for molding materials due to its excellent

thermal properties. Among its mostly remarkable physical and chemical properties, however, one rather annoying characteristic that may have limited the expansive usage of PE was its poor adhesion property. Here the adhesion between diamond-like Carbon (DLC) and high-density polyethylene (HDPE) was investigated. The peel strength of DLC-deposited HDPE was found to be 20 times as high as that of non-treated HDPE. Further improvement in adhesion was observed in fluorinated DLC (F-DLC). By applying fluorine (C_2F_6) etching to DLC, the peel strength eventually increased up to 60 times as compared with that of pure HDPE without any pretreatment. From the surface observation and the experimental results of the surface free energy of modified HDPE, it is surmised that the mechanism behind this phenomenon is principally due to the formation of nano-scale anchors that were formed during the DLC deposition process. Further etching of the HDPE substrate by fluorine radicals eventually increased the number of the anchors, leading to a significant improvement in the adhesion between HDPE and F-DLC.

Recently the demand for polymeric materials has been increasing and functionalization of polymers is much desired for wider applications. Polyethylene (PE) is a semi-crystalline polyolefin widely used as, for example, plastic films for food packaging and flexible pipes for sewage systems. Due to its excellent physical and chemical properties, its lightness, low cost, and easiness in molding, PE is one of the most used semi-crystalline polymers. The poor adhesion of PE on one hand, has created a best plastic glove to handle strong adhesives such as Super Glue, the super-bonding cyanoacrylate glue. On the other hand, there has been substantial interest in developing bonding methods to enhance the adhesion property of PE [86–88]. Accordingly, the processes such as corona discharge, flame treatment, plasma treatment, and primer treatment have been widely studied and introduced. These pretreatments were especially used in order to modify the poor-bonding surface of PE films, but their usage is relatively limited because of their complex, sometimes inconvenient, and unsafe modification mechanism. Processes such as corona and flame treatments also have the risk of degradation due to the gradual deoxidation on the surface. Primers are also considered difficult when applied to only small selected area of the polymer substrate. Here in this section, the improvement of the adhesive property of PE by the deposition of diamond-like carbon (DLC) and fluorinated DLC (F-DLC) was introduced. DLC is an amorphous carbon film which possesses excellent physical properties such as high hardness, high gas barrier property, and low friction coefficient. The structure of DLC consists of a mixture of diamond (sp^3) and graphite (sp^2), terminated by hydrogen. Though the structure of DLC and PE are basically different, there should be similarity between DLC and PE, as they are both composed of hydrogen and carbon atoms. It was therefore expected that depositing DLC had a considerable effect on the adhesion properties of PE. Moreover, by depositing stable DLC film on PE, a widespread introduction of the surface modification on selected places of the PE substrate became highly possible, thus leading to the control of the adhesion property of PE. Further enhancement of adhesion was analyzed and tested by adding fluorine into the DLC film. This film, called fluorinated DLC

(F-DLC) film as defined in the previous section, is a thin functional film which until today is known to possess, for example, optical transparency, water repellency, and high antithromogenicity [41]. By gradually incorporating fluorine into DLC films, the control of the adhesion force was expected owing to the surface modification mechanism discussed later. Here, a high-density polyethylene (HDPE), the widespread polyethylene of the polyethylene family was used. After the deposition of the thin functional DLC and F-DLC on HDPE, it was found that the modified HDPE can adhere to various substrates ranging from metals to polymers, at the same time presenting excellent surface properties originated by DLC and F-DLC in addition to the highly flexible mechanical properties originated by HDPE. Moreover, DLC and F-DLC films were deposited on HDPE substrates and the peel strength was examined by T-peel testing. Furthermore, the mechanism of how the film deposition enhanced the peel strength of HDPE was investigated through the surface observation of the peeled surfaces conducted by scanning electron microscopy (SEM) and contact angle measurement.

6.2.1.1 Peel Strength

Figure 6.11 show the peel strength results of differently treated HDPE: HDPE without any pretreatment, HDPE directly bonded by an instant adhesive (Aron Alpha or Super Glue, the superbonding cyanoacrylate glue) without epoxy resin, HDPE stuck by adhesive tape developed for the adhesion of Polyolefin materials, HDPE pretreated by primers, and DLC-deposited HDPE. The DLC-deposited HDPE had approximately equal peel strength to primer-treated HDPE. When compared to HDPE without any pretreatment, the peel strength of DLC-deposited HDPE was about 20 times higher. The peel strength of F-DLC-deposited HDPE is shown in Fig. 6.12. F100 refers to plasma etching by C_2F_6 . As the amount of fluorine inside the film increased, the peel strength increased. Especially in F80 and F100, adherend failure (breaking of HDPE substrates themselves) occurred, indicating that the peel strength was actually even higher than the fracture strength of the HDPE substrate.

Fig. 6.11 Peel strength results of differently treated HDPE [118]

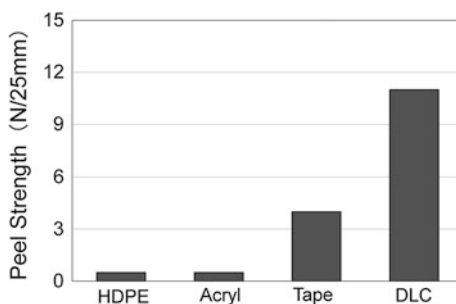
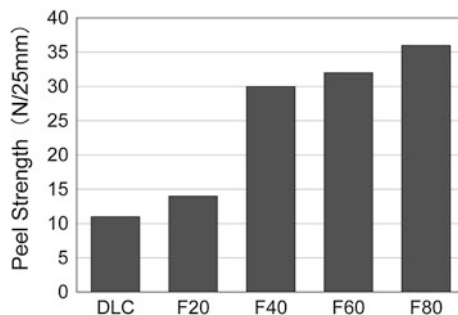


Fig. 6.12 Peel strength results of F-DLC-deposited HDPE [118]



6.2.1.2 SEM Images of HDPE

The SEM micrographs of HDPE before and after DLC deposition, and after peeling test were studied. The SEM micrograph of HDPE surface after peeling test was presented in Fig. 6.13. Before DLC deposition, HDPE surface is covered with nano-scale fibrils, which are considered the crystalline segments of polyethylene. After depositing DLC, the number of fibrils is seemingly increased. Since DLC well copies the surface characteristics of the substrate surface, the observation of DLC surface must be almost equivalent to the direct observation of the HDPE surface. From the SEM image of HDPE after T-peel testing, numerous nano-scars were found, indicating local tension existed during the T-peel testing.

6.2.1.3 Surface Free Energy

The surface free energies of DLC-deposited HDPE, F60-deposited HDPE, C_2F_6 -etched (F100) HDPE, epoxy resin, and HDPE were analyzed. They were ~ 45 , ~ 41 , ~ 29 , ~ 43 , ~ 39 [mJ/m^2], respectively. By increasing the fluorine content in DLC, the contact angle of both purified water and methylene iodide increased, eventually decreasing the surface free energy. Even though C_2F_6 -etched HDPE (F100) was not verified as HDPE with thin F-DLC film, it had the lowest surface free energy (i.e. the highest contact angle).

Polyethylene is a semi-crystalline polymer, composed of a crystalline region and an amorphous region. There is a significant difference between these two regions in physical properties such as Young's modulus and fracture strain. Due to the difference, the crystallization of PE often brings about a drastic change in mechanical properties. In the field of adhesion, it has been said that the amorphous parts distributed on the surface of PE had a significant effect on adhesion. Such unique surface was named "Weak Boundary Layer (WBL)", and it was frequently reported that the adhesion improvement of PE was caused by the ablation of the WBL. However, Briggs questioned the existence of WBL, and it was widely considered that the adhesion improvement was caused not only by WBL but also by different mechanisms [89], which are yet to be analyzed and discussed since

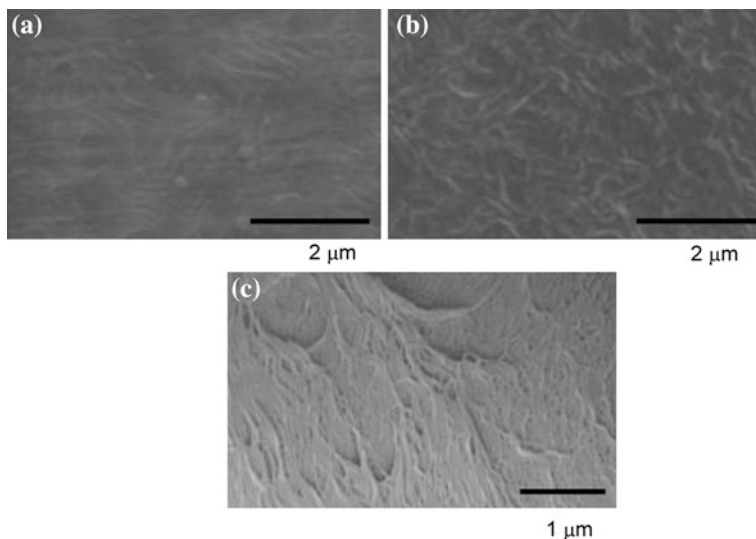


Fig. 6.13 SEM images of HDPE before deposition, after deposition, and after the T-peel testing [118]

they are not understood completely. From the above-mentioned contact angle measurements results, it was found that, for F-DLC-deposited HDPE, the peel strength increased with the decrease in the surface free energy by doping fluorine into DLC. Surface free energy generally shows the wetting capability of the substrate, which is directly related to the intermolecular interactions between substrate and adhesive. The surface free energy of epoxy resin, however, is below the value of DLC and it was considered that the enhancement of adhesion cannot be explained sufficiently only by the surface free energy. The T-peel test is to examine adhesion between substrate and adhesive, and therefore the sample has normally three layers (i.e. an adhesive layer sandwiched by two substrates). In the above experiments, since thin films (DLC or F-DLC) are already deposited on top of the substrate, the sample has actually five layers. It was therefore necessary to identify which layer of five was peeled off by the T-peel testing. During all the peel tests, it was eventually analyzed that there was a separation of DLC (or F-DLC) film from HDPE substrate. The results indicate that the process of DLC deposition on HDPE substrate significantly affects the surface of HDPE, enhancing the adhesion force between DLC and HDPE. From SEM images, nano-fibrils of 10–20 nm in diameter were found distributed over the surface of HDPE. These nano-scale anchors can be directly related to the enhancement of adhesion of HDPE. Moshonov et al. calculated the wettability and measured the improved peel strength of PE caused by C_2H_2 glow plasma discharge [90]. Even though their experimental methods and the parameters such as discharge power were different from the ones in this experiment, it was possible for C_2H_2 to be generated during the DLC deposition. The process can be described as follows: HDPE surface was

first etched by C, H radicals at the beginning of DLC deposition, forming nano-scale hills and holes on the HDPE surface. Then almost simultaneously, DLC film was deposited and accumulated, filling the holes. After deposition, the hardened thin film adhered physically to the substrate, thus finally presenting the strong peel strength. The increase in the peel strength by the introduction of fluorine could be due to the etching caused by this relatively large halogen atom. Strobel found that the C_2F_6 plasma generated CF_x radicals in plasma environment, at the same time fluorinating the PE surface [56]. By including fluorine during the process, CF_x radicals were generated to etch the surface of HDPE at the beginning of the film deposition. Thus the peel strength of F-DLC-deposited HDPE became higher, as the fluorine content of F-DLC increased.

In conclusion, the adhesion modification of HDPE by DLC and F-DLC films was carefully investigated. By depositing DLC and F-DLC films, the peel strength of HDPE increased 60 times. Surface free energy could not sufficiently explain the tendency of the adhesion enhancement, revealing that the enhancement was not solely caused by the molecular interactions. From the SEM images, plenty of intertwined nano-fibrils were observed and it was concluded that the improvement in adhesion was presumably due to the formation of nano-scale anchors on the HDPE substrate at the beginning of the DLC and F-DLC film deposition.

6.2.2 Fracture

DLC films coated on polymer substrates have been extensively used and investigated because recently, quite a few applications for the use of these polymer-DLC composites have been proposed. Under these circumstances, fracture of DLC is another critical problem that should be solved before practical use. The DLC-polymer applications range from e.g. DLC-coated polyethylene terephthalate film (DLC-PET), through DLC-coated polycarbonate (DLC-PC) to other DLC-coated rubbers. In this section, thin DLC films coated on several polymer substrates possessing different chemical structures and Young's moduli were investigated. The DLC-polymer films were stretched to different strains and the extended surface was investigated by optical microscopy and scanning electron microscopy (SEM) to study the fracture mechanism of the DLC-coated polymer films. Intriguing horizontally and vertically aligned micro-cracks and micro-buckling were observed, constructing periodic lattice-like fracture patterns on the surface of the extended DLC-polymer films. It was found that the lattice patterns were significantly influenced by Young's moduli of both polymer substrates and DLC films, and that the patterns were also dependent on the adhesion between the DLC films and the polymers.

Recently the demand for polymeric materials has been increasing and highly functionalized polymers are much desired for wider applications such as flexible materials with high gas barrier properties. In order to functionalize polymers, Diamond-like Carbon (DLC) coating is one of many useful approaches that are

industrially broadly used for the surface modification. DLC is characterized by many unique properties, including high hardness, high wear resistance, low friction coefficient, chemical inertness and high gas barrier properties, which are used as commercial materials including DLC-coated PET bottles, improved tribological rubber surfaces and highly biocompatible polymers especially for medical purposes [91, 92]. However there are obvious structural differences between polymers and DLC, particularly on a microscopic scale. Polyethylene (PE), the most fundamental C–H based polymer, consists of plenty of two dimensional macromolecules partly connected to each other by crystallization (i.e. through relatively weak van der Waals force) and the distance between two molecules are typically ~ 2.5 , ~ 4.9 and ~ 7.4 Å, while DLC are intrinsically three dimensional carbon networks (i.e. connected through strong chemical bonding force) and the typical distance between two carbons is 2.5 Å, which is shorter (i.e. denser and heavier) than PE. Considering the use of the composite materials made of polymers and DLC, such structural differences between the two materials cannot be neglected and hence the resulting composite presents complex physical properties which are necessary to be investigated systematically. However, there have been few reports that dealt with the structural and mechanical behavior of DLC films coated on polymer materials, particularly when the polymer–DLC composites were mechanically and cooperatively deformed. Fracture behavior of thin hard films coated on metals has been investigated by several groups. Shear strength and crack surface were observed by Agarawal et al. on copper coated by thin ceramic film [93]. They found transverse cracks when mechanically stretched. Ye et al. introduced three types of cracking processes on thin films due to residual strain in brittle substrates and weak interface between the films and substrates [94]. Chen et al. observed periodic cracking on thin TiN coated on stainless steel [95], while Ogwu et al. examined similar periodic cracking on thin DLC film coated on stainless steel when exposed to biological fluids [96]. Fracture surface and characterization of mechanical properties of DLC film were discussed by Choi et al., Cho et al. and Aoki et al. [97–99]. The deformation of the substrates becomes more significant as well as problematic, when softer polymeric materials are used as substrates instead of traditionally utilized hard metals. There have been a few papers that directly dealt with polymer–DLC composites. Ollivier et al. assessed the adhesion between DLC films and polyethylene terephthalate (PET) films through simple tensile testing and surface microscopy. Aoki and Ohtake improved the wear resistance of DLC films by using segment-structured DLC films on aluminum substrates [97]. They developed this method after they studied the morphology of the DLC surface that presented a segmented surface (lattice-like fracture) automatically generated when DLC was coated on polymers. The composites of softer materials (polymers) and harder materials (DLC) should present complex physical behavior and when they are deformed by mechanical tension, the fracture properties of thin DLC films should be strongly dependent on the chemical and physical properties of both polymer substrates and DLC films. We therefore focused on The moduli of materials, of both polymers and DLC, were carefully analyzed and how the resulting polymer–DLC composites acted in terms

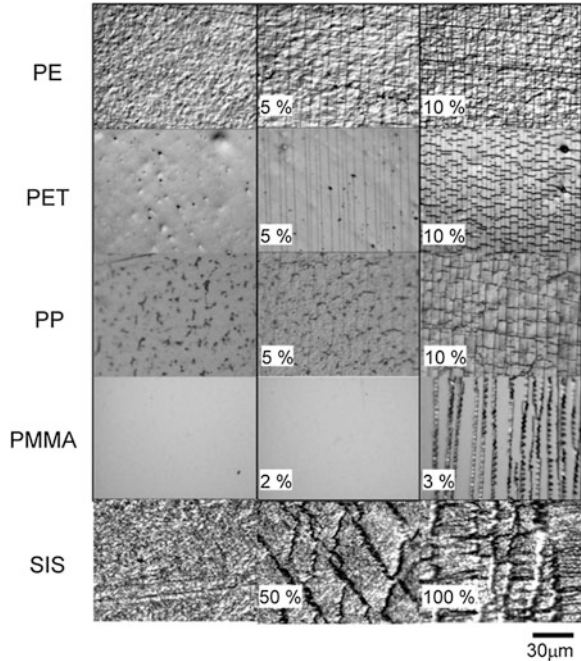
of fracture behavior was investigated when they were mechanically deformed. The moduli of materials were changed by choosing different materials possessing different Young's moduli. Two different polymers with similar Young's moduli but with different adhesion to DLC films were selected to investigate the adhesion effects of polymer–DLC composites on fracture properties. Periodic fracture patterns of thin DLC films coated on soft polymers have been observed, showing lattice-like fracture surfaces of the DLC. It was also found that the periodicity and mechanism of fracture surfaces were strongly related to the moduli of polymers and DLC as well as the adhesion between both materials.

The following polymers were used in the experiments: polyethylene (PE), polyethylene terephthalate (PET), polystyrene-block-polyisoprene-block-polystyrene copolymer (SIS), polydimethylsiloxane (PDMS) and polypropylene (PP). PDMS at "Silastic Medical" grade were used, which was already cut in shape for the experiments. Young's moduli of PE, PET, SIS, PDMS, and PP were measured using tensile testing machine, which were 1,500, 600, 460, 6, and 1.4 MPa, respectively.

6.2.2.1 The Influence of Young's Moduli of Polymer Substrates on Fracture Mechanics of DLC Films

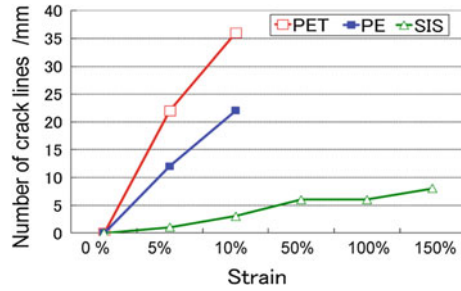
Figure 6.14 shows the surface micrographs of DLC on PE, PET, PP, PMMA, and SIS samples. The samples were extended to 0 % (unstretched), 5 and 10 % of natural length for PE and PET samples in a step-strain fashion by the tensile tester in the transverse direction of the figures. SIS samples were very elastic and since fracture was not clearly observed at low deformation, they were further extended to 50, 100 and 150 % and unloaded step by step down to 100 and 50 %. All materials presented unusual fracture surfaces and showed almost regularly aligned perpendicular and horizontal straight fracture lines, eventually constructing lattice-like fracture surfaces. The fracture mechanics were found to be very different between polymer samples of different Young's moduli. First, the surface of DLC-coated PE samples (DLC-PE) whose Young's modulus was ~ 460 MPa was observed. DLC-PE was extended to 105 % and showed vertical crack lines and horizontal buckling lines, producing a periodic lattice fracture pattern. These vertical and horizontal lines were identified as micro-cracks and micro-buckling by SEM. The SEM micrograph of the magnified fracture surface of PET–DLC composite stretched 10 % in strain clearly revealed horizontal crack lines and vertical buckling lines that appeared on the surface. The fracture surface patterns of polymer–DLC composites were therefore indeed characterized by the crack and buckling lines crossed orthogonal to each other. The sample was further extended to 10 % and the distance between cracks in the lattice pattern became narrower than that of 5 % extended sample. The cracks appeared due to the tensile stress in the normal direction of the stretching force, followed by the buckling parallel to the stretching force due to the compression perpendicular to the extension. The compression was due to the contraction strain against extension strain in the

Fig. 6.14 Surface micrographs of stretched and fractured samples of PE, PET, PP, PMMA, and SIS coated by DLC by optical microscopy [119]



direction of the stretching force, obeying Poisson's ratio. Next, the PET samples which were harder substrates than PE were tested and they showed only vertical crack lines at the extension rate of 5 % of natural length. After further extension of the PET samples to 10 %, horizontal buckling lines appeared and the perpendicular crack lines increased, resulting in the narrow lattice pattern similar to that of PE but narrower than PE's at the same amount of extension. Last but not least, the SIS sample, the softest rubber material in this experiment, showed only few cracks and bucklings up to 5 % or even till 10 % of natural length. Therefore the SIS samples were stretched to 50, 100 and 150 % of their natural length and eventually recovered to 100, 50 % and the surfaces at all strains were investigated. In the extension range from 0 to 100 %, there were only a few diagonal crack lines and no buckling lines were observed. At the extension over 100 %, horizontal bucklings began to appear, and at the same time, the diagonal cracks became more vertical. The vertical cracks became more pronounced when the samples were in the unloading process (down to the strains of 100 and 50 %). It should be noted that the number of cracks in the SIS samples stretched to 150 % was smaller than that of the PE samples only stretched to 5 % and hence the length and the width of the lattice pattern of SIS samples were broader than those of the PE samples. The number of crack lines as a function of strain was counted by optical microscopy for PET, PE, and SIS samples (all coated with DLC) and was plotted in Fig. 6.15. The crack number increased with strain for each sample. It was found that PET, the hardest material, had the highest crack number, followed by PE and SIS, the

Fig. 6.15 The number of crack lines as a function of strain counted by optical microscopy for stretched PET, PE, and SIS samples (all coated with DLC) [119]



softer and the softest materials, respectively. At the strain of 10 %, PET possessed over 10 times of the crack number as compared with the lowest SIS. As a result, it was found that the fracture surface of DLC films on polymer substrates was characterized by the lattice-like fracture pattern due to the well-aligned vertical crack lines and the horizontal buckling lines and that the lattice pattern of the DLC films on harder polymer substrates showed narrower length and width in their “lattice” periodicity. The mechanism of the lowering of the lattice periodicity can be qualitatively explained by considering tensile modulus of the polymer substrate as presented in Fig. 6.16. Assuming the quality of DLC to be consistent through all polymer samples, the DLC should be broken almost at a constant critical stress S_c . In the case of DLC coated on harder polymer substrates, as soon as one crack appears, the next crack will appear when the polymer under the crack deforms till it reaches the critical stress S_c . If the polymer used as a substrate is harder, the critical stress S_c is attained at lower strain, thus the next crack appears at lower strain. Similarly if the polymer is softer, the higher strain is required to reach S_c , thus ending in higher strain for the next crack to appear. In such ways, the number of cracks on DLC films on top of harder polymer substrates would be higher than that of DLC on softer polymer substrates. In other words, the DLC film on harder polymer substrates develops more cracks to relax the tensile stress. However, in the case of DLC films on softer polymer substrates, the polymer substrates right under the DLC cracks can be highly deformed to relax the tensile stress, concurrently declining the total number of cracks over the fracture surface of the composites in the end.

6.2.2.2 The Influence of Young’s Moduli of DLC Films on Fracture Properties of DLC Films

The surface micrographs of DLC on PDMS and the micrographs of F-DLC on PDMS samples were analyzed as above. PDMS were used to investigate the detailed strain impact on fracture behavior since PDMS was flexible and widely used for medical purposes and its mechanical and fracture properties needed to be urgently clarified. The same experimental condition was selected for the extension of PDMS samples as the one for the extension of DLC on SIS samples as

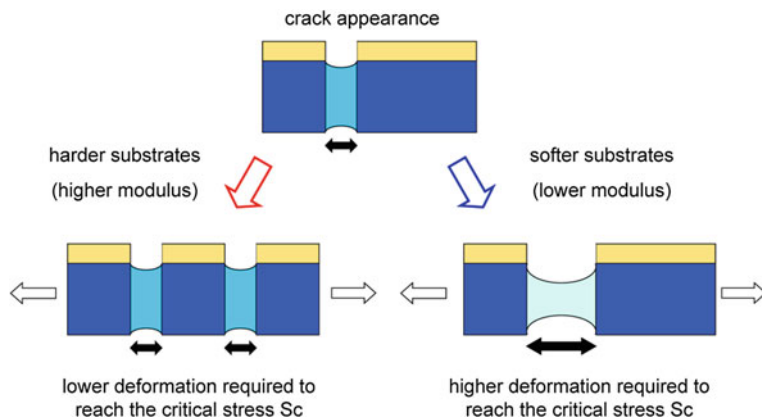


Fig. 6.16 A qualitative description of the fracture mechanism. The increase in the distance between cracks (i.e. the lower number of *crack lines*) takes place when softer polymers are used as a substrate [119]

mentioned in 6.2.2.1. Observing the fracture surface of DLC films on PDMS samples which were softer than PE and PET but harder than SIS, it was found that the fracture surface showed the lattice pattern with broader crack distance than PE or PET but narrower than SIS, which was consistent with the discussion and conclusion on tensile moduli in the previous Sect. 6.2.2.1. Comparing the fracture results of softer F-DLC on PDMS samples with those of the harder DLC on PDMS samples, there were less cracks and more bucklings in F-DLC. At the strain of especially 100 and 150 % of F-DLC samples, the bucklings of F-DLC films were clearly observed which could not be seen in the DLC samples. The bucklings were likely to be directly formed by tracing the bucklings of the surface of PDMS substrates which could be seen through the cracks. The number of crack lines as a function of strain for DLC-coated PDMS and F-DLC-coated PDMS was analyzed. The crack number increased with strain for each sample. Although the crack number was almost similar for both samples up to the strain of 10 %, a substantial difference arose at higher strains. The DLC-coated PDMS, the harder carbon film, had higher crack number than the softer F-DLC coated PDMS. At the strain of 100 %, the crack number of DLC-PDMS was ~ 1.3 times larger than that of F-DLC-PDMS and the number seemed to be leveling off over the strain of 100 %. Basically, the fracture behavior could be explained similarly to the one observed above. Since F-DLC was more flexible than DLC, it was easily imagined that F-DLC could be stretched to higher strains without producing cracks than DLC. Hence, the harder DLC relaxed the tensile stress by producing more cracks than F-DLC as in Fig. 6.17. The softer F-DLC could be highly deformed to relax the stress, and the number of cracks was suppressed. In other words, F-DLC films were softer than usual DLC films, accordingly demonstrating higher ability to follow the extension of the substrates. Also, since F-DLC was more flexible, F-DLC could more easily follow the bucklings of the polymer substrates.

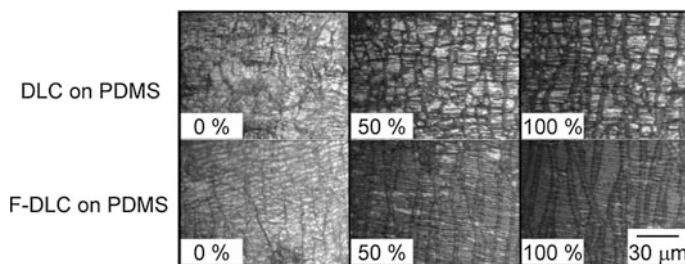


Fig. 6.17 Surface micrographs of stretched samples of PDMS coated with harder DLC and softer F-DLC [119]

6.2.2.3 The Influence of Adhesion Between Polymer Substrates and DLC Films

The surface micrographs of DLC on PE samples as well as on PP samples were compared. Here again, the same condition was used for the extension of PE and PP samples as the one for the extension of DLC on PE and PET samples in the previous sections. Comparing these two samples, it was found that the lattice pattern of the PP samples were significantly larger and broader than that of the PE samples at every extension. It should be noted, however, that the Young's modulus of PP was higher than that of PE, which should come to the conclusion that the lattice pattern of the PP samples should be narrower. Here in this case however, considerably bad adhesion between DLC films and PP substrates, as compared with that of PE, presumably overrode the influence of the small effect of the slightly higher Young's moduli of PP substrates. The number of crack lines as a function of strain for PE and PP samples was analyzed. The crack number increased with strain for each sample, and PE, which possessed stronger adhesion to DLC, had higher crack number than PP. The PE–DLC composites of good adhesion produced more cracks to relax the applied tensile stress. However, in the case of bad adhesion, as observed in the PP–DLC composites, debonding between the PP and DLC could occur at lower strain, where stress concentration took place and hence the stress was absorbed by softer polymers at the debonded place. For example, Fig. 6.18 showed the schematic image of peeled interface at the midpoint of PP–DLC composites, where PP deforms to reach the critical stress S_c . The PP could be highly deformed and hence the composites could be extended without creating cracks in DLC films until the stress reaches S_c . Therefore the number of the cracks of the composites with bad adhesion was smaller than that of the composites with good adhesion.

To summarize, the fracture mechanics has been analyzed and discussed in terms of Young's moduli and the adhesion of the DLC films coated on several polymers. The semi-crystalline polymers (PET, PP, and PE) and the elastomers (SIS and PDMS) used here were flexible and elastomeric as compared with hard materials such as ceramics, metals or glassy polymers. It was found that the fracture behavior

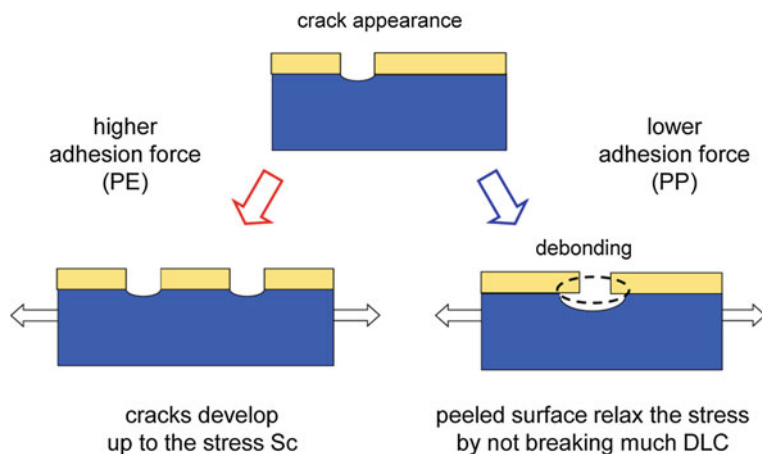


Fig. 6.18 A qualitative description of the fracture mechanism in different adhesion forces using PE (good adhesion) and PP (bad adhesion) [119]

of such polymer–DLC composites was characterized by lattice-like cracks and micro-buckling aligned regularly over the extended surface of the thin DLC films. The growth process and the number of crack and buckling lines were found to be highly dependent on Young’s moduli of both the DLC and the polymer substrates, and also dependent on the adhesion between DLC and polymers.

6.3 Permeation Properties of DLC on Polymers

6.3.1 Gas Permeation Property

The high-gas-barrier properties of the a-C:H films have been introduced and are now actively applied for films and containers in food and beverage markets. The consumption of polyethylene terephthalate (PET) bottles has noticeably increased because of the magnificent characters of PET bottles: they are highly transparent, light in weight, unbreakable, convenient, cost-effective, resealable and recyclable. Instead, PET bottles are gradually taking the place of metal cans and glass bottles. Carbonated soft drinks, tea, water, soy sauce and edible oil are currently mostly packed in PET bottles. PET bottles were first introduced in Japan for soy-sauce containers in 1976. Since the commercial debut of PET bottles for the soft drink market in 1978, the total amount of PET bottle usage has rapidly expanded to approximately 250 billion units in 2004, corresponding to 10 million tons of PET resin, and with a further growth by an average of over 10 % annually. It is expected to reach beyond 300 billion units in 2006. PET is, as mentioned above, a well-balanced material for beverage containers from the viewpoint of strength,

clarity, gas retention, flavor retention, flexibility, moldability, and cost effectiveness.

Comparing the oxygen transmission rate (OTR), carbon dioxide transmission rate (CO₂TR) and vapor transmission rate (VTR) of general plastic materials for food packaging, the gas barrier property of PET is better than that of high-density polyethylene as well as that of polypropylene [92]. The barrier property, however, is still not sufficient to contain taste-controlled beverages such as beer, juice, and wine because the permeation of oxygen, carbon dioxide gases, water vapor, and flavors is still not negligible. The permeation causes continuous ingress and release of the gases through the bottle surface, resulting in serious deterioration of the beverages in the flavor. For example, when substantial oxygen gas enters the bottle, odor formation and loss of vitamins occur, while the release of carbon dioxide corresponds to the loss of the fizziness in carbonated soft drinks. To prevent the gas permeation of plastic materials to protect the quality of the content, materials possessing high-gas-barrier properties should be introduced to the bottle. The existing ways to improve the gas barrier properties of PET bottles are generally classified into four major approaches: multilayers, coatings, scavenging agents, and composite fortifications. The multilayer technology is an easy way to produce a gas barrier bottle, but the improvement of the gas barrier properties through this technology is not that significant, but has serious problems in recycling. From the viewpoint of productivity, cost and recyclability, coating is the most reliable, suitable and promising method to improve the gas barrier property of PET bottles. Blocking the passage of gas molecules through PET wall using ultrathin gas barrier films minimizes the negative impact on the recycling process due to very low level contamination by different materials. Many coating materials have been subjected to practical trials. As a result, diamond-like carbon (DLC) and silicon oxide are the currently favored materials in this industry. DLC is principally formed through plasma enhanced chemical vapor deposition (PECVD) methods, while silicon dioxide is fabricated through sputter deposition, electron beam evaporation (PVD) or PECVD methods. Silicon oxide coating has a longer history than DLC coating for the gas barrier improvement of transparent plastic films, and has been studied using PVD and PECVD techniques since the early 1980s. However, the intrinsic brittleness of silicon oxide films requires rather complicated conversion processes in order to withstand mechanical stress and stretching on a PET bottle surface. Recent progress for forming a cushion layer between PET and silicon oxide layer enabled the production of commercial level silica coated PET bottles. Recently, high gas barrier PET bottles coated by DLC [more precisely defined as amorphous hydrocarbon (a-C:H)] have been commercially available in the market. Thus, worldwide competition between two superior barrier coating technologies is in progress. Coating process deals with covering the PET bottle with an ultrathin high-gas-barrier material to establish a-C:H-coated PET bottles. Gas molecules can pass through the wall of uncoated bottles, while a-C:H films coated on the bottles block the passage [92]. Also, this ultrathin coating is an ideal way to minimize the negative impact of the extremely low contamination of a-C:H films on the recycling process of virgin PET materials. Moreover,

newly synthesized high-gas-barrier a-C:H films were introduced under atmospheric pressure prepared by atmospheric-pressure glow (APG) plasma chemical vapor deposition (CVD), which possibly becomes the next-generation technique for the film-coating industry.

6.3.2 Gas Barrier Properties and the Principle and the Method of Gas Barrier Evaluation

The permeation of gas molecules through a polymeric membrane is a result of combined process of sorption, diffusion and desorption. The molecules pass through thermally fluctuated micro voids existing among tangled polymer chains. The permeability coefficient refers to the number of molecules passing through the film, per unit of time, area, thickness, and pressure difference.

$$P = \frac{QL}{tAp} \quad (6.2)$$

where P = permeability coefficient ($\text{cm}^3 \cdot \text{cm}/\text{cm}^2 \text{ s MPa}$), Q = amount of gas permeated (cm^3 at standard condition), L = averaged thickness of film (cm), t = time (sec), A = permeation area (cm^2), and p = pressure difference (MPa). The gas barrier property of polymer films is usually expressed in permeability coefficient, while the gas transmission property of PET bottles for e.g. oxygen and carbon dioxide is often simply indicated as the gas transmission rate of the whole bottle, for example, in the unit of $\text{cm}^3/\text{day} \cdot \text{bottle}$. The oxygen transmission rates can be determined using a modification of the ASTM Standard Method D 3985-81 with an Ox-Tran apparatus (Mocon, Inc., Minneapolis, USA) where a coulometric detector detects the permeated oxygen in a stream of dry nitrogen circulating through the system. The carbon dioxide transmission rate is measured by a "dry ice method". PET bottles containing dry ice for the inside pressure of 0.27 MPa are kept at room temperature and measured weight regularly. The loss of carbon dioxide can be calculated from the change in the weight.

6.3.3 The Coating of DLC and the Coated DLC

The gas barrier property of DLC films has not been sufficiently investigated, while other fundamental characteristics including high hardness and chemical inertness are well known. Recently, several reports have suggested high gas barrier properties of DLC films on plastic films [100]. Kirin Brewery Co., Ltd. has developed a unique technology using DLC coating for high gas barrier PET bottles since early 1990s, and succeeded in making the first high barrier DLC-coated PET bottles in 1994 in a cooperative process development with Samco International, Inc. The

technology was based on a PECVD method under vacuum conditions. Since their first official presentation on the excellent properties of DLC-coated PET bottles in 1997, many machine manufactures have made extensive efforts for the commercialization of high gas barrier PET bottles using dry vacuum process, which had been formally regarded as an impractical and costly process. Kirin's DLC coating process applied the deposition of a very thin DLC film to the inner surface of PET bottles by generating capacitively coupled plasma between specifically designed inner and outer electrodes. The inner electrode was grounded while the outer electrode was connected to the power supply. The first step of the process was to place a bottle in a vacuum chamber that functions as the outer electrode. Radio frequency power of 13.56 MHz was then applied to the outer electrode to generate a low temperature plasma state of hydrocarbons while acetylene (C_2H_2) gas was injected into the bottle. The ions and radicals reacted to deposit on the inner surface of the bottle in a negative self-bias potential over the outer electrode. The advantages of the use of DLC film for PET bottles were primarily derived from its flexible nature along with its high gas barrier property and chemical inertness. The detailed composition of the DLC coating was obtained in the combination of elastic recoil detection analysis (ERDA) and Rutherford backscattering analysis (RBS). The result showed relatively high hydrogen content for DLC films. This ensured excellent adhesion and crack resistance. The amorphous identity of the DLC was also confirmed in Fourier transform infrared absorption (FT-IR) measurement and transmission electron microscopy (TEM) observation. The results indicated that the DLC coating obtained was basically composed of a three-dimensional amorphous carbon and hydrogen network [101]. A typical Raman spectrum result of the DLC film presented a relatively sharper peak at 1,530 cm (the G peak) and a broad shoulder peak at 1,350 cm (the D peak). The lower area ratio of a two-Gaussian fit (the area of the G line over the area of the D line) and the lower shifted G position suggested that the DLC film had a mixture of sp^2 and sp^3 bonding structures [10, 102, 103]. Microscopic observation revealed the surface of the DLC film was extremely smooth and the thickness ranged from 10 to 30 nm for 2.0 s of coating, depending on coating conditions.

6.3.4 Gas Barrier Property of DLC-Coated PET Bottles

Table 6.2 shows the oxygen transmission rate (OTR) and carbon dioxide transmission rate (CO_2TR) of DLC-coated bottles at different temperatures. Gas barrier properties of DLC-coated PET bottles were significantly improved as expressed in the numbers of barrier improvement factor (BIF). As temperature increased, the DLC-coated and the uncoated bottles showed lower barrier properties for both OTR and CO_2TR . The result indicated that, although DLC coating was known as a thermally stable material, thermal molecular movement had an influence on the gas permeation property of the whole coated bottle. Table 6.2 also showed the values of activation energy E_p , determined in an Arrhenius plot, for the gas

Table 6.2 Oxygen transmission rate (OTR) and carbon dioxide transmission rate (CO₂TR) of uncoated and DLC-coated PET bottles at different temperatures [92]

	Uncoated PET		a-C:H-coated PET		BIF ^a	
	O ₂	CO ₂	O ₂	CO ₂	O ₂	CO ₂
Temperature (°C)						
20		0.0032		0.00034		9.4
23	0.07		0.0035		20.0	
30	0.1132	0.0048	0.0043	0.00044	26.3	11.0
40	0.2167	0.0071	0.0061	0.00059	35.5	12.1
E _p ^b (cal/mol)	12231	7286	6044	5186		

transmission, indicating that the DLC coating layer improved thermal stability to the barrier property of the whole bottle. Since the DLC coating layer had a high thermal stability, the E_p values for the whole DLC-coated bottle ranged from 50 to 70 % of those for the whole uncoated bottle.

6.3.5 Evaluation of the Food Containing and Preservation Performance of DLC-Coated PET Bottles

As indicated in Table 6.2 in the previous section, the DLC coating provided quite a high level of gas barrier enhancement, and the DLC-coated bottles were comparable to glass bottles in terms of quality protection against gas permeation. Based on the results of sensory evaluation and chemical analysis, the DLC-coated PET bottles proved an excellent quality retention performance, which was even comparable to glass bottles. The results strongly supported that the DLC coating could provide a sufficient property for the use of beer, one of the most sensitive product to oxygen permeation in the PET-bottle market. The coating of the DLC film on the inside surface of the PET bottle well preserved fresh flavors of the products because the film prevented the sorption and the migration between the bottle wall and the contents. The sorption test using various aroma components showed that the sorption amount in the DLC-coated PET bottles was only 5–10 % of that in uncoated PET bottles. As partially described above, the chemically inert nature of the DLC coating can provide safe and long shelf life with food and beverage.

6.3.6 Industrial Coating Methods for High Barrier DLC-PET

In the commercial coating process using a PECVD method for PET, a great number of process parameters related to each other must be controlled including

raw material gas rate, gas pressure, input power, and dimensions of electrodes. These parameters are required to be set differently depending on the size and shape of targeted bottles or films and the barrier requirement for products. Therefore the coating conditions should be well optimized. A high-speed commercial DLC coating machine for these purposes was introduced, which was manufactured by Mitsubishi Heavy Industries, Inc. The machine had a capacity of producing 18,000 bottles per hour with DLC and is now being in operation. It automatically monitors the operating conditions including chamber pressure, input and scattered power profiles, gas flow rate, and photoemission in order to ensure the product quality. Sidel Inc. has developed another type of DLC coating technology: Actis (amorphous carbon treatment on internal surface). It also uses acetylene gas as a source of carbon coating. A microwave-assisted process excites the gas into plasma, which deposits a layer of carbon about 0.15 μm thick on the inside of the bottle. Sidel claimed that Actis increased the carbon dioxide barrier of PET bottles by up to seven times. Toyo Seikan Kaisha Ltd., Toppa Printing Co., Ltd., and SIG Corpoplast GmbH Co. developed and realized silicon dioxide coatings using PECVD methods. Interestingly, all of these commercially successful coatings were applied to the inside of bottles, while several unsuccessful coating technologies have tried to coat the outside of bottles.

6.3.7 Future Prospects

The future of DLC coatings for many types of containers can be considered in view of market needs and technical development. In these aspects, further use of DLC coatings seems quite promising. For example, the potential market for high barrier PET bottles lies widespread and worldwide, including the large market of beer, juice, wine, and carbonated soft drinks, and is estimated to be 10 % of the whole PET bottle market, which would reach approximately 30 billion units. At present, in Japan, DLC coated PET bottles for hot tea drinks have been sold in the market, and 50 million units of such bottles came into the market in 2005. Future market needs were also promisingly found in high barrier containers made of plastics instead of PET. The candidates for such plastics include polyethylene, polypropylene, and biodegradable plastics. These plastics are used in large quantities; however, they often have poor barrier properties. From the technical perspective, a DLC film less than 10 nm thickness was expected to achieve sufficient barrier improvement for PET bottles. This thin DLC structure would exhibit much more colorless clarity than the current DLC structure with slightly tinted color, which limited the applications of the current DLC products to some specific product categories [104]. The current vacuum process is another drawback in the present market since the achievement of process vacuum requires high capital investment, long process time (decreased throughput), and wide space occupation due to a pumping system and other systems. Atmospheric plasma treatment could be the solution for this problem. In the laboratory scale trial, remarkably high

barrier DLC coating was successfully obtained using an atmospheric plasma method. Thus, the future development of DLC coatings is expected to improve the performance and cost effectiveness, and subsequently to contribute towards broader applications of plastic containers for food and beverage. The future use of DLC and modified DLC coatings seems promising in the medical field. The short-term data on DLC and modified DLC coatings obtained so far in *in vitro* and *in vivo* experiments indicate that their biocompatibility and hemocompatibility are excellent. The investigation of their long-term biological performance is further required before being able to use them in practical applications.

In conclusion, DLC films containing a certain amount of hydrogen worked effectively with certain polymers as a high-barrier coating material, which could provide the following advantages:

1. Gas barrier properties: blocks oxygen and carbon dioxide.
2. Flavor barrier: blocks migration and sorption.
3. UV barrier: increase absorbance of ultraviolet ray.
4. Chemical inertness: chemical stability with no interaction with ingredients.
5. Recyclability: no obstacle to the recycling process for polymeric materials.
6. Others: maintaining existing benefits of polymers.

6.4 Permeation Property for the Drug Controlled Release

As was previously mentioned, we have witnessed the evolution of an intense public controversy regarding late thrombosis following implantation of drug eluting stent (DES) in patients with obstructive coronary artery disease. To overcome the problem, DES should possess sufficient biocompatibility and non-thrombogenicity with a controlled drug release system. A new DES composed of biocompatible polymers coated with DLC coating was proposed. In this study, the drug release profile of the newly proposed drug eluting system was thoroughly investigated. Three polymers were selected as base drug-reservoir materials: hydrophilic 2-methacryloyloxyethyl phosphorylcholine (MPC), hydrophobic poly (ethylene-co-vinyl acetate) (EVA), and less hydrophobic polyurethane (PU). The three polymers are currently used or studied for biomedical materials, while MPC and DLC were already confirmed as excellent biocompatible materials with anti-thrombogenicity. After coating the lattice-like patterned DLC on both polymers containing drug, samples were soaked into 2 ml of medium of phosphate-buffered saline with 10 % ethanol. The drug release rate was measured by a spectrophotometer. The percentile cover area of patterned DLC on polymers was varied from 0 % (without DLC) to 100 % (fully covered). The sample without DLC coating presented an initial burst of the drug release from the polymer matrix, whereas the DLC-coated samples inhibited the initial burst release from polymers within the

first five days of the experiments. It was found that the drug eluting profiles could be effectively controlled by changing the cover area of micro-patterned DLC coatings on polymers, which may be applicable to the next-generation DES system that eventually prevents late thrombosis.

An effective way of controlling drug release using polymeric matrix coated with thin DLC film was introduced. The control of the drug release was efficiently achieved by combining several types of soft polymers with micro-patterned hard DLC. It was found that by selecting appropriate polymers, well-adhered DLC/polymer composites with combining merits of flexibility, moldability, absorbability, biocompatibility, low friction, high gas, and liquid barrier effects, etc. were obtained, where the former three merits typically originated from polymers and the latter three resulted from DLC. The new DLC/polymer composites could therefore be extensively utilized in the field of intravascular medical devices such as stents and catheters. The earliest use of bare metal stents (BMS) has markedly improved the treatment of coronary artery disease, while restenosis due to neointimal proliferation has been a major concern, which eventually promoted urgent development of the second-stage stents, called drug eluting stents (DES), containing antithrombotic drug. DES was successful in preventing cellular proliferation, thrombus formation, and inflammation, hence recently having been practically used in clinical practice and surgery [105, 106]. After approximately a year of indwelling DES, however, almost all drugs were evacuated and unprotected polymer surface was directly exposed to blood, causing possible thrombogenicity [107–110]. DLC, a biocompatible and antithrombotic carbonaceous material was examined for the surface coating of drug-containing polymers, targeting the next-generation stents that may control the drug release rate, accompanied by the enhancement of the biocompatibility. For the industrial use, DLC has already been coated on materials adding high gas barrier property. The research on combining hard DLC with soft polymers has not been much explored, largely due to the potential cumbersome procedures of solving difficult problems that may be caused by the differences between DLC and polymers in chemical and physical properties including hardness, adhesion, and barrier properties. A few degradable polymers were already investigated as the composite partners of DLC and the polymers were found useful for the establishment of a degradation-controlled drug release system, but some incomplete healing sites were found after 180 days of testing [107]. Other applications of DLC for soft materials can only be found in industrial uses for mechanical and tribological purposes by using e.g. segment-structured DLC on polymers. After several years of investigations on biocompatibility and anti-thrombogenicity of DLC [16, 41, 79, 111, 112], a new coronary artery stent was proposed, which consisted of DLC-coated polymer containing drug. In this section, the fabrication of micro-patterned DLC was introduced, which was carried out on silicon wafer and polymers, and the microstructure of DLC was observed. After confirming the micro-structures, DLC was then coated on polymer films containing drug before measuring the drug release rates.

6.4.1 Surface Morphology of Micro-Patterned DLC on Silicon

The surface of micro-patterned DLC deposited on substrates through metallic mesh with several sizes of micropores was observed. Figure 6.19 shows the optical micrographs of the surfaces of unprocessed smooth silicon wafer, metallic mesh and micro-patterned DLC. From Fig. 6.19b, the pore size of metallic mesh was found to be about $35\ \mu\text{m}^2$. From Fig. 6.19c, the size of deposited micro-patterned DLC was found approximately the same as that of micropores of metallic mesh, indicating the direct deposition of DLC through the pores. The ratio of DLC-deposited area to the whole surface area of the substrates was $\sim 35\%$ determined through the optical microscope image analysis. The surface profile of DLC-coated films was measured using Dektak surface profilometer. The width of micro-patterned DLC blocks was approximately $35\ \mu\text{m}$, which corresponds to the experimental results of the optical micrographs. The thickness of the coated DLC was found from 10 to 20 nm, which was thinner than the thickness expected from the deposition time ($\sim 100\ \text{nm}$). This is supposed to be due to the plasma inhibition of the metallic mesh, causing micro-shielding of the plasma as well as decrease in the entire number of carbon radicals. The difference in the thickness of DLC may not bring about any detrimental effects on the barrier property of DLC as the molecular weight of the drug is much higher than that of gas molecules and the gas barrier property can be sufficiently achieved over 10 nm of DLC thickness.

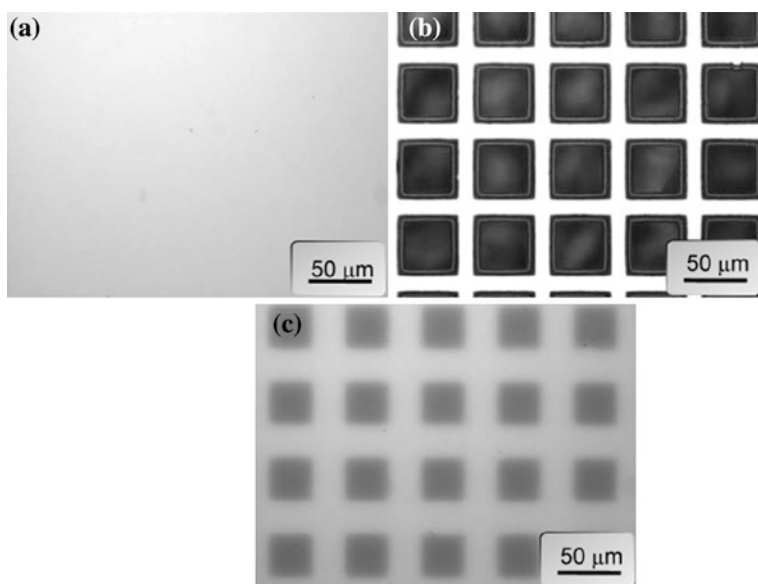


Fig. 6.19 Optical micrographs of substrates: **a** silicon wafer, **b** micro-pore mesh, and **c** micro-patterned DLC deposited on silicon wafer [120]

6.4.2 Chemical Structures of Polymer Films Containing Curcumin as Drug

The FT-IR spectra of three polymer films were obtained for the original polymer film, the polymer film containing 10 % of curcumin, and the polymer film with 20 % of curcumin. The spectra of each polymer film without curcumin were firstly interpreted to discern curcumin signals from the original signals emitted by polymers. While analyzing FT-IR spectra, it was important to know the difference in molecular structures of three polymers. The major difference lied in the possession of hydrogen-bonded group. MPC had hydrogen-bonded OH group, while PU consisted of hydrogen-bonded NH group, and EVA had no hydrogen-bonding group in its molecular structure. Curcumin possessed OH group which may also be directly detected by FT-IR. In more detail, the broad signal detected around 3400 cm^{-1} in the MPC signal could be affiliated with -OH vibrations from hydrogen-bonded OH groups. The strong peaks at 2,959, 2,866, and $1,474\text{ cm}^{-1}$ were attributed to the stretching of $\text{-CH}_2\text{-}$ groups. One of the major peaks of MPC was a stretching vibration peak observed at 1724 cm^{-1} by $\text{C}=\text{O}$ of ester. The three peaks at 1,234, 1,152, and $1,076\text{ cm}^{-1}$ were due to $\text{-POCH}_2\text{-}$. The strong peaks at 2,917, 2,849 and $1,372\text{ cm}^{-1}$ in the EVA signal indicated the stretching and the deformation of methyl groups. The accurate peak at $1,735\text{ cm}^{-1}$ was attributed to $\text{C}=\text{O}$ of ester. The peak at $1,239\text{ cm}^{-1}$ indicates a C-O single bond. The spectrum of PU was also analyzed, where the strong peaks at 2,920 and $2,852\text{ cm}^{-1}$ came from the stretching of $\text{-CH}_2\text{-}$ groups. Two carbonyl bands, one at $1,701\text{ cm}^{-1}$ and the other at $1,730\text{ cm}^{-1}$ are assigned to $\text{C}=\text{O}$ groups. The peak at $3,324\text{ cm}^{-1}$ was due to the N-H group participating in hydrogen bonding. The band of the non-hydrogen-bonded N-H group appeared as a broad peak at $3,480\text{ cm}^{-1}$. The peak at $1,620\text{ cm}^{-1}$, which indicated the existence of aromatic $\text{C}=\text{C}$, was found in the spectra of each polymer film containing curcumin, and as the contents of curcumin increased, the intensity of the signal from the aromatic $\text{C}=\text{C}$ also increased. Pure hydrophobic EVA film showed no peak around $3,400\text{ cm}^{-1}$. As the amount of curcumin increased in EVA, the signal around $3,400\text{ cm}^{-1}$, indicating hydrogen bonding, increased due to the injected curcumin in EVA. In this way, a somewhat quantitative evaluation of the amount of the injected curcumin could be made by FT-IR.

6.4.3 Surface Morphology of Curcumin-Eluting Polymer Films

In Table 6.3, samples used in the drug eluting experiments were all listed. For the sample names, "DLC" as suffix was added to the original sample name when the polymer was entirely covered with DLC, while the suffix "DP" was added for the samples with micro-patterned DLC. The numbers in the names represented the

content of curcumin. The ratio of the DLC-coated area was approximately 35 %. Optical micrographs of the polymers and the polymers with DLC or with micro-patterned DLC (DP) containing 10 or 20 % of curcumin were presented in Fig. 6.19. There were no distinct differences in the size and the shape of micro-patterned DLC coated on the three polymers and on silicon wafer (Fig. 6.19c). Figure 6.19a shows the surface of the MPC polymer films. As curcumin was hydrophilic, it was highly compatible with MPC polymer, so that the entire surface looked flat and homogeneous without any aggregates of curcumin comprised even for higher curcumin-containing samples. There were not any noticeable differences between the films before and after DLC deposition, revealing the thermal stability of MPC films even after DLC deposition process at a higher temperature (~ 60 °C). The surface of EVA films was shown in Fig. 6.19b. Since EVA was much more hydrophobic than MPC, the surface of EVA with curcumin looked more uneven and heterogeneous than that of MPC. Many aggregates of curcumin were observed on the surface of EVA and the number of the aggregates increased as the concentration of curcumin increased. EVA and curcumin therefore seemed incompatible. The undulated surface of DLC-deposited EVA films was observed owing to the low thermal stability of EVA under strong internal stress of DLC. It was found that the melting point of EVA was 50 °C measured by differential scanning calorimetry (DSC). DLC deposition temperature could reach 50 °C where EVA could be softened and be pulled by the strong internal stress of DLC. The micro-patterned DLC surface on EVA was quite even because the segmentation of DLC could prevent or ease the internal stress caused by the entire coating of DLC. Figure 6.19c showed the surface of PU films. The surface of PU films was quite homogeneous, which was fairly similar to the surface of hydrophilic MPC films. As PU was more hydrophilic than EVA due to the N–H group participating in hydrogen bonding, the hydrophilic curcumin could be more or less dispersed over an entire volume of the PU substrates to construct a uniform surface. At even higher curcumin contents, the aggregates of curcumin appeared and were slightly observed. After DLC coating, as on EVA surface, the undulated PU surface was monitored but the roughness of the PU surface was lower than that of EVA surface. This could be due to the higher modulus, higher thermal stability of PU than those of EVA. PU and EVA are both thermoplastic materials and the melting temperatures (T_m), above which the samples would melt and be easily molded, were 210 °C for PU and 50 °C for EVA. The plasma processing temperature could reach ~ 60 °C which was above the T_m of EVA. The surface of EVA was thermally transformed to ease the internal stress, which resulted in constructing the undulated surface. The surface roughness of DLC-coated MPC, EVA and PU was analyzed. The surface roughness of MPC, regardless of the content of DLC and curcumin, was very low according to the measurements by AFM. The surface roughness of unprocessed EVA and PU films was also lower than 20 nm. By containing curcumin, the surface roughness became slightly higher than the unprocessed films, but still lower than 40 nm. After DLC coating, however, the surface roughness of both EVA and PU films became meaningfully higher, reaching even higher than 160 nm for EVA, and 120 nm for PU with 20 %

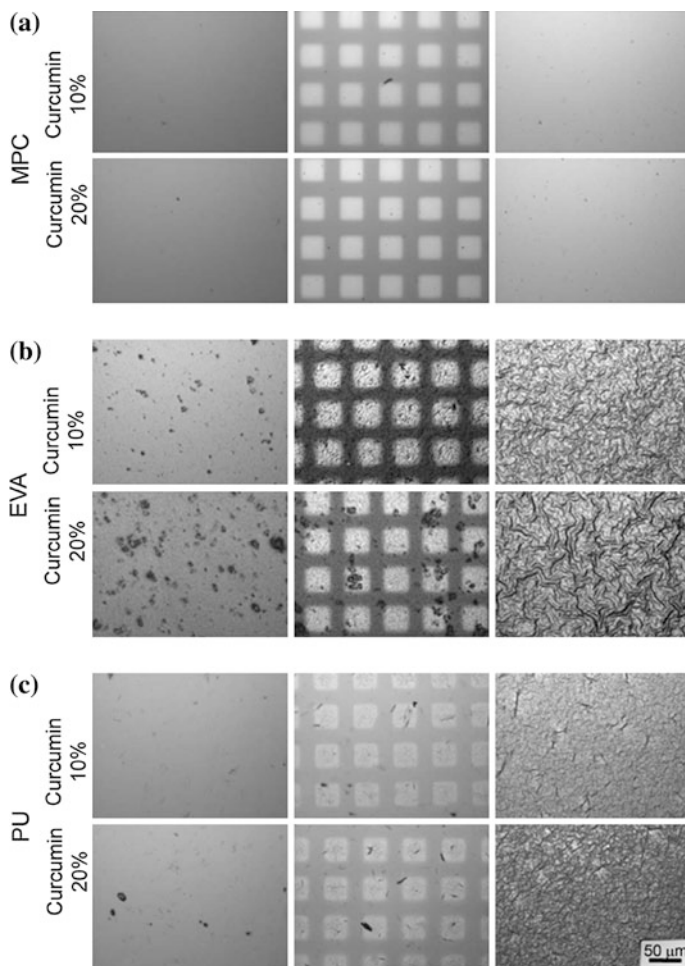


Fig. 6.20 Optical micrographs of substrates with curcumin: **a** MPC, **b** EVA, and **c** PU [120]

of curcumin. Hasebe et al. [60] reported that the surface roughness of DLC would not make any significant influence on the thrombogenicity of the materials if the roughness was within the range from ~ 4 to ~ 100 nm in Ra, which was introduced in the previous section. The effect of the surface roughness over 100 nm on thrombogenicity was not yet fully understood. Therefore after DLC coating on EVA and PU, it was necessary to carefully examine the thrombogenicity of the DLC-coated materials. Apparently, the surface of polymers with micro-patterned DLC was smoother than that of polymers with fully deposited DLC, hence micro-patterning would be a promising candidate for the drug-releasing system.

Table 6.3 Specimens coated with DLC including curcumin for the drug eluting experiments [120]

Sample name	Polymer	DLC coating area [%]	Curcumin contents [%]
MPC10	MPC	0	10
MPC10DP	MPC	35	10
MPC10DLC	MPC	100	10
MPC20	MPC	0	20
MPC20DP	MPC	35	20
MPC20DLC	MPC	100	20
EVA10	EVA	0	10
EVA10DP	EVA	35	10
EVA10DLC	EVA	100	10
EVA20	EVA	0	20
EVA20DP	EVA	35	20
EVA20DLC	EVA	100	20
PU10	PU	0	10
PU10DP	PU	35	10
PU10DLC	PU	100	10
PU20	PU	0	20
PU20DP	PU	35	20
PU20DLC	PU	100	20

6.4.4 Release Profile of Curcumin from Polymers

The cumulative release of curcumin from MPC polymers to the medium as a function of time was plotted in Fig. 6.21. Figure 6.21a showed the drug release results of MPC polymers containing 10 % of curcumin and Fig. 6.21b shows the results of MPC polymers with 20 % of curcumin. Squares represented the drug release from MPC polymers without coating, while triangles showed the results of MPCDP and circles presented the results of MPCDLC. The rest of the figures (Figs. 6.22 and 6.23) are plotted in this manner, where Figs. 6.22 and 6.23 showed the results of EVA and PU, respectively. In the experiments, as expected, the initial burst release was observed for polymers without coating, which implies that the content ratio of curcumin indeed reached well beyond the solubility of the curcumin in the polymers. Generally, it was understandable that if polymers possessed a high amount of drug (i.e. high drug concentration), the drug would be eluted rapidly especially in the early time of the drug release just after the specimens being immersed in medium. Therefore the initial burst could be detected in MPC10, MPC20, EVA10, and EVA20 samples. Higuchi was the first to derive an equation to describe the release of drug from an insoluble matrix as the square root of a time-dependent process based on Fickian diffusion [113]. The drug release experimental results of various samples were also analyzed using the drug release equation of the Higuchi model which has been utilized to study the release of drugs contained in semi-solid and/or solid matrixes [114]. To analyze the drug elution from a planar system of a homogeneous matrix, the relation of the drug

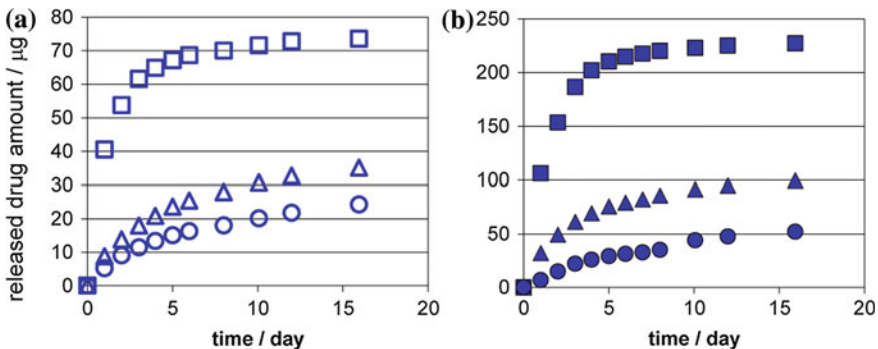


Fig. 6.21 Drug release profiles of MPC (square), MPCDP (triangle), and MPCDLC (circle) varying the concentrations of curcumin: a 10 % and b 20 % [120]

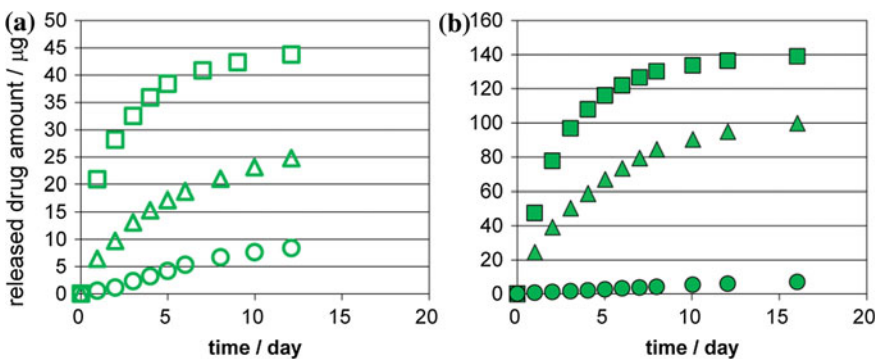


Fig. 6.22 Drug release profiles of EVA (square), EVADP (triangle), and EVADLC (circle) varying the concentrations of curcumin: a 10 % and b 20 % [120]

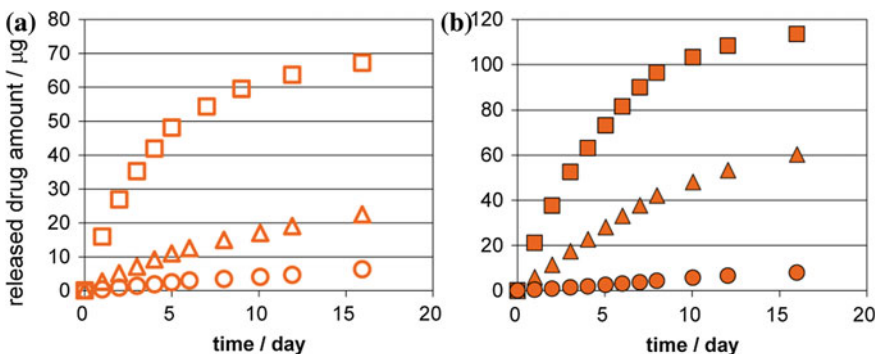


Fig. 6.23 Drug release profiles of PU (square), PUDP (triangle), and PUDLC (circle) varying the concentrations of curcumin: a 10 % and b 20 % [120]

release amount (Q) and the release time (t) could be described as follows: where Q is the amount of drug released in time t and K_H is the Higuchi dissolution constant. Since MPC10, MPC20, EVA10, and EVA20 exhibited the initial burst release, the release profiles from the four samples could not be fitted well with the Higuchi equation and the deviation from the model was indeed observed after 5 days of elution. The Higuchi model therefore was only applied to the initial results of several early days of the measurements to evaluate the release rate (K_H) of the samples. For the other -DLC and -DP samples, the Higuchi model fitted the experimental data quite well throughout the testing. In this manner, K_H of every sample was calculated from the drug release profiles plotted in Figs. 6.20, 6.21, and 6.22. Figure 6.23 showed the results of K_H . It was clear that K_H decreased with increasing the DLC-deposited area of the polymer films. Figure 6.23a showed the K_H of each polymer containing 10 % of curcumin. Comparing the results of the three polymers without DLC deposition, MPC film presented the largest K_H . The K_H of EVA was almost the same as that of PU, indicating the fastest release rate in MPC and the lower release rate in EVA and PU. The results also revealed that the dissolution of drug was strongly affected by the compatibility between the matrix polymer and the medium. The used medium was water while MPC was hydrophilic, whereas EVA was rather hydrophobic and PU was in between. Based on this standpoint, the water uptake of MPC was the greatest, which led to the rapid elution of curcumin. DLC deposition efficiently inhibited the drug release from each polymer film, where K_H was almost the same for polymers with micro-patterned DLC, as the largest K_H was observed in MPC, followed by EVA and PU. Furthermore in the same way, K_H of each polymer decreased more with overall DLC deposition. It was confirmed that the drug release rate was effectively controlled by varying the area coated with DLC. Figure 6.23b showed the K_H of each polymer containing 20 % of curcumin. The similar results to the specimen with 10 % of curcumin were observed. Increasing the concentration of the curcumin resulted in producing higher drug release rate for all three polymers. The K_H of MPC20 was about 3 times as large as that of MPC10. K_H of EVA20 and PU20 was about 2.7 and 1.6 times larger than those with 10 % curcumin, respectively. The increased amount of K_H by adding curcumin content was the highest in MPC due to the hydrophilicity. The increased amount of K_H was higher in EVA20 than in PU20. As was mentioned previously, there were no hydrogen bonds in the chemical structure of EVA, implicating the lower binding force with curcumin with high K_H , while a larger amount of curcumin stayed in the PU matrix that consisted of hydrogen-bonded NH group.

To summarize, the micro-patterning of DLC coated on several types of soft polymers was investigated. The shape of DLC blocks deposited by CVD method was confirmed by optical microscopy, which was found to be well fabricated on polymers. The thickness of micro-patterned DLC blocks was ~ 30 nm, while that of overall DLC deposition was ~ 100 nm. The surface roughness was measured for each sample and the roughness became higher when the drug and the polymer became less compatible from the viewpoint of solubility. Moreover, the surface roughness substantially decreased when micro-patterning of DLC was

implemented on polymers. The drug release rate from DLC-coated polymers was well controlled with varying the deposition area of micro-patterned DLC. Here again, it was found that the compatibility between polymer, medium, and drug, affected the eventual drug release rates. The results may be applicable to the next-generation DES system that possessed both biocompatibility and well controlled dissolution behavior of drug preventing the late thrombosis. Further studies would also be to evaluate the availability of this novel drug-delivery system for three-dimensional medical devices without the risk of film breakdown in various clinical settings.

References

1. Aisenber, S., Chabot, R.: Ion-beam deposition of thin films of diamondlike carbon. *J. Appli. Phys.* **42** (7):2953-&. (1971). doi:[10.1063/1.1660654](https://doi.org/10.1063/1.1660654)
2. Thomson, L.A., Law, F.C., Rushton, N., Franks, J.: Biocompatibility of diamond-like carbon coating. *Biomaterials* **12**(1), 37–40 (1991)
3. Airoidi, F., Colombo, A., Tavano, D., Stankovic, G., Klugmann, S., Paolillo, V., Bonizzoni, E., Briguori, C., Carlino, M., Montorfano, M., Liistro, F., Castelli, A., Ferrari, A., Sgura, F., Di Mario, C.: Comparison of diamond-like carbon-coated stents versus uncoated stainless steel stents in coronary artery disease. *Am. J. Cardiol.* **93**(4), 474–477 (2004). doi:[10.1016/j.amjcard.2003.10.048](https://doi.org/10.1016/j.amjcard.2003.10.048)
4. Gutensohn, K., Beythien, C., Bau, J., Fenner, T., Grewe, P., Koester, R., Padmanaban, K., Kuehnl, P.: In vitro analyses of diamond-like carbon coated stents: Reduction of metal ion release, platelet activation, and thrombogenicity. *Thromb. Res.* **99**(6), 577–585 (2000). doi:[10.1016/s0049-3848\(00\)00295-4](https://doi.org/10.1016/s0049-3848(00)00295-4)
5. Schroeder, A., Francz, G., Bruinink, A., Hauert, R., Mayer, J., Wintermantel, E.: Titanium containing amorphous hydrogenated carbon films (a-C:H/Ti): surface analysis and evaluation of cellular reactions using bone marrow cell cultures in vitro. *Biomaterials* **21**(5), 449–456 (2000). doi:[10.1016/s0142-9612\(99\)00135-0](https://doi.org/10.1016/s0142-9612(99)00135-0)
6. Tran, H.S., Puc, M.M., Hewitt, C.W., Soll, D.B., Marra, S.W., Simonetti, V.A., Cilley, J.H., DelRossi, A.J.: Diamond-like carbon coating and plasma or glow discharge treatment of mechanical heart valves. *J. Invest. Surg.* **12**(3), 133–140 (1999)
7. Allen, M., Myer, B., Rushton, N.: In vitro and in vivo investigations into the biocompatibility of diamond-like carbon (DLC) coatings for orthopedic applications. *J. Biomed. Mater. Res.* **58**(3), 319–328 (2001). doi:[10.1002/1097-4636\(2001\).58:3<319::aid-jbm1024>3.0.co;2-f](https://doi.org/10.1002/1097-4636(2001).58:3<319::aid-jbm1024>3.0.co;2-f)
8. Grill, A., Meyerson, B.S., Patel, V.V.: Diamond-like carbon-films by rf plasma-assisted chemical vapor-deposition from acetylene. *IBM J. Res. Dev.* **34**(6), 849–857 (1990)
9. Lifshitz, Y.: Diamond-like carbon—present status. *Diam. Relat. Mater.* **8**(8–9), 1659–1676 (1999). doi:[10.1016/s0925-9635\(99\)00087-4](https://doi.org/10.1016/s0925-9635(99)00087-4)
10. Ferrari, A.C., Robertson, J.: Interpretation of Raman spectra of disordered and amorphous carbon. *Phys. Rev. B* **61**(20), 14095–14107 (2000). doi:[10.1103/PhysRevB.61.14095](https://doi.org/10.1103/PhysRevB.61.14095)
11. Cuong, N.K., Tahara, M., Yamauchi, N., Sone, T.: Diamond-like carbon films deposited on polymers by plasma-enhanced chemical vapor deposition. *Surf. Coat. Technol.* **174**, 1024–1028 (2003). doi:[10.1016/s0257-8972\(03\)00360-8](https://doi.org/10.1016/s0257-8972(03)00360-8)
12. Leu, M.S., Chen, S.Y., Chang, J.J., Chao, L.G., Lin, W.: Diamond-like coatings prepared by the filtered cathodic arc technique for minting application. *Surf. Coat. Technol.* **177**, 566–572 (2004). doi:[10.1016/s0257-8972\(03\)00928-9](https://doi.org/10.1016/s0257-8972(03)00928-9)
13. Sui, J.H., Cai, W., Zhao, L.C.: Surface modification of NiTi alloys using diamond-like carbon (DLC) fabricated by plasma immersion ion implantation and deposition (PIID).

- Nucl. Instr. Meth. Phys. Res. Sect. B-Beam Interact. Mater. Atoms **248**(1), 67–70 (2006). doi:[10.1016/j.nimb.2006.04.054](https://doi.org/10.1016/j.nimb.2006.04.054)
14. Ahmed, S.F., Moon, M.-W., Lee, K.-R.: Effect of silver doping on optical property of diamond like carbon films. *Thin Solid Films* **517**(14), 4035–4038 (2009). doi:[10.1016/j.tsf.2009.01.135](https://doi.org/10.1016/j.tsf.2009.01.135)
 15. Choi, H.W., Dauskardt, R.H., Lee, S.-C., Lee, K.-R., Oh, K.H.: Characteristic of silver doped DLC films on surface properties and protein adsorption. *Diam. Relat. Mater.* **17**(3), 252–257 (2008). doi:[10.1016/j.diamond.2007.12.034](https://doi.org/10.1016/j.diamond.2007.12.034)
 16. Hasebe, T., Shimada, A., Suzuki, T., Matsuoka, Y., Saito, T., Yohena, S., Kamijo, A., Shiraga, N., Higuchi, M., Kimura, K., Yoshimura, H., Kuribayashi, S.: Fluorinated diamond-like carbon as antithrombogenic coating for blood-contacting devices. *J. Biomed. Mater. Res. Part A* **76A**(1), 86–94 (2006). doi:[10.1002/jbm.a.30512](https://doi.org/10.1002/jbm.a.30512)
 17. Hasebe, T., Yohena, S., Kamijo, A., Okazaki, Y., Hotta, A., Takahashi, K., Suzuki, T.: Fluorine doping into diamond-like carbon coatings inhibits protein adsorption and platelet activation. *J. Biomed. Mater. Res. Part A* **83A**(4), 1192–1199 (2007). doi:[10.1002/jbm.a.31340](https://doi.org/10.1002/jbm.a.31340)
 18. Jones, B.J., Mahendran, A., Anson, A.W., Reynolds, A.J., Bulpett, R., Franks, J.: Diamond-like carbon coating of alternative metal alloys for medical and surgical applications. *Diam. Relat. Mater.* **19**(7–9), 685–689 (2010). doi:[10.1016/j.diamond.2010.02.012](https://doi.org/10.1016/j.diamond.2010.02.012)
 19. Kim, H.G., Ahn, S.H., Kim, J.G., Park, S.J., Lee, K.R.: Effect of Si-incorporation on wear-corrosion properties of diamond-like carbon films. *Thin Solid Films* **482**(1–2), 299–304 (2005). doi:[10.1016/j.tsf.2004.11.164](https://doi.org/10.1016/j.tsf.2004.11.164)
 20. Kwok, S.C.H., Jin, W., Chu, P.K.: Surface energy, wettability, and blood compatibility phosphorus doped diamond-like carbon films. *Diam. Relat. Mater.* **14**(1), 78–85 (2005). doi:[10.1016/j.diamond.2004.07.019](https://doi.org/10.1016/j.diamond.2004.07.019)
 21. Kwok, S.C.H., Zhang, W., Wan, G.J., McKenzie, D.R., Bilek, M.M.M., Chu, P.K.: Hemocompatibility and anti-bacterial properties of silver doped diamond-like carbon prepared by pulsed filtered cathodic vacuum arc deposition. *Diam. Relat. Mater.* **16**(4–7), 1353–1360 (2007). doi:[10.1016/j.diamond.2006.11.001](https://doi.org/10.1016/j.diamond.2006.11.001)
 22. Lee, K.R., Kim, M.G., Cho, S.J., Eun, K.Y., Seong, T.Y.: Structural dependence of mechanical properties of Si incorporated diamond-like carbon films deposited by RF plasma-assisted chemical vapour deposition. *Thin Solid Films* **308**, 263–267 (1997). doi:[10.1016/s0040-6090\(97\)00411-2](https://doi.org/10.1016/s0040-6090(97)00411-2)
 23. Maguire, P.D., McLaughlin, J.A., Okpalugo, T.I.T., Lemoine, P., Papakonstantinou, P., McAdams, E.T., Needham, M., Ogwu, A.A., Ball, M., Abbas, G.A.: Mechanical stability, corrosion performance and bioresponse of amorphous diamond-like carbon for medical stents and guidewires. *Diam. Relat. Mater.* **14**(8), 1277–1288 (2005). doi:[10.1016/j.diamond.2004.12.023](https://doi.org/10.1016/j.diamond.2004.12.023)
 24. Ogwu, A.A., Okpalugo, T.I.T., Ali, N., Maguire, R.D., McLaughlin, J.A.D.: Endothelial cell growth on silicon modified hydrogenated amorphous carbon thin films. *J. Biomed. Mater. Res. Part B-Appli. Biomater.* **85B**(1), 105–113 (2008). doi:[10.1002/jbm.b.30922](https://doi.org/10.1002/jbm.b.30922)
 25. Okpalugo, T.I.T., Ogwu, A.A., Maguire, P.D., McLaughlin, J.A.D.: Platelet adhesion on silicon modified hydrogenated amorphous carbon films. *Biomaterials* **25**(2), 239–245 (2004). doi:[10.1016/s0142-9612\(03\)00494-0](https://doi.org/10.1016/s0142-9612(03)00494-0)
 26. Okpalugo, T.I.T., Ogwu, A.A., Okpalugo, A.C., McCullough, R.W., Ahmed, W.: The human micro-vascular endothelial cells in vitro interaction with atomic-nitrogen-doped diamond-like carbon thin films. *J. Biomed. Mater. Res. Part B-Appli. Biomater.* **85B**(1), 188–195 (2008). doi:[10.1002/jbm.b.30934](https://doi.org/10.1002/jbm.b.30934)
 27. Papakonstantinou, P., Zhao, J.F., Lemoine P., McAdams, E.T., McLaughlin, J.A.: The effects of Si incorporation on the electrochemical and nanomechanical properties of DLC thin films. *Diamond Relat. Mater.* **11** (3–6):1074–1080. (2002). doi:[10.1016/s0925-9635\(01\)00656-2](https://doi.org/10.1016/s0925-9635(01)00656-2)
 28. Yokota, T., Terai, T., Kobayashi, T., Meguro, T., Iwaki, M.: Cell adhesion to nitrogen-doped DLCs fabricated by plasma-based ion implantation and deposition method using

- toluene gas. *Surf. Coat. Technol.* **201**(19–20), 8048–8051 (2007). doi:[10.1016/j.surfcoat.2006.03.051](https://doi.org/10.1016/j.surfcoat.2006.03.051)
29. Mohanty, M., Anilkumar, TV., Mohanan, PV., Muraleedharan, CV., Bhuvaneshwar, GS., Derangere, F., Sampeur, Y., Suryanarayanan R.: Long term tissue response to titanium coated with diamond like carbon. *Biomolecular Engineering* **19** (2–6):125–128. (2002). doi:[Pii s1389-0344\(02\)00026-6](https://doi.org/10.1016/S1389-0344(02)00026-6)
 30. Affatato, S., Frigo, M., Toni, A.: An in vitro investigation of diamond-like carbon as a femoral head coating. *J. Biomed. Mater. Res.* **53**(3), 221–226 (2000)
 31. Du, C., Su, X.W., Cui, F.Z., Zhu, X.D.: Morphological behaviour of osteoblasts on diamond-like carbon coating and amorphous C-N film in organ culture. *Biomaterials* **19**(7–9), 651–658 (1998). doi:[10.1016/S0142-9612\(97\)00159-2](https://doi.org/10.1016/S0142-9612(97)00159-2)
 32. Hauert, R.: A review of modified DLC coatings for biological applications. *Diam. Relat. Mater.* **12**(3–7), 583–589 (2003). doi:[10.1016/S0925-9635\(03\)00081-5](https://doi.org/10.1016/S0925-9635(03)00081-5)
 33. Lappalainen, R., Heinonen, H., Anttila, A., Santavirta, S.: Some relevant issues related to the use of amorphous diamond coatings for medical applications. *Diam. Relat. Mater.* **7**(2–5), 482–485 (1998). doi:[10.1016/S0925-9635\(98\)80003-4](https://doi.org/10.1016/S0925-9635(98)80003-4)
 34. Linder, S., Pinkowski, W., Aepfelbacher, M.: Adhesion, cytoskeletal architecture and activation status of primary human macrophages on a diamond-like carbon coated surface. *Biomaterials* **23**(3), 767–773 (2002). doi:[10.1016/S0142-9612\(01\)00182-X](https://doi.org/10.1016/S0142-9612(01)00182-X)
 35. Cui, F.Z., Li, D.J.: A review of investigations on biocompatibility of diamond-like carbon and carbon nitride films. *Surf. Coat. Technol.* **131**(1–3), 481–487 (2000). doi:[10.1016/S0257-8972\(00\)00809-4](https://doi.org/10.1016/S0257-8972(00)00809-4)
 36. Dearnaley, G., Arps, J.H.: Biomedical applications of diamond-like carbon (DLC) coatings: A review. *Surf. Coat. Technol.* **200**(7), 2518–2524 (2005). doi:[10.1016/j.surfcoat.2005.07.077](https://doi.org/10.1016/j.surfcoat.2005.07.077)
 37. Grill, A.: Diamond-like carbon coatings as biocompatible materials an overview. *Diamond Relat. Mater.* **12** (2):166–170. (2003). doi:[Pii s0925-9635\(03\)00018-9](https://doi.org/10.1016/S0925-9635(03)00018-9)
 38. Mitura, E., Mitura, S., Niedzielski, P., Has, Z., Wolowiec, R., Jakubowski, A., Szmidt, J., Sokolowska, A., Louda, P., Marciniak, J., Koczy, B.: Diamond-like carbon coatings for biomedical applications. *Diam. Relat. Mater.* **3**(4–6), 896–898 (1994). doi:[10.1016/0925-9635\(94\)90295-X](https://doi.org/10.1016/0925-9635(94)90295-X)
 39. Roy, R.K., Lee, K.-R.: Biomedical applications of diamond-like carbon coatings: A review. *J. Biomed. Mater. Res. Part B-Appl. Biomater.* **83B**(1), 72–84 (2007). doi:[10.1002/jbm.b.30768](https://doi.org/10.1002/jbm.b.30768)
 40. Evans, A.C., Franks, J., Revell, P.J.: Diamond-like carbon applied to bioengineering materials. *Surf. Coat. Technol.* **47**(1–3), 662–667 (1991). doi:[10.1016/0257-8972\(91\)90338-W](https://doi.org/10.1016/0257-8972(91)90338-W)
 41. Saito, T., Hasebe, T., Yohena, S., Matsuoka, Y., Kamijo, A., Takahashi, K., Suzuki, T.: Antithrombogenicity of fluorinated diamond-like carbon films. *Diam. Relat. Mater.* **14**(3–7), 1116–1119 (2005). doi:[10.1016/j.diamond.2004.09.017](https://doi.org/10.1016/j.diamond.2004.09.017)
 42. Schaefer, O., Lohrmann, C., Winterer, J., Kotter, E., Langer, M.: Endovascular treatment of superficial femoral artery occlusive disease with stents coated with diamond-like carbon. *Clin. Radiol.* **59**(12), 1128–1131 (2004). doi:[10.1016/j.crad.2004.05.016](https://doi.org/10.1016/j.crad.2004.05.016)
 43. Babapulle, M.N., Joseph, L., Belisle, P., Brophy, J.M., Eisenberg, M.J.: A hierarchical Bayesian meta-analysis of randomised clinical trials of drug-eluting stents. *Lancet* **364**(9434), 583–591 (2004). doi:[10.1016/S0140-6736\(04\)16850-5](https://doi.org/10.1016/S0140-6736(04)16850-5)
 44. McFadden, E.P., Stabile, E., Regar, E., Cheneau, E., Ong, A.T.L., Kinnaird, T., Suddath, W.O., Weissman, N.J., Torguson, R., Kent, K.M., Pichard, A.D., Satler, L.F., Waksman, R., Serruys, P.W.: Late thrombosis in drug-eluting coronary stents after discontinuation of antiplatelet therapy. *Lancet* **364**(9444), 1519–1521 (2004). doi:[10.1016/S0140-6736\(04\)17275-9](https://doi.org/10.1016/S0140-6736(04)17275-9)

45. Xu, ZH., Rowcliffe, D.: Nanoindentation on diamond-like carbon and alumina coatings. *Surf. Coat. Technol.* **161** (1):44–51. (2002). doi:[Pii s0257-8972\(02\)00364-x10.1016/s0257-8972\(02\)00364-x](https://doi.org/10.1016/s0257-8972(02)00364-x)
46. Dorner-Reisel, A., Schurer, C., Irmer, G., Simon, F., Nischan, C., Muller, E.: Diamond-like carbon coatings with Ca-O-incorporation for improved biological acceptance. *Anal. Bioanal. Chem.* **374**(4), 753–755 (2002). doi:[10.1007/s00216-002-1546-x](https://doi.org/10.1007/s00216-002-1546-x)
47. Ho, J.Y., Matsuura, T., Santerre, J.P.: The effect of fluorinated surface modifying macromolecules on the surface morphology of polyethersulfone membranes. *J. Biomater. Sci.-Polymer Ed.* **11**(10), 1085–1104 (2000)
48. Grischke, M., Bewilogua, K., Trojan, K., Dimigen, H.: Application-oriented modifications of deposition processes for diamond-like-carbon-based coatings. *Surf. Coat. Technol.* **74–75**(1–3), 739–745 (1995). doi:[10.1016/0257-8972\(94\)08201-4](https://doi.org/10.1016/0257-8972(94)08201-4)
49. Grischke, M., Hieke, A., Morgenweck, F., Dimigen, H.: Variation of the wettability of DLC-coatings by network modification using silicon and oxygen. *Diam. Relat. Mater.* **7**(2–5), 454–458 (1998). doi:[10.1016/s0925-9635\(97\)00237-9](https://doi.org/10.1016/s0925-9635(97)00237-9)
50. Memming, R.: Properties of polymeric layers of amorphous hydrogenated carbon produced by a plasma-activated chemical vapor-deposition process. I. spectroscopic investigations. *Thin Solid Films* **143**(3), 279–289 (1986). doi:[10.1016/0040-6090\(86\)90181-1](https://doi.org/10.1016/0040-6090(86)90181-1)
51. Frank, R.D., Dresbach, H., Thelen, H., Sieberth, H.G.: Glutardialdehyde induced fluorescence technique (GIFT): A new method for the imaging of platelet adhesion on biomaterials. *J. Biomed. Mater. Res.* **52**(2), 374–381 (2000). doi:[10.1002/1097-4636\(200011\)52:2<374:aid-jbm18>3.0.co;2-z](https://doi.org/10.1002/1097-4636(200011)52:2<374:aid-jbm18>3.0.co;2-z)
52. Gorbet, M.B., Sefton, M.V.: Biomaterial-associated thrombosis: roles of coagulation factors, complement, platelets and leukocytes. *Biomaterials* **25**(26), 5681–5703 (2004). doi:[10.1016/j.biomaterials.2004.01.023](https://doi.org/10.1016/j.biomaterials.2004.01.023)
53. Hu, W.J., Eaton, J.W., Tang, L.P.: Molecular basis of biomaterial-mediated foreign body reactions. *Blood* **98**(4), 1231–1238 (2001). doi:[10.1182/blood.V98.4.1231](https://doi.org/10.1182/blood.V98.4.1231)
54. Jones, M.I., McColl, I.R., Grant, D.M., Parker, K.G., Parker, T.L.: Protein adsorption and platelet attachment and activation, on TiN, TiC, and DLC coatings on titanium for cardiovascular applications. *J. Biomed. Mater. Res.* **52**(2), 413–421 (2000). doi:[10.1002/1097-4636\(200011\)52:2<413:aid-jbm23>3.0.co;2-u](https://doi.org/10.1002/1097-4636(200011)52:2<413:aid-jbm23>3.0.co;2-u)
55. Ma, Y.J., Yang, H.N., Guo, J., Sathe, C., Agui, A., Nordgren, J.: Structural and electronic properties of low dielectric constant fluorinated amorphous carbon films. *Appl. Phys. Lett.* **72**(25), 3353–3355 (1998). doi:[10.1063/1.121601](https://doi.org/10.1063/1.121601)
56. Strobel, M., Corn, S., Lyons, C.S., Korba, G.A.: Plasma fluorination of polyolefins. *J. Poly. Sci. Part a-Poly. Chem.* **25**(5), 1295–1307 (1987). doi:[10.1002/pola.1987.080250508](https://doi.org/10.1002/pola.1987.080250508)
57. Butler, M.A., Buss, R.J., Galuska, A.: Properties of micrometer-thick plasma-polymerized tetrafluoroethylene films. *J. Appl. Phys.* **70**(4), 2326–2332 (1991). doi:[10.1063/1.349428](https://doi.org/10.1063/1.349428)
58. Elam, J.H., Nygren, H.: Adsorption of coagulation proteins from whole-blood on to polymer materials—relation to platelet activation. *Biomaterials* **13**(1), 3–8 (1992). doi:[10.1016/0142-9612\(92\)90086-4](https://doi.org/10.1016/0142-9612(92)90086-4)
59. Bottani, C.E., Lamperti, A., Nobili, L., Ossi, P.M.: Structure and mechanical properties of PACVD fluorinated amorphous carbon films. *Thin Solid Films* **433**(1–2), 149–154 (2003). doi:[s0040-6090\(03\)00323-710.1016/s0040-6090\(03\)00323-7](https://doi.org/10.1016/s0040-6090(03)00323-7)
60. Hasebe, T., Ishimaru, T., Kamijo, A., Yoshimoto, Y., Yoshimura, T., Yohena, S., Kodama, H., Hotta, A., Takahashi, K., Suzuki, T.: Effects of surface roughness on anti-thrombogenicity of diamond-like carbon films. *Diam. Relat. Mater.* **16**(4–7), 1343–1348 (2007). doi:[10.1016/j.diamond.2006.12.009](https://doi.org/10.1016/j.diamond.2006.12.009)
61. Trippe, S.C., Mansano, R.D., Costa, F.M., Silva, R.F.: Mechanical properties evaluation of fluor-doped diamond-like carbon coatings by nanoindentation. *Thin Solid Films* **446**(1), 85–90 (2004). doi:[10.1016/j.tsf.2003.08.069](https://doi.org/10.1016/j.tsf.2003.08.069)
62. Yu, G.Q., Tay, B.K., Sun, Z., Pan, L.K.: Properties of fluorinated amorphous diamond like carbon films by PECVD. *Appl. Surf. Sci.* **219**(3–4), 228–237 (2003). doi:[10.1016/s0169-4332\(03\)00644-5](https://doi.org/10.1016/s0169-4332(03)00644-5)

63. Agraharam, S., Hess, D.W., Kohl, P.A., Allen, S.A.B.: Plasma chemistry in fluorocarbon film deposition from pentafluoroethane/argon mixtures. *J. Vacuum Sci. Technol. Vac. Surf. Films* **17**(6), 3265–3271 (1999). doi:[10.1116/1.582053](https://doi.org/10.1116/1.582053)
64. Hynes, A.M., Shenton, M.J., Badyal, J.P.S.: Pulsed plasma polymerization of perfluorocyclohexane. *Macromolecules* **29**(12), 4220–4225 (1996). doi:[10.1021/ma951747q](https://doi.org/10.1021/ma951747q)
65. Goodman, S.L., Grasel, T.G., Cooper, S.L., Albrecht, R.M.: Platelet shape change and cytoskeletal reorganization on polyurethaneureas. *J. Biomed. Mater. Res.* **23**(1), 105–123 (1989). doi:[10.1002/jbm.820230109](https://doi.org/10.1002/jbm.820230109)
66. Phillips, D.R., Charo, I.F., Parise, L.V., Fitzgerald, L.A.: The platelet membrane glycoprotein-iiib-iiiia complex. *Blood* **71**(4), 831–843 (1988)
67. Courtney, J.M., Lamba, N.M.K., Sundaram, S., Forbes, C.D.: Biomaterials for blood-contacting applications. *Biomaterials* **15**(10), 737–744 (1994). doi:[10.1016/0142-9612\(94\)90026-4](https://doi.org/10.1016/0142-9612(94)90026-4)
68. Sheppard, J.I., McClung, W.G., Feuerstein, I.A.: Adherent platelet morphology on adsorbed fibrinogen—effects of protein incubation-time and albumin addition. *J. Biomed. Mater. Res.* **28**(10), 1175–1186 (1994). doi:[10.1002/jbm.820281008](https://doi.org/10.1002/jbm.820281008)
69. Whicher, S.J., Brash, J.L.: Platelet—foreign surface interactions—release of granule constituents from adherent platelets. *J. Biomed. Mater. Res.* **12**(2), 181–201 (1978). doi:[10.1002/jbm.820120205](https://doi.org/10.1002/jbm.820120205)
70. Keogh, J.R., Velander, F.F., Eaton, J.W.: Albumin-binding surfaces for implantable devices. *J. Biomed. Mater. Res.* **26**(4), 441–456 (1992). doi:[10.1002/jbm.820260403](https://doi.org/10.1002/jbm.820260403)
71. Kottkemarchant, K., Anderson, J.M., Umemura, Y., Marchant, R.E.: Effect of albumin coating on the invitro blood compatibility of dacron arterial prostheses. *Biomaterials* **10**(3), 147–155 (1989). doi:[10.1016/0142-9612\(89\)90017-3](https://doi.org/10.1016/0142-9612(89)90017-3)
72. Niimi, Y., Yamane, S., Yamaji, K., Tayama, E., Sueoka, A., Nose, Y.: Protein adsorption and platelet adhesion on the surface of an oxygenator membrane. *ASAIO J.* **43**(5), M706–M710 (1997)
73. Tang, L.P., Eaton, J.W.: Fibrin(OGEN) mediates acute inflammatory responses to biomaterials. *J. Exp. Med.* **178**(6), 2147–2156 (1993). doi:[10.1084/jem.178.6.2147](https://doi.org/10.1084/jem.178.6.2147)
74. Calvete, J.J.: Clues for understanding the structure and function of a prototypic human integrin—the platelet glycoprotein IIB/IIIa complex. *Thromb. Haemost.* **72**(1), 1–15 (1994)
75. McNicol, A., Israels, S.J.: Platelets and anti-platelet therapy. *J. Pharm. Sci.* **93**(4), 381–396 (2003). doi:[10.1254/jphs.93.381](https://doi.org/10.1254/jphs.93.381)
76. Haidopoulos, M., Turgeon, S., Sarra-Bournet, C., Laroche, G., Mantovani, D.: Development of an optimized electrochemical process for subsequent coating of 316 stainless steel for stent applications. *J. Mater. Sci-Mater Med.* **17**(7), 647–657 (2006). doi:[10.1007/s10856-006-9228-4](https://doi.org/10.1007/s10856-006-9228-4)
77. Kihara, S., Yamazaki, K., Litwak, K.N., Litwak, P., Kameneva, M.V., Ushiyama, H., Tokuno, T., Borzelleca, D.C., Umezu, M., Tomioka, J., Tagusari, O., Akimoto, T., Koyanagi, H., Kurosawa, H., Kormos, R.L., Griffith, B.P.: In vivo evaluation of a MPC polymer coated continuous flow left ventricular assist system. *Artif. Organs* **27**(2), 188–192 (2003). doi:[10.1046/j.1525-1594.2003.t01-2-06993.x](https://doi.org/10.1046/j.1525-1594.2003.t01-2-06993.x)
78. Yang, P., Huang, N., Leng, Y.X., Chen, J.Y., Fu, R.K.Y., Kwok, S.C.H., Leng, Y., Chu, P.K.: Activation of platelets adhered on amorphous hydrogenated carbon (a-C:H) films synthesized by plasma immersion ion implantation-deposition (PIII-D). *Biomaterials* **24**(17), 2821–2829 (2003). doi:[10.1016/s0142-9612\(03\)00091-7](https://doi.org/10.1016/s0142-9612(03)00091-7)
79. Hasebe, T., Matsuoka, Y., Kodama, H., Saito, T., Yohena, S., Kamijo, A., Shiraga, N., Higuchi, A., Kuribayashi, S., Takahashi, K., Suzuki, T.: Lubrication performance of diamond-like carbon and fluorinated diamond-like carbon coatings for intravascular guidewires. *Diam. Relat. Mater.* **15**(1), 129–132 (2006). doi:[10.1016/j.diamond.2005.08.025](https://doi.org/10.1016/j.diamond.2005.08.025)

80. Maitz, M.F., Gago, R., Abendroth, B., Camero, M., Caretti, I., Kreissig, U.: Hemocompatibility of low-friction boron-carbon-nitrogen containing coatings. *J. Biomed. Mater. Res. Part B-Appl. Biomater.* **77B**(1), 179–187 (2006). doi:[10.1002/jbm.b.30435](https://doi.org/10.1002/jbm.b.30435)
81. Hecker, J.F., Edwards, R.O.: Effects of roughness on the thrombogenicity of a plastic. *J. Biomed. Mater. Res.* **15**(1), 1–7 (1981). doi:[10.1002/jbm.820150104](https://doi.org/10.1002/jbm.820150104)
82. Hecker, J.F., Scandrett, L.A.: Roughness and thrombogenicity of the outer surfaces of intravascular catheters. *J. Biomed. Mater. Res.* **19**(4), 381–395 (1985). doi:[10.1002/jbm.820190404](https://doi.org/10.1002/jbm.820190404)
83. Tsunoda, N., Kokubo, K., Sakai, K., Fukuda, M., Miyazaki, M., Hiyoshi, T.: Surface roughness of cellulose hollow fiber dialysis membranes and platelet adhesion. *ASAIO J.* **45**(5), 418–423 (1999). doi:[10.1097/00002480-199909000-00010](https://doi.org/10.1097/00002480-199909000-00010)
84. Zingg, W., Neumann, A.W., Strong, A.B., Hum, O.S., Absolom, D.R.: Effect of surface-roughness on platelet-adhesion under static and under flow conditions. *Can. J. Surg.* **25**(1), 16–19 (1982)
85. Tepe, G., Schmehl, J., Wendel, H.P., Schaffner, S., Heller, S., Gianotti, M., Claussen, C.D., Duda, S.H.: Reduced thrombogenicity of nitinol stents—in vitro evaluation of different surface modifications and coatings. *Biomaterials* **27**(4), 643–650 (2006). doi:[10.1016/j.biomaterials.2005.06.004](https://doi.org/10.1016/j.biomaterials.2005.06.004)
86. Beholz, L.G., Aronson, C.L., Zand, A.: Adhesion modification of polyolefin surfaces with sodium hypochlorite in acidic media. *Polymer* **46**(13), 4604–4613 (2005). doi:[10.1016/j.polymer.2005.03.086](https://doi.org/10.1016/j.polymer.2005.03.086)
87. Choi, D.M., Park, C.K., Cho, K., Park, C.E.: Adhesion improvement of epoxy resin/polyethylene joints by plasma treatment of polyethylene. *Polymer* **38**(25), 6243–6249 (1997). doi:[10.1016/s0032-3861\(97\)00175-4](https://doi.org/10.1016/s0032-3861(97)00175-4)
88. Medard, N., Soutif, J.C., Poncin-Epaillard, F.: CO₂, H₂O, and CO₂/H₂O plasma chemistry for polyethylene surface modification. *Langmuir* **18**(6), 2246–2253 (2002). doi:[10.1021/la011481i](https://doi.org/10.1021/la011481i)
89. Brewis, D.M., Briggs, D.: Adhesion to polyethylene and polypropylene. *Polymer* **22**(1), 7–16 (1981). doi:[10.1016/0032-3861\(81\)90068-9](https://doi.org/10.1016/0032-3861(81)90068-9)
90. Moshonov, A., Avny, Y.: The use of acetylene glow-discharge for improving adhesive bonding of polymeric films. *J. Appl. Polym. Sci.* **25**(5), 771–781 (1980). doi:[10.1002/app.1980.070250506](https://doi.org/10.1002/app.1980.070250506)
91. Nakahigashi, T., Tanaka, Y., Miyake, K., Oohara, H.: Properties of flexible DLC film deposited by amplitude-modulated RF P-CVD. *Tribol. Int.* **37**(11–12), 907–912 (2004). doi:[10.1016/j.triboint.2004.07.007](https://doi.org/10.1016/j.triboint.2004.07.007)
92. Shirakura, A., Nakaya, M., Koga, Y., Kodama, H., Hasebe, T., Suzuki, T.: Diamond-like carbon films for PET bottles and medical applications. *Thin Solid Films* **494**(1–2), 84–91 (2006). doi:[10.1016/j.tsf.2005.08.366](https://doi.org/10.1016/j.tsf.2005.08.366)
93. Agrawal, D.C., Raj, R.: Measurement of the ultimate shear-strength of a metal ceramic interface. *Acta Metall.* **37**(4), 1265–1270 (1989). doi:[10.1016/0001-6160\(89\)90120-x](https://doi.org/10.1016/0001-6160(89)90120-x)
94. Ye, T., Suo, Z., Evans, A.G.: Thin-film cracking and the roles of substrate and interface. *Int. J. Solids Struct.* **29**(21), 2639–2648 (1992). doi:[10.1016/0020-7683\(92\)90227-k](https://doi.org/10.1016/0020-7683(92)90227-k)
95. Chen, B.F., Hwang, J., Yu, G.P., Huang, J.H.: In situ observation of the cracking behavior of TiN coating on 304 stainless steel subjected to tensile strain. *Thin Solid Films* **352**(1–2), 173–178 (1999). doi:[10.1016/s0040-6090\(99\)00342-9](https://doi.org/10.1016/s0040-6090(99)00342-9)
96. Ogwu, A.A., Coyle, T., Okpalugo, T.I.T., Kearney, P., Maguire, P.D., McLaughlin, J.A.D.: The influence of biological fluids on crack spacing distribution in Si-DLC films on steel substrates. *Acta Mater.* **51**(12), 3455–3465 (2003). doi:[10.1016/s1359-6454\(03\)00166-6](https://doi.org/10.1016/s1359-6454(03)00166-6)
97. Aoki, Y., Ohtake, N.: Tribological properties of segment-structured diamond-like carbon films. *Tribol. Int.* **37**(11–12), 941–947 (2004). doi:[10.1016/j.triboint.2004.07.011](https://doi.org/10.1016/j.triboint.2004.07.011)
98. Cho, S.J., Chung, J.W., Lee, K.R.: Characterization of the mechanical properties of diamond-like carbon films. *Diam. Relat. Mater.* **14**(8), 1270–1276 (2005). doi:[10.1016/j.diamond.2004.11.034](https://doi.org/10.1016/j.diamond.2004.11.034)

99. Choi, H.W., Lee, K.R., Wang, R.Z., Oh, K.H.: Fracture behavior of diamond-like carbon films on stainless steel under a micro-tensile test condition. *Diam. Relat. Mater.* **15**(1), 38–43 (2006). doi:[10.1016/j.diamond.2005.07.002](https://doi.org/10.1016/j.diamond.2005.07.002)
100. Higson, S.P.J., Vadgama, P.M.: Diamond-like carbon-coated films for enzyme electrodes—characterization of biocompatibility and substrate diffusion limiting properties. *Anal. Chim. Acta* **300**(1–3), 77–83 (1995). doi:[10.1016/0003-2670\(94\)00380-5](https://doi.org/10.1016/0003-2670(94)00380-5)
101. Kimura, A., Kodama, H., Suzuki, T.: Diamond-like carbon films deposited on polyethylene terephthalate substrates by radio frequency plasma chemical vapor deposition method. *J. Vac. Sci. Technol. A* **21**(2), 515–517 (2003). doi:[10.1116/1.1537717](https://doi.org/10.1116/1.1537717)
102. Tsai, H.C., Bogy, D.B., Kundmann, M.K., Veirs, D.K., Hilton, M.R., Mayer, S.T.: Structure and properties of sputtered carbon overcoats on rigid magnetic media disks. *J. Vac. Sci. Technol. a-Vac. Surf. Films* **6**(4), 2307–2315 (1988). doi:[10.1116/1.575581](https://doi.org/10.1116/1.575581)
103. Yoshikawa, M., Katagiri, G., Ishida, H., Ishitani, A., Akamatsu, T.: Raman-spectra of diamondlike amorphous-carbon films. *J. Appl. Phys.* **64**(11), 6464–6468 (1988). doi:[10.1063/1.342063](https://doi.org/10.1063/1.342063)
104. Yamamoto, S., Kodama, H., Hasebe, T., Shirakura, A., Suzuki, T.: Oxygen transmission of transparent diamond-like carbon films. *Diam. Relat. Mater.* **14**(3–7), 1112–1115 (2005). doi:[10.1016/j.diamond.2004.10.025](https://doi.org/10.1016/j.diamond.2004.10.025)
105. Sousa, J.E., Costa, M.A., Sousa, A., Abizaid, A.C., Seixas, A.C., Abizaid, A.S., Feres, F., Mattos, L.A., Falotico, R., Jaeger, J., Popma, J.J., Serruys, P.W.: Two-year angiographic and intravascular ultrasound follow-up after implantation of sirolimus-eluting stents in human coronary arteries. *Circulation* **107**(3), 381–383 (2003). doi:[10.1161/01.cir.0000051720.59095.6d](https://doi.org/10.1161/01.cir.0000051720.59095.6d)
106. Stone, G.W., Ellis, S.G., Cox, D.A., Hermiller, J., O’Shaughnessy, C., Mann, J.T., Turco, M., Caputo, R., Bergin, P., Greenberg, J., Popma, J.J., Russell, M.E., Investigators, T.-I.: A polymer-based, paclitaxel-eluting stent in patients with coronary artery disease. *N. Engl. J. Med.* **350**(3), 221–231 (2004). doi:[10.1056/NEJMoa032441](https://doi.org/10.1056/NEJMoa032441)
107. Drachman, D.E., Edelman, E.R., Seifert, P., Groothuis, A.R., Bornstein, D.A., Kamath, K.R., Palasis, M., Yang, D.C., Nott, S.H., Rogers, C.: Neointimal thickening after stent delivery of paclitaxel: Change in composition and arrest of growth over six months. *J. Am. Coll. Cardiol.* **36**(7), 2325–2332 (2000). doi:[10.1016/s0735-1097\(00\)01020-2](https://doi.org/10.1016/s0735-1097(00)01020-2)
108. Suzuki, T., Kopia, G., Hayashi, S., Bailey, L.R., Llanos, G., Wilensky, R., Klugherz, B.D., Papandreou, G., Narayan, P., Leon, M.B., Yeung, A.C., Tio, F., Tsao, P.S., Falotico, R., Carter, A.J.: Stent-based delivery of sirolimus reduces neointimal formation in a porcine coronary model. *Circulation* **104**(10), 1188–1193 (2001). doi:[10.1161/hc3601.093987](https://doi.org/10.1161/hc3601.093987)
109. Togni, M., Windecker, S., Cocchia, R., Wenaweser, P., Cook, S., Billinger, M., Meier, B., Hess, O.M.: Sirolimus-eluting stents associated with paradoxical coronary vasoconstriction. *J. Am. Coll. Cardiol.* **46**(2), 231–236 (2005). doi:[10.1016/j.jacc.2005.01.062](https://doi.org/10.1016/j.jacc.2005.01.062)
110. Virmani, R., Guagliumi, G., Farb, A., Musumeci, G., Grieco, N., Motta, T., Mihalscik, L., Tsepili, M., Valsecchi, O., Kolodgie, F.D.: Localized hypersensitivity and late coronary thrombosis secondary to a sirolimus-eluting stent should we be cautious? *Circulation* **109**(6), 701–705 (2004). doi:[10.1161/01.cir.0000116202.41966.d4](https://doi.org/10.1161/01.cir.0000116202.41966.d4)
111. Hasebe, T., Hotta, A., Kodama, H., Kamijo, A., Takahashi, K., Suzuki, T.: Recent advances in diamond-like carbon films in the medical and food packing fields. *New Diamond Front. Carbon Technol.* **17**(6), 263–279 (2007)
112. Roy, R.K., Choi, H.W., Yi, J.W., Moon, M.W., Lee, K.R., Han, D.K., Shin, J.H., Kamijo, A., Hasebe, T.: Hemocompatibility of surface-modified, silicon-incorporated, diamond-like carbon films. *Acta Biomater.* **5**(1), 249–256 (2009). doi:[10.1016/j.actbio.2008.07.031](https://doi.org/10.1016/j.actbio.2008.07.031)
113. Higuchi, T.: Correction. *J. Pharm. Sci.* **50** (12):874 (1961). doi:[10.1002/jps.2600501018](https://doi.org/10.1002/jps.2600501018)
114. Costa, P., Manuel, J., Lobo, S.: Modeling and comparison of dissolution profiles. *Eur. J. Pharm. Sci.* **13**(2), 123–133 (2001). doi:[10.1016/s0928-0987\(01\)00095-1](https://doi.org/10.1016/s0928-0987(01)00095-1)
115. Kodama, H., Nakaya, M., Shirakura, A., Hotta, A., Hasebe, T., Suzuki, T.: Synthesis of practical high-gas-barrier carbon films at low and atmospheric pressure for PET bottles. *New Diamond Front. Carbon Technol.* **16**(2), 107–119 (2006)

116. Asakawa, R., Nagashima, S., Nakamura, Y., Hasebe, T., Suzuki, T., Hotta, A.: Combining polymers with diamond-like carbon (DLC) for highly functionalized materials. *Surf. Coat. Technol.* **206**(4), 676–685 (2011). doi:[10.1016/j.surfcoat.2011.02.064](https://doi.org/10.1016/j.surfcoat.2011.02.064)
117. Hasebe, T., Nagashima, S., Kamijo, A., Yoshimura, T., Ishimaru, T., Yoshimoto, Y., Yohena, S., Kodama, H., Hotta, A., Takahashi, K., Suzuki, T.: Depth profiling of fluorine-doped diamond-like carbon (F-DLC) film: Localized fluorine in the top-most thin layer can enhance the non-thrombogenic properties of F-DLC. *Thin Solid Films* **516**(2–4), 299–303 (2007). doi:[10.1016/j.tsf.2007.06.033](https://doi.org/10.1016/j.tsf.2007.06.033)
118. Hoshida, T., Tsubone, D., Takada, K., Kodama, H., Hasebe, T., Kamijo, A., Suzuki, T., Hotta, A.: Controlling the adhesion between diamond-like carbon (DLC) film and high-density polyethylene (HDPE) substrate. *Surf. Coat. Technol.* **202**(4–7), 1089–1093 (2007). doi:[10.1016/j.surfcoat.2007.07.087](https://doi.org/10.1016/j.surfcoat.2007.07.087)
119. Tsubone, D., Hasebe, T., Kamijo, A., Hotta, A.: Fracture mechanics of diamond-like carbon (DLC) films coated on flexible polymer substrates. *Surf. Coat. Technol.* **201**(14), 6423–6430 (2007). doi:[10.1016/j.surfcoat.2006.12.008](https://doi.org/10.1016/j.surfcoat.2006.12.008)
120. Enomoto, K., Hasebe, T., Asakawa, R., Kamijo, A., Yoshimoto, Y., Suzuki, T., Takahashi, K., Hotta, A.: Controlling the drug release rate from biocompatible polymers with micro-patterned diamond-like carbon (DLC) coating. *Diam. Relat. Mater.* **19**(7–9), 806–813 (2010). doi:[10.1016/j.diamond.2010.01.053](https://doi.org/10.1016/j.diamond.2010.01.053)

Chapter 7

Surface Modification of Biodegradable Polyesters for Soft and Hard Tissue Regeneration

Hesameddin Mahjoubi, Sara Abdollahi and Marta Cerruti

Abstract Synthetic biodegradable polyesters are commonly used in biomedical applications, especially as three-dimensional porous scaffolds for soft and hard tissue engineering. In addition to straightforward fabrication procedures, good mechanical strength and adjustable degradation properties all contribute to the appeal of these polymers. Still, scaffolds synthesized from polyesters are hydrophobic in nature and lack cell recognition signals. Coating or modifying their surface with molecules that enhance cellular adhesion and activity is therefore necessary to make them suitable as biomaterials, while preserving their bulk properties. This chapter reviews current strategies used to modify the surface of polyester-based scaffolds, with a specific focus on the modifications necessary to stimulate soft and hard tissue regeneration. The methods reviewed mostly involve two steps. During the first step, the polymer hydrophilicity is increased by generating carboxylic, amino or hydroxyl groups on the surface by either chemically or photochemically breaking the polymeric ester bonds, or by plasma treatment. This step also allows introducing functional groups on the polymeric surface, which can be used as anchors to bind biomolecules in the next step. In the second step, biomolecules of different types are bound to the previously modified polymer surface, to stimulate a specific tissue response. After providing an overview and many recent examples of the strategies used to achieve both steps, the chapter concludes by summarizing the main achievements to date and the challenges that still remain open.

Hesameddin Mahjoubi and Sara Abdollahi contributed equally to this chapter.

H. Mahjoubi · S. Abdollahi · M. Cerruti (✉)
Materials Engineering, McGill University, 3610 University St,
Montreal, QC H3A 0C5, Canada
e-mail: marta.cerruti@mcgill.ca

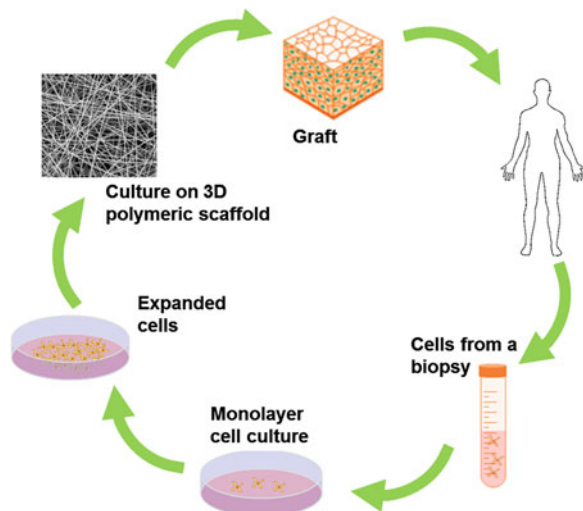
7.1 Introduction

7.1.1 The Importance of Surfaces in Tissue Engineering

Tissue engineering is an emerging discipline at the junction of engineering, biology and medicine, which is changing the traditional ways of improving people's health by restoring, maintaining, or enhancing tissue and organ functions [1]. The main goal of tissue engineering is to recreate living tissue in the lab, for applications that can be either therapeutic (for example, replace a damaged organ in a patient), or diagnostic (for example, check the metabolism and toxicity of drugs). To achieve this goal, cells related to the tissue to be recreated are harvested from the target organ and cultured in a petri dish. Once enough cells are generated, they are seeded onto porous structures called scaffolds and kept in an incubator to grow. Then they are implanted in the patient's body in order to enhance regeneration of the damaged tissue or organ (Fig. 7.1).

Most of the current research in tissue engineering focuses on improving the scaffolds used for tissue culture. Optimal scaffolds should not only provide a physical support for the cells, but also an environment for their proliferation, growth and differentiation, which can finally lead to successful tissue regeneration. Said in a different way, scaffolds should mimic the extra cellular matrix (ECM), which is the natural support over which cells bind and grow in the body. To achieve this, the scaffold should meet four basic requirements: (1) they should be biocompatible, so no infection occurs when they are implanted in the patient body; (2) they need to be porous, to support two dimensional (2D) expansion and three dimensional (3D) growth of the cells, and the pores must be interconnected, to allow for easy delivery of nutrients to the cells and waste removal; (3) they should

Fig. 7.1 Basic principles of tissue engineering

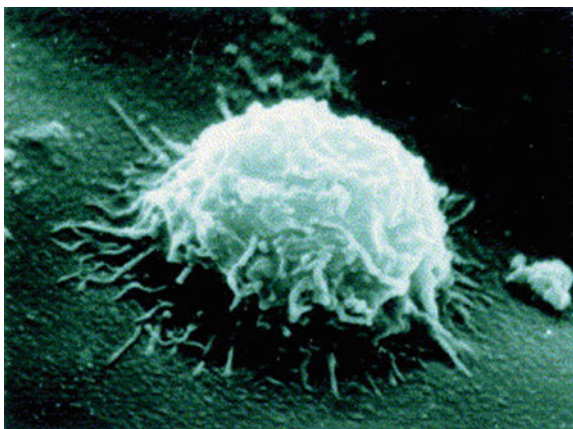


be mechanically stable, so they do not deform and collapse before complete regeneration of tissue; and (4) they should be biodegradable, i.e. gradually decompose as the tissue is regenerated, meanwhile producing residues that can be removed by normal metabolic activity of the body. In addition to these basic requirements, it is crucial that the scaffold's surface elicit the desired response from the cells in contact with it. Indeed, *it is the scaffold's surface that determines the initial cellular response to the implant, and therefore its acceptance and durability in the body* [2].

Many biological reactions happen at interfaces [3]. As chemists have known for more than a century, surfaces can provide catalytic sites that can lower reaction energy barriers, and enhance turnover rate. In a similar way, biological surfaces can expose enzymatic sites, facilitate interactions between biomolecules, and encourage specific aspects of cellular activity. The ECM represents one of the most important examples of a biological surface: cells anchor on it through actin filaments, and their proliferation and differentiation is affected by the presence of several signaling complexes on the ECM, such as growth and differentiation factors [4]. Cells respond to biomaterial surfaces somewhat similarly to ECM, and spread and anchor on them if they recognize them as a suitable environment (Fig. 7.2).

Serum proteins adsorb on a biomaterial's surface within minutes from its implantation, and these in turn influence the type and quantity of cells that adhere and spread on it [5]. A successful scaffold for tissue engineering will thus be able to attract the desired type of proteins and cells at its interface, to regenerate the originally damaged tissue. To achieve this, scaffold's surface properties such as wettability, surface charge, and morphology need to be carefully controlled [6]. In addition, the scaffold's surface can be modified to generate functional groups for the immobilization of drugs, receptors, enzymes, signaling molecules, antibodies or other biologically active molecules for different biomedical applications.

Fig. 7.2 Scanning electron microscopy picture of a myoblast cell (length is approximately 10 μm) interacting with a synthetic biomaterial surface [3]



7.1.2 Scaffold Materials for Soft and Hard Tissue Regeneration

The material chosen to fabricate the scaffolds influences both surface and mechanical properties of the implants, and therefore material selection is dictated by the final scaffold application. For example, a scaffold to be used in bone tissue engineering must be able to bear loads, and therefore should have sufficient mechanical strength [7]. For soft tissue regeneration, such as skin, the material should be able to act as a barrier, allow for water flow above it, and be adherent to the tissues underneath [8]. Materials currently used to prepare scaffolds for hard or soft tissue regeneration can be divided into three main categories: bioceramics, natural and synthetic polymers.

Bioceramics are produced by sintering or melting inorganic raw materials to create an amorphous or crystalline solid piece, which can be used as an implant. Products used for scaffold applications are usually porous. Bioceramics can be further classified in three groups. (1) Nonresorbable ceramics: these are relatively inert, and include alumina, zirconia and silicon nitride. Implants made with this type of bioceramics are mainly used as fixtures in medical applications and they need to be removed from the body during a second surgery. (2) Bioactive or surface active ceramics: examples include Bioglass[®] or porous hydroxyapatite $\text{Ca}_{10}(\text{PO}_4)_6(\text{OH})_2$ —these materials are mostly used for surface modification and fabrication of scaffolds with enhanced surface properties; (3) Biodegradable or resorbable ceramics, like coralline hydroxyapatite [9] and ferrite calcium phosphates [10]. These materials degrade after some time of implantation in the body, and can be completely resorbed.

Among the natural polymers, both polypeptides such as collagen, gelatin and silk, and polysaccharides such as agarose, alginate and chitosan have been used. These polymers are biocompatible and enzymatically biodegradable. The main advantage for using natural polymers is that they contain bio-functional molecules that aid the attachment, proliferation, and differentiation of cells. Their main disadvantage lies in the difficulty of controlling their degradation rate; this is mainly dependent on enzymes, whose level may vary from patient to patient. Additionally, natural polymers are often mechanically weak, although cross-linking has shown to enhance their structural stability [11].

Synthetic polymers are chemically synthesized, which implies that properties such as mechanical strength and degradation rate can be tuned by changing composition and synthesis parameters. Also, since most of them degrade hydrolytically, the degradation rate of scaffolds made with these polymers does not vary significantly between different patients. The most common synthetic polymers are polyesters such as poly(glycolic) acid (PGA), poly(d,l-lactic) acid (PDLA), poly(l-lactic) acid (PLLA), and poly(d,l-lactic acid-co-glycolic acid) (PLGA) [12]. Other types include polyanhydrides, polycarbonates, and polyphosphazenes [11–13]. Most of these polymers degrade forming acidic compounds that are naturally occurring in the body. Although these products are not toxic, high concentrations

of them may increase local acidity, resulting in inflammation or fibrous encapsulation [12, 14, 15]. Despite this potential disadvantage, synthetic polymers are among the most promising materials for biomedical applications due to their low production costs and the ease of controlling their properties.

Among biodegradable synthetic polymers, polyesters such as PDLLA and PLGA have been explored extensively because of their excellent biodegradability and non-toxicity, which allowed them to be FDA approved [16]. However, their inherent hydrophobicity hinders the interactions between scaffolds made with these polymers and biomolecules, proteins and cells—especially if compared with hydrophilic biomaterials such as polyvinyl alcohol [17]. Surface treatments are thus necessary to optimize the properties of these polymers for biomedical applications.

This chapter will focus on surface modifications of scaffolds made with polyesters for orthopedic and soft tissue regeneration. Surface treatments of these scaffolds aim first at increasing their hydrophilicity, while maintaining their biocompatibility and bulk properties. Both physical methods such as plasma treatment and chemical methods such as hydrolysis can be used to achieve this goal. The functional groups introduced with either method can then be used as anchors to bind specific biomolecules, such as cell signaling molecules and proteins, to improve cell adhesion, proliferation and growth. Compared with relatively recent reviews on surface modification of biomaterials [5, 18–21], the present book chapter aims at giving a more in-depth perspective on the modifications adopted so far on polyesters, and providing examples from recent literature relative to applications in soft (mainly skin and cartilage) and hard (mainly bone) tissue engineering. After reviewing plasma treatments (Sect. 7.2) and chemical methods (Sect. 7.3) used to increase scaffold hydrophilicity and generating anchoring groups, we will provide examples of modifications that have increased the scaffolds' biological activity (Sect. 7.4). In the last section of this review (Sect. 7.5), we will summarize the most important trends of research so far and describe what is left to be done to achieve a complete control of scaffold's surface properties. The large number of examples proposed from the most recent literature together with the final summary and perspective should provide the reader with a comprehensive, up-to-date understanding of the importance and potential of surface modifications for biomaterial development.

7.2 Plasma Treatment

Treating polymeric materials with plasma is perhaps the only method that allows modifying their surface without resorting to wet chemistry. In this section we will quickly describe the principles of plasma surface modification, and we will then provide examples of plasma surface modification of biodegradable polyesters used as thin films or scaffolds for soft and hard tissue engineering.

7.2.1 The Principles of Plasma Surface Modification

Plasma is a state of matter composed of highly excited atomic, molecular, ionic, and radical species, achieved by gas excitation with radio frequency [22], or electrons from a hot filament discharge [23]. Since plasma processing has been widely used in microelectronics, coating and painting, the underlying physics and chemistry of plasma is relatively well-known [24]. Plasma is generated by ionizing atoms or molecules in a medium. The ionization takes place when the components of the plasma absorb enough energy from an external excitation source or by collisions with one another. There are many different plasma sources, but the most common ones are gas discharge [23], pulsed vacuum arcs initiated on the surface of a consumable cathode [25–27], and laser [28].

Plasma surface modification techniques can be categorized into plasma sputtering, etching, cleaning, implantation and deposition. In plasma sputtering and cleaning, the surface is bombarded with inert gases such as neon or argon; some of the material surface is etched away, and a clean layer is eventually exposed [29]. Plasma implantation can introduce elements on the surface of the materials by bombarding them with ions coming from a target material [30, 31]. In plasma deposition different groups such as amine and carboxyl groups are deposited on the surface of polymer to change its surface charge and prepare it for attachment of other functional groups and bio molecules [32].

Plasma's highly reactive chemical environment can modify the surface of materials exposed to it. Indeed plasma engineering has been used to modify almost any type of materials, and change their surface chemical, physical, tribological, electrical, or mechanical properties. Plasma treatments are reproducible and relatively inexpensive, and they can be monitored precisely, and work extremely well on 2D polymer films [86–90]. In biomedical engineering, plasma treatments have been used for many diverse applications, ranging from surface treatment of devices in contact with human blood such as blood bags and vascular grafts to prevent thrombosis [33, 34], sterilization of surgical tools [35], and enhancing anti-bacterial properties [36].

7.2.2 Plasma Treatment of Polyesters for Soft and Hard Tissue Engineering

The advantages of plasma treatment such as easy preparation, achievement of a homogenous surface layer, and sterilization during the treatment, make this method a strong candidate for surface modifications of polyester-based implants and devices. Most commonly, plasma modification of biodegradable polyesters involves their exposure to gases like air, NH_3 , SO_2 and CO_2 . These treatments aim at introducing polar functionalities on the polymer surfaces, such as hydroxyl, carboxyl, amino and sulfate groups, to increase their hydrophilicity. For example,

Yang et al. [32] showed that plasma treatment using N_2 , NH_3 and/or O_2 gas could decrease the water contact angle on PDLA films from a starting value of 78° all the way to 17° in just 2 min of exposure, thus indicating a very large increase in hydrophilicity of the polymer surface. The NH_3 plasma-treated PDLA samples were then exposed to a collagen-containing solution. 3T3 fibroblast adhesion and spreading was compared on these materials and on PDLA samples coated with collagen without the plasma pretreatment, as well as on PDLA treated with NH_3 plasma only. Cell spreading and growth was maximized by the combination of plasma treatment and collagen exposure (Fig. 7.3). This was attributed to the fact that collagen was present in larger amounts and was more stably anchored to the plasma-treated PDLA. Positively charged groups present on collagen were suspected to be responsible for the greater interactions with negatively charged cells [32].

Shen et al. [37] investigated immobilization of basic fibroblast growth factor (bFGF) on PLGA after plasma treatment. They introduced acid carboxylic functional groups on the surface of PLGA scaffolds via a CO_2 plasma, and incubated the samples in a solution containing bFGF. They characterized the composition of PLGA films before and after CO_2 plasma treatment with X-ray photoelectron spectroscopy (XPS) and water contact angle, and observed an increase in the fraction of carboxylated species and in hydrophilicity of the PLGA films with longer plasma treatments. To characterize cell adhesion on these surfaces, they cultivated 3T3 fibroblasts on them, and then applied a constant shear stress. They

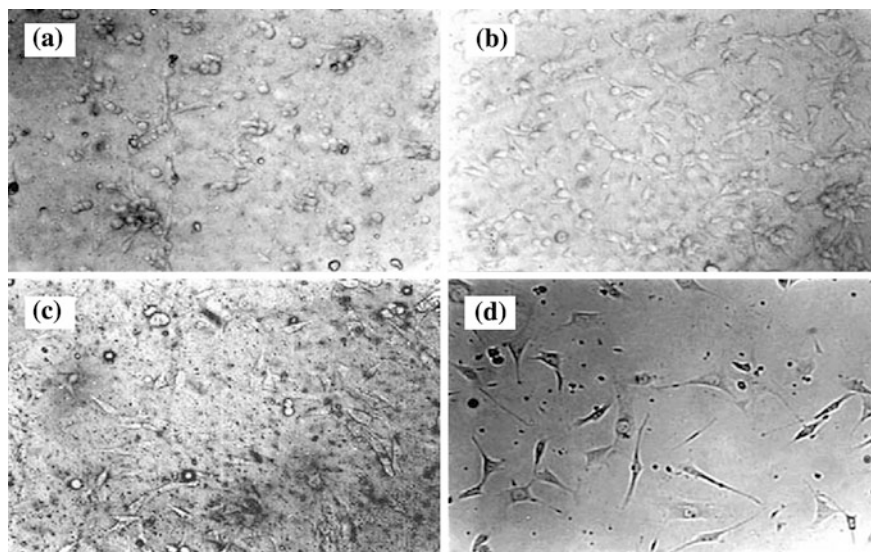


Fig. 7.3 Photomicrograph (x150) of 3T3 fibroblasts cultured on different PDLA films for 9 h. **a** control; **b** sample modified by NH_3 plasma (50 W, 20 Pa, 300 s); **c** sample modified by collagen coating, and **d** sample modified by ammonia plasma pre-treatment collagen anchorage [32]

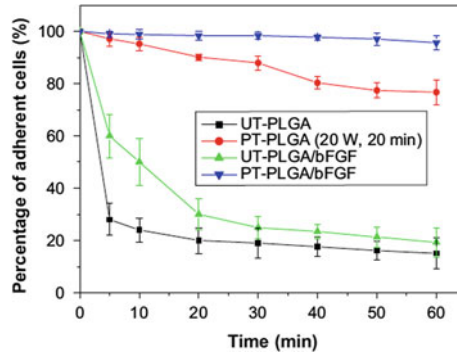


Fig. 7.4 The fraction of adherent 3T3 fibroblasts on different PLGA films as a function of time under 36.5 N/m^2 of shear stress. While on untreated PLGA films (UT-PLGA) about 76 % of cells detached within 10 min and on PLGA samples just coated with bFGF (UT-PLGA/bFGF) about 80 % detached after 60 min, only ~ 23 % of cells detached from plasma treated PLGA (PT-PLGA) and less than 5 % on bFGF coated, plasma treated PLGA (PT-PLGA/bFGF) after 60 min [37]

found that plasma treatment followed by bFGF coating drastically increased the amount of cells remaining on the surface, compared with uncoated PLGA or PLGA coated with bFGF without the plasma pretreatment (Fig. 7.4).

In another work, Shen et al. [38] studied immobilization of human bone morphogenetic protein-2 (rhBMP-2) on PLGA scaffolds. BMP-2 is a powerful osteogenic factor that promotes proliferation, migration and osteogenic differentiation of stem cells. In this paper, the authors modified PLGA scaffolds with different plasma treatments, such as O_2 , NH_3 and CO_2 , and then incubated them in rhBMP-2 solution to bind the protein onto the surface of the scaffolds. In order to measure the amount of the attached protein on the surface of non-treated and plasma treated PLGA scaffolds, they used a modified enzyme-linked immunosorbent (ELISA) assay method used by other researchers [39, 40]. The results revealed that O_2 plasma allowed for the largest binding of rhBMP-2 (Fig. 7.5). The adsorption of rhBMP-2 allowed mouse OCT-1 osteoblast-like cells to better attach and spread on the scaffolds.

Khorasani et al. [41] studied the radio frequency (RF) oxygen plasma surface treatment of PLLA and PLGA used in nerve tissue engineering. Their water drop contact angle results showed a large increase in polymer hydrophilicity: 1 h of plasma treatment caused a decrease in contact angle from 85° to 10° for PLLA, and from 74.5° to 36.6° for PLGA. B65 nervous tissue cells showed much larger adhesion and growth both on PLLA and PLGA treated samples compare to the untreated ones (Fig. 7.6).

Demina et al. [42] investigated the effect of direct current (DC) discharge plasma modification on composite films made of chitosan, gelatin and PLLA (CGP). This composite has a homogenous bulk structure due to the strong molecular interactions between its components, and thus keeps its chemical and

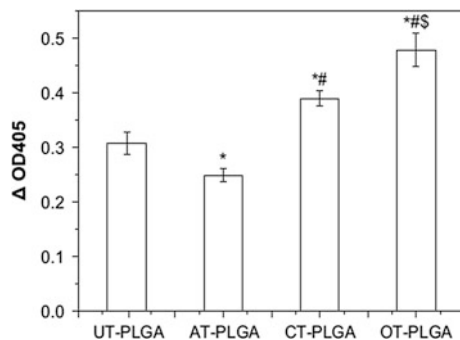


Fig. 7.5 Untreated (UT-PLGA), ammonia treated (AT-PLGA), CO₂ treated (CT-PLGA) and O₂ treated (OT-PLGA) PLGA films with a diameter of 7 mm were loaded with 100 ml rhBMP-2 solution (15 mg/ml) for 1 h. rhBMP-2 binding ability is shown here based on ELISA assay results. * $p < 0.05$ against UT-PLGA films; # $p < 0.05$ against AT-PLGA films; \\$ $p < 0.05$ against CT-PLGA films [38]

Fig. 7.6 B65 cell attachment on: (a) untreated PLGA; (b) O₂ plasma treated PLGA (magnification 400x) [41]

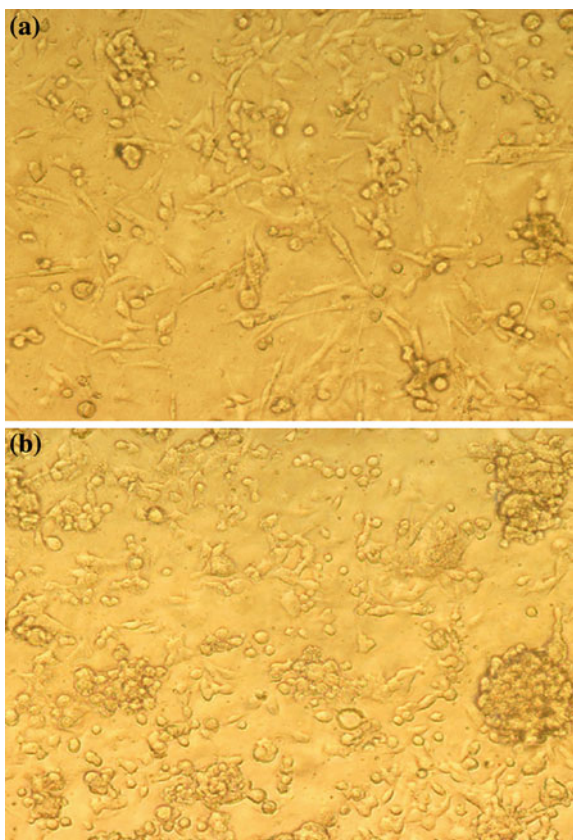
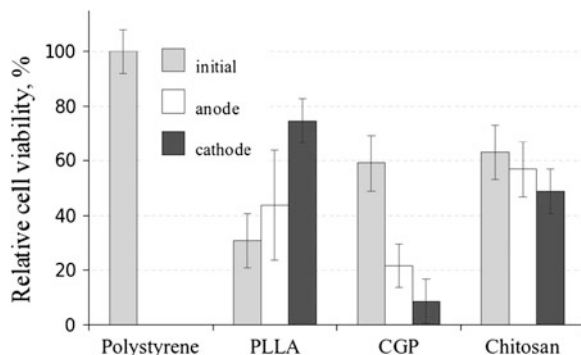


Fig. 7.7 Relative viability of L929 mouse fibroblasts cultured on the PLLA, CGP, and chitosan films for 1 week. Results of MTT-test expressed as mean \pm standard deviation for three replicates. Viability of the cells cultivated on polystyrene plates was used as a control (100 %) [42]



mechanical properties during in vivo degradation. To see the effect of DC discharge plasma treatment on CGP films, a set of samples was treated while connected to the anode side of the DC plasma, and another other set to the cathode. The same treatments were performed on PLLA and chitosan films. The water contact angle measurements showed more than 55° decrease from untreated to plasma-treated CGP samples. Mouse fibroblasts (L929) viability was tested on all the films. Cell viability decreased on CGP after plasma treatment, while it increased on treated PLLA samples (Fig. 7.7). This result indicated that while cell viability on PLLA was mainly affected by changes in wettability, which increased upon plasma treatment, other physicochemical properties such as surface morphology and charge affected cell viability on CGP samples. Differences in cell viability observed upon changes in surface morphology and charge was observed by other researchers as well [43, 44].

All these examples show why plasma treatments are becoming more and more common ways to modify the surface of polyesters and biomaterials in general: they allow changing surface properties without altering the bulk properties of the material, thereby offering a high degree of quality control, reliability and reproducibility that is difficult to achieve with other methods. The main drawback of plasma treatment is its difficulty in penetrating pores, which is a major obstacle when trying to modify the surface of 3D scaffolds [45–48].

7.3 Chemical Modifications

Similar to plasma treatment, chemical modifications have the goal of increasing the hydrophilicity of polyesters while generating surface reactive groups that can be used as anchors to immobilize biomacromolecules. In this section we will describe the two main avenues available for chemical modification of polyester scaffolds, i.e. wet chemistry or photochemistry.

7.3.1 Wet Chemistry Modifications

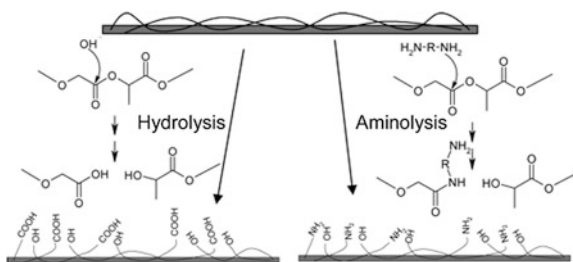
The two most commonly used and simplest wet chemical techniques to modify polyesters are aminolysis and alkali hydrolysis. In both cases, the abundant ester bonds are hydrolyzed, and either amide or carboxylate groups are formed, along with hydroxyl and primary or secondary amine functional groups [49, 50].

Alkali hydrolysis is performed by simply immersing the scaffolds in solutions of concentrated NaOH, for periods ranging from minutes [51] to hours [52]. This treatment leads to cleavage of the ester $-COO-$ bonds and formation of carboxyl and hydroxyl groups. Aminolysis is most commonly achieved by exposing the scaffolds to diamine solutions, which can react with the ester bonds and form amide bonds and amino groups. Both treatments are schematically shown in Fig. 7.8.

Aminolysis can be performed with reactants other than diamines. For example, PDLLA can be exposed to poly(ethyleneimine) [53], which leads to the formation of a surface containing a high density of positively charged secondary and tertiary amino groups that can be used as a starting point for further modification with negatively and positively charged biopolymers using the layer-by-layer assembly technique described in Sect. 7.4.4.

The introduction of carboxyl/hydroxyl and amino/amide groups on the scaffolds changes both their chemical properties and topography. Croll et al. [49] performed a thorough physico-chemical study of the changes in chemical properties of thin PLGA films upon both hydrolysis and aminolysis, and found that both treatments caused a decrease in advancing contact angle of approximately five degrees after few minutes of treatment; the decrease was faster for alkali hydrolysis. Major changes in surface topography and a large increase in surface roughness accompanied this modification, as shown in Fig. 7.9 [51]. Indeed, if aminolysis is performed for several hours on PLLA fibers, complete breakdown can occur, leading to the formation of irregularly shaped particles in the nano to micron size range [54]. Thapa et al. prepared a silastic mold to reproduce the nanofeatures obtained on PLGA films treated with NaOH, in an attempt to decouple to changes in chemical surface features and topography induced by the treatment. They found that the increase in nanometer roughness achieved with NaOH treatment was alone responsible for an increase in density of bladder smooth muscle cell attachment to

Fig. 7.8 Schematic representation of alkali hydrolysis and aminolysis to achieve functionalization of PLGA films adapted from [49]



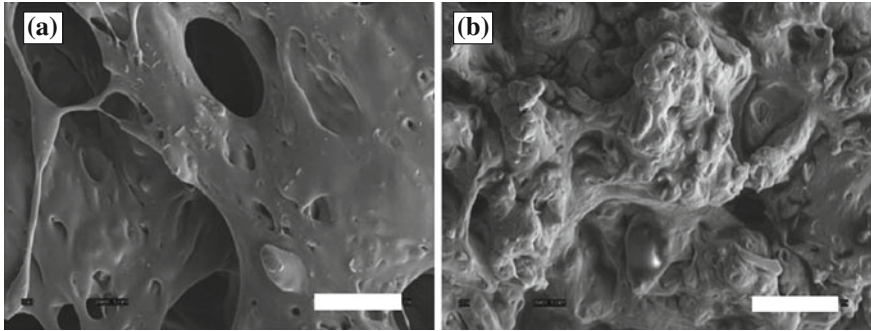


Fig. 7.9 SEM images showing increase in surface roughness upon NaOH treatment: PLGA porous films before (a), and after (b) 10 min exposure to 1 N NaOH. Scale bars are 10 μ m. Adapted from [51]

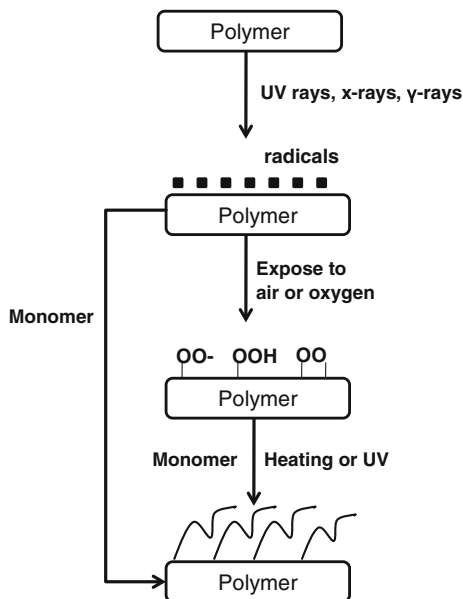
PLGA films [55]. This result shows the complexity of the changes occurring upon chemical treatments of polyester materials, and how hard it is to pinpoint the variables responsible for a specific biological response to the modified surfaces.

Although in most cases chemical modifications were performed on polymeric films, a few reports show examples of extension of this technique to 3D scaffolds [51, 52]. For example, Zhang et al. [56] extended the 2D immobilization of the Arg-Gly-Asp (RGD) peptide on film surfaces to 3D scaffold constructs on which amino functional groups were prior introduced with 1,6-hexanediamine. In a later study [57], they conjugated bone morphogenetic protein-2 (BMP-2) to 3D poly(ϵ -caprolactone) (PCL) scaffolds following aminolysis and demonstrated the effectiveness of this technique for surface modification versus simple adsorption. The group of Zhu et al. [58] took a similar approach to create functional groups in a first aminolysis step followed by grafting of fibronectin on poly(L-lactide-co-caprolactone) (PLLC) scaffolds for epithelium regeneration. 3D PLLA surfaces have also been chemically modified by hydrolysis. Hydrolyzed PLLA scaffolds rich in COOH and OH has been shown to promote hydroxyapatite formation after incubation in SBF [59]. When carrying out chemical surface modifications, reaction conditions must be properly controlled in order to maintain the inherent properties of the polymer and avoid accelerated degradation. Furthermore, thorough rinsing is necessary to remove excess reactants from the porous structure [18, 19].

7.3.2 Photochemical Modification

The photochemical strategy uses high-energy photons (ultraviolet (UV) rays, x-rays, γ -rays) to break chemical bonds and introduce initiators (free radicals) on the chemically inert surface of polyesters [18, 60]. Upon exposure of the free radicals to air or oxygen and in the presence of a monomer and heat or UV light, a

Fig. 7.10 Photochemical modification for graft copolymerization on polymer surface (Adapted from [19])



polymeric layer is grafted (Fig. 7.10). This technique has been often used to modify the surface of polyesters with polymers rich in reactive groups (for example, carboxylic groups in polyacrylic acids), which serve as anchors to subsequently bind biomolecules [61].

To create a biomimetic film for meniscus regeneration, poly(3-hydroxybutyrate-*co*-3-hydroxyvalerate) (PHBV), a polyester extracted from microorganisms, was photo-grafted with polyacrylamide, a spacer subsequently used for collagen immobilization [62]. In the first step, the amide-modified PHBV was generated by dipping the polymeric films into benzophenone and aqueous acrylamide solutions followed by UV lamp irradiation under nitrogen purge. In a second step, the films were functionalized with collagen, a main constituent of meniscal ECM, via the hydrophilic polyacrylamide spacers.

PHBV was similarly studied by Grondahl et al. [63] for grafting acrylic acid (AAc), this time using gamma irradiation. The extent of modification and introduction of carboxylic acid groups was controlled through adjustment of AAc concentration, thus avoiding a radiation dose that could have resulted in polymer degradation. The polymeric coating obtained was apt for subsequent covalent attachment of glucosamine.

The photochemical technique can also be applied for bulk modification. Shibata et al. [64], for instance, synthesized linear polyesters having pendant azido groups. They used UV irradiation to generate unstable nitrene radicals. These radicals then reacted with the surrounding polymer backbone and yielded cross-links. The reactive nitrene radicals could attack other chemical bonds as well (C–H, N–H and O–H), and be reduced to corresponding amines. Thus, the photo-crosslinking of

azidopolyesters occurred without the use of any photo- or radical-initiator. This technique established an important design strategy for advanced materials, since the azidopolyester can be used as a photolithography material.

Gamma irradiation was applied by Bat et al. [65] to cross-link trimethylene carbonate and d,l-lactide (co)polymers using pentaerythritol triacrylate as cross-linking agent. This is an effective and simple method to prepare form stable and creep resistant materials with low glass transition temperatures and tunable degradation properties.

Overall, photochemical modification is advantageous because of its low operation cost and mild reaction conditions compared to other chemical modification techniques [5]. In addition, the target species can be selectively immobilized at specific regions of the substrate [18]. The need for specialized equipment that provides an irradiation source is the inconvenience of this approach [66]. Furthermore, similar to wet chemical methods, high energy treatments can weaken the polymer's mechanical properties and accelerate degradation. These factors have so far limited the application of photochemical modification mostly to 2D substrates rather than 3D scaffolds [18].

7.4 Functionalization with Biomolecules

Functional groups such as carboxylates, hydroxyls, and amino groups are introduced on the surface of polyesters with plasma or chemical techniques not only to increase their hydrophilicity, but also to provide anchors to bind specific biomolecules that can improve the performance of the materials when implanted in the body. A few examples of biomolecules bound to polyesters were provided in Sects. 7.2 and 7.3. Here we describe more specifically the main techniques used to perform this step, and we give more examples showing the changes in biological properties upon functionalization.

7.4.1 Physical Adsorption

One of the most common methods for protein immobilization on a polymeric scaffold consists in immersing it in a solution containing the molecule of interest and simply allowing the molecule to physisorb on the material's surface [18]. ECM proteins like fibronectin, collagen, laminin, or molecules such as gelatin have often been coated on polymeric scaffolds with this technique, to make them more biomimetic [5, 67]. Since a protein layer may not form at all or be uneven and unstable if the protein solution is simply cast on a hydrophobic surface [66], polyesters are often treated with plasma or chemicals before contacting them with the protein-containing solutions.

7.4.1.1 ECM Protein Coating

Collagen, fibronectin and laminins are among the most commonly used proteins to modify the surface of scaffolds intended to be used for soft and hard tissue regeneration. Gamboa-Martínez et al. [68] prepared macroporous PLLA scaffolds and coated their walls with a thin network of fibrin, without any chemical or physical pretreatment. The scaffolds were simply evacuated and then exposed to a fibrinogen solution and later to a thrombin solution. The result was scaffolds coated with a network of fibrin fibrils (Fig. 7.11). This coating doubled the elastic modulus of the scaffolds (from 0.29 MPa for pure PLLA to 0.65 MPa for the coated scaffolds), and improved the uniformity of mouse pre-osteoblastic cells seeded on the scaffolds.

Zhang et al. [69] used a salt leaching method to construct PDLLA/biphasic calcium phosphate bone scaffolds. The applicability of this construct for drug delivery was then analyzed by coating the scaffold with the hydrophilic polymer poly(ethylene glycol) (PEG) and the antibiotic vancomycin. The surface modification of the scaffold with the mixed coating took place by simple adsorption, by immersing the scaffolds in a solution of PEG/antibiotic after evacuation. The drug on the scaffold surface was active as demonstrated by a standardized bacterial assay. *In vitro* drug release showed that the antibiotic release profile could be controlled by the concentration of the PEG solution used during the co-adsorption.

Another composite scaffold, in this case made from PCL and mesoporous bioactive glass (MBG) was developed by Yun et al. [70]. MBG is an attractive addition in scaffolds for hard tissue regeneration because it encourages hydroxyapatite (HA) growth, which is the mineral component of bone, when immersed in body fluid. However, the bioactive glass component induces local pH variations during its dissolution, which can result in inflammation *in vivo*. In this study, the MBG-PCL constructs were immersed in a solution of collagen and simulated body fluid (SBF) in an attempt to create a mixed coating of hydroxyapatite and collagen,

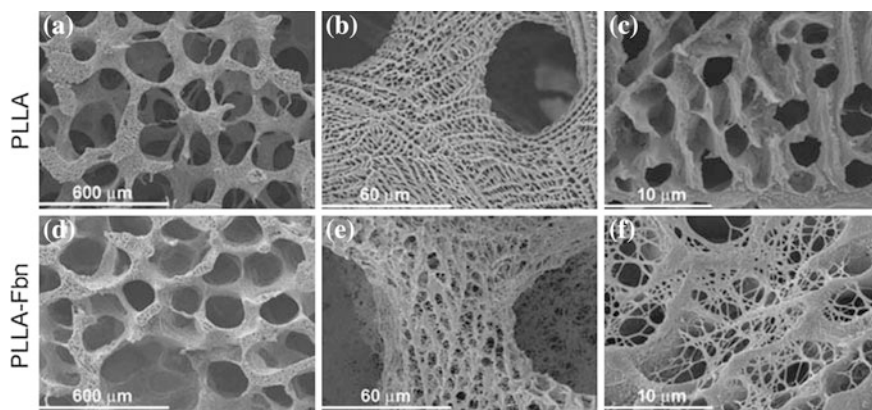


Fig. 7.11 SEM images of PLLA and fibrin coated PLLA scaffolds [68]

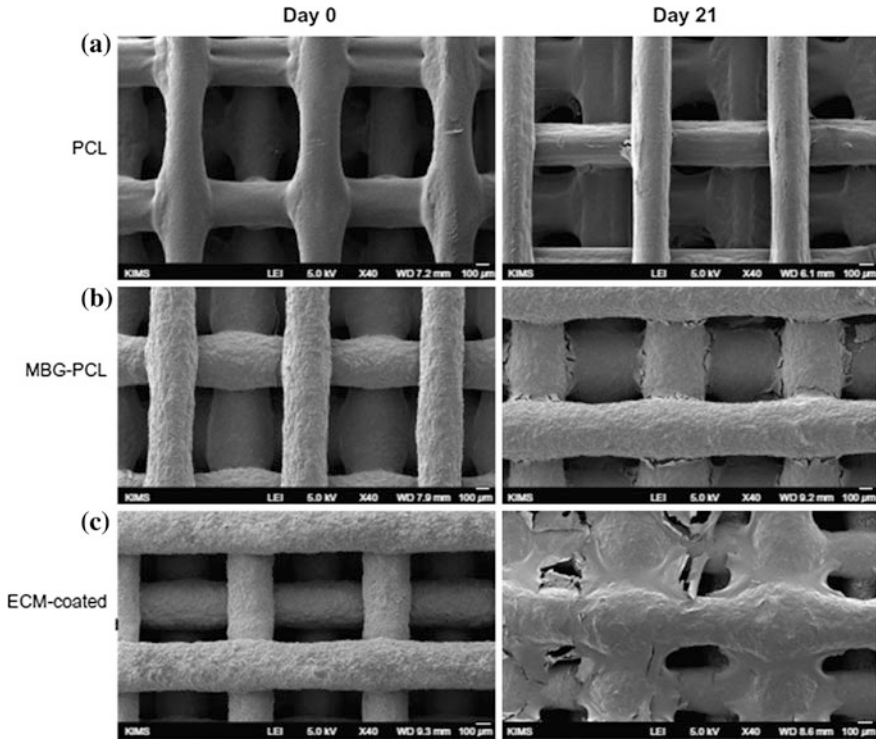


Fig. 7.12 Field emission SEM images of PCL, MBG-PCL, and ECM-coated PCL scaffolds (*left*), and same scaffolds after 21 days of MC3T2-E1 culture [70]

and eliminate the potential negative side effects of MBG. Both osteoblast attachment and mineralization were significantly improved after this adsorptive surface modification method (Fig. 7.12).

Finally, another study [71] employed a 100 μl poly(dopamine) solution as coating agent in an attempt to increase the cell affinity for synthetic polyester films such as PCL, PLLA, and PLGA. Although not an ECM protein, this coating was inspired by the repeated 3,4-dihydroxy-L-phenylalanine-lysine (DOPA-K) motif found in mussel adhesive proteins. The presence of the physisorbed poly(dopamine) coating increased chondrocyte adhesion 1.35–2.69-fold compared with the untreated substrates. The coating was then further extended to 3D polyurethane scaffolds with success.

7.4.1.2 Osteogenic Proteins

Several researchers have coated scaffolds for bone repair with BMP-2. A recent example was provided by Dupont et al. [72], who coated synthetic PCL cylindrical scaffolds with adeno-associated virus encoding BMP-2 to promote endogenous

bone repair. The researchers did not pretreat the scaffold surface before exposure to biomolecules; however they physically adsorbed both the biomimetic peptide GFOGER and collagen type I before adding particles of adenoassociated viral vectors encoding for BMP-2 (scAAV2.5-BMP2). Two sets of experiments were performed, with and without preseeding of human mesenchymal stem cells (hMSCs) on the scaffolds prior to implantation in rat femoral defects. The results showed more mineral formation on the scaffolds containing BMP after 12 weeks of implantation (Fig. 7.13). BMP2 scaffolds preseeded with hMSCs did not display significant differences of bone ingrowth in comparison with those containing no hMSCs. Overall, scaffolds coated with BMP2, whether preseeded with hMSCs or not, showed a significant increase of mineral formation and mechanical properties at all time points.

Another recent study [73] involved the direct physisorption of BMP2 on PLGA scaffolds either as-prepared or pre-coated with an hydroxyapatite layer by immersion in SBF. The osteogenic differentiation of hMSCs was then assessed on both the uncoated and hydroxyapatite-coated scaffolds. Mineralized scaffolds were

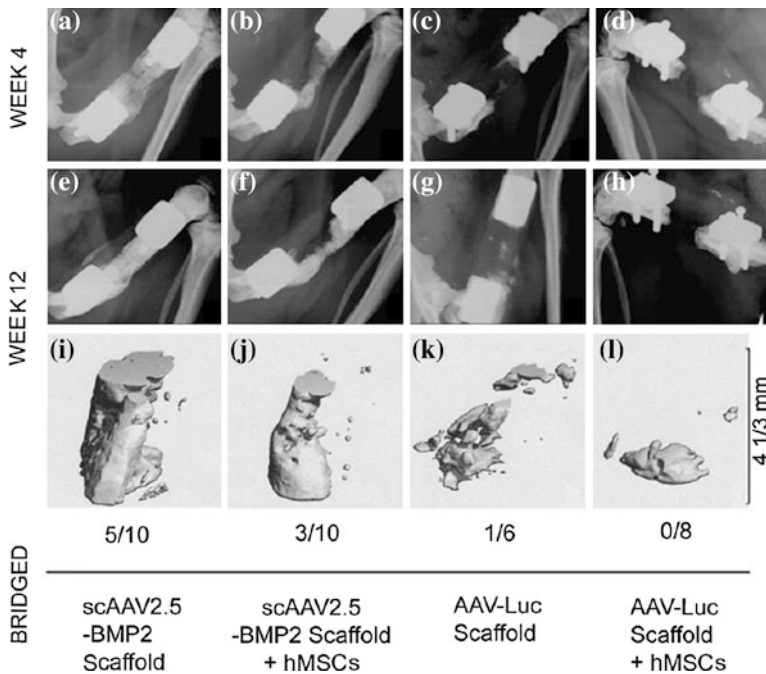


Fig. 7.13 Mineral formation post-mortem (12 weeks) on rat femoral defects, with scaffolds containing scAAV2.5-BMP2 particles, without (a, e, i) or with (b, f, j) the pre-seeding with hMSCs, compared with control samples coated with AAV-luciferase (AAV-Luc) without (c, g, k) or with (d, h, l) pre-seeding with hMSCs. Bony bridge formation was observed on 5/10 defects for scAAV2.5-BMP2 scaffolds, 3/10 for scAAV2.5-BMP2 scaffolds + hMSCs scaffolds, 1/6 defects for AAV-Luc scaffolds and 0/8 for AAV-Luc + hMSCs scaffolds [72]

more hydrophilic and adsorbed more BMP2. It was found that the hydroxyapatite/BMP2 combination enhanced the osteogenic response of hMSCs. Another example of the coating of polyester scaffolds with BMP2 is provided by Yanoso-Scholl et al. [74]. These authors coated PLLA scaffolds with beta-tricalcium phosphate (TCP), and then physisorbed on the PLLA/beta-TCP composites a mix of BMP2 and vascular endothelial growth factor (VEGF). Although the retention efficiency of the growth factors was suboptimal, a 1.8-fold increase in neo vessel formation was nevertheless observed in scaffolds containing the growth factors.

7.4.1.3 Limitations

Although these recent examples show successful enhancement of mechanical and biological properties of scaffolds coated with biomacromolecules (alone or in conjunction with pre-mineralization treatments), physical adsorption has its limitations. For example, the orientation of the adsorbed proteins is random and influenced by factors such as surface topography, charge, and wettability [75, 76]. In addition, the protein may lose its structural conformation upon adsorption [18]. Oriented immobilization of ECM proteins on the material's surface can overcome this challenge, and is thus the topic of the next section [77].

7.4.2 Covalent Immobilization

Covalent immobilization of biological molecules is an effective method to modify the surface properties of polymers controllably and permanently. Proteins can be covalently bonded by reacting their amino, carboxyl, hydroxyl and thiol functionalities with complementary reactive groups [18, 78]. Unlike physical adsorption, this approach allows oriented protein immobilization [78]. Though similar to coating, the chemically inert polymeric surface needs modification prior to biomolecule immobilization.

One of the most common methods to covalently immobilize biomolecules on polymer surfaces is to crosslink them using carbodiimides such as *N,N*-(3-Dimethylaminopropyl)-*N,N*-ethylcarbodiimide (EDC) [52, 79, 80]. These are referred to as zero length cross-linking agents because they form bonds without addition of other atoms or spacers [81]. In a recent example, Ghasemi-Mobarakeh et al. [52] covalently crosslinked a mix of ECM proteins found in basement membranes (collagen IV, fibronectin, heparin sulphate proteoglycans, AKA "matrigel") to PCL nanofibrous scaffolds. Before crosslinking, carboxylate groups were formed on PCL surfaces by alkaline hydrolysis. The importance of cross-linking was proved by characterizing nerve precursor cells (NPC) adhesion and proliferation on scaffolds that were built with PCL fibers, fibers treated with alkaline hydrolysis (PCL-H), fibers made by simple blending PCL with matrigel (PCL-B), and PCL fibers covalently modified with matrigel (PCL-F). The results

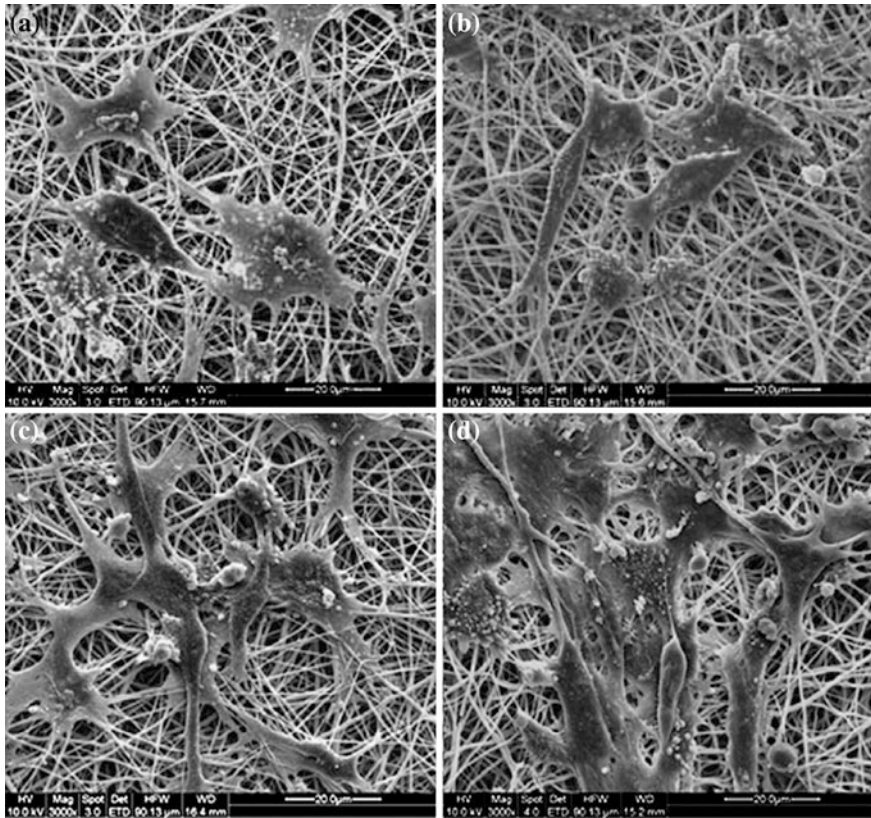


Fig. 7.14 SEM of NPC cultured for 4 days on PCL (A), PCL-H(B), PCL-B(C), and PCL-F(D) [52]

of the study showed that cells adhered and proliferated to a greater extent on fibers modified by covalent crosslinking, while simple blending was ineffective (Fig. 7.14).

EDC was used to covalently bind cationized gelatin (CG) gelatin to electrospun PLLA nanofibers (NF) also by Chen et al. [82]. In this case, surface carboxylation was achieved using a DC-pulsed plasma system [83]. The goal of this work was to prove the potential of this modified scaffold for cartilage tissue engineering. XPS characterization successfully confirmed CG binding to PLLA NF membranes (CG-PLLA NFMs). Rabbit articular chondrocytes showed enhanced viability, proliferation and differentiation on CG-PLLA NFMs. In-vivo tests in New Zealand white rabbits carried out with chondrocyte-seeded CG-PLLA NFMs showed only a small inflammatory reaction (Fig. 7.15). Also, the seeded chondrocytes maintained their ability to generate and secrete cartilage ECM markers after 4 weeks of in vivo culture, which confirmed the ability of CG-PLLA NFM to induce ectopic cartilage formation after long-term in vivo implantation.

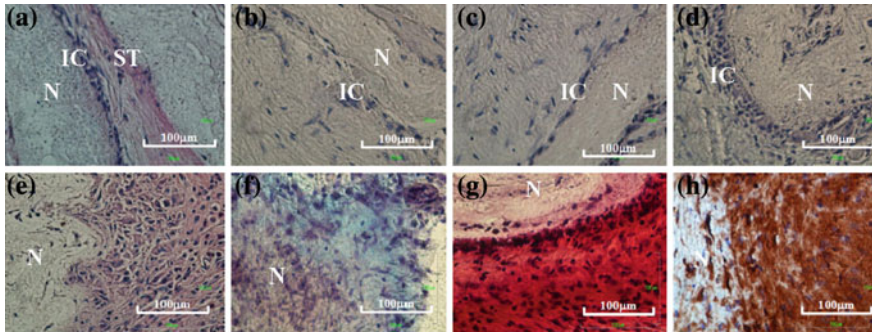
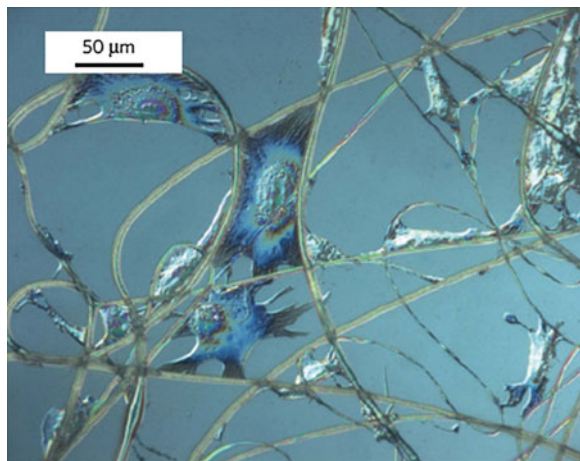


Fig. 7.15 Histological images of (a–d) control CG-PLLA NFM and (e–h) chondrocyte-seeded CG-PLLA NFM 4 weeks post-implantation. Sections were stained with H&E (a, e), Alcian blue (b, f) Safranin O (c, g), and immunohistochemically for collagen type II (d, h). *N* nanofiber; *IC* inflammatory cells; *ST* surrounding tissue. Bar 100 μm [82]

In a very recent example, Grafahrend et al. [84] covalently functionalized electrospun PLGA fibers with the cell-adhesion-mediating peptide sequence Gly-Arg-Gly-Asp-Ser (GRGDS). Covalent crosslinking was not performed directly on PLGA, but on the additive star-shaped poly(ethylene oxide-stat-propylene oxide) containing isocyanate end groups (NCO-sP(EO-stat-PO)), which was mixed with PLGA during electrospinning. Isocyanate end groups allowed for covalent binding with amino groups from GRGDS, and the resulting fibers had several advantages over plain PLGA because they were hydrophilic and resisted non-specific protein adsorption thanks to the presence of sP(EO-stat-PO), and able to support cell adhesion and proliferation because of the presence of the RGD domain in the GRGDS peptide. Indeed, human fibroblast cells did not adhere on scaffolds composed by just PLGA and sP(EO-stat-PO), while thrived on those covalently modified with GRGDS (Fig. 7.16).

Fig. 7.16 Optical microscope image of human dermal fibroblasts after 24 h in cell culture on GRGDS-functionalized PLGA/sP(EO-stat-PO) fibers [84]



Covalent immobilization has been tested also to bind inorganic particles to polyester scaffolds. Koo et al. [85] first introduced carboxylate groups on a PLLA scaffolds by chemical modification (treatment in NaOH); then they aminated the surface using ethylenediamine (EDA), covalently bound to the carboxylate groups through EDC coupling. Nanohydroxyapatite (N-HAp) was modified with ethylene glycol methacrylate phosphate (EGMP), and the phosphonate groups on N-HAp could be crosslinked with the amino groups on the PLLA surface again with the use of EDC (Fig. 7.17). Using XPS, the authors showed a higher surface Ca atomic ratio (4.6 %) when N-HAp was surface immobilized on the scaffolds rather than bulk-mixed (0.4 %). The covalently immobilized N-HAp provides a favorable environment for enhanced *in vivo* bone tissue growth in comparison to the unmodified and N-HAp bulk-modified surfaces. The phosphonic acid groups on the immobilized N-HAp surface could also provide opportunities for functionalization with other biomolecules.

Wu et al. [86] even used covalent immobilization as a means to create a stable gelatin gradient on the surface of PLLA scaffolds in order to obtain a continuous increment of signaling for chondrocytes adhesion and viability. To aminolyze the PLLA surface, 1,6-hexanediamine/propanol solution was continuously injected by a micropump into a glass vial where the scaffold stood vertically fixed (Fig. 7.18). The reaction time difference along the longitude of the PLLA scaffold resulted in an increase of $-NH_2$ groups from the bottom upward, thus enabling a graded coupling with gelatin.

One of the challenges of covalent biomolecule immobilization on polymeric surfaces is that chemicals and crosslinkers can result in the loss of the protein's natural conformation [66]. Furthermore, the complex architecture of the scaffold surface and buried ligand sites may lead to below optimal cell-receptor

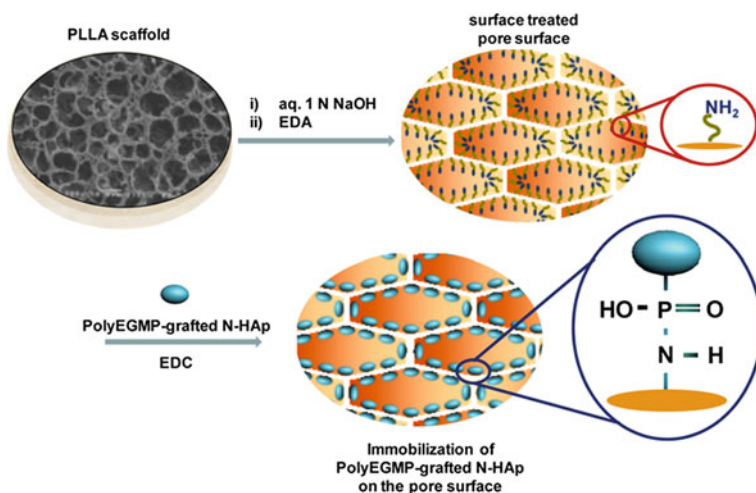
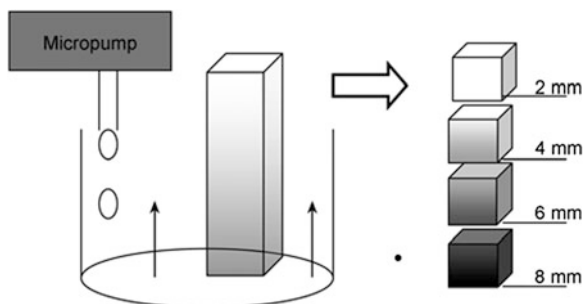


Fig. 7.17 Surface immobilization of N-HAp on PLLA scaffolds [85]

Fig. 7.18 Creation of an amino gradient along the surface of PLLA scaffold [86]



interactions [18]. This technique is nevertheless effective and surface immobilized proteins can be quantified [87].

7.4.3 Entrapment

Entrapment was first introduced by Desai and Hubbell as a non-covalent but stable technique to modify polyester surfaces with biomacromolecules [88]. The two-step method first involves swelling the polymer in a mixture of solvent and non-solvent of the polymer, containing the molecules. A gel-like layer then forms on the surface of the polymer, within which proteins diffuse. These proteins are then “entrapped” in the gel through immersion of the polymer in a pure non-solvent (Fig. 7.19) [89].

Different molecules have been confined in polyester films or scaffolds through entrapment. In one of the earliest examples, Quirk et al. modified PLLA films with both PEG and a cell adhesive peptide conjugate poly(L-lysine)-RGD (PLL-RGD). Their results showed that bovine aortal endothelial cell adhesion was drastically decreased in the presence of PEG alone, due to the suppression of non-specific protein adsorption on the PLLA surface, while the entrapment of both PEG and PLL-RGD allowed cells to adhere on the PLLA [89].

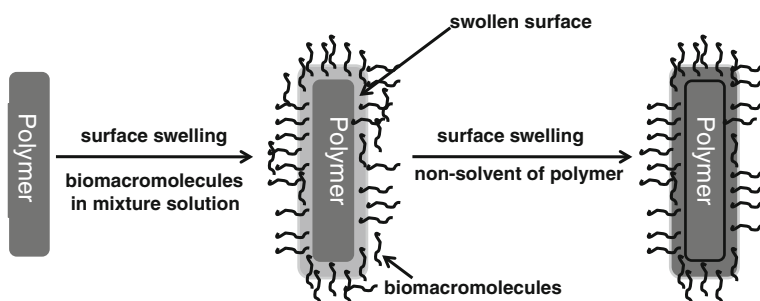


Fig. 7.19 Surface modification by entrapment (adapted from [5])

Another early work using entrapment is that by Liu et al. [90], who modified PDLLA films with baicalin, a flavonoid compound purified from the herbal medicinal plant *Scutellaria baicalensis Georgi*, known for its antioxidant and anti-inflammatory properties. The entrapment procedure consists of (1) firstly immersing the polymer film in an acetone/water mixture (solvent/nonsolvent), (2) exposing the film to the baicalin solution, and finally (3) rinsing with distilled water and phosphate buffered saline (PBS). The behavior of osteoblasts on the modified films was then compared with controls. The results of MTT assay and alkaline phosphatase activity reveal higher cell attachment, greater cell proliferation and viability, and an overall improvement in biocompatibility for the surface-modified PDLLA.

Recently, a similar entrapment of PEG on PDLLA nanofibrous mats prepared by electrospinning was reported by Xie et al. [54]. Water contact angles before and after entrapment indicated an increase in the hydrophilicity of the surface of the mats. In this case, although PEG was the sole entrapped species, an improvement in biocompatibility after surface modification was visible following canine fibroblast cell seeding and cell viability tests by MTT assay.

In another recent study, Duan et al. [91] designed 3D composite scaffolds for bone tissue engineering from calcium phosphate (Ca-P) nanoparticles and PHBV. Selective laser sintering (SLS), which is a form of rapid prototyping technique, was used to create the structures. The high crystallinity of PHBV makes it such that the overall surface is hydrophobic, impairing cell affinity and weakening cell-scaffold interactions. Gelatin was therefore physically entrapped in the scaffold to increase its hydrophilicity. A decrease in contact angle proved the efficacy of the modification. At the same time, the entrapment did not affect surface morphology and mechanical properties, as demonstrated by SEM analysis (Fig. 7.20) and compression tests, respectively.

Entrapment is thus a commonly used method for protein immobilization, where the amount of entrapped biomolecules can be controlled through adjustment of solvent composition and reaction time [18, 91]. Limitations of the technique include random orientation and over-crowding of the proteins [76].

7.4.4 Self-Assembly

The most common technique that exploits molecular self-assembly for surface modification is layer-by-layer self-assembly. This consists of alternate depositions of oppositely charged polyanions and polycations on the polymer surface (Fig. 7.21) [92, 93]. Prior to the multilayer build-up, initial charges are usually introduced on the substrate. The thickness and charge of the assembly can be precisely controlled. Additionally, the nature of polyelectrolytes, pH, and ionic strength of the deposition solutions are adjustable and affect both the physical and chemical properties of the coating [92].

Fig. 7.20 SEM images of Ca–P/PHBV scaffold surface before (a) and after (b) gelatin entrapment [91]

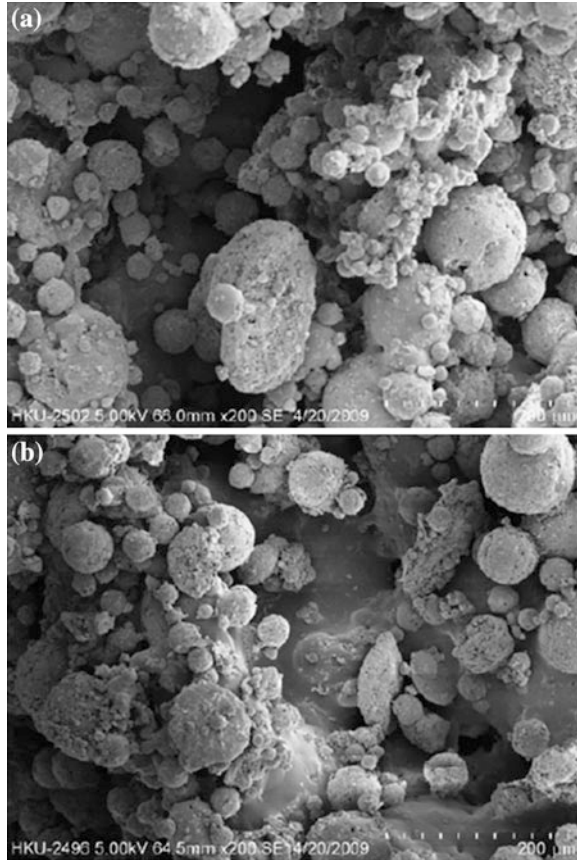
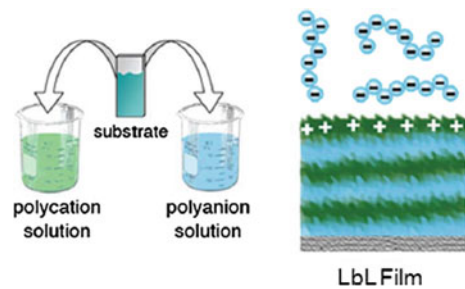


Fig. 7.21 Constructing layer by layer film by adsorption of positively and negatively charged species [93]



Layer-by-layer assembly has been used by several authors to coat polyester films or scaffolds with ECM proteins or other naturally occurring polypeptides. Most commonly, positively charged polypeptides are deposited in alternating layers with negatively charged polyelectrolytes such as poly(styrene sulfonate) (PSS) [94, 95].

Li et al. [94] used layer-by-layer deposition to coat electrospun PCL scaffolds with gelatin. The deposition started with the immersion of the PCL scaffolds for 20 min in a 2 mg/mL gelatin solution in 20 mM acetic buffer. This was followed by rinsing the matrix with water and dipping for another 20 min in a 3 mg/mL PSS sodium salt solution in 20 mM acetic buffer. The aforementioned process was repeated to reach the desired number of layers. When the gelatin-surface modified scaffolds were mineralized in SBF, a drastically higher amount of bonelike calcium phosphate was deposited on their surface. The incorporation of gelatin thus promoted nucleation and growth of calcium phosphate. The authors also showed that MC3T3-E1 preosteoblastic cells adhered and spread to a greater extent on the mineralized scaffolds compared to the pure PCL scaffolds (Fig. 7.22).

A different kind of self-assembly strategy was adopted by Stendahl et al. [96] for PLLA fiber surface modification. The authors synthesized a triblock molecule containing cholesterol, an oligomer of L-lactic acid, and lysine moieties (Fig. 7.23). The cholesterol and oligo-lactic acid segments are hydrophobic, and thus have an affinity for PLLA, while the hydrophilic dendron is displayed on the outer surface upon self-assembly. Cholesterol has the added advantages of

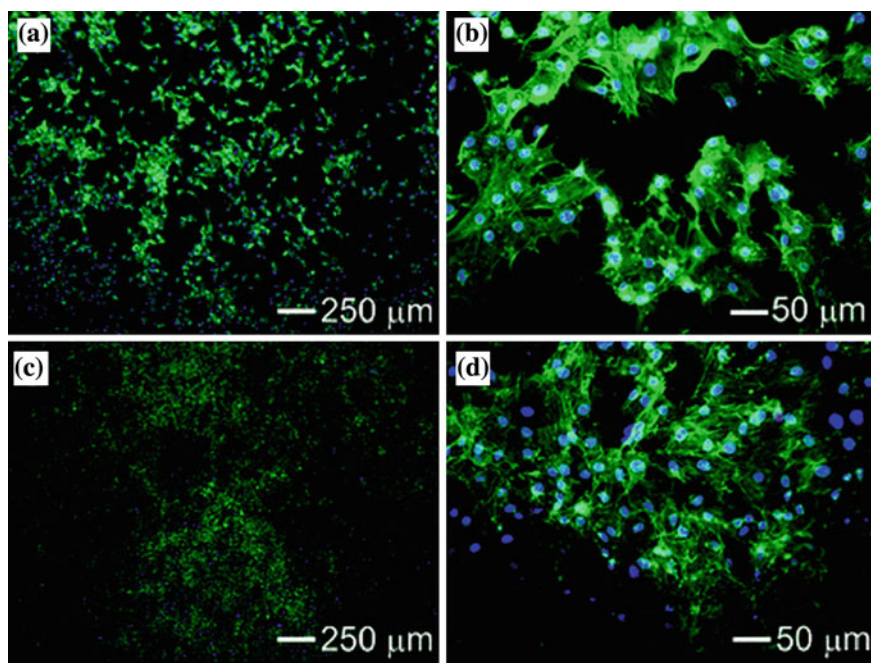


Fig. 7.22 Fluorescence micrographs of MC3T3-E1 cells cultured for 7 days on (a, b) membranes of electrospun PCL fibers and (c, d) membranes of electrospun PCL fibers coated with gelatin and then calcium phosphate. The F-actin was stained with fluorescein isothiocyanate-phalloidin (green color), while the cell nucleus was stained with 4'-6-diamidino-2-phenylindole (DAPI) (purple color) [94]

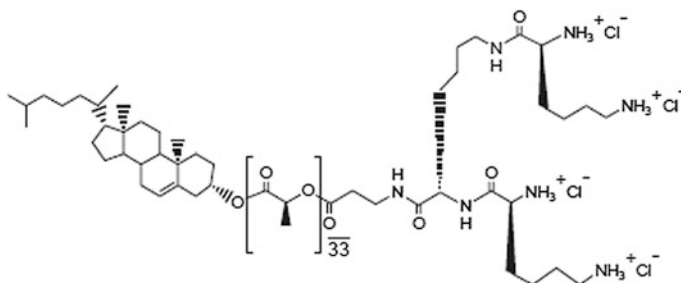


Fig. 7.23 The amphiphilic triblock molecule made from a rigid cholesterol segment, a flexible oligomer of L-lactic acid, and an L-lysine dendron used to modify PLLA scaffold fibers [96]

generating ordered layers on PLLA, and having a strong affinity to plasma membranes. The study showed that the ordered self-assembled layer formed on PLLA resulted in biomaterials that were more biocompatible. Indeed, both the adhesion and proliferation of 3T3 mouse calvaria cells was enhanced on the surface modified structures.

Self-assembly is a simple and conceptually intriguing technique, since it exploits the chemical properties of biomolecules to generate truly “bottom-up” structures. The structures are stable without the need for extra cross-linkers, and therefore this method can be applied not only to modify material surfaces, but also to create bulk structures that include biological functionalities [97].

7.5 Conclusions and Perspective

In this chapter we have shown that many different techniques can be used to modify the surface of polyesters for biomedical applications. Such modifications are necessary in order to make the materials suitable for interactions with cells and implantation. Indeed, polyesters are hydrophobic materials, which might attract unwanted proteins on their surface if implanted as they are. Also, since they do not have any biological activity, they cannot provoke a specific reaction in the surrounding tissue. Therefore, although biodegradable and bioresorbable in most cases, in a certain sense these materials should be compared to *bioinert* materials. Altering their surface properties and binding biological molecules on their surface allows them to overcome this limitation.

Table 7.1 summarizes the biomolecules bound to 2D or 3D polyester scaffolds discussed in this chapter. As we can see, many examples relate to proteins found in the ECM. Synthetic polyesters are used as scaffolds to simulate the organic matrix on which osteoblasts lay down hydroxyapatite (for bone tissue engineering), or chondrocytes, fibroblasts or endothelial cells start building soft tissue (for cartilage and skin engineering). ECM proteins therefore can be used to make the scaffolds *biomimetic*, and imitate the physiological matrix that cells meet in the body, thus promoting their attachment and spreading. Other examples related to proteins

Table 7.1 Summary of the biomolecules bound to polyester 2D or 3D scaffolds reviewed in this chapter. The table highlights the technique used for immobilization and the application studied in each work

Class	Specific example	Primary surface modification	Secondary binding step	Obtained better attachment/ spreading/functions for	Matrix	Ref.	
ECM proteins	Collagen	NH ₃ plasma	Physisorption	Fibroblasts	2D	[32]	
		Photochemical grafting of polyacrylamide	Covalent coupling	Chondrocytes	2D	[62]	
	Mix of ECM proteins (matrigel)	None	Physisorption		Osteoblasts	2D, 3D	[70]
		Hydrolysis	Covalent coupling		Nerve precursor cells	2D	[52]
		DC plasma	Covalent coupling		Chondrocytes	2D	[83]
		Aminolysis	Covalent coupling		Chondrocytes	2D	[86]
	Bioactive proteins or peptides	Fibronectin	None	Entrapment	Fibroblasts	2D	[91]
			None	Layer-by-layer assembly	Preosteoblastic cells	3D	[94]
		Fibrin	Aminolysis	Covalent coupling	Epithelial cells	2D	[58]
		Basic fibroblast growth factor (bFGF)	None	Physisorption	Preosteoblastic cells	2D	[68]
Bone morphogenetic protein-2 (BMP-2)		CO ₂ plasma	Physisorption	Fibroblasts	2D	[37]	
		Various plasmas	Physisorption	Osteoblasts	2D	[38]	
Drugs or drug-like compounds	RGD-containing molecules	Aminolysis	Covalent coupling	Chondrocytes	2D	[57]	
		None or apatite coating	Physisorption	Mesenchymal stem cells	3D	[73]	
		Physorption of collagen and GFOGER	Physisorption	In-vivo bone formation	3D	[70]	
		Coating with TCP	Physisorption	Chondrocytes	2D	[74]	
	Poly(dopamine)	Alkaline hydrolysis	Covalent coupling	Nerve precursor cells	3D	[56]	
		Formation of isocyanate groups on polymer mixed with PLGA	Covalent coupling	Fibroblasts	3D	[84]	
	Glycosamine compounds	None	Entrapment		Endothelial cells	3D	[89]
		None	Physisorption		Chondrocytes	2D, 3D	[71]
		Photochemical grafting of polyacrylic acids	Covalent coupling		None	2D	[63]
		None	Physisorption		Osteoblasts (no detrimental effect observed)	3D	[69]
Baicalin	None	Entrapment		Osteoblasts	3D	[90]	

belonging to the extended family of growth factors. Incorporating these molecules on the surface of a polymeric scaffold makes it *bioactive*: the molecules are able to elicit specific functions in the cells that adhere on the substrates, and improve the success of the implant. Finally, the last few examples listed in the table relate to the binding of drugs. In this case, the overall goal is to achieve controlled release of these substances. Binding the drugs to a biodegradable scaffold surface allows for a controlled local delivery, since the scaffold is to be implanted at the site where the drug needs to be delivered. In this case, we could say that the scaffolds are transformed into *local delivery vectors*.

Table 7.1 also shows the techniques used to bind the biomolecules to the polymeric surfaces. Pros and cons of these methods as well as all those presented in this chapter are summarized in Table 7.2.

By looking at Table 7.1, we can observe that the most prevalent methods used for biomolecule attachment are physisorption and covalent binding, which are also the simplest methods to (a) achieve a continuous coverage (in the case of physisorption) and (b) control the orientation of the molecules bound to the polymer surface (in the case of covalent binding) (see Table 7.2). Both methods require a preliminary surface modification step, i.e. introducing anchoring groups that the biomolecules will interact with or will be crosslinked to. As shown in Table 7.2, there is no ideal preliminary surface modification technique. Methods explored so far are either limited mostly to 2D film modification (plasma and photochemical treatment) or, if they allow for 3D modification, they tend to degrade the polymeric bulk structure (chemical treatment based on hydrolysis or aminolysis). Since 3D and not 2D structures are mainly implanted *in vivo*, there is clearly a strong need to find a new way to improve the preliminary surface modification step. We recently showed a different type of chemical modification based on diazonium salts. This method allowed us to generate anchoring groups on a PDLLA 3D scaffold without modifying its bulk structure. The amino groups introduced with this technique were used to covalently bind phosphonate-containing molecules without the use of crosslinkers, which improved scaffold mineralization when immersed in SBF [98].

The second step of the functionalization, i.e. the biomolecule attachment, could be improved as well. Even covalent binding, despite offering a better control of protein orientation compared to simple physisorption, cannot always ensure that the protein will maintain its natural configuration. In fact, covalent bonding works with crosslinkers that can bind to any amino, carboxylates, or thiol groups present in the protein. Since there are many of them, the protein can end up being bound in different ways depending on which of the groups react more easily, or in a more open configuration than in its natural state. Although not ideal, in some cases this could be an advantage, especially for bone tissue engineering—in fact, the same phenomenon happens when proteins interact with the ECM. It is well known that the same proteins (e.g. osteopontin) are able to inhibit mineralization when in solution, while promote it when bound to the ECM [99]. In view of this, one could consider modifying scaffold surfaces not necessarily with the physiological biomolecules, but with synthetic analogues that are designed to mimic the density and

Table 7.2 Summary of advantages and disadvantages of techniques used for primary surface modification and for biomolecule immobilization on polyester-based biomaterials

Type of surface modification	Technique	Advantages	Disadvantages
Preliminary surface modification step	Plasma coating	Does not alter bulk properties of material Reproducible Can be used to increase hydrophilicity Can generate surface groups to be used for further modification	Cannot easily penetrate inside pores Mostly limited to 2D substrates
	Hydrolysis and aminolysis	Can be used to increase hydrophilicity Can be used to change surface morphology Can generate surface groups to be used for further modification	Degrades polymeric matrix
	Photochemical modification	Can modify 3D scaffolds Can be used to graft polymers that are suitable for further modification Possibility of photolithography and controlled attachment	Material damage if too high radiation is used Need for specialized equipment
Biomolecule immobilization	Physical adsorption	Easiness Applicable to any biomolecule	Mostly limited to 2D substrates Random protein orientation Proteins may lose their conformation Bond is not very stable
	Covalent immobilization	Stable bonds formed Allows oriented protein immobilization	Protein may lose native conformation Active sites may be buried inside the scaffold
	Entrapment	Easiness Applicable to any biomolecule	Random protein orientation Possible overcrowding
	Self-assembly	Easiness (in the layer-by-layer approach)	May need to construct molecules from scratch to induce self-assembly
		Does not require crosslinkers Possibility of oriented protein immobilization	

spacing of important functional sites present on the natural proteins when they are bound to the ECM. Several researchers have worked on understanding the amount and density of negatively charged amino acids in the structure of proteins involved in bone mineralization [99]. A recent study showed that by controlling the density of hydroxyl and carboxylate groups on a hydrogel, a hydroxyapatite-like layer could be easily produced when the hydrogels were immersed in Ca and P-containing solutions [100]. If a similar strategy was applied to modify the surface of a scaffold with the correct density of functional groups, one could obtain a biomaterial able to improve mineralization without using natural proteins. Such controlled density could be obtained using photolithography, or by covalent binding of small molecules containing the groups of interest, e.g. amino acids.

Possibly a similar method could be used to mimic more complex functions of natural proteins, and not only their ability to induce mineralization. Binding small peptides mimicking the active sites of natural proteins goes in this direction. Most of the work done so far in this respect involves binding peptides containing the cell adhesive RGD sequence. Still, active peptides other than RGD have been recently discovered. For example, D'Andrea et al. [101] found a short peptide part of VEGF responsible for its activity. Leslie-Barbick et al. [102] then bound this peptide to PEG hydrogels, and found that it was able to promote vascularization better than the whole VEGF, most likely because it suffered less from steric hindrance from the hydrogel. Peptides are much easier to bind to scaffold surfaces with the correct orientation than the whole growth factor, they are stable in harsher solvents, which implies that they could be incorporated in synthetic scaffolds even during their preparation, and are definitely less expensive. For all these reasons, we predict that in the near future many more researchers will work on binding small peptides rather than the complete biomolecules to polyester-based scaffolds.

As a final remark, we would like to point out that all the work described in this chapter on surface functionalization of polyester scaffolds aims at making materials that are able to better communicate with the body, by exposing signaling molecules able to elicit a specific response. However, true communication can be achieved only if the scaffolds were able to not only talk the same language of the body, but also listen to its response. The next generation of scaffolds and biomaterials will have both functional groups bound to their surfaces able to provide correct signals, and sensors able to track changes in physiological variables. Ideally, scaffolds should be able to dynamically respond to these changes, for example by releasing drugs on demand. A scaffold that was at the same time biomimetic, bioactive, local delivery vector, and able to sense physiological changes could cause a real paradigm shift in tissue engineering.

References

1. Sipe, J.D., Tissue engineering and reparative medicine. *Reparative Medicine: Growing Tissues and Organs*, 961 (2002)

2. Hench, L.L.: *Biomaterials. Science* **208**, 4446 (1980)
3. Castner, D.G., Ratner, B.D.: *Biomedical surface science: Foundations to frontiers. Surf. Sci.* **500**(1–3), 28–60 (2002)
4. Kim, S.-H., Turnbull, J., Guimond, S.: *Extracellular matrix and cell signalling: the dynamic cooperation of integrin, proteoglycan and growth factor receptor. J. Endocrinol.* **209**, 2 (2011)
5. Jiao, Y.P., Cui, F.Z.: *Surface modification of polyester biomaterials for tissue engineering. Biomed. Mater.* **2**(4), R24–R37 (2007)
6. Zeb, G., et al.: *Decoration of graphitic surfaces with Sn nanoparticles through surface functionalization using diazonium chemistry. Langmuir* **1**, 13042–13050 (2012)
7. Sabir, M., Xu, X., Li, L.: *A review on biodegradable polymeric materials for bone tissue engineering applications. J. Mater. Sci.* **44**(21), 5713–5724 (2009)
8. Metcalfe, A.D., Ferguson, M.W.J.: *Tissue engineering of replacement skin: the crossroads of biomaterials, wound healing, embryonic development, stem cells and regeneration. J. Roy. Soc. Interf.* **4**, 14 (2007)
9. Aragon, J., et al.: *Development and characterization of a novel bioresorbable and bioactive biomaterial based on polyvinyl acetate, calcium carbonate and coralline hydroxyapatite. Mater. Res. -Ibero-Am. J. Mater.* **14**, 1 (2011)
10. Le Guehennec, L., Layrolle, P., Daculsi, G.: *A review of bioceramics and fibrin sealant. Eur. Cells Mater.* **8**, 1–11 (2004)
11. Dhandayuthapani, B., et al.: *Polymeric scaffolds in tissue engineering application: A review. Int. J. Polymer Sci.* **2011**, 1–19 (2011)
12. Thomson, R.C., et al.: *Biodegradable polymer scaffolds to regenerate organs. Biopolymers* **122**, 245–274 (1995)
13. Cheung, H.-Y., et al.: *A critical review on polymer-based bio-engineered materials for scaffold development. Compos. B-Eng.* **38**, 3 (2007)
14. Seal, B.L., Otero, T.C., Panitch, A.: *Polymeric biomaterials for tissue and organ regeneration. Mater. Sci. Eng. R-Reports* **34**, 4–5 (2001)
15. Gunatillake, P.A., Adhikari, R.: *Biodegradable synthetic polymers for tissue engineering. Eur. Cells Mater.* **5**, 1–16 (2003)
16. Wang, S.G., Cui, W.J., Bei, J.Z.: *Bulk and surface modifications of polylactide. Anal. Bioanal. Chem.* **381**(3), 547–556 (2005)
17. Lin Y et al (2006) *Surface modification of poly (L-lactic acid) to improve its cytocompatibility via assembly of polyelectrolytes and gelatin. Acta Biomater* **2**(2):155–164
18. Vasita, R., Shanmugam, I.K., Katt, D.S.: *Improved biomaterials for tissue engineering applications: Surface modification of polymers. Curr. Top. Med. Chem.* **8**(4), 341–353 (2008)
19. Ma, Z.W., Mao, Z.W., Gao, C.Y.: *Surface modification and property analysis of biomedical polymers used for tissue engineering. Colloids Surf. B-Biointerf.* **60**(2), 137–157 (2007)
20. Jacobs, T., et al.: *Plasma surface modification of biomedical polymers: Influence on cell-material interaction. Plasma Chem. Plasma Process.* **32**(5), 1039–1073 (2012)
21. Ratner, B.D.: *Plasma deposition for biomedical applications—a brief review. J. Biomater. Sci. Polymer Edn.* **4**(1), 3–11 (1992)
22. Urano, Y., et al.: *Production of 1-m size uniform plasma by modified magnetron-typed RF discharge with a subsidiary electrode for resonance. Thin Solid Films* **316**, 1–2 (1998)
23. Raizer, Y.P.: *J. Atmos. Terr. Phys.* **55**(10), 1487 (1993). (Gas discharge physics: 1991, p. 449. Springer. Heidelberg, DM 148.00 hb, ISBN 3-540-19462-2)
24. Ohl, A., Schroder, K.: *Plasma-induced chemical micropatterning for cell culturing applications: a brief review. Surf. Coat. Technol.* **116**, 820–830 (1999)
25. Boxman, R.L., Goldsmith, S., Greenwood, A.: *Twenty-five years of progress in vacuum arc research and utilization. IEEE Trans. Plasma Sci.* **25**(6), 1174–1186 (1997)
26. Yushkov, G.Y., et al.: *Effect of multiple current spikes on the enhancement of ion charge states of vacuum arc plasmas. J. Appl. Phys.* **87**(12), 8345–8350 (2000)

27. Oks, E.M., Yushkov, G.Y., Anders, A.: A summary of recent experimental research on ion energy and charge states of pulsed vacuum arcs. 23rd international symposium on discharges and electrical insulation in vacuum, 2008. ISDEIV 2008
28. Amoruso, S., et al.: Characterization of laser-ablation plasmas. *J. Phys. B-Atomic Molecular Opt. Phys.* **32**(14), R131–R172 (1999)
29. Chan, C.M., Ko, T.M., Hiraoka, H.: Polymer surface modification by plasmas and photons. *Surf. Sci. Rep.* **24**(1–2), 3–54 (1996)
30. Inagaki, N., *Plasma Surface Modification and Plasma Polymerization*. Pennsylvania, Technomic Publishing Company, Inc (1996)
31. Chu, P.K., et al.: Plasma immersion ion implantation, Aña fledgling technique for semiconductor processing. *Mater. Sci. Eng. R: Reports* **17**(6–7), 207–280 (1996)
32. Yang, J., Bei, J.Z., Wang, S.G.: Enhanced cell affinity of poly (D, L-lactide) by combining plasma treatment with collagen anchorage. *Biomaterials* **23**, 12 (2002)
33. Kiaei, D., Hoffman, A.S., Horbett, T.A.: Tight-binding of albumin to glow-discharge treated polymers. *J. Biomater. Sci. Polymer Edn* **4**, 1 (1992)
34. Garfinkle, A.M., et al.: Effects of a tetrafluoro ethylene glow-discharge on patency of small diameter dacron vascular grafts. *Trans. Am. Soc. Artif. Inter. Organs* **30**, 169 (1984)
35. Gombotz, W.R., Hoffman, A.S.: Gas-discharge techniques for biomaterial modification. *CRC Crit. Rev. Biocompat.* **4**, 1 (1987)
36. Bazaka, K., et al.: Plasma-assisted surface modification of organic biopolymers to prevent bacterial attachment. *Acta Biomater.* **7**(5), 2015–2028 (2011)
37. Shen, H., et al.: The immobilization of basic fibroblast growth factor on plasma-treated poly(lactide-co-glycolide). *Biomaterials* **29**, 15 (2008)
38. Shen, H., et al.: The bioactivity of rhBMP-2 immobilized poly(lactide-co-glycolide) scaffolds. *Biomaterials* **30**, 18 (2009)
39. Chen, B., et al.: Homogeneous osteogenesis and bone regeneration by demineralized bone matrix loading with collagen-targeting bone morphogenetic protein-2. *Biomaterials* **28**, 6 (2007)
40. Han, B., et al.: Collagen-targeted BMP3 fusion proteins arrayed on collagen matrices or porous ceramics impregnated with Type I collagen enhance osteogenesis in a rat cranial defect model. *J. Orthopaedic Res.* **20**, 4 (2002)
41. Khorasani, M.T., Mirzadeh, H., Irani, S.: Plasma surface modification of poly (L-lactic acid) and poly (lactic-co-glycolic acid) films for improvement of nerve cells adhesion. *Radiat. Phys. Chem.* **77**, 3 (2008)
42. Demina, T., et al.: DC discharge plasma modification of chitosan/gelatin/PLLA films: Surface properties, chemical structure and cell affinity. *Surf. Coat. Technol.* **207**, 508–516 (2012)
43. van Wachem, P.B., et al.: Adhesion of cultured human endothelial cells onto methacrylate polymers with varying surface wettability and charge. *Biomaterials* **8**(5), 323–328 (1987)
44. Chen, H., et al.: Electrospun chitosan-graft-poly (ϵ -caprolactone)/poly (ϵ -caprolactone) cationic nanofibrous mats as potential scaffolds for skin tissue engineering. *Int. J. Biol. Macromol.* **48**(1), 13–19 (2011)
45. Demirbilek, M.E., et al.: Oxidative stress parameters of L929 cells cultured on plasma-modified PDLLA scaffolds. *Appl. Biochem. Biotechnol.* **164**, 6 (2011)
46. Tian, H., et al.: Biodegradable synthetic polymers: Preparation, functionalization and biomedical application. *Progress in Polymer Science* **37**, 2 (2012)
47. De Bartolo, L., et al.: Evaluation of cell behaviour related to physico-chemical properties of polymeric membranes to be used in bioartificial organs. *Biomaterials* **23**, 12 (2002)
48. Groth, T., et al.: Interaction of human skin fibroblasts with moderate wettable polyacrylonitrile-copolymer membranes. *J. Biomed. Mater. Res.* **61**, 2 (2002)
49. Croll, T.I., et al.: Controllable surface modification of poly(lactic-co-glycolic acid) (PLGA) by hydrolysis or aminolysis I: Physical, chemical, and theoretical aspects. *Biomacromolecules* **5**(2), 463–473 (2004)

50. Zhu, Y.B., et al.: Immobilization of biomacromolecules onto aminolyzed poly(L-lactic acid) toward acceleration of endothelium regeneration. *Tissue Eng.* **10**, 1–2 (2004)
51. Park, G.E., et al.: Accelerated chondrocyte functions on NaOH-treated PLGA scaffolds. *Biomaterials* **26**(16), 3075–3082 (2005)
52. Ghasemi-Mobarakeh, L., et al.: Bio-functionalized PCL nanofibrous scaffolds for nerve tissue engineering. *Mater. Sci. Eng. C* **30**(8), 1129–1136 (2010)
53. Zhu, H.G., Ji, J., Shen, J.C.: Construction of multilayer coating onto poly-(DL-lactide) to promote cytocompatibility. *Biomaterials* **25**, 1 (2004)
54. Xie, Z., et al.: Electrospun poly(D, L)-lactide nonwoven mats for biomedical application: Surface area shrinkage and surface entrapment. *J. Appl. Polym. Sci.* **122**(2), 1219–1225 (2011)
55. Thapa, A., et al.: Nano-structured polymers enhance bladder smooth muscle cell function. *Biomaterials* **24**(17), 2915–2926 (2003)
56. Zhang, H.N., Lin, C.Y., Hollister, S.J.: The interaction between bone marrow stromal cells and RGD-modified three-dimensional porous polycaprolactone scaffolds. *Biomaterials* **30**(25), 4063–4069 (2009)
57. Zhang, H.N., et al.: Chemically-conjugated bone morphogenetic protein-2 on three-dimensional polycaprolactone scaffolds stimulates osteogenic activity in bone marrow stromal cells. *Tissue Eng. Part A* **16**(11), 3441–3448 (2010)
58. Zhu, Y.B., et al.: Esophageal epithelium regeneration on fibronectin grafted poly(L-lactide-co-caprolactone) (PLLC) nanofiber scaffold. *Biomaterials* **28**(5), 861–868 (2007)
59. Jao, Y.P., et al.: Effect of hydrolysis pretreatment on the formation of bone-like apatite on poly(L-lactide) by mineralization in simulated body fluids. *J. Bioactive Compat. Polymers* **22**(5), 492–507 (2007)
60. Poncinepaillard, F., Chevet, B., Brosse, J.C.: Modification of isotactic polypropylene by a cold-plasma or an electron-beam and grafting of the acrylic-acid onto these activated polymers. *J. Appl. Polym. Sci.* **53**(10), 1291–1306 (1994)
61. Steffens, G.C., et al.: High density binding of proteins and peptides to poly(D, L-lactide) grafted with polyacrylic acid. *Biomaterials* **23**(16), 3523–3531 (2002)
62. Ke, Y., et al.: Bioactive surface modification on amide-photografted poly(3-hydroxybutyrate-co-3-hydroxyvalerate). *Biomed. Mater.* **6**, 2 (2011)
63. Grondahl, L., Chandler-Temple, A., Trau, M.: Polymeric grafting of acrylic acid onto poly(3-hydroxybutyrate-co-3-hydroxyvalerate): Surface functionalization for tissue engineering applications. *Biomacromolecules* **6**(4), 2197–2203 (2005)
64. Shibata, Y., et al.: Azidation of polyesters having pendent functionalities by using NaN_3 or DPPA-DBU and photo-crosslinking of the azidopolyesters. *Polym. J.* **43**(3), 272–278 (2011)
65. Bat, E., et al.: Crosslinking of trimethylene carbonate and D, L-Lactide (Co-) polymers by gamma irradiation in the presence of pentaerythritol triacrylate. *Macromol. Biosci.* **11**(7), 952–961 (2011)
66. Ma, Z., Mao, Z., Gao, C.: Surface modification and property analysis of biomedical polymers used for tissue engineering. *Colloids Surf. B* **60**(2), 137–157 (2007)
67. Shin, H., Jo, S., Mikos, A.G.: Biomimetic materials for tissue engineering. *Biomaterials* **24**(24), 4353–4364 (2003)
68. Gamboa-Martinez, T.C., Gomez Ribelles J.L., Gallego Ferrer, G.: Fibrin coating on poly (L-lactide) scaffolds for tissue engineering. *J. Bioactive Compat. Polymers*, **26**(5), 464–477 (2011)
69. Zhang, L.F., et al.: Hydrophilic poly (ethylene glycol) coating on PDLLA/BCP bone scaffold for drug delivery and cell culture. *Mater. Sci. Eng., C* **28**(1), 141–149 (2008)
70. Yun, H.S., et al.: Biomimetic component coating on 3D scaffolds using high bioactivity of mesoporous bioactive ceramics. *Int. J. Nanomed.* **6**, 2521–2531 (2011)
71. Tsai, W.B., et al.: Poly(dopamine) coating of scaffolds for articular cartilage tissue engineering. *Acta Biomater.* **7**(12), 4187–4194 (2011)
72. Dupont, K., et al.: Synthetic scaffold coating with adeno-associated virus encoding BMP2 to promote endogenous bone repair. *Cell Tissue Res.*, pp. 1–14

73. Davis, H.E., et al.: Osteogenic response to BMP-2 of hMSCs grown on apatite-coated scaffolds. *Biotechnol. Bioeng.* **108**(11), 2727–2735 (2011)
74. Yanoso-Scholl, L., et al.: Evaluation of dense poly(lactic acid)/beta-tricalcium phosphate scaffolds for bone tissue engineering. *J. Biomed. Mater. Res., Part A* **95A**(3), 717–726 (2010)
75. Dee, K.C., Puleo, D.A., Bizios, R.: An introduction to tissue-biomaterial interactions, Hoboken, N.J., Wiley-Liss, p. 228
76. Fu, K., Klibanov, A.M., Langer, R.: Protein stability in controlled-release systems. *Nat. Biotechnol.* **18**(1), 24–25 (2000)
77. Neff, J.A., Caldwell, K.D., Tresco, P.A.: A novel method for surface modification to promote cell attachment to hydrophobic substrates. *J. Biomed. Mater. Res.* **40**(4), 511–519 (1998)
78. Goddard, J.M., Hotchkiss, J.H.: Polymer surface modification for the attachment of bioactive compounds. *Prog. Polym. Sci.* **32**(7), 698–725 (2007)
79. Edlund, U., Sauter, T., Albertsson, A.C.: Covalent VEGF protein immobilization on resorbable polymeric surfaces. *Polym. Adv. Technol.* **22**(1), 166–171 (2011)
80. Li, L., Wu, J., Gao, C.: Gradient immobilization of a cell adhesion RGD peptide on thermal responsive surface for regulating cell adhesion and detachment. *Colloids Surf., B* **85**(1), 12–18 (2011)
81. Nakajima, N., Ikada, Y.: Mechanism of amide formation by carbodiimide for bioconjugation in aqueous-media. *Bioconjug. Chem.* **6**(1), 123–130 (1995)
82. Chen, J.-P., Su C.-H.: Surface modification of electrospun PLLA nanofibers by plasma treatment and cationized gelatin immobilization for cartilage tissue engineering. *Acta Biomaterialia*, **7**, 1 (2011)
83. Chen, J.P., Chiang, Y.P.: Surface modification of non-woven fabric by DC pulsed plasma treatment and graft polymerization with acrylic acid. *J. Membrane Sci.* **270**, 1–2 (2006)
84. Grafahrend, D., et al.: Degradable polyester scaffolds with controlled surface chemistry combining minimal protein adsorption with specific bioactivation. *Nat. Mater.* **10**(1), 67–73 (2011)
85. Koo, A.N., et al.: Enhanced bone regeneration by porous poly(L-lactide) scaffolds with surface-immobilized nano-hydroxyapatite. *Macromol. Res.* **18**(10), 1030–1036 (2010)
86. Wu, J.D., et al.: Covalently immobilized gelatin gradients within three-dimensional porous scaffolds. *Chin. Sci. Bull.* **54**(18), 3174–3180 (2009)
87. Brandley, B.K., Schnaar, R.L.: Covalent attachment of an Arg-Gly-Asp sequence peptide to derivatizable polyacrylamide surfaces—support of fibroblast adhesion and long-term growth. *Anal. Biochem.* **172**(1), 270–278 (1988)
88. Desai, N.P., Hubbell, J.A.: Solution technique to incorporate polyethylene oxide and other water-soluble polymers into surfaces of polymeric biomaterials. *Biomaterials* **12**(2), 144–153 (1991)
89. Quirk, R.A., et al.: Controlling biological interactions with poly(lactic acid) by surface entrapment modification. *Langmuir* **17**(9), 2817–2820 (2001)
90. Liu, W.G., et al.: Effects of baicalin-modified poly(D, L-lactic acid) surface on the behavior of osteoblasts. *J. Mater. Sci. Mater. Med.* **14**(11), 961–965 (2003)
91. Duan, B., et al.: Surface modification of three-dimensional Ca-P/PHBV nanocomposite scaffolds by physical entrapment of gelatin and its in vitro biological evaluation. *Front. Mater. Sci.* **5**(1), 57–68 (2011)
92. Bertrand, P., et al.: Ultrathin polymer coatings by complexation of polyelectrolytes at interfaces: suitable materials, structure and properties. *Macromol. Rapid Commun.* **21**(7), 319–348 (2000)
93. Hammond, P.T.: Engineering materials layer-by-layer: Challenges and opportunities in multilayer assembly. *AIChE J.* **57**(11), 2928–2940 (2011)
94. Li, X., et al.: Coating Electrospun Poly(ϵ -caprolactone) fibers with gelatin and calcium phosphate and their use as biomimetic scaffolds for bone tissue engineering. *Langmuir* **24**(24), 14145–14150 (2008)

95. Zhu, Y., Sun, Y.: The influence of polyelectrolyte charges of polyurethane membrane surface on the growth of human endothelial cells. *Colloids Surf. B* **36**(1), 49–55 (2004)
96. Stendahl, J.C., et al.: Modification of fibrous poly(L-lactic acid) scaffolds with self-assembling triblock molecules. *Biomaterials* **25**(27), 5847–5856 (2004)
97. Cui, H., Webber, M.J., Stupp, S.I.: Self-assembly of peptide amphiphiles: From molecules to nanostructures to biomaterials. *Pept. Sci.* **94**(1), 1–18 (2010)
98. Mahjoubi, H., Cerruti, M.: Homogeneous surface modification of poly (D, L-lactic acid) scaffolds for orthopedic applications: a non-destructive method based on diazonium chemistry. *Chem. Mater.* (2012)
99. George, A., Veis, A.: Phosphorylated proteins and control over apatite nucleation, crystal growth, and inhibition. *Chem. Rev.* **108**(11), 4670–4693 (2008)
100. Song, J., Malathong, V., Bertozzi, C.R.: Mineralization of synthetic polymer scaffolds: A bottom-up approach for the development of artificial bone. *J. Am. Chem. Soc.* **127**(10), 3366–3372 (2005)
101. D'Andrea, L.D., et al.: Targeting angiogenesis: Structural characterization and biological properties of a de novo engineered VEGF mimicking peptide. *Proceedings of the national academy of sciences of the United States of America*, 102(40), 14215–14220 (2005)
102. Leslie-Barbick, J.E., et al.: The promotion of microvasculature formation in poly(ethylene glycol) diacrylate hydrogels by an immobilized VEGF-mimetic peptide. *Biomaterials* **32**(25), 5782–5789 (2011)

Chapter 8

Thin Film Biosensors

Hatice Ceylan Koydemir, Haluk Külâh and Canan Özgen

Abstract New generation biosensors are analytical compact devices made of thin films. Sensitivity, specificity, rapid response time, ease-of-use, and low cost are the major advantages of these biosensors. All of these properties are closely related with thicknesses of the films used in fabrication of the sensor. The detection principle of a biosensor is mainly based on the interaction of the biological analyte with the surface-modified thin film. The thin film acts as a physicochemical—optical, mechanical, magnetic, and electrical—transducer and converts the signal resulting from the recognition of the biological analyte into another measurable signal. In this chapter, first, the roles of thin films in biosensor applications will be discussed. Then, different types of thin films used in the fabrication of biosensors will be explained. The methods to form organic thin films on sensitive layers for adsorption of biological analytes will be given together with four main methods of detection as: optical, mechanical, magnetic, and electrical. Finally, recent developments will be outlined.

H. Ceylan Koydemir (✉) · H. Külâh
METU-MEMS Center, Middle East Technical University, 06800 Çankaya, Ankara, Turkey
e-mail: hceylan@metu.edu.tr

H. Külâh
e-mail: kulah@metu.edu.tr

H. Ceylan Koydemir · C. Özgen
Department of Chemical Engineering, Middle East Technical University, 06800 Çankaya,
Ankara, Turkey
e-mail: cozgen@metu.edu.tr

H. Külâh
Department of Electrical and Electronics Engineering, Middle East Technical University,
06800 Çankaya, Ankara, Turkey

8.1 Introduction

There has been an extended interest on biosensors for rapid and reliable detection of biological particles or molecules since the development of the first glucose biosensor in 1960s by Professor Leland C Clark Jr [1]. The trend in 1970s was towards macro scale commercialization of disposable/single-use glucose sensors. Since then, numerous biosensors have been developed for different applications (e.g., pathogen, toxin, rare cell, and DNA detection, glucose monitoring, and blood analysis) to offer high sensitivity and high selectivity for several types of target analytes. The developments in the research papers on biosensors and the increase in the resources of laboratories have changed the demand for miniaturized biosensors that are finding wider use in portable devices with increased functionality. Nowadays, miniaturization of sensors from millimeter scale to nanometer scale has been investigated with the developments in molecular medicine, nanotechnology, and micro fabrication technology to create solutions that will improve the life quality. The working principle of biosensors is mainly based on adsorption of biological molecule to be detected on a sensitive surface, made of a thin film modified with receptor probes. The thin film acts as a physicochemical (optical, mechanical, magnetic, or electrical) transducer, which converts the signal resulting from the recognition of the biological analyte into another measurable signal. These biosensors are complex structures of thin films, which give enormous functionalities to the sensors.

Thin films can be made from organic and/or inorganic materials, such as metals, glass, polymers, silicon, or metal oxides. Biological particles or chemicals can also be used as thin films.

Each layer made out of different materials adds different properties to the whole structure of a biosensor: thin films can be used as sacrificial layers, barrier (insulation) layers, and recognition (sensitive) layers. Sacrificial layers have the role in the fabrication of biosensors to form 3D patterns. Barrier (insulation) layers play a significant role in determination of high sensitivity by enhancing signal to noise ratio. Recognition (sensitive) layer, i.e. the thin film surface on which biological particles adsorbed, is the most important part of a biosensor. On this surface, atomic interactions, surface free energies, and forces are different from the bulk of the material, and any reaction can start here. Surface activation can be necessary to immobilize biological analytes on sensitive layer. For this purpose, use of self-assembled monolayer (SAM) is a powerful tool.

In this chapter, first focus will be given to the roles, types, and modification methods of thin films in biosensor applications in a broader context with the aim of introducing a general perspective. Then, four main detection methods will be discussed with their current constraints and advantages in the miniaturization. Lastly, recent developments on thin film biosensors will be given by focusing on sample preparation, isolation, purification, and amplification of target analytes, diagnosis, cell separation, biomimetic structures, and cell culturing at micro scale.

8.2 Thin Films as Intelligent and Functional Layers

New generation biosensors are used in different applications ranging from point of care diagnosis to homeland security. Rapid response time, low cost, portability, high sensitivity, and high selectivity are desired main features of the biosensors to improve people's life quality, to have appropriate treatment, and to decrease mortality rates. Novel design and innovative fabrication of these miniaturized systems require a deep knowledge on properties (i.e., electrical, optical, mechanical, and magnetic) changing with the size of structures of materials used. Fabrication of these biosensors is based on coating and patterning thin and/or thick films to make a compact device, and it is possible to form 1D (e.g., nano-wires, and nano-tubes), 2D, and 3D structures with the today's micro fabrication technology. Figure 8.1 shows a typical biosensor fabrication flow to form such structures. Each layer of the sensor can have a different role determining the degree of specificity, sensitivity, and response time of the biosensor.

Thin films can be used to functionalize (e.g., controlling hydrophobicity, bio-affinity, biocompatibility, and electrical activity) the surface of biosensors with or without using surface treatment processes. For example, Parylene C, which is a polymer commonly used in the packaging of integrated circuits, is a hydrophobic polymer with a water contact angle of 87° and its surface can be made hydrophilic with oxygen plasma treatment [3]. The controllable hydrophobicity of Parylene C allows it to be used in the fabrication of microfluidic devices where the capillary flow dynamics gain importance. Ultrananocrystalline diamond, oxide coatings (e.g., SiO_2 , TiO_2 , and Al_2O_3), silicon nitride (Si_3N_4), and polymers (e.g., Parylene C, and polyetherurethane) are good examples of biocompatible layers [4]. These biocompatible coatings enable the implantation of biosensors for different applications from controllable drug delivery to chronic cardiovascular diseases [5, 6]. On the contrary, in some cases, it is necessary to form a barrier to cease the flow of current, or to stop etching process. Si_3N_4 is a good example to the barrier type thin

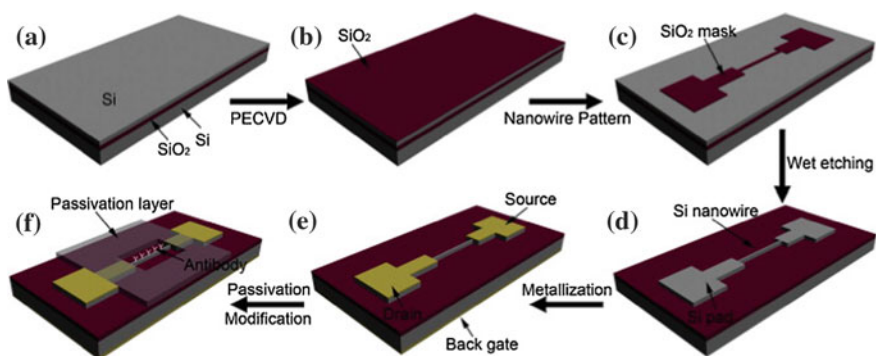


Fig. 8.1 A schematic flow diagram demonstrating fabrication of a biosensor developed by Kong et al. [2] [Reprinted with permission from [2] Copyright (2012) Elsevier]

films and used as insulation layer and/or chemical barrier in integrated circuit (IC) fabrication due to its high resistivity and inertness to most of the chemicals.

Electrical, optical, mechanical, and magnetic properties of the thin films are generally different and sometimes even better than the properties of thick materials, resulting in improved performance of the sensor. For instance, in the study of Sokolov et al. [7], micro patterned polydimethylsiloxane (PDMS) layer of pressure sensor has returned to off state in ~ 100 ms while its bulk film counterpart shows a 50-fold delay time for the same amount of applied pressure. Besides these, the increase in surface-to-volume ratio provides an advantage to thin film materials in biosensor implementations [8, 9].

The use of thin films in the micro-fabrication of sensors can reduce the amount of coated materials. Especially when precious metals like gold, platinum, and titanium are used, the thickness of these coatings in biosensors is around 500 nm at most. Thus, the use of thin films enables the use of typical metal sources for at least one thousand times in sputtering depending on the thickness of the layer and the operation conditions, which reduces the cost of the sensors by saving metal amount.

In the development of biosensors for diagnostic applications, World Health Organization presented a rule of thumb that a biosensor must be ASSURED, that is it must be Affordable, Sensitive, Specific, User-friendly, Rapid and robust, Equipment free, and Deliverable to end-users [10]. Therefore, it is necessary to evaluate new trends in the aspect of specificity, sensitivity, cost effectiveness, disposability, low weight, and ease of use and access. It is sure that the materials used in the innovative fabrication of biosensors improve the novel design and result in enhancement of the sensitivity and specificity of the miniaturized device. Therefore, selection of materials plays significant role to meet the ASSURED criteria. The following two subsections are devoted to the introduction of thin film materials, which are used in the micro fabrication processes as inorganic materials and in the functionalization of the surfaces to adsorb biological molecules as organic films.

8.3 Thin Film Materials

Different types of thin films are used in the micro fabrication of biosensors. Metals [e.g., gold (Au), platinum (Pt), titanium (Ti), chromium (Cr), silver (Ag), aluminum (Al)] are coated with the use of mainly four different techniques: sputtering, evaporation, electroplating, and electroless coating. These metal layers can be used to form bonding pads, to form active surfaces for adhesion of biological analytes or materials, or to form adhesion layer between two layers. For example, gold is used to form electrodes mostly due to its high conductivity, inertness with most of the chemicals (e.g., acids and solvents), high melting point, and biocompatibility. Titanium is mostly used to enhance adhesion between the substrate [e.g., silicon (Si) or glass] and the top metal layer (e.g., Pt, Au) in integrated circuit industry. Its

unique properties, such as inertness to body fluids and compatibility with tissues, broaden its applications in the biological studies. As an example in the study of Farra et al. [5], a wirelessly controlled microchip, whose outermost layer is coated with titanium to make it biocompatible, is successfully implanted to a human for drug delivery applications with no adverse immune reaction [11].

Other than the metals, the different allotropes of carbon have also been utilized in the fabrication of biosensors. Diamond, which is known for its superior electrochemical properties, chemical inertness, hardness, and thermal conductivity, is widely studied in recent years [12]. In the formation of diamond films, chemical vapor deposition (CVD) techniques are used due to the ability of various growth conditions to have significantly improved film properties. Functionalization of the diamond surface can be done either before or after the fabrication of the film to modify its surface with biological analytes or materials by chemisorption. In the study of Marcon et al. [13], the surface of boron-doped diamond was terminated with oxidized, amine, alkyl, trifluoromethyl, and vinyl linkers after the fabrication of the film with the use of plasma treatments and chemicals. Then, these surfaces were used to analyze the cell adhesion density with the consideration of the effect of contact angle on adsorption. It was revealed that, the cell densities on oxidized and amine-terminated surfaces were much higher than the other functionalized surfaces due to surface hydrophilicity. Conversely, as mentioned above, the diamond film can be modified during the fabrication of the thin film. In the study of Wang et al. [14], hydrogen terminated diamond surface was formed with the use of diaryl carbenes during the growth of film by CVD. Graphene, whose carbon atoms are in the shape of honeycomb crystal lattice, is another allotrope of carbon. The properties, such as low cost, ease of processing, safety, and high surface to volume ratio, make the graphene an excellent material in the electrochemical detection of biological analytes or materials [15].

Another type of thin films commonly used in the fabrication of biosensors is polymers, which are used commonly for forming channels, preventing non-specific binding of biological analytes or materials, and forming hydrophobic/hydrophilic layers. PDMS, polyethylene (PE), perfluoropolyether (PFPE), polyimide (PI), Parylene C, polyetheretherketone (PEEK), cyclic olefin/copolymer (COC/COP), poly(methylmethacrylate) (PMMA), polypropylene (PP), polystyrene (PS) are the mostly used ones [16]. Among them, PDMS is preferred in rapid prototyping of biosensors since it is optically clear, chemically inert, and easy to make micro channels with soft lithography, and does not necessitate a clean room environment. However, the difference between the methods and materials used in the fabrication of biosensors in academic environment and the ones in the commercialized products increases day by day. This difference results in inefficiency of the commercialization of the developed biosensors. Therefore, materials and/or methods that are compatible with manufacturing of commercialized products should be taken into consideration [16]. Parylene C is more compatible to IC technology compared to PDMS, especially for packaging of post-complementary metal oxide semiconductor (CMOS) biosensors. This is due to the advantages of Parylene C such as low water permeability, biocompatibility, transparency, and

non-conductivity [17, 18]. Additionally, there are coatings such as indium tin oxide (ITO) and zinc oxide (ZnO), which are not only electrically conductive but also transparent. These transparent conductive layers provide analysis of the biological analytes with both electrical devices and microscopes. In the study of Choi et al. [19], the applicability of ITO for biosensor applications was demonstrated with the use of endothelial cell growth on transparent conductive electrodes. It was concluded that the use of ITO enables monitoring intricate networks and cellular activities with both optical detection and electrical impedance measurements. An example to transparent conductive polymers is poly (3,4-ethylenedioxythiophene) poly(styrene sulfonate) (PEDOT:PSS), which is water soluble and has stable electrical conductivity even after a thousand hours of exposure to 100 °C air treatment [20].

8.4 Methods of Forming Molecular Recognition Surfaces

The organic thin films have crucial importance in the development of chemical and biological sensors. In order to improve functionality and sensitivity of the sensor, it is necessary to deposit the organic thin films with conformal coverage and uniformity. The organic thin films, which deposit biomolecules such as horseradish peroxidase, nucleic acids, cells and proteins, have different applications ranging from microfluidic sensors to DNA microarrays. The growth of organic films on the sensitive surfaces can be done with four different methods: Langmuir film formation, Langmuir–Blodgett film formation, SAMs grown from solution, SAMs grown from vapor, and organic molecular beam epitaxy [21]. Among them, the deposition of the organic films is usually performed by SAMs because of the ease of preparation and the various functionality of the SAM structure either laterally or vertically. Additionally, the selection of the right surface chemistry to form organic films depends on the physicochemical properties of the material to be activated and the end chemical groups of the biomolecules (e.g., NH_3^- , OH^- , and SH^-).

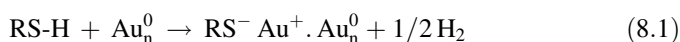
Biological molecules (e.g., antibody, enzyme, cell, and nucleic acid) can be adsorbed to the surface by either physisorption or chemisorptions. In the physisorption, which is known as physical adsorption, the molecules bind to the surface by van der Waals forces. The energy of binding is about 10–100 meV and the interaction between the adsorbate and the surface is so weak that the molecules adsorbed on the surface may be removed at the first rinsing step. Electrostatic and hydrophobic interactions are examples to the physisorption. On the other hand, the binding energy of molecules to the surface in chemisorption, at which a chemical reaction occurs between the adsorbate and the surface, is about 1–10 eV, which enables the formation of stable monolayer molecules. Biological molecules can be chemisorbed to the functionalized surface depending on the end group of the chain, or cross-linking agents are used for further modification of the surface to have appropriate functional groups at the end of the monolayer. There are two

Table 8.1 Targets and some examples of cross linkers used in the formation of SAMs [22, 23]

Cross-linking targets	Example	References
Amine to amine	Disuccinimidyl glutarate (DSG)	[24]
	Disuccinimidyl suberate (DSS)	[25]
	Dithiobis[succinimidylpropionate] (DSP)	[26]
Amine to sulfhydryl	3,3'-Dithiobis[sulfosuccinimidylpropionate] (DTSSP)	[27]
	Sulfosuccinimidyl 6-(3'-[2-pyridyldithio]-propionamido) hexanoate (Sulfo-LC-SPDP)	[28]
	Sulfosuccinimidyl-4-(N-maleimidomethyl) cyclohexane-1-carboxylate (Sulfo-SMCC)	[29]
	N- κ -Maleimidoundecanoyl-oxysulfosuccinimide ester (Sulfo-KMUS)	[30]
Carboxyl to amine	Dicyclohexylcarbodiimide (DCC)	[31]
	1-Ethyl-3-[3-dimethylaminopropyl] carbodiimide hydrochloride (EDC)	[32]
Hydroxyl to sulfhydryl	N-(p-malimidophenyl) isocyanate (PMPI)	[33]
Sulfhydryl to sulfhydryl	Polyethylene glycol (PEG) polymers	[34]
Sulfhydryl to carbohydrate	N-[β -Maleimidopropionic acid] hydrazide, trifluoroacetic acid salt (BMPH)	[35]

types of cross-linkers: homobifunctional cross-linkers and heterobifunctional cross-linkers. In the former one, the end groups of cross-linking targets are the same, while in the other one, the end groups differ (Table 8.1).

Gold is the most commonly used material to form sensitive surfaces in chemical and biological sensors due to its high electrical conductivity, chemical inertness, and biocompatibility. Gold surface can be made functional by using thiol (-SH) modified molecules or activating the surface by using thiol molecules. The energy for chemisorption of thiol group on gold is about 50 kcal/mol and the probable chemical reaction that occurs on the gold surface is given in Eq. (8.1) as,



The reaction results in the formation of gold (I) thiolate (RS^-) species [36]. However, the other product, hydrogen cannot be observed during experiments. There can be two possibilities for this; it can be either due to its small amount or due to its transfer to aqueous solution. The complete mechanism is not completely understood, but the formation of thiolate on gold substrate is clear and this adsorption process makes short range, dispersive, London-type, van der Waals forces more important [36]. Some frequently used groups to form SAMs on gold layer are thiols ($\text{HS}-(\text{CH}_2)_n\text{-X}$), dithiols ($\text{XS}-(\text{CH}_2)_n\text{-SX}$), sulfides ($\text{X}(\text{CH}_2)_m\text{S}(\text{CH}_2)_n\text{X}$), and disulfides ($\text{X}(\text{CH}_2)_m\text{S-S}(\text{CH}_2)_n\text{X}$), at which m and n are the numbers for alkyl chain and X is chain with the formula of either $-\text{H}$, $-\text{NH}_2$, $-\text{CH}_3$, $-\text{OH}$, or $-\text{COOH}$ [37, 38] (Fig. 8.2).

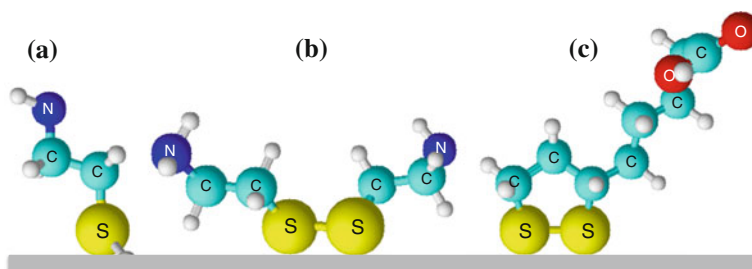


Fig. 8.2 Some of the small molecules containing thiol groups adsorbed on metal surface **a** 2-mercapto-ethylamine **b** Cystamine **c** Lipoic acid [39]

On the other hand, inorganic surfaces or particles (e.g., glass and silica) can be functionalized by using silane compounds to form functional groups (e.g., NH_3^- , OH^- , and SH^-) on the surface in order to conjugate biomolecules to inorganic layers (Table 8.2). In the functionalization of the surface, the reaction with the silane coupling groups results in hydrolysis and the formed intermediate product binds to the inorganic surface via hydrogen bonding. The product of hydrolysis is water and it is necessary to remove water from the surface by heating or vacuuming to form stable layers.

8.5 Sensing Strategies for Biomolecular Detection

In biosensors, which are used for the identification of biological molecules, after chemisorptions of molecules on the biosensor surface, the physicochemical difference of the presence of the biological molecule must be identified by using a

Table 8.2 List of most commonly used functional silane compounds [40]

Functional silane compound	Formed end group on the surface	Possible further modification
3-aminopropyltriethoxysilane (APTS)	Amine	Amine Hydroxyl
3-aminopropyltrimethoxysilane	Amine	Amine Hydroxyl
Carboxyethylsilanetriol	Carboxyl	Amine
N-(Trimethoxysilylpropyl)ethylenediamine triacetic acid (TMS-EDTA)	EDTA	Metal salts
3-Glycidoxypropyltrimethoxysilane (GOPTS)	Epoxy	Amine Hydroxyl Sulfhydryl
3-Glycidoxypropyltriethoxysilane	Epoxy	Amine Hydroxyl Sulfhydryl
Isocyanatopropyltriethoxysilane (ICPTES)	Isocyanate	Hydroxyl

detection strategy. Until now, extensive studies have been performed by scientists in multidisciplinary teams to develop different detection methods as optical, electrical, mechanical, and magnetic detection (Fig. 8.3).

Optical detection has been the base of all detection methods over decades due to its dependency on visual detection and its unique advantage of rapid response time. The detection principle is based on the measurement of change in the wavelength of light beams directed on the compound of interest. The signal transduction has been performed by using Surface Plasmon Resonance (SPR), Localized Surface Plasmon Resonance (LSPR), fluorescence, or other methods. Among them, the fluorescence detection is still commonly used for the analysis of molecules in microchips due to its simplicity and reliability. However, its miniaturization is limited due to its complexity and necessity of applicable compounds, such as light source. The recent developments on light emitting diodes (LEDs) provide an alternative light source to the fluorescence detection and enable the miniaturization of optical systems and their combinations with biomedical sensors. This is due to the advantages provided by small size LEDs like necessity of low power driving currents and low fabrication cost [41]. On the other hand, it is necessary to focus light generated from LEDs by using complex optic tools to be able to use their radiation power in confocal imaging of biomolecules because light generated from LEDs spreads over micron scale and LEDs cannot be used alone as a point light source [42]. Another alternative light source is organic light-emitting diodes (OLED). In comparison to LEDs, OLEDs, which are composed of

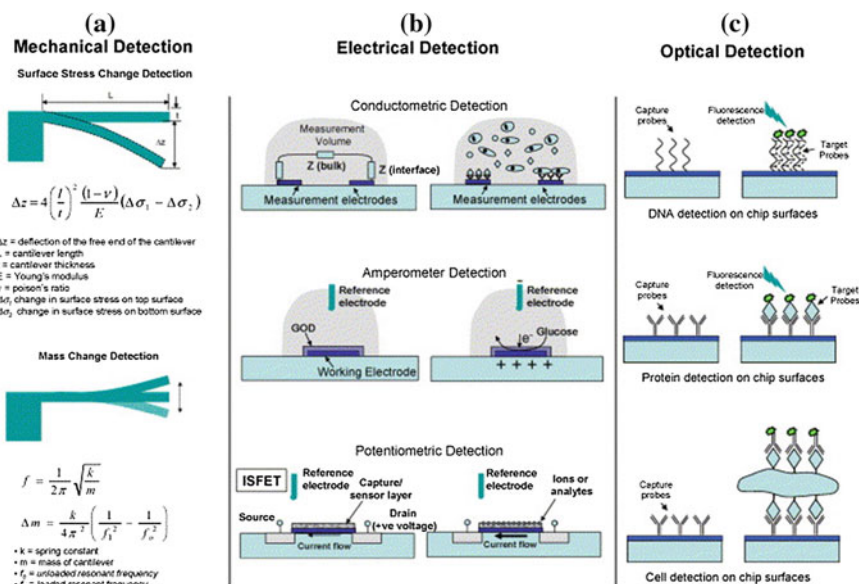


Fig. 8.3 Detection strategies used in the biosensors [Reprinted with permission from [44] Copyright (2004) Elsevier]

thin films, can be fabricated by using micro fabrication processes and they are more compatible to microfluidic devices than LEDs due to their flat surface in detection of biological analytes [43].

Mechanical detection of biological particles or molecules is based on the detection of mass of the particle or molecule adsorbed on the sensitive surface (Fig. 8.4). The presence of the particle can be determined by measuring either the amount of the deflection or the resonant shift, which results from the adsorption of the particle. However, there are some intrinsic limitations of this detection method: detection limit, operation conditions, and signal to noise ratio. Firstly, it is necessary to adsorb sufficient amount of particles or molecules on the deflected surface to produce surface stress, although attomolar detection limits can be achievable with resonant MEMS and nano-electro-mechanical-systems (NEMS) sensors. In addition, it is important on which part of the deflected surface the particle is adsorbed, since the momentum of the mass affects the stress. The adsorption place on the sensor does not matter in the case of resonant sensor; however, it can be a problematic issue in cantilever-based sensors. The other important limitation in the mechanical detection is the operation conditions of sensors. Deflection based sensors have the advantage over the resonant sensors for the detection of biological particles or molecules in liquid since the stress does not depend on viscous damping. However, detection in liquid medium is an important design consideration for resonant sensors since they are affected from viscous damping.

There are new studies to enhance the efficiency of resonant sensors in liquid environment by coating the surface with hydrophobic layers [46]. On the other hand, mechanical sensors are affected from environmental fluctuations (e.g., air, wind, temperature, vibrations) during the measurement of the mass and they can cause a decrease in signal to noise ratio and result in inaccurate measurements. This problem is solved by operating the sensitive surface in vacuum environment [47].

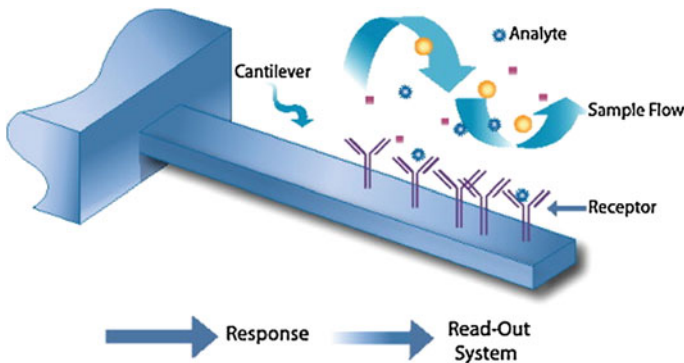


Fig. 8.4 A schematic drawing demonstrating the working principle of cantilever based sensing [Reprinted with permission from [45]. Copyright (2012) Elsevier]

Magnetic detection is another method for detection of biological particles or molecules. Paramagnetic or super paramagnetic particles are efficient in the particle or molecule separation from a biological fluid. Their sizes are ranging from nm to μm and they show hysteresis loop, which demonstrates a relationship between the flux density and applied magnetic force. The most widely used application of magnetic particles in biological studies is the separation of biological molecules from a liquid mixture. The big advantage of using magnetic particles in separation is that, there is no need of centrifugation; it is enough to use an external magnetic force to agglomerate particles. This advantage reduces handling time in sample preparation. Moreover, it is possible to isolate biological particles by functionalized magnetic particles, which limits the nonspecific adsorption.

Electrical detection is one of the mostly studied detection method in biosensors. It provides a rapid response time, high sensitivity, and high selectivity while enabling the miniaturization of devices, which further enables the development of point of care (POC) devices. In addition, this detection method is compatible with IC and MEMS technologies since the electrodes or layers are the products of standard micro fabrication processes and can be fabricated in batch mass production. There are different detection strategies in electrical detection and among them capacitive and electrochemical detections offer promise of development of portable systems by coupling with nanometer size particles. In capacitive detection, recent studies show that, it is possible to sense DNA hybridization in 10 nm scale nano-gaps with high selectivity. On the other hand, electrochemical detection provides rapid detection of biological particles or molecules with high sensitivity and selectivity at low cost [48].

Representative examples of detection methods and recent developments in thin film biosensors will be discussed in the following section.

8.6 Recent Developments in Thin Film Biosensors

Research and development studies in micro and nano technologies over the last three decades enabled and accelerated the fabrication of new generation biosensors by combining the knowledge in the fields ranging from electronics to biology. These studies have provided new platforms, which are composed of functional thin films, to overcome with the challenges faced in the analysis, detection, monitoring, and examining the behavior of biological analytes in different mediums by adding lots of advantages compared to conventional methods.

In the following sections, newly developed medical technologies, which are lab-on-a-chip and human-on-a-chip systems, will be explained with their applications.

8.6.1 Lab-on-a-Chip Systems

The ultimate aim in micro fabrication technology in combination with molecular medicine is to provide a new platform, a lab-on-a-chip system, which is capable of doing whole work on a single microchip similar to the one done at today’s clinical/biological/chemical laboratories with a higher sensitivity and clinical selectivity. For this purpose, researchers from different expertise fields form multidisciplinary teams and work together to develop a part or parts of this miniaturized system and to integrate them further to form lab-on-a-chip systems (Fig. 8.5).

Lab-on-a-chip systems offer potential for rapid and accurate detection of target analyte for an early diagnosis of diseases, such as cancer and infectious diseases (e.g., sepsis). Different biological molecules are used as target analyte. Among them, cells, proteins, phages, and genes are the most commonly used biological particles in the diagnosis. Although there are systems developed for cell-based detection, the need of portable devices for POC diagnosis has forced the scientists to develop complex devices by using nucleic acids as target analytes.

These lab-on-a-chip systems are mainly composed of three units: sample preparation, amplification, and detection.

8.6.1.1 Sample Preparation

Sample preparation is the most time-consuming step in the detection of target analyte and includes the steps of sample collection, cell lysis, and nucleic acid extraction. In this step, target cells taken from a patient or source, are separated, sorted, and lysed to analyze the contents of cells, and nucleic acid is extracted.

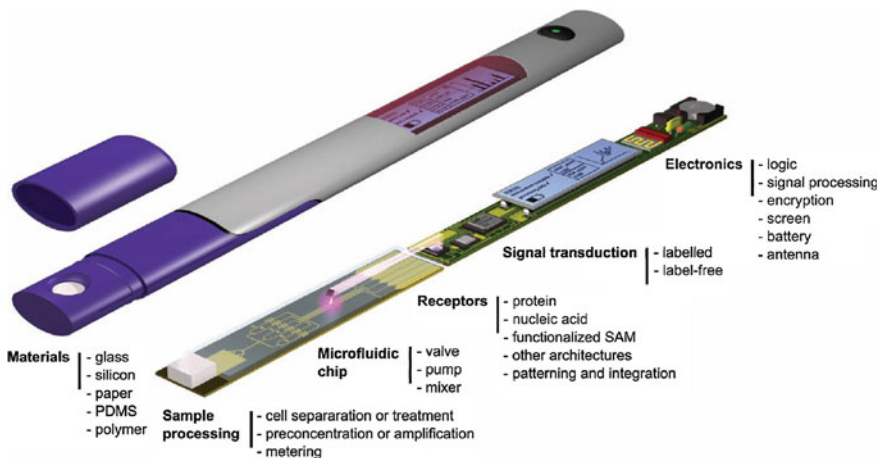


Fig. 8.5 A schematic of ideal lab-on-a-chip system for POC diagnosis. (Reproduced with permission from IBM, copyright 2010 IBM Corporation [49])

Different samples taken from eye, nose, throat, perineum, groin, axilla, or skin, such as tear, blood, or saliva can be used in the detection of diseases. These differences lead to different challenges, which must be accomplished for each specific target analyte in the design of biosensors for sample preparation. The dependency on operator interaction and necessity of reagents and/or solution containing target analyte to perform the detection assay are rate-limiting steps, which can bring some challenges in automaticity of the biosensors and necessity of rapid detection [50]. Clogging of microfluidic channels with cell and protein residues after isolation of target analytes is another issue that can be a challenge for the sample preparation kits with micro channels. Additionally, the concentrations of samples can demonstrate variability from patient to patient, are dependent on time, and the amount of sample type taken from the body [49]. Therefore, the developed sample preparation units are unique to a specific target analyte and a sample type. Thus, it is necessary to make more research to solve problems in the commercialization of biosensors in the field of sample preparation [49]. Therefore, there is an endless effort to develop a complete lab-on-a-chip system for POC diagnosis.

The thin films are combined with the micro-machined structures to perform micro/nano transport or cell separation. In transportation or separation of particles, different forces or approaches are used, such as biological, dielectrophoretic, centrifugal, magnetic, and non-Newtonian fluid forces (Fig. 8.6). In the study of Tarhan et al. [51], streptavidin functionalized silicon micro needles were combined with microtubules, and used as biotin carriers on kinesin-coated glass surface, while in the study of Bottier et al. [52] kinesin coated oil droplets were transported on the microtubules. In the study of Beech, red blood cells in shape from discocyte to stomatocyte were separated by using deterministic lateral displacement mechanism continuously [53]. A PDMS biosensor, at which the bottom of microchannel has pillars of height ranging from 12 to 3 μm , was used for separation of cells in size, shape, and deformability. The separation and sorting were successfully performed by changing pressure level inside the microchannel. In another PDMS device, the dynamics of non-Newtonian fluid were used for separation of platelets from blood with an efficiency of 99.9 % [54].

The first attempt to integrate cell isolation, cell lysis, nucleic acid purification and recovery was done by Hong et al. [56] (Fig. 8.7). Two microfluidic chips fabricated with soft lithography were integrated with mechanical micro valves and electrophoresis to demonstrate the applicability of parallelization of steps used in sample preparation in a single chip. Easley et al. [57] took the integrated chip one step further and developed a microfluidic device for the detection of nucleic acids, which was capable of accepting crude biological samples, such as blood, and provided the result in less than 30 min. The process speed was enhanced by using nanoliter volume reactors for the amplification of nucleic acid with the use of PCR. In the study of Bienvenue et al. [58], a simple and robust device was developed for the nucleic acid extraction from sperm cells to be used in forensic applications. This device included cell sorting, cell lysis, isolation, and purification of DNA.

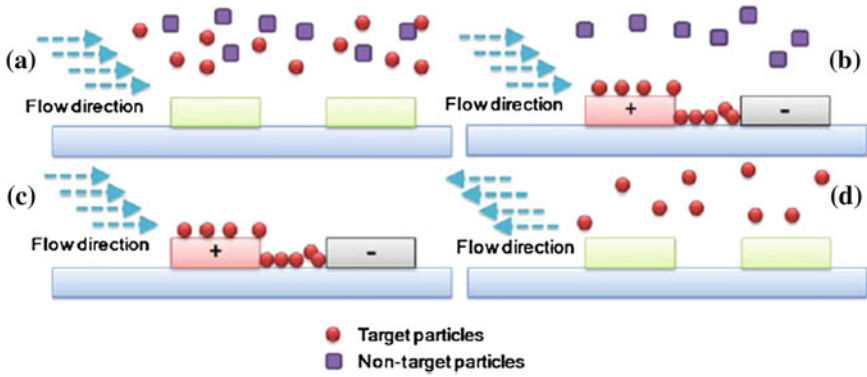


Fig. 8.6 A schematic showing the trapping and release of particle separation with dielectrophoretic force [Reprinted (adapted) with permission from [55] Copyright (2010) Springer]

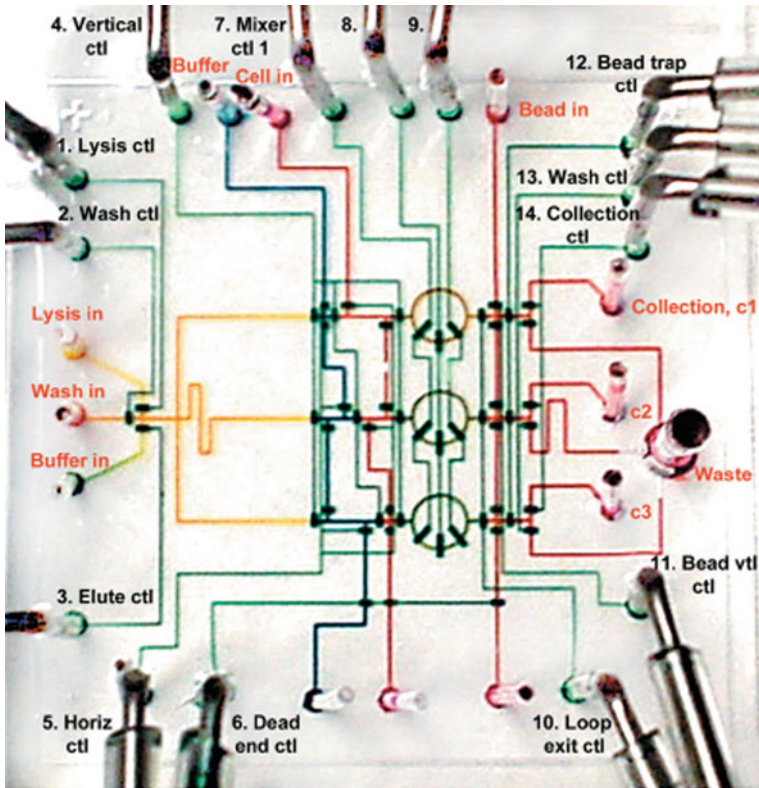


Fig. 8.7 DNA purification chip developed by Hong et al. [56]. [Reprinted (adapted) with permission from [56] Copyright (2004) Nature]

The cell lysis process can be performed in different ways, such as the use of enzymes and mechanical forces. In the study of Lee et al. [59], a sample preparation chip was integrated with Laser-Irradiated Magnetic Bead System (LIMBS) to lyse cell and nucleic acid isolation and they demonstrated that it was possible to perform cell lysis in 40 s even for *Staphylococcus epidermis* and *Escherichia coli* BL 21, which are belonging to Gram-positive bacteria and Gram negative bacteria, respectively. A laser beam (808 nm) with high power and titration had been used to combine thermal and mechanical forces in cell lysis. However, it was not possible to concentrate nucleic acids after cell lysis and the use of crude sample such as blood due to the geometry of the developed chip. In the study of Cho et al. [60], the drawbacks of the LIMBS based chip were eliminated with a new design and by the use of lab-on-a-disc sample preparation chip, rather than complex microfluidic structures like a spider network. A single laser diode was successfully used for cell lysis and operation of micro valves made from iron-oxide nanoparticle doped paraffin film in the developed system and the processing time from plasma separation to nucleic acid extraction was only 12 min. In the study of Baier et al. [50], a disposable microfluidic chip with a desktop system was developed to have an automatic sample preparation system without any handling process at any step. For this purpose, the reagents and the necessary mixtures were loaded to the chip before performing the process by using the openings on the valves. Although good results were taken with the developed system, the evaporation and incomplete release of reagents or mixtures into the microfluidic chip for the assay are handicaps in lab-on-a-chip devices that will be used in POC diagnosis. The loading of reagent before performing assay manually or with the use of analyzer can be solutions to these weak points and they decrease the possibility of operator failure. However, it is important not to lose the focus of lab-on-a-chip systems and is necessary to develop novel solutions to have low cost, miniaturized, and portable POC systems. The liquid and lyophilized forms can be used in the storage of the reagents. Different approaches can be used in the release of pre-stored reagents [61]. In the study of Hoffmann et al. [62], glass ampoules were used to store reagents into the microfluidic systems. The reagent was released by using centrifugal forces and filtered to prevent the glass particles to go through to the micro channels. The disadvantage of the use of the glass ampoules was the encapsulation of temperature sensitive substances since it was necessary to heat the glass to form ampoules. Hitzbleck et al. [63] investigated the formation of a dry reagent storage capsule integrated with a microfluidic chip by using standard micro fabrication processes. They developed a reagent integrator, which had an inlet and two dilution channels with an area of 1 mm² to store nano grams amounts of biological particles. Although the experiments were performed just after four hours of reagent loading with an inkjet nozzle, it took around six minutes to complete release of reagent. This approach offers promise in the field of integrated lab-on-chip systems without operator intervention.

It is important to store the reagents so that the contents must not change during the stored period because of some intrinsic concerns such as evaporation, contamination, and degradation of biological particles with temperature. These issues

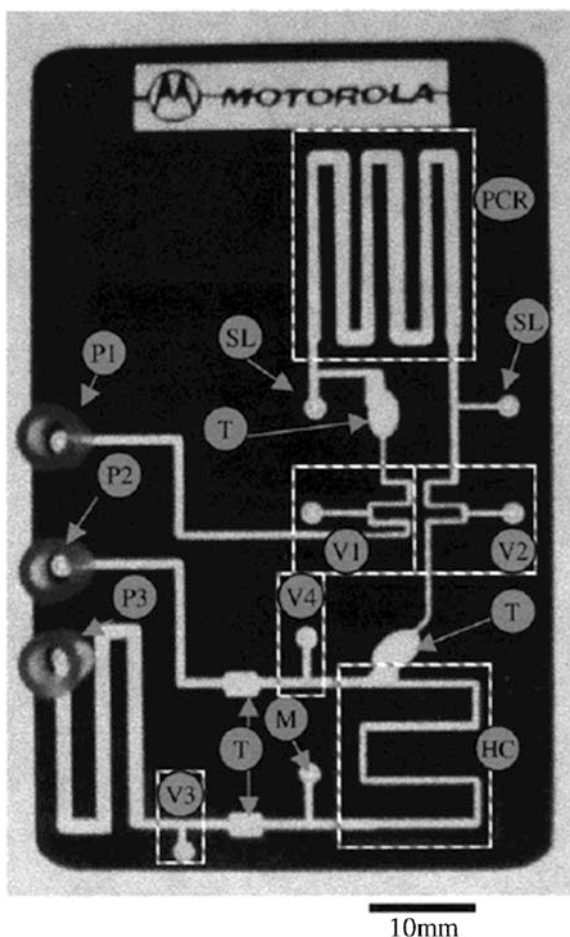
must be ensured not only for the reagent storage but also for the parts faced with the sample to prevent contamination and to guarantee reliable and accurate sample preparation. Therefore, all precautions must be taken in a cost effective way for the storage of reagents and shipment of lab-on-a-chip systems.

8.6.1.2 Amplification

High sensitivity and high selectivity are essential features of lab-on-a-chip systems for POC diagnosis. Diagnosis of any target pathogen starts with the processing of the crude sample to obtain the nucleic acid of the pathogen, which contains the genetic information, by using sample preparation methods. The presence or absence of the correct sequence in the solution can be analyzed by sequence specific interaction with a complementary probe or genome sequence profiling. Although there is a great effort by some companies to develop genome sequence profiling of whole nucleic acid sequence on miniaturized portable systems, the development process could not be completed yet. However, the detection with the use of former analysis method, which is known as hybridization, is possible in miniaturized systems with the sensing strategies described above or in their combinations. The sensitivity of the sensing strategy depends on the amount of nucleic acid in the analysis solution and the surface activation processes, which improve the signal. Amplification of signal is the key for high sensitivity which can enable the single cell detection and/or a few copy of nucleic acid detection, by multiplying the target nucleic acid sequence or using biological particles as reporter, such as enzymes [64]. Amplification of nucleic acids in a single chip does not only increase the high sensitivity, but also prevents contamination and decreases handling steps, volume of valuable reagents, and cost.

Polymerase Chain Reaction (PCR) is a common cost-effective choice to amplify nucleic acids for further detection. The target nucleic acid sequence is multiplied by enzymatic activity and it is based on thermal cycling of three steps: denaturation, annealing, and elongation [61]. The complete process can be ended with 30–40 thermal cycles and each cycle takes one to three minutes [65]. The total time is spent for reactions at each cycle and heating and cooling steps of the cycles. Since the required reaction time cannot be decreased, the effective way is to reduce time for heating and cooling by using miniaturized systems [61, 66]. The first PCR amplification in a micro fabricated chamber was studied by Northrup et al. [67] in 1993 and there is an extended amount of studies which resulted with impressive amplification limits. The micro fabricated PCR units can be classified in two groups according to the place that amplification occurs: stationary PCR and flow-through PCR [68]. In stationary PCR, the amplification takes place in a micro chamber, which has a heater on the chip. Therefore, it necessitates a novel design, while it provides good temperature control. On the contrary, the flow through PCR, the amplification reaction occurs in the micro channels, which needs syringe pump control (Fig. 8.8). In the study of Chung et al. [69], a palmtop system, which has a triangular loop channel for PCR steps with an inlet and an outlet and at which the

Fig. 8.8 Monolithic integrated polycarbonate DNA assay device. Serpentine PCR channel (PCR), hybridization channel (HC), Pluronic valves (V1–V4), Pluronic traps (T), hydrophobic air-permeable membrane (M), PCR reagent loading holes (SL), sample driving syringe pump (P1), waste-withdrawing syringe pump (P2), and wash syringe pump (P3). Figure and legend [Reprinted (adapted) with permission from [70]. Copyright (2002) American Chemical Society]



flow was controlled by thermo siphon effect, was fabricated from polycarbonate pellet by using chemical–mechanical polishing (CMP) and worked with a thermal cyclers system. They demonstrated that the disposable microfluidic PCR chip was capable of amplifying 127 bp target gene in 10 min. In the study of Jung et al. [68], the advantages of two groups of the PCR units were combined on a system composed of microfluidic chip with dimensions 18×50 mm, thermal blocks, and a motor for rotation. The PDMS based disposable microchip was rotated on thermal blocks, which have 94, 58 and 72 °C for denaturation, annealing, and extension steps, respectively. Therefore, there was not any time-consuming step due to the settling of temperature at each step. The experimental results were demonstrated that the amplification of target genes, which were RNA sequences of influenza A H3N2, H5N1, and H1N1, was performed in 25.5 min. In conclusion, the microfluidic PCR chips can be integrated with sample preparation units to have sample-in-answer-out systems.

As an alternative to PCR, there are other miniaturized amplification methods, which are performed at constant temperature, and therefore they do not necessitate any ramping temperature cycles: nucleic acid sequence-based amplification (NASBA), strand displacement amplification (SDA), loop-mediated isothermal amplification (LAMP), helicase-dependent amplification (HDA), and rolling circle amplification (RCA).

NASBA is used for amplification of RNA sequences (i.e., mRNA, rRNA, genomic RNA and ssDNA) at 41 °C with the use of three enzymes: avian myeloblastosis virus reverse transcriptase, RNase H, and T7 RNA polymerase [64, 71]. In short, the forward primer binds to RNA template and complementary DNA was synthesized by reverse transcriptase. RNase H, which affects only hybridized RNA, destroys RNA in RNA-DNA hybrid. Then, the reverse primer binds to the DNA to form new RNA-DNA hybrid. T7 RNA polymerase attacks to the new hybrid to form new RNA template [72]. As in PCR, NASBA is also a cyclic process to amplify sequences exponentially. Since three enzymes work sequentially for specific purposes, it is important to use certain amounts from these enzymes to proceed the reactions. In this account, it is more complex than the conventional PCR methods [71]. The first miniaturized system was developed by Gulliksen et al. [71] in 2004. The system was made of silicon and glass and it has three reactors with volumes 10, 50, and 300 nl. The reagents were manually loaded to the chambers and the inner surfaces of chambers were coated with SigmaCote to prevent nonspecific adsorption of enzymes. As a target sequence, HPV 16 was amplified successfully and it was demonstrated that the results of NASBA amplification in the micro fabricated device were in good agreement with the ones in conventional method although the reactor volumes were decreased by 2,000 in order. In the study of Furuberg et al. [73], a prototype composed of an inlet, a waste chamber, ten parallel amplification units, in which there are three capillary valves and two reaction chambers, was manufactured by using COC. After fabrication, the surfaces were activated with polyethylene glycol (PEG). NASBA amplification was performed in parallel 500 nl reactors by using pre-stored dry reagents. It was shown that the enzymes could be stored, dried, and rehydrated in the reactors of the chip. In the study of Dimov et al. [74], NASBA amplification was integrated with RNA isolation and real time detection with molecular beacon fluorescent probes for the first time in literature. The integrated system was made out of PDMS and silica beads were adhered to the surface of RNA purification chamber. The amplification results demonstrated that it was possible to take result of detection in real time, just after NASBA amplification started. *E. Coli* was used as a target analyte and the time-to-result for this pathogen from sample preparation to detection was 30 min.

SDA is an isothermal method used for amplification of DNA. Multiple enzymes (e.g., a restriction enzyme and DNA polymerase) and four primers are used to form amplified products of a target DNA sequence and displace the copied sequence. The amplification process starts with denaturation of target double strand DNA and a primer with restriction enzyme attach to the single strand sequence to synthesize strand by using DNA polymerase. The strands generated

are displaced by a bumper primer. Another restriction enzyme, which is stable to high temperatures, marks the double stranded molecules with a single-strand nick and DNA polymerase extends the new strand to form target copy [64]. SDA is commonly used for cells, which are difficult to make culturing, such as *Chlamydia trachomatis*. Yang et al. [75] described an integrated micro laboratory device combined with CMOS circuit and a SDA module to detect analytes starting from isolation of cells. The device had a stacking structure made out of PMMA, acrylic adhesive layer, polyimide and CMOS circuit on a glass substrate. It was demonstrated that Shiga-like toxin gene detection from *E. Coli* was performed in 2.5 h, including dielectrophoretic concentration of bacteria, cell lysis, and SDA at 60 °C.

LAMP is an amplification method of DNA strands with high sensitivity and rapidity [76]. It takes less than an hour to amplify a strand of DNA to 10^9 copies. DNA polymerase and four primers are necessary to perform this amplification process. However, it is also possible to amplify RNA sequences by adding reverse transcriptase to the process [77]. Fang et al. [78] integrated LAMP with micro fluidics to detect target analytes in a portable device. The device was fabricated from PDMS by using glass as substrate and demonstrated to analyze DNA samples with 400 nl volume in less than one hour for an isothermal amplification process at 63 °C. In the study of Liu et al. [79], a disposable cassette composed of three layers of polycarbonate, two PDMS valves, and two thin film heaters was developed to perform LAMP reaction in micro chambers. The detections of 10 target copies of DNA sequence of *E. Coli* and RNA sequence of HIV included in Eiken LoopAmp kit were successfully performed with the use of developed cassette at 63 °C.

HDA is also used for amplification of DNA sequences at a constant temperature of 65 °C. The working principle of HDA is the same with the PCR, except with the operating temperature. Its advantage compared to PCR is that, it does not need a thermal cycler, which increases process time because of heating and cooling transient stages. However, HDA requires optimally designed primers. Mahalanabis et al. [80, 81] integrated sample preparation with real time HDA to detect amplified products with a fluorescent reporter, for the first time in literature. The disposable cartridge was made out of COP and composed of micro solid phase extraction column to isolate DNA from crude sample, hydrophobic vents, micro channels and four reaction chambers; one of them was for control purposes. They presented that the disposable cartridge could detect at least 10 colonies of *E. Coli* in a medium.

RCA is an amplification method, which uses the feature of circular DNA. Two different approaches of RCA are single primed RCA and double primed RCA. In the former, the rolling circle DNA template works together with a primer, which results 10^2 – 10^3 copies of ssDNAs that are lengthy and have repeated sequences. In the later, two primers are used and the amplified product is 10^9 distinct copies of target sequence [82]. Mahmoudian et al. [83] presented, for the first time, a micro system made out of PMMA that combines single primed RCA, circle-to-circle amplification and capillary electrophoresis on a chip. This system had T-shaped micro channels and four reservoirs. The longest channel was preloaded with

polyethylene oxide polymer and SYBR gold fluorescent dye. The sample preparation was performed in an off-chip system and it was shown that the device was capable of amplifying and detecting as few as 25 ng DNA sequence of *Vibrio cholerae* in less than 65 min at 37 °C. In the study of Sato et al. [84], micro beads were used in on-chip reaction of RCA to enable rinsing procedures. The primer probe tagged micro beads were placed in the channels of device and RCA amplification was performed at 30 °C. After production of lengthy DNA sequences on micro bead, fluorescence staining was done to detect DNA sequences by taking images with either CCD camera or confocal microscope. The capability of device was demonstrated by detecting 88 ng Rsa I-fragmented *Salmonella Enterica* DNA.

In addition to the above mentioned amplification methods, there are others named as new amplification techniques, which may have different applications in micro systems. Recombinase polymerase amplification (RPA) [85], multiple displacement amplification (MDA) [86], and exponential amplification reaction (EXPAR) [87] are some of them [64]. These and the above mentioned amplification methods offer a promise in the way of detecting rare cells in a growth medium. However, it is crucial to integrate them with sample preparation and detection modules in order to have portable diagnostic systems.

In the following section, recent developments in the systems used for the detection of different diseases, which pose serious threats to public health, and chemicals such as drugs will be given.

8.6.1.3 Detection

The rapid and accurate diagnosis is critical for diseases, specially for heart diseases, cancerous diseases and infectious diseases like MRSA, HIV, and tuberculosis diseases, which directly affect the immune system. Many of these diseases have an increasing threat around the world [10].

Heart diseases are the leading cause of death in the developed countries. It affects millions of people around the world and the number of affected people further increases with ageing. The cost of coronary heart disease alone was about 108 million US\$ to United States in 2008 while the total cost of heart diseases to Europe in 2006 was about €110 billion, which is a real financial burden to the clinics [88, 89]. One of the most commonly encountered heart diseases is acute myocardial infarction (AMI), which is known as heart attack and it is due to temporally cease of blood supply to heart, which results in an injury of heart cells. The signs of AMI must be followed for the suspicious patients of AMI. For this purpose, the information taken from electrocardiogram and the level of cardiac specific biomarkers in the patient's blood must be examined [90]. Some of these specific biomarkers are Troponin-I, myoglobin, MB band of creatine kinase (CK-MB), and D-dimer. Although there are newly developed commercial products for immunosensing of the biomarkers, the problems behind the integration of the commercial products with the existing clinical routine tests, their cost to clinics

and the limited portability limit the usage of these commercial products in the clinics. Therefore, lab-on-a-chip systems have been developed by scientists for point of care diagnosis of AMI in the field of heart diseases. For this purpose, CMOS compatible silicon nanowire biosensor without labeling [2], resonant sensor [91], nanoparticle based electrochemiluminescence sensor [92] have been developed to detect cardiac Troponin-I marker, which is generally around 0.5 ng ml^{-1} in normal serum and increases upon AMI, with a lowest detection limit of 0.002 ng ml^{-1} [92]. In recent years, the use of amperometric methods has been preferred in the commercialized products for POC diagnosis, as in the case of i-STAT (Abbott Point of Care, U.S.A) at which only $16 \text{ }\mu\text{L}$ blood sample is necessary to detect the level of Troponin-I [90].

On the other hand, cancer comes in the second for the cause of death and the overall annual cost of cancer to the US alone is about \$263.8 billion for 2010 [93]. The expected growth and ageing of population can increase the cost of medical treatments, which is a growing burden for the clinical resources. According to United States Cancer Statistics Data for the years between 2003 and 2007, the top 10 cancer sites diagnosed for every 100,000 people are prostate (153.6), female breast (120.5), lung and bronchus (68.1), colon and rectum (48.9), corpus and uterus (23.8), urinary bladder (21.3), non-hodgkin lymphoma (19.3), melanomas of the skin (18.3), kidney and renal pelvis (14.9), and ovary (12.8) [94]. It is important to diagnose the disease at an early stage to reduce incidence and morbidity and mortality rates, improve prognosis and the quality of life of the patient. In the identification of the prostate cancer, almost all detection methods have been used. In the study of Waggoner et al. [95], a micromechanical trampoline resonator was developed and the resonator surface area of $\sim 54 \text{ }\mu\text{m}^2$ was functionalized by using APTS chemistry. The lowest detection limit with this sensor was 50 fg ml^{-1} prostate specific antigen (PSA). A lower detection limit, 1 aM (0.1 fg ml^{-1}) was achieved by using functionalized gold nanorods and detecting the resonance shift difference with LSPR [96]. In the study of Chuah et al. [97], magnetic and electrochemical detection methods are combined to detect PSA on thin gold surface by using horseradish peroxidase as signal amplifier and the lowest detected PSA concentration was found to be 100 fg ml^{-1} [97]. On the other hand, Toner's group developed a microfluidic device which is capable of sensing 5 CTCs/ml with accurate identification and it is composed of pillars with surfaces which were functionalized with specific antibodies to capture different types of rare circulating tumor cells (CTCs) [i.e., prostate, colon, localized prostate, breast, pancreas, and non-small-cell lung cancer (NSCLC)] [98]. The ovarian cancer is the fifth leading cause of death among women in US [94]. The increase in epithelial ovarian cancer antigen-125 (CA-125) is the indicator of the disease and the normal limit of CA-125 in the blood of healthy patient is less than 35 units per milliliter. In the study of Viswanathan et al. [99], the electrochemical detection of a protein biomarker related to the ovarian cancer was performed by using molecular imprinted nano sensor. In the fabrication of the sensor, membrane is used as substrate and gold electroless deposition is performed to have pillars in nano scale dimensions. Then a thin film of CA-125 is coated on the pillars by using protein imprinting.

The presence of the marker was analyzed by the occurrence of oxidation reaction of $[\text{Fe}(\text{CN})_6]^{-4}$. The detection limit of 0.5 units per milliliter was achieved, that allows the biosensor developed to be used as screening test.

Infectious diseases result from pathogenic microorganisms like those that bacteria, virus and fungi, and they are transmitted from human to human. Although human being has bacteria in the flora, the increase in the number of bacteria in the body results in disease that directly affects the immune system. HIV, tuberculosis, malaria, meningococcal meningitis, and influenza are some examples to infectious diseases. In a recent study, a smart phone was combined with a microfluidic chip for detection of *Staphylococcus aureus* and *Escherichia coli* with loop-mediated isothermal amplification (LAMP) for point of care testing [42]. Another device for point of care diagnosis of infectious diseases was developed by Zhu et al. [100]. In their study, a cellular phone was combined with a fluorescent microscopy to detect white blood cells and *Giardia Lamblia* parasite with a sample volume 100 μl .

In developing biosensors for point of care diagnosis, the first aim is to have rapid and accurate diagnosis with small amount of sample taken from the patient. However, it is important to reduce the cost of the biosensors to make use of the biosensors in the economically developed countries. For this purpose, alternative materials (e.g., paper, wax, tape, cellulose powder, etc.) are suggested to use in forming microfluidic analysis systems by Whitesides's group [101–103]. For example, in the study of Wong et al. [101], human blood plasma isolation was performed by using an egg beater and then the sample was analyzed for cholesterol assay on patterned paper. Then, an electrochemical assay on paper was studied by Nie et al. [104] by combining micro fluidics to determine heavy metal ions and glucose. The capability of producing programmable diagnostic patterns with paper was demonstrated by Martinez et al. [105].

8.6.2 Human-on-a-Chip Systems

Biosensors have place in medical applications not only for detection but also for understanding the behavior of biological structures like cells, organs, and tissues at different environments. “Organ-on-a-chip” micro devices that can mimic or reproduce the tissue–tissue interfaces are good examples of such biosensors, which are complexly integrated mechanical, biological, and chemical structures. These micro devices, which resemble closely to organs, can be used in the development of experimental model systems for drug screening and toxicology applications of chemicals to reduce cost and time consumed with animal-based experiments and clinical trials.

Current method in culturing of cells for drug discovery applications is in vitro, and it is based on incubating multi-well plate systems at which the medium with its cells and drug is static. However, the behavior of tissue cells in vivo can be different from the one in vitro system due to the dynamic complexity of the drug delivery. Therefore, various amounts of organs have been studied to miniaturize tissues and monitor cell behavior for long periods ranging from bone to muscle.

In this aspect, inspiration from nature has been achieved by scientists in the designs of “organ-on-a-chip” to develop “human-on-a-chip” systems.

8.6.2.1 E-Skin-on-a-Chip

The thermal and electronic conductivity and pressure sensitivity of the skin have been researched for many years. Although there are different attempts to mimic the structure of skin for practical applications, the most suitable ones were developed with micro fabrication techniques [106]. Kim et al. [106] developed an electronic membrane, which was like a tattoo to measure electrical activity resulted from brain, heart and skeletal muscles actions. This compact electronic device was composed of electrodes, sensors, power supply, and wireless components. The capability of device was shown by measuring ECG, EMG, and EEG from chest, leg, and forehead of the body, respectively. Another promising study related to the electronic skin (e-skin) was developed by Bao’s research group [7]. The micro fabricated device was an Organic Field Effect Transistors (OFET) based e-skin, which can transduce the physical or chemical events occurring on the surface to electronic signal (Fig. 8.9). In this e-skin, the semiconductor layer made of Si/SiO₂ is for detection of chemical or biological species such as TNT, cysteine and pH while the dielectric layer, which is composed of PDMS micro pillars, serves as pressure sensors on a biocompatible or biodegradable substrate (e.g., ITO/PET). The response time (~ 100 ms) for human physiological detection limit of sensation and detection of part-per-million to part-per-billion concentrations of chemicals or biological analytes were achieved by using this OFET device.

8.6.2.2 Intestine-on-a-Chip

The gastrointestinal tract is the place where the digested products enter the systemic circulation. In drug development, the knowledge of effects and pathways of

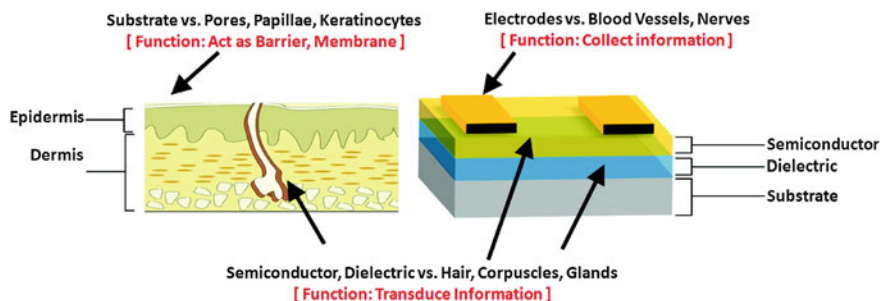


Fig. 8.9 A schematic drawing showing the similar tasks between OFET-based-e-skin device and human skin [Reprinted with permission from [7] Copyright (2012) American Chemical Society]

drug from uptake to removal from the human body is crucial to analyze drug toxicity [107]. In this account, researchers have also investigated miniaturization of gastrointestinal structure to understand the dynamics of drug toxicity. In the study of Kimura et al. [108], the prolonged (21 days) cultivation of gastrointestinal cells has been performed by using a PDMS chip with on-chip pumping and micro fluidics and the chemical transport in gastrointestinal cell culture was analyzed with the transport of Rhodamine 123 in colon carcinoma cell line, Caco-2 cells. Mahler et al. [107] developed an intestine-on-a-chip system, which composed of digestion, a mucus layer and physiologically realistic cell populations. The device was mimicked and designed so that the residence time and the distribution of flow in channels and chambers were similar to gastrointestinal tract. In the fabrication, standard micro fabrication techniques were used. The device capability and the effects of drug on toxicity was demonstrated with a decrease in gastrointestinal and liver cell glutathione for an orally taken drug, acetaminophen. The mimicking of gastrointestinal villi in micro scale was performed by Sung et al. [109]. The 3D microstructures were fabricated with collagen/PEG, and Caco-2 cells were fed to cover the micro gastrointestinal villi by cell proliferation.

8.6.2.3 Liver-on-a-Chip

Drugs can have some adverse effects on human body although they are designed for the treatment of some illnesses. One of the most important adverse effects is drug toxicity, which can mostly affect the liver and can cause changes in liver functions, even liver failure [110]. The drug toxicity in liver is known as hepatotoxicity and it is necessary to test toxicity of drugs with reliable and cost effective tools. The miniaturization of cell cultures offers a promise for these tests. Among the developed approaches, 3D cell cultures have potential to mimic biological tissues. In the study of Domansky et al. [111], a 3D tissue culturing platform was developed to understand liver pathology in drug development. The organ-on-a-chip platform was designed and fabricated in an array format. The behavior of cell culture was monitored with the transfer and consumption of oxygen and the experimental findings were compared with the developed dynamic model. It was demonstrated that the oxygen uptake of cells followed a first order reaction with a constant of $0.27 \pm 0.03 \text{ ml min}^{-1}$. Moreover, hepatocytes were cultured for seven days. To demonstrate suitability of device for long term culturing, Liver Sinusoidal Endothelial Cells (LSECs) and hepatocytes were cultured for 13 days and it was observed that LSECs continued the expression of SE-1 antibody. In the study of Khetani and Bhatia [112], PDMS based multiwell elastomeric culture system was developed to analyze hepatotoxicity. The proof of device capability to culturing was demonstrated by hepatocyte-fibroblast co-culturing for several weeks with maintaining functional expressions. In addition to 3D tissue culturing micro devices, it is important to take into consideration the cell-cell interactions for having cultured cells similar to in vivo tissue cells. In this account, Toh et al. [113] studied on 3D microfluidic channel based micro culture

system, which was made from transparent materials, such as PDMS and glass, and enabled the imaging of cell–cell interaction by using confocal microscope. Midwoud et al. [114] presented integration of intestinal micro sliced tissue into a miniaturized flow system, for the first time in literature. It was demonstrated that the sliced tissue remained its functions at least three hours of incubation medium. Moreover, the incorporation of intestine and liver tissue slices was performed to investigate the effects of organs on each other in a sequentially connected microfluidic system.

8.6.2.4 Tumor-on-a-Chip

The culturing of cancerous cells is also an essential issue in drug discovery, especially for circulating tumor cells (CTCs). It is important to select drug type and predict the behavior of the chemicals or drugs on the targeted tissue in connection with other organs. The *in vitro* culturing of cancerous cells can provide a platform to determine the drug type for individual patients [115]. Frimat et al. [116] presented single cell culturing of cancerous cells in a microfluidic device by a cellular valve structure. PDMS was used in the fabrication of device with eight parallel serpentine micro channels, which had 40 μm width and 200 trapping zone. The capability of device was demonstrated by using the single cell capturing and culturing of cells with diameters ranging from 14.6 to 17.9 μm (i.e., Human SW480 epithelial, MCF-7 epithelial like breast cancer cells, and HT29 colon carcinoma cells). However, it needs more research on retrieving of captured single cells from the fluidic device for further off-chip experiments and for limiting cellular interactions between neighboring cells. Hong et al. [117] developed a microfluidic platform, which allows sequential trapping of single cells in a culture chamber on the side of channels. This device provides an environment to analyze single cell culturing or cell–cell interactions. In the study of Sung et al. [118], a compact microfluidic system was developed to culture multiple cell lines and to have almost same residence time with the physiological residence time of the blood flow in three regions (i.e., colon tumor, liver, and marrow). Then, the cancer cells were loaded into the colon tumor and liver and the effect of drug, Tegafur, on cells was analyzed in comparison with the observed effects at 96-well micro plate. It was revealed that the toxicity effect of Tegafur on liver cells was observed only with the cultures in microfluidic device. The isolation, detection and culturing of CTCs was miniaturized by Kang et al. [115]. The microfluidic device was made of PDMS with 100 μm in height micro channels with side chambers to collect magnetic particle adhered CTCs. The nonspecific adsorption of cells to the walls of channels was prevented by using Pluronic-F108 and cell residues was filtered with micro pillars located at the beginning part of the channel. The device was capable of isolating breast cancer cells introduced into one-milliliter blood of mouse and expansion of these cells for culturing in a 96-well tissue culture plates in seven days.

8.6.2.5 Blood-Vessel-on-a-Chip

Blood vessels are intricate network of the circulatory system, which plays a crucial role in transportation of nutrients, chemicals, and waste throughout the body. The miniaturization of such a complex network in a chip is a big challenge since vessels provides interaction between different organs. Raghavan et al. [119] studied the control of endothelial tubulogenesis by growing them in micro channels filled with collagen. The lumen tubes were formed in one centimeter in length and the diameter of these tubes were controlled with either channel diameter or collagen concentration. The cell migration and the interaction of cells in a co-culture medium to form capillary tubes were investigated by Chung et al. [120]. The proof of interaction was demonstrated by culturing three different cells: endothelial, cancer and muscle cells. It was concluded that muscle cells caused to cease endothelial cell activity while the effect of cancer cells on capillary morphogenesis depended on the type of cancer cells. Another factor, which can affect the structure and function of vessels, is physiological conditions, such as pressure, temperature, and chemicals. A microfluidic platform was developed by Günther et al. [121]. The device provided a well-defined environment to determine the artery structure and function in long term culturing of cells. Shao et al. [122] studied the effect of stress on epithelial cells and for this purpose; they developed a microfluidic device, which enables the experiments in both static and dynamic conditions. It was concluded that the endothelial cells gave different morphological responses to laminar and turbulent shear stresses.

Although promising results were obtained from simple and cost effective micro devices, the real phenomenon is much more complex than the one faced in experiments. Therefore, these integrated micro devices provide an opportunity to understand the dynamics of tissue cells in different environments.

8.6.2.6 Muscle-on-a-Chip

In vitro culturing models can be used in understanding behavior of cells in physiological conditions rather than animal experiments [110, 123]. Skeletal muscle plays a crucial role in the maintenance of glucose homeostasis. Models containing skeletal muscle cells can help to elucidate the complex mechanisms of insulin resistance in type 2 diabetes [124]. The systems integrated with micro electric parts provide platforms for monitoring the physiological activity of the cells. However, it is important to culture cells on the contact points, at which electrical pulses were applied to the cells, for long periods, since the cells tend to detach from the surface after a few days of inoculation. Therefore, it is necessary to design novel micro devices for culturing cells, which have similar characteristics with their counterparts in in vivo experiments.

In the study of Nagamine et al. [125], a skeletal muscle cell-based device was micro fabricated to culture muscle cells by using myotube/gel sheet patched Pt electrode arrays [125]. This organ-on-a-chip was enabled the determination of

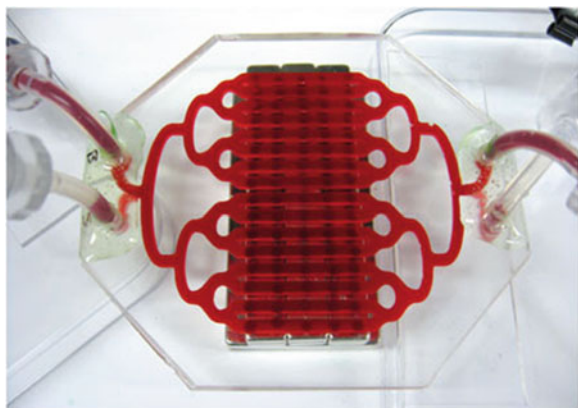
contraction effect of glucose transporter, GLUT4, which is responsible for transport of glucose in the control of insulin, at translocations of myotubes by periodic electrical pulse stimulation of muscle cells. In the study of Kaji et al. [126], a micro device was developed to stimulate C2C12 cells cultured on porous membrane and to study the glucose uptake relation with contractile activity with fluorescence-labeled glucose. The electrical stimulation resulted in the contraction of myotubes on the membrane and this resulted to a proportional relationship with glucose uptake. Bajaj et al. [127] studied the differentiation of C2C12 skeletal cells with the geometric structures used in micro devices patterned with a protein, fibronectin. Linear, circular, and hybrid pattern were used as geometrical structure and the hybrid pattern with 30° angle was demonstrated as the optimal structure to maximize differentiation of the cells.

8.6.2.7 Other Tissues

Along with the above mentioned organ-on-a-chip systems, there are numerous attempts to develop miniaturized in vitro models of tissues. Some of them will be mentioned here to show the capabilities of micro engineered devices. In the study of Huh et al. [128], a PDMS microfluidic device with its alveolar epithelial cell culture and air–liquid interface was developed to reconstitute the human alveolar-capillary interface. Although there are some differences between the micro device and the real lung such as barrier thickness and changes in airflow, the lung-on-a-chip can be used in the analysis of mechanical forces on epithelial cell growth. Blake et al. [129] presented a micro device to culture brain slice on a chip, which enables the insertion of probes through the edges of brain slices.

Researchers from Wyss Institute for Biologically Inspired Engineering at Harvard University have been working on spleen-on-a-chip for sepsis therapy to separate pathogens with nano magnetic beads from contaminated blood (Fig. 8.10). Up to now, the anticoagulated whole human blood was passed through

Fig. 8.10 Spleen-on-a-chip
[Reprinted by permission
from Macmillan Publishers
Ltd: [Nature] [131],
Copyright (2011)]



the device without any clotting with a flow rate of 36–360 ml/h and the capability of device was demonstrated with separation of 99.8 % of fungal pathogens in blood [130].

8.7 Conclusion

Thin films made of either organic or inorganic materials are critical functional components of biosensors. Physical and chemical vapor deposition, electroplating, and electroless coating are processes to deposit films layer-by-layer on a substrate. The thickness, composition, and uniformity of the films are the major factors that determine the specificity and sensitivity of biosensors. There are different detection strategies to sense biomolecules and among them, electrical detection has been the most preferred one because of ease of miniaturization of electrodes and compatibility with integrated circuits and thin film biosensors. However, new developments in thin film deposition techniques have enabled the combination of biosensors with miniaturized optical devices such as OLEDs in detection of biomolecules. Diagnosis by using of low-cost, sensitive, and reliable biosensors is of particular interest to detect the markers or indicators of some of the most commonly encountered mortal diseases around the world to reduce mortality and morbidity rates, to improve life quality of patient, and to reduce cost to clinics. However, the commercialization of lab-on-a-chip systems for point of care diagnosis still needs much improvement for automation. Other than the diagnosis, in the last decade, human-on-a-chip systems have also gained importance in order to develop personal drugs and to have efficient treatment. As research continues to be made in the microenvironment, it is certain that the thin films biosensors will be everywhere, even on and in our body with intelligent sensors.

References

1. Newman, J., Setford, S.: Enzymatic biosensors. *Mol. Biotechnol.* **32**(3), 249–268 (2006). doi:[10.1385/mb:32:3:249](https://doi.org/10.1385/mb:32:3:249)
2. Kong, T., Su, R., Zhang, B., Zhang, Q., Cheng, G.: CMOS-compatible, label-free silicon-nanowire biosensors to detect cardiac troponin I for acute myocardial infarction diagnosis. *Biosens. Bioelectron.* **34**(1), 267–272 (2012). doi:[10.1016/j.bios.2012.02.019](https://doi.org/10.1016/j.bios.2012.02.019)
3. Tan, C.P., Craighead, H.G.: Surface engineering and patterning using parylene for biological applications. *Materials* **3**(3), 1803–1832 (2010). doi:[10.3390/ma3031803](https://doi.org/10.3390/ma3031803)
4. Li, W., Kabius, B., Auciello, O.: Science and technology of biocompatible thin films for implantable biomedical devices. In: 2010 Annual International Conference of the IEEE Engineering in Medicine and Biology Society. IEEE Engineering in Medicine and Biology Society Conference Proceedings, pp. 6237–6242. (2010). doi:[10.1109/IEMBS.2010.5628056](https://doi.org/10.1109/IEMBS.2010.5628056)
5. Farra, R., Sheppard, N.F., McCabe, L., Neer, R.M., Anderson, J.M., Santini, J.T., Cima, M.J., Langer, R.: First-in-human testing of a wirelessly controlled drug delivery microchip. *Sci. Transl. Med.* **4**(122), 121–122 (2012)

6. Ainslie, K.M., Desai, T.A.: Microfabricated implants for applications in therapeutic delivery, tissue engineering, and biosensing. *Lab Chip* **8**(11), 1864–1878 (2008). doi:[10.1039/b806446f](https://doi.org/10.1039/b806446f)
7. Sokolov, A.N., Tee, B.C.K., Bettinger, C.J., Tok, J.B.H., Bao, Z.: Chemical and engineering approaches to enable organic field-effect transistors for electronic skin applications. *Acc. Chem. Res.* **45**(3), 361–371 (2011). doi:[10.1021/ar2001233](https://doi.org/10.1021/ar2001233)
8. Chiang, T.-C.: Superconductivity in thin films. *Science* **306**(5703), 1900–1901 (2004). doi:[10.1126/science.1106675](https://doi.org/10.1126/science.1106675)
9. Dew-Hughes, D.: The critical current of superconductors: An historical review. *Low Temp. Phys.* **27**(9–10), 713–722 (2001). doi:[10.1063/1.1401180](https://doi.org/10.1063/1.1401180)
10. Ceylan Koydemir, H., Kulah, H., Ozgen, C., Alp, A., Hascelik, G.: MEMS biosensors for detection of methicillin resistant *Staphylococcus aureus*. *Biosens. Bioelectron.* **29**(1), 1–12 (2011). doi:[10.1016/j.bios.2011.07.071](https://doi.org/10.1016/j.bios.2011.07.071)
11. Maloney, J.M., Uhlund, S.A., Polito, B.F., Sheppard Jr, N.F., Pelta, C.M., Santini Jr, J.T.: Electrothermally activated microchips for implantable drug delivery and biosensing. *J. Controlled Release* **109**(1–3), 244–255 (2005). doi:[10.1016/j.jconrel.2005.09.035](https://doi.org/10.1016/j.jconrel.2005.09.035)
12. Carlisle, J.A.: Diamond films: Precious biosensors. *Nat. Mater.* **3**(10), 668–669 (2004). doi:[10.1038/nmat1225](https://doi.org/10.1038/nmat1225)
13. Marcon, L., Spriet, C., Coffinier, Y., Galopin, E., Rosnoble, C., Szunerits, S., Hélot, L., Angrand, P.-O., Boukherroub, R.: Cell adhesion properties on chemically micropatterned boron-doped diamond surfaces. *Langmuir* **26**(19), 15065–15069 (2010). doi:[10.1021/la101757f](https://doi.org/10.1021/la101757f)
14. Wang, H., Griffiths, J.-P., Egdell, R.G., Moloney, M.G., Foord, J.S.: Chemical functionalization of diamond surfaces by reaction with diaryl carbenes. *Langmuir* **24**(3), 862–868 (2008). doi:[10.1021/la702701p](https://doi.org/10.1021/la702701p)
15. Shao, Y.Y., Wang, J., Wu, H., Liu, J., Aksay, I.A., Lin, Y.H.: Graphene based electrochemical sensors and biosensors: A review. *Electroanalysis* **22**(10), 1027–1036 (2010). doi:[10.1002/elan.200900571](https://doi.org/10.1002/elan.200900571)
16. Becker, H., Gartner, C.: Polymer microfabrication technologies for microfluidic systems. *Anal. Bioanal. Chem.* **390**(1), 89–111 (2008). doi:[10.1007/s00216-007-1692-2](https://doi.org/10.1007/s00216-007-1692-2)
17. Lin, L., Mason, A.J.: Post-CMOS parylene packaging for on-chip biosensor arrays. In: *Sensors, 2010 IEEE*, pp. 1613–1616, 1–4 Nov 2010. doi:[10.1109/ICSENS.2010.5690397](https://doi.org/10.1109/ICSENS.2010.5690397)
18. Yildirim, E., Kulah, H.: Analysis and characterization of an electrostatically actuated in-plane parylene microvalve. *J. Micromech. Microeng.* **21**(10), 105009 (2011). doi:[10.1088/0960-1317/21/10/105009](https://doi.org/10.1088/0960-1317/21/10/105009)
19. Choi, C.K., English, A.E., Jun, S.-I., Kihm, K.D., Rack, P.D.: An endothelial cell compatible biosensor fabricated using optically thin indium tin oxide silicon nitride electrodes. *Biosens. Bioelectron.* **22**(11), 2585–2590 (2007). doi:[10.1016/j.bios.2006.10.006](https://doi.org/10.1016/j.bios.2006.10.006)
20. Ouyang, B.Y., Chi, C.W., Chen, F.C., Xi, Q.F., Yang, Y.: High-conductivity poly(3,4-ethylenedioxythiophene): poly(styrene sulfonate) film and its application in polymer optoelectronic devices. *Adv. Funct. Mater.* **15**(2), 203–208 (2005). doi:[10.1002/adfm.200400016](https://doi.org/10.1002/adfm.200400016)
21. Schreiber, F.: Structure and growth of self-assembling monolayers. *Prog. Surf. Sci.* **65**(5–8), 151–257 (2000). doi:[10.1016/S0079-6816\(00\)00024-1](https://doi.org/10.1016/S0079-6816(00)00024-1)
22. Greg, T.H.: Homobifunctional crosslinkers. In: *Bioconjugate Techniques*, 2nd edn. Academic Press, New York, pp. 234–275 (2008) doi:[10.1016/B978-0-12-370501-3.00004-7](https://doi.org/10.1016/B978-0-12-370501-3.00004-7) (Chap. 4)
23. Greg, T.H.: Heterobifunctional crosslinkers. In: *Bioconjugate Techniques*, 2nd edn. Academic Press, New York, pp. 276–335 (2008) doi:[10.1016/B978-0-12-370501-3.00005-9](https://doi.org/10.1016/B978-0-12-370501-3.00005-9) (Chap. 5)
24. Besselink, G.A.J., Schasfoort, R.B.M., Bergveld, P.: Modification of ISFETs with a monolayer of latex beads for specific detection of proteins. *Biosens. Bioelectron.* **18**(9), 1109–1114 (2003). doi:[10.1016/S0956-5663\(02\)00243-9](https://doi.org/10.1016/S0956-5663(02)00243-9)

25. Wang, C., Trau, D.: A portable generic DNA bioassay system based on in situ oligonucleotide synthesis and hybridization detection. *Biosens. Bioelectron.* **26**(5), 2436–2441 (2011). doi:[10.1016/j.bios.2010.10.028](https://doi.org/10.1016/j.bios.2010.10.028)
26. Arya, S.K., Chornokur, G., Venugopal, M., Bhansali, S.: Dithiobis (succinimidyl propionate) modified gold microarray electrode based electrochemical immunosensor for ultrasensitive detection of cortisol. *Biosens. Bioelectron.* **25**(10), 2296–2301 (2010). doi:[10.1016/j.bios.2010.03.016](https://doi.org/10.1016/j.bios.2010.03.016)
27. Chang, S.-C., Pereira-Rodrigues, N., Henderson, J.R., Cole, A., Bedioui, F., McNeil, C.J.: An electrochemical sensor array system for the direct, simultaneous in vitro monitoring of nitric oxide and superoxide production by cultured cells. *Biosens. Bioelectron.* **21**(6), 917–922 (2005). doi:[10.1016/j.bios.2005.02.015](https://doi.org/10.1016/j.bios.2005.02.015)
28. Kim, N., Park, I.-S.: Application of a flow-type antibody sensor to the detection of *Escherichia coli* in various foods. *Biosens. Bioelectron.* **18**(9), 1101–1107 (2003). doi:[10.1016/S0956-5663\(02\)00240-3](https://doi.org/10.1016/S0956-5663(02)00240-3)
29. Capobianco, J.A., Shih, W.-H., Leu, J.-H., Lo, G.C.-F., Shih, W.Y.: Label free detection of white spot syndrome virus using lead magnesium niobate–lead titanate piezoelectric microcantilever sensors. *Biosens. Bioelectron.* **26**(3), 964–969 (2010). doi:[10.1016/j.bios.2010.08.004](https://doi.org/10.1016/j.bios.2010.08.004)
30. Viswanathan, S., Rani, C., Vijay Anand, A., Ho, J.-a: Disposable electrochemical immunosensor for carcinoembryonic antigen using ferrocene liposomes and MWCNT screen-printed electrode. *Biosens. Bioelectron.* **24**(7), 1984–1989 (2009). doi:[10.1016/j.bios.2008.10.006](https://doi.org/10.1016/j.bios.2008.10.006)
31. Cha, J., Han, J.I., Choi, Y., Yoon, D.S., Oh, K.W., Lim, G.: DNA hybridization electrochemical sensor using conducting polymer. *Biosens. Bioelectron.* **18**(10), 1241–1247 (2003). doi:[10.1016/S0956-5663\(03\)00088-5](https://doi.org/10.1016/S0956-5663(03)00088-5)
32. Lee, K.-H., Su, Y.-D., Chen, S.-J., Tseng, F.-G., Lee, G.-B.: Microfluidic systems integrated with two-dimensional surface plasmon resonance phase imaging systems for microarray immunoassay. *Biosens. Bioelectron.* **23**(4), 466–472 (2007). doi:[10.1016/j.bios.2007.05.007](https://doi.org/10.1016/j.bios.2007.05.007)
33. Wang, Y., He, X., Wang, K., Ni, X., Su, J., Chen, Z.: Electrochemical detection of thrombin based on aptamer and ferrocenylhexanethiol loaded silica nanocapsules. *Biosens. Bioelectron.* **26**(8), 3536–3541 (2011). doi:[10.1016/j.bios.2011.01.041](https://doi.org/10.1016/j.bios.2011.01.041)
34. Yin, H., Zhou, Y., Zhang, H., Meng, X., Ai, S.: Electrochemical determination of microRNA-21 based on graphene, LNA integrated molecular beacon, AuNPs and biotin multifunctional bio bar codes and enzymatic assay system. *Biosens. Bioelectron.* **33**(1), 247–253 (2012). doi:[10.1016/j.bios.2012.01.014](https://doi.org/10.1016/j.bios.2012.01.014)
35. Ishikawa, F.N., Chang, H.K., Curreli, M., Liao, H.I., Olson, C.A., Chen, P.C., Zhang, R., Roberts, R.W., Sun, R., Cote, R.J., Thompson, M.E., Zhou, C.W.: Label-free, electrical detection of the SARS virus N-protein with nanowire biosensors utilizing antibody mimics as capture probes. *ACS Nano* **3**(5), 1219–1224 (2009). doi:[10.1021/mn900086c](https://doi.org/10.1021/mn900086c)
36. Sellers, H., Ulman, A., Shnidman, Y., Eilers, J.E.: Structure and binding of alkanethiolates on gold and silver surfaces: implications for self-assembled monolayers. *J. Am. Chem. Soc.* **115**(21), 9389–9401 (1993). doi:[10.1021/ja00074a004](https://doi.org/10.1021/ja00074a004)
37. Frank, S.: Structure and growth of self-assembling monolayers. *Prog. Surf. Sci.* **65**(5–8), 151–257 (2000)
38. Love, J.C., Estroff, L.A., Kriebel, J.K., Nuzzo, R.G., Whitesides, G.M.: Self-assembled monolayers of thiolates on metals as a form of nanotechnology. *Chem. Rev.* **105**(4), 1103–1169 (2005). doi:[10.1021/cr0300789](https://doi.org/10.1021/cr0300789)
39. Greg, T.H.: The chemistry of reactive groups. In: *Bioconjugate Techniques*. Academic Press, San Diego, pp. 137–166 (1996). doi:[10.1016/B978-012342335-1/50003-8](https://doi.org/10.1016/B978-012342335-1/50003-8)
40. Hermanson, G.T.: Silane coupling agents. In: *Bioconjugate Techniques*, 2nd edn. Academic Press, New York, pp. 562–581 (2008). doi:[10.1016/B978-0-12-370501-3.00013-8](https://doi.org/10.1016/B978-0-12-370501-3.00013-8) (Chap. 13)
41. Gotz, S., Karst, U.: Recent developments in optical detection methods for microchip separations. *Anal. Bioanal. Chem.* **387**(1), 183–192 (2007). doi:[10.1007/s00216-006-0820-8](https://doi.org/10.1007/s00216-006-0820-8)

42. Stedtfeld, R.D., Tourlousse, D.M., Seyrig, G., Stedtfeld, T.M., Kronlein, M., Price, S., Ahmad, F., Gulari, E., Tiedje, J.M., Hashsham, S.A.: Gene-Z: A device for point of care genetic testing using a smartphone. *Lab Chip* **12**, 1454–1462 (2012). doi:[10.1039/C2LC21226A](https://doi.org/10.1039/C2LC21226A)
43. Yao, B., Luo, G., Wang, L., Gao, Y., Lei, G., Ren, K., Chen, L., Wang, Y., Hu, Y., Qiu, Y.: A microfluidic device using a green organic light emitting diode as an integrated excitation source. *Lab Chip* **5**(10), 1041–1047 (2005). doi:[10.1039/B504959H](https://doi.org/10.1039/B504959H)
44. Bashir, R.: BioMEMS: State-of-the-art in detection, opportunities and prospects. *Adv. Drug Deliv. Rev.* **56**(11), 1565–1586 (2004). doi:[10.1016/j.addr.2004.03.002](https://doi.org/10.1016/j.addr.2004.03.002)
45. Johnson, B.N., Mutharasan, R.: Biosensing using dynamic-mode cantilever sensors: A review. *Biosens. Bioelectron.* **32**(1), 1–18 (2012). doi:[10.1016/j.bios.2011.10.054](https://doi.org/10.1016/j.bios.2011.10.054)
46. Eroglu, D., Kulah, H.: Quality factor enhancement of lateral microresonators in liquid media by hydrophobic coating. *J. Microelectromech. Syst.* **20**(5), 1068–1070 (2011). doi:[10.1109/jmems.2011.2160936](https://doi.org/10.1109/jmems.2011.2160936)
47. Burg, T.P., Godin, M., Knudsen, S.M., Shen, W., Carlson, G., Foster, J.S., Babcock, K., Manalis, S.R.: Weighing of biomolecules, single cells and single nanoparticles in fluid. *Nature* **446**(7139), 1066–1069 (2007). doi:[10.1038/nature05741](https://doi.org/10.1038/nature05741)
48. Ceylan Koydemir, H., Kulah, H., Ozgen, C.: A micro electrochemical sensor for the detection of methicillin resistance in *Staphylococcus aureus*. Paper presented at the Biosensors 2012: 22nd Anniversary World Congress on Biosensors, Cancun, Mexico (2012)
49. Gervais, L., de Rooij, N., Delamarque, E.: Microfluidic chips for point-of-care immunodiagnosics. *Adv. Mater.* **23**(24), H151–H176 (2011). doi:[10.1002/adma.201100464](https://doi.org/10.1002/adma.201100464)
50. Baier, T., Hansen-Hagge, T.E., Gransee, R., Crombe, A., Schmahl, S., Paulus, C., Drese, K.S., Keegan, H., Martin, C., O’Leary, J.J., Furuberg, L., Solli, L., Gronn, P., Falang, I.M., Karlgard, A., Gulliksen, A., Karlsen, F.: Hands-free sample preparation platform for nucleic acid analysis. *Lab Chip* **9**(23), 3399–3405 (2009). doi:[10.1039/B910421F](https://doi.org/10.1039/B910421F)
51. Tarhan, M.C., Yokokawa, R., Bottier, C., Collard, D., Fujita, H.: A nano-needle/microtubule composite gliding on a kinesin-coated surface for target molecule transport. *Lab Chip* **10**(1), 86–91 (2010). doi:[10.1039/B913312G](https://doi.org/10.1039/B913312G)
52. Bottier, C., Fattaccioli, J., Tarhan, M.C., Yokokawa, R., Morin, F.O., Kim, B., Collard, D., Fujita, H.: Active transport of oil droplets along oriented microtubules by kinesin molecular motors. *Lab Chip* **9**(12), 1694–1700 (2009). doi:[10.1039/B822519B](https://doi.org/10.1039/B822519B)
53. Beech, J.P., Holm, S.H., Adolfsson, K., Tegenfeldt, J.O.: Sorting cells by size, shape and deformability. *Lab Chip* **12**(6), 1048–1051 (2012). doi:[10.1039/C2LC21083E](https://doi.org/10.1039/C2LC21083E)
54. Nam, J., Lim, H., Kim, D., Jung, H., Shin, S.: Continuous separation of microparticles in a microfluidic channel via the elasto-inertial effect of non-Newtonian fluid. *Lab Chip* **12**(7), 1347–1354 (2012). doi:[10.1039/C2LC21304D](https://doi.org/10.1039/C2LC21304D)
55. Zhang, C., Khoshmanesh, K., Mitchell, A., Kalantar-zadeh, K.: Dielectrophoresis for manipulation of micro/nano particles in microfluidic systems. *Anal. Bioanal. Chem.* **396**(1), 401–420 (2010). doi:[10.1007/s00216-009-2922-6](https://doi.org/10.1007/s00216-009-2922-6)
56. Hong, J.W., Studer, V., Hang, G., Anderson, W.F., Quake, S.R.: A nanoliter-scale nucleic acid processor with parallel architecture. *Nat. Biotechnol.* **22**(4), 435–439 (2004). doi:[10.1038/nbt951](https://doi.org/10.1038/nbt951)
57. Easley, C.J., Karlinsey, J.M., Bienvenue, J.M., Legendre, L.A., Roper, M.G., Feldman, S.H., Hughes, M.A., Hewlett, E.L., Merkel, T.J., Ferrance, J.P., Landers, J.P.: A fully integrated microfluidic genetic analysis system with sample-in–answer-out capability. *Proc. Nat. Acad. Sci.* **103**(51), 19272–19277 (2006). doi:[10.1073/pnas.0604663103](https://doi.org/10.1073/pnas.0604663103)
58. Bienvenue, J.M., Duncalf, N., Marchiarullo, D., Ferrance, J.P., Landers, J.P.: Microchip-based cell lysis and DNA extraction from sperm cells for application to forensic analysis. *J. Forensic Sci.* **51**(2), 266–273 (2006). doi:[10.1111/j.1556-4029.2006.00054.x](https://doi.org/10.1111/j.1556-4029.2006.00054.x)
59. Lee, J.-G., Cheong, K.H., Huh, N., Kim, S., Choi, J.-W., Ko, C.: Microchip-based one step DNA extraction and real-time PCR in one chamber for rapid pathogen identification. *Lab Chip* **6**(7), 886–895 (2006). doi:[10.1039/B515876A](https://doi.org/10.1039/B515876A)

60. Cho, Y.-K., Lee, J.-G., Park, J.-M., Lee, B.-S., Lee, Y., Ko, C.: One-step pathogen specific DNA extraction from whole blood on a centrifugal microfluidic device. *Lab Chip* **7**(5), 565–573 (2007). doi:[10.1039/B616115D](https://doi.org/10.1039/B616115D)
61. Focke, M., Kosse, D., Muller, C., Reinecke, H., Zengerle, R., von Stetten, F.: Lab-on-a-foil: microfluidics on thin and flexible films. *Lab Chip* **10**(11), 1365–1386 (2010). doi:[10.1039/C001195A](https://doi.org/10.1039/C001195A)
62. Hoffmann, J., Mark, D., Lutz, S., Zengerle, R., von Stetten, F.: Pre-storage of liquid reagents in glass ampoules for DNA extraction on a fully integrated lab-on-a-chip cartridge. *Lab Chip* **10**(11), 1480–1484 (2010). doi:[10.1039/B926139G](https://doi.org/10.1039/B926139G)
63. Hitzbleck, M., Gervais, L., Delamarche, E.: Controlled release of reagents in capillary-driven microfluidics using reagent integrators. *Lab Chip* **11**(16), 2680–2685 (2011). doi:[10.1039/C1LC20282K](https://doi.org/10.1039/C1LC20282K)
64. Asiello, P.J., Baeumner, A.J.: Miniaturized isothermal nucleic acid amplification, a review. *Lab Chip* **11**(8), 1420–1430 (2011). doi:[10.1039/C0LC00666A](https://doi.org/10.1039/C0LC00666A)
65. Schoder, D., Schwalwiess, A., Schaubberger, G., Kuhn, M., Hoorfar, J., Wagner, M.: Physical characteristics of six new thermocyclers. *Clin. Chem.* **49**(6), 960–963 (2003). doi:[10.1373/49.6.960](https://doi.org/10.1373/49.6.960)
66. Shen, K., Chen, X., Guo, M., Cheng, J.: A microchip-based PCR device using flexible printed circuit technology. *Sens. Actuators B Chemical* **105**(2), 251–258 (2005). doi:[10.1016/j.snb.2004.05.069](https://doi.org/10.1016/j.snb.2004.05.069)
67. Northrup, M.A., Ching, M.T., White, R.M., Watson, R.T., (1993) DNA amplification with a microfabricated reaction chamber. Paper presented at the 7th International Conference Solid-State Sensors and Actuators (Transducers '93), Yokohama, Japan, 7–10 June 1993
68. Jung, J.H., Choi, S.J., Park, B.H., Choi, Y.K., Seo, T.S.: Ultrafast rotary PCR system for multiple influenza viral RNA detection. *Lab Chip* **12**(9), 1598–1600 (2012). doi:[10.1039/C2LC21269B](https://doi.org/10.1039/C2LC21269B)
69. Chung, K.H., Park, S.H., Choi, Y.H.: A palmtop PCR system with a disposable polymer chip operated by the thermosiphon effect. *Lab Chip* **10**(2), 202–210 (2010). doi:[10.1039/B915022F](https://doi.org/10.1039/B915022F)
70. Liu, Y., Rauch, C.B., Stevens, R.L., Lenigk, R., Yang, J., Rhine, D.B., Grodzinski, P.: DNA amplification and hybridization assays in integrated plastic monolithic devices. *Anal. Chem.* **74**(13), 3063–3070 (2002). doi:[10.1021/ac020094q](https://doi.org/10.1021/ac020094q)
71. Gulliksen, A., Solli, L., Karlsen, F., Rogne, H., Hovig, E., Nordstrøm, T., Sirevåg, R.: Real-time nucleic acid sequence-based amplification in nanoliter volumes. *Anal. Chem.* **76**(1), 9–14 (2003). doi:[10.1021/ac034779h](https://doi.org/10.1021/ac034779h)
72. Deiman, B., van Aarle, P., Sillekens, P.: Characteristics and applications of nucleic acid sequence-based amplification (NASBA). *Mol. Biotechnol.* **20**(2), 163–179 (2002). doi:[10.1385/mb:20:2:163](https://doi.org/10.1385/mb:20:2:163)
73. Furuberg, L., Mielnik, M., Gulliksen, A., Solli, L., Johansen, I.R., Voitel, J., Baier, T., Riegger, L., Karlsen, F.: RNA amplification chip with parallel microchannels and droplet positioning using capillary valves. *Microsys. Technol. Micro. Nanosystems Inf Storage Process. Sys.* **14**(4–5), 673–681 (2008). doi:[10.1007/s00542-007-0515-x](https://doi.org/10.1007/s00542-007-0515-x)
74. Dimov, I.K., Garcia-Cordero, J.L., O'Grady, J., Poulsen, C.R., Viguier, C., Kent, L., Daly, P., Lincoln, B., Maher, M., O'Kennedy, R., Smith, T.J., Ricco, A.J., Lee, L.P.: Integrated microfluidic tmRNA purification and real-time NASBA device for molecular diagnostics. *Lab Chip* **8**(12), 2071–2078 (2008). doi:[10.1039/B812515E](https://doi.org/10.1039/B812515E)
75. Yang, J.M., Bell, J., Huang, Y., Tirado, M., Thomas, D., Forster, A.H., Haigis, R.W., Swanson, P.D., Wallace, R.B., Martinsons, B., Krihak, M.: An integrated, stacked microlaboratory for biological agent detection with DNA and immunoassays. *Biosens. Bioelectron.* **17**(6–7), 605–618 (2002). doi:[10.1016/S0956-5663\(02\)00023-4](https://doi.org/10.1016/S0956-5663(02)00023-4)
76. Notomi, T., Okayama, H., Masubuchi, H., Yonekawa, T., Watanabe, K., Amino, N., Hase, T.: Loop-mediated isothermal amplification of DNA. *Nucleic Acids Res.* **28**(12), e63 (2000). doi:[10.1093/nar/28.12.e63](https://doi.org/10.1093/nar/28.12.e63)

77. Mori, Y., Notomi, T.: Loop-mediated isothermal amplification (LAMP): A rapid, accurate, and cost-effective diagnostic method for infectious diseases. *J. Infect. Chemotherapy* **15**(2), 62–69 (2009). doi:[10.1007/s10156-009-0669-9](https://doi.org/10.1007/s10156-009-0669-9)
78. Fang, X.E., Liu, Y.Y., Kong, J.L., Jiang, X.Y.: Loop-mediated isothermal amplification integrated on microfluidic chips for point-of-care quantitative detection of pathogens. *Anal. Chem.* **82**(7), 3002–3006 (2010). doi:[10.1021/ac1000652](https://doi.org/10.1021/ac1000652)
79. Liu, C.C., Mauk, M.G., Bau, H.H.: A disposable, integrated loop-mediated isothermal amplification cassette with thermally actuated valves. *Microfluid. Nanofluid.* **11**(2), 209–220 (2011). doi:[10.1007/s10404-011-0788-3](https://doi.org/10.1007/s10404-011-0788-3)
80. Mahalanabis, M., Do, J., Almuayad, H., Zhang, J.Y., Klapperich, C.M.: An integrated disposable device for DNA extraction and helicase dependent amplification. *Biomed. Microdevices* **12**(2), 353–359 (2010). doi:[10.1007/s10544-009-9391-8](https://doi.org/10.1007/s10544-009-9391-8)
81. Mahalanabis, M., Do, J., Almuayad, H., Zhang, J.Y., Klapperich, C.M.: An integrated disposable device for DNA extraction and helicase dependent amplification, vol 12, p. 353, 2010. *Biomedical Microdevices* **13**(3), 599–602 (2011). doi:[10.1007/s10544-011-9518-6](https://doi.org/10.1007/s10544-011-9518-6)
82. Kuhn, H., Demidov, V.V., Frank-Kamenetskii, M.D.: Rolling-circle amplification under topological constraints. *Nucleic Acids Res.* **30**(2), 574–580 (2002). doi:[10.1093/nar/30.2.574](https://doi.org/10.1093/nar/30.2.574)
83. Mahmoudian, L., Kaji, N., Tokeshi, M., Nilsson, M., Baba, Y.: Rolling circle amplification and circle-to-circle amplification of a specific gene integrated with electrophoretic analysis on a single chip. *Anal. Chem.* **80**(7), 2483–2490 (2008). doi:[10.1021/ac702289j](https://doi.org/10.1021/ac702289j)
84. Sato, K., Tachihara, A., Renberg, B., Mawatari, K., Tanaka, Y., Jarvius, J., Nilsson, M., Kitamori, T.: Microbead-based rolling circle amplification in a microchip for sensitive DNA detection. *Lab Chip* **10**(10), 1262–1266 (2010). doi:[10.1039/b927460j](https://doi.org/10.1039/b927460j)
85. Lutz, S., Weber, P., Focke, M., Faltin, B., Hoffmann, J., Muller, C., Mark, D., Roth, G., Munday, P., Armes, N., Piepenburg, O., Zengerle, R., von Stetten, F.: Microfluidic lab-on-a-foil for nucleic acid analysis based on isothermal recombinase polymerase amplification (RPA). *Lab Chip* **10**(7), 887–893 (2010). doi:[10.1039/b921140c](https://doi.org/10.1039/b921140c)
86. Marcy, Y., Ishoey, T., Lasken, R.S., Stockwell, T.B., Walenz, B.P., Halpern, A.L., Beeson, K.Y., Goldberg, S.M.D., Quake, S.R.: Nanoliter reactors improve multiple displacement amplification of genomes from single cells. *PLoS Genet.* **3**(9), 1702–1708 (2007). doi:[10.1371/journal.pgen.0030155](https://doi.org/10.1371/journal.pgen.0030155)
87. Tan, E., Erwin, B., Dames, S., Ferguson, T., Buechel, M., Irvine, B., Voelkerding, K., Niemi, A.: Specific versus nonspecific isothermal dna amplification through thermophilic polymerase and nicking enzyme activities†. *Biochemistry* **47**(38), 9987–9999 (2008). doi:[10.1021/bi800746p](https://doi.org/10.1021/bi800746p)
88. Heidenreich, P.A., Trogdon, J.G., Khavjou, O.A., Butler, J., Dracup, K., Ezekowitz, M.D., Finkelstein, E.A., Hong, Y., Johnston, S.C., Khera, A., Lloyd-Jones, D.M., Nelson, S.A., Nichol, G., Orenstein, D., Wilson, P.W.F., Woo, Y.J.: Forecasting the future of cardiovascular disease in the United States. *Circulation* (2011). doi:[10.1161/CIR.0b013e31820a55f5](https://doi.org/10.1161/CIR.0b013e31820a55f5)
89. EUROPA: Cardiovascular diseases: European commission. http://ec.europa.eu/health-eu/health_problems/cardiovascular_diseases/index_en.htm (2012). Accessed 01 April 2012
90. Mohammed, M.-I., Desmulliez, M.P.Y.: Lab-on-a-chip based immunosensor principles and technologies for the detection of cardiac biomarkers: A review. *Lab Chip* **11**(4), 569–595 (2011). doi:[10.1039/C0LC00204F](https://doi.org/10.1039/C0LC00204F)
91. Kim, W.-J., Kim, B.K., Kim, A., Huh, C., Ah, C.S., Kim, K.-H., Hong, J., Park, S.H., Song, S., Song, J., Sung, G.Y.: Response to cardiac markers in human serum analyzed by guided-mode resonance biosensor. *Anal. Chem.* **82**(23), 9686–9693 (2010). doi:[10.1021/ac101716p](https://doi.org/10.1021/ac101716p)
92. Shen, W., Tian, D., Cui, H., Yang, D., Bian, Z.: Nanoparticle-based electrochemiluminescence immunosensor with enhanced sensitivity for cardiac troponin I using N-(aminobutyl)-N-(ethylisoluminol)-functionalized gold nanoparticles as labels. *Biosens. Bioelectron.* **27**(1), 18–24 (2011). doi:[10.1016/j.bios.2011.05.022](https://doi.org/10.1016/j.bios.2011.05.022)

93. NHLBI: NHLBI Fact book, fiscal year 2008. Bethesda (MD): National Heart, Lung, and Blood Institute (2009)
94. Group USCSW: United States cancer statistics: 1999–2007 incidence and mortality web-based report. U.S. Department of Health and Human Services, Centers for Disease Control and Prevention and National Cancer Institute. www.cdc.gov/uscs (2010)
95. Waggoner, P.S., Varshney, M., Craighead, H.G.: Detection of prostate specific antigen with nanomechanical resonators. *Lab Chip* **9**(21), 3095–3099 (2009). doi:[10.1039/B907309B](https://doi.org/10.1039/B907309B)
96. Truong, P.L., Kim, B.W., Sim, S.J.: Rational aspect ratio and suitable antibody coverage of gold nanorod for ultra-sensitive detection of a cancer biomarker. *Lab Chip* **12**(6), 1102–1109 (2012). doi:[10.1039/C2LC20588B](https://doi.org/10.1039/C2LC20588B)
97. Chuah, K., Lai, L.M.H., Goon, I.Y., Parker, S.G., Amal, R., Justin Gooding, J.: Ultrasensitive electrochemical detection of prostate-specific antigen (PSA) using gold-coated magnetic nanoparticles as ‘dispersible electrodes’. *Chem. Commun.* **48**(29), 3503–3505 (2012). doi:[10.1039/C2CC30512G](https://doi.org/10.1039/C2CC30512G)
98. Nagrath, S., Sequist, L.V., Maheswaran, S., Bell, D.W., Irimia, D., Ulkus, L., Smith, M.R., Kwak, E.L., Digumarthy, S., Muzikansky, A., Ryan, P., Balis, U.J., Tompkins, R.G., Haber, D.A., Toner, M.: Isolation of rare circulating tumour cells in cancer patients by microchip technology. *Nature* **450**(7173), 1235–1239 (2007). doi:[10.1038/nature06385](https://doi.org/10.1038/nature06385)
99. Viswanathan, S., Rani, C., Ribeiro, S., Delerue-Matos, C.: Molecular imprinted nanoelectrodes for ultra sensitive detection of ovarian cancer marker. *Biosens. Bioelectron.* **33**(1), 179–183 (2012). doi:[10.1016/j.bios.2011.12.049](https://doi.org/10.1016/j.bios.2011.12.049)
100. Zhu, H., Yaglidere, O., Su, T.-W., Tseng, D., Ozcan, A.: Cost-effective and compact wide-field fluorescent imaging on a cell-phone. *Lab Chip* **11**(2), 315–322 (2011). doi:[10.1039/C0LC00358A](https://doi.org/10.1039/C0LC00358A)
101. Wong, A.P., Gupta, M., Shevkoplyas, S.S., Whitesides, G.M.: Egg beater as centrifuge: isolating human blood plasma from whole blood in resource-poor settings. *Lab Chip* **8**(12), 2032–2037 (2008). doi:[10.1039/B809830C](https://doi.org/10.1039/B809830C)
102. Martinez, A.W., Phillips, S.T., Whitesides, G.M., Carrilho, E.: Diagnostics for the developing world: microfluidic paper-based analytical devices. *Anal. Chem.* **82**(1), 3–10 (2009). doi:[10.1021/ac9013989](https://doi.org/10.1021/ac9013989)
103. Martinez, A.W., Phillips, S.T., Whitesides, G.M.: Three-dimensional microfluidic devices fabricated in layered paper and tape. *Proc. Nat. Acad. Sci.* **105**(50), 19606–19611 (2008). doi:[10.1073/pnas.0810903105](https://doi.org/10.1073/pnas.0810903105)
104. Nie, Z., Nijhuis, C.A., Gong, J., Chen, X., Kumachev, A., Martinez, A.W., Narovlyansky, M., Whitesides, G.M.: Electrochemical sensing in paper-based microfluidic devices. *Lab Chip* **10**(4), 477–483 (2010). doi:[10.1039/B917150A](https://doi.org/10.1039/B917150A)
105. Martinez, A.W., Phillips, S.T., Nie, Z., Cheng, C.-M., Carrilho, E., Wiley, B.J., Whitesides, G.M.: Programmable diagnostic devices made from paper and tape. *Lab Chip* **10**(19), 2499–2504 (2010). doi:[10.1039/C0LC00021C](https://doi.org/10.1039/C0LC00021C)
106. Kim, D.-H., Lu, N., Ma, R., Kim, Y.-S., Kim, R.-H., Wang, S., Wu, J., Won, S.M., Tao, H., Islam, A., Yu, K.J., Kim, T.-i, Chowdhury, R., Ying, M., Xu, L., Li, M., Chung, H.-J., Keum, H., McCormick, M., Liu, P., Zhang, Y.-W., Omenetto, F.G., Huang, Y., Coleman, T., Rogers, J.A.: Epidermal electronics. *Science* **333**(6044), 838–843 (2011). doi:[10.1126/science.1206157](https://doi.org/10.1126/science.1206157)
107. Mahler, G.J., Esch, M.B., Glahn, R.P., Shuler, M.L.: Characterization of a gastrointestinal tract microscale cell culture analog used to predict drug toxicity. *Biotechnol. Bioeng.* **104**(1), 193–205 (2009). doi:[10.1002/bit.22366](https://doi.org/10.1002/bit.22366)
108. Kimura, H., Yamamoto, T., Sakai, H., Sakai, Y., Fujii, T.: An integrated microfluidic system for long-term perfusion culture and on-line monitoring of intestinal tissue models. *Lab Chip* **8**(5), 741–746 (2008). doi:[10.1039/B717091B](https://doi.org/10.1039/B717091B)
109. Sung, J.H., Yu, J., Luo, D., Shuler, M.L., March, J.C.: Microscale 3-D hydrogel scaffold for biomimetic gastrointestinal (GI) tract model. *Lab Chip* **11**(3), 389–392 (2011). doi:[10.1039/C0LC00273A](https://doi.org/10.1039/C0LC00273A)

110. Ghaemmaghami, A.M., Hancock, M.J., Harrington, H., Kaji, H., Khademhosseini, A.: Biomimetic tissues on a chip for drug discovery. *Drug Discovery Today* **17**(3–4), 173–181 (2012). doi:[10.1016/j.drudis.2011.10.029](https://doi.org/10.1016/j.drudis.2011.10.029)
111. Domansky, K., Inman, W., Serdy, J., Dash, A., Lim, M.H.M., Griffith, L.G.: Perfused multiwell plate for 3D liver tissue engineering. *Lab Chip* **10**(1), 51–58 (2010). doi:[10.1039/B913221J](https://doi.org/10.1039/B913221J)
112. Khetani, S.R., Bhatia, S.N.: Microscale culture of human liver cells for drug development. *Nat Biotech* **26**(1), 120–126 (2008). doi:[10.1038/nbt1361](https://doi.org/10.1038/nbt1361)
113. Toh, Y.-C., Zhang, C., Zhang, J., Khong, Y.M., Chang, S., Samper, V.D., van Noort, D., Hutmacher, D.W., Yu, H.: A novel 3D mammalian cell perfusion-culture system in microfluidic channels. *Lab Chip* **7**(3), 302–309 (2007). doi:[10.1039/B614872G](https://doi.org/10.1039/B614872G)
114. van Midwoud, P.M., Merema, M.T., Verpoorte, E., Groothuis, G.M.M.: A microfluidic approach for in vitro assessment of interorgan interactions in drug metabolism using intestinal and liver slices. *Lab Chip* **10**(20), 2778–2786 (2010). doi:[10.1039/C0LC00043D](https://doi.org/10.1039/C0LC00043D)
115. Kang, J.H., Krause, S., Tobin, H., Mammoto, A., Kanapathipillai, M., Ingber, D.E.: A combined micromagnetic-microfluidic device for rapid capture and culture of rare circulating tumor cells. *Lab Chip* (2012). doi:[10.1039/C2LC40072C](https://doi.org/10.1039/C2LC40072C)
116. Frimat, J.-P., Becker, M., Chiang, Y.-Y., Marggraf, U., Janasek, D., Hengstler, J.G., Franzke, J., West, J.: A microfluidic array with cellular valving for single cell co-culture. *Lab Chip* **11**(2), 231–237 (2011). doi:[10.1039/C0LC00172D](https://doi.org/10.1039/C0LC00172D)
117. Hong, S., Pan, Q., Lee, L.P.: Single-cell level co-culture platform for intercellular communication. *Integrative Biology* **4**(4), 374–380 (2012). doi:[10.1039/C2IB00166G](https://doi.org/10.1039/C2IB00166G)
118. Sung, J.H., Shuler, M.L.: A micro cell culture analog (μ CCA) with 3-D hydrogel culture of multiple cell lines to assess metabolism-dependent cytotoxicity of anti-cancer drugs. *Lab Chip* **9**(10), 1385–1394 (2009). doi:[10.1039/B901377F](https://doi.org/10.1039/B901377F)
119. Raghavan, S., Nelson, C.M., Baranski, J.D., Lim, E., Chen, C.S.: geometrically controlled endothelial tubulogenesis in micropatterned gels. *Tissue Eng. Part A* **16**(7), 2255–2263 (2010). doi:[10.1089/ten.tea.2009.0584](https://doi.org/10.1089/ten.tea.2009.0584)
120. Chung, S., Sudo, R., Mack, P.J., Wan, C.-R., Vickerman, V., Kamm, R.D.: Cell migration into scaffolds under co-culture conditions in a microfluidic platform. *Lab Chip* **9**(2), 269–275 (2009). doi:[10.1039/B807585A](https://doi.org/10.1039/B807585A)
121. Gunther, A., Yasotharan, S., Vagaon, A., Lochovsky, C., Pinto, S., Yang, J., Lau, C., Voigtlaender-Bolz, J., Bolz, S.-S.: A microfluidic platform for probing small artery structure and function. *Lab Chip* **10**(18), 2341–2349 (2010). doi:[10.1039/C004675B](https://doi.org/10.1039/C004675B)
122. Shao, J., Wu, L., Wu, J., Zheng, Y., Zhao, H., Jin, Q., Zhao, J.: Integrated microfluidic chip for endothelial cells culture and analysis exposed to a pulsatile and oscillatory shear stress. *Lab Chip* **9**(21), 3118–3125 (2009). doi:[10.1039/B909312E](https://doi.org/10.1039/B909312E)
123. Tourovskaya, A., Li, N.Z., Folch, A.: Localized acetylcholine receptor clustering dynamics in response to microfluidic focal stimulation with agrin. *Biophys. J.* **95**(6), 3009–3016 (2008). doi:[10.1529/biophysj.107.128173](https://doi.org/10.1529/biophysj.107.128173)
124. Kelley, D.E., He, J., Menshikova, E.V., Ritov, V.B.: Dysfunction of mitochondria in human skeletal muscle in type 2 diabetes. *Diabetes* **51**(10), 2944–2950 (2002). doi:[10.2337/diabetes.51.10.2944](https://doi.org/10.2337/diabetes.51.10.2944)
125. Nagamine, K., Kawashima, T., Sekine, S., Ido, Y., Kanzaki, M., Nishizawa, M.: Spatiotemporally controlled contraction of micropatterned skeletal muscle cells on a hydrogel sheet. *Lab Chip* **11**(3), 513–517 (2011). doi:[10.1039/C0LC00364F](https://doi.org/10.1039/C0LC00364F)
126. Kaji, H., Ishibashi, T., Nagamine, K., Kanzaki, M., Nishizawa, M.: Electrically induced contraction of C2C12 myotubes cultured on a porous membrane-based substrate with muscle tissue-like stiffness. *Biomaterials* **31**(27), 6981–6986 (2010). doi:[10.1016/j.biomaterials.2010.05.071](https://doi.org/10.1016/j.biomaterials.2010.05.071)
127. Bajaj, P., Reddy, B., Millet, L., Wei, C., Zorlutuna, P., Bao, G., Bashir, R.: Patterning the differentiation of C2C12 skeletal myoblasts. *Integrative Biology* **3**(9), 897–909 (2011). doi:[10.1039/C1IB00058F](https://doi.org/10.1039/C1IB00058F)

128. Huh, D., Matthews, B.D., Mammoto, A., Montoya-Zavala, M., Hsin, H.Y., Ingber, D.E.: Reconstituting organ-level lung functions on a chip. *Science* **328**(5986), 1662–1668 (2010). doi:[10.1126/science.1188302](https://doi.org/10.1126/science.1188302)
129. Blake, A.J., Rodgers, F.C., Bassuener, A., Hippensteel, J.A., Pearce, T.M., Pearce, T.R., Zarnowska, E.D., Pearce, R.A., Williams, J.C.: A microfluidic brain slice perfusion chamber for multisite recording using penetrating electrodes. *J. Neurosci. Methods* **189**(1), 5–13 (2010). doi:[10.1016/j.jneumeth.2010.02.017](https://doi.org/10.1016/j.jneumeth.2010.02.017)
130. Ingber, D.: Spleen-on-a-chip, sepsis therapeutic device. Hansjörg Wyss Institute for Biologically Inspired Engineering at Harvard University. <http://www.darpa.mil/WorkArea/DownloadAsset.aspx?id=2147485154> (2012). Accessed 30 April 2012
131. Baker, M.: Tissue models: A living system on a chip. *Nature* **471**(7340), 661–665 (2011). doi:[10.1038/471661a](https://doi.org/10.1038/471661a)

Chapter 9

Thin Film Coatings as Electrodes in Neuroscience

Saida Khan, Ahsan Mian and Golam Newaz

Abstract Neural electrodes are essential tools widely used in both basic neuroscience studies and clinical applications to treat various neurodegenerative diseases. In this chapter we explore the common and novel thin film materials used in fabrication of neural electrodes. Discussion will include the physical and chemical properties of thin film coating materials that make them advantageous compared to hard and solid electrodes like silicon etc. To assess the biocompatibility requirements for the neural electrodes, it is important to understand the anatomy of the brain and the neural environment. This chapter will discuss the typical immune response around the implant with coatings and the tests for biocompatibility. How nanotechnology offers huge potential in the fabrication of high performance electrodes with thin film coating are addressed in terms of the current state of the art materials and fabrication technology. At the end, the future trends in research related to thin film coatings will be presented briefly.

9.1 Introduction

Every year, thousands are disabled by neurological diseases and injury, resulting in the loss of functioning neuronal circuits and regeneration failure. Several therapies offer significant promise for the restoration of neuronal function, including the use of growth factors to prevent cell death following injury [1], stem cells to rebuild parts of the nervous system [2], and the use of functional electrical stimulation to bypass CNS lesions [3, 4]. All these different treatment options can be performed

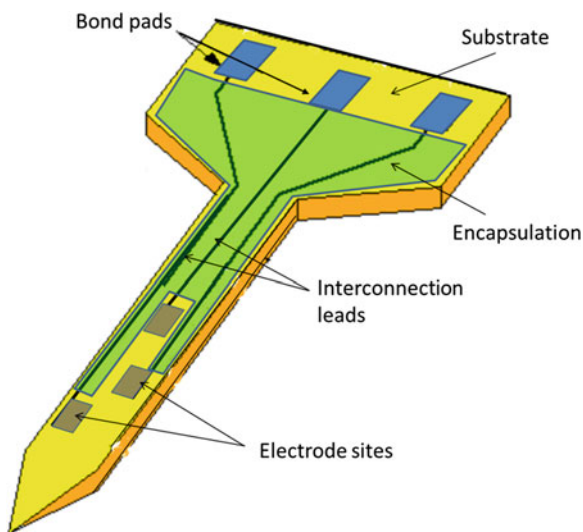
S. Khan (✉) · G. Newaz
Wayne State University, Detroit, Michigan
e-mail: saida_rahman@yahoo.com

A. Mian
Wright State University, Dayton, Ohio

locally using an implantable electronic device. Though most of the ideas related to neural implants are still in fiction, a considerable amount of research effort is focused in their design and development. Current developments in this field, especially with implantable microelectrodes, have already arisen hope in opening up great opportunities for treating patients who have lost the ability to move and talk because of stroke, spinal cord injury or neuro-degenerative diseases, such as Parkinson's disease. The field has potential with possibilities to restore vision and hearing ability of people who suffer blindness or deafness due to damaged nerve functions.

Generally speaking, neural implants are designed and fabricated at the micro scale to ensure that they are as non-invasive as possible. The electrodes are designed to stimulate the neurons in the proximity of the electrodes or record the communication between neurons using safe and low electrical current. A schematic diagram of a neural electrode array is shown in Fig. 9.1. The implants also communicate with an external source such as a microphone if sounds modality is considered, which records and processes the wirelessly received inputs. Since, the dimensions of neural cells range from tens to hundreds of micrometer; it is desirable to be able to conveniently change the number and spacing of electrode sites for various applications. Micro-electrode arrays are generally created using silicon based fabrication processes. While the response from this fabrication process is positive, these electrode arrays can break during tests due to the brittle nature of silicon. The rigid electrodes often cause tissue damage, inflammatory reaction, and scar formations. Recently, polymeric materials are being studied extensively as a substrate material due to their higher flexibility and improved bio-compatibility. Handling of flexible polymer material seems to be easier during neural recordings as tested by Kim et al. [5]. With the advances in microfabrication and thin film deposition technology achieving high spatial resolution is

Fig. 9.1 A schematic diagram of a neural electrode array



being possible; however, achieving good electromechanical properties is a balance between the materials, geometry and fabrication techniques. Low surface area of the electrodes leads to their low charge injection capacity and high impedance. Obviously, changing the actual surface area is unpractical, so to overcome that, the effective surface area is enlarged by use of coating materials such as Titanium Nitride, Iron Oxide or PEDOT. These coatings improve the electromechanical properties but have other undesired limitations such as instability over long term use, complex deposition methods, or toxicity. As a recent progress, surface modification of the flexible metallic (e.g. platinum) electrodes by adding a thin layer of carbon nanotube (CNT), polymer nanotube or conducting polymer has shown to improve the bio-compatibility, ease of handling and use, and durability better than silicon based substrate.

Various research groups working in the field of development of neural implant devices or neuro-prosthesis have focused their work in different areas. There are a number of problems that must be studied during the development of neural implant devices. There are material issues, fabrication issues, biocompatibility issues, surgical technique issues, and so on. For example, in the 36th Annual Neural Prosthesis Workshop and the annual meeting of the National Institute of Health's (NIH) Deep Brain Stimulation (DBS) Consortium, the six plenary sessions were: Progress in Deep Brain Stimulation, Novel Interface Technologies for Stimulation, Surgical Considerations for Neural Interfaces, Chronic Recording Microelectrodes, Neural Interfaces for Sensory Information, Spinal Cord Interfaces, and Future Efforts in Neural Interfaces. If we start from the bottom up, the most important issue is the materials biocompatibility. The device must be able to perform with an appropriate host response in its intended application. Two other critical factors in the development and long-term effectiveness of all implantable devices are: spatial resolution and good electromechanical properties.

Thin film technology in general reduce the materials cost by more efficient utilization of active materials. It is also possible to tune the film properties like porosity, crystal structures and film surface roughness by controlling the deposition variables. A combination of coating and substrate materials are used depending on the overall design and application of the electrode device. Using flexible polymers as backbone structure, thin film technology made possible fabrication of implants with high charge injection properties and low impedance. Electrochemical reactions in thin film are facilitated by faster ionic transport and smaller current paths.

The present chapter is organized as follows. First, the neural environment is introduced along with various electrode materials that are compatible with the environment and thin film technology. These materials are identified and listed by reviewing recent research articles. Various physical, chemical, electrical, and mechanical properties that are required for a good electrode material are also discussed. Since the recent trend is targeted towards developing flexible electrodes due to their many advantages, the materials that have shown superior properties for substrate and encapsulation are presented next along with their relative advantages and disadvantages. Next, current state of the art coatings used on electrode

surfaces for further improvement of the electrochemical properties of stimulation and recording electrodes are discussed. The improvement of such properties is discussed with an emphasis on various surface coatings of electrodes. Then, several common techniques used in fabricating thin film electrodes and their surface modifications are briefly presented. Different methods for testing biocompatibility and bio-stability of various electrode materials are also depicted. The chapter is concluded with future trends of highly stable microelectrode and biocompatible materials for chronic neural stimulation and recording.

9.2 Neural Environment

Neurons are extraordinary among cells for various reasons. First, they are polarized, possessing receptive dendrites on one end and axons with synaptic terminals at other with high selectivity to the substrate. Second, the neuronal cell is electrically and chemically excitable. Third, nerve cells in specific zones of the brain form specific signaling networks that mediate specific behaviors. Fourth, by electrical and chemical stimulations, it is possible to accomplish physiological and anatomical changes, including pruning of preexisting connections, and even growth of new connections. All these facts are the basis of relentless research efforts in the creation of neuronal prosthesis for neuronal recovery processes (Fig. 9.2).

The astrocytes and microglia are the two major contributors in the brain's immunological reactions. These cells are very important in the study of biocompatibility and are mainly responsible for developing scar tissue around the implant or electrode sites. The development of tissue scars in a controlled process

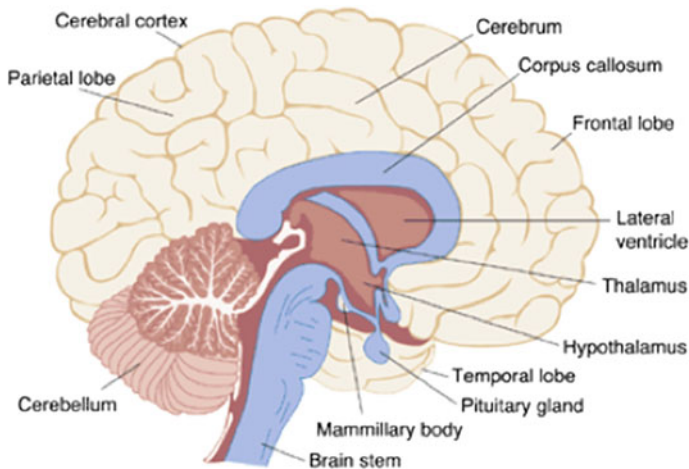


Fig. 9.2 Neural environment http://creationwiki.org/Human_brain

facilitates the implantation of the microelectrode at a fixed position in the brain. However, uncontrolled scar tissue formation may cause encapsulation of the electrode with thick tissue introducing additional impedance in the current path and eventually complete separation of the electrode from the surrounding neurons.

9.3 Requirements for Electrode Materials

Different materials such as platinum, alloys of platinum and indium, iridium, iridium oxide, titanium nitride, conductive polymers and carbon derivatives such as graphene, carbon nanotubes, etc. have been used for the fabrication of electrode arrays. Following are some properties that are important when selecting an electrode material.

- Smaller geometry for selectivity.
- Safe charge injection capability with small power consumption.
- Reversible reaction during charge injection that do not form toxic product at electrode-tissue interface.
- Low polarization and impedance at the phase boundary for efficient injection of charge.
- Long term mechanical stability and corrosion resistance for chronic stimulation applications.
- Biocompatibility of the electrode material or the coating.
- Visible to MRI, X-ray and other noninvasive diagnostic techniques.

Basically for biological application electrodes function as transducers between physiologic and electronic systems, as illustrated in Fig. 9.3.

In the neural environment, neurons communicate using bioelectric potentials that are carried in electrolytic media (cerebrospinal fluid) in the form of ionic currents via chemical species. The communication at the electrode-neuron interface or signal transduction by the electrode involves the inter-conversion of energy

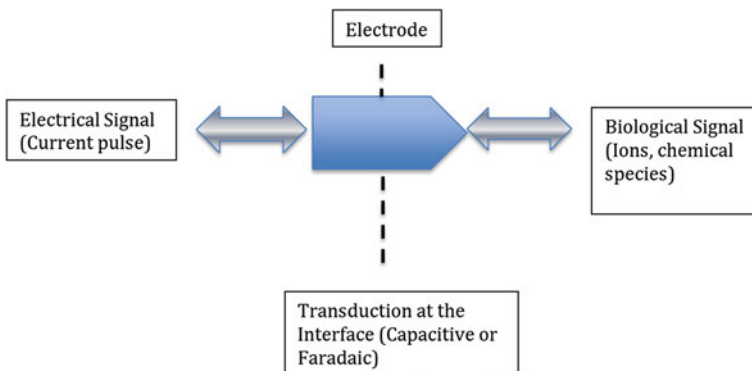


Fig. 9.3 Transduction of signals at electrode interface [101]

Table 9.1 Studies with neural stimulation device

Research group	Electrode material	Electrode geometry	Research subject
Hesse et al. [104]	Platinum	$0.1 \text{ nm} \times 0.1 \text{ m}^2$	Cat retina
Humayun et al. [105–108]	Platinum	400 nm diameter disc and 25–1 25 nm wires	Human retina
Walter et al. [109]	Platinum and Titanium Nitride	100 μm (Pt.) and 50 nm (TiN) diameter	Rabbit retina
Grumet et al. [110]	Platinum	10 nm diameter disc	Rabbit retina
Rizzo et al. [111, 112]	AIROF	100 and 400 μm diameter disc	Human retina
McCreery [113]	Activated Ir	GSA of $1,000 \pm 200 \mu\text{m}^2$	Cat VCN
Branner [114]	Pt	Electrode tip 0.005 mm^2	Cat sciatic nerve

that is present in the form of ionic carriers and in the form of electronic carriers (electrons and holes). This takes place by means of capacitive coupling (without net charge transfer) and or by charge transfer reactions (Faradic) in which electrons in the electrode are transferred to and from ions in the solution. The electrode–electrolyte interface is still not fully understood. Two most common models that are used to describe the electrochemical behavior are capacitive mechanism (charging and discharging of the electrode double layer, no electron transfer) and Faradaic mechanism (chemical oxidation or reduction, reversible or irreversible).

Several examples of electrodes used in electrode stimulation studies with different geometries and materials are presented in Table 9.1.

9.4 Types of Electrodes in Neuroscience

Thin film microelectrodes used in neuroscience research can be categorized in the following major types:

1. Stimulating Electrodes [6–11]
2. Recording Electrodes [10–14] (Fig. 9.4)
3. Sensing Electrodes [15, 16].

9.4.1 Stimulating Electrodes

Stimulating electrodes uses a small current pulse to initiate a functional response by depolarizing the membranes of Neurons. Depolarization is achieved by the flow of ionic current between two or more electrodes: the working electrode and the

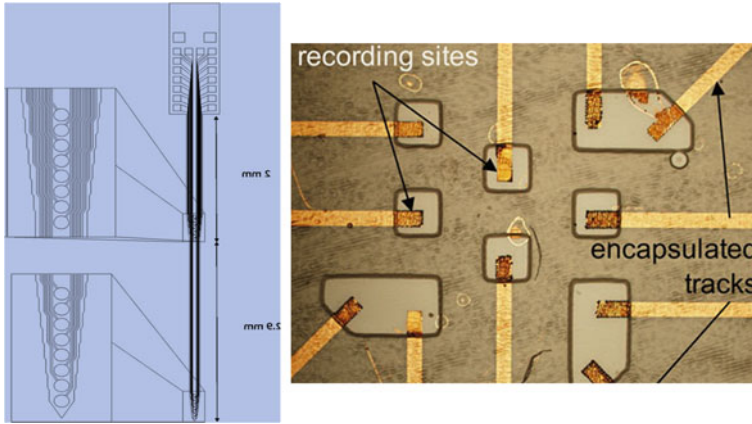


Fig. 9.4 Penetrating electrode [102] and surface electrode [103]

return electrodes. The working electrode interacts with the target cell or tissue being in its close proximity.

The stimulation used in most neural applications, is applied in a series in the form of biphasic current pulses. For the safety of the neural tissue it is very important that the current is charge-balance is to maintain the electrode potential within an optimum range. High voltage can cause irreversible reduction and oxidation reactions that may degrade the electrode and damage tissue. Other factors important to consider are pulse width and charge injection limit of the electrodes. The stimulus waveforms must be limited to current and charge densities that allow charge injection by reversible processes and at a finite rate [17].

9.4.2 Recording Electrodes

Recording electrodes are used to record signals related to neuronal activities as the input of various prosthetic device intended to treat patients with paralysis or other neurodegenerative disease [12, 14, 18]. The recording can also be used as feedback signals from the neurons that are being stimulated using stimulating electrodes like in the cases of adaptive DBS [19] and functional stimulation for epilepsy [20].

The activity of neurons is recorded as an extracellular potential, or action potential, with microelectrodes implanted in close proximity to the target neurons. For single cell recording, the microelectrodes used are very small in size with geometric surface area (GSA) in the range of 2000–4000 μm^2 or smaller. Recording electrodes are typically characterized by their impedance at 1 kHz, we will find the mention of this impedance in Table 9.2. For recording electrodes, unlike stimulating electrodes, current flow and the electrochemical changes across the electrode–electrolyte interface are not critical factors. The two most important

Table 9.2. Recent research in electrode materials

Materials type	Thin film electrode	Fabrication technique	Comments	Reference
Metal	Pt	Sputtering	Low charge injection limit, but good biocompatibility	[87, 88]
	IrOx	Electrochemical activation (AIROF) [115], reactive laser ablation [116] or reactive sputtering (SIROF) [117, 118]	High charge injection limit, low impedance, resistance to dissolution and corrosion in a saline environment [3, 4]	[88, 119] [115, 116] [117, 118]
Conducting Polymer	Gold	Sputtering	Deposition parameters have effect on metal adhesion and film structure (granular vs. columnar). Dense columnar films have lower impedance of the interface and increased charge injection properties	[85, 86]
	Gold Nanoparticle/CNT	Layer by layer	3-fold improvement in impedance and 1 order of magnitude increase in charge storage capacity	[120]
	PEDOT/Nafion composite	Facile electrochemical deposition	Average diffusion coefficient of hole carriers in the film $4.8 \times 10^{-12} \text{ m}^2/\text{s}$	[121]
	PPy, PEDOT polyaniline	Electrochemical deposition In-situ polymerization	High safe charge injection properties and good biocompatibility Low protein absorption/better biocompatibility and corrosion protection of pt electrode	[90] [93]
Carbon	Conducting polymer nanotube	Electrochemical polymerization	Nano-structured polymer decrease the impedance of microelectrode by about two orders of magnitude and increase the charge transfer capacity by three orders of magnitude compared to polymer film	[122]
	Carbon nanotube (CNT)	Thermal/chemical vapor deposition	Safe and high charge injection limit with good cell adhesion/biocompatibility	[123, 124]
	Polypyrrole(PPy)/graphene(GO)	Electrochemical deposition	The impedance of the PPy/GO coated Pt electrode is 10 % of the bare Pt electrode at 1 kHz and charge capacity density is more than two orders of the magnitude of Pt electrode	[94]
	Polypyrrole/CNT	Electrochemical deposition	High safe charge injection limit of 7.5 mC/cm^2 and low electrode impedance at 1 kHz along with good stability and neuro-compatibility	[95]

considerations for recording electrodes are, (1) maintaining consistent neural recordings for long term [21, 22] and (2) the quality of recordings. The distance and impedance between a neuron and electrode affect the quality of the recorded signals. For chronic implants, these two are affected by the brain's micro-motion [23, 24] and the thickness and composition of the connective tissue sheath surrounding the electrode, which may vary with time following implantation. Fabrication and design issues are certainly important for performance, however, addressing immunologic response resulted from surgical procedure [25] and brain's immune system [26–28] are two areas receiving a great deal of attention from the research community.

9.4.3 Sensing Electrodes

Sensing electrodes are tiny lab on a chip used to detect neurochemical and electrophysiological signals to understand the role of the specific chemical in normal and altered brain function. Chemical detection can be achieved by analyzing the *in vivo* cyclic voltammograms from electrode sites coated with ion selective membranes. The array of neurochemicals detected by voltammetric methods using sensing electrodes include dopamine [29–31], norepinephrine [32], serotonin [33–37], ascorbate [38, 39], uric acid [40], adenosine [41, 42], and acetylcholine [43].

The electrodes are predominantly made of very small diameter carbon nanofibers [44] coated by a thin layer of ion selective membrane that allow diffusion of analytes of interest to electrode surfaces. The membranes are made of organic polymers and include Nafion [45], fibronectin [46], base-hydrolyzed cellulose acetate (BCA) [47], polypyrrole [48], chitosan [49], and carbon nanotubes [33, 50]. Nafion is a material of interest because of its ease of deposition on Carbon fiber Micro-electrodes (CFM) surfaces, durability and its cation-selective permeability. Nafion is also resistant to electrode fouling [51] Base-hydrolyzed cellulose is also used as a fouling-resistant coating material for sensing electrodes because of its ability to exclude large biomolecules [47]. Fibronectin is another ion-sensitive coating materials with high biocompatibility and chemical conductivity [44].

9.5 Electrode Characterization

An understanding of the electrochemical mechanisms, how neural stimulation and recording electrodes works at the electrode-tissue interface, is very important for the development of chronically implanted devices. Common techniques for characterizing electrochemical properties relevant to stimulation and recording will be discussed in this section [17]. The common techniques for electrochemical characterization of electrodes in neuroscience are cyclic voltammetry (CV), impedance spectroscopy, and potential transient measurements.

9.5.1 Cyclic Voltammetry

Cyclic voltammetry (CV) is a very useful technique that uses three-electrode measurement in which the potential of a test electrode, with respect to a noncurrent-carrying reference electrode, is swept cyclically at a constant rate between two potential limits. The current is allowed to flow between the test electrode and a counter electrode. The potential works as the driving force for reactions at the test electrode, while the rate of the reactions is proportional to the current. The information received from the CV is: (1) the presence and reversibility of electrochemical reactions, (2) the quantity of electroactive material on the electrode, and (3) the stability of the electrode. For a given electrode material CV response depends on variables like the sweep rate, the effective geometric area of the electrode, and the roughness/porosity of the electrode [17].

CV provides information about the charge storage capacity (CSC) of an electrode. The time integral of the cathodic current in a slow-sweep-rate cyclic voltammogram over a potential range within the water electrolysis window is equal to the CSC which is a measure of the total amount of charge available for a stimulation pulse. For Pt and Ir oxide electrodes, the water window is typically taken as -0.6 – 0.8 V with Ag|AgCl as the reference electrode. The shaded region in the AIROF CV in Fig. 9.5 represents a CSC of 35 mC cm^{-2} , calculated at a sweep rate of 50 mV s^{-1} [52].

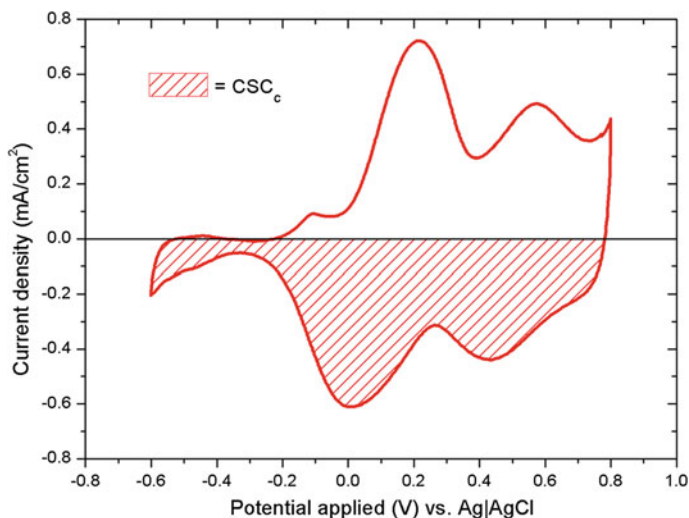


Fig. 9.5 Charge storage capacity (CSC) from cyclic voltammetry of IrO₂ electrodes

9.5.2 Impedance Spectroscopy

Electrochemical impedance spectroscopy (EIS) provides useful information about the recording capability of an electrode by measuring the electrical impedance and phase angle obtained with sinusoidal voltage or current excitation of the electrode. It is also helpful to estimate the resistive contribution of tissue conductivity to the overall electrode impedance. The measurement is made over a broad frequency range, typically $<1-10^5$ Hz. A linear current–voltage response is obtained at each frequency. For voltage excitation, the root-mean-square magnitude of the excitation source is typically ~ 10 mV, not exceeding 50 mV. EIS is a safe method for the *in vivo* assessment of an electrode.

9.5.3 Voltage Transients

Voltage transient measurements estimate the maximum charge that can be injected in a current-controlled stimulation pulse. The experimental setup consists of a three electrode configuration with a test electrode, a large-area return electrode and a noncurrent-carrying reference electrode. The voltage transients are analyzed to determine the maximum polarization, both the most negative (E_{mc}) and most positive (E_{ma}), across the electrode–electrolyte interface which are then compared with established maximum safe potentials to polarize the electrode.

9.6 Substrate and Encapsulation Materials

In this section, various state of the art substrate and encapsulation materials are discussed. Substrate refers to the mechanical structure that supports the entire electrode components including interconnecting metal lines, thin film interlayers, encapsulating materials, etc. Encapsulation refers to the layer of insulating materials that is deposited to isolate metal electrodes from neural environments. Both the substrate and encapsulation materials have to be biocompatible, biostable and possess good dielectric properties. A material is said to be biocompatible if it does not induce a toxic, allergic or immunologic reaction. Similarly, a good biostable material must not change physically or chemically under the influence of any biological fluids or metabolic substances.

The very common and widely used substrate materials are silicon (Si) and glass for rigid neural electrodes where silicon dioxide (SiO_2) and silicon nitride (Si_3N_4) are used as protective or encapsulation layers. The recent trend is to develop polymer based flexible electrodes that can deform easily to contour the brain environment. The flexible electrodes are being adopted to avoid or reduce tissue damage, inflammatory reaction, scar formations, and micromotion caused by rigid

electrodes [21, 53]. Different polymeric materials such as polyimide [54, 55] benzocyclobutene (BCB) [56], polydimethylsioxane (PDMS) [5, 57, 58] and parylene [59, 60] are recently being investigated as both substrate and encapsulations materials. Polyimide is a proven biocompatible material with appropriate mechanical properties for ease of insertion and good adhesion with metal. The major disadvantage of polyimide is its permeability to environmental moisture and ions that could lead to the loss of its dielectric property causing short circuiting. Hence long term use of polyimide based devices may be questionable. Due to its low moisture absorption and chemical stability, BCB has been studied for potential substrate and encapsulation material. A thermoplastic material parylene and a rubber based material PDMS are both superior materials due to their excellent biocompatibility and very low moisture absorption. However, parylene is gaining more interests due to its ease of manufacturing through room temperature vapor deposition process. Thus the parylene based structure can be very conformal coated with almost no residual stress. The major disadvantage of this material is its poor adhesion with some metals. To promote adhesion, a secondary barrier material such as chromium [21, 53] can be used.

9.7 Current State of the Art Electrodes

The research efforts in the development of brain implantable microelectrode are driven by the following factors:

1. Single site electrode to multisite electrode for better efficiency
2. Rigid substrate to flexible substrate to match the brain's mechanical properties
3. Smaller geometry and higher charge injection properties
4. Biocompatibility
5. Corrosion/degradation, water absorption, swelling
6. Immune response and associated decrease in performance.

A comprehensive review of the literature on treatments involving electrical stimulation of neural tissue is presented in the reviews by Li and Mogul [61], Normann [62], Perlmutter and Mink [63], Clark [64], Shepherd and McCreery [65], Jackson et al. [66], Rutten [67], Jezernik et al. [68], Prochazka et al. [69], Hoffer et al. [70]. A very informative discussion on the foreign-body response to implanted electrodes and potential adverse consequences is provided in the review by Polikov et al. [21]. Table 9.2 below contains brief information about very recent research and findings that addressed the above mentioned problems. From the materials selection point, the most suitable materials can be categorized into three major types;

1. Metal: Pt, IrO_x, gold etc., primarily deposited by sputtering technique.
2. Carbon: CNT, Graphene etc., primarily deposited by chemical vapor deposition.
3. Conducting polymers: PPy, PEDOT, Polyaniline etc., primarily fabricated by electrochemical deposition or insitu polymerization.

9.7.1 *Metallic Electrodes*

Platinum is the most widely used and biocompatible material used in electrodes for neural implants [71]. It is used as the structural material of the electrode in bulk form and as thin film electrode on other substrate material as well [17]. Among other novel electrode materials that have been widely studied, IrO₂ is the most promising candidate material for development of neural prostheses. Iridium oxide was found to be having very high charge injection limit with minimum power consumption [72, 73]. It delivers charge in faradic mechanism and the reversible reaction does not form a toxic interface with the neurons [74]. It is possible to deposit very thin film of IrO₂ both in crystalline and amorphous form using vapor deposition techniques [75, 76] on different substrates. Biocompatibility of sputtered deposited IrO₂ has been extensively studied in vitro and found biocompatible with cultured neurons [77–79].

9.7.2 *Carbon Nanotube Electrodes*

It is discussed in the previous section that various biocompatible and biostable metallic materials such as gold and platinum have been used for years as electrode materials. However, as the electrode size becomes smaller, the electrode impedance increases significantly causing ineffective neural recording and stimulation. To overcome this problem, carbon nanofibers (CNF) and carbon nanotube (CNT) [77, 80] based electrodes are getting attention due to its intriguing physico-chemical properties. They are also the materials of choice for creating nanoscale topography. Many groups [81–83] have studied the cytotoxicity of carbon nanofibers with neuronal cells.

The CNT electrodes are shown to improve electrode characteristics because of the fact that the nanoscale CNTs have very high surface to volume ratio that increases the effective interfacial area thereby reducing electrode impedance. Moreover, CNTs have been demonstrated to be a good biocompatible and biostable material with improved neural activity and neuronal growth. The material is highly electrically conductive and exhibits effective electrical stimulation with long-term endurance; hence CNT electrodes can be used for chronic neural recordings or stimulations. CNTs are typically grown on metal conductors using chemical vapor deposition (CVD) process. To create well aligned CNTs, a very high temperature is to be maintained (typically around 650°) in the CVD chamber [78]. Hence, CNT based electrodes have been successfully created only using rigid substrates such as silicon or glass that can withstand the high temperature required for a CVD process. Since the most of the flexible substrates are based on polymer that have relatively low melting or decomposition temperatures, high temperature CVD is not suitable to grow CNTs on flexible substrates. There are several alternative techniques of creating CNT microelectrodes on flexible substrates such as transferring well-grown CNTs to flexible substrates by microwave welding, stamp transfer, polymer binding

and electrodeposition coating. However, these techniques do not always ensure good adhesion between the CNTs and the substrate; thus caution has to be taken for long term applicability of these electrodes. Recently, CNTs have been successfully grown on metal surface of polyimide substrate based microelectrodes using low temperature (400 °C) CVD process. This method seems highly compatible with the flexible microelectrode fabrication process and will be explained in a later section.

9.7.3 Conducting Polymer Electrodes

The conducting polymers (CP) or carbon derivatives are usually deposited on a metal primarily on Platinum electrode to enhance the charge injection properties and corrosion properties. Schimdt group is a pioneer in studying conductive polymers as a candidate for thin film neural electrode [84]. CPs including polypyrrole (PPy), polythiophene (PTh) and PTh derivative poly(ethylene dioxythiophene) (PEDOT) are being studied for improved long-term efficacy and performance of both neural stimulation and recording electrodes. The main characteristic of CPs is a conjugated backbone with high degree of π -orbital overlap. This structure can be modified by acceptor or donor electrons (also called oxidation or reduction, respectively) thereby creating p-type or n-type materials, respectively. It has been observed that electrical conductivities of a polymer can be improved by as much as 15 orders of magnitude by changing just dopant concentrations.

The following section discusses several of the fabrication techniques in brief.

9.8 Fabrication of Thin Film Electrodes

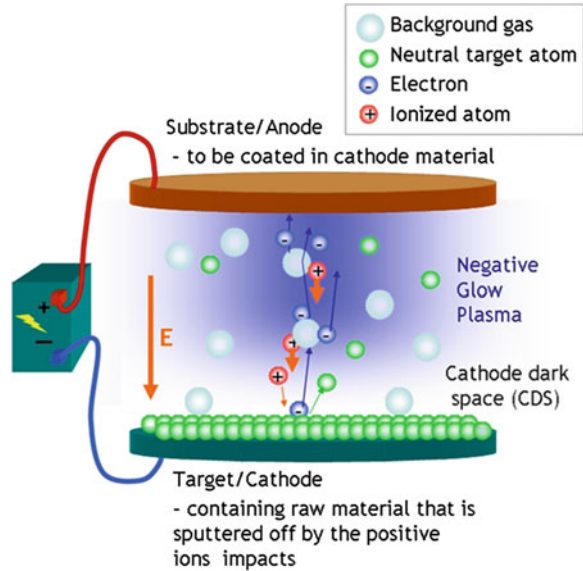
It is mentioned in the [Sect. 9.7.3](#) that there are many methods to fabricate neural electrodes depending upon the electrode configurations and type of surface coatings. In most cases, the electrodes are fabricated layer-by-layer deposition of thin films. Thin electrode films are then patterned and etched using conventional photolithography process to create electrodes with certain configurations. In this section, common thin film deposition processes are discussed. Then a common technique used in fabricating flexible electrodes is briefly presented.

9.8.1 Common Thin Film Deposition Processes

9.8.1.1 Sputtering

Various metallic materials such as platinum (Pt), iridium oxide (IrOx), gold (Au), etc. are deposited using a physical vapor deposition (PVD) method called sputtering. A schematic representation of the technique is shown in [Fig. 9.6](#). The method

Fig. 9.6 A schematic diagram of DC plasma sputtering (Source <http://upload.wikimedia.org/wikipedia/commons/2/2a/DCplasmaSputtering.jpg>)



involves ejecting material from a “target” that is to be deposited onto a “substrate” by bombarding the target surface with neutral target atoms. Substrate materials can be of any shape however, free from small steps such as planar silicon or micro-scale Kevlar fiber [85, 86]. Ionized sputtered particles fly from the target and impact on the substrates or vacuum chamber. To facilitate ion movement, chamber gas pressure is controlled depending upon the type of target materials and required coating morphology. At higher gas pressures, the ions collide with the gas atoms that act as a moderator and move diffusively, reaching the substrates or vacuum chamber wall and condensing after undergoing a random walk. The sputtering gas is often an inert gas such as argon. Researchers have spent years to identify critical process parameters such as gas pressure, RF power, deposition time, etc. for creating coatings with required surface morphology, microstructure and thickness [85]. Although the process is complex due to the presence of many process parameters, experts have large degree of control over the growth and microstructure of the film.

Adhesion between the substrate material and the metal coating is very critical for the neural applications as long term implanting may result in delamination thereby causing implant failure. The substrate surfaces are usually cleaned sequentially prior to deposition using acetone, methanol, isopropanol, and DI water to remove particles and organic residues [85–88] to promote adhesion. In many cases, the adhesion between the electrode material and the substrate material is enhanced by adding an interlayer between them. For example, a thin layer of titanium can be used to promote adhesion of the gold films to silicon substrates [85].

9.8.1.2 Electrochemical Deposition/Polymerization

Electroactive conducting polymers such as polypyrrole (PPy) [89], PEDOT [90–92], polyaniline [93] and their composites such as PPy/graphene oxide (GO) [94], PPy/carbon nanotube [95] are used to modify metallic electrode surfaces using electrochemical deposition process. Such surface modifications are to (1) improve sensitivity; (2) impart selectivity; (3) suppress the effect of interfering reactions; and (4) immobilize indicator molecules [96]. Electrochemical deposition of polymer is often called as electrochemical polymerization.

In general, electrochemical deposition of polymer is done using electrochemical polymerization equipment. A schematic diagram of the equipment is shown in Fig. 9.7. The monomer compound of the polymer to be deposited is first dissolved into a solvent containing a suitable supporting electrolyte. An appropriate voltage is applied to the electrode pair that are being immersed into the electrolyte solution. The monomer is oxidized or reduced to create polymer that is deposited in the form of powder or a film on the surface of the anode or cathode, respectively. If the monomer is oxidized and polymerized on the anode surface, it is called an electrochemical oxidation polymerization. On the other hand if the monomer is reduced and polymerized on the surface of the cathode, it is called electrochemical reduction polymerization. The reference electrode may or may not be necessary for all types of films.

The type of polymer to be deposited on anode or cathode surface depends on the composition of electrolyte, solvent type, electrode type, and monomer. A list of various thin film polymers deposited on different electrode materials are shown in Table 9.3. Other parameters that may influence the deposited film quality are the composition of the electrolyte, the applied voltage, the current density, distance between electrodes, and the polymerization temperature [91].

Fig. 9.7 A schematic diagram of electrochemical deposition setup (oxidation type)

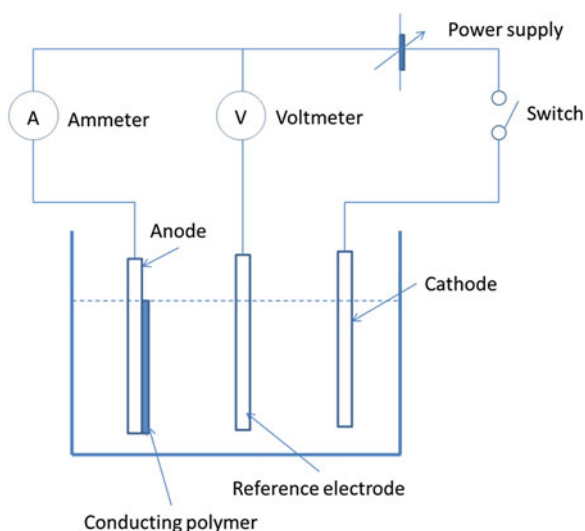


Table 9.3 A list of various thin film polymers deposited on different electrode materials

Film to be deposited	Substrate/backbone material/film electrode	Counter electrode	Reference electrode	Monomer	Supporting electrolyte	Reference
PEDOT	Conductive glass	Nickel (Ni) plate	Silver (Ag) wire	0.1 mol/l 3, 4-ethylenedioxythiophene (EDOT)	Four-fluorinated boric acid tetrabutylammonium tetrafluoroborate (TBAFB ₄)	[91]
Ppy	Aluminum or Al 2024-T3	Platinum plate	Ag/AgCl	0.05 M pyrrole	0.05 M Tiron or 0.05 M Na-pTS	[89]
PPy/ Poly(vinyl alcohol (PVA)	ITO coated glass with spin coated PVA on it	Ni plate	Ag wire	0.1 mol/l pyrrole	TBAFB ₄	[125]
Ppy/GO	Platinum (Pt)	Pt foil	Pt foil	0.05 mol/l pyrrole	Aquas solution of 0.05 mol/l poly(sodium 4-styrene-sulphonate) (PSS) and 0.5 or 1.0 gm/l GO	[94]
Paratoluene sulphonate (pTS) doped PEDOT	Pt	Pt	-	0.1 M EDOT	Aquas solution of acetonitrile with 0.05 M pTS dopant	[126]

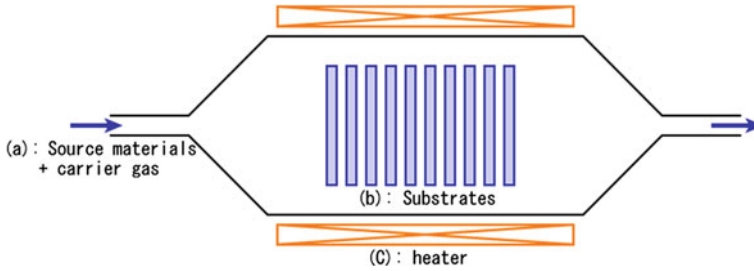
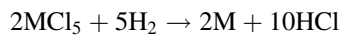


Fig. 9.8 A schematic diagram showing a typical CVD process (Source <http://upload.wikimedia.org/wikipedia/commons/9/9e/ThermalCVD.PNG>)

9.8.1.3 Chemical Vapor Deposition

Chemical vapor deposition (CVD) (see Fig. 9.8) is a chemical process to deposit high-purity thin film on a substrate. One or more precursor gases are delivered into a reaction chamber at approximately ambient temperature. The substrate that is subjected to be thin-film deposited is maintained a high temperature that depends on the type of deposited material. As precursor gases pass over or come into contact with the heated substrate, they react or decompose forming a solid phase that is deposited onto the substrate. Volatile by-products produced in the process are removed by gas flow through the reaction chamber. CVD processes are widely used in the microfabrication industry to deposit various metallic thin films such as molybdenum, tantalum, titanium, nickel, and tungsten. In general, for an arbitrary metal M the precursor gases used are metal chloride (MCl_5) and hydrogen (H_2) that undergo the following chemical reaction to create M film:



Currently, the CVD process is also being used to deposit CNT thin films on metal surface for neural electrodes. In this case, a mixture of C_2H_2 and H_2 is used as a precursor gas.

9.8.2 Flexible Electrode Fabrication

A crystalline polymer parylene-C has received tremendous attention due to its unique combination of physical, chemical, and mechanical properties. It is being used as both structural and encapsulation materials because of its improved biocompatibility and inertness, [53, 59]. Due to the poor adhesion of parylene to metallic materials, a thin layer of interlayer can be used to improve adhesion between them [60]. A simple two-mask photolithography based fabrication process of a microelectrode arrays is shown schematically in Fig. 9.9 [53].

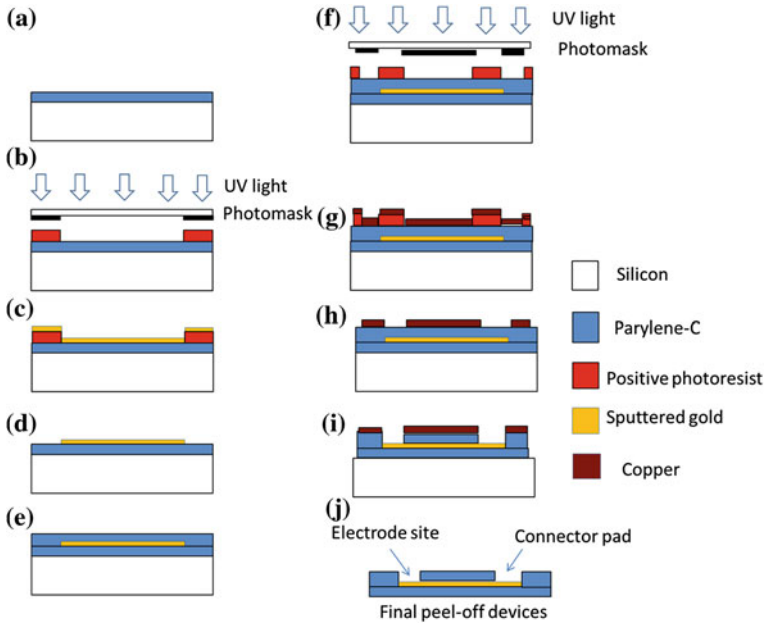


Fig. 9.9 Fabrication steps of flexible microelectrode arrays

In the first step, silicon substrate is vapor deposited with parylene-C (Fig. 9.9a). To create the array geometry, a positive photoresist is spun over parylene followed by photo-exposure and development (Fig. 9.9b). Sputtering technique is then used to successively deposit chromium and gold on parylene (Fig. 9.9c). Chromium is used in this case to promote adhesion between gold and parylene. The unwanted metal is then removed using lift-off technique where the wafer is sonicated in an acetone bath (Fig. 9.9d). A second layer of parylene is deposited next on the entire wafer surface to encapsulate the patterned metal lines. The next several steps (Fig. 9.9f–i) are used to selectively remove parylene thereby exposing metal surfaces for recording sites and interconnecting bond pads. First, a thin positive photoresist layer is spun, exposed, and developed (Fig. 9.9f). A thin copper layer is then deposited using sputtering technique (Fig. 9.9g) that is later used as a parylene etch mask. The unwanted copper is then lifted-off thereby creating electrode outline and openings for recording sites and bond pads (Fig. 9.9h). Reactive ion etching of parylene is carried out to remove it from not only the recording sites and bond pads, but also from edges to define the final outline of the device (Fig. 9.9i). After wet-etching of copper, the devices are manually peeled off from the wafer surface (Fig. 9.9j).

Similar processing steps have also been adopted to create polyimide based flexible microelectrodes [54]. In this case, glass slide is used as handle substrate and sputtered titanium/platinum is used as electrode material. For both the

parylene and polyimide based electrodes, the exposed recording sites can be coated with conducting polymer, CNT, polymer nanotube, etc. to have further improvement in neuronal cell response.

9.8.3 CNT Electrode Fabrication

It is discussed previously that CVD based fabrication of CNT electrode requires high temperature substrate materials. Recently, researchers [80] were successfully able to deposit CNT film on metal at relatively low temperature (400 °C). Since polyimide (PI) melting point is around 550 °C, CNT electrode can be fabricated using polyimide as a substrate material. Figure 9.10 illustrates the process flow of fabricating CNT microelectrodes on a PI substrate. The process steps are described as follows. A thin layer of adhesion layer followed by a layer of gold (Au) are deposited on PI film (Fig. 9.10a). Both layers are then patterned to form microelectrodes, interconnecting wires, and bond pads (Fig. 9.10b–d). A titanium (Ti) adhesion layer followed by a thin catalyst layer of nickel (Ni) are deposited using a shadow mask having openings only above microelectrode sites (Fig. 9.10e). The Ni catalyst layer is used to promote adhesion between CNTs and the metal electrode surface. This adhesion is critical for long term stability of the CNT layer in neural environment. Then, CNTs are grown above the Ni catalyst by thermal CVD with using C_2H_2/H_2 as precursor gases. Finally, all regions except for the electrode areas and the wire-bonding pads are encapsulated by a relatively thick layer of electrochemically deposited parylene.

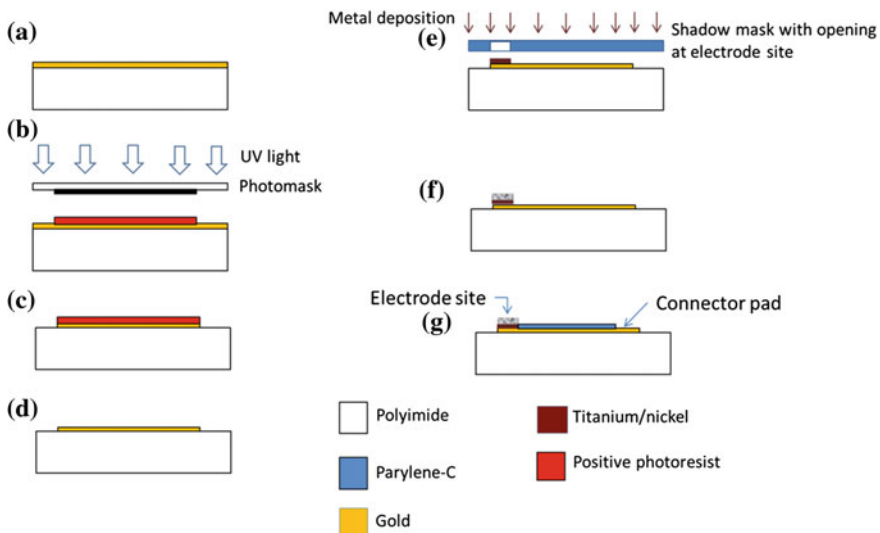


Fig. 9.10 Fabrication steps of CNT electrode for flexible microelectrode arrays (adapted from Ref. [80])

9.9 Degradation of Thin Film Electrodes in Neural Environment

The major drawback of thin film microelectrodes is they are prone to degradation in chronic application. This section reviews the degradation mechanism of the common thin film coatings used in brain implantable microelectrodes.

Electrolysis of water is the most common irreversible processes responsible for platinum electrode dissolution due to the oxidative formation of soluble metal complexes coupled with pH changes and gas formation. Oxidation of organics, such as glucose and tyrosine, and saline oxidation, have been identified, as other possible irreversible or harmful electrochemical reactions that might be responsible for degradation [10, 11] of implanted neural stimulation electrodes like Pt dissolution [11, 97] and iridium oxide delamination [98]. It is important to establish the maximum charge density for stimulation specific to the thin film material. It has been found that application of current pulse higher than a safe maximum results in polarization of the IrO₂ electrode beyond the potential window for electrolysis of water (−0.6–0.8 V versus Ag|AgCl) and delamination of the film [98].

For thin film conductive polymer electrodes, water absorption and volume change due to mass transport are possible reasons of degradation [99]. A comparison between electrodeposited PPy/Cl, PPy/PSS and PPy/SWCNT films on Pt after stimulation showed a significant delamination for PPy/Cl films after stimulation. PPy/PSS films did not show significant delamination, but the edge of the film was swollen and noticeably deformed [95]. The volume change due to electrode cycling may result in adhesion failure of the conducting polymer films on the electrode substrate [100].

9.10 Biocompatibility Testing

To achieve functionality and reliability of the device, interaction of the brain cells with the device at the interface must be studied with respect to biocompatibility. Before any experiments with these neural implant devices are conducted in living animals, characterization should be conducted upon cultured cells. Cell viability is a preliminary study of biocompatibility. Therefore, culturing of cells on the proposed materials is essential to test the cytotoxicity.

However, the concept of biocompatibility is not limited to non-toxicity, but encloses a wide spectrum of physical and chemical surface properties and whole behavioral aspects in the biological environment around the implant as well. Therefore, three areas need to be considered [101]:

- The bio-safety which include body's response to the electrode
- The bio-functionality which include the electrodes performance in the body

Table 9.5 Some additional tests suggested by FDA

Device categories		Biological effect			
Body contact	Contact duration: A-limited (<24 h) B-prolonged (24 h to 30 days) C-permanent (>30 days)	Chronic toxicity	Carcinogenicity	Reproductive/developmental	Biodegradable
Implant device	Tissue/ bone	A			
		B			
		C	X	X	X
	Blood	A			
		B			
		C	X	X	X

X ISO evaluation tests for consideration

O Additional tests which may be applicable

- In addition, bio-stability is important since the implant must not be susceptible to attack of biological fluids, proteases, macrophages or any substances of metabolism. Stability of implant material is important not only for stable function, but also because degradation products may be harmful for the host organism.

All these aspects of biocompatibility should be investigated in culture before any material or device can be tested in vivo. For the development of an implantable neural electrode the general tests of biocompatibility consists of the following steps:

- in vitro
- in vivo testing
- animal models
- cytotoxicity

The information presented in Tables 9.4 and 9.5 are taken from the website of the US Food and Drug administration (FDA: <http://www.fda.gov/MedicalDevices/DeviceRegulationandGuidance/GuidanceDocuments/ucm080742.htm>) that entails the general guideline for the initial evaluation tests for any medical device biocompatibility.

9.11 Conclusions

Key materials for thin film coatings for microelectrodes are Pt, IrO_x and gold. These systems use microelectronic fabrication technique such as sputtering and can be mass produced. Conductive polymers such as PEDOT and gold coated Parylene are very good options. PEDOT is utilized via electrochemical deposition while gold coating can be accomplished on Parylene using sputtering. Carbon nanotube systems can be developed via thermal/chemical vapor deposition. Other coating materials discussed in the article have good potential. However, their efficacy is closely tied to acute microelectrode applications. Chronic applications require more stable material systems as the ones mentioned above. Biocompatibility of all of these materials require further evaluation for their long-term application in neural devices.

9.12 Future Trends

Chronic neural stimulation requires highly stable microelectrode and biocompatible materials with high charge injection capability. Conductive polymers coating is a major trend that must be exploited that meets these goals. Conductive polymer, poly (3,4-ethylenedioxythiophene) PEDOT has excellent promise as it has charge injection limit similar to IrO_x. Well-coated PEDOT electrodes can be very stable under chronic stimulation conditions, suggesting that PEDOT is a promising electrode material to be further developed for chronic neural stimulation applications. Parylene-C shows promise as selective insulation of microelectrodes to provide greater intensity at the electrode probes for neural activity. Flexibility of Parylene has also been exploited for micro channeling for drug delivery. Chemical vapor deposited Parylene-C films show potential for implantable dielectric encapsulation material. Gold-coated parylene is an important trend in new neural devices. Gold with CNT can increase sensitivity several fold.

Finally, carbon nanotube modified microelectrodes have been used to increase the sensitivity, promote electron transfer, and reduce cell coverage or fouling. Most methods have focused on nanotube coatings of somewhat larger electrodes and slower electrochemical techniques that are not good for measurements in vivo. However, nanotube modified coatings will continue to offer new coating designs and offers the potential for tailored systems for superior microelectrode performance, both from optimizing electrochemical property improvements and also from durability for chronic implantation.

References

1. Vincent, A.M., Feldman, E.L.: Control of cell survival by IGF signaling pathways. *Growth Hormon. IGF Res.* **12**(4), 193–197 (2002)
2. Horner, P.J., Gage, F.H.: Regenerating the damaged central nervous system. *Nature* **407**(6807), 963–970 (2000)
3. Grill, W.M., et al.: At the interface: convergence of neural regeneration and neural prostheses for restoration of function. *J. Rehabil. Res. Dev.* **38**(6), 633–639 (2001)
4. Peckham, P.H., et al.: An advanced neuroprosthesis for restoration of hand and upper arm control using an implantable controller. *J. Hand Surg.* **27**(2), 265–276 (2002)
5. Kim, Y.-H., et al.: Function-inspection scheme for an injured peripheral nerve using a polymer based microelectrode array. *Sens. Actuators A* **139**(1–2), 58–65 (2007)
6. Tehovnik, E.J.: Direct and Indirect Activation of Cortical Neurons by Electrical Microstimulation. *J. Neurophysiol.* **96**(2), 512–521 (2006)
7. Tehovnik, E.J.: Electrical stimulation of neural tissue to evoke behavioral responses. *J. Neurosci. Methods* **65**(1), 1–17 (1996)
8. McIntyre, C.C.: Selective microstimulation of central nervous system neurons. *Ann. Biomed. Eng.* **28**(3), 219–233 (2000)
9. Basser, P.J.: N C E S E T. *Annu. Rev. Biomed. Eng.* **2**(1), 377–397 (2000)
10. Merrill, D.R.: Electrical stimulation of excitable tissue: design of efficacious and safe protocols. *J. Neurosci. Methods* **141**(2), 171–198 (2005)
11. Robblee, L.S.: *Electrochemical Guidelines for Selection of Protocols and Electrode Materials for Neural Stimulation. Neural Prostheses: Fundamental Studies*, p. 25 (1990)
12. Lebedev, M.A.: Brain-machine interfaces: past, present and future. *Trends Neurosci (Regular ed.)* **29**(9), 536–546 (2006)
13. Friehs, G.M.: Brain-machine and brain-computer interfaces. *Stroke*(1970) **35**(11_suppl_1), 2702–2705 (2004)
14. Donoghue, J.P.: Connecting cortex to machines: recent advances in brain interfaces. *Nature Neurosci.* **5**(supp), 1085–1088 (2002)
15. Hashemi, P., et al.: Chronically implanted, Nafion-Coated Ag/AgCl reference electrodes for neurochemical applications. *ACS Chem. Neurosci.* **2**(11), 658–666 (2011)
16. Johnson, M.D., et al.: Chemical sensing capability of MEMS implantable multichannel neural microelectrode arrays in engineering in medicine and biology society, 2003. In: *Proceedings of the 25th Annual International Conference of the IEEE.* (2003)
17. Cogan, S.F.: Neural stimulation and recording electrodes. *Annu. Rev. Biomed. Eng.* **10**(1), 275–309 (2008)
18. Donoghue, J.P.: Assistive technology and robotic control using motor cortex ensemble-based neural interface systems in humans with tetraplegia. *J. Physiol.* **579**(3), 603–611 (2007)
19. McCreery, D.: Microelectrode array for chronic deep-brain microstimulation and recording. *IEEE Trans. Biomed. Eng.* **53**(4), 726–737 (2006)
20. Gluckman, B.J.: Adaptive electric field control of epileptic seizures. *J. Neurosci.* **21**, 590 (2001)
21. Polikov, V.S., Tresco, P.A., Reichert, W.M.: Response of brain tissue to chronically implanted neural electrodes. *J. Neurosci. Methods* **148**(1), 1–18 (2005)
22. Johnson, M.D.: Repeated voltage biasing improves unit recordings by reducing resistive tissue impedances. *IEEE Trans. Neural Syst. Rehabil. Eng.* **13**(2), 160–165 (2005)
23. Niparko, J.K.: Surgical implantation and biocompatibility of central nervous system auditory prostheses. *Ann. Otol. Rhinol. Laryngol* **98**, 965 (1989)
24. Kim, Y.-T.: Chronic response of adult rat brain tissue to implants anchored to the skull. *Biomaterials* **25**(12), 2229–2237 (2004)
25. Edell, D.J.: Factors influencing the biocompatibility of insertable silicon microshafts in cerebral cortex. *IEEE Trans. Biomed. Eng.* **39**(6), 635–643 (1992)

26. Turner, J.N.: Cerebral astrocyte response to micromachined silicon implants. *Exp. Neurol.* **156**(1), 33–49 (1999)
27. Szarowski, D.H.: Brain responses to micro-machined silicon devices. *Brain Res.* **983**(1–2), 23–35 (2003)
28. Biran, R.: Neuronal cell loss accompanies the brain tissue response to chronically implanted silicon microelectrode arrays. *Exp. Neurol.* **195**(1), 115–126 (2005)
29. Phillips, P.E.M., et al.: Subsecond dopamine release promotes cocaine seeking. *Nature* **422**(6932), 614–618 (2003)
30. Cheer, J.F., et al.: Phasic dopamine release evoked by abused substances requires cannabinoid receptor activation. *J. Neurosci.* **27**(4), 791–795 (2007)
31. Uchiyama, Y., et al.: Phospholipid mediated plasticity in exocytosis observed in PC12 cells. *Brain Res.* **1151**, 46–54 (2007)
32. Yavich, L., Jäkälä, P., Tanila, H.: Noradrenaline overflow in mouse dentate gyrus following locus coeruleus and natural stimulation: real-time monitoring by in vivo voltammetry. *J. Neurochem.* **95**(3), 641–650 (2005)
33. Swamy, B.E.K., Venton, B.J.: Carbon nanotube-modified microelectrodes for simultaneous detection of dopamine and serotonin in vivo. *Analyst* **132**(9), 876–884 (2007)
34. Perez, X.A., Andrews, A.M.: Chronoamperometry to determine differential reductions in uptake in brain synaptosomes from serotonin transporter knockout mice. *Anal. Chem.* **77**(3), 818–826 (2004)
35. Singh, Y.S., et al.: Boron-doped diamond microelectrodes reveal reduced serotonin uptake rates in lymphocytes from adult rhesus monkeys carrying the short allele of the 5-HTTLPR. *ACS Chem. Neurosci.* **1**(1), 49–64 (2009)
36. Montañez, S., et al.: Differential in vivo clearance of serotonin in rat dorsal raphe nucleus and CA3 region. *Brain Res.* **955**(1–2), 236–244 (2002)
37. Jackson, B.P., Dietz, S.M., Wightman, R.M.: Fast-scan cyclic voltammetry of 5-hydroxytryptamine. *Anal. Chem.* **67**(6), 1115–1120 (1995)
38. Hocevar, S.B., et al.: Simultaneous in vivo measurement of dopamine, serotonin and ascorbate in the striatum of experimental rats using voltammetric microprobe. *Front. Biosci.* **11**, 2782–2789 (2006)
39. Rice, M.E.: Ascorbate regulation and its neuroprotective role in the brain. *Trends Neurosci.* **23**(5), 209–216 (2000)
40. Bravo, R., Stickle, D.M., Brajter-Toth, A.: Determination of uric acid in urine by fast-scan voltammetry (FSV) using a highly activated carbon fiber electrode. *Methods Mol. Biol.* **186**, 195–208 (2002)
41. Swamy, B.E.K., Venton, B.J.: Subsecond Detection of Physiological Adenosine Concentrations Using Fast-Scan Cyclic Voltammetry. *Anal. Chem.* **79**(2), 744–750 (2006)
42. El-Nour, K.A., Brajter-Toth, A.: Development of adenosine sensor: effect of physiological buffers on activity and sensitivity in adenosine determinations by fast scan voltammetry. *Analyst* **128**(8), 1056–1061 (2003)
43. Burmeister, J.J., et al.: Ceramic-based multisite microelectrode arrays for simultaneous measures of choline and acetylcholine in CNS. *Biosens. Bioelectron.* **23**(9), 1382–1389 (2008)
44. Singh, Y.S.: Head-to-Head Comparisons of Carbon Fiber Microelectrode Coatings for Sensitive and Selective Neurotransmitter Detection by Voltammetry. *Anal. chem.* (Washington) 110803090708049 (2011)
45. Rice, M.E., Nicholson, C.: Measurement of nanomolar dopamine diffusion using low-noise perfluorinated ionomer-coated carbon fiber microelectrodes and high-speed cyclic voltammetry. *Anal. Chem.* **61**(17), 1805–1810 (1989)
46. Trouillon, R., et al.: Comparative study of poly(styrene-sulfonate)/poly(L-lysine) and fibronectin as biofouling-preventing layers in dissolved oxygen electrochemical measurements. *Analyst* **134**(4), 784–793 (2009)

47. Marinesco, S., Carew, T.J.: Improved electrochemical detection of biogenic amines in Aplysia using base-hydrolyzed cellulose-coated carbon fiber microelectrodes. *J. Neurosci. Methods* **117**(1), 87–97 (2002)
48. Cheng, Q., Brajter-Toth, A.: Permselectivity and high sensitivity at ultrathin monolayers. Effect of film hydrophobicity. *Anal. Chem.* **67**(17), 2767–2775 (1995)
49. Cruz, J., Kawasaki, M., Gorski, W.: Electrode coatings based on chitosan scaffolds. *Anal. Chem.* **72**(4), 680–686 (2000)
50. Wang, J., Musameh, M., Lin, Y.: Solubilization of carbon nanotubes by nafion toward the preparation of amperometric biosensors. *J. Am. Chem. Soc.* **125**(9), 2408–2409 (2003)
51. Cahill, P.S., et al.: Microelectrodes for the measurement of catecholamines in biological systems. *Anal. Chem.* **68**(18), 3180–3186 (1996)
52. Hasenkamp, W., et al.: Electrodeposition and characterization of iridium oxide as electrode material for neural recording and stimulation, in World Congress on Medical Physics and Biomedical Engineering, 7–12 Sept 2009, Munich, Germany. In: Dössel, O., Schlegel (eds.), pp. 472–475 Springer, Berlin, Heidelberg, (2009)
53. Metallo, C., White, R.D., Trimmer, B.A.: Flexible parylene-based microelectrode arrays for high resolution EMG recordings in freely moving small animals. *J. Neurosci. Methods* **195**(2), 176–184 (2011)
54. Myllymaa, S., Myllymaa, K., Lappalainen, R.: Flexible implantable thin film neural electrodes, in Recent advances in biomedical engineering. Naik, G.R., (ed.) Intech. pp. 165–190, (2009)
55. Stieglitz, T., Gross, M.: Flexible BIOMEMS with electrode arrangements on front and back side as key component in neural prostheses and biohybrid systems. *Sens Actuators B: Chem* **83**(1–3), 8–14 (2002)
56. Keekeun, L., Stephen, M., Jiping, H.: Biocompatible benzocyclobutene-based intracortical neural implant with surface modification. *J. Micromech. Microeng.* **15**(11), 2149 (2005)
57. Liang, G., et al.: A PDMS-based conical-well microelectrode array for surface stimulation and recording of neural tissues. *IEEE Trans. Biomed. Eng.* **57**(10), 2485–2494 (2010)
58. Meacham, K., et al.: A lithographically-patterned, elastic multi-electrode array for surface stimulation of the spinal cord. *Biomed. Microdev.* **10**(2), 259–269 (2008)
59. Schmidt, E., McIntosh, J., Bak, M.: Long-term implants of parylene-C coated microelectrodes. *Med. Biol. Eng. Comput.* **26**(1), 96–101 (1988)
60. Seymour, J.P., et al.: The insulation performance of reactive parylene films in implantable electronic devices. *Biomaterials* **30**(31), 6158–6167 (2009)
61. Li, Y., Mogul, D.J.: Electrical control of epileptic seizures. *J. Clin. Neurophysiol.* **24**(2), 197–204 (2007). doi:[10.1097/WNP.0b013e31803991c3](https://doi.org/10.1097/WNP.0b013e31803991c3)
62. Normann, R.A.: Technology Insight: future neuroprosthetic therapies for disorders of the nervous system. *Nat Clin Pract Neuro* **3**(8), 444–452 (2007)
63. Perlmutter, J.S., Mink, J.W.: Deep brain stimulation. *Annu. Rev. Neurosci.* **29**(1), 229–257 (2006)
64. Clark, G.M.: The multiple-channel cochlear implant: the interface between sound and the central nervous system for hearing, speech, and language in deaf people—a personal perspective. *Philos. Trans. R. Soc. B: Biol. Sci.* **361**(1469), 791–810 (2006)
65. Shepherd, R.K., McCreery, D.B.: Basis of electrical stimulation of the cochlea and the cochlear nucleus. *Adv. Otorhinolaryngol.* **64**, 186–205 (2006)
66. Jackson, A., et al.: The neurochip BCI: towards a neural prosthesis for upper limb function. *IEEE Trans. Neural Syst. Rehabil. Eng.* **14**(2), 187–190 (2006)
67. Ruten, W.L.C.: Selective electrical interfaces with the nervous system. *Annu. Rev. Biomed. Eng.* **4**(1), 407–452 (2002)
68. Jezernik, S.: Electrical stimulation for the treatment of bladder dysfunction: Current status and future possibilities. *Neurol. Res. (New York)* **24**(5), 413–430 (2002)
69. Prochazka, A.: Neural prostheses. *J. Physiol* **533**(1), 99–109 (2001)
70. Hoffer, J.A.: Neural signals for command control and feedback in functional neuromuscular stimulation: a review. *J. Rehabil. Res. Dev.* **33**, 145 (1996)

71. Ereifej, E.S., et al.: Characterization of astrocyte reactivity and gene expression on biomaterials for neural electrodes. *J. Biomed. Mater. Res. Part A* **99A**(1), 141–150 (2011)
72. Beebe, X., Rose T.: Charge injection limits of activated iridium oxide electrodes with 0.2 ms pulses in bicarbonate buffered saline (neurological stimulation application). *Biomed. Eng. IEEE Trans.* **35**(6), 494–495 (1988)
73. Weiland, J.D., Anderson, D.J., Humayun, M.S.: In vitro electrical properties for iridium oxide versus titanium nitride stimulating electrodes. *Biomed. Eng. IEEE Trans.* **49**(12), 1574–1579 (2002)
74. Lee, I.-S., et al.: Formation of nano iridium oxide: material properties and neural cell culture. *Thin Solid Films*, **475**(1), 32–336 (2005)
75. Thanawala, S.: Characterization of Sputtered IrO₂ Thin Films on Planar and Laser Micro-structured Platinum Thin Film Surfaces for Neural Stimulation Applications, in *Biomedical Engineering*. Wayne State University, Detroit (2006)
76. Thanawala, S., et al.: Characterization of iridium oxide thin films deposited by pulsed-direct-current reactive sputtering. *Thin Solid Films* **515**(18), 7059–7065 (2007)
77. Lin, C.-M., et al.: Flexible carbon nanotubes electrode for neural recording. *Biosens. Bioelectron.* **24**(9), 2791–2797 (2009)
78. Ren, Z.F., et al.: Synthesis of large arrays of well-aligned carbon nanotubes on glass. *Science* **282**(5391), 1105–1107 (1998)
79. Khan, S., Newaz, G.: A comprehensive review of surface modification for neural cell adhesion and patterning. *J. Biomed. Mater. Res., Part A* **93A**(3), 1209–1224 (2010)
80. Yung-Chan, C., et al.: An active, flexible carbon nanotube microelectrode array for recording electrocorticograms. *J. Neural Eng.* **8**(3), 034001 (2011)
81. Sorkin, R., et al.: Compact self-wiring in cultured neural networks. *J. Neural Eng.* **3**(2), 95–101 (2006)
82. Matsumoto, K., et al.: Neurite outgrowths of neurons with neurotrophin-coated carbon nanotubes. *J. Biosci. Bioeng.* **103**(3), 216–220 (2007)
83. McKenzie, J.L., et al.: Decreased functions of astrocytes on carbon nanofiber materials. *Biomaterials* **25**(7–8), 1309–1317 (2004)
84. Gomez, N., Lee, J.Y., Nickels, J.D., Schmidt, C.E.: Micropatterned polypyrrole: a combination of electrical and topographical characteristics for the stimulation of cells. *Adv. Funct. Mater.* **17**(10), 1645–1653 (2007)
85. Frommhold, A., Tarte, E.: Effect of film structure on the electrochemical properties of gold electrodes for neural implants. *Electrochim. Acta* **56**(17), 6001–6007 (2011)
86. Lawrence, S.M., Dhillon, G.S., Horch, K.W.: Fabrication and characteristics of an implantable, polymer-based, intrafascicular electrode. *J. Neurosci. Methods* **131**(1–2), 9–26 (2003)
87. Tokuda, T., et al.: CMOS-based multichip networked flexible retinal stimulator designed for image-based retinal prosthesis. *IEEE Trans. Electron Dev.* **56**(11), 2577–2585 (2009)
88. Negi, S., et al.: In vitro comparison of sputtered iridium oxide and platinum-coated neural implantable microelectrode arrays. *Biomed. Mater.* **5**(1), 015007 (2010)
89. Tallmana, D.E., et al.: Direct electrodeposition of polypyrrole on aluminum and aluminum alloy by electron transfer mediation. *J. Electrochem. Soc.* **149**(3), C173–C179 (2002)
90. Guimard, N.K., Gomez, N., Schmidt, C.E.: Conducting polymers in biomedical engineering. *Prog. Polym. Sci.* **32**(8–9), 876–921 (2007)
91. Onoda, M., Abe, Y., Tada, K.: Experimental study of culture for mouse fibroblast used conductive polymer films. *Thin Solid Films* **519**(3), 1230–1234 (2010)
92. Wang, K., et al.: Neural Stimulation with a Carbon Nanotube Microelectrode Array. *Nano Lett.* **6**(9), 2043–2048 (2006)
93. Di, L., et al.: Protein adsorption and peroxidation of rat retinas under stimulation of a neural probe coated with polyaniline. *Acta Biomater.* **7**(10), 3738–3745 (2011)
94. Deng, M., et al.: Electrochemical deposition of polypyrrole/graphene oxide composite on microelectrodes towards tuning the electrochemical properties of neural probes. *Sens. Actuators B: Chem.* **158**(1), 176–184 (2011)

95. Lu, Y., et al.: Electrodeposited polypyrrole/carbon nanotubes composite films electrodes for neural interfaces. *Biomaterials* **31**(19), 5169–5181 (2010)
96. Cui, X., et al.: Electrochemical deposition and characterization of conducting polymer polypyrrole/PSS on multichannel neural probes. *Sens. Actuators, A* **93**(1), 8–18 (2001)
97. Agnew, W.F.: Histopathologic evaluation of prolonged intracortical electrical stimulation. *Exp. Neurol.* **92**(1), 162–185 (1986)
98. Cogan, S.F., et al.: Over-pulsing degrades activated iridium oxide films used for intracortical neural stimulation. *J. Neurosci. Methods* **137**(2), 141–150 (2004)
99. Jager, E.W.H., Smela, E., Inganäs, O.: Microfabricating conjugated polymer actuators. *Science* **290**(5496), 1540–1545 (2000)
100. Abidian, M.R., et al.: Conducting-polymer nanotubes improve electrical properties, mechanical adhesion, neural attachment, and neurite outgrowth of neural electrodes. *Small* **6**(3), 421–429 (2010)
101. Mckenna, A.S.a.T.M. (ed.): *Enabling Technologies for Cultured Neural Networks*. Academic Press, New York (1994)
102. McCarthy, P., Otto, K., Rao, M.: Robust penetrating microelectrodes for neural interfaces realized by titanium micromachining. *Biomed. Microdevices* **13**(3), 503–515 (2011)
103. Lacour, S., et al.: Flexible and stretchable micro-electrodes for in vitro and in vivo neural interfaces. *Med. Biol. Eng. Comput.* **48**(10), 945–954 (2010)
104. Hesse, L., et al.: Implantation of retina stimulation electrodes and recording of electrical stimulation responses in the visual cortex of the cat. *Graefes Arch. Clin. Exp. Ophthalmol.* **238**(10), 840–845 (2000)
105. Humayun, M.S., et al.: Pattern electrical stimulation of the human retina. *Vision. Res.* **39**(15), 2569–2576 (1999)
106. O’Hearn, T.M., et al.: Electrical stimulation in normal and retinal degeneration (rd1) isolated mouse retina. *Vision. Res.* **46**(19), 3198–3204 (2006)
107. Shyu, J.S., et al.: Electrical stimulation in isolated rabbit retina. *IEEE Trans. Neural Syst. Rehabil. Eng.* **14**(3), 290–298 (2006)
108. Samip, S., et al.: Electrical properties of retinal–electrode interface. *J. Neural Eng.* **4**(1), S24 (2007)
109. Walter, P., Heimann, K.: Evoked cortical potentials after electrical stimulation of the inner retina in rabbits. *Graefes Arch. Clin. Exp. Ophthalmol.* **238**(4), 315–318 (2000)
110. Grumet, A.E., Wyatt Jr, J.L., Rizzo 3rd, J.F.: Multi-electrode stimulation and recording in the isolated retina. *J. Neurosci. Methods* **101**(1), 31–42 (2000)
111. Rizzo 3rd, J.F., et al.: Perceptual efficacy of electrical stimulation of human retina with a microelectrode array during short-term surgical trials. *Invest. Ophthalmol. Vis. Sci.* **44**(12), 5362–5369 (2003)
112. Rizzo 3rd, J.F., et al.: Methods and perceptual thresholds for short-term electrical stimulation of human retina with microelectrode arrays. *Invest. Ophthalmol. Vis. Sci.* **44**(12), 5355–5361 (2003)
113. McCreery, D.B.: Chronic microstimulation in the feline ventral cochlear nucleus: physiologic and histologic effects. *Hear. Res.* **149**(1–2), 223–238 (2000)
114. Branner, A.: Selective stimulation of cat sciatic nerve using an array of varying-length microelectrodes. *J. Neurophysiol.* **85**, 1585 (2001)
115. Weiland, J.D., Anderson, D.J.: Chronic neural stimulation with thin-film, iridium oxide electrodes. *Biomed. Eng. IEEE Trans.* **47**(7), 911–918 (2000)
116. El Khakani, M.A., Chaker, M.: Reactive pulsed laser deposition of iridium oxide thin films. *Thin Solid Films*, **335**(1–2), 6–12 (1998)
117. Wang, K., Chung-Chiu, L., Durand, D.M.: Flexible Nerve Stimulation Electrode With Iridium Oxide Sputtered on Liquid Crystal Polymer. *Biomed. Eng. IEEE Trans.* **56**(1), 6–14 (2009)
118. Cogan, S.F., et al., Sputtered iridium oxide films for neural stimulation electrodes. *J. Biomed. Mater. Res. Part B Appl. Biomater.* **89B**(2), 353–361 (2009)

119. Pan, Y. et al.: Optimization of sputtering condition of IrOx thin film stimulation electrode for retinal prosthesis application. *J. Phys.: Conf. Ser.* **352**(1) (2012)
120. Zhang, H., et al.: Layered Nanocomposites from Gold Nanoparticles for Neural Prosthetic Devices. *Nano Lett.* **12**(7), 3391–3398 (2012)
121. Wang, P., Olbricht, W.L.: PEDOT/Nafion composite thin films supported on Pt electrodes: Facile fabrication and electrochemical activities. *Chem. Eng. J.* **160**(1), 383–390 (2010)
122. Abidian, M.R., Martin, D.C.: Experimental and theoretical characterization of implantable neural microelectrodes modified with conducting polymer nanotubes. *Biomaterials* **29**(9), 1273–1283 (2008)
123. Ben-Jacob, E., Hanein, Y.: Carbon nanotube micro-electrodes for neuronal interfacing. *J. Mater. Chem.* **18**(43), 5181–5186 (2008)
124. Wang, K., et al.: Neural stimulation with a carbon nanotube microelectrode array. *Nano Lett.* **6**(9), 2043–2048 (2006)
125. Onoda, M., Abe, Y., Tada, K.: New fabrication technique of conductive polymer/insulating polymer composite films and evaluation of biocompatibility in neuron cultures. *Thin Solid Films* **518**(2), 743–749 (2009)
126. Lu, Y., et al.: Poly(vinyl alcohol)/poly(acrylic acid) hydrogel coatings for improving electrode–neural tissue interface. *Biomaterials* **30**(25), 4143–4151 (2009)

Chapter 10

Scanning Electrochemical Microscopy Applied to Cancer Related Studies

Isabelle Beaulieu and Janine Mauzeroll

Abstract This book chapter will not only provide an overview of the SECM principles but will also focus on SECM and cancer. More precisely we will look at biomarkers involved in cancer and SECM experiments concerning mammalian cancer cells. A description of selected SECM modes will also be included as well as an introduction to Bio-SECM.

10.1 Introduction

Scanning probe microscopy (SPM) encompasses several techniques such as atomic force microscopy (AFM), scanning tunneling microscopy (STM) and scanning electrochemical microscopy (SECM). All of these techniques can be used in imaging applications while a probe is moved above a sample and monitors its topography.

In AFM, surface induced mechanical forces are monitored at a tip that is fixed on a cantilever (Fig. 10.1b) [1], which lead to subtle (0.1 Å) deflection of the cantilever. The studied sample is placed on a piezoelectric controlled positioning system that moves in the x , y and z directions. The cantilever deflections are measured by recording the position of a focused laser beam that is reflected off of the cantilever surface. Movement of the cantilever causes a change in the amount of light reflected on the photocells, which creates a differential electrical signal [1]. The extent of the cantilever deflection for a certain force and the sensitivity is determined by the spring constant of the cantilever [2]. To avoid sample destruction, the force applied by the cantilever on the surface has to be small enough to prevent atomic bond breaking [3]. Since interatomic spring constants in

I. Beaulieu · J. Mauzeroll (✉)
Department of Chemistry, McGill University, 801 Sherbrooke Street West,
Montreal, QC H3A 2K6, Canada
e-mail: janine.mauzeroll@mcgill.ca

solids are on the order of 10 N/m, the stiffness of the cantilever needs to be significantly lower [2, 3].

STM measures the tunneling current that occurs between a sharp metal tip and a conducting sample as the tip is brought close to and rastered across a surface (Fig. 10.1a) [1]. Tunneling is a form of electronic conduction that occurs when the tip is so close to the surface (i.e., 5–10 Å apart) that the wave functions of the tip overlap with those of the surface atoms. This current flow is not based on a faradaic process and does not produce a chemical change. The electrons tunnel from filled electronic states in the sample to empty states in the tip when the

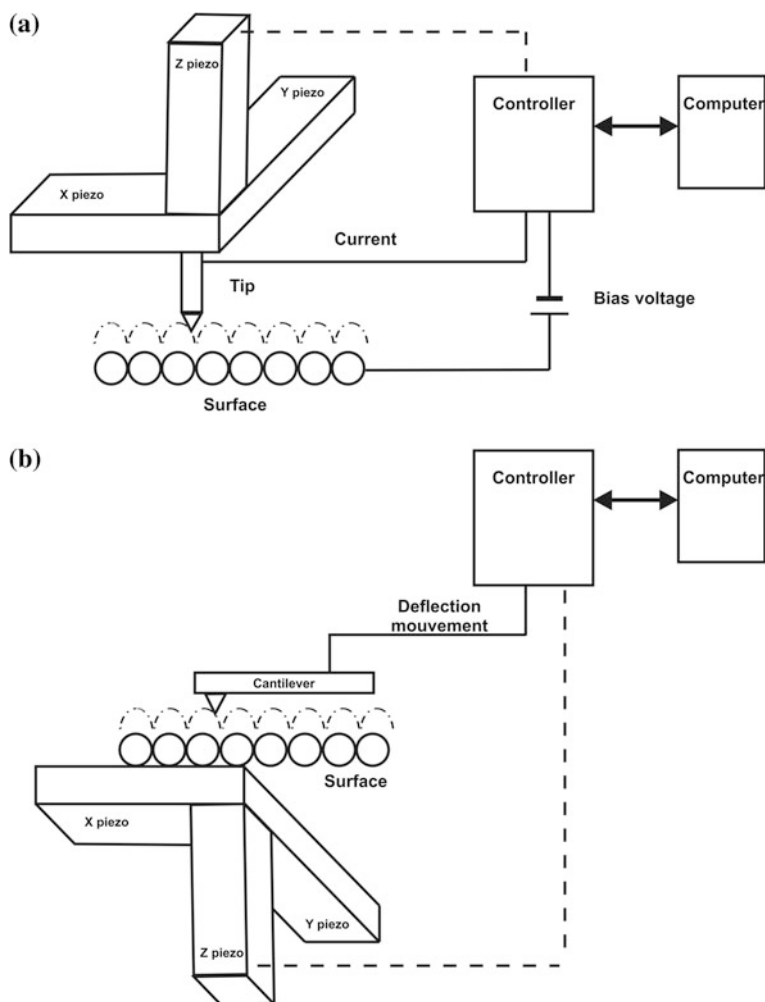


Fig. 10.1 Schematic illustrations of **a** a scanning tunneling microscope and **b** an atomic force microscope. Tripod representation of piezoelectric elements is for illustrative purposes only. Reproduced with permission from [1]. Copyright (1993) John Wiley and Sons

sample versus tip voltage is negative, and from the tip to empty sample electronic states when the bias is positive. The tunneling current depends exponentially on the tip-sample separation with a typical 10 fold change per Å. STM depends on the density of electronic states of the sample and tip. The most common STM mode is the constant current mode where an image of a surface is acquired by moving the tip in the z-direction until a tunneling current flows and then scanning the tip across the surface (in the x - y plane) while maintaining the current constant by moving the tip up and down, i.e., by varying z . Atomic-resolution x - y - z motion of the tip is accomplished by using piezoelectric controlled positioners [4].

Finally, SECM (Fig. 10.2) measures the faradaic current recorded at an microelectrode positioned within hundreds of nanometers of a surface. SECM provides quantitative information about the electrochemical reactions that occur within the confined volume between the tip and the surface [5]. The tip can be moved normal to the surface (the z direction) to probe the diffusion layer, the so-called approach curve. The tip can also be scanned across the surface (x and y directions) in order to record a single line scan or a full image. The tip and substrate are immersed in an electrochemical cell that usually also contains other (e.g., auxiliary and reference) electrodes. The instrument necessary to make such studies requires a movement of the tip with a resolution as low as Å level, which is attainable with precise motors such as piezoelectric or stepping motors [6]. In recent years, electrochemists started using SECM to work with biological samples like enzymes [7–9] and cells [9–12]. The sensitivity of the tip allows the detection

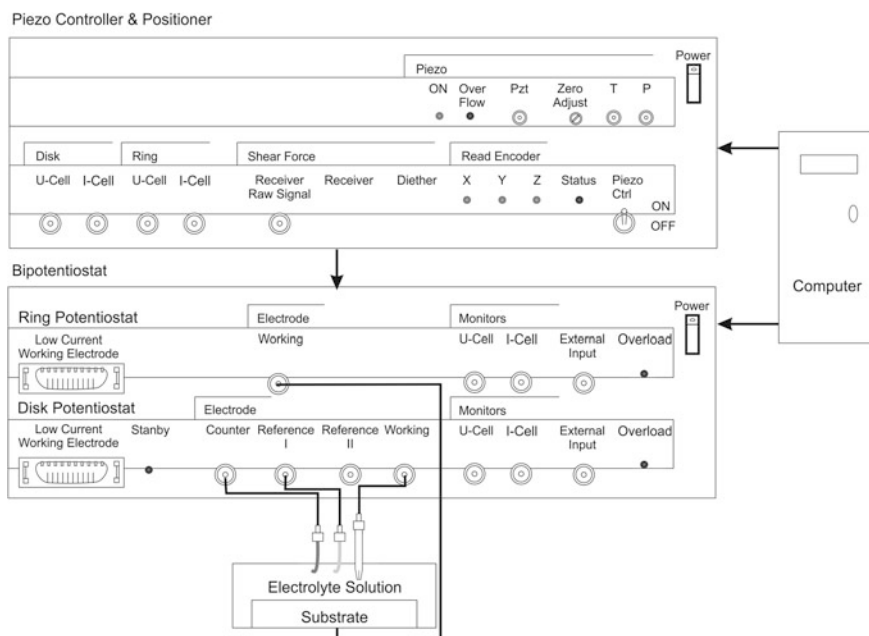


Fig. 10.2 Schematic illustration of a scanning electrochemical microscope

of small electrochemically active molecules such as neurotransmitters [13–15], reactive oxygen species [16] or other biomarkers [17, 18]. This is the reason why this book chapter will not only provide an overview of the SECM principles but will also focus on SECM and cancer. More precisely we will look at biomarkers involved in cancer and SECM experiments concerning mammalian cancer cells.

10.2 SECM Principles

Unlike other electrochemical instruments employing macroelectrodes, SECM uses a microelectrode to make quantitative electroanalytical measurements. Several reviews have been written about the behavior of the far away from the surface [19–23]. To perform SECM measurements, three electrodes are employed: a working electrode (or tip), the auxiliary electrode (or counter electrode) that balances the current produced at the working electrode and the reference electrode that fixes the potential bias set point. All three electrodes are placed in a vessel called an electrochemical cell that contains a redox mediator solution of concentration c and electrolyte salts to ensure high solution conductivity. When a potential far exceeding the standard potential of the dissolve redox mediator is applied between the working and the reference electrodes, the mediator is consumed at the tip surface via an oxidation or reduction reaction. The electrochemical reaction leads to a current flow between the working and auxiliary electrodes, which is detected at the tip. The recorded data of the current versus the potential forms a sigmoidal plot called a voltammogram (Copyright [24]).

The limiting current observed on the sigmoidal voltammogram occurs because the electrochemical process is governed by mass transfer. This implies that the dissolved redox mediator diffuses from the bulk solution to the electrode surface where the electrochemical process has reduced its concentration to essentially zero. Mathematically, the steady state diffusion-controlled current of a voltammogram acquired at a microelectrode of disk radius a (m) embedded in an insulating sheath, is given by [25]:

$$I_{ss} = 4nFDca\beta(RG)$$

where n is the number of electrons involved in the electrochemical process, F is the Faraday constant ($96.48534 \times 10^3 \text{ C mol}^{-1}$), D is the diffusion coefficient of the electroactive species in solution ($\text{m}^2 \text{ s}^{-1}$) and c is the concentration of the electroactive species (mol m^{-3}). Although other geometry exists, SECM experiments are often carried out with disk-shaped electrodes, because they have the best sensitivity. The current dependence on the radius of the insulating sheath, r_g , often referred in the SECM literature as $RG = r_g/a$ is expressed by $\beta(RG)$ factor. Common $\beta(RG)$ values are: $\beta(10) = 1.02$, $\beta(5) = 1.04$, $\beta(2) = 1.11$, $\beta(1) = 1.43$ [25]. Moreover, the current is practically not affected by convection in the bulk of the solution since the diffusion of the species to the small disk ($\sim Dc/a$) is

relatively large. Also, the current enters a steady state quite rapidly for a small disk ($\sim a^2/D$) this means that while scanning a surface with this kind of electrode, the system can be considered as a steady-state system. Lastly, because tips used for most experiments have a size of nm to μm , the recorded currents are quite low (pA to nA) [24].

10.2.1 Probe

We cannot emphasize enough the importance of the microelectrodes in SECM measurements. This is the reason why so many electrochemists focus on their fabrication and characterization. Their goal is to develop the smallest of probes with, if possible, a reproducible fabrication process. This is extremely challenging because of the fragility of the tip. Of course through the years, new fabrication methods have appeared on the electrochemical scene. The specific fabrication process differs depending on the nature of the material used (e.g. gold, platinum, carbon and borosilicate, quartz or soda glass) and the kind of analysis done [26]. The resulting electrode geometry varies, for example it can be disk-type [27–29], ring-type [30], cone-shaped [31, 32] or needle-type [33]. A multitude of articles and reviews have been written about different fabrication processes which include sealing/polishing [27] and laser-pulling [32] and showcase a variety of electrodes [5, 34–36].

Overall the choice of a working electrode in SECM depends on the type of measurement needed to be performed such as imaging, sensing process more complex than electron transfer or quantitative kinetic data acquisition [37]. For example, biosensors can be employed as a working electrode. A biosensor is composed of a recognition element that detects a molecule in a matrix [38]. Then a transducer transforms the biological signal into an electrical one and the data is displayed by the processor [38–41]. Like other electrodes, biosensors can include different type of material as recognition elements, among them, enzymes, antibodies and antigens are commonly used [38]. Those kinds of sensors can be used to analyze radicals, ions and small molecules to name a few [38, 41]. As for transducers; nanowires, carbon nanotubes, nanorods and quantum dots are being included into recent devices [38, 41]. One of the first biosensor was created by Clark to detect oxygen [42] and later was instrumental in the advent of the glucose sensor [43]. The type of biosensors used for electrochemical measurements are mainly amperometric, potentiometric and conductometric devices as mentioned in a nice review by Grieshaber et al. [41]. Amperometric sensors include the oxygen and glucose (through detection of hydrogen peroxide) sensors, more examples are cited in a review by Borgmann et al. [38]. As for potentiometric and conductometric biosensors, they can respectively detect hybridization of single-stranded oligonucleotide near a PVC membrane and enzymatic reactions [41].

10.2.2 Motors

Scanning probe microscopies involve displacements in x , y and z directions. In SECM, the probe displacement in the z axis has to be of nanometer-scale precision, which practically requires mounting the microelectrode on a high resolution piezoelectric actuator. The x and y travel distances can range from a few hundred microns to a few millimeters [44] and achieved by a variety of motor combinations. For example, HeKa produces a system called Elproscan that has a closed loop XY translation stage on which the sample is positioned. The entire stage changes direction thanks to a DC servo stepper motor controlled by a computer. There is also a stepper motor for z axis movement and a Z-piezo for fine positioning to move the stage on which the electrode is mounted. The global resolution of the positioning system is 1.0 nm [45]. Other systems are also available commercially such as the CHI900B SECM from CH Instruments Inc. This instrument also includes a combination of stepper motors and a XYZ piezo block for rough positioning and precise displacements respectively [44]. The positioning system has a global resolution of 1.6 nm [45]. Most instruments now use close-loop positioners that correct movement hysteresis using sensors that are optical-, capacitive- or strain- based in nature. This is particularly important in large-distance imaging of surfaces or in measurements where the exact surface area is scanned twice in order to deconvolute the contributions of surface topography and reactivity to the tip current [44].

10.2.3 Modes

SECM proved to be a versatile analytic method. In fact, different SECM modes offer diverse possibilities. In this section, we will review a few of those modes: feedback, imaging, generation-collection SG/TC and TG/SC, direct, redox-competition, surface interrogation and penetration and ion transfer modes [46]. In depth discussion of other operational modes are also available [37, 44, 47–50].

10.2.3.1 Feedback Mode

In feedback mode, when the UME approaches an insulating surface, the diffusion of the electroactive species towards the tip is hindered by the physical presence of the surface. The hindered diffusion leads to an overall decrease of the tip current with decreasing tip to substrate distance [so-called negative feedback (Fig. 10.3)]. If the surface is conductive, during a reduction process at the UME, the surface potential will regenerate the original electroactive species by re-oxidizing it. The established redox cycle during the positive feedback mode of SECM produces an additional flux of material that overrides the hindered diffusion process and results

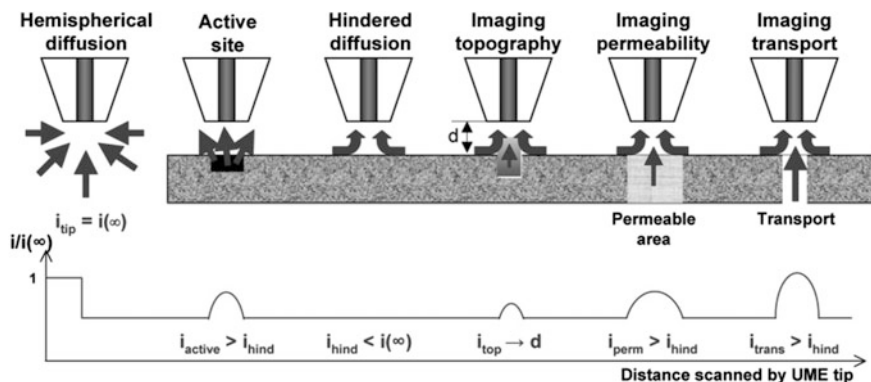


Fig. 10.3 A selection of modes of operation of a SECM, illustrating how the current response, expressed as a normalized quantity, hinges upon imaging certain features. *Arrows* represent the flow of the electroactive species (or ions) to the UME. Reproduced with permission from [50]. Copyright (2006) IOP Publishing

in a progressive increase in tip current with decreasing tip to substrate distance. A plot of the tip current with decreasing tip to substrate distance is called an approach curve. Experimental approach curves can readily be compared to theoretical approach curves obtained by solving the diffusion equations for a given microelectrode geometry [25, 51]. Typically the current and distances reported on approach curves are given in dimensionless form (I_N , L). The measured microelectrode current (i_T) and tip to substrate distances (d) are respectively normalized by the microelectrode current acquired far away from the surface ($i_{T,\infty}$) and the microelectrode radius (a). Normalized approach curves have differential behavior based on the concentration and diffusion coefficient of electroactive species, substrate kinetics and microelectrode geometry. Practically approach curves are often used to preposition the microelectrode at a known d prior to imaging [24].

10.2.3.2 SECM Imaging Modes

1. Constant height

In order to acquire an SECM image, the tip is brought in close proximity to the surface. Pre-positioning of the electrode prior to imaging is most often achieved using a feedback mode approach curve. When the tip is within a tip to substrate distance that is on the order of the tip radius, the microelectrode scans across the sample in x and y plane at a defined height. Constant height imaging is particularly sensitive to substrate tilts. As such slope correction protocols are often integrated prior to SECM imaging. For example, having defined a rectangular area of the substrate to be imaged, three negative approach curves are performed at the corners of the image. Since the microelectrode current scales with the tip to substrate

distance, the slope in the x and y direction are then defined based on the current variations recorded between two corners. The z position of the microelectrode is then adjusted at each point of the image based on the value of these two slopes. The image is acquired because of the current changes detected by the electrode. SECM imaging in constant height mode has some disadvantages. The main problem is related to irregular surfaces whose topography deviates from the linear slope correction. Significant topographical features create artifacts because their effect competes with the substrate reactivity. Also, during feedback based constant height imaging, the electrode is placed within a tip radius of the surface. Important surface roughness or tilting can lead to tip crash or break during imaging [52]. In fact, as people try to produce electrodes of smaller size to get a better resolution imaging, the risk of crashing the tip increases greatly when the scanning is done at constant height [52].

2. Constant distance

Constant-height mode is not always the best option for imaging due to its limitations. However the constant-distance mode allows control of the distance between the tip and the sample, which gives a more accurate detection of the current variations. During scans at a constant distance, the electrode follows the contour of the sample and is protected against a potential crash on the surface. It also allows simultaneous acquisition of the electrochemical response and determination of sample topography [52]. This is particularly important while scanning above living cells to avoid damaging the studied sample (Fig. 10.4). The cells are not completely flat on the surface and the reactivity is not always stable across the entire cell surface therefore topography cannot be a factor during the measurement because all the reactivity variations need to be detected. The constant distance SECM is a good solution to maintain the distance between the electrode and the cell constant during the scan by using the distance dependent feedback signal [54]. Shear force is a nice way of controlling the distance in this mode. It consists in fixing piezoelectric elements near the tip of the probe [53]. Systems have evolved lately using different types of piezos such as piezo dither [55–59] and piezo tuning fork [60–63].

3. 4D shearforce-based constant-distance mode scanning electrochemical microscopy (4D SF/CD-SECM)

(4D SF/CD-SECM) is designed to measure currents at the tip at different points of the x , y -scanning grid but at constant distances of the interrogated surface depending of its topography [64]. The distance of the tip from the surface depends on the signal received and is created by a shear-force interaction between the resonance of the tip vibrating and the surface. This kind of measurement is achieved by dividing the sample surface in a grid of multiple points. At each grid point, a distance calibration curve is performed using the shear-force controller. Distance calibration curve are acquired once the tip is in contact with the surface. During the retraction steps, pairs of tip current and position are recorded for each

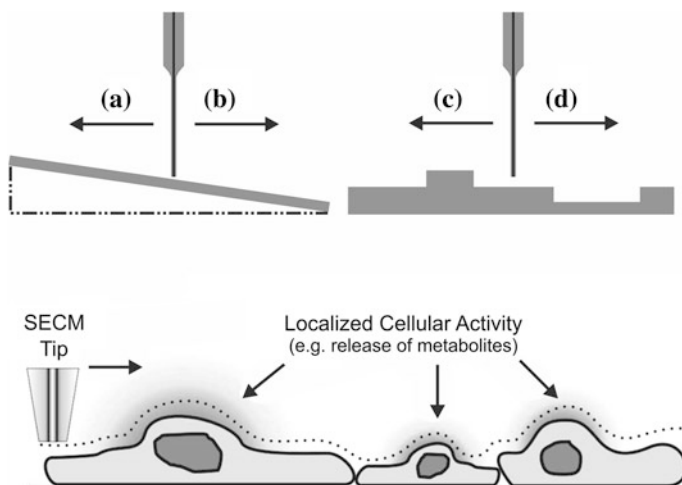


Fig. 10.4 Top Panel: There is a risk of tip crash when the tip is scanned at constant height across a tilted surface (a) or when the height of three-dimensional structures on the sample surface significantly exceeds the diameter of the SECM tip itself (c). On the other hand, the feedback or collection efficiency is lost if the tip is scanned away from a tilted surface © 2002 WILEY-VCH Verlag GmbH & Co. KGaA, Weinheim (b) or during scanning across grooves or holes (d). Reproduced with permission from [52]. Bottom Panel: Illustration of SECM imaging of live cells in constant distance mode. Dotted line represents the probe scan path. Reprinted with permission from [53]. Copyright (2010) American Chemical Society.

distances of determined increment and tabulated. Having established the tip to substrate distance for a given grid point the tip can be moved back vertically to larger separations that would not conventionally be accessible through shear force control. Finally, it requires the use of shear force only intermittently resulting in reduced analysis time [64].

10.2.3.3 Generation-Collection Modes

Tip collection mode has been really useful to measure transport phenomenon in artificial and biological membranes [65–71]. When the chemical process at the surface are slow, the tip collection is a nice mode for measurements since its efficiency relies mainly on the tip sensitivity to relevant species. But this mode might be difficult to use over heterogeneous surfaces with variable reactivity making the mass transport between the tip and the surface harder to define [50].

1. Sample-generation/tip-collection (SG/TC) mode

While doing SECM measurements in the sample generation-tip collection mode, the tip detects the reactivity of the sample. A pre-determined potential is applied at the tip to collect the sample generated electrochemically active species.

The principle is quite simple, when the tip is positioned above an active part of the sample, it detects an increase of current and when it is positioned above an inactive area, it detects a background current (same thing applies to TG/SC mode) [72].

2. Tip-generation/sample-collection (TG/SC) mode

As for the tip-generation sample collection mode, the opposite reasoning to SG/TC mode applies. In this mode, the electroactive species are generated at the tip and detected at a larger substrate electrode [73]. A possible problem with this mode is the fact that small currents are generated and they can get lost in the background noise created when the needed potential is applied on the sample. This collection mode as the advantage of having a better sensitivity than the feedback mode but its resolution is inferior [8, 72]. The larger substrate allows a great collection efficiency [74] for stable species therefore experiments can quickly be done under steady state conditions [59, 73, 75–78]. Also the mass transport is well-defined for TG/SC which simplifies numerical modeling designs [74].

10.2.3.4 Direct Mode

In the direct mode of SECM, the tip has the role of a microscopic size counter-electrode. As for the macroscopic sized sample, it acts as the working electrode. Due to a limitation through the counter electrode reaction and a confinement of the electric field between the tip and the perpendicular surface area of the sample, electrochemical processes at the sample surface are restricted to an area approximately the size of the tip and located opposite to the SECM tip position [72].

10.2.3.5 Redox-Competition Mode

The redox-competition mode is illustrated in Fig. 10.5. This mode of SECM requires the use of a bipotentiostat. During the experiment, the tip competes with the sample for the same analyte. When the electrode is near an area of the sample where there is electrocatalytic activity, the measured current decreases [80]. This mode is particularly useful if one wants to do imaging when an irreversible reaction, such as oxygen reduction, is involved. For each point of the image, an oxidative potential is applied at the electrode to locally generate O_2 . As soon as the generation step is stopped, the potential of the electrode is switched to a reductive potential and competes with the substrate to collect the generated O_2 . If the experiment is performed above an electrocatalytic surface, a fraction of the generated O_2 will be consumed at the surface to form hydrogen peroxide. Therefore, the collection efficiency at the microelectrode will be lower above an active surface and the collection current will also be lower. To create the image, the current transients from all the points over which the electrode is positioned are recorded [79]. One of the main advantage of this mode compared to TG/SC, is the possibility to use it on large samples without being limited by the tip diameter [79, 80].

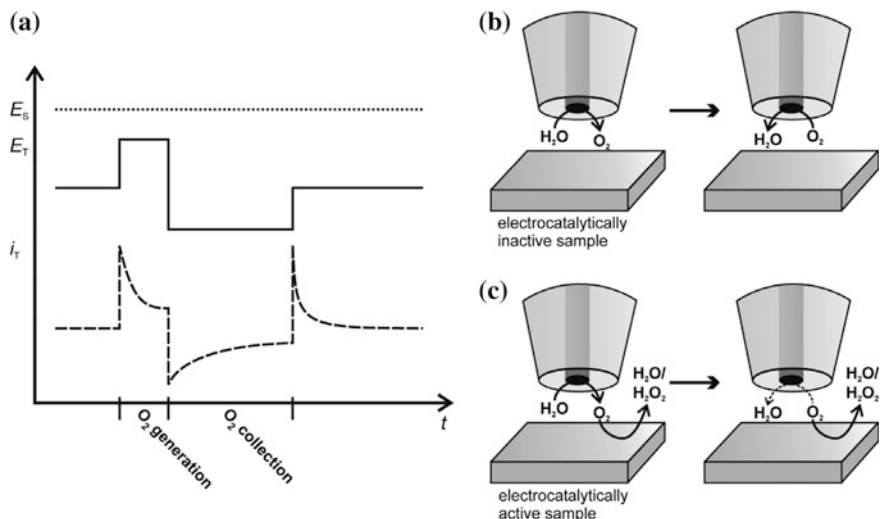


Fig. 10.5 General principle of the RC mode. **a** Pulse program at the UME: $E_s(t)$ (dotted line), $E_T(t)$ (solid line), and $i_T(t)$ (dashed line). **b** O₂ is generated and re-collected at the UME above an electrocatalytically inactive substrate. **c** O₂ is generated at the UME and partly consumed at an electrocatalytically active substrate. As a result, the current at the UME decreases. Reprinted with permission from [79]. Copyright (2008) Oldenbourg Wissenschaftsverlag

10.2.3.6 Surface Interrogation Mode

In this SECM mode, the tip is approached to a substrate of similar diameter. This tip is approached to the sample surface while the latter is being polarized to produce a reaction and a deposit on the electrode. The sample surface potential is then returned to open circuit to allow one of the redox species generated at the working electrode (tip) to react with its counterpart redox species adsorbed at the substrate electrode. During this surface interrogation the current measured through a feedback process varies accordingly to the amount of species adsorbed on the tip substrate. In other words, in this mode for the same electrochemical system the generation and detection of reactive species happen concomitantly in solution and is made possible through SECM feedback mode [81].

10.2.3.7 Penetration Mode

The name of this mode is self-explanatory. A small electrode is used to penetrate into a polymer film. The film contains a redox mediator and the variation of distance in the z axis allows for the determination of concentration differences, kinetics and mass transport variations [82, 83] depending of the depth of the electrode in the film. When the tip is inside a homogenous polymeric film, it is possible to make the same kind of voltammetric measurements than in solution. In

fact, as the tip goes through this film, reasonably conductive, and approaches the surface on which it is deposited, the feedback effects transpire and are comparable to those happening in solution though tunneling effects may occur for distances of <1 nm [49]. What makes this mode interesting is the possibility to use it with biological samples such as nuclei, [84] liposomes, [85] and cells [11] to detect intracellular electroactive molecules, differences of potential and ions crossing the cell membrane. Such experiments can provide information about the distribution of electroactive species inside the cell, potentials, and ion transfers across biological membranes [44].

10.2.3.8 Ion Transfer Mode

In this mode, the steady state diffusion controlled current, when the tip is away from the surface, and the feedback currents are generated during ion-transfer processes. A micropipette holds two unmixable solutions that create an interface and serve as an amperometric tip. Another interface is used as a sample but it can either be of liquid or solid nature. This setup can be useful for high-resolution SECM imaging of the liquid/liquid and liquid/membrane interfaces [49].

10.2.4 Different Substrate Used and Their Target Analysis

SECM instruments have been used for electrochemical measurements in many applications on a variety of materials such as charge transfer kinetic mechanisms [86], dissolution processes [87], corrosion of metals [88] and kinetic studies of adsorption and desorption [89], to name a few. The relatively new approach of electrochemist groups is their use of SECM to study biological systems [50]. It is possible to study different processes among them: neurotransmitter release [90], enzymatic activity and DNA hybridation [18], photosynthesis, respiration or redox activity at single-cell level [10].

10.2.5 Bio-SECM: Adaptation of the Instrument for Biosystem Analysis

A Bio-SECM is a SECM that has been modified to incorporate an inverted microscope. There are different models mostly homemade but HeKa Elektronik Dr. Schulze GmbH (Lambrecht/Pfalz, Germany) is offering two commercial models HeKa ELP 2 and HeKa ELP 3. The adaptation of conventional SECM into a bioanalytical tool made it more convenient to study electrochemical reactions on seeded cells [11, 14, 56, 69, 91, 92]. The inverted microscope gives the possibility

to identify suitable cells, with typical morphology of healthy cells and position the tip more quickly above the cells [26]. It is also possible to use a fluorescence microscope, which adds a non-negligible advantage of following the cell state by using specific viability fluorescent dyes. This allows one to corroborate electrochemical data with fluorescence images captured with a CCD camera.

10.3 SECM Studies Applied to Cancer

10.3.1 Biomarkers

Everyone has heard about cancer or knows someone affected by it. But what is cancer exactly? Cancer is a genetic disease appearing after alterations or changes in the DNA sequence of important genes [93]. By important genes we mean oncogenes stimulating cell division and survival or tumor suppressor genes controlling the cell cycle and regulating apoptosis (programmed cell death). When these genes are altered, cell functions are not regulated as they should and normal cells change into cancer cells that starts proliferating uncontrollably creating tumors [40].

An increasing number of people are affected by cancer every year and it is well known that early detection improves chances of successful outcome. This is the reason why researchers have been working towards developing more sensitive and specific methods for early cancer diagnosis [94]. A good strategy for improved screening is to look at cancer biomarkers. They are molecular changes detectable in patients' biological fluids, like blood or urine, but are not present in healthy people [40, 94, 95]. These biomarkers come from the tumor or are the results of the body reacting to the presence of a cancer [40]. Research in proteomic and genetic allows the discovery of promising biomarkers that could have clinical use. However, biomarkers have to be approved by the Food and Drug Administration (FDA) through clinical validation before they can be used and that process can be long and difficult [96]. Here are examples of commonly used biomarkers that successfully made it through: human chorionic gonadotropin- β (hCG β -subunit) for testicular cancer, cancer antigen 19-9 (CA19-9) for pancreatic cancer, cancer antigen 125 (CA125) for ovarian cancer, carcinoembryonic antigen (CEA) for colon cancer, prostate-specific antigen (PSA) for prostate cancer and cancer antigen 15-3 (CA15-3) for breast cancer [40, 96]. The use of biomarkers offers a great advantage of not being as invasive as biopsies. Also, the extraction of tissue is not always efficient in primary stage of cancer because cancer cells can be missed, in that case biomarkers can be better for early detection [94, 97]. Moreover, it is possible to use arrays to make multianalyte detection simultaneously by doing multiple immunoassays. Wilson and Nie used electrodes on which a different antigen was immobilized to detect seven tumor markers and obtained comparable results than with single-analyte enzyme-linked immunosorbent assays

(ELISA) [98]. Also, Ju's group developed a disposable device for automated detection of four tumor markers through amperometric immunoassay. In this case, antigen immobilized on working electrodes compete against antigens circulating in the sample for antibodies labeled with an enzyme, horseradish peroxidase (HRP), present in a limited quantity. The detection is done by amperometric monitoring of the enzymatic reduction of the HRP substrate, H_2O_2 [99]. Such multianalyte arrays diminish the detection time at a relatively low cost. The main problem with biomarkers is that they are often present in small amounts at a scale of pL and in order to make a diagnosis it is a prerequisite to have sensitive detection method with low enough detection limits [41]. As discussed below, this is where SECM could be relevant since it has been proven that single molecule can be detected [100–102] and could come in handy for diagnosis of cancer at an early stage.

10.3.2 SECM Studies on Cancer Biomarkers

10.3.2.1 Cytokine

Cytokines are small molecules that are mainly produced by leukocytes [104, 105] but also by tumor cells [106]. These proteins play a role in cell-to-cell communication by transmitting signals between cells [107]. Among them, there is the interleukin- 1β (IL- 1β) which is a pro-inflammatory cytokine present in the vicinity of almost all the tumors [108]. This same IL- 1β is involved in many diseases, for examples it is known to stimulate colon cancer cell growth [109], breast cancer progression [110] and cell proliferation in prostate cancer [106]. Also, when it's secreted at high concentration it promotes invasiveness of tumor cells [111].

The cytokine IL- 1β secreted by two cancer cell lines, used as leukocyte models, was studied on a cellular chip. This chip combines cell-collagen gel spots and SECM-enzyme linked immunosorbent assay (SECM-ELISA) [103]. During culture, the leukocyte models human monocytic leukemia (THP-1) and human promyelocytic leukemia (HL-60), were activated with phorbol 12-myristate-13-acetate (PMA) and lipopolysaccharides (LPS). As can be seen on Fig. 10.6a, a first antibody (Anti-IL- 1β) is attached to a glass substrate, this antibody links the IL- 1β secreted by the leukocytes in the collagen matrix. After removal of this matrix, the cytokine is trapped by a second antibody marked with a biotin to form a sandwich; this is the ELISA (Fig. 10.6b). Then this biotin combines with an avidin molecule labeling an enzyme (HRP). As mentioned earlier, the HRP uses H_2O_2 as a substrate. The enzymes catalyze the reduction of the hydrogen peroxide and then the ferrocenemethanol (FcMeOH) used as a redox mediator acts as an electron donor. The concentration variation of the oxidized form of ferrocenemethanol (FcMeOH⁺) is detected by measuring the reduction current generated at the electrode scanning over the spots. Even though the authors conclude the quantification of IL- 1β was challenging, they had results comparable to other methods found in literature [112, 113] and they did so by using sample volume of 1 μL [103].

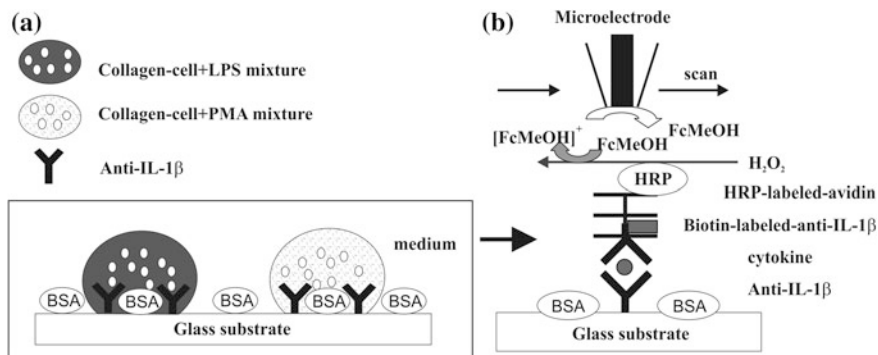


Fig. 10.6 Assembly of the sandwich structure on the antibody-immobilized glass substrate for cytokine assay of IL-1. Cell–collagen gel mixture droplets containing PMA or LPS were spotted, followed by further decoration for SECM imaging (a). A schematic diagram of the operating principle of the SECM-cytokine assay system (b). Reprinted with permission from [103]. Copyright (2006) Elsevier

10.3.2.2 Single Nucleotide Polymorphisms

Single nucleotide polymorphisms (SNPs) are the most frequent genetic variations [114, 115]. A SNP is a difference of a single nucleotide in the genome. Nucleotides are Adenosine (A), Thymine (T), Cytosine (C) and Guanine (G). For example, a SNP would be a mismatch due to a substitution between an A and a C. So SNP are biomarkers that can help locate genes related to diseases [114, 116–118]. Also, if the polymorphism happens in a repair gene section of the DNA, damage reparation can be altered and lead to cancer [119, 120].

Electrochemical measurements have been done to detect mismatch in DNA. Kraatz's group recently used electrochemical impedance spectroscopy (EIS) and SECM for this detection [121]. We will focus on the SECM part of their study. A 25 base fragment of hybridized ds-DNA films (forming a base-paired double helix) was printed on a gold substrate. SECM approach curves were done above the golden surface and the DNA spots with a Pt tip in a solution containing a redox mediator $K_4[Fe(CN)_6]$ in presence or absence of Zn^{2+} . The Zn^{2+} is used solely for signal amplification purpose. Above the bare surface, a positive feedback current was recorded compared to a negative feedback when the tip approached the ds-DNA. This negative current is mainly due to the diffusion limitation of the mediator to the tip caused by the presence of the ds-DNA. In the presence of Zn^{2+} , the signal amplification helped to better discriminate the mismatches ds-DNA film. Interestingly, the electrochemical results obtained were similar to those previously reported optical studies. This method shows that it is possible to study mismatches independently of their position, in this case they evaluated the entire 25 base sequence unlike other electrochemical experiments for which people looked at three positions only (top, center, bottom) [121].

10.3.2.3 Proenzyme

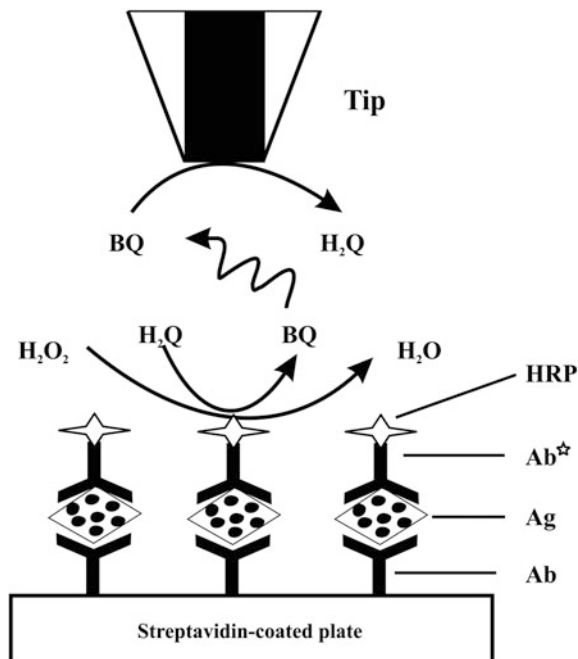
A pepsinogen is inactive; this is why we call it a proenzyme until it is converted into pepsin, its enzymatic active form [122]. Pepsinogens, like PG 1 and 2, are proteins secreted by gastric cells that can be measured in the plasma and the serum [123]. A low concentration of PG1 and low ratio of PG1/PG2 are considered to be biomarkers of atrophic chronic gastritis, a condition precursor of gastric cancer [84, 123–125]. SECM-ELISA type experiment is done to detect both pepsinogens [126]. The sandwich immunocomplexes are also done with HRP as previously described in the Cytokine section. This time, the ELISAs are done with anti-PG1 and anti-PG2 IgG antibodies to form microspots. Two method of microspot formation are used and compared. The first method consists of using a typical immunoassay procedure by immobilizing the antibodies on hydrophobic glass slides. A 50 μm diameter glass capillary is used to deposit the anti-PGs in small spots on the surface and then different concentrations of PG1 and PG 2 are added on the spots. The second method demands the use of silicon stencil made by lithography to create arrays containing pyramidal holes. The holes formed by chemical etching have $100 \times 100 \mu\text{m}$ dimensions. This stencil is deposited on a Polydimethylsiloxane (PDMS) surface and PDMS separators are added on the silicon to make sure all the holes are isolated before adding the anti-PGs in the holes. After the immunoreaction, the PDMS separators and the silicon template are removed. SECM dual imaging of PG1 and PG2, linked to different microspots, is done by scanning the electrode above the surfaces, glass or PDMS, in presence of the FcMeOH mediator. Once again, the detected reaction was previously explained in the Cytokine section. Both microspots fabrication methods allowed the detection of the pepsinogens, with limited cross-contamination, but the method using the pyramidal hole array gave sharper results [126].

10.3.2.4 Antigens

An antigen is an element that can induce the production of antibodies by lymphocytes [127]. Antigens specifically bind antibodies [128] equivalent to our daily lock and key combinations. The first antigen used as a cancer biomarker through an immunoassay was the carcinoembryonic antigen (CEA) [129, 130]. Matsue's group detected CEA with antigen/antibody sandwich microspots using SECM imaging just like they did with the pepsinogens. Doing so they could detect as low as 10^4 CEA molecules in a spot of 20 μm radius [131].

Also, it's been demonstrated that SECM GC mode can be useful for immunoassay to detect the circulating CA15-3 antigen [132]. The HRP enzyme was also used in the ELISA but this time around the detection was done in the presence of a hydroquinone (H_2Q) as a redox mediator. As can be seen on Fig. 10.7, the HRP in presence of H_2O_2 , catalyzes the conversion of the H_2Q into benzoquinone (BQ). The reduction current generated by the BQ at the electrode corresponds to the amount of CA15-3 immobilized in the sandwich. With this method, it was

Fig. 10.7 Assembly of the sandwich structure on the streptavidin-coated substrate and the schematic of SECM detection. Reprinted with permission from [132]. Copyright (2006) Elsevier



determined that the limit of detection is 2.5 U/mL, which is sensitive enough to detect CA15-3 antigens [9, 132].

In another study, SECM imaging was used to detect CD10 antigens [133]. These antigens can be expressed in different form of cancer like acute lymphoblastic leukemias, follicular lymphomas and Burkitt-like lymphomas [134]. To carry the experiment, a gold electrode coated with anti-CD10 antibodies is used as sample. Then to amplify the signal, gold nanoparticles are activated with glutathione to allow bonding with the HRP enzyme. When the CD10 antigen is present, the sandwich is formed on the electrode with a secondary antibody and the nanoparticles bonded to the HRP. A 10 μm platinum electrode was used to measure the reduction current of mediator $\text{Fe}(\text{CN})_6^{3-}$ to $\text{Fe}(\text{CN})_6^{4-}$ at the same time than imaging with the SG/GC mode. Optimal conditions allowed to have a linear response in a range from 1.0×10^{-11} up to 6.0×10^{-11} M with a detection limit of 4.38×10^{-12} M [133].

10.3.3 Studies on Mammalian Cancer Cells

As much as it is interesting to study biomarkers, the validation process can be dreadful [96]. Therefore, it can be advantageous to immobilize cells and evaluate the production and the diffusion of molecules in the vicinity of these cells. Many

molecules have been studied in electrochemistry such as reactive oxygen species (ROS), reactive nitrogen species (RNS) and nitric oxide synthases (NOS) [16, 135]. Detecting species produced by the cell itself restricts the cytotoxicity issues that can be induced by exogenous mediators that are potentially toxic. This is one of the reasons why people often choose to use oxygen to evaluate cell viability [12]. SECM offers great advantages to detect ROS at varied location on the cell membrane even at low levels and it is relatively specific [135]. But one of the main disadvantages during biological measurement is the biological molecules tendency to stick on the surface of the electrode [135] causing a decrease in the signal detected.

Reactive oxygen species are often studied because of their implication in cellular homeostasis and functions. Therefore monitoring ROS as principal indicator is interesting because of their production by all types of cells. This is the reason why SECM measurements are made on a variety of cells. Here are some examples of cancer cells studies.

10.3.3.1 MCF-10A and MDA-MB-231 Breast Cells

SECM has been used to measure the redox activity of individual human breast cells. In this experiment, Mirkin's group used a chemical mediator called quinone that takes part in intracellular redox activity after crossing the membrane [136]. The microelectrode is positioned close to the membrane in order to record the reactions in microsecond timescale. This experiment is extremely interesting because it reveals that the redox activity of breast cancer cells is different than the one seen in non-cancerous cells. With non-transformed or metastatic cells, the redox activity yield rate constants change accordingly to the alteration of expression or activity of the protein kinase C α which is an enzyme involved in the mechanism of cell metastasis. The SECM 2D scans allow to spatially resolve the redox map of an individual cell or field of cells. Therefore, this method allows one to distinguish breast cancer cells in the middle of non-transformed cells [136].

10.3.3.2 Hepatoblastoma Hep G2 Cells

Bard's group first studied the cytotoxicity of menadione on hepatocytes by using SECM's substrate generation/tip collection mode. They exposed the cells to menadione and detected the product made after it conjugates with glutathione. Glutathione acts as an antioxidant and protects the cell against oxidative product damages. This menadione-S-glutathione conjugate called thiodione is exported from the cells by an ATP-dependent pump. The SECM experiments made it possible to electrochemically observe and image the efflux of the thiodione from single cells and within groups of confluent living cells. Consequently, they could determine the amount of molecules of thiodione per cell per second exported from

a single layer of Hep G2 cells by using a simulation constant flux model. See Fig. 10.8 for a timeline exportation of thiodione from adjacent cells [69].

10.3.3.3 HeLa Cervical Cells

In Bard's group, menadione has been used for numerous years as an inducer of oxidative stress in living cells [69, 91, 137]. Menadione is a hydrophobic molecule that passes through the cell membrane passively and is cytotoxic. As mentioned

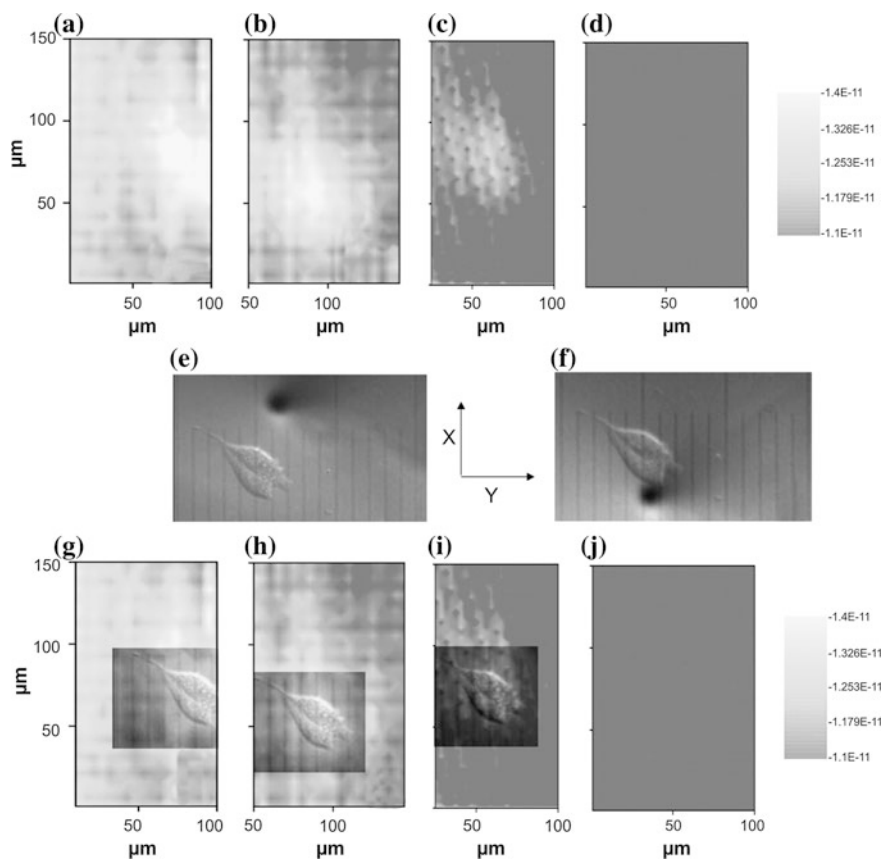


Fig. 10.8 Time-dependent profile of the export of thiodione from two adjacent human liver cells as detected by SECM imaging. **a–d** SECM images of the Hep G2 cell. The tip potential was held at 0.55 V versus $\text{Hg}/\text{Hg}_2\text{SO}_4$ and scanned at 150 $\mu\text{m}/\text{sec}$. The quiet time was 2 s. **e** and **f** Simultaneous optical micrograph of the Hep G2 cell being imaged. The black spot on the micrograph is the 10- μm Pt UME at two different positions, (**e** and **f**). One division corresponds to 10 μm . **g–j** Superimposed optical micrograph on the SECM image. These images were acquired after 43 min of incubation in the 80 μM menadione solution. All images were normalized with respect to scale. Reprinted with permission from [69]. Copyright (2004) National Academy of Sciences, U.S.A

earlier, once inside the cell, a detoxification process occurs and the menadione is conjugated to glutathione to form thiodione. This new molecule is then actively transported outside the cell by a pump called MRP1. The SECM system allowed them to measure the extracellular level of thiodione after its release. They managed to compare their experimental data with a computer simulation and determined the kinetic of menadione uptake and thiodione expulsion. Also, to make sure the MRP1 was really responsible for the transport, they used an inhibitor MK571 to moderate the pump's activity by competing with glutathione conjugate transport (Fig. 10.9) and a monoclonal antibody QCRL-4 that selectively blocks the MRP1 pumps. The thiodione flux decrease confirmed that thiodione was indeed actively transported by MRP1, and that glutathione is an essential substrate for MRP1-mediated transport. Therefore, one can say SECM can be a useful tool in quantitative studies of MRP1 inhibitors and suggests that monoclonal antibodies can be used to inhibit the transport of these pumps, and potentially limit the effects of multidrug resistance [137].

The beauty of the SECM is the possibility to make measurements at the single-cell level. In Matsue's group, they exploited this feature to measure the respiratory activities of cultured HeLa cells. They used the SECM to detect the oxygen

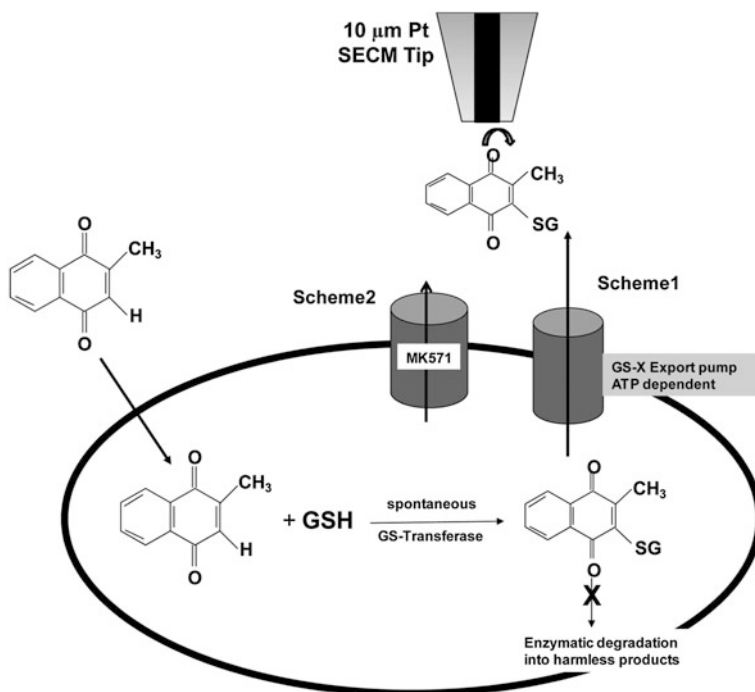


Fig. 10.9 Schematic diagram of cellular response to menadione in the presence or absence of MRP1 blocker MK571. Reprinted with permission from [137]. Copyright (2012) National Academy of Sciences, U.S.A

surrounding the cell and produced images of the localized distribution of oxygen. In this present study, they combined the utilization of a fluorescent probe, Calcein-AM, and SECM to assess changes in a single HeLa cell respiration after it's been exposed to inhibiting chemicals like KCN and Antimycin A. Calcein-AM stains all living cells green and emits fluorescence after being transformed to Calcein by esterases found in the cytoplasm. If the cell membrane is altered, the Calcein leaks and there is no fluorescence. So this probe is useful to visualize the damage done by the drugs to the membrane integrity. With this study, they could demonstrate that SECM made it possible to monitor the decrease of cellular respiration after the addition of inhibitors. When combining fluorescence measurements with SECM, the acquired information could help in elucidating drug action mechanism [138].

10.3.3.4 T24 Bladder Cells

Ding's group discovered a periodicity in the ROS evolution of human bladder cancer (T24) cells by time-lapse SECM (Fig. 10.10) [139]. They defined the extracellular profile of ROS when generated and released by a cell and when the cell is not releasing ROS. They could do so by comparing their experimental approach curves with simulated ones. The cell releases more or less ROS to maintain a good homeostasis. While an untreated cell actively released ROS its distribution was found to be steady with a long release/unrelease cycle. After administrating cisplatin to induce apoptosis, the periodicity of the ROS generation cycle is significantly accelerated and more species are released in the extracellular surrounding. This shows a modification in cell homeostasis. With ROS released from the cells as the redox mediator, SECM provides an excellent label-free method to monitor the physiological activities of single cancer cells [139].

10.3.3.5 Chinese Hamster Ovarian Cells and Human Epithelial Carcinoma A431 Cells

The epidermal growth factor receptor (EGFR) was imaged on the cell membrane of Chinese hamster ovarian cells (CHO) and human epithelial carcinoma A431 cells with SECM [140]. The EGFR has an important role in cancer cell development. A malfunction of this membrane protein causes unregulated proliferation, apoptosis inhibition, angiogenesis and possible metastasis [142]. Once again, SECM-ELISA type method was utilized with SG/TC and feedback modes to measure the amount of EGFR expressed in cell membrane. To do so, the receptor was attached to a first antibody (anti-EGFR) which was linked to a second antibody labelled with an alkaline phosphatase (ALP) molecule. The ALP hydrolyses the *p*-aminophenylphosphate monosodium salt (PAPP) present in the media into *p*-aminophenol (PAP). The antibody setup can be viewed on Fig. 10.11a. The latter was detected at the microelectrode by applying at +0.3 V potential versus an Ag/AgCl reference electrode. Doing so, single-cell imaging was accomplished and the

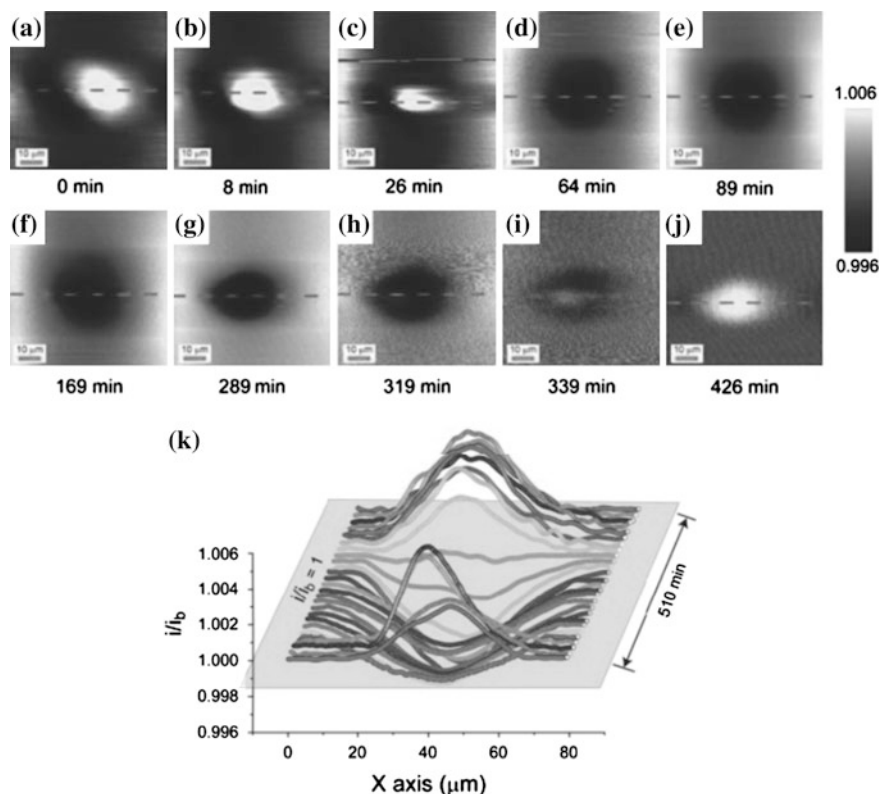


Fig. 10.10 ROS evolution of an untreated T24 cell revealed by time-lapse SECM images. **a–j** are representative conventional SECM images out of 27 images in total, which were taken by a $5\ \mu\text{m}$ diameter Pt UME at $-0.800\ \text{V}$ versus Ag/AgCl scanning over the same area in each image ($80 \times 80\ \mu\text{m}$) at certain time intervals (15–30 min). The scale bar presents the normalized current. The acquisition time of images (**a**) and (**b**) was 3 min for with 128×128 pixels, while that for images (**c–j**) was 12 min with 256×256 pixels. **k** Cross-section lines extracted from all the 27 time-lapse SECM images. The location of the cross-section line is illustrated in images (**a–j**) by the dashed red line. A correction of baseline tilting was made for the cross-section lines. i_b is the current value when the UME was far away from the cell. The duration of this set of time-lapse SECM experiments was 510 min. Reproduced with permission from [139]. Copyright (2012) by Elsevier

expression level of EGFR was statistically determined for CHO, CHO over-expressing EGFR and A431 cells. With the CHO cells having the lowest density of receptors and the A431 having the highest amount [140].

Later on, the same group showed optical and SECM images of EGFR expressed in patterned cells (Fig. 10.11b) [141]. The patterns of each cell lines can be view in the optical micrograph and the gradient of EGFR density is well visible from one cell line compared to the others on Fig. 10.11b.

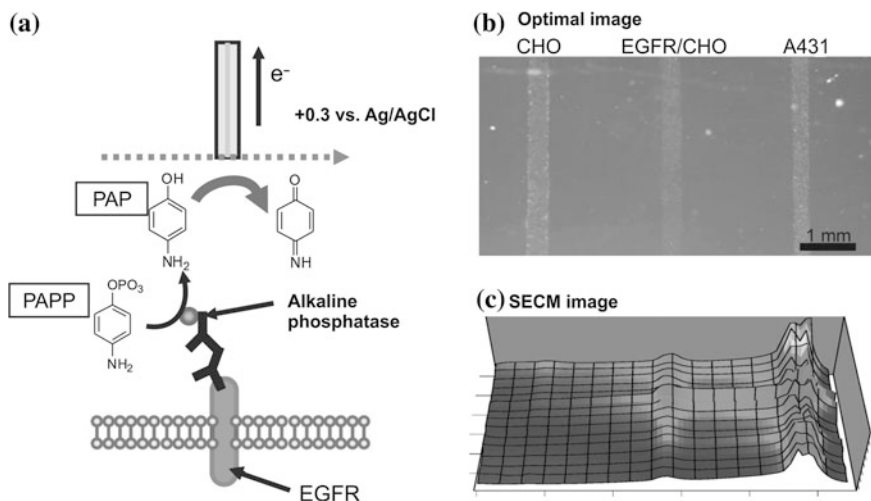


Fig. 10.11 **a** Schematic diagrams of EGFR detection using generation-collection mode. Adapted from [140] Copyright (2009) American Chemical Society. SECM image of the EGFR expression level of patterned different kinds of cells. **b** Optical microscopy image. **c** SECM image. The electrode was set at 20 mm above the substrate, and the scan rate was $100 \mu\text{m s}^{-1}$. The scan range was $7.0 \times 3.0 \text{ mm}$, and the step size was $100 \mu\text{m}$. Reproduced from [141] with permission of the PCCP Owner Societies

10.4 Conclusion

Analytical method development is intrinsically linked to our increased understanding of cancer. Several imaging techniques have already proven critical in early diagnostic and disease progression analysis: Positron Emission Tomography (PET), Ultrasound, and Magnetic Resonance Imaging (MRI).

PET is a 3D diagnostic imaging technic in nuclear medicine that produces images of functional process of the body [143]. This diagnostic tool uses chemical tracers such as neurotransmitters [144] and Fluorodeoxyglucose F18 (FDG) which is a radiolabelled glucose analogue [145]. Although it appeared in the 1970s [143, 146], PET research led to its gradual application in clinical use, oncology being its most important application [143] where it is used for: tumor detection [147], differential diagnosis of benign and malignant tumors [143], tumor metabolism and growth measurements [148], tumor staging and evaluation of tumor response [149], radiation treatment planning and development of new anticancer drugs [143]. Overall PET strives to image specific molecular targets that are associated with cancer to allow earlier diagnosis and better management of oncology patients.

Many imaging systems used for clinical purposes depend on electromagnetic radiation interaction with tissues or fluids [150]. As for ultrasonic imaging, it is mainly based on high-frequency sound waves being scattered, refracted, attenuated and reflected [151]. Since the sound waves bounce off tissues, it is possible to

image tissue stiffness allowing to distinguish between normal cells and cancer cells. As reported in the literature, tumors are stiffer than normal tissue [152] which makes them detectable by palpation. Palpation has its limitations since lesions are often too small or not positioned in a way to be felt [153, 154]. In cases like these ultrasound elastography can be a solution as it has been used to examine breast, prostate and liver [155]. This method can also be used endoscopically and can be used to image lymph nodes, oesophageal cancer, pancreatic cancer, adrenal and submucosal tumors [150, 156].

There are several reasons why MRI has emerged as a key technique in cancer diagnosis and management. First, MRI avoids the use of potentially damaging ionizing radiation and radioactive materials. It derives its signals from the interaction of tissues with a magnetic field and radiofrequency energy. For example, MRI can image nuclei atoms containing an odd number of protons and/or neutrons. As such, water molecules and protons on fat molecules are commonly imaged in MRI [157]. Second, the quality of the MRI images consistently has enhanced contrast among a variety of soft tissues. MRI has enhanced contrast in part because of a flexible parameterization that can be tuned to exploit different tissue-specific properties. Third, MRI generates tomographic images either as a true three-dimensional (3D) volume or by reconstruction from a stack of two-dimensional (2D) slices. This tomography can be acquired from any plane without patient or instrument movement.

PET and MRI are high-cost and low-throughput last line tools that are overbooked and critical to all cancer treatments. Ultrasound is definitely a lower cost technique but overall its throughput is relatively low. It is important to pursue the development of low cost and/or high-throughput first line of defense analytical methods capable of achieving early cancer diagnostics. As such, multianalyte protein arrays, high sensitivity mass spectrometry and electrochemical methods are attractive candidates.

The development of multianalyte protein arrays is tied to advances in microfluidics, arrays, sensors, and nanomaterials. Parallel acquisition of measurements of many analytes requires the use of arrays containing 100–10,000 μm sized features [158]. Microarray principle is based on receptors bound on the surface intercepting analytes and generating a signal. Each array area can be specific for different analytes making simultaneous analysis possible [159]. The detection of the signal is usually done electrochemically, gravimetrically or optically label free or not [160, 161]. Different labels include fluorescent dyes, quantum dots and metal colloids [161]. For example, DNA microarrays proved to be useful for cancer classification, diagnosis and prognosis [162]. They are used in different cancer research settings namely breast [163], prostate [164] and pediatric [165] cancers. Tissue microarrays (TMA) are also well known as diagnosis tools in Hodgkin's lymphomas, breast, prostate and bladder cancers among others [166, 167]. These TMA's present great advantages as they are an amplification of tissue resources and more biomarkers analysis can be performed for each sample. They are also great for reproducibility, rapid analysis and more economical since less reagent is needed [167]. On the other hand, the selected sample needs to be

representative of the total tissue or population, the results need statistical validation of the final cohort [167] the use of arrays in general require complex training protocols [158].

Mass Spectroscopy (MS) is an analytical chemistry staple capable of quantifying the exact mass of protein or peptide fragment from protein. Protein and peptides need to be ionized in order to be detected in MS. There are several sample introduction and ionization methods available, but for the specific case of protein/peptide samples direct or laser ionization are often used. The accelerated ions produced are then injected in a time of flight component, which achieves ion separation based on the time taken by individual ions to reach the detector. The time of flight of an ion is dependent on its charge to mass ratio. Aside from time of flight MS, tandem methods exist that can establish peptide sequences [168]. Hyphenation with chromatographic chips array MS can also be used in tandem with chromatographic chip arrays to selectively bind subsets of proteins from complex samples. The surfaces can be washed to remove nonspecifically bound proteins and substances that can interfere with the ionization process (salt, detergents, etc.). This type of analysis provides high throughput via automation and requires minimal sample preparation.

Finally electrochemistry is another analytical method that has potential for early cancer diagnostic applications for cancer biomarkers and in live cell assays. In this Chapter we have focused on an electrochemical imaging approach that can study cancer biomarkers and cancer cells. In terms of cancer biomarkers, SECM has been applied to cytokines, single nucleotide polymorphism, proenzymes and antigens. It has also been used to monitor the metabolic state of cancer cells through studies performed on reactive oxygen species, multidrug resistance and cancer protein membrane expression.

References

1. Haggerty, L., Lenhoff, A.M.: STM and AFM in biotechnology. *Biotechnol. Prog.* **9**(1), 1–11 (1993)
2. Rugar, D., Hansma, P.: Atomic force microscopy. *Phys. Today* **43**(10), 23–30 (1990)
3. Giessibl, F.J.: Principles and applications of the qPlus Sensor. In: Morita S, Giessibl F.J., Wiesendanger R. (Eds.) *Noncontact atomic force microscopy*, pp. 121–142. Springer, Berlin
4. Lieber, C.M., Wu, X.L.: Scanning tunneling microscopy studies of low-dimensional materials: probing the effects of chemical substitution at the atomic level. *Acc. Chem. Res.* **24**(6), 170–177 (1991)
5. Amemiya, S., et al.: Scanning electrochemical microscopy. *Ann. Rev. Anal. Chem.* **1**, 95–131 (2008)
6. Bard, A.J., et al.: Scanning electrochemical microscopy. Introduction and principles. *Anal. Chem.* **61**(2), 132–138 (1989)
7. Wittstock, G., et al.: SECM feedback imaging of enzymatic activity on agglomerated microbeads. *Electroanalysis* **13**(8–9), 669–675 (2001)
8. Wittstock, G.: Modification and characterization of artificially patterned enzymatically active surfaces by scanning electrochemical microscopy. *Fresen. J. Anal. Chem.* **370**(4), 303–315 (2001)

9. Roberts, W.S., et al.: Advances in the application of scanning electrochemical microscopy to bioanalytical systems. *Biosens. Bioelectron.* **23**, 301–318 (2007)
10. Amemiya, S., et al.: Biological applications of scanning electrochemical microscopy: chemical imaging of single living cells and beyond. *Anal. Bioanal. Chem.* **386**(3), 458–471 (2006)
11. Sun, P., et al.: Nanoelectrochemistry of mammalian cells. *Proc. Nat. Acad. Sci.* **105**(2), 443–448 (2008)
12. Zheng, X.T., Li, C.M.: Single cell analysis at the nanoscale. *Chem. Soc. Rev.* **41**(6), 2061–2071 (2012)
13. Hengstenberg, A., et al.: Spatially resolved detection of neurotransmitter secretion from individual cells by means of scanning electrochemical microscopy. *Angew. Chem. Int. Ed.* **40**(5), 905–908 (2001)
14. Kurulugama, R.T., et al.: Scanning electrochemical microscopy of model neurons: constant distance imaging. *Anal. Chem.* **77**(4), 1111–1117 (2005)
15. Wightman, R.M.: Probing cellular chemistry in biological systems with microelectrodes. *Science* **311**(5767), 1570–1574 (2006)
16. Borgmann, S.: Electrochemical quantification of reactive oxygen and nitrogen: challenges and opportunities. *Anal. Bioanal. Chem.* **394**(1), 95–105 (2009)
17. Shiku, H., Ohya, H., Matsue, T.: Scanning electrochemical microscopy applied to biological systems. In: Bard A.J., Stratmann, M. (eds.) *Encyclopedia of electrochemistry*, pp 257–275. Wiley-VCH, NY
18. Gyurecsányi, R.E., et al.: Chemical imaging of biological systems with the scanning electrochemical microscope. *Bioelectrochemistry* **63**(1–2), 207–215 (2004)
19. Wightman, R.M., Wipf, D.O.: Voltammetry at ultramicroelectrodes. In: Bard A.J. (ed.) *Electroanalytical chemistry*, pp 267–353. Marcel Dekker, New York (1989)
20. Montenegro, M.I., Queirós, M.A., Daschbach, J.L. (eds.): *Microelectrodes: Theory and Applications*. NATO ASI Series, Kluwer Academic Publishers, Dordrecht (1991)
21. Heinze, J.: Ultramicroelectrodes in electrochemistry. *Angew. Chem. Int. Ed. Engl.* **32**(9), 1268–1288 (1993)
22. Forster, R.J.: Microelectrodes: new dimensions in electrochemistry. *Chem. Soc. Rev.* **23**(4), 289–297 (1994)
23. Zoski, C.G.: Steady-state voltammetry at microelectrodes. In: Vanýsek P. (ed.) *Modern techniques in electroanalysis*, pp. 241–312. Wiley, New York (1996)
24. Bard, A.J.: Introduction and principles. In: Bard A.J., Mirkin, M.V. (eds.) *Scanning electrochemical microscopy*, CRC Press, USA (2001)
25. Lefrou, C., Cornut, R.: Analytical expressions for quantitative scanning electrochemical microscopy (SECM). *Chem. Phys. Chem.* **11**(3), 547–556 (2010)
26. Beaulieu, I., et al.: Biological scanning electrochemical microscopy and its application to live cell studies. *Anal. Chem.* **83**(5), 1485–1492 (2011)
27. Sun, P., Mirkin, M.V.: Kinetics of electron-transfer reactions at nanoelectrodes. *Anal. Chem.* **78**(18), 6526–6534 (2006)
28. Velmurugan, J., Sun, P., Mirkin, M.V.: Scanning electrochemical microscopy with gold nanotips: the effect of electrode material on electron transfer rates. *J. Phys. Chem. C* **113**(1), 459–464 (2008)
29. Bonazza, H.L., Fernández, J.L.: An efficient method for fabrication of disk-shaped scanning electrochemical microscopy probes with small glass-sheath thicknesses. *J. Electroanal. Chem.* **650**(1), 75–81 (2010)
30. Shin, H., et al.: Batch fabrication of atomic force microscopy probes with recessed integrated ring microelectrodes at a wafer level. *Anal. Chem.* **79**(13), 4769–4777 (2007)
31. Avdic, A., et al.: Fabrication of cone-shaped boron doped diamond and gold nanoelectrodes for AFM-SECM. *Nanotechnology* **22**(14), 1–6 (2011)
32. Shao, Y., et al.: Nanometer-sized electrochemical sensors. *Anal. Chem.* **69**(8), 1627–1634 (1997)

33. Hussien, E.M., Schuhmann, W., Schulte, A.: Shearforce-based constant-distance scanning electrochemical microscopy as fabrication tool for needle-type carbon-fiber nanoelectrodes. *Anal. Chem.* **82**(13), 5900–5905 (2010)
34. Zoski, C.G.: Ultramicroelectrodes: design, fabrication, and characterization. *Electroanalysis* **14**(15–16), 1041–1051 (2002)
35. Zoski, C.G.: UME fabrication/characterization basics. In: Cynthia G.Z. (ed.) *Handbook of electrochemistry*, pp. 189–260. Elsevier, Amstertam (2007)
36. Fu-Ren, F., Christophe D.: Preparation of Tips for Scanning Electrochemical Microscopy. In: Allen B.J., Michael M.V. (eds.) *Scanning electrochemical microscopy*, Second edn. pp 25–52, CRC Press, USA (2012)
37. Mirkin, M.V., et al.: Scanning electrochemical microscopy in the 21st century. Update 1: five years after. *Phys. Chem. Chem. Phys.* **13**(48), 21196–21212 (2011)
38. Borgmann, S., et al.: Amperometric biosensors, in advances in electrochemical science and engineering. Wiley-VCH Verlag GmbH & Co. KGaA. pp 1–83 (2011)
39. Bohunicky, B., Mousa, S.A.: Biosensors: the new wave in cancer diagnosis. *Nanotechnol. Sci. Appl.* **4**(1), 1–10 (2011)
40. Rasooly, A., Jacobson, J.: Development of biosensors for cancer clinical testing. *Biosens. Bioelectron.* **21**(10), 1851–1858 (2006)
41. Grieshaber, D., et al.: Electrochemical biosensors - sensor principles and architectures. *Sensors* **8**(3), 1400–1458 (2008)
42. Clark Jr, L.C., Clark, E.W.: A personalized history of the clark oxygen electrode. *Int. Anesthesiol. Clin.* **25**(3), 1–29 (1987)
43. Clark Jr, L.C., Lyons, C.: Electrode systems for continuous monitoring in cardiovascular surgery. *Ann. NY. Acad. Sci.* **102**(1), 29–45 (1962)
44. Sun, P., Laforge, F.O., Mirkin, M.V.: Scanning electrochemical microscopy in the 21st Century. *Phys. Chem. Chem. Phys.* **9**(7), 802–823 (2007)
45. Bard, A.J., Mirkin, M.V.: *Scanning Electrochemical Microscopy*, Second Edn. (2012)
46. Bertocello, P.: Advances on scanning electrochemical microscopy (SECM) for energy. *Energy Environ. Sci.* **3**(11), 1620–1633 (2010)
47. Barker, A.L., et al.: Scanning electrochemical microscopy: beyond the solid/liquid interface. *Anal. Chim. Acta* **385**(1–3), 223–240 (1999)
48. Mirkin, M.V.: High resolution studies of heterogeneous processes with the scanning electrochemical microscope. *Microchim. Acta* **130**(3), 127–153 (1999)
49. Mirkin, M.V., Horrocks, B.R.: Electroanalytical measurements using the scanning electrochemical microscope. *Anal. Chim. Acta* **406**(2), 119–146 (2000)
50. Edwards, M.A., et al.: Scanning electrochemical microscopy: principles and applications to biophysical systems. *Physiol. Meas.* **27**(12), R63–R108 (2006)
51. Kwak, J., Bard, A.J.: Scanning electrochemical microscopy. Theory of the feedback mode. *Anal. Chem.* **61**(11), 1221–1227 (1989)
52. Ballesteros Katemann, B., Schulte, A., Schuhmann, W.: Constant-distance mode scanning electrochemical microscopy (SECM)—part i: adaptation of a non-optical shear-force-based positioning mode for SECM tips. *Chem. A Eur. J.* **9**(9), 2025–2033 (2003)
53. Zhao, X., Diakowski, P.M., Ding, Z.: Deconvoluting topography and spatial physiological activity of live macrophage cells by scanning electrochemical microscopy in constant-distance mode. *Anal. Chem.* **82**(20), 8371–8373 (2010)
54. Eckhard, K., Schuhmann, W.: Alternating current techniques in scanning electrochemical microscopy (AC-SECM). *Analyst* **133**(11), 1486–1497 (2008)
55. Hengstenberg, A., Kranz, C., Schuhmann, W.: Facilitated tip-positioning and applications of non-electrode tips in scanning electrochemical microscopy using a shear force based constant-distance mode. *Chem. A Eur. J.* **6**(9), 1547–1554 (2000)
56. Bauermann, P., Schuhmann, L.W., Schulte, A.: An advanced biological scanning electrochemical microscope (Bio-SECM) for studying individual living cells. *Physical Chemistry Chemical Physics* **6**(15), 4003–4008 (2004)

57. Etienne, M., et al.: Feedback-independent Pt nanoelectrodes for shear force-based constant-distance mode scanning electrochemical microscopy. *Anal. Chem.* **78**(20), 7317–7324 (2006)
58. Eckhard, K., Schuhmann, W., Maciejewska, M.: Determination of optimum imaging conditions in AC-SECM using the mathematical distance between approach curves displayed in the impedance domain. *Electrochim. Acta* **54**(7), 2125–2130 (2009)
59. Cougnon, C., et al.: Development of a phase-controlled constant-distance scanning electrochemical microscope. *Anal. Chem.* **81**(9), 3654–3659 (2009)
60. Zu, Y., et al.: Scanning optical microscopy with an electrogenerated chemiluminescent light source at a nanometer tip. *Anal. Chem.* **73**(10), 2153–2156 (2001)
61. Lee, Y., Ding, Z., Bard, A.J.: Combined scanning electrochemical/optical microscopy with shear force and current feedback. *Anal. Chem.* **74**(15), 3634–3643 (2002)
62. Garay, M.F., et al.: Retrospective chemical analysis of tree rings by means of the scanning electrochemical microscopy with shear force feedback. *Phys. Chem. Chem. Phys.* **6**(15), 4028–4033 (2004)
63. Takahashi, Y., et al.: Transfected single-cell imaging by scanning electrochemical optical microscopy with shear force feedback regulation. *Anal. Chem.* **81**(23), 9674–9681 (2009)
64. Nebel, M., et al.: 4D shearforce-based constant-distance mode scanning electrochemical microscopy. *Anal. Chem.* **82**(18), 7842–7848 (2010)
65. Nebel, M., et al.: Local reactivity of diamond-like carbon modified PTFE membranes used in SO₂ sensors. *Electrochim. Acta.* **55**(27), 7923–7928 (2010)
66. Baltes, N., Heinze, J.: Imaging local proton fluxes through a polycarbonate membrane by using scanning electrochemical microscopy and functionalized alkanethiols. *Chem. Phys. Chem.* **10**(1), 174–179 (2009)
67. Scott, E.R., Phipps, J.B., White, H.S.: Direct imaging of molecular transport through skin. *J. Invest. Dermatol.* **104**(1), 142–145 (1995)
68. Mauzeroll, J., et al.: Detection of Tl(I) transport through a gramicidin – dioleoylphosphatidylcholine monolayer using the substrate generation – tip collection mode of scanning electrochemical microscopy. *Langmuir* **18**(24), 9453–9461 (2002)
69. Mauzeroll, J., et al.: Menadione metabolism to thiodione in hepatoblastoma by scanning electrochemical microscopy. *Proc. Natl. Acad. Sci.* **101**(51), 17582–17587 (2004)
70. Macpherson, J.V., Unwin, P.R.: Scanning electrochemical microscopy as an in vitro technique for measuring convective flow rates across dentine and the efficacy of surface blocking treatments. *Electroanalysis* **17**(3), 197–204 (2005)
71. Roberts, W.S., et al.: Detection and imaging the expression of the trans-membrane protein CD44 in RT112 cells by use of enzyme-labeled antibodies and SECM. *Biosens. Bioelectron.* (In press)
72. Stoica, L., Neugebauer, S., Schuhmann, W.: Scanning electrochemical microscopy (SECM) as a tool in biosensor research. In: Renneberg R., Lisdat F. (eds.) *Biosensing for the 21st Century*, pp. 455–492, Springer, Berlin (2008)
73. Lee, C., Kwak, J., Anson, F.C.: Application of scanning electrochemical microscopy to generation/collection experiments with high collection efficiency. *Anal. Chem.* **63**(14), 1501–1504 (1991)
74. Martin, R.D., Unwin, P.R.: Theory and experiment for the substrate generation/tip collection mode of the scanning electrochemical microscope: application as an approach for measuring the diffusion coefficient ratio of a redox couple. *Anal. Chem.* **70**(2), 276–284 (1998)
75. Zhou, F., Unwin, P.R., Bard, A.J.: Scanning electrochemical microscopy. 16. Study of second-order homogeneous chemical reactions via the feedback and generation/collection modes. *J. Phy. Chem.* **96**(12), 4917–4924 (1992)
76. Unwin, P.R., Bard, A.J.: Scanning electrochemical microscopy. 9. Theory and application of the feedback mode to the measurement of following chemical reaction rates in electrode processes. *J. Phy. Chem.* **95**(20), 7814–7824 (1991)

77. Demaille, C., Unwin, P.R., Bard, A.J.: Scanning electrochemical microscopy. 33. Application to the study of ECE/DISP reactions. *J. Phy. Chem.* **100**(33), 14137–14143 (1996)
78. Sánchez-Sánchez, C.M., et al.: Scanning electrochemical microscopy for studying electrocatalysis on shape-controlled gold nanoparticles and nanorods. *Electrochim. Acta* **55**(27), 8252–8257 (2010)
79. Pust, S.E., Maier, W., Wittstock, G.: Investigation of localized catalytic and electrocatalytic processes and corrosion reactions with scanning electrochemical microscopy (SECM). *Zeitschrift für Physikalische Chemie* **222**(10), 1463–1517 (2008)
80. Eckhard, K., et al.: Redox competition mode of scanning electrochemical microscopy (RC-SECM) for visualisation of local catalytic activity. *Phy. Chem. Chem. Phy.* **8**(45), 5359–5365 (2006)
81. Rodríguez-López, J.n., Alpuche-Avilés, M.A., Bard, A.J.: *Interrogation of Surfaces for the Quantification of Adsorbed Species on Electrodes: Oxygen on Gold and Platinum in Neutral Media*†. *J. Am. Chem. Soc.* **130**(50), 16985–16995 (2008)
82. Mirkin, M.V., Fan, F.-R.F., Bard, A.J.: Scanning electrochemical microscopy part 13. Evaluation of the tip shapes of nanometer size microelectrodes. *J. Electroanal. Chem.* **328**(1–2), 47–62 (1992)
83. Fan, F.R.F., Mirkin, M.V., Bard, A.J.: Polymer films on electrodes. 25. Effect of polymer resistance on the electrochemistry of poly(vinylferrocene): scanning electrochemical microscopic, chronoamperometric, and cyclic voltammetric studies. *J. Phy. Chem.* **98**(5), 1475–1481 (1994)
84. Guo, J., Amemiya, S.: Permeability of the nuclear envelope at isolated xenopus oocyte nuclei studied by scanning electrochemical microscopy. *Anal. Chem.* **77**(7), 2147–2156 (2005)
85. Zhan, W., Bard, A.J.: Scanning electrochemical microscopy. 56. Probing outside and inside single giant liposomes containing Ru(bpy)₃²⁺. *Anal. Chem.* **78**(3), 726–733 (2005)
86. Lu, X., Wang, Q., Liu, X.: Review: recent applications of scanning electrochemical microscopy to the study of charge transfer kinetics. *Anal. Chim. Acta* **601**(1), 10–25 (2007)
87. Macpherson, J.V., et al.: In-situ imaging of ionic crystal dissolution using an integrated electrochemical/AFM probe. *J. Am. Chem. Soc.* **118**(27), 6445–6452 (1996)
88. Niu, L., et al.: Application of scanning electrochemical microscope in the study of corrosion of metals. *J. Mater. Sci.* **44**(17), 4511–4521 (2009)
89. Unwin, P.R., Bard, A.J.: Scanning electrochemical microscopy. 14. Scanning electrochemical microscope induced desorption: a new technique for the measurement of adsorption/desorption kinetics and surface diffusion rates at the solid/liquid interface. *J. Phy. Chem.* **96**(12), 5035–5045 (1992)
90. Schulte, A., Nebel, M., Schuhmann, W.: Scanning electrochemical microscopy in neuroscience. *Ann. Rev. Anal. Chem.* **3**, 299–318 (2010)
91. Mauzeroll, J., Bard, A.J.: Scanning electrochemical microscopy of menadione-glutathione conjugate export from yeast cells. *Proc. National Acad. Sci.* **101**(21), 7862–7867 (2004)
92. Takahashi, Y., et al.: Topographic, electrochemical, and optical images captured using standing approach mode scanning electrochemical/optical microscopy. *Langmuir* **22**(25), 10299–10306 (2006)
93. Soper, S.A., et al.: Point-of-care biosensor systems for cancer diagnostics/prognostics. *Biosens. Bioelectron.* **21**(10), 1932–1942 (2006)
94. Tothill, I.E.: Biosensors for cancer markers diagnosis. *Semin. Cell Dev. Biol.* **20**(1), 55–62 (2009)
95. Chatterjee, S.K., Zetter, B.R.: Cancer biomarkers: knowing the present and predicting the future. *Future oncol.* **1**(1), 37–50 (2005)
96. Ludwig, J.A., Weinstein, J.N.: Biomarkers in cancer staging, prognosis and treatment selection. *Nat. Rev. Cancer* **5**(11), 845–856 (2005)
97. Hanash, S.M., Pitteri, S.J., Faca, V.M.: Mining the plasma proteome for cancer biomarkers. *Nature* **452**(7187), 571–579 (2008)

98. Wilson, M.S., Nie, W.: Multiplex measurement of seven tumor markers using an electrochemical protein chip. *Anal. Chem.* **78**(18), 6476–6483 (2006)
99. Wu, J., et al.: A disposable multianalyte electrochemical immunosensor array for automated simultaneous determination of tumor markers. *Clin. Chem.* **53**(8), 1495–1502 (2007)
100. Bard, A.J., Fan, F.-R.F.: Electrochemical detection of single molecules. *Acc. Chem. Res.* **29**(12), 572–578 (1996)
101. Fan, F.-R.F., Bard, A.J.: Electrochemical detection of single molecules. *Science* **267**(5199), 871–874 (1995)
102. Fan, F.-R.F., Kwak, J., Bard, A.J.: Single molecule electrochemistry. *J. Am. Chem. Soc.* **118**(40), 9669–9675 (1996)
103. Kasai, S., et al.: Cytokine assay on a cellular chip by combining collagen gel embedded culture with scanning electrochemical microscopy. *Anal. Chim. Acta* **566**(1), 55–59 (2006)
104. Whiteside, T.L.: Cytokines and cytokine measurements in a clinical laboratory. *Clin. Diagn. Lab. Immunol.* **1**(3), 257–260 (1994)
105. Curfs, J.H., Meis, J.F., Hoogkamp-Korstanje, J.A.: A primer on cytokines: sources, receptors, effects, and inducers. *Clin. Microbiol. Rev.* **10**(4), 742–780 (1997)
106. Coussens, L.M., Werb, Z.: Inflammation and cancer. *Nature* **420**(6917), 860–867 (2002)
107. Bouraoui, Y., et al.: Pro-inflammatory cytokines and prostate-specific antigen in hyperplasia and human prostate cancer. *Cancer Detect. Prev.* **32**(1), 23–32 (2008)
108. Mantovani, A., et al.: Cancer-related inflammation. *Nature* **454**(7203), 436–444 (2008)
109. Kaler, P., Augenlicht, L., Klampfer, L.: Macrophage-derived IL-1 β stimulates Wnt signaling and growth of colon cancer cells: a crosstalk interrupted by vitamin D3. *Oncogene* **28**(44), 3892–3902 (2009)
110. Valdivia-Silva, J.E., et al.: Effect of pro-inflammatory cytokine stimulation on human breast cancer: Implications of chemokine receptor expression in cancer metastasis. *Cancer Lett.* **283**(2), 176–185 (2009)
111. Apte, R.N., et al.: Effects of micro-environment- and malignant cell-derived interleukin-1 in carcinogenesis, tumour invasiveness and tumour-host interactions. *Eur. J. Cancer* **42**(6), 751–759 (2006)
112. Mita, Y., et al.: Induction of toll-like receptor 4 in granulocytic and monocytic cells differentiated from HL-60 cells. *Br. J. Haematol.* **112**(4), 1041–1047 (2001)
113. Fragaki, K., et al.: A novel leishmania infantum nuclear phosphoprotein Lepp 12 which stimulates IL1-beta synthesis in THP-1 transfectants. *BMC Microbiol.* **3**(1), 1–13 (2003)
114. Collins, F.S., Brooks, L.D., Chakravarti, A.: A DNA polymorphism discovery resource for research on human genetic variation. *Genome Res.* **8**(12), 1229–1231 (1998)
115. Hinds, D.A., et al.: Whole-genome patterns of common DNA variation in three human populations. *Science* **307**(5712), 1072–1079 (2005)
116. Fan, J.B., et al.: Highly parallel SNP genotyping. Cold Spring Harbor Laboratory Press, NY, pp 69–78 (2003)
117. Sachidanandam, R., et al.: A map of human genome sequence variation containing 1.42 million single nucleotide polymorphisms. *Nature* **409**(6822), 928–933 (2001)
118. Halushka, M.K., et al.: Patterns of single-nucleotide polymorphisms in candidate genes for blood-pressure homeostasis. *Nat. Genet.* **22**(3), 239–247 (1999)
119. Goode, E.L., Ulrich, C.M., Potter, J.D.: Polymorphisms in DNA repair genes and associations with cancer risk. *Cancer Epidemiol. Biomark. Prev.* **11**(12), 1513–1530 (2002)
120. Ford, B.N., et al.: Identification of single nucleotide polymorphisms in human DNA repair genes. *Carcinogenesis* **21**(11), 1977–1981 (2000)
121. Alam, M.N., Shamsi, M.H., Kraatz, H.-B.: Scanning positional variations in single-nucleotide polymorphism of DNA: an electrochemical study. *Analyst* **137**(18), 4220–4225 (2012)
122. Hirschowitz, B.I.: Pepsinogen: its origins secretion and excretion. *Physiol. Rev.* **37**(4), 475–511 (1957)

123. Abnet, C.C., et al.: Plasma pepsinogens, antibodies against helicobacter pylori, and risk of gastric cancer in the Shanghai Women's Health Study Cohort. *Br. J. Cancer* **104**(9), 1511–1516 (2011)
124. di Mario, F., Cavallaro, L.G.: Non-invasive tests in gastric diseases. *Digestive and Liver Disease* **40**(7), 523–530 (2008)
125. Dinis-Ribeiro, M., et al.: *Meta*-analysis on the validity of pepsinogen test for gastric carcinoma, dysplasia or chronic atrophic gastritis screening. *J. Med. Screen.* **11**(3), 141–147 (2004)
126. Yasukawa, T., et al.: Enzyme immunosensing of Pepsinogens 1 and 2 by scanning electrochemical microscopy. *Biosens. Bioelectron.* **22**(12), 3099–3104 (2007)
127. Zabriskie, J.B.: *Essential clinical immunology*. Cambridge University Press, Cambridge (2009)
128. Roitt, I.M., Delves, P.J.: *Roitt's essential immunology*. 10th edn. p. 481 (2001)
129. Thomson, D.: The carcinoembryonic antigen (CEA) radioimmunoassay. *Proc. Roy. Soc. Med.* **65**(7), 635–636 (1972)
130. Malyankar, U.M.: Tumor-associated antigens and biomarkers in cancer and immune therapy. *Int. Rev. Immunol.* **26**(3–4), 223–247 (2007)
131. Shiku, H., Matsue, T., Uchida, I.: Detection of microspotted carcinoembryonic antigen on a glass substrate by scanning electrochemical microscopy. *Anal. Chem.* **68**(7), 1276–1278 (1996)
132. Zhang, X., Peng, X., Jin, W.: Scanning electrochemical microscopy with enzyme immunoassay of the cancer-related antigen CA15-3. *Anal. Chim. Acta* **558**(1–2), 110–114 (2006)
133. Song, W., Yan, Z., Hu, K.: Electrochemical immunoassay for CD10 antigen using scanning electrochemical microscopy. *Biosens. Bioelectron.* **38**(1), 425–429 (2012)
134. Uherova, P., et al.: The clinical significance of CD10 antigen expression in diffuse large B-cell lymphoma. *Am. J. Clin. Pathol.* **115**(4), 582–588 (2001)
135. Bogeski, I., et al.: Redox regulation of calcium ion channels: chemical and physiological aspects. *Cell Calcium* **50**(5), 407–423 (2011)
136. Rotenberg, S.A., Mirkin, M.V.: Scanning electrochemical microscopy: detection of human breast cancer cells by redox environment. *J. Mammary Gland Biol. Neoplasia* **9**(4), 375–382 (2004)
137. Koley, D., Bard, A.J.: Inhibition of the MRP1-mediated transport of the menadione-glutathione conjugate (Thiodione) in HeLa cells as studied by SECM. *Proc. Natl. Acad. Sci.* **109**(29), 11522–11527 (2012)
138. Kaya, T., et al.: Monitoring the cellular activity of a cultured single cell by scanning electrochemical microscopy (SECM). A comparison with fluorescence viability monitoring. *Biosens. Bioelectron.* **18**(11), 1379–1383 (2003)
139. Zhang, M.M.N., Long, Y.-T., Ding, Z.: Cisplatin effects on evolution of reactive oxygen species from single human bladder cancer cells investigated by scanning electrochemical microscopy. *J. Inorg. Biochem.* **108**, 115–122 (2012)
140. Takahashi, Y., et al.: Electrochemical detection of epidermal growth factor receptors on a single living cell surface by scanning electrochemical microscopy. *Anal. Chem.* **81**(7), 2785–2790 (2009)
141. Takahashi, Y., et al.: Electrochemical detection of receptor-mediated endocytosis by scanning electrochemical microscopy. *Phy. Chem. Chem. Phys.* **13**(37), 16569–16573 (2011)
142. Pantaleo, M.A., et al.: Experimental results and related clinical implications of PET detection of epidermal growth factor receptor (EGFr) in cancer. *Ann. Oncol.* **20**(2), 213–226 (2009)
143. Langer, A.: A systematic review of PET and PET/CT in oncology: a way to personalize cancer treatment in a cost-effective manner? *BMC Health Services Research* **10**(283), 1–16 (2010)
144. Volkow, N.D., et al.: PET evaluation of the dopamine system of the human brain. *J. Nucl. Med.* **37**(7), 1242–1256 (1996)

145. Allison, D.B., et al.: Microarray data analysis: from disarray to consolidation and consensus. *Nat. Rev. Genet.* **7**(1), 55–65 (2006)
146. Czernin, J., Phelps, M.E.: Positron emission tomography scanning: current and future applications. *Annu. Rev. Med.* **53**(1), 89–112 (2002)
147. Groves, A.M., et al.: Non- ^{18}F FDG PET in clinical oncology. *Lancet Oncol.* **8**(9), 822–830 (2007)
148. Shields, A.: Positron emission tomography measurement of tumor metabolism and growth: its expanding role in oncology. *Mol. Imag. Biol.* **8**(3), 141–150 (2006)
149. Bomanji, J.B., Costa, D.C., Ell, P.J.: Clinical role of positron emission tomography in oncology. *Lancet Oncol.* **2**(3), 157–164 (2001)
150. Fass, L.: Imaging and cancer: a review. *Mol. Oncol.* **2**(2), 115–152 (2008)
151. Lawrence, J.P.: Physics and instrumentation of ultrasound. *Crit. Care Med.* **35**(8 SUPPL.), S314–S322 (2007)
152. Paszek, M.J., et al.: Tensional homeostasis and the malignant phenotype. *Cancer Cell* **8**(3), 241–254 (2005)
153. Lerner, R.M., Huang, S.R., Parker, K.J.: “Sonoelasticity” images derived from ultrasound signals in mechanically vibrated tissues. *Ultrasound Med. Biol.* **16**(3), 231–239 (1990)
154. Zhi, H., et al.: Comparison of ultrasound elastography, mammography, and sonography in the diagnosis of solid breast lesions. *J. Ultrasound Med.* **26**(6), 807–815 (2007)
155. Ophir, J., et al.: Elastographic Imaging. *Ultrasound Med Biol* **26**(1), S23–S29 (2000)
156. Reddy, Y., Willert, R.P.: Endoscopic ultrasound: what is it and when should it be used? *Clin. Med. J. Roy. Coll. Physicians* **9**(6), 539–543 (2009)
157. Korosec, F.R.: *Basic principles of MRI and MR angiography*. In: Carr, J.C., Carroll, T.J. (eds.) *Magnetic resonance angiography*, pp. 3–38. Springer, New York (2012)
158. Walt, D.R.: Miniature analytical methods for medical diagnostics. *Science* **308**(5719), 217–219 (2005)
159. Dufva, M., Christensen, C.B.V.: Diagnostic and analytical applications of protein microarrays. *Expert Rev. Proteomics* **2**(1), 41–48 (2005)
160. Sassolas, A., Leca-Bouvier, B.D., Blum, L.J.: DNA biosensors and microarrays. *Chem. Rev.* **108**(1), 109–139 (2007)
161. Bally, M., et al.: Optical microarray biosensing techniques. *Surf. Interface Anal.* **38**(11), 1442–1458 (2006)
162. Young, R.A.: Biomedical discovery with DNA arrays. *Cell* **102**(1), 9–15 (2000)
163. Cooper, C.: Applications of microarray technology in breast cancer research. *Breast Cancer Res.* **3**(3), 1–18 (2001)
164. Grouse, L.H., Munson, P.J., Nelson, P.S.: Sequence databases and microarrays as tools for identifying prostate cancer biomarkers. *Urology* **57**(4, Supplement 1), 154–159 (2001)
165. Triche, T.J., Schofield, D., Buckley, J.: DNA microarrays in pediatric cancer. *Cancer J.* **7**(1), 2–15 (2001)
166. Simon, R., Mirlacher, M., Sauter, G.: Tissue microarrays in cancer diagnosis. *Expert Rev. Mol. Diagn.* **3**(4), 421–430 (2003)
167. Dolled-Filhart, M.P., Gustavson, M.D.: Tissue microarrays and quantitative tissue-based image analysis as a tool for oncology biomarker and diagnostic development. *Expert Opin. Med. Diagn.* **6**(6), 569–583 (2012)
168. Conrad, D., Goyette, J., Thomas, P.: Proteomics as a method for early detection of cancer: a review of proteomics, exhaled breath condensate, and lung cancer screening. *J. Gen. Intern. Med.* **23**, 78–84 (2008)

Index

A

Adhesion, 42, 183, 186, 192, 194, 205, 315
Alkaline phosphatase, 14, 36, 52, 55, 127, 130, 251, 252
Aminolysis, 239, 240, 255–257
Antimicrobial properties, 105, 106, 117
Antioxidant, 251, 348
Anti-thrombogenicity, 190
Artificial hearts, 15, 34, 191

B

Bioactive glass, 20, 44–46, 156, 243
Bioceramic, 38, 44, 232
Biocompatibility, 8, 11, 20, 25–28, 30, 32–36, 38, 41, 44–52, 57–60, 74, 123, 156, 171, 172, 174–176, 178, 180, 184, 188, 191, 212, 213, 221, 251, 267–269, 271, 301, 303, 305, 312, 313, 318, 321, 323
Biodegradable, 9, 123, 211, 229, 231–234, 254, 256, 287
Biofoam, 69, 70, 80, 81
Biofunctional coating, 9, 105
Biomimetic, 39, 41, 109, 118, 120, 131, 154, 241, 242, 245, 254, 258, 266
Biomaterialization, 39, 120, 129, 131
Biomolecules, 105, 111–117, 129, 132, 229, 231, 233, 241, 242, 245, 246, 249, 251, 254, 256, 258, 270, 272, 273, 292, 309
Biosensors, 50, 163–165, 265–269, 272, 275, 277, 286, 292, 335
Bone regeneration, 38, 106, 128, 130
Brownian motion, 150, 151, 158
Burkitt-like lymphomas, 347

C

Cantilever, 274, 331, 332
Carbon nanotube, 9, 52, 303, 313, 316, 324
Carboxyl, 112–114, 127, 130, 234, 239, 246
Cell-cell interactions, 289
Cerebrospinal fluid, 305
Chemisorptions, 270, 272
Chromatographic chip arrays, 355
Collagen, 126, 127, 243, 255
Corrosion, 1, 12, 13, 15, 16, 25, 31
Cytotoxic, 14, 18, 21, 24, 30, 31–33, 36, 47, 50

D

Delamination, 77, 108, 178, 315, 321
Dental implants, 15, 38, 39, 105–111, 117, 121–123, 126–129
Diamond, 9, 33, 36, 171–173, 184, 269
Dielectrophoresis, 150, 151
DNA hybridization, 116, 275, 280
DNA sequence, 282, 283, 284, 343

E

Early cancer diagnosis, 343
Electrode surface, 158, 309, 316, 334
Electrodeposition, 108, 314
Electroosmosis, 159, 162
Electrophoresis, 9, 145, 147–150, 155, 157, 162, 165
ELISA, 236, 344, 346, 351
Entrapment, 250, 251
Epitaxy, 270

F

Feedback mode, 336, 337, 341, 351
 Fiber metal mesh, 70–72, 74–76
 Fibrinogen, 34, 36, 175, 176, 178, 184, 185, 187–191, 243
 Fibronectin, 57, 59, 108, 117–119, 127, 128, 240, 242, 243, 246, 291, 309
 Flavor barrier, 212
 Flexible substrate, 312, 313
 Fluorescence image, 343
 Fracture, 15, 17, 20, 24, 36, 41, 44, 46, 60, 91, 92, 106, 171, 174, 196, 197, 199–201, 203–205

G

Gas barrier, 207–210, 213, 214
 Glucose monitoring, 266
 Gription, 69, 70, 83, 84
 Growth mechanism, 4

H

HVOF, 8, 28
 Hydroxyapatite, 38, 39, 41
 Hydroxyl groups, 112, 115, 229, 239

I

Immunoassay, 343, 344, 346
 Impedance spectroscopy, 305, 311, 345
 In vitro, 16, 21, 23, 51, 290
 In vivo, 14, 23, 24, 34, 42–45, 81
 Inflammation, 14, 18, 20, 21, 33, 34, 174, 243

K

Knee implant, 23, 76

L

Lab-on-a-chip, 9, 275–277, 279, 280, 285
 Large-distance imaging, 336
 Liquid medium, 145, 147, 148, 150, 153, 274

M

Magnetic particles, 275
 Magnetic resonance imaging, 353
 Mass spectroscopy, 355
 Membrane, 13, 57, 117, 118, 122, 123, 129, 130, 153, 165, 175, 178, 189, 193, 208, 285, 287, 291, 309, 335, 342, 348, 351, 355

Mesoporous silica, 156, 157
 Migration, 43, 44, 52, 55, 77, 90, 147, 210, 212, 236, 290
 Miniaturization, 2, 31, 146, 266, 273, 275, 288, 290, 292
 Molecular linkers, 113
 Molecular recognition surfaces, 270
 Morphology, 18, 23, 28, 32–36, 38, 39, 41, 47, 51, 54, 55, 105, 156, 185, 187, 200, 231, 238, 251, 315, 343

N

Neurological diseases, 301
 Neuron, 305, 309
 Neurotransmitter, 334, 342, 353
 Nitinol, 27–31, 176, 177, 191

O

Oligonucleotide, 116, 335
 Orthopaedic implant, 70–73, 76, 84, 85
 Osteoblast, 13, 14, 21, 25, 35, 47
 Osteocalcin, 44, 47, 108, 118, 120, 130
 Osteoconduction, 14, 44
 Osteogenic proteins, 244
 Osteopontin, 117, 118, 130

P

Paraffin, 279
 Peel strength, 195, 196, 199
 Penetration, 28, 82, 123, 136, 341
 Permeability coefficient, 208
 Photosynthetic organism, 164
 Physisorption, 245, 255, 256, 270
 Plasma modification, 334, 336
 Plasma spray, 8, 70, 72, 77–79
 Polyester, 229, 233, 234, 238, 240, 241, 250, 252
 Polyethylene, 194–196, 200
 Polymerase chain reaction, 14, 280
 Proenzyme, 346, 355
 Protein adsorption, 107, 116, 184, 187–190

R

Random impingements, 151
 Recyclability, 207, 212
 Redox, 334, 336, 340–342, 344–346, 348, 351
 Regenerex, 69, 70, 79
 Resonant sensors, 274, 285

S

- Scaffold, 45, 60, 79, 85, 87, 88, 127, 231–233, 240, 242, 243, 245, 247, 249, 251, 256, 258
- Scanning electrochemical microscopy, 9, 338
- Self-assembly, 112, 125, 251, 253, 254
- Shape memory alloys, 27, 31
- Silane, 113, 114, 123, 127, 128, 131, 272
- Simulated body fluid, 32, 39, 45, 54, 56, 109
- Single nucleotide polymorphisms, 345
- Spinal cord interfaces, 303
- Statherin, 120, 131
- Stem cells, 18, 37, 42, 45, 48, 55, 60, 125, 236, 245, 301
- StikTite, 69, 70, 84
- Stimulating electrodes, 306, 307
- Superhydrophilic surface, 108
- Supersaturation, 109, 130
- Surface energy, 55, 105, 108, 179, 189, 190
- Surface free energy, 190, 197–199
- Surface Interrogation, 336, 341
- Surface roughness, 182–194

T

- Thin film deposition, 3, 314
- Ti-6Al-4V, 17, 20, 42, 113
- Tissue microarrays, 354
- Tissue regeneration, 11, 230, 232
- Topography, 239, 246, 313, 331
- Tritanium, 69, 82, 83

U

- UV barrier, 212